SLAC-R-204

SLAC-204
(T/E)

PROCEEDINGS OF

SUMMER INSTITUTE ON PARTICLE PHYSICS

July 11-22, 1977

QUARK SPECTROSCOPY AND HADRON DYNAMICS

Program Directors

David W. G. S. Leith

and

Frederick J. Gilman

Ed. by Martha C. Zipf

Sponsored by Stanford University and Stanford Linear Accelerator Center
under contract with the Energy Research and Development Administration.
Contract EY-76-C-03-0515

November 1977

Printed in the United States of America. Available from National Technical
Information Service, U.S. Department of Commerce,
5285 Port Royal Road, Springfield, Va. 22161
Prices: Printed copy $15.00; Microfiche $3.00

PREFACE

This volume contains the Proceedings of the fifth SLAC Summer Institute on Particle Physics which was held at the Stanford Linear Accelerator Center July 11-22, 1977. The topic for this year's Institute, "Quark Spectroscopy and Hadron Dynamics," was covered by usage of the format of previous years with a one-week long intense, pedagogic review of the material followed by a three-day topical conference.

The Institute was attended by 317 physicists from 18 countries. Over half of the participants were experimentalists. The meeting derives its importance not only from the topicality of the subjects and the high quality of the lectures, but also from the fact that there are few continuing meetings in the United States in which the frontiers of the field are regularly reviewed and which make a positive effort to encourage strong participation from the experimental physicist community

The lectures covered the spectroscopy of quarks and leptons, discussed why the quarks are not observed freely in nature, and reviewed the properties of hadronic systems built from the various quark building blocks. Once again, the afternoon discussion sessions were well attended and provided an opportunity for informal, and often exciting, exchanges of ideas on the day's lecture material. During the topical conference there were fifteen reports on the leading work in th field with many last minute results from SPEAR, DORIS, and FNAL.

Again, the smooth running of the Institute and the informal, friendly atmosphere which characterized the meeting were due, in large part, to the careful planning and hard work of the Coordinator, Martha C. Zipf, assisted by Delores Adams and Joan Meister.

David W. G. S. Leith and Frederick J. Gilman

Program Directors

Table of Contents

PART II. Topical Conference (continued)

WIS-77/56-PH
November 1977

Quarks and Leptons*

Haim Harari

Weizmann Institute of Science, Rehovot, Israel

and

Stanford Linear Accelerator Center, Stanford
California, U.S.A.

A review based on lectures delivered at the SLAC Summer Institute, July 1977. To be published in Physics Reports.

*Supported in part by the United States-Israel Binational Science Foundation and the Israel Commission for Basic Research, and by the U.S. Energy Research and Development Administration.

Abstract

We review the physics of quarks and leptons within the framework of gauge theories for the weak and electromagnetic interactions. The Weinberg-Salam $SU(2) \times U(1)$ theory is used as a "reference point" but models based on larger gauge groups, especially $SU(2)_L \times SU(2)_R \times U(1)$, are discussed. We distinguish among three "Generations" of fundamental fermions: The first generation (e^-, ν_e, u, d), the second generation (μ^-, ν_μ, c, s) and the third generation (τ^-, ν_τ, t, b). For each generation we discuss the classification of all fermions, the charged and neutral weak currents, possible right-handed currents, parity and CP-violation, fermion masses and Cabibbo-like angles and related problems. We review theoretical ideas as well as experimental evidence, emphasizing open theoretical problems and possible experimental tests. The possibility of unifying the weak, electromagnetic and strong interactions is a grand unification scheme is reviewed. The problems and their possible solutions are presented, generation by generation, but a brief subject-index (following the table of contents) enables the interested reader to follow any specific topic throughout the three generations.

Table of Contents

Table I: A brief subject index to those topics which are discussed in several different sections. Topics which are discussed only in one section (e.g. $\mu^- \to e^-\gamma$ or the T-family) are not included in the table. They can be easily found by consulting the Table of Contents.

Subject	Sections containing detailed dicussion	Sections containing brief reference
Cabibbo Angles		
Quark Sector	(3.1)(3.10)(4.7)	
Lepton Sector	(3.8)(4.3)	(3.1)
CP Violation	(3.9)(4.10)	(4.5)(4.7)
Fermion Masses	(2.7)(3.10)	
Grand Unification	(2.8)(2.9)(2.10)(3.11)	(4.1)
Higgs Particles	(2.6)	(3.8)(3.9)
Models		
$SU(2)_L \times SU(2)_R \times U(1)$	(2.6)	(2.1)(2.10)(4.4)(4.5)(4.8)(5.1)
$SU(3) \times U(1)$		(3.5)(4.1)(5.2)
Multimuon Events		(3.2)(3.3)(4.5)(4.8)(4.9)(5.2)
Neutral Currents		
General Phenomenology	(2.2)(2.3)(2.4)(2.6)	(3.4)(5.2)
Flavor Conservation	(3.5)(3.6)	(3.4)
Right-Handed Currents		
Quark Sector	(3.2)(3.3)(4.11)	(2.4)(3.9)(5.2)
Lepton Sector		(2.3)(3.8)(4.4)
Weak Decays of New Mesons	(4.8)(4.9)	(3.2)(3.3)(3.6)

1. Introduction

1.1 Quark and Lepton Spectroscopy

At the time of this writing we have clear evidence for the existence of four different flavors of quarks and five flavors of leptons. There is indirect evidence for, at least, one additional quark and one additional lepton. In the last few years, various authors have entertained speculations involving even larger numbers of quarks and leptons. The proliferation of quarks and leptons has been sudden and largely unexpected. For ten years (1964-1974), the world of particle physics was more or less content with three quarks and four leptons. However, now we regard the number of fundamental fermions as yet another unknown parameter in our theoretical picture of the structure of matter.

With the proliferation of quarks and leptons, a new field of investigation has opened up. Suddenly, the old μ-e puzzle is generalized to the much more complex problem of understanding the quark and lepton mass spectrum. The problem of computing the Cabibbo angle expands into the question of calculating several such angles in the quark and lepton sectors of the theory and a possible connection is established between these angles and CP violation. An important (but poorly understood) relation probably exists between the masses of the fundamental fermions and the Cabibbo angles. Several hints seem to connect quarks and leptons to each other and one wonders about the study of all fundamental fermions under the roof of a common "grand unification" gauge group of the strong, electromagnetic and weak interactions. Some of these problems have been with us in one form or another for several decades, but the theoretical and experimental developments of the last few years have provided a new dimension to each one of them.

Hadron spectroscopy is still very much alive. It is still interesting, as well as important, to classify the observed hadrons, study strong, weak and electromagnetic transitions between hadronic levels, understand the quark rules which govern hadronic collisions, and search for exotic hadrons. Theoretically, the study of the hadron as a system of confined quarks is one of the most important unsolved problems of physics. Quantum-Chromo-Dynamics (QCD) is the candidate theory for explaining quark confinement, and some of its features (such as asymptotic freedom) are tested in deep inelastic collisions and in processes which are forbidden by the Zweig-Iizuka rule. All of these topics relate to hadron spectroscopy.

At the same time, we begin to see glimpses of the next spectorscopy: the spectroscopy of quarks and leptons. Here we try to understand the mass pattern of the fundamental fermions (rather than the composite hadrons). We study weak transitions between fundamental fermions (sometimes by extracting the necessary information from weak hadronic transitions). We ask questions such as: How many types of quarks exist? How many leptons? What are their symmetry properties? What is the gauge group of the weak and electromagnetic interactions? To which representations of this gauge group do we assign the left-handed and the right-handed fundamental fermions? What are the properties of the gauge vector Bosons and the Higgs scalar particles in such a theory? What are the experimental values of all Cabibbo-like angles? How can we calculate these angles? Can we incorporate the phenomenon of CP-violation into our gauge theory, and predict its observed magnitude?

The present review is devoted to the open problems of quark and lepton spectroscopy. Some of these problems are listed above while others will be raised throughout our discussion. Whenever the answers

are known, we try to provide them. When they are not known (in most cases!) we outline some of the possible directions of attacking the problem. Whenever possible, we discuss experimental tests of the various ideas and models.

1.2 Theoretical Framework: A "Minimal" SU(2) x U(1) Theory

We do not yet know which is the ultimate gauge algebra of the weak and electromagnetic interactions [1]. It is likely, but not certain, that the correct algebra includes SU(2) x U(1) as a sub-algebra (perhaps in a trivial way, i.e. the correct algebra is SU(2) x U(1)). We will devote some of our attention to models based on different gauge algebras. However, all the algebras considered by us include SU(2) x U(1). Consequently, we choose to use SU(2) x U(1) as the basic theoretical framework for our discussion [2].

Unless otherwise stated, we will therefore always assume that the *weak and electromagnetic interactions are described by a renormalizable* gauge theory based on SU(2) x U(1). The theory contains four gauge bosons W^+, W^-, Z^0 and γ, corresponding to the four generators of the algebra. Except for the fermion masses, the fine structure constant α and the $W^{\pm}$-mass, the theory contains one parameter - the Weinberg *angle* θ_W *defined by the relation:*

$$\begin{aligned} Z_\mu &= W^3_\mu \cos\theta_W + B_\mu \sin\theta_W \\ A_\mu &= -W^3_\mu \sin\theta_W + B_\mu \cos\theta_W \ . \end{aligned} \qquad (1.1)$$

Where Z_μ, A_μ, W^3_μ, B_μ are respectively, the vector fields of the neutral weak gauge boson, the photon, the third component of the SU(2) triplet of gauge fields, and the U(1) gauge field.

From time to time we will speculate on the properties of the Higgs scalar particles of the theory. However, unless otherwise stated, we will assume the simplest allowed Higgs structure. In the "standard" left-handed SU(2) x U(1) model, this involves four fields transforming like two SU(2) doublets. Three of these fields "convert" into the longitudinal modes of the vector fields when the W^+, W^-, Z acquire their masses, while one neutral scalar Higgs state remains as a physical particle. The simplest Higgs structure (as well as other patterns based only on SU(2) doublets) provide us with the well-known mass relation:

$$M_Z = \frac{M_{W^\pm}}{\cos\theta_W} \quad ; \quad M_{W^\pm} = \frac{37\ \text{GeV}}{\sin\theta_W} \ . \qquad (1.2)$$

Whenever necessary, we will assume that the SU(3) gauge group of color is the underlying algebra of the interactions between quarks and gluons. This assumption is not crucial to most of our discussion, and it becomes relevant only when we discuss the possible unification of strong, weak and electromagnetic interactions.

We summarize: unless otherwise specified we assume throughout this review -

(i) SU(2) x U(1) gauge theory of weak and electromagnetic interactions.

(ii) Simplest possible Higgs particle structure.

(iii) Color SU(3) gauge theory of quarks and gluons.

1.3 Outline of Review

Our discussion does not follow the historical order of developments in the physics of quarks and leptons. Instead, we follow a path which is, pedagogically, more appealing to us and which could have been the historical order!

We introduce the fundamental fermions in three "generations":

First generation: ν_e, e^-, u, d.

Second generation: ν_μ, μ^-, c, s.

Third generation: ν_τ, τ^-, t, b.

For each generation we discuss all theoretical and experimental questions which arise, even if, historically, some of these questions may have emerged only after the discovery of a subsequent generation. Thus, the discussion of topics such as parity violation in Atomic physics or quark-lepton unification by an SU(5) or an SO(10) algebra precedes not only a discussion of the charmed quarks, but also the muon or the strange quark.

For each generation we study all known processes involving the fundamental fermions of that (and preceding) generation. At each stage we introduce the new physics ingredients which are necessary for a discussion of the appropriate generation, and review the combined pattern or quarks and leptons up to that point.

Due to our "quasi-historical" approach, certain topics are discussed several times in different chapters. In order to enable the reader who is interested in one specific issue to find all references to it, we have included a brief subject index which appears immediately after the table of contents.

The detailed plan of the review is the following: Chapters 2, 3 and 4 are devoted, respectively, to the first, second and third generation of fermions. Chapter 5 mentions some open problems.

In Section 2.1 we briefly review the properties of charged currents involving first-generation fermions. This is followed in Section 2.2 by a discussion of neutral currents and their implications for the classification of right handed fermions. We emphasize that neutral current experiments enable us to obtain information about the classification of a given fermion into a multiplet of the gauge group, even if other fermions in the same multiplet are not observed. Sections 2.3 and 2.4 are devoted, respectively, to the properties of the right handed electron and the right handed u and d quarks. The complete SU(2) x U(1) picture of left and right-handed first-generation fermions is then reviewed in Section 2.5, reaching the tentative conclusion that the standard Weinberg-Salam model is extremely successful, except for the lack of observed violation of parity in atomic physics experiments. This last difficulty leads us to search for a somewhat larger gauge group which, however, duplicates the Weinberg-Salam model for charged current processes as well as neutrino-induced neutral currents. Such a model is the $SU(2)_L \times SU(2)_R \times U(1)$ scheme which we discuss in detail in Section 2.6.

In Section 2.7 we turn to the mass spectrum of first-generation fermions. We observe that the spectrum is essentially well "understood", at least qualitatively. (We realize that the pattern of the second generation turns this "understanding" into a totally unexplained mystery, but that happens only in Section 3.10.) The possibility of relating quarks and leptons to each other is motivated in Section 2.8, followed by a discussion of several unification schemes in Sections 2.9 and 2.10. We distinguish between "simple unification" schemes which unify only the weak and electromagnetic interactions, using a simple (or "pseudosimple") Lie algebra and "grand unification" schemes which relate the strong, weak and electromagnetic interactions. We show that all "simple unification" schemes must involve an SU(3) subalgebra. Among "grand unification" models we emphasize those based on SU(5) and SO(10). We conclude Chapter 2 by a brief summary of the first-generation fermions.

Our discussion of the second generation of fermions begins in Section 3.1, in which the left-handed fermions are classified and the Cabibbo angle is introduced. The possibility of right-handed doublets of quarks is discussed in Sections 3.1, 3.2 and 3.3. Section 3.2 is devoted to arguments against the existence of a $(c,d)_R$ doublet. In Section 3.3 we discuss experimental tests for the existence of a $(c,s)_R$ doublet. We conclude that, at present, there is no compelling evidence for or against such a doublet.

Flavor conserving neutral currents involving second-generation fermions are briefly discussed in Section 3.4, followed by a general analysis of flavor conservation by neutral currents in Section 3.5. We review the theoretical conditions for "natural" flavor conservation, and conclude, in Section 3.6, that there is strong evidence not only against $|\Delta S| = 1$ neutral currents, but also against $|\Delta C| = 1$ neutral currents. The SU(2) x U(1) classification of second-generation fermions is summarized in Section 3.7.

Possible Cabibbo-like angles and mixing effects in the leptonic sector are introduced in Section 3.8. Various mechanisms for transitions such as $\mu^- \to e^-\gamma$ are briefly discussed.

One of the most attractive features of some gauge models is the inclusion of a CP-violating interaction within the framework of the theory. At the level of the first two generations of fermions, CP-violation can be introduced only through the couplings of the Higgs mesons or through right-handed currents. All of these issues are analyzed in Section 3.9, where we also conclude that the "standard" left-handed model can accommodate CP-violation only at the six-quark level. A brief discussion of the masses of second-generation fermions is given in Section 3.10. Unfortunately, all we can do in this discussion is to expose our total ignorance and our lack of ability to compute either the fermion masses or the Cabibbo angle. While the main ingredients of the concept of "grand unification" are introduced already in Chapter 2, we devote Section 3.11 to grand unification schemes which relate the first and second generation fermions to each other. We emphasize the E(7) model, but conclude that it leads to an unacceptable value of the Weinberg angle. Section 3.12 contains a brief summary of the second-generation fermions.

Our discussion of the third generation of fermions begins with a general introduction in Section 4.1. We mention several possible patterns for the fifth and sixth quark, and conclude that the assumption that the third generation is similar to its two predecessors, is an attractive, but unproven, possibility. We then introduce the third-generation fermions one by one. Section 4.2 contains a discussion of the properties of the τ-lepton with an emphasis on its decay modes. In Section 4.3 we show that it is almost certain that the τ-lepton is accompanied by its own neutral lepton. Whether this lepton is very light (<300 MeV) or heavy (>2 GeV), we do not know. There are many possible models for the leptonic sector including six or more leptons. We mention some of them in Section 4.4. Section 4.5 is devoted to a general discussion of possible experimental and theoretical motivations for the introduction of the top and bottom (t and b) quarks. The "quarkonium" family of $b\bar{b}$ or $t\bar{t}$ mesons is discussed in Section 4.6 with special emphasis on the properties of the recently discovered Υ and Υ' particles. We indicate that the $b\bar{b}$ assignment for Υ is slightly favored over $t\bar{t}$.

Sections 4.7-4.10 contain a detailed discussion of the left-handed six-quark model. The model is introduced in Section 4.7 where three Cabibbo-like angles are introduced and their numerical values are estimated. Sections 4.8 and 4.9 are devoted to a discussion of

the weak production and weak decays of mesons including b-quarks and t-quarks, respectively. A detailed discussion of CP-violation in the K-$\bar{K}$ system and the electric dipole moment of the neutron is presented in Section 4.10. In Section 4.11 we briefly consider right-handed currents involving the six quarks of the first three generations. Using a variety of theoretical and experimental arguments, we conclude that within SU(2) x U(1), such currents are unlikely. Finally, we summarize the third-generation fermions in Section 4.12.

Our final chapter is devoted to a brief overall summary and to the discussion of open experimental and theoretical problems. In Section 5.1 we discuss our present overall view of the correct gauge theory of quarks and leptons. We consider $SU(2)_L \times SU(2)_R \times U(1)$ to be the most likely candidate. In Section 5.2 we review several experimental issues which remain open. These include the trimuon events observed in neutrino scattering, the question of parity violation in neutral currents, the search for right handed charged currents, the decays of the τ lepton, some open problems in the ψ-family and Υ-family and the question of neutrino masses. Our review concludes in Section 5.3 with a short list of outstanding theoretical problems. which is the correct gauge group? Do we have any theoretical guide-line for the total number of quarks and leptons? How can we calculate the masses and angles which are generated by the spontaneous symmetry breaking mechanism? What is the connection between quarks and leptons? The answer to any of these profound questions will undoubtedly provide us with a significantly better understanding of the world of quarks and leptons.

2. First Generation Fermions: ν_e, e^-, u, d

2.1 Charged Weak Currents and the Classification of Left-Handed Fermions

The first generation of fermions includes two leptons (ν_e and e^-), and two quarks (u and d). The charged currents represent the $\nu_e \leftrightarrow e^-$ transition and the $u \leftrightarrow d$ transition.

Information concerning $\nu_e \leftrightarrow e^-$ is obtainable from β-decay and μ-decay:

$$n \to p + e^- + \bar{\nu}_e \tag{2.1}$$

$$\mu^- \to \nu_\mu + e^- + \bar{\nu}_e \ . \tag{2.2}$$

In both cases all data are consistent with a pure left-handed V-A leptonic charged current:

$$J^- \propto \bar{\nu}_e \, \gamma_\alpha (1-\gamma_5) e^- \ . \tag{2.3}$$

Small contributions from non-vectorial currents (S,P,T) are not completely excluded. However, in the absence of any good theoretical reason to consider such terms,we are probably safe in ignoring them. The contribution of right-handed V+A currents is either absent or very small. Here we could envisage interesting theoretical models in which a right-handed $\bar{\nu}_e e^-$ term is actually small, but non-vanishing. Two examples of such schemes are:

(i) In an $SU(2)_L \times SU(2)_R \times U(1)$ gauge theory [3] (see Section 2.6) we could have $M_{W_R^\pm} >> M_{W_L^\pm}$, yielding right handed charged-current effects which are usually suppressed by a factor : $(M_{W_L^\pm}/M_{W_R^\pm})^4$.

(ii) In an SU(2) x U(1) model, the right handed electron could be in a doublet with a heavy neutral lepton N_e while a right-handed

ν_e is in a different SU(2) multiplet (assuming that it is not massless). We could then have a small Cabibbo-like angle ε, mixing the right-handed N_e and ν_e. The right handed $\nu_e \leftrightarrow e$ transition would then be suppressed by a factor $\sin^2\varepsilon$.

Both of these possibilities are not excluded. The most we could do within the framework of such models, would be to use the data in order to set an upper bound on $M_{W_L^\pm}/M_{W_R^\pm}$ or on $\sin\varepsilon$. In both cases the bound will depend on other factors, such as the classification of u, d and μ.

Having mentioned these possibilities we will say no more about them, and assume that the left handed ν_e and e transform like a double of SU(2) x U(1):

$$\begin{pmatrix}\nu_e\\ e^-\end{pmatrix}_L \qquad (2.4)$$

while the right-handed electron e_R^- is not in the same SU(2) x U(1) multiplet as ν_{eR}.

Note that we have not used here the information coming from the only measured purely leptonic process involving first generation leptons:

$$\bar{\nu}_e + e^- \to \bar{\nu}_e + e^- \quad . \qquad (2.5)$$

This process involves charged as well as neutral currents, and the present quality of the data enables us only to draw conclusions concerning the neutral currents, assuming that the charged currents are purely left-handed. We discuss $\bar{\nu}_e e^-$ elastic scatterin in Section 2.3.

The charged current involving u and d quarks cannot be studied directly. Like all quark currents, it can be determined only with the aid of several theoretical assumptions. Experimentally, β-decay data enable us to compute G_A/G_V where G_A and G_V are defined by the phenomenological form of the hadronic current

$$J^- \propto \bar{p}\gamma_\alpha(G_V + G_A\gamma_5)n \qquad (2.6)$$

The vector and axial-vector quark couplings are related to G_A/G_V by the Adler-Weisberger relation [4]. Its success hints that the charged quark current is of the form:

$$J^- \propto \bar{u}\gamma_\alpha(1 - \gamma_5)d \quad . \qquad (2.7)$$

This conclusion is supported by several other successes of the SU(2) x SU(2) algebra of currents [5]. These include several different sum rules for deep inelastic scattering, relations between deep inelastic ep and νp scattering and several current algebra predictions. All of these support the charged quark current of equation (2.7). However, small contributions from other terms cannot be excluded, and the two simple models outlined above in the leptonic case, could again yield small right handed $u \leftrightarrow d$ transitions.

Barring such a situation, we assert that the left-handed u and d are in an SU(2) x U(1) doublet:

$$\begin{pmatrix}u\\ d\end{pmatrix}_L \qquad (2.8)$$

while u_R and d_R are in two different SU(2) x U(1) multiplets.

The approximate equality ("universality") of the couplings of the $u \leftrightarrow d$ and $\nu_e \leftrightarrow e^-$ transitions is a necessary consequence of the gauge theory. The deviation from universality is presumably due to impurities in the eigenstates of the weak SU(2) x U(1) multiplets, and the Cabibbo mixing of states explains this deviation (see Sections 3.1).

We conclude that the left-handed first-generation fermions fall, to a good approximation, into two SU(2) x U(1) doublets:

$$\begin{pmatrix} \nu_e \\ e^- \end{pmatrix}_L \qquad \begin{pmatrix} u \\ d \end{pmatrix}_L \tag{2.9}$$

We now turn to the classification of right-handed fermions.

2.2 Neutral Weak Currents and the Classification of Right Handed Fermions

The SU(2) x U(1) classification of right handed fermions could be studied, in principle, by observing right-handed charged current transitions involving ν_e, e, u, d, etc. No such transitions have been clearly observed. Within the SU(2) x U(1) theory this still leaves two possibilities:

(i) The right-handed fermions ν_{eR}, e_R, u_R, d_R belong to SU(2) x U(1) singlets. Consequently, they do not couple to $W^{\pm}$ and do not participate in right-handed charged current transitions.

(ii) Some or all of the right-handed fermions belong to SU(2) x U(1) doublets (or higher multiplets). The right-handed charged currents are not experimentally observed at a given energy because the other fermions in the same multiplets are heavy, and cannot be produced at that energy.

At any given energy below the threshold for producing the alleged heavy right-handed fermions, it is not possible to distinguish between these two alternatives on the basis of charged current processes.

On the other hand, neutral current experiments do not necessitate the presence of the elusive heavy fermion (or fermions) which belong to the same representation. The weak neutral current in SU(2) x U(1) has the form:

$$J_{neutral} = J_3 - 2\sin^2\theta_W J_{em} \tag{2.10}$$

where J_3 is the third component of the SU(2)-vector, and θ_W is the Weinberg angle (Equation 1.1). Consequently, any neutral current measurement involving a fundamental fermion f, provides us with a measurement of $I_3(f)$. When the vector and axial vector neutral currents are separately determined, we may deduce the values of $I_3(f_L)$ and $I_3(f_R)$ for the left- and right-handed fermion f. Note, however, that the Weinberg angle θ_W has to be determined before we can translate neutral current data into statements about $I_3(f_R)$.

In general, the determination of $I_3(f_R)$ does not uniquely determine the SU(2) x U(1) multiplet of the right handed fermion (e.g. $I_3 = 0$ could correspond to $I = 0$ or $I = 1$, etc.). However, if we limit ourselves to SU(2) singlets and doublets, $I_3(f_R)$, of course, determines the multiplet.

The crucial point here is the fact that we do not have to perform any high energy experiments in order to determine $I_3(f_R)$, even if the other fermion in the same doublet is extremely heavy. Thus, if an atomic physics experiment or a nuclear reactor experiment tells us that $I_3(e_R) = -\frac{1}{2}$, we know that a heavy right-handed neutral lepton with $I_3 = +\frac{1}{2}$ must exist. This is one of the most fascinating aspects of the properties of neutral currents in a gauge theory: a "table-top" atomic physics experiment can tell us about the existence of a new fundamental fermion with a mass of a few GeV!

In order to translate these principles into practical calculations [6], we now define the following left-handed and right-handed neutral current couplings for each fermion f:

$$J_{neutral} \propto g_f^L \bar{f}\gamma_\alpha(1-\gamma_5)f + g_f^R \bar{f}\gamma_\alpha(1+\gamma_5)f \quad . \tag{2.11}$$

In SU(2) x U(1) we have:

$$g_f^L = 2I_3(f_L) - 2\sin^2\theta_W Q(f) \tag{2.12}$$

$$g_f^R = 2I_3(f_R) - 2\sin^2\theta_W Q(f) \tag{2.13}$$

where Q(f) is the electric charge of f .

For the left-handed first-generation fermions we assume (Section 2.1):

$$I_3(\nu_{eL}) = \frac{1}{2} \; ; \; I_3(e_L^-) = -\frac{1}{2} \; ; \; I_3(u_L) = \frac{1}{2} \; ; \; I_3(d_L) = -\frac{1}{2} \; . \tag{2.14}$$

There is no evidence for a right-handed ν_e . All known experiments involve only ν_{eL} . Consequently, we can shed no light on the existence and assignment of ν_{eR} . The quantities that we wish to study are: $I_3(e_R)$, $I_3(u_R)$ and $I_3(d_R)$. For convenience, we introduce the notation:

$$\alpha_f = 2I_3(f_R) \; ; \quad x = \sin^2\theta_W \quad . \tag{2.15}$$

Hence:

$$\begin{aligned} g_e^L &= -1 + 2x \; ; & g_e^R &= \alpha_e + 2x \\ g_u^L &= 1 - \frac{4}{3}x \; ; & g_u^R &= \alpha_u - \frac{4}{3}x \\ g_d^L &= -1 + \frac{2}{3}x \; ; & g_d^R &= \alpha_d + \frac{2}{3}x \; . \end{aligned} \tag{2.16}$$

The next two sections are devoted to a phenomenological discussion of the parameters α_e, α_u, α_d and x .

2.3 The Right-Handed Electron

The most direct information concerning the properties of the right-handed electron comes from neutrino-electron elastic scattering. Four such processes can be, in principle, measured:

$$\bar{\nu}_e + e^- \to \bar{\nu}_e + e^- \tag{2.17}$$

$$\nu_e + e^- \to \nu_e + e^- \tag{2.18}$$

$$\bar{\nu}_\mu + e^- \to \bar{\nu}_\mu + e^- \tag{2.19}$$

$$\nu_\mu + e^- \to \nu_\mu + e^- \quad . \tag{2.20}$$

The processes (2.17), (2.18) involve charged currents as well as neutral currents, while (2.19), (2.20) are pure neutral current reactions (to lowest order). Assuming the standard V-A form for the charged $\nu_e \leftrightarrow e$ currents and neglecting terms of order m_e/E_ν , we find:

$$\sigma(\bar{\nu}_e e^- \to \bar{\nu}_e e^-) = KE_\nu[(g_e^R)^2 + \tfrac{1}{3}(2 + g_e^L)^2] \tag{2.21}$$

$$\sigma(\nu_e e^- \to \nu_e e^-) = KE_\nu[\tfrac{1}{3}(g_e^R)^2 + (2 + g_e^L)^2] \tag{2.22}$$

$$\sigma(\bar{\nu}_\mu e^- \to \bar{\nu}_\mu e^-) = KE_\nu[(g_e^R)^2 + \tfrac{1}{3}(g_e^L)^2] \tag{2.23}$$

$$\sigma(\nu_\mu e^- \to \nu_\mu e^-) = KE_\nu[\tfrac{1}{3}(g_e^R)^2 + (g_e^L)^2] \tag{2.24}$$

where

$$K = \frac{G^2 m_e}{2\pi} \tag{2.25}$$

Experimentally, the process (2.17) has been measured [7] using the $\bar{\nu}_e$ flux coming out of a nuclear reactor. In that case, m_e/E_ν is not negligible and additional experimental factors enter. The limits on g_e^R and g_e^L for two different intervals of the neutrino energy

are shown in Fig. 1.

The reaction (2.18) has not been measured. Reactions (2.19) and (2.20) were studied in the Gargamelle Bubble Chamber [8]. Three $\bar{\nu}_\mu e$ events and no $\nu_\mu e$ events were seen, yielding a measured rate for (2.19) and an upper limit for (2.20). The corresponding restrictions on g_e^L and g_e^R are shown in Fig. 2. Additional data on the same reaction have been recently analyzed but not yet published by the Aachen-Padova collaboration [9]. Their recent data are consistent with Fig. 2. The present data for the reactions (2.17)-(2.20) are summarized in Fig. 3. We find that there are two overlap regions which are consistent with all data. Since Equations (2.21)-(2.24) are invariant under $g_e^R \leftrightarrow -g_e^R$, the two allowed regions are symmetric with respect to the g_e^L axis. The most probable value for g_e^L and g_e^R are:

$$g_e^L = -0.5 \pm 0.2 \qquad (2.26)$$

$$g_e^R = \pm(0.5 \pm 0.2) \ . \qquad (2.27)$$

Since we know that -

$$g_e^L = -1 + 2x \qquad (2.28)$$

we determine x to be:

$$x = 0.25 \pm 0.1 \ . \qquad (2.29)$$

Consequently, the two solutions for g_e^R yield the following values for $\alpha_e = 2I_e(e_R)$:

I. $\alpha_e = 0 \ ; \quad I_3(e_R) = 0$

II. $\alpha_e = -1 \ ; \quad I_3(e_R) = -\frac{1}{2}$.

On the basis of the "world's data" on neutrino-electron scattering we find that the right-handed electron may be either in an

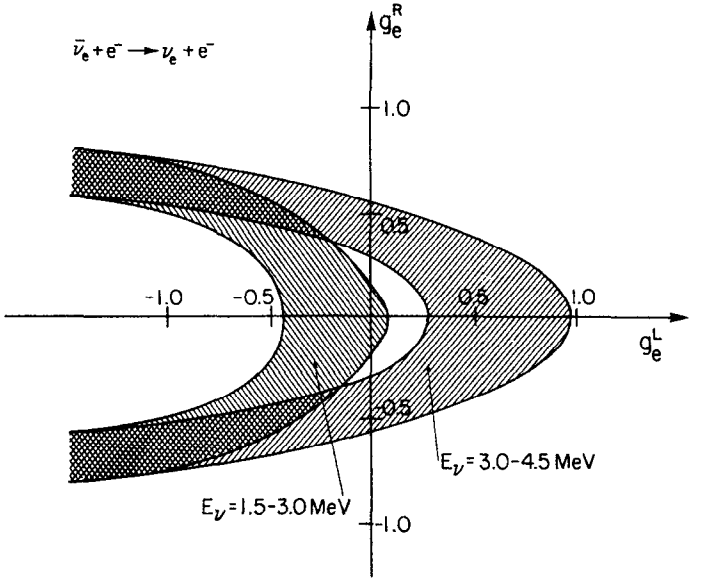

Figure 1: The allowed range of g_e^L and g_e^R as determined from $\sigma_{el}(\bar{\nu}_e e)$. The two shaded regions correspond to data from two different ranges of neutrino energy [7].

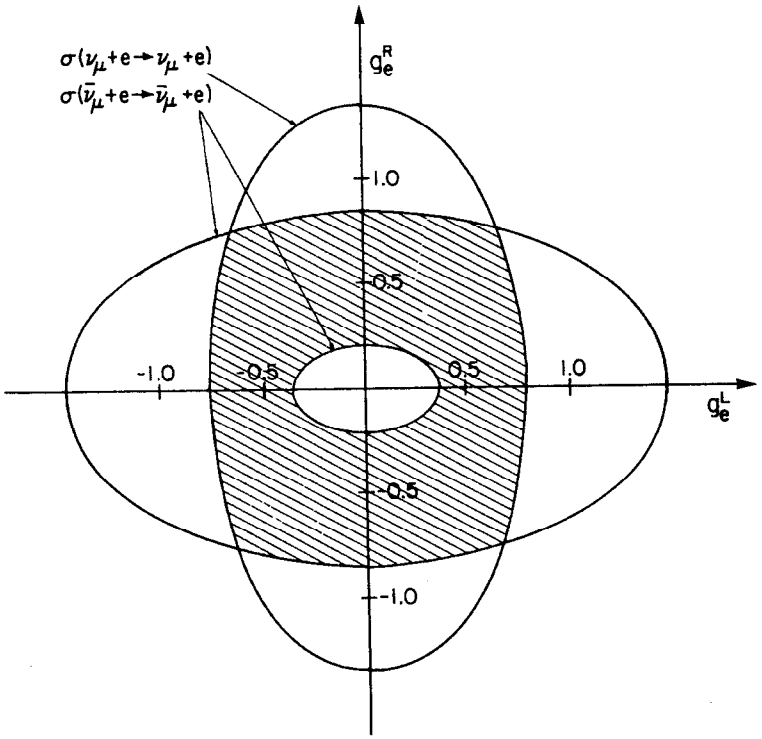

Figure 2: The allowed range of g_e^L and g_e^R as determined from $\sigma_{el}(\nu_\mu e)$ and $\sigma_{el}(\bar{\nu}_\mu e)$ [8].

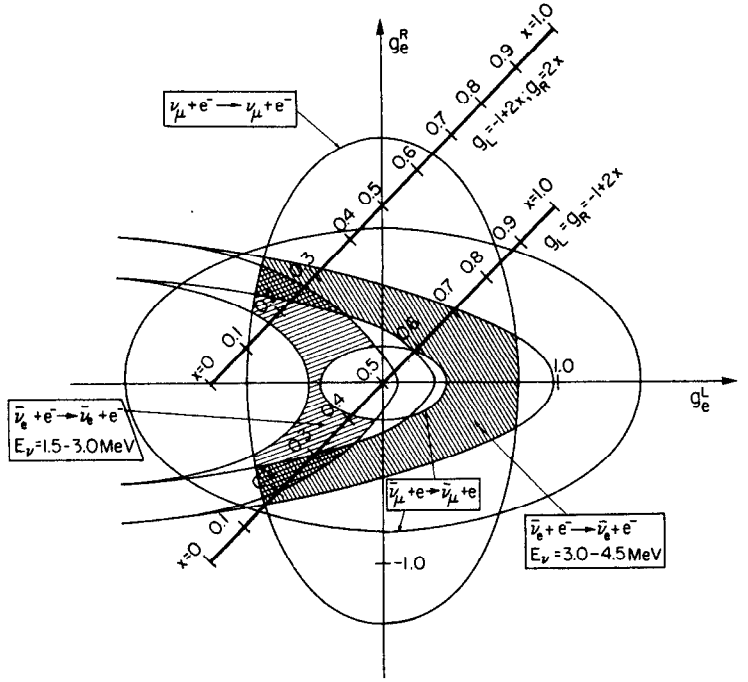

Figure 3: The allowed range of g_e^L and g_e^R, as determined from all available data on νe scattering. The two diagonal lines represent a left-handed SU(2) x U(1) model ($g_L = g_R - 1$) and a vector SU(2) x U(1) model ($g_L = g_R$). In both cases $x = \sin^2\theta_W \sim 0.25$.

SU(2) x U(1) singlet or in a doublet, while in both cases

$x = \sin^2\theta_W \sim 0.25$.

Note that solution I ($\alpha_e = 0$) corresponds to the "standard" Weinberg-Salam left-handed model. Solution II ($\alpha_e = -1$) leads to:

$$g_e^L - g_e^R = 0 \qquad (2.30)$$

and to a vanishing axial vector coupling of the electron to the neutral current. A new heavy neutral right-handed lepton is predicted, in this case, as the $I_3 = +\frac{1}{2}$ member of the doublet containing the right-handed electron.

Notice that both solutions happen to correspond to $(g_e^L)^2 = (g_e^R)^2$. Consequently, in both cases, $\sigma_{el}(\bar{\nu}_\mu e) = \sigma_{el}(\nu_\mu e)$. However, in the case of solution I ($\alpha_e = 0$) the ratio $\sigma(\bar{\nu}_\mu e)/\sigma(\nu_\mu e)$ is extremely sensitive to the value of $\sin^2\theta_W$. The general expression is:

$$\frac{\sigma_{el}(\bar{\nu}_\mu e)}{\sigma_{el}(\nu_\mu e)} = \frac{16x^2+(1-4x)+3\alpha(\alpha+4x)}{16x^2+3(1-4x)+\alpha(\alpha+4x)} = \begin{cases} \dfrac{16x^2+(1-4x)}{16x^2+3(1-4x)} & \text{For } \alpha=0 \\ 1 & \text{For } \alpha=1 \end{cases} \qquad (2.31)$$

An accurate measurement of this ratio would provide, in this case, a good determination of θ_W (Figure 4). For solution II, $\sigma(\bar{\nu}_\mu e)/\sigma(\nu_\mu e) = 1$ regardless of the value of θ_W . The unpublished data of Reference [9] seems to indicate that $\sigma_{el}(\bar{\nu}_\mu e) \neq \sigma_{el}(\nu_\mu e)$. It would be interesting to have better data on this issue.

An additional measurement of the neutral weak current of the electron is provided by the search for parity violation in atomic physics phenomena. Such parity violations can be due to products of vector and axial vector terms, where one term represents the electron neutral current while the other represents the nucleon (or u and d) neutral current.

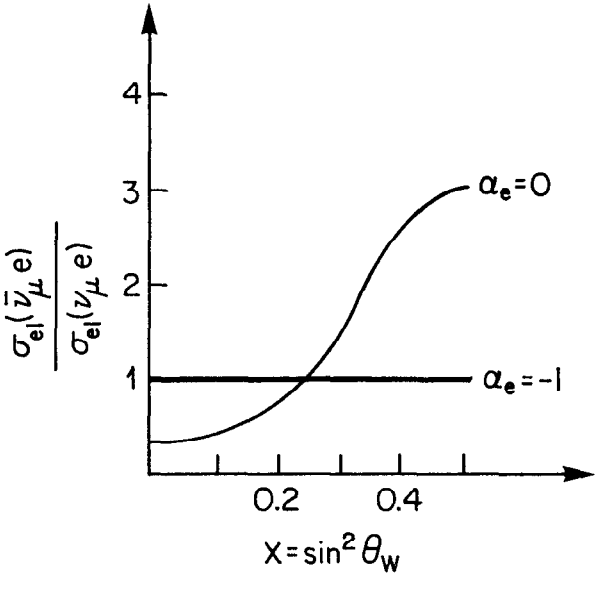

Figure 4: Dependence of $\sigma_{el}(\bar{\nu}_\mu e)/\sigma_{el}(\nu_\mu e)$ on $x = \sin^2\theta_W$ for a left-handed SU(2) x U(1) model ($\alpha_e = 0$) and a vector model ($\alpha_e = -1$) .

In general, the effects of atomic parity violation would be proportional to [10]:

$$J_e^A J_q^V + J_e^V J_q^A$$

where the indices A,V, e, q stand for axial vector, vector, electron and quark respectively. However, in heavy atoms the contribution of the J_q^A term is very small (proportional to the recoil of the nucleus), and the dominant term is given by:

$$J_e^A J_q^V \propto (g_e^L - g_e^R)\ [(g_u^L + g_u^R)\ (2Z+N) + (g_d^L + g_d^R)(Z + 2N)] \qquad (2.32)$$

Here Z and N are, respectively, the number of protons and neutrons in the atom under discussion.

The experiments carried out, so far [11], used Bismuth atoms (Z = 83, N = 126). Assuming $x = 0.25$, we get from Equation (2.16):

$$g_u^L = 0.67\ ;\quad g_d^L = -0.83\ ;\quad g_u^R = \alpha_u - 0.33\ ;\quad g_d^R = \alpha_d + 0.17\ . \qquad (2.33)$$

Hence, the right-hand side of Equation (2.32) is:

$$K = (1 + \alpha_e)\ (-126 + 292\alpha_u - 335\alpha_d)\ . \qquad (2.34)$$

In the case of the standard Weinberg-Salam left-handed model ($\alpha_e = \alpha_u = \alpha_d = 0$), we have $K = 126$. Experimentally, the latest results are [11] (in the same units):

$$K = 16 \pm 24 \text{ (Oxford)}$$

$$K = -8 \pm 24 \text{ (Seattle)}\ .$$

The conversion of the directly measured rotation angle to a value of our K-parameters requires assumptions on the atomic wave-function. There are some indications of ambiguities in these calculations. It is still possible that the discrepancy between the measured effect and the predictions of the Weinberg-Salam model is much smaller than that suggested here. We will have to wait for a more accurate experiment in order to be certain that the discrepancy is indeed substantial.

One intriguing possibility is, of course, that the correct value is $K = 0$. This could be due to the electron coupling, yielding:

$$\alpha_e = 2I_3(e_R) = -1 \qquad (2.35)$$

and preferring the solution II of Fig. 3. It could also be due to the quark coupling, namely:

$$-126 + 292\alpha_u + 335\alpha_d = 0\ . \qquad (2.36)$$

This is an unlikely possibility, but we return to it briefly in Section 2.4. A third possibility is that the weak neutral current actually conserves parity. Such a hypothesis, together with the νN and $\bar{\nu}N$ scattering data, would force us outside SU(2) x U(1), and necessitate more than one neutral weak boson. We return to this possibility in Section 2.6.

We summarize our conclusions concerning the right-handed electron:

Within SU(2) x U(1), neutrino-electron elastic scattering data yield $\sin^2\theta_W \sim 0.25$ and allow the right-handed electron to be in an SU(2) singlet ($\alpha_e = 0$) or doublet ($\alpha_e = -1$) . Atomic parity violation experiments indicate that the second possibility (e_R in a doublet) is more likely.

2.4 The Right-Handed u and d Quarks

Information on the properties of right-handed u and d quarks can be obtained from several different processes. The most important among these are deep inelastic neutrino and antineutrino neutral-current processes.

The measured experimental quantities are:

$$R_\nu = \frac{\sigma(\nu + N \to \nu + \text{anything})}{\sigma(\nu + N \to \mu^- + \text{anything})} \qquad (2.37)$$

$$R_{\bar\nu} = \frac{\sigma(\bar\nu + N \to \bar\nu + \text{anything})}{\sigma(\bar\nu + N \to \mu^+ + \text{anything})} \qquad (2.38)$$

Experimentally, an average over the four available experiments [12], ignoring energy variation, gives:

$$R_\nu = 0.28 \pm 0.04$$

$$R_{\bar\nu} = 0.38 \pm 0.05 \ .$$

All experiments are, more or less, consistent with these values.

If we assume that deep inelastic neutrino scattering can be described by the quark-parton model and if we temporarily neglect the contribution of the "ocean" of $q\bar{q}$ pairs in the nucleon, we obtain:

$$R_\nu = \frac{1}{4}\left(L + \frac{1}{3}R\right) \qquad (2.39)$$

$$R_{\bar\nu} = \frac{1}{4}\left(L + 3R\right) \qquad (2.40)$$

where

$$L = (g_u^L)^2 + (g_d^L)^2 = \left(1 - \frac{4}{3}x\right)^2 + \left(-1 + \frac{2}{3}x\right)^2 \qquad (2.41)$$

$$R = (g_u^R)^2 + (g_d^R)^2 = \left(\alpha_u - \frac{4}{3}x\right)^2 + \left(\alpha_d + \frac{2}{3}x\right)^2 \ . \qquad (2.42)$$

Experimentally, the quark-parton model is in reasonable agreement with experiment. However, the contribution of the $q\bar{q}$ "ocean" amounts to 10% or so of the cross section. In particular, the ratio:

$$\frac{\sigma(\nu + N \to \mu^- + \text{anything})}{\sigma(\bar\nu + N \to \mu^+ + \text{anything})} \qquad (2.43)$$

is predicted to be 1/3 in the absence of "ocean" contributions. The measured values [13] are around 0.4-0.45, yielding:

$$B = \frac{\int_0^1 [q(\xi) - \bar{q}(\xi)]\,d\xi}{\int_0^1 [q(\xi) + \bar{q}(\xi)]\,d\xi} \sim 0.8 \qquad (2.44)$$

where $q(\xi)$, $\bar{q}(\xi)$ are the usual momentum distribution functions for quarks and antiquarks in the nucleon and ξ is the momentum fraction carried by the quark. $B = 1$ corresponds to a vanishing "ocean" contribution.

In the presence of "ocean" contributions (but neglecting $s\bar{s}$, $c\bar{c}$ pairs in the "ocean"), Equations (2.39), (2.40) are modified as follows:

$$R_\nu = \frac{1}{4}\left[L + R\left(\frac{2-B}{2+B}\right)\right] \sim \frac{1}{4}\left(L + 0.42R\right) \qquad (2.45)$$

$$R_{\bar\nu} = \frac{1}{4}\left[L + R\left(\frac{2+B}{2-B}\right)\right] \sim \frac{1}{4}\left(L + 2.3R\right) \qquad (2.46)$$

It is easy to see that R is not very sensitive to the values of α_u and α_d. In fact, Fig. 5 shows R as a function of x for all four combinations of $\alpha_u = 1,0$ and $\alpha_d = 0,-1$ (using Equation (2.45) and assuming $B = 0.8$). In the experimentally interesting range ($R_\nu = 0.28 \pm 0.04$), all four curves yield similar values of x. We may therefore use the experimental value of R in order to determine the approximate value of $x = \sin^2\theta_W$, before we begin our discussion of α_u and α_d. In all cases we obtain $0.2 < x < 0.5$. For $\alpha_d = 0$, $\alpha_u = 0$ we actually find

$$x = 0.29 \pm 0.08$$

in magnificent agreement with the value determined in Section 2.3 from purely leptonic processes.

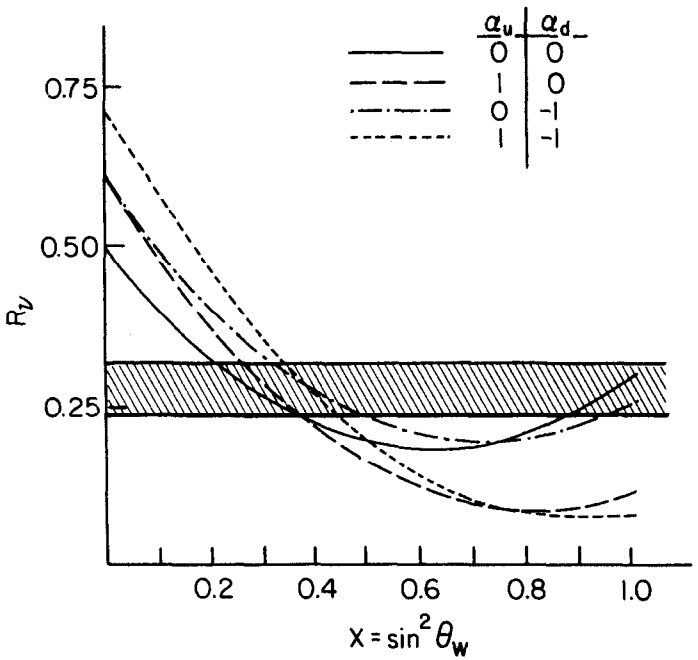

Figure 5: R_ν as a function of $x = \sin^2\theta_W$ for four different sets of α_u, α_d values. The shaded region represents the experimental value of R_ν . For all α_u, α_d values, $0.2 < x < 0.5$.

Having determined x, we may now use the measured value of R_ν in order to determine the allowed range for α_u, α_d (using Equations (2.46), (2.41), (2.42)). Figure 6 shows the allowed values of α_u, α_d for two representative x-values: $x = 0.25$ and $x = 0.35$. For all acceptable x-values, $\alpha_d = -1$ is excluded. We therefore conclude that the right-handed d-quark probably belongs to an SU(2) x U(1) singlet. In the case of $x = 0.25$, $\alpha_u = 1$ is also excluded and the only allowed solution is $\alpha_d = \alpha_u = 0$, as required by the standard left-handed Weinberg-Salam model. However, for $x = 0.35$, $\alpha_u = 1$ is not ruled out. Consequently, we cannot completely reject the possibility that the right-handed u-quark is in an SU(2) x U(1) doublet. (Note that for $\alpha_u = 1$, $\alpha_d = 0$, Fig. 5 actually gives $x = 0.32 \pm 0.05$.)

It might be interesting to see whether any of the allowed regions of α_u, α_d would lead to vanishing parity violation in the atomic Bismuth experiment. The condition for the vanishing of the quark vector neutral current is (Equation (2.32)):

$$292\alpha_u - 335\alpha_d = 332x + 43 \simeq \begin{cases} 126 \ (x = 0.25) \\ 159 \ (x = 0.35) \ . \end{cases} \qquad (2.47)$$

The only α_u, α_d values consistent with Equation (2.47) as well as with the observed value of R_ν are:

$$\alpha_u \sim 0 \ , \quad \alpha_d \sim -0.4 \ . \qquad (2.48)$$

These values do not correspond to any physically interesting situation.

Elastic neutrino-nucleon and antineutrino nucleon experiments could serve as additional constraints [14] on α_u, α_d and x . However, present data [15] cannot exclude any of the otherwise allowed possibilities. A substantial improvement in the elastic data (expected soon!) should provide additional information.

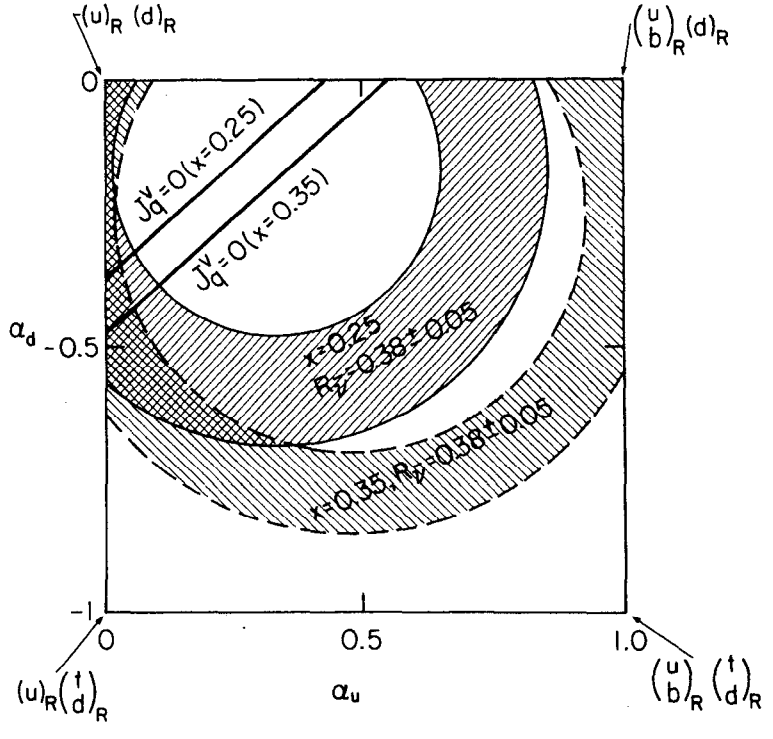

Figure 6: The allowed range of α_u, α_d as determined by the experimental value of $R_{\bar{\nu}}$. The two shaded regions correspond to $x = 0.25$ and $x = 0.35$, respectively. The two diagonal lines represent the condition for a vanishing quark vector current J_q^V, for the same x-values.

We conclude that, within the SU(2) x U(1) theory, all data are consistent with $x = \sin^2\theta_W \sim 0.25\text{-}0.30$ and the right-handed u and d quarks being in SU(2) singlets ($\alpha_u = \alpha_d = 0$). The assignment of the right-handed u to a doublet ($\alpha_u = 1$) is not completely ruled out, provided that x is somewhat larger. The smallness of parity violation effects in the Bismuth experiment is probably not due to the hadronic vertex. It is presumably due to the electron vertex, implying $\alpha_e = -1$ (see Section 2.3).

2.5 Summary: SU(2) x U(1) Classification of First Generation Fermions

We now summarize the conclusions of the previous four sections, trying to remain within an SU(2) x U(1) theory:

(i) The left-handed first-generation fermions belong to two doublets:

$$\begin{pmatrix} \nu_e \\ e^- \end{pmatrix}_L \qquad \begin{pmatrix} u \\ d \end{pmatrix}_L \tag{2.49}$$

(ii) The Weinberg angle can be determined from elastic neutrino-electron scattering and, independently, from the deep inelastic neutral current process $\nu + N \to \nu +$ anything. In both cases, $\sin^2\theta_W$ can be approximately deduced without determining whether the right-handed e, u or d belong to singlets or doublets! We find:

$$x = \sin^2\theta_W = 0.25 \pm 0.1 \quad (\nu e \text{ elastic scattering}) \tag{2.50}$$

$$0.2 < \sin^2\theta_W < 0.5 \quad (\nu+N \to \nu + \text{anything}) \tag{2.51}$$

We can therefore assume that:

$$0.2 < \sin^2\theta_W < 0.35 \ . \tag{2.52}$$

(iii) If we accept the contradiction between the pure left-handed model and the atomic Bismuth experiment, we must conclude that, within

SU(2) x U(1), the right-handed electron is probably in a doublet:

$$\begin{pmatrix} N_e \\ e^- \end{pmatrix}_R \qquad (2.53)$$

The singlet assignment for e_R is consistent with all the elastic ν-e data, but would lead to substantial parity violation in atoms.

(iv) The right-handed d quark is in an SU(2) x U(1) singlet.

(v) The right-handed u quark is probably in a singlet, although the doublet assignment is not completely ruled out.

The most likely SU(2) x U(1) classification, consistent with all data, is:

$$\begin{pmatrix} \nu_e \\ e^- \end{pmatrix}_L \quad \begin{pmatrix} u \\ d \end{pmatrix}_L \quad \begin{pmatrix} N_e \\ e^- \end{pmatrix}_R \quad (u)_R \quad (d)_R \qquad (2.54)$$

where the only allowed modification is the assignment of u_R to a doublet.

Further experimental tests of these assignments and of the value of $\sin^2\theta_W$ will be provided by:

(a) Better data on all four νe elastic processes (Equations (2.17)-(2.20)).

(b) Additional atomic-physics parity-violation experiments. In particular, the above assignment does <u>not</u> lead to a vanishing neutral axial-vector <u>quark</u> current. Consequently, it would lead to significant parity violation effects in light atoms, particularly in hydrogen!

(c) Elastic νN and $\bar{\nu}N$ experiments could provide further tests for the classification of u_R and d_R.

(d) Deep inelastic scattering of polarized electrons on nucleons provides another probe of the neutral weak current [16]. In this process, an asymmetry is expected from the above SU(2) x U(1) assignment (see also Table II in Section 2.6).

(e) A different type of asymmetry can be measured in the reaction $e^+ + e^- \to \mu^+ + \mu^-$. The forward-backward asymmetry of the produced $\mu^+\mu^-$ pairs depends on the neutral axial vector current couplings of the electron and muon [17]. No asymmetry is expected in an SU(2) x U(1) model, if the right-handed electron belongs to a doublet.

On a phenomenological level, our analysis gave quite satisfactory results. We have a unique SU(2) x U(1) classification of all left-handed and right-handed first-generation fermions, with a unique value of the Weinberg angle. Several additional experimental tests are expected soon.

From the theoretical point of view, the resulting scheme is unsatisfactory: The symmetry between quarks and leptons is destroyed by the right-handed couplings; triangle anomalies are not cancelled; incorporation of the quarks and leptons in a larger unification scheme appears to be very difficult. Our theoretical prejudices tell us that we should be able to do better!

2.6 A Possible Extended Gauge Group: $SU(2)_L \times SU(2)_R \times U(1)$

In the previous section we have seen that the study of all available data involving first-generation fermions has yielded a unique consistent solution based on SU(2) x U(1). The solution treated electrons and quarks in a different way. It corresponded to a pure left-handed model in the quark sector and to a vector-like scheme in the lepton sector. While this may be the correct answer, our theoretical prejudices guide us in a different direction.

In order to pursue other possibilities we note that the standard Weinberg-Salam left-handed model is, so far, in very good agreement

with all neutral current data involving neutrinos (namely: with all neutral current data except the atomic Bismuth experiment). On the other hand, "all" neutral current data which do not involve neutrinos (namely: the atomic Bismuth experiments) are consistent with parity conserving neutral currents.

Is it possible that all neutral currents conserve parity? The answer is yes! Within SU(2) x U(1), a parity conserving neutral current must give $\sigma_{el}(\nu p) = \sigma_{el}(\bar{\nu} p)$, $\sigma(\nu + N \to \nu + \text{any}) = \sigma(\bar{\nu} + N \to \bar{\nu} + \text{any})$, etc. These results are inconsistent with the data. Hence, either parity is violated by neutral currents or SU(2) x U(1) should be enlarged. If SU(2) x U(1) is enlarged, parity conserving neutral currents could yield different νN and $\bar{\nu} N$ elastic (or inelastic) cross sections. The neutral weak interaction could then conserve parity, but the initial neutrino (or antineutrino) beam would be left- (or right-) handed, thus introducing a nonsymmetric situation.

The challenge facing us would then be the following: Construct a theory in which all neutral currents conserve parity, while all neutrino-related weak processes are described by the usual phenomenology of the Weinberg-Salam left-handed model. Such a theory should treat quarks and leptons in the same way and should have only one Weinberg angle.

All of these requirements can be satisfied by a theory based on the gauge group $SU(2)_L \times SU(2)_R \times U(1)$ [18]. Various versions of such a theory were considered by several authors during the last few years [19-22].

The $SU(2)_L \times SU(2)_R \times U(1)$ theory necessitates seven gauge Bosons. The generators of $SU(2)_L$ and $SU(2)_R$ are denoted by W_L^+, W_L^3, W_L^- and W_R^+, W_R^3, W_R^-. The U(1) generator is denoted by B. The $SU(2)_L$ and $SU(2)_R$ coupling constants are assumed to be equal, obeying a left-right symmetry. We denote the SU(2) coupling by g and the U(1) coupling by g'. The charged W_L and W_R Bosons are chosen not to mix with each other. This can be easily arranged, e.g., if the Higgs mesons χ_L and χ_R belong to a $(\frac{1}{2}, 0)$ and $(0, \frac{1}{2})$ multiplets of $SU(2)_L \times SU(2)_R$, with vacuum expectation values:

$$\langle \chi_L \rangle = \langle \chi_R \rangle = \begin{pmatrix} 0 \\ \lambda \end{pmatrix} \quad . \tag{2.55}$$

In the absence of any other Higgs particles the mass matrix for W_L^+ and W_R^+ will be diagonal and:

$$M^2_{W_L^\pm} = M^2_{W_R^\pm} = \frac{1}{2} \lambda^2 g^2 \quad . \tag{2.56}$$

The $(\text{mass})^2$ matrix for the three neutral Bosons W_L^3, W_R^3 and B has the form [20]:

$$\frac{1}{2} \lambda^2 \begin{pmatrix} g^2 & 0 & -gg' \\ 0 & g^2 & -gg' \\ -gg' & -gg' & 2g'^2 \end{pmatrix} \quad . \tag{2.57}$$

The eigenstates and eigenvalues are:

$$A = \sin\theta_W (W_L^3 + W_R^3) + \sqrt{\cos 2\theta_W}\, B \quad ; \qquad M_A^2 = 0$$

$$Z_V = \frac{1}{\sqrt{2}} \sqrt{\cos 2\theta_W}\, (W_L^3 + W_R^3) - \sqrt{2} \sin\theta_W B; \quad M^2_{Z_V} = \frac{1}{2} \lambda^2 (g^2 + 2g'^2) \tag{2.58}$$

$$Z_A = \frac{1}{\sqrt{2}} (W_L^3 - W_R^3) \; ; \qquad M^2_{Z_A} = \frac{1}{2} \lambda^2 g^2 \quad .$$

The relations between g, g' and e, θ_W are:

$$g = \frac{e}{\sin\theta_W} \quad ; \quad g' = \frac{e}{\sqrt{\cos 2\theta_W}} \tag{2.59}$$

where e is the electromagnetic coupling constant and θ_W is a Weinberg-like angle. The masses of the two neutral Z-Bosons are related by:

$$M_{Z_A}^2 = M_{Z_V}^2 \cos 2\theta_W \qquad (2.60)$$

Notice that the left- and right-handed neutral Bosons are mixed in a "maximal" way, creating a pure vector and a pure axial-vector neutral Boson Z_V and Z_A.

All left-handed fermions are assigned to $(\frac{1}{2}, 0)$ representations. All right-handed fermions are in $(0, \frac{1}{2})$ representations. The fermion masses (or, at least, mass differences) must be generated by Higgs mesons belonging to the $(\frac{1}{2}, \frac{1}{2})$ multiplet. Such Higgs particles would also couple to the gauge Bosons and will spoil the simple $W^{\pm}$ and Z eigenstates which emerged from our previous discussion. We assume that the vacuum expectation values of the $(\frac{1}{2}, \frac{1}{2})$ Higgs mesons are very small relative to λ and that, consequently, the physical $W^{\pm}$ and Z states are not very different from the ones listed above.

At this point, we have to introduce into the theory some ingredient which would give us the usual left-handed charged currents and eliminate any presently observable right-handed charged currents. This can be done in two different ways:

(i) We may introduce yet another Higgs multiplet which will affect the masses of $W_R^{\pm}$ without contributing to any other vector Boson mass. This could be done [19,20] by introducing Higgs fields δ_L and δ_R belonging to the (1,0) and (0,1) representations of $SU(2)_L \times SU(2)_R$. These new Higgs fields do not contribute to the masses of the neutral vector Bosons, but they may influence the charged-Boson masses. We assume:

$$\langle \delta_L \rangle = \begin{pmatrix} 0 \\ 0 \\ 0 \end{pmatrix} \qquad \langle \delta_R \rangle = \begin{pmatrix} 0 \\ \Lambda \\ 0 \end{pmatrix} \qquad (2.61)$$

If $\Lambda >> \lambda$, we have:

$$M_{W_R^{\pm}} >> M_{W_L^{\pm}} \qquad (2.62)$$

while we still preserve the relations:

$$M_{Z_A}^2 = M_{W_L^{\pm}}^2 \; ; \quad M_{Z_V}^2 = \frac{M_{W_L^{\pm}}^2}{\cos 2\theta_W} \; . \qquad (2.63)$$

In such a scheme all right-handed charged current transitions are suppressed by, at least, factors of λ^2/Λ^2. We may, for instance, assign u_R and d_R to the same $(0, \frac{1}{2})$ multiplet, leading to deviations of order λ^4/Λ^4 from the usual V-A theory in β-decay. We can always choose λ/Λ to be sufficiently small so that the model is consistent with all present experiments. The set of Higgs particles which is introduced in this model suffers from an important theoretical drawback [23]: its pattern does not survive higher-order loop corrections. In this sense, the pattern of spontaneous breaking of parity invariance is not natural. Several ideas have been proposed in order to rectify this difficulty [23], but the situation is still somewhat unclear.

(ii) A second option would be [21] to keep $M_{W_L^{\pm}} = M_{W_R^{\pm}}$ but exploit the orthogonality of $W_L^{\pm}$ and $W_R^{\pm}$. In that case we must assign heavy fermions to some of the right handed doublets which contain e_R, u_R, d_R. All charged current neutrino-initiated processes would follow the usual V-A theory, since the left-handed neutrinos in the beam would couple only to $W_L^{\pm}$, which then couples only to u_L, d_L, etc. On the other hand, the successful V-A description of nucleon β-decay tells us that $W_R^{\pm}$ does not contribute significantly and that at least (u_R, d_R) or (ν_{eR}, e_R^-) cannot be in a $(0, \frac{1}{2})$ multiplet of $SU(2)_L \times SU(2)_R \times U(1)$. Some heavy fermions are then needed in order to form doublets with e_R or u_R, d_R.

In both versions of the theory, the weak neutral-current Lagrangian would be:

$$L = \frac{g}{\sqrt{2}} [J_A^3 Z_A + \frac{1}{\sqrt{\cos 2\theta_W}} (J_V^3 - \sin^2\theta_W J_{em}) Z_V] \quad . \tag{2.64}$$

The effective Hamiltonian of the weak neutral current would then have the form:

$$H_{weak}^{N.C.} = \frac{g^2}{2} \left[\frac{1}{M_{Z_A}^2} J_A J_A + \frac{1}{\cos 2\theta_W \cdot M_{Z_V}^2} J_V J_V \right] = \frac{g^2}{2M_{W_L^\pm}^2} (J_A J_A + J_V J_V) . \tag{2.65}$$

It is clear that the neutral-current interactions conserve parity. Furthermore, the equal coefficients of $J_A J_A$ and $J_V J_V$ guarantee that the left-handed component of the $\bar{\nu}\nu$ neutral current couples only to the left-handed component of the $\bar{e}e$ or $\bar{u}u$ or $\bar{d}d$ current. Consequently:

(i) All neutral current processes involving left-handed neutrinos obey the phenomenological description of the standard left-handed Weinberg-Salam model, yielding the same relations between $\sin^2\theta_W$ and the measured experimental quantities. Thus, $\sin^2\theta_W \sim 0.2$-0.35, as found in our analysis of Sections 2.3 and 2.4.

(ii) All neutral current processes in which neutrinos do not participate, are manifestly parity conserving, yielding no parity violation in any atomic physics process and no asymmetry in deep inelastic scattering of polarized electrons on protons.

(iii) All charged current processes involving first-generation fermions obey the usual V-A theory.

The most remarkable property of the $SU(2)_L \times SU(2)_R \times U(1)$ model, is the identity between its predictions for neutrino-induced neutral-current processes and the predictions of the standard left-handed Weinberg-Salam theory. This identity is not accidental. In fact, it is a special case of a general theorem [22,24] which states the following: Consider a gauge theory based on a group $G' \times G'' \times U(1)$ in which all Higgs particles are either G'-singlets or G''-singlets. In such a theory, all neutral current processes involving a neutral particle which is a G''-singlet, will be fully described by the $G' \times U(1)$ subgroup. The detailed proof can be found elsewhere [24], but the situation is intuitively clear: If a particle transforms as a G''-singlet, it couples only to the vector-Bosons and Higgs particles which are G''-singlets. In such a case, its interactions cannot possibly be influenced by the nature of G''. Hence, the left-handed neutrino which is an $SU(2)_R$ singlet, does not couple to $W_R^\pm$, W_R^3, χ_R or δ_R. Its interactions are entirely described by $SU(2)_L \times U(1)$.

In Table II we present a comparison of the predictions of four models:

(a) The standard left-handed Weinberg-Salam model ("Standard Model").

(b) An $SU(2) \times U(1)$ vector model in which all fermions are in doublets and all neutral weak currents conserve parity ("Vector Model").

(c) An $SU(2) \times U(1)$ model with the assignments of Section 2.5: e_R in doublet; u_R, d_R in singlets; ("Asymmetric Model").

(d) The $SU(2)_L \times SU(2)_R \times U(1)$ model described in the present section ("Left-Right Model").

It is clear from the table that the standard and vector models are ruled out, respectively, by the atomic Bismuth experiment and the neutral-current $\bar{\nu}/\nu$ ratio. The two other models (described, respectively, in Sections 2.5 and 2.6) are consistent with all present data, but differ in their predictions for the last three processes in the table [17,22]. Any one of these processes could distinguish between these models. Our theoretical prejudices favor the $SU(2)_L \times SU(2)_R \times U(1)$ model.

Table II: Some Features of Four Possible Gauge Models

	"Standard"	"Vector"	"Asymmetric"	"Left-Right"	
Gauge Group	$SU(2) \times U(1)$	$SU(2) \times U(1)$	$SU(2) \times U(1)$	$SU(2)_L \times SU(2)_R \times U(1)$	
Bosons	$W^{\pm}$, Z, γ	$W^{\pm}$, Z, γ	$W^{\pm}$, Z, γ	$W_L^{\pm}$, $W_R^{\pm}$, Z_V, Z_A, γ	
Left-handed Fermions	$\begin{pmatrix}\nu_e\\ e^-\end{pmatrix}_L \begin{pmatrix}u\\ d\end{pmatrix}_L$	$\begin{pmatrix}\nu_e\\ e^-\end{pmatrix}_L \begin{pmatrix}u\\ d\end{pmatrix}_L$	$\begin{pmatrix}\nu_e\\ e^-\end{pmatrix}_L \begin{pmatrix}u\\ d\end{pmatrix}_L$	$\begin{pmatrix}\nu_e\\ e^-\end{pmatrix}_L \begin{pmatrix}u\\ d\end{pmatrix}_L$ in $\left(\frac{1}{2}, 0\right)$	
Right-handed Fermions	$(e^-)_R (u)_R (d)_R$	$\begin{pmatrix}N_e\\ e^-\end{pmatrix}_R \begin{pmatrix}u\\ b\end{pmatrix}_R \begin{pmatrix}t\\ d\end{pmatrix}_R$	$\begin{pmatrix}N_e\\ e^-\end{pmatrix}_R (u)_R (d)_R$	$\begin{pmatrix}\nu_e\\ e^-\end{pmatrix}_R \begin{pmatrix}u\\ d\end{pmatrix}_R$ in $\left(\frac{1}{2},0\right)$	$\begin{pmatrix}N_e\\ e^-\end{pmatrix}_R \begin{pmatrix}u\\ b\end{pmatrix}_R \begin{pmatrix}t\\ d\end{pmatrix}_R$ in $\left(0,\frac{1}{2}\right)$
Minimal Higgs-system	Two Doublets	Doublets Triplets	Doublets Triplets	$\left(\frac{1}{2},\frac{1}{2}\right)$ small VEV $\left(\frac{1}{2},0\right), \left(0,\frac{1}{2}\right)$ medium VEV (0,1) large VEV	$\left(\frac{1}{2},\frac{1}{2}\right)$ small VEV $\left(\frac{1}{2},0\right), \left(0,\frac{1}{2}\right)$ medium VEV
Boson-Mass Relations	$M_Z^2(1-x)=M_W^2$	$M_Z^2(1-x)\leq M_W^2$	$M_Z^2(1-x)\leq M_W^2$	$M_{W_R^{\pm}}^2 > M_{W_L}^2 = M_{Z_A}^2$ $M_{Z_V}^2(1-2x)=M_{Z_A}^2$	$M_{W_R^{\pm}}=M_{W_L^{\pm}}=M_{Z_A}$ $M_{Z_V}^2(1-2x)=M_{Z_A}^2$

Table II: Continued

	"Standard"	"Vector"	"Asymmetric"	"Left-Right"
$\frac{\sigma(\bar{\nu}_\mu e)}{\sigma(\nu_\mu e)}$	$\frac{1-4x+16x^2}{3-12x+16x^2}$	1	1	Same as "Standard"
$\frac{\sigma(\bar{\nu}N\to\bar{\nu}X)}{\sigma(\nu N\to\nu X)}$	$\frac{(2-B)(1-2x)+\frac{40}{9}x^2}{(2+B)(1-2x)+\frac{40}{9}x^2}$	1 (wrong)	Same as "Standard"	Same as "Standard"
P-violation in Heavy Atoms (J_A^e)	Yes (wrong)	No	No	No
P-violation in Hydrogen (J_A^q)	Yes	No	Yes	No
Asymmetry in polarized ep scattering	Yes	No	Yes	No
Front-Back Asymmetry in $e^+e^-\to\mu^-\mu^+$	Yes	No	Yes	Yes

2.7 The Mass Spectrum of First-Generation Fermions

The four first-generation fermions exhibit a very simple and reasonable mass spectrum. All its qualitative features can be more or less "understood" by simply considering the different interactions involved:

(i) The u and d quarks are heavier than the ν_e and e leptons. This is presumably due to the strong (QCD) interactions of quarks which somehow generate the quark-lepton mass differences.

(ii) The ν_e-e and the u-d mass differences are of the same sign and roughly the same order of magnitude. Both are presumably due to electromagnetic differences, since the two fermions within each doublet have identical weak and strong interactions. We have:

$$m(e) - m(\nu_e) \sim 0.5 \text{ MeV}$$

$$m(d) - m(u) \sim 2.5 \text{ MeV}.$$

We thus see that, at least superficially, the qualitative mass pattern is as simple as it could be, and all mass differences simply reflect the different interactions enjoyed by different fermions.

These simple remarks exhaust our understanding of the mass spectrum. From this point onward, we are only able to ask questions:

(a) Is the neutrino massless? If so, why? There must be some symmetry principle which prevents the neutrino from acquiring a mass. We do not know what it is. There may be a symmetry which forbids neutrino mass-terms to all orders, leading to a vanishing mass. Alternatively, it is conceivable that some symmetry prevents low order mass terms, and small high order terms are allowed. In that case a small but finite neutrino mass may be generated. The present limit [25]:

$$m(\nu_e) < 60 \text{ eV}$$

still allows concoctions such as $m(\nu_e) \sim \alpha^2 m(e)$. The (approximate?) masslessness of the neutrino is probably related to the left-right asymmetry observed in the weak charged currents, but we do not know of any satisfactory explanation of either phenomenon.

(b) What are the masses of u and d? The mass difference can be safely estimated. The masses themselves are either:

$$m(u) \sim m(d) \sim 300 \text{ MeV} \tag{2.66}$$

as obtained from "mechanical" mass formulae ($m(u) \sim \frac{1}{3} m(p)$) or:

$$m(u) \sim m(d) \sim \text{few MeV} \tag{2.67}$$

as obtained from calculations [26] of the symmetry breaking of chiral SU(2) x SU(2). It seems that in different contexts we must use different u and d masses. This may mislead us when we try to relate u, d masses to c, s masses, etc.

(c) Isospin symmetry ($m(u) \sim m(d)$) appears natural when only first-generation fermions are considered. It presumably follows from

$$e << g_{st} \tag{2.68}$$

where e and g_{st} are the electromagnetic and strong (QCD) coupling constants, respectively. However, the peculiar pattern of second generation masses leads us to consider isospin symmetry as an exception rather than the rule. It is possible that isospin symmetry represents the overall smallness of the u and d masses, rather than the smallness of their mass difference [27].

(d) The alleged simplicity of the first-generation mass spectrum is valid only if no heavy fermions (such as N_e, b, t) appear in the same doublets with e, u, d. Among the models of Table I only two have this feature: The standard model and the $SU(2)_L \times SU(2)_R \times U(1)$ model with $M_{W_R^\pm} >> M_{W_L^\pm}$. In all other models, additional fermions play an important role.

(e) Finally, we must make the most obvious remark: If our "explanation" of first-generation masses is valid, the mechanism which generates the masses of the second and third generations must be completely different, and it involves totally new physics ingredients. Alternatively, if all fermion masses are generated in the same manner, the simplicity of the first-generation spectrum must be regarded as accidental. Both of these possibilities are unattractive. We return to discuss them in Section 3.9, but we can offer no solution.

2.8 The Quark-Lepton Connection: Introduction

The building blocks of matter are quarks and leptons. Are they related to each other?

Six different arguments are usually mentioned as a motivation for considering a possible connection between quarks and leptons:

(i) To the extent probed by presently available momenta, quarks and leptons are "pointlike", $J = \frac{1}{2}$ fermions.

(ii) Quarks and leptons appear to respond to the weak interactions in an analogous way. Left-handed quarks and leptons are in SU(2) x U(1) doublets. Right-handed quarks and leptons do not seem to participate in the observed charged currents. There is a general similarity between the observed spectra of quarks and leptons, generation by generation.

(iii) The quantization of electric charge in the quark sector is clearly related to that of the lepton sector. This is not guaranteed by SU(2) x U(1). Within SU(2) x U(1) there is no reason for any special relationship between, say, the electron charge and the proton charge (or between Q(e) and Q(u), etc.).

(iv) The Weinberg angle θ_W is a free parameter in SU(2) x U(1) or $SU(2)_L$ x $SU(2)_R$ x U(1). Hence, the weak and electromagnetic interactions are not truly unified in such models. In a true unification scheme we should be able to compute θ_W from the symmetry properties of the unifying gauge group. Such a unification scheme may include the strong, weak and electromagnetic interactions and involve a quark-lepton connection.

(v) The strengths of the weak and electromagnetic interactions become comparable at $s \gtrsim M_W^2$. The effective strong interaction coupling constant in asymptotically free QCD decreases logarithmically at high momenta. At sufficiently high energies, perhaps of order 10^{17} GeV [28], the strong interactions presumably become comparable to the weak and electromagnetic ones. At such high energies, we may have an overall symmetry unifying all of these interactions, and relating the quarks to the leptons.

(vi) Empirically, the sum of electric charges of the first-generation fermions vanishes (counting the three quark-colors):

$$Q(\nu_e) + Q(e^-) + 3Q(u) + 3Q(d) = 0 \quad . \qquad (2.69)$$

A similar relation holds for second-generation fermions, etc. In a pure left-handed Weinberg-Salam model, this is actually a necessary condition for the elimination [29] of the triangle anomalies [30]. In other models, the anomalies are automatically cancelled, regardless of the sum of fermion charges. The fact remains, however, that the sum vanishes. One possible explanation for this may be the fact that in any model which contains the electric charge and which assigns quarks and leptons to the same multiplet of a simple group, the sum of quark and lepton charges must vanish. This may very well be the reason for the validity of Equation (2.69).

It is clear that a successful "grand unification scheme" of strong, weak and electromagnetic interactions would automatically account for

all of the six items which we have just enumerated. However, we should perhaps study them separately, in order to see whether "grand unification" is indeed necessary for each one of them.

The first two points (i), (ii), are qualitative statements concerning the similarity between quarks and leptons. They do not impose any specific mathematical connection between them, although the similarity would perhaps be more natural in theories in which such a connection exists. In any event, even if we accept that points (i) and (ii) guide us towards a quark-lepton connection, there is no reason to insist that it must assume the form of a grand unification group, assigning quarks and leptons to the same multiplet.

The next two items (iii), (iv) clearly point at a "truly unifying" gauge group larger than $SU(2) \times U(1)$ or $SU(2)_L \times SU(2)_R \times U(1)$. The gauge group has to be either a simple group G or a "pseudosimple" direct product of the form $G \times G$ with a discrete symmetry relating the coupling constant of the two G's. It must unify the weak and electromagnetic interactions, but need not be related to the strong interactions. In such a situation, charge quantization becomes universal and the Weinberg angle is uniquely determined, without introducing quarks and leptons into the same multiplet. We refer to such a theory as "simple unification".

Only the last two items (v), (vi), seem to require "grand unification" of strong, weak and electromagnetic interactions. In fact, the possible equality of strong and weak coupling constants actually sets the energy scale in which the symmetry limit of such a grand unification scheme may be realized. This energy scale ($\sim 10^{17}$ GeV) forces us to extrapolate our present ideas over many orders of magnitude. Most of the resulting symmetry relations are unlikely to be ever tested.

Summarizing our discussion, we find that we have:

(a) Qualitative motivation for a quark-lepton analogy (points (i), (ii)).

(b) Strong motivation for "simple unification" which, however, may leave quarks and leptons unrelated (points (iii), (iv)).

(c) Some motivation for "grand unification" (points (v),(vi)).

We must remember, however, that "grand unification" automatically achieves "simple unification" while the reverse is, of course, not true.

We now proceed to discuss the general features of "simple unification" and "grand unification".

2.9 "Simple Unification"

A "simple unification" scheme is based on a gauge group G such that:

(i) G is simple or pseudosimple (i.e. direct product of isomorphic groups, with equal coupling constants).

(ii) $G \supset SU(2) \times U(1)$

(iii) G commutes with $SU(3)_c$ and, therefore, does not connect quarks to leptons.

Any "simple unification" group would have additional weak gauge bosons, presumably heavier than $W^{\pm}$ and Z, but hopefully in the general mass range of 10^2-10^4 GeV, well below the mass range required by "grand unification" (see Section 2.10). The quantization of all electric charges follows a pattern which is determined by the gauge group, thus explaining the relation between quark and lepton charges. The Weinberg angle is determined by the group, and is given by [28]:

$$\sin^2\theta_W = \frac{\sum_i I_{3i}^2}{\sum_i Q_i^2} \qquad (2.70)$$

Where the summation is done over all quarks or all leptons in any representation of G. I_3 and Q are the diagonal neutral generators obeying a relation of the form:

$$Q = I_3 + \sum_j \alpha_j G_j \qquad (2.71)$$

while the corresponding vector fields A_μ and $W_{3\mu}$ obey:

$$A_\mu = W_{3\mu} \sin\theta_W + \sum_j \beta_j W_j \qquad (2.72)$$

G_j are all the diagonal generators of G which are orthogonal to I_3; W_j are their corresponding vector fields; α_j and β_j are numerical coefficients.

An important consequence of any "simple unification" scheme are the conditions:

$$\sum_{\text{quarks}} Q_i = 0 \quad ; \quad \sum_{\text{leptons}} Q_i = 0 \qquad (2.73)$$

for all quarks or all leptons in any given representation of G. Starting with the u, d quarks with charges $\frac{2}{3}$, $-\frac{1}{3}$ we immediately conclude that any "simple unification" theory must include, as a subgroup, an SU(3) gauge group of the weak and electromagnetic interactions. Moreover, if we restrict our attention to models in which all quark charges are $\frac{2}{3}$ or $-\frac{1}{3}$ (excluding $\frac{5}{3}$, $-\frac{4}{3}$, etc.) we find that the quarks must always come in SU(3)-triplets. Each triplet will then include an SU(2) doublet ($Q = \frac{2}{3}$, $-\frac{1}{3}$) and SU(2) singlet ($Q = -\frac{1}{3}$). The full "simple unification" group may be larger than SU(3) but it must contain an SU(3) subgroup in such a way as to guarantee that all quarks are in triplets of that SU(3) subgroup [31]. This can be achieved with G = SU(6), SU(3) x SU(3), SU(3) x SU(3) x SU(3), etc. The full scheme would then be based on:

$$G \supset SU(3) \supset SU(2) \times U(1) \ . \qquad (2.74)$$

It is easy to see that all such theories will have several common properties:

(i) We must have at least four (possibly many more) gauge Bosons beyond those of SU(2) x U(1). Their masses are likely to be, at least, several hundred GeV.

(ii) The first generation of quarks must be supplemented by, at least, one additional $Q = -\frac{1}{3}$ quark.

(iii) Leptons and quarks must belong to inequivalent representations. Leptons belong, at least, to SU(3) octets.

(iv) We must either have positively charged leptons, or have leptons and antileptons in the same SU(3) multiplet, leading to lepton number nonconservation.

(v) The Weinberg angle is determined. If the operator I_3 in Equations (2.70), (2.71), (2.72) is identified with the third generator or an SU(2) subgroup of SU(3), we have:

$$\sin^2\theta_W = \frac{3}{4} \qquad (2.75)$$

in clear contrast with experiment. However, if G is sufficiently large, we may identify I_3 in several different ways within G. Thus, if $G = SU(3)_L \times SU(3)_R$ and if I_3 of Equations (2.70), (2.71), (2.72) is a generator of $SU(3)_L$, we may obtain [32]:

$$\sin^2\theta_W = \frac{3}{8} \qquad (2.76)$$

which is perhaps not completely ruled out by experiment (see Sections 2.3, 2.4, 2.5). We do not know how to construct a reasonable "simple unification" scheme with a value of $\sin^2\theta_W$ smaller than $\frac{3}{8}$.

(vi) Any value of the Weinberg angle which is determined by G will not be substantially modified by renormalization effects, once we move away from the mass region of the heavy vector Bosons. Thus,

the theoretical value of θ_W can be directly confronted with experiment. Furthermore, the determined value of θ_W will remain unchanged if the simple unification group G is embedded in a grand unification group G*. All renormalization effects of G* will not modify the value of θ_W which has already been determined by G!

(vii) There will, in principle, be flavor changing neutral currents, connecting the two $Q = -\frac{1}{3}$ quarks in the same SU(3) triplet. The experimental effects of these currents may be small, due to large W-masses or additional discrete symmetries or cleverly chosen values of Cabibbo angles, or other means. However, there is no "natural" flavor conservation built into the theory (see Section 3.5).

Our overall conclusion is that "simple unification" schemes are extremely restrictive. They have several features which are somewhat unpleasant: θ_W is too large; no natural flavor conservation by neutral currents; unequal number of $Q = \frac{2}{3}$ and $Q = -\frac{1}{3}$ quarks; either positive charge leptons or lepton number nonconservation. The least unlikely candidate for "simple unification" is $SU(3)_L \times SU(3)_R$ [32]. While we do not consider it to be a very attractive gauge group, we cannot rule it out at the present time.

2.10 Grand Unification

A grand unification scheme [33], [34] is based on a group G* such that:

(i) G* is simple or pseudosimple.

(ii) $G^* \supset SU(2) \times U(1) \times SU(3)_{color}$

The gauge Bosons of G* include the twelve gauge Bosons of $SU(2) \times U(1) \times SU(3)_c$ ($W^{\pm}$, Z, γ and eight gluons) as well as many additional Bosons, some of which must transform nontrivially under both SU(2) and $SU(3)_c$.

The "grand unification" group G* may or may not include a "simple unification" subgroup G such that G commutes with $SU(3)_c$ and:

$$G^* \supset G \times SU(3)_c \supset SU(2) \times U(1) \times SU(3)_c \qquad (2.77)$$

If it does, the entire discussion of Section 2.9 applies to G*, including the determination of θ_W, the requirements concerning an SU(3) subgroup and the restrictions on the quark and lepton spectrum. However, it is entirely possible that G* does not contain any "simple unification" subgroup. In that case, all results of the previous section are inapplicable to G*.

All grand unification schemes have several important common features:

(i) The mass scale in which the grand unification scheme achieves its symmetric limit can be estimated by studying the momentum dependence of the "running" coupling constant in asymptotically free QCD. Various estimates [28], [35] range between 10^{15} and 10^{19} GeV. At least some of the gauge Bosons which generate G* presumably acquire masses of that order, in the process of spontaneous symmetry breaking.

(ii) G* must contain a set of gauge Bosons [33], [34] which carry the quantum number of both $SU(2)_{weak}$ and $SU(3)_{color}$. The minimal set of such Bosons transform as a (2,3) multiplet of SU(2) x SU(3). Together with the conjugate states in a $(2,\bar{3})$ multiplet, we must have, at least, twelve such Bosons. These Bosons convert a quark state into a lepton state and vice versa. They are sometimes referred to as "leptoquarks". They must be extremely heavy and they may be "confined" if all color-carrying states are "confined".

(iii) Quarks and leptons may be assigned to the same irreducible representation of G*. This immediately means that baryon number and

lepton number cannot commute with all generators of G*. Thus, baryon number and lepton number, if they are to be conserved, must be identified within G*. Any exactly conserved quantum number within a gauge theory corresponds to a massless gauge Boson. Consequently, if baryon and/or lepton number are exactly conserved, we must have at least one additional neutral massless gauge Boson, in addition to the photon and the (confined?) gluons. Such a massless Boson does not seem to exist in nature. We therefore conclude that baryon number and/or lepton number cannot be exactly conserved in a grand unification scheme[33,34]. This leads to the prediction that the proton is not stable. Its decay modes depend on the specific theory, but they may be e.g.:

$$p \to e^+ + \pi^o \qquad \text{or} \qquad p \to \nu + \nu + \bar{\nu} + \pi^o \ . \tag{2.78}$$

In order to preserve agreement between the observed lower limit of the proton's lifetime ($\sim 10^{30}$ years) and a given grand unification scheme, we may need to postulate that the masses of the gauge bosons which mediate processes such as $p \to e^+ + \pi^o$ are somewhere between 10^{15} and 10^{19} GeV, depending on the model. This is consistent with estimates of the energy scale of grand unification, but it is certainly far removed from any present or future experimental studies.

(iv) The Weinberg angle is, again, determined by the following expression (see Section 2.9, Equations (2.70), (2.71), (2.72)):

$$\sin^2\theta_W = \frac{\sum_i I_{3i}^2}{\sum_i Q_i^2} \tag{2.79}$$

where now the summation is over all quarks and leptons in the same representation of G*. *In general, the value of θ_W obtained in such* a way will be valid only at the grand unification mass (10^{15}-10^{19} GeV). In order to estimate θ_W at currently available energies, we have to compute the renormalization corrections to θ_W. This cannot be done in a reliable way, and it involves a wild extrapolation. Crude estimates based on the procedure of Georgi, Quinn and Weinberg [28] indicate that $\sin^2\theta_W$ may move from 0.375 at the grand unification mass to 0.2-0.3 or so at present energies [35]. However, such a substantial renormalization correction appears only when G* does not contain a "simple unification" subgroup G. If such a subgroup G exists, θ_W is determined by G and its value cannot be changed in the process of spontaneous symmetry breaking from G* to G.

Note that a complete list of all fermions in one representation of G* determines the symmetry value of $\sin^2\theta_W$. Hence, any grand unification scheme based on the first generation fermions ν_e, e, u, d, with no additions, would give:

$$\sin^2\theta_W = \frac{3}{8} \ [\text{if } I_3(f_R) = 0]$$
$$\sin^2\theta_W = \frac{3}{4} \ [\text{if } I_3(f_R) = I_3(f_L)] \ . \tag{2.80}$$

We now briefly mention several specific grand unification schemes which are of interest:

(i) The SU(5) Model [36]: The minimal grand unification scheme is based on SU(5). This is the smallest simple algebra containing SU(2) x U(1) x SU(3), and the only one which has the minimal number of leptoquarks (twelve). The left-handed first-generation fermions and antifermions are assigned to a reducible $10 + \bar{5}$ representation:

$$\bar{5} \supset (2,1) + (1,\bar{3}) = (\nu_e, e^-)_L + (\bar{d})_L \tag{2.81}$$

$$10 \supset (2,3) + (1,\bar{3}) + (1,1) = (u,d)_L + (\bar{u})_L + (e^+)_L \ . \tag{2.82}$$

The subsequent SU(2) x U(1) classification is, of course, that of the standard left-handed Weinberg-Salam model (which disagrees with the

atomic physics parity violation experiments; see Sections 2.3, 2.5). The neutrino must be massless. The Weinberg angle is $\sin^2\theta_W = \frac{3}{8}$, but it may be renormalized down to around 0.2 (see [35]). The leptoquark masses must be of the order of 10^{19} GeV and the Higgs particles must also be extremely heavy in order to protect the present limit on the proton lifetime. In SU(5), not only baryon and lepton number, but even fermion number, is not conserved. The theory has no anomalies.

(ii) The SO(10) Model [34], [35]: A more atttractive scheme is based on SO(10). This is the smallest simple group which contains $SU(2)_L \times SU(2)_R \times U(1) \times SU(3)_c$ and is therefore the natural grand unification scheme for the $SU(2)_L \times SU(2)_R \times U(1)$ theory of weak and electromagnetic interactions (see Section 2.6). The left-handed first-generation fermions and antifermions are assigned to the 16-dimensional spinor representation of SO(10). We may consider several different symmetry breaking chains:

(a) $SO(10) \supset SU(5) \supset SU(2)_L \times U(1) \times SU(3)$

Here the 16-dimensional representation of SO(10) has the following SU(5) decomposition:

$$16 \supset 10 + \bar{5} + 1 \qquad (2.83)$$

This provides us with the feature of including all left-handed fermions and antifermions of one generation in one irreducible representation (unlike the SU(5) case). The additional singlet is the left-handed antineutrino which could have a mass.

(b) $SO(10) \supset SU(2)_L \times SU(2)_R \times U(1) \times SU(3)_c$.

In this chain the 16-dimensional representation has the following content:

$$16 \supset (2,1,3) + (2,1,1) + (1,2,\bar{3}) + (1,2,1) \ . \qquad (2.84)$$

The four terms in Equation (2.84) correspond, respectively, to $(u,d)_L$; $(\nu_e,e^-)_L$; $(\bar{u},\bar{d})_L$; $(\bar{\nu}_e,e^+)_L$.

(c) $SO(10) \supset SU(2)_L \times SU(2)_R \times SU(4)_c$.

Here the 16-dimensional multiplet decomposes into:

$$16 \supset (2,1,4) + (1,2,\bar{4}) \ . \qquad (2.85)$$

$SU(4)_c$ is the generalized color group, including lepton number as a "fourth color". This was advocated a long time ago by Pati and Salam [33] who pioneered the study of grand unification schemes.

The different symmetry breaking chains of SO(10) can be summarized by the diagram:

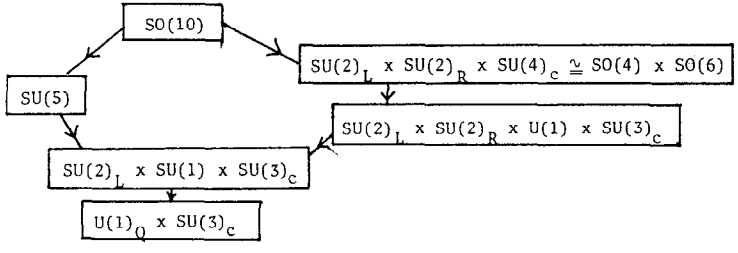

The SO(10) scheme predicts $\sin^2\theta_W = \frac{3}{8}$. The renormalization correction may modify this value to about 0.25-0.3. Chanowitz, Ellis and Gaillard have actually argued [35] that the renormalization corrections to θ_W in SO(10) are smaller than those in SU(5), yielding a more satisfactory value of θ_W. Here, again, leptoquarks must be extremely heavy, fermion number is not conserved and the theory is anomaly-free.

(iii) Gursey and collaborators [37] have proposed models based on the exceptional groups E(6) and E(7). We return to these models in Section 3.11. At this point we remark, however, that all such models include a "simple unification" subgroup and are therefore subject to

our discussion in Section 2.8. In particular, the E(7) scheme predicts $\sin^2\theta_W = \frac{3}{4}$, a value which is not substantially modified by renormalization, and is inconsistent with experiment.

We believe that the most attractive grand unification scheme for first-generation fermions is the SO(10) model. It provides a reasonable value of θ_W, "explains" why the sum of quark and lepton charges equals zero, provides a natural classification of the observed quarks and leptons and reduces naturally to $SU(2)_L \times SU(2)_R \times U(1)$. It suffers from the disadvantages of all grand unification schemes: Extremely heavy gauge Bosons, baryon and lepton number violations, and a grand unification mass which necessitates extrapolations over 15-20 orders of magnitude.

2.11 Summary: First-Generation Fermions

The first-generation fermions raise many of the fundamental problems of the physics of quarks and leptons. Their left-handed SU(2) x U(1) classification is simple and straightforward. Their right-handed classification is less clear. Present data dictate either leptonic right-handed doublets and quark right-handed singlets, or a gauge group which is larger than SU(2) x U(1). An attractive possibility is a version of $SU(2)_L \times SU(2)_R \times U(1)$ whose predictions coincide with those of the left-handed Weinberg-Salam model for all charged current and all neutral current reactions involving neutrinos, while at the same time all neutral currents conserve parity. Future asymmetry measurements in hydrogen atoms, polarized ep scattering, and $e^+e^- \to \mu^+\mu^-$ will test these ideas.

The mass spectrum of first-generation fermions appears to be qualitatively simple and "explainable". Whether this is an illusion we will know only when we understand the masses of the next generations.

The motivation for connecting quarks and leptons already exists at the level of the first-generation fermions. The group SO(10) seems to be the most attractive candidate for a grand unfication of first-generation fermions. It incorporates $SU(2)_L \times SU(2)_R \times U(1)$ in a natural way and has several other advantages. However, like all grand unification attempts, it suffers from several difficulties and unpleasant features.

3. Second-Generation Fermions: ν_μ, μ^-, c, s

3.1 Charged Weak Currents and the Classification of Second-Generation Fermions

The second generation of fermions includes two leptons (ν_μ and μ^-) and two quarks (c and s). The muon was the first fermion of that generation to be discovered. When it was identified as a lepton, the central problems of the second generation of fermions were already clearly states: Why do these fermions exist? What distinguishes them from first-generation fermions? First we had the μ^-, duplicating all properties of e^-, except its mass. Later, ν_μ was found, presumably duplicating ν_e. The strange and charmed quarks seem to duplicate the strong, weak and electromagnetic properties of the down and up quarks, respectively (again-except for their masses). The central mystery of the second generation, namely-the reason for its existence, remains unsolved, forty years after the discovery of the muon. More on that in Section 3.10.

The charged weak currents of the second generation involve the $\nu_\mu \leftrightarrow \mu^-$ and the $c \leftrightarrow s$ transitions. However, we now have, for the first time, a possibility of "generation mixing". There is nothing, apriori, to stop the mixing of e^- and μ^-, ν_e and ν_μ, u and c, d and s. Every such pair contains two particles with identical values of all the conserved quantum numbers of the non-strong interactions. Consequently, if the usual particle labels define the "physical" mass eigenstates, the SU(2) x U(1) representations may contain mixtures of such states.

In the leptonic case we will temporarily assume $m(\nu_e) = m(\nu_\mu)$. In that case, the mass does not select specific eigenstates ν_e and ν_μ. We can then define the left-handed ν_e and ν_μ to be the SU(2) x U(1) companions of the left-handed e^- and μ^-, respectively, and no further mixing is allowed among left-handed leptons. We return to this question in detail in Section 3.8 and consider the case $m(\nu_e) \neq m(\nu_\mu)$. Until then, we assume equal neutrino masses and no mixing of left-handed leptons. The decay

$$\mu^- \to e^- + \bar{\nu}_e + \nu_\mu \tag{3.1}$$

is consistent with a pure V-A transiton. Hence, the $\mu^- \leftrightarrow \nu_\mu$ transition presumably involves only left-handed leptons. The relevant charged current is:

$$J^-_\alpha \propto \bar{\nu}_\mu \gamma_\alpha (1-\gamma_5) \mu^- \tag{3.2}$$

and the left-handed ν_μ, μ are in an SU(2) x U(1) doublet:

$$\begin{pmatrix} \nu_\mu \\ \mu^- \end{pmatrix}_L \quad . \tag{3.3}$$

The quark case is, of course, different. We define u, d, c, s to be the mass eigenstates (also the strong interaction eigenstates). If we then postulate that all four left-handed quarks are in SU(2) x U(1) doublets, we may choose either u and c or d and s to define the two SU(2) x U(1) doublets. We then have the following equivalent SU(2) x U(1) assignments of the four left-handed quarks of the first two generations:

$$\begin{pmatrix} u \\ d' \end{pmatrix}_L \quad \begin{pmatrix} c \\ s' \end{pmatrix}_L \qquad \text{or} \qquad \begin{pmatrix} u' \\ d \end{pmatrix}_L \quad \begin{pmatrix} c' \\ s \end{pmatrix}_L \tag{3.4}$$

where

$$\begin{aligned} d' &= d\cos\theta + s\sin\theta \\ s' &= -d\sin\theta + s\cos\theta \end{aligned} \qquad \text{or} \qquad \begin{aligned} u' &= u\cos\theta - c\sin\theta \\ c' &= u\sin\theta + c\cos\theta \end{aligned} \tag{3.5}$$

and θ is the Cabibbo angle. For $\theta \neq 0$ we now have not only $u \leftrightarrow d$, $c \leftrightarrow s$ charged current transitions, but also $u \leftrightarrow s$, $c \leftrightarrow d$ transitions of strength $G\sin\theta$. We will consider every one of these four transitions separately. The two transitions involving u-quarks are well studied:

(i) $u \leftrightarrow d$. We have already discussed this transition in Section 2.1 and noted that it is consistent with being a pure left-handed transition. We are now in a position to use the strength of the $u \leftrightarrow d$ transition in order to determine θ. The properties of the gauge theory dictate equal couplings for the charged currents:

$$\bar{\nu}_\mu \gamma_\alpha (1-\gamma_5) \mu^- \qquad \text{and} \qquad \bar{u} \gamma_\alpha (1-\gamma_5) d' \tag{3.6}$$

Hence, the strength of the $u \leftrightarrow d$ transition should be given by $G_\mu \cos\theta$ where G_μ is the coefficient of the $\nu_\mu \leftrightarrow \mu$ term. Experimentally, the vector couplings of nucleon β-decay and μ-decay yield [38]:

$$\cos^2\theta = 0.948 \pm 0.004 \ . \tag{3.7}$$

(ii) $u \leftrightarrow s$. The strangeness changing charged current can be studied in semi-leptonic hyperon decays and K-decays such as $K^- \to \mu^- \bar{\nu}_\mu$, $K \to \pi \ell \nu$, $\Lambda \to p e^- \bar{\nu}_e$, $\Xi^- \to \Lambda e^- \bar{\nu}_e$, etc. All of these transitions are consistent with a V-A current:

$$\bar{u} \gamma_\alpha (1-\gamma_5) s \tag{3.8}$$

with strength $G\sin\theta$ where [38]:

$$\sin\theta = 0.229 \pm 0.003 \ . \tag{3.9}$$

While there is no evidence for any right-handed $u \leftrightarrow s$ transition, its existence (with a strength smaller than $G\sin\theta$) cannot be excluded (see also our discussion in Section 2.1). The value of the Cabibbo angle as determined from the $|\Delta S| = 1$ charged current is in extremely good agreement with the β-decay determination of $\cos^2\theta$. Several recent discussions of the separate determination of $\cos\theta$ and $\sin\theta$ yield [38]:

$$1 - (\sin^2\theta + \cos^2\theta) \leq 0.004 \ . \tag{3.10}$$

The calculation of Sirlin [39] actually leads to an even more stringent limit:

$$1 - (\sin^2\theta + \cos^2\theta) \leq 0.001 \ . \tag{3.11}$$

This "maximal allowed deviation from a four-quark Cabibbo theory" will play an important role in our discussion of the left-handed six quark model (Section 4.7).

The V and A structure of transitions involving the charmed quark ($c \leftrightarrow d$, $c \leftrightarrow s$) has not been directly studied, so far. We have, however, indirect considerations which enable us to determine the properties of these transitions. The next two sections are devoted, respectively, to the $\bar{c}d$ and $\bar{c}s$ charged currents.

3.2 The Case Against a Right-Handed $\bar{c}d$ Charged Current

The $c \leftrightarrow d$ charged-current transition can be directly studied in the decay process:

$$c \to d + e^+ + \nu_e \tag{3.12}$$

or the production process:

$$\nu_\mu + d \to \mu^- + c \ . \tag{3.13}$$

We have four different indications which favor a predominantly left-handed $c \leftrightarrow d$ transitions:

(i) D-meson decays. The charmed D-mesons should decay through a $c \leftrightarrow s$ or $c \leftrightarrow d$ transition. The $c \to s$ left-handed transition is of strength $G\cos\theta$ while the $c \leftrightarrow d$ left-handed

coupling is $G\sin\theta$. Consequently, if all c-decays are left-handed we expect:

$$\frac{\Gamma(c \to d + e^+ + \nu_e)}{\Gamma(c \to s + e^+ + \nu_e)} \sim \sin^2\theta \sim 0.05 \ . \qquad (3.14)$$

On the other hand, if we have a $c \leftrightarrow d$ right-handed transition of strength G we would expect:

$$\Gamma(c \to d + e^+ + \nu_e) \sim \Gamma(c \to s + e^+ + \nu_e) \ . \qquad (3.15)$$

Experimentally, one should measure the ratio:

$$\frac{\Gamma(D \to e^+ + \nu_e + \bar{K} + \text{anything})}{\Gamma(D \to e^+ + \nu_e + \text{anything})} \ . \qquad (3.16)$$

This ratio would be around 95% for the standard left-handed model, but around 50% for a model with a full-strength right-handed $c \leftrightarrow d$ transition. Semileptonic D-decays have been observed both in e^+e^- collisions and in neutrino reactions. The fraction of decays containing K-mesons seems to be substantial and probably larger than 50%. However, the semileptonic data [40] are not yet sufficiently precise in order to definitely distinguish between a branching ratio of 50% and 95%. A somewhat less definitive prediction involves the overall (semileptonic and nonleptonic) ratio:

$$\frac{\Gamma(D \to \bar{K} + \text{anything})}{\Gamma(D \to \text{anything})} \ . \qquad (3.17)$$

Here, again, the ratio would be either 95% or 50%, but in order to obtain this prediction we have to assume that we have no special enhancement or suppression mechanisms of specific nonleptonic channels. Such effects exist, of course, in nonleptonic K-decays and hyperon decays, where $\Delta I = \frac{1}{2}$ amplitudes are strongly enhanced, leading to a small semileptonic branching ratio. We believe, however, that such enhancement effects are not very prominent in D-decays in view of the "reasonable" semileptonic branching ratio [41]:

$$\frac{\Gamma(D \to \text{semileptonic})}{\Gamma(D \to \text{all})} \sim 0.2 \qquad (3.18)$$

We therefore consider the ratio (3.17) to be a reasonable test for the existence of right handed $c \leftrightarrow d$ transitions. Experimentally, it seems that most D-decays do contain K-mesons and that the 95% estimate is probably preferred [42].

Finally, we have an upper limit [43] on:

$$\frac{\Gamma(D^0 \to \pi^+ + \pi^-)}{\Gamma(D^0 \to K^+ + \pi^-)} \leq 0.07 \ . \qquad (3.19)$$

This, again, indicates the absence of right-handed $\bar{c}d$ terms which might yield:

$$\Gamma(D^0 \to \pi^+ + \pi^-) \sim \Gamma(D^0 \to K^- + \pi^+) \ . \qquad (3.20)$$

We summarize: The percentage of K-meson events in two-body nonleptonic D-decays is definitely above 90%. It is almost certainly around 90% in overall D-decays, and it is probably around the same value in semileptonic decays. All of these indicate, with varying degrees of experimental and theoretical certainty, that there is no substantial $c \leftrightarrow d$ right-handed transition.

(ii) Charmed particle production by neutrinos. Events of the type:

$$\nu_\mu + N \to \mu^- + \mu^+ + \text{anything} \qquad (3.21)$$

are presumably mostly due to the production of a charged particle followed by its semileptonic decay. The average ξ-value (momentum fraction) of the $\mu^-\mu^+$ events in νN scattering is significantly larger than the corresponding ξ-value for $\bar{\nu}N$ [44]. The absolute rate of $\mu^-\mu^+$

events is larger in νN than in $\bar{\nu}N$ [44]. Both of these facts indicate that most of the $\mu^-\mu^+$ events in νN scattering occur when the charmed quark is produced off a valence quark:

$$\nu_\mu + d \to \mu^- + c \ . \qquad (3.22)$$

By studying the y-distribution of these events we may then determine whether they are produced via a left-handed $d \leftrightarrow c$ transition (yielding a constant y-dependence) or a right-handed transition (yielding a $(1-y)^2$ dependence). Furthermore, the production rate would be much higher in the case of a right-handed transition.

The production rate of $\mu^-\mu^+$ events in νN scattering is [44] somewhat less than 1%, consistent with a production fraction of the order of $\sin^2\theta \sim 0.05$ times a decay branching ratio of the order of 10%. Should we have a right-handed $d \to c$ transition of strength G, approximately 25% of all νN events would contain charmed particles and the rate of $\mu^-\mu^+$ events would be larger than 2%. This seems somewhat large when compared with the observed $\mu^-\mu^+$ rate.

The y-distribution of $\mu^-\mu^+$ events in νN collisions is *consistent with a pure left-handed current and inconsistent with a* dominant right handed $c \leftrightarrow d$ transition [44]. We, therefore, conclude that the neutrino data favors a left-handed $c \leftrightarrow d$ transition.

(iii) $\underline{K^0_S\text{-}K^0_L \text{ mass difference}}$. The mass of the charmed quark was originally estimated [45], within the standard left-handed model of Glashow, Iliopoulos and Maiani (GIM) [46] from the observed $K^0_S\text{-}K^0_L$ mass difference. The estimate is based on the diagram of Fig. 7a. One obtains:

$$\Delta M = K(m_c^2 - m_u^2)\cos^2\theta \sin^2\theta \ , \qquad (3.23)$$

where the constant K involves factors (of G, M_W, etc.) which are irrelevant to the present argument. Inserting the experimental

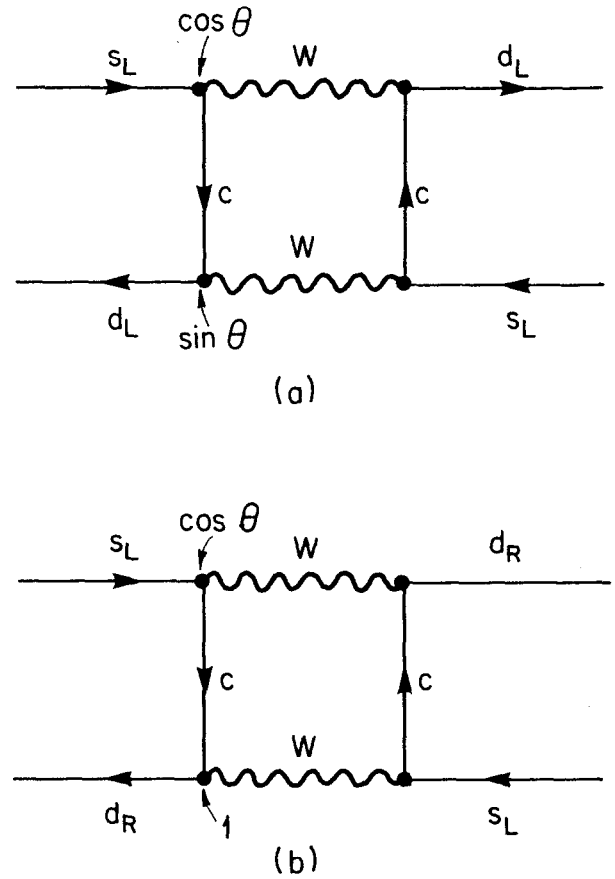

Figure 7: Dominant contribution to $K^0_S\text{-}K^0_L$ mass difference in (a) left-handed model; (b) a model with a right-handed $c \leftrightarrow d$ transition.

values of ΔM and θ one obtains the successful estimate [45]:

$$m_c \sim 1.5 \text{ GeV} \tag{3.24}$$

If we now have a right-handed $c \leftrightarrow d$ coupling of strength G, the expression for ΔM acquires a contribution (Fig. 7b):

$$\Delta M = K(m_c^2 - m_u^2)\cos^2\theta \cdot 2\left\{ \ell n \frac{M_W}{m_c} - 1 \right\} \quad . \tag{3.25}$$

where K is the same factor as in Equation (3.23). It is easy to see that the latter contribution to ΔM is larger than the first one by a factor of 100. Consequently, the estimate of m_c, based on a right-handed $c \leftrightarrow d$ coupling and the experimental value of ΔM, yields the totally unacceptable value $m_c \sim 150$ MeV . This argues very strongly against such a right-handed current [47].

(iv) Nonleptonic K-decays. Golowich and Holstein [48] have presented another interesting argument against a right-handed $c \leftrightarrow d$ transition. They studied the transformation properties of the weak Hamiltonian H_W for nonleptonic K-decays, under chiral SU(2) x SU(2). In a V-A theory, the $\Delta I = \frac{1}{2}$, $\frac{3}{2}$ pieces of H_W transform like the $(\frac{1}{2}, 0)$, $(\frac{3}{2}, 0)$ representations of SU(2) x SU(2). Consequently:

$$[H_W, Q+Q_5] = 0 \quad \text{and} \quad [H_W, Q_5] = -[H_W, Q_5] \tag{3.26}$$

where Q, Q_5 are, respectively, the vector and axial vector charges. In a theory with a substantial V+A current connecting $c \leftrightarrow d$, the $\Delta I = \frac{1}{2}$ piece of H_W will contain a term:

$$\bar{s}\gamma_\alpha(1-\gamma_5)c \cdot \bar{c}\gamma_\alpha(1+\gamma_5)d \ . \tag{3.27}$$

Such a term belongs to the $(0, \frac{1}{2})$ representation of SU(2) x SU(2) and obeys:

$$[H_W^{1/2}, Q-Q_5] = 0 \quad \text{and} \quad [H_W^{1/2}, Q_5] = [H_W^{1/2}, Q] \ . \tag{3.28}$$

If the $\Delta I = \frac{1}{2}$ piece of H_W is dominated by this term we have the following situation:

(i) In the standard left-handed model:

$$[H_W^{3/2}, Q_5] = -[H_W^{3/2}, Q] \ ; \ [H_W^{1/2}, Q_5] = -[H_W^{1/2}, Q] \ . \tag{3.29}$$

(ii) In a model with a right-handed $c \leftrightarrow d$ current:

$$[H_W^{3/2}, Q_5] = -[H_W^{3/2}, Q] \ ; \ [H_W^{1/2}, Q_5] = [H_W^{1/2}, Q] \ . \tag{3.30}$$

We can then distinguish between the two models by measuring the relative sign of the $I = \frac{1}{2}$ and $I = \frac{3}{2}$ amplitudes in K-decays. These amplitudes are related by PCAC to the corresponding $[H_W, Q_5]$ commutators, and their measured values clearly favor the case (i), again ruling out a substantial $c \leftrightarrow d$ right-handed term [48].

The four arguments listed above are more than sufficient for excluding a right-handed SU(2) x U(1) doublet of the form:

$$\begin{pmatrix} c \\ d \end{pmatrix}_R \tag{3.31}$$

None of these arguments can, at present, exclude a right-handed $c \leftrightarrow d$ transition of strength $G\sin\theta$, namely, a comparable amount of left and right-handed $c \leftrightarrow d$ couplings. Such a possibility can be excluded only by much better data on the production of charmed mesons by neutrinos, or by a detailed analysis of decays such as:

$$D^+ \to \mu^+ + \nu \ ; \ D \to \rho + e^+ + \nu_e \ . \tag{3.32}$$

The last two arguments (concerning the K_S^0-K_L^0 mass difference and nonleptonic decays) are important because they lead to a general result: In an SU(2) x U(1) model, no heavy quark can have a left-handed coupling of order G to the s-quark (or d-quark) and at the same time a right-handed coupling of order G to the d-quark (or s-quark).

This is a significant constraint on models involving third generation quarks.

3.3 Is There a Right-Handed $\bar{c}s$ Charged Current?

The left-handed c and s quarks are presumably connected by a charged current of strength $G\cos\theta$, leading to predominant strange particle decays of charmed mesons (see Section 3.2). Do we also have right-handed $c \leftrightarrow s$ transitions of strength G?

The phenomenological analysis of this problem is more difficult than the corresponding discussion of right-handed $c \leftrightarrow d$ terms in Section 3.2. A right-handed $(c,d)_R$ doublet would lead to an almost pure V + A coupling for $c \leftrightarrow d$ (because of the $\sin\theta$ suppression of the left-handed coupling). On the other hand, a $(c,s)_R$ doublet would yield approximately equal amounts of V + A and V - A couplings, leading to an almost pure vector interaction. While in the $c \leftrightarrow d$ case it was sufficient to exclude a dominant V + A term, here we try to exclude an equal amount of V + A and V - A.

At present, there is no convincing experimental or theoretical indication against a right-handed $c \leftrightarrow s$ term. There are, however, four items that we would like to discuss in this connection:

(i) F^+-decays. Certain rare decays of the F^+-meson [49] provide a relatively clean test of the V, A structure of the $c \leftrightarrow s$ transition [50]. The decay $F^+ \to \mu^+\nu$ can proceed only via an axial vector coupling. It is forbidden if the $\bar{c}s$ current is pure vector and is suppressed by a factor $\sin^4\theta$ if we have a right-handed doublet $(c,s)_R$. Similarly, the decay $F^+ \to (3\pi)^+$ is strongly suppressed in the presence of a $(c,s)_R$ doublet. Both of these tests will be decisive [50], but they involve extremely rare decay modes of the F^+.

(ii) $D \to K^* e \nu_e$. The decay $D \to K^* e^+ \nu_e$ is, presumably, the dominant semileptonic decay of the D-meson. It is also the simplest decay which could proceed by both V and A currents. A detailed measurement of the electron momentum spectrum in this decay could distinguish between V - A, V + A or pure V [51]. The present data [52] (which represents $D \to e^+ +$ anything, without K*-detection) is consistent with a pure V - A transition. However, pure V cannot yet be excluded.

We must emphasize that all the tests concerning F^+ and D decays test the effective V, A structure of the meson weak current rather than the "bare" weak couplings of the c and s quarks. The connection could, in principle, be made using methods similar to those of Adler and Weisberger [4], but the application of such methods for the $\bar{c}s$ current is not straightforward.

(iii) $\bar{\nu}+N \to \mu^+ + \mu^- +$ anything. A somewhat more direct test of the $c \leftrightarrow s$ current involves the production of $\mu^-\mu^+$ pairs in $\bar{\nu}N$ reactions. Assuming that such pairs emerge from the production and decay of charmed particles, the dominant mechanism will be:

$$\bar{\nu} + \bar{s} \to \mu^+ + \bar{c} \quad \Big\lfloor \to \mu^- + \bar{s} + \bar{\nu}_\mu \qquad (3.33)$$

where the struck $\bar{s}$ belongs to the $q\bar{q}$ "ocean" in the nuclear target. The observed rate of antineutrino $\mu^+\mu^-$ events, as well as their ξ distribution, are consistent with this assumption [44]. We may then use the y-distribution in order to determine the V, A structure of the production mechanism. For a pure V-A model the struck $\bar{s}$ and the produced $\bar{c}$ will be right-handed, yielding a constant y-dependence. A pure V + A (not wanted by anyone) would produce a $(1-y)^2$ dependence. A pure vector (representing approximately equal left-handed and right-handed $c \leftrightarrow s$ terms) would give:

$$\frac{d\sigma}{dy} \sim 1 + (1-y)^2 \qquad (3.34)$$

The present data [44] is consistent with a constant, is inconsistent with $(1-y)^2$, but probably cannot exclude $[1 + (1-y)^2]$. Better data on $\bar{\nu}$-production of $\mu^+\mu^-$ pairs is likely to be the best way of settling this issue.

(iv) $\Delta I = \frac{1}{2}$ enhancement in nonleptonic strange particle decays. It has been known for a long time that $\Delta I = 1/2$ matrix elements of the effective weak Hamiltonian for nonleptonic decays of strange particles are strongly enhanced relative to $\Delta I = \frac{3}{2}$ nonleptonic matrix elements and relative to semileptonic transitions. There is some circumstantial evidence that the enhancement comes from "single quark operators" such as the one shown in Fig. 8a. Such terms contribute only to the $\Delta I = \frac{1}{2}$ nonleptonic decay. The case in which both couplings in Fig. 8a are left-handed or right-handed, contributes to the renormalization of the quark wave-function rather than to the nonleptonic decay matrix element. The right-left coupling not only contributes, but is proportional to the mass of the intermediate charmed quark and is therefore presumably enhanced over other terms. Since we excluded a substantial right-handed $c \leftrightarrow d$ coupling the most logical possibility [53] would be to have a right-handed $c \leftrightarrow s$ coupling of order G followed by a left-handed $c \leftrightarrow d$ coupling of strength $G\sin\theta$. Whether the strength of such a term is sufficient for explaining the $\Delta I = \frac{1}{2}$ enhancement we do not know, but it is certainly an interesting possibility. One immediate corollary of this mechanism is the prediction that nonleptonic charmed particle decays will not have such an enhancement because the intermediate quark mass (m_s) is much smaller (Fig. 8b). Consequently, semileptonic branching ratios for D, F and the charmed baryons would be substantially larger than the corresponding branching ratios for K^0_S, Λ, Σ and Ξ.

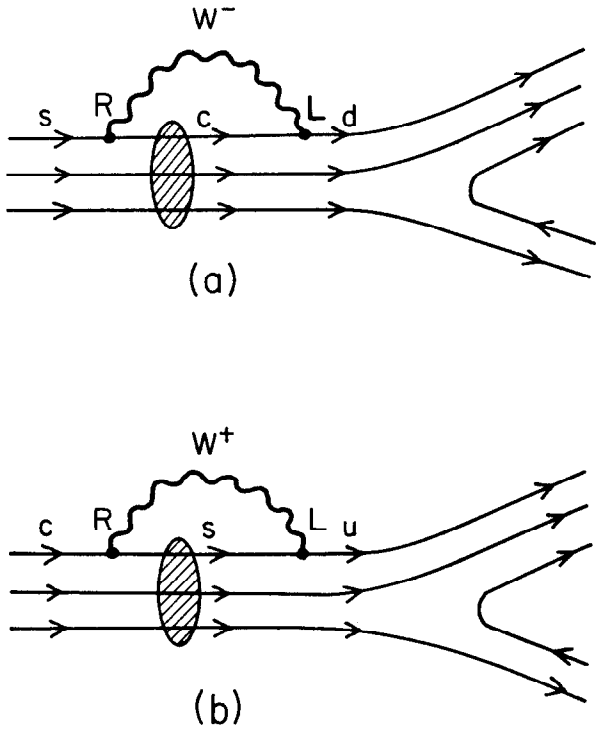

Figure 8: Possible contributions to (a) strangeness changing and (b) charm changing nonleptonic decays. The diagrams represent a weak Hamiltonian which is a "single-quark" operator, guarranteeing a $\Delta I = \frac{1}{2}$ rule. The shaded "blob" represents gluon exchanges.

Experimentally, this is verified in the case of D-decays [41]. It is interesting to note that in the $SU(2)_L \times SU(2)_R \times U(1)$ model discussed in Section 2.6, such a mechanism cannot operate. In such a model $W_R^{\pm}$ and $W_L^{\pm}$ are orthogonal eigenstates, and we cannot have a right-left term in Fig. 8.

Our overall conclusion is that there is no direct experimental evidence for or against a $(c,s)_R$ doublet. However, several tests involving the decays $F^+ \to \mu^+\nu_\mu$, $F^+ \to 3\pi$, $D \to K^* e\nu_e$ as well as the production of $\mu^+\mu^-$ pairs by antineutrinos, may help us to resolve this question. The only theoretical motivation for a $(c,s)_R$ doublet comes from a speculation involving the $\Delta I = 1/2$ enhancement in nonleptonic $|\Delta S| = 1$ decays. On the other hand, we will see in Section 3.7 that there are indirect theoretical arguments against a $(c,s)_R$ doublet.

3.4 Flavor Conserving Neutral Currents

Flavor conserving neutral currents involving second-generation fermions are, experimentally, extremely elusive. An exception is, of course, the neutral current involving ν_μ which is measured in $\nu_\mu e^-$ and $\nu_\mu N$ scattering, and which was already discussed in detail in Sections 2.3, 2.4. The neutral current of the muon will hopefully be probed when the asymmetry in $e^+e^- \to \mu^+\mu^-$ is detected (see Section 2.6 and Table II).

Flavor conserving neutral currents involving s and c quarks are more difficult to detect. It is unlikely that the contribution of the $s\bar{s}$ or $c\bar{c}$ pairs in the $q\bar{q}$ "ocean" will ever be isolated in $\nu + N \to \nu +$ anything. The only other method of detecting such currents would be through the decays $\phi \to \nu\bar{\nu}$, $\psi \to \nu\bar{\nu}$. We can express such decays in terms of the neutral current couplings:

$$g_c^L = 1 - \frac{4}{3}x \quad ; \quad g_c^R = \alpha_c - \frac{4}{3}x$$
$$g_s^L = -1 + \frac{2}{3}x \quad ; \quad g_s^R = \alpha_s + \frac{2}{3}x \qquad (3.35)$$

defined in analogy with Equation (2.16) in Section 2.2. The $\psi \to \nu\bar{\nu}$ decay branching ratio is given by [54]:

$$\frac{(\psi \to \nu_\mu \bar{\nu}_\mu)}{(\psi \to \mu^+\mu^-)} = \frac{9G^2M_\psi^4}{256\,\pi^2\alpha^2}\left(1 + \alpha_c - \frac{8}{3}x\right)^2 = 8 \times 10^{-7}\left(1 + \alpha_c - \frac{8}{3}x\right)^2 \qquad (3.36)$$

The total decay rate of ψ to all types of massless neutrinos is obtained by multiplying Equation (3.36) by the number of different types of neutrinos. For $\alpha_c = 0$, $x = 0.25$ and three types of neutrinos (ν_e, ν_μ, ν_τ) we get:

$$\Gamma(\psi \to \nu\bar{\nu}) = 1.5 \times 10^{-3}\ \text{eV} . \qquad (3.37)$$

The $\psi \to \nu\bar{\nu}$ decay rate can, <u>in principle</u>, be measured by studying the process:

$$e^+ + e^- \to \psi' \to \pi^+ + \pi^- + \text{Missing Mass}$$

where the missing mass is m_ψ and no hadrons or photons are emitted from the decay of ψ. It is unlikely, however, that such a measurement would achieve the required sensitivity in the foreseeable future.

It is interesting to note that the decay $\psi \to \nu\bar{\nu}$ is exactly forbidden in the standard left-handed model, when $\sin^2\theta_W$ assumes its "grand unification" value of 3/8. In a vector SU(2) x U(1) theory we have $\alpha_c = 1$, but the "grand unification" value is $\sin^2\theta_W = 3/4$, again leading to a forbidden $\psi \to \nu\bar{\nu}$ decay. This peculiar coincidence reflects the fact that the <u>vector</u> weak coupling of $I_3 = +1/2$ quarks (u, c, etc.) vanishes in most "grand unification" schemes, including all the schemes mentioned in this review (SU(5), SO(10), E(7), etc.). There is an interesting analogy here between the vanishing vector

electromagnetic coupling of $I_3 = +1/2$ leptons (neutrinos) and the vanishing of the vector weak coupling of $I_3 = +1/2$ quarks. One can prove that these two facts actually follow from each other in a large class of grand unification schemes, which includes all interesting models [55]. We do not know how important or profound this observation is.

The decay $\phi \to \nu\bar{\nu}$ is even more difficult to detect than $\psi \to \nu\bar{\nu}$, and it is practically hopeless.

We therefore conclude that a direct study of flavor conserving neutral currents involving s or c quarks is unlikely in the foreseeable future.

3.5 "Natural" Conservation of Flavor by Neutral Weak Currents

When a generator of a Lie algebra acts on a component of a given irreducible representation, it transforms it into another component of the same irreducible representation. In a gauge theory, the vector Boson fields generate the gauge algebra. Consequently, they can only connect states belonging to the same representation. If two different flavors of quarks with equal electric charges belong to two different representations of the gauge algebra, the neutral-current generators cannot connect them.

In the standard left-handed model we can always select u and c or s and d to be the unmixed states in SU(2) x U(1) doublets (see Section 3.1). We can do so, regardless of the specific value of the Cabibbo angle θ. Hence, in such a theory, there will be no strangeness changing $(\bar{s}d)$ or charm changing $(\bar{c}u)$ neutral currents. This is, of course, the famous GIM mechanism [46], which originally led to the prediction of charm. The conservation of flavor by the neutral current is "natural" in the sense that it occurs for any value of θ and does not require a specific value for any mass or angle parameter.

Our ability to assign u and c or s and d as pure SU(2) x U(1) states, regardless of the value of θ, follows from the assumption that the equal-charge quarks were assigned to identical SU(2) x U(1) multiplets. Consequently, any linear combination of them would also entirely reside in such a multiplet. Had we assigned, say, u and c into a doublet and a singlet, respectively, the SU(2) x U(1) eigenstates would have been uniquely determined by the value of θ and we would have no freedom in rearranging u and c to belong to two different SU(2) x U(1) representations. In such a case, charm-changing neutral currents would exist, and their strength would depend on the value of the u-c mixing angle.

The general conditions for "natural" flavor conservation has been studied by several authors [56]. Within SU(2) x U(1) we can define neutral-current coupling matrices G^L and G^R, generalizing our definitions of the couplings g_f^L and g_f^R in Section 2.2. We then have the matrix relation:

$$G^L = I_3^L - 2\sin^2\theta_W Q \qquad (3.38)$$

$$G^R = I_3^R - 2\sin^2\theta_W Q \ .$$

If we use the basis of the "physical" (mass eigenstates) quarks, flavor conservation means that G_L and G_R must be diagonal. However, if we consider all quark flavors with a common charge Q, "natural" flavor conservation means that G^L and G^R be diagonal for any set of values of the (generalized) Cabibbo angles. This can happen only if G^L and G^R are multiplets of the unit matrix for all quarks of the same charge. Hence, all equal-charge quarks must have the same I_3^L-values and the same I_3^R-values.

If we further want to exclude effective flavor changing neutral currents of order $G\alpha$ we have to consider single loop contributions to the effective coupling. The effective matrix element to order $G\alpha$ may include all neutral second order operators, namely:

$$(I_3^L)^2 \ , \ (I^L)^2 \ , \ (I_3^R)^2 \ , \ (I^R)^2 \ .$$

Hence, the required condition is that all equal-charge quarks have identical values of I^L and identical values of I^R. The leading term in the effective neutral weak interaction will then be of order $G\alpha \ (m_q^2/M_W^2)$, consistent with the observed magnitude of the K_L^o-K_S^o mass difference and the $K_L^o \to \mu^+\mu^-$ decay [56].

Additional constraints are required if we want to prevent effective flavor-changing neutral currents due to the exchange of neutral Higgs particles.

An important theoretical question is whether we must demand that any gauge theory obeys "natural" flavor conservation. The success of the GIM mechanism is impressive, and the smallness of charm changing neutral currents is gradually being established. It would be extremely ugly if these would be mere accidents. However, even if we adopt the point of view that there is nothing accidental about flavor conservation, we still have two options:

(i) Adhere to the conditions listed above. This would practically limit us to SU(2), U(1) or their products, as the candidate algebras of weak and electromagnetic interactions. All larger groups such as SU(3), and all "simple unification" schemes are excluded [35].

(ii) We might use a larger gauge group, but impose "natural" flavor conservation by introducing additional discrete symmetries. Such a mechanism exists, for instance, in the SU(3) x U(1) model [57].

Our own prejudice is that "natural" flavor conservation should be a property of the correct gauge theory, and that the introduction of a special discrete symmetry for the sole purpose of enforcing it, is somewhat artificial. We do not feel that imposing "natural" flavor conservation by the neutral Higgs particles is necessarily a mandatory requirement.

3.6 Experimental Evidence Against $|\Delta S| = 1$ and $|\Delta C| = 1$ Neutral Currents

The smallness of $|\Delta S| = 1$ neutral weak interactions has been known for many years. The two outstanding examples are, of course [25]:

$$m(K_L^o) - m(K_S^o) \sim 3.5 \times 10^{-6} \text{ eV} \qquad (3.39)$$

$$\frac{(K_L^o \to \mu^+\mu^-)}{(K_L^o \to \text{all})} \sim 10^{-8} \ . \qquad (3.40)$$

Both of these results are significantly below the expected values from an effective neutral interaction of order G . Both are consistent with estimates of order $G\alpha \ (m_c^2/M_W^2)$, and are smaller than flavor-conserving neutral weak processes by seven orders of magnitude. It is these experimental observations which led to the prediction of charm, and they form the basis to our belief in the GIM mechanism [46].

Now that charmed particles have been discovered, we are immediately led to ask whether charm changing neutral currents are also absent. There are two simple methods for searching for such currents, and both have yielded negative results:

(i) D^o-$\bar{D}^o$ Mixing. A charm changing neutral current could produce D^o-$\bar{D}^o$ mixing through a diagram such as Fig. 9. The amount of D^o-$\bar{D}^o$ mixing depends on the relative strength of D^o decay and the

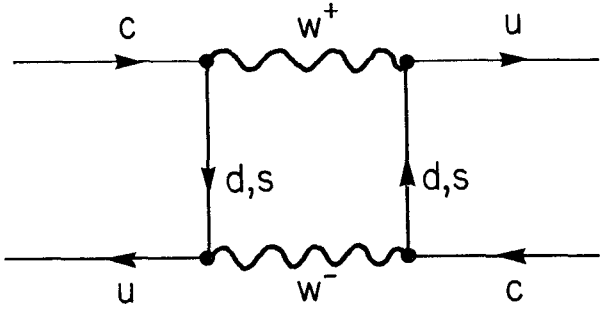

Figure 9: A contribution to D^o-$\bar{D}^o$ mixing.

$D^o \leftrightarrow \bar{D}^o$ transition. If the $D^o \leftrightarrow \bar{D}^o$ transition is of order G we would expect substantial (if not complete) D^o-$\bar{D}^o$ mixing. If charm changing neutral currents are absent, we expect, of course, no mixing [58].

The dominant decay modes of D^o include $\bar{K}$ particles. Most $\bar{D}^o$ decays include K's. In the case of D^o-$\bar{D}^o$ mixing we would expect a K with the "wrong" strangeness to be produced in D^o-decay. In particular, one may study the process:

$$e^+ + e^- \rightarrow D^o + K^\pm + \text{anything} \qquad (3.41)$$
$$\hookrightarrow K^\pm \pi^\mp$$

In this process, the two detected charged K-mesons will have opposite charges in the absence of D^o-$\bar{D}^o$ mixing (neglecting effects proportional to $\sin^4\theta \sim 0.004$). In the case of complete D^o-$\bar{D}^o$ mixing there will be no correlation between the charges of the two K-meson. It is convenient to define:

$$\varepsilon = \frac{N_{opposite} - N_{same}}{N_{opposite} + N_{same}} \qquad (3.42)$$

where $N_{opposite}$, N_{same} are, respectively, the number of events showing K-meson pairs with opposite charges and the same charges. For complete mixing: $\varepsilon = 0$. In the absence of mixing: $\varepsilon = 1$. The preliminary experimental determination gave [59]:

$$\varepsilon = 0.76 \pm 0.17 .$$

Thus, complete mixing is excluded. The existence of a $|\Delta C| = 1$ neutral current of order G is extremely unlikely, and the leading $|\Delta C| = 1$ term may well be of the same order of magnitude as the $|\Delta S| = 1$ neutral interaction.

(ii) $\nu + u \to \nu + c$. The production of charmed particles by a neutral-current neutrino interaction can be identified by detecting a "wrong sign" lepton. The detected process would be:

$$\nu_\mu + N \to \mu^+ + \text{anything (no } \mu^-) \qquad (3.43)$$

or

$$\nu_\mu + N \to e^+ + \text{anything (no } \mu^-) \; . \qquad (3.44)$$

In both cases, such a final state would emerge from:

$$\nu + u \to \nu + c \hookrightarrow \begin{cases} \mu^+ + \text{anything} \\ e^+ + \text{anything} \; . \end{cases} \qquad (3.45)$$

One should remember, of course, that "wrong sign" leptons may come from $\bar{\nu}_\mu$ or $\bar{\nu}_e$ contamination in the neutrino beam.

The best available limit on reaction (3.45) is given by the Brookhaven-Columbia bubble chamber experiment [60]:

$$\frac{\sigma(\nu + N \to \nu + \text{charm})}{\sigma(\nu + N \to \mu^- + \text{anything})} \cdot \frac{\Gamma(\text{charm} \to e^+ + \text{anything})}{\Gamma(\text{charm} \to \text{anything})} \leq 5 \times 10^{-4} \; . \qquad (3.46)$$

This, again, completely excludes $|\Delta C| = 1$ neutral currents of order G .

There are other, more difficult, methods of studying $|\Delta C| = 1$ neutral currents, such as looking for a charm theshold in R_ν (as defined in equation 2.37). No evidence for any such effects was found, so far.

We may thus safely conclude that no $|\Delta C| = 1$ neutral currents exists to lowest order. The GIM mechanism is probably operative, giving further support to the notion of "natural" flavor conservation by neutral currents (Section 3.5).

3.7 Summary: SU(2) x U(1) Classification of Second Generation Fermions

The discussion of the previous sections leads us to the following conclusions concerning the SU(2) x U(1) classification of second generation fermions:

(i) The left-handed fermions are in doublets:

$$\begin{pmatrix} \nu_\mu \\ \mu^- \end{pmatrix}_L \qquad \begin{pmatrix} c \\ s' \end{pmatrix}_L \qquad (3.47)$$

where s' is the Cabibbo-rotated s quark.

(ii) There is no evidence for any charged right-handed current involving a second-generation fermion. There is substantial evidence against right-handed currents with an effective coupling of order G, connecting $\nu_\mu \leftrightarrow \mu^-$, $u \leftrightarrow s$, $c \leftrightarrow d$. A $c \leftrightarrow s$ right-handed doublet cannot be excluded, at present. Note, however, that the "natural" conservation of strangeness and charm by neutral currents implies that d_R and s_R on one hand, and u_R and c_R on the other hand, must have identical I and I_3 values. Consequently, if $(c,s)_R$ form a doublet, u_R and d_R must be in doublets, contrary to our analysis in Section 2.4. Such a possibility is unlikely.

Within the SU(2) x U(1) model, all eight fermions of the first and second generation must be in left-handed doublets. At the same time, all possible right-handed doublets are excluded except:

$$\begin{pmatrix} c \\ s \end{pmatrix}_R \qquad (3.48)$$

and even this is unlikely, in view of our last argument.

There is no evidence against the suggestion that the weak and electromagnetic properties of the second-generation fermions are

identical to those of the first generation. If this hypothesis is correct, we would be left, again, with only one possible SU(2) x U(1) classification, duplicating the classification of the first generation (see Section 2.5). Alternatively, we could extend the gauge group into $SU(2)_L$ x $SU(2)_R$ x U(1) and have left-handed doublets in the (1/2,0) representation and right-handed doublets in the (0,1/2) (see Section 2.6). The present data concerning second-generation fermions (except for ν_μ) sheds no light on this question and adds no information concerning $\sin^2\theta_W$.

3.8 Flavor Conservation and Cabibbo-Like Angles in the Leptonic Sector

The "generation mixing" introduced by the Cabibbo angle is due to the fact that the "mass eigenquarks" do not coincide with the SU(2) x U(1) eigenquarks. The transformation between the two sets of eigenquarks is given by the Cabibbo rotation. In the leptonic case, a similar situation would occur if we could uniquely define "mass eigenleptons". We now consider several cases:

(i) $m(\nu_e) = m(\nu_\mu)$ in a left-handed model. In this case (including, of course, the possibility of $m(\nu_e) = m(\nu_\mu) = 0$) the "mass eigenleptons" can be arbitrarily chosen. The Cabibbo rotation becomes meaningless, and we actually define ν_e and ν_μ to be the SU(2) x U(1) left-handed partners of e^- and μ^-, respectively. In that case, all couplings between fermions and gauge Bosons will automatically conserve μ-number and e-number. If all right-handed leptons are in singlets and if we temporarily ignore the Higgs mesons, μ-number would be conserved to all orders of the weak interactions, without having to postulate it as a special symmetry. A sufficiently complex set of Higgs mesons would then be the only agent which could lead to μ-number nonconservation in a left-handed SU(2) x U(1) model [61]. Typical one loop and two loop diagrams contributing to $\mu \to e\gamma$ in such a theory are shown in Fig. 10. The two-loop contribution is probably dominant and one finds [61]:

$$\frac{(\mu^- \to e^- + \gamma)}{(\mu^- \to e^- + \bar{\nu}_e + \nu_\mu)} \sim O\left(\frac{\alpha}{\pi}\right)^3 \tag{3.49}$$

This is comparable with the present experimental upper limit. Note, however, that with the minimal set of Higgs particles no such contributions exist and $\mu \leftrightarrow e\gamma$ is forbidden.

(ii) $m(\nu_e) \neq m(\nu_\mu)$ in a left-handed model. If the two neutrinos have different masses, the "mass eigenleptons" will, in general, be different from the SU(2) x U(1) eigenleptons. In that case, the entire Cabibbo formalism is reproduced. The left-handed doublets will be:

$$\begin{pmatrix} \nu_e' \\ e^- \end{pmatrix}_L \qquad \begin{pmatrix} \nu_\mu' \\ \mu^- \end{pmatrix}_L \tag{3.50}$$

where

$$\begin{aligned} \nu_e' &= \nu_e \cos\phi + \nu_\mu \sin\phi \\ \nu_\mu' &= -\nu_e \sin\phi + \nu_\mu \cos\phi \end{aligned} \tag{3.51}$$

ν_e, ν_μ are the "mass-eigenleptons" and ϕ is a leptonic Cabibbo angle. We continue to assume that all right-handed leptons are singlets. The mixing of neutrinos will allow μ-number violating transitions, through diagrams such as Fig. 11. However, the rate for $\mu^- \to e^- + \gamma$ in such a model is hopelessly small [62]:

$$\frac{(\mu^- \to e^- + \gamma)}{(\mu^- \to e^- + \bar{\nu}_e + \nu_\mu)} = O\left\{\frac{\alpha}{\pi} \cdot \frac{\Delta m_\nu^2}{M_W^2} \sin 2\phi\right\} . \tag{3.52}$$

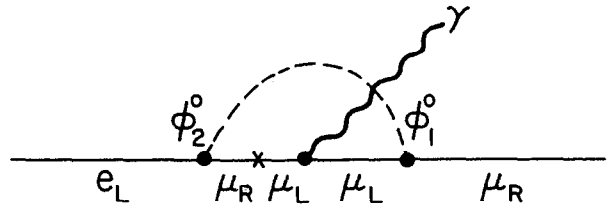

(a)

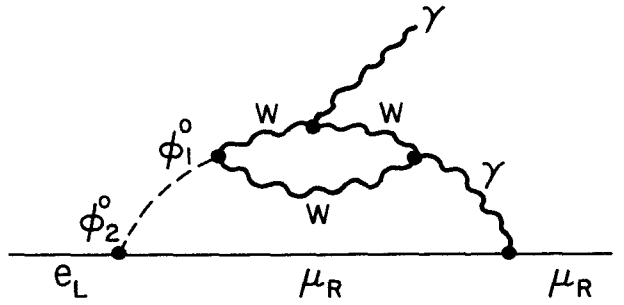

(b)

Figure 10: Typical (a) one-loop and (b) two-loop contributions to $\mu^- \to e^-\gamma$ in a model involving a non-minimal Higgs structure [61]. The two-loop diagram is probably dominant.

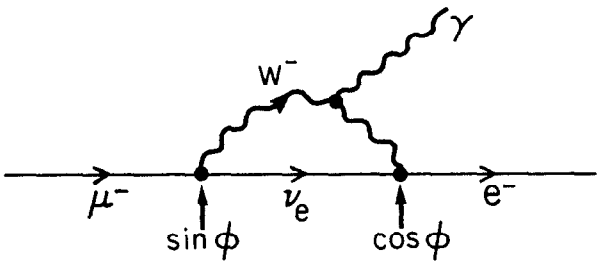

Figure 11: A mechanism for the reaction $\mu^- \to e^-\gamma$ in a model involving Cabibbo-like mixing in the leptonic sector.

For the present upper limit on $m(\nu_\mu)$ we obtain a ridiculously small branching ratio of less than 10^{-19}. It is clear that any effect which is proportional to Δm_ν^2 is unlikely to be detected in this case! The ν_e-ν_μ mixing leads to other effects such as "neutrino oscillations" [63]. This would happen in the following way: Neutrinos emitted in $\pi^+ \to \mu^+ + \bar{\nu}$ decay would be the ν_μ' mixture of ν_e and ν_μ. The resulting neutrino beam will be a time-dependent mixture of the two mass eigenstates ν_e and ν_μ. The probability of finding the SU(2) x U(1) eigenlepton ν_e' then depends on the time evolution of the beam. Consequently, the ratio between produced e^+ and μ^+ will vary along the beam line. Such effects can be, in principle, detected in neutrino experiments.

(iii) μ-number Violation in a Right-handed Model. We now consider a model (see Section 2.5) in which both the left-handed and the right-handed e^- and μ^- are in SU(2) x U(1) doublets:

$$\begin{pmatrix}\nu_e\\ e^-\end{pmatrix}_L \quad \begin{pmatrix}\nu_\mu\\ \mu^-\end{pmatrix}_L \quad \begin{pmatrix}N_e'\\ e^-\end{pmatrix}_R \quad \begin{pmatrix}N_\mu'\\ \mu^-\end{pmatrix}_R \quad . \tag{3.53}$$

For simplicity, ν_e and ν_μ may be massless. N_e' and N_μ' are neutral SU(2) x U(1) eigenleptons representing a mixture of "mass eigenleptons" N_e and N_μ [64]:

$$\begin{aligned} N_e' &= N_e\cos\chi + N_\mu\sin\chi \\ N_\mu' &= -N_e\sin\chi + N_\mu\cos\chi \quad . \end{aligned} \tag{3.54}$$

The mechanism which violates μ-number conservation is, in this case, identical to the one described above in the case $m(\nu_\mu) \neq m(\nu_e)$. The theoretical expression for the $\mu \to e+\gamma$ branching ratio is similar:

$$\frac{(\mu^- \to e^- + \gamma)}{(\mu^- \to e^- + \bar{\nu}_e + \nu_\mu)} \sim 0 \left[\frac{\alpha}{\pi} \cdot \frac{m(N_\mu)^2 - m(N_e)^2}{M_W^2} \cdot \sin 2\chi\right] \quad . \tag{3.55}$$

However, it is now entirely possible that $m(N) \sim$ few GeV. Consequently, we may obtain $\mu^- \to e^- + \gamma$ branching ratios around 10^{-8} - 10^{-10}, comparable with present experimental upper limits. The left-handed N-leptons (about which we assumed nothing, so far) may also mix with the neutrino, leading to additional contributions to $\mu^- \to e^- + \gamma$ [65].

There are, of course, many other variations of the SU(2) x U(1) theory, leading to different forms of μ-number violation. The common feature of all such theories is the fact that in the absence of Cabibbo mixing, μ-number is automatically conserved (except for the Higgs couplings). Consequently, all μ-number violations are proportional to the mixing parameters as well as to the $(\text{mass})^2$ differences of the mixed states. In order to obtain a nontrivial effect, these masses have to be of the order of GeV or so, implying the existence of heavy neutral right-handed leptons.

In an $SU(2)_L$ x $SU(2)_R$ x U(1) theory, the μ-number violation effects discussed here are basically unchanged. The only minor differences involve (i) replacing M_W by M_{W_L} and M_{W_R} according to the involved coupling, and (ii) elimination of contributions from right-left diagrams in which the two W-couplings to the leptons are of opposite handedness.

3.9 CP Violation in a Gauge Theory

The charged weak current of the standard Weinberg-Salam left-handed model can be written as:

$$J = (\bar{u}\bar{c})\ \gamma_\mu(1-\gamma_5)\ A\begin{pmatrix} d \\ s \end{pmatrix} \qquad (3.56)$$

where A is a unitary 2 x 2 matrix. In principle, such a unitary matrix can be fully parametrized in terms of four real parameters. However, three of these parameters can be "absorbed" into the definitions of the quark states, u, d, c, s. In other words, we can redefine u as $ue^{i\phi}$ without suffering any observable consequences. Four quark states can absorb only three phase parameters - one for each quark except for one overall phase. We therefore remain with an A-matrix which is fully determined by one real parameter. A is then necessarily an orthogonal matrix and the single parameter can be chosen as the Cabibbo angle θ :

$$A = \begin{pmatrix} \cos\theta & \sin\theta \\ -\sin\theta & \cos\theta \end{pmatrix} . \qquad (3.57)$$

All matrix elements of weak currents involving the four quarks and the four vector gauge particles (W^+, W^-, Z^o, γ) will be relatively real in such a theory. Consequently, CP is necessarily conserved in a gauge theory based on the left-handed model of first and second-generation quarks.

One might suggest that the interaction responsible for CP violation is not an integral part of the gauge theory of weak and electromagnetic interactions. In that case, all the fundamental questions which were solved by the introduction of gauge theories must be reopened. It is not clear, for instance, that a gauge theory with an external CP-violating piece remains renormalizable, etc.

It would be much more attractive to be able to account for CP-violations within the framework of the gauge theory, in a fashion that preserves all the beautiful features of the theory. This could be achieved if the matrix elements of the weak current would contain complex phases which cannot be eliminated by redefining the physical states, and which are, therefore, experimentally observable.

There are, at least, three ways to achieve this within the framework of the SU(2) x U(1) gauge theory (but not within the simplest four-quark verison of the standard left-handed model). We now discuss them briefly:

(i) CP-violation and Higgs Mesons. We may remain with only four quarks and only left-handed currents but introduce the complex phase parameter into the interactions of the Higgs particles [66]. The "minimal" set of Higgs particles in the Weinberg-Salam model includes four scalar states. Three of them are "eaten up" by the three massive vector gauge Bosons and one remains as a physical particle. The couplings of this particle cannot induce CP-violation. It is clear, however, that we can also introduce a larger set of Higgs particles. Such an assumption is neither elegant nor necessary, but it is perfectly consistent with all the requirement of the theory. Weinberg [66] has pointed out that the (otherwise ugly) possibility of increasing the number of Higgs particles, enables us to introduce an arbitrary relative phase parameter between the interactions of different Higgs particles. Such a phase will produce CP-violation through the interference of diagrams involving different virtual Higgs particles. This is the only way of incorporating CP-violation into the standard left-handed model without introducing new quarks or new currents. The attractive feature of this idea is the natural smallness of the CP-violating amplitude, relative to other weak amplitudes. The resulting CP-violating amplitude successfully "imitates" the predictions of the superweak theory, in accordance with experiment. The unattractive

feature is the explicit dependence on the properties of the Higgs particles, and the required non-minimal set of such particles.

(ii) CP-violation and Right-handed Currents. If we do not appeal to the Higgs particles, we may still introduce CP-violation at the level of second generation quarks. This can be done by the introduction of right-handed weak currents and in particular the $c \leftrightarrow s$ right-handed transition discussed in Section 3.3. The idea is simple: the 2 x 2 matrix A which we have discussed above, has "lost" three of its arbitrary parameters through a redefinition of the quark states u, d, c, s. If, however, some of the same quarks also participate in a right-handed current, we do not have any more freedom to absorb the phase parameters of the additional current into the redefined quark states. In other words, a relative phase between the left-handed transitions and the right-handed matrix elements cannot be, in general, eliminated. This method of violating CP was first suggested by Mohapatra [67] several years ago, and was later discussed by other authors [68]. It also leads to predictions which imitate the "superweak" results for the K^o-$\bar{K}^o$ system, but the typical strength of the CP-violating interaction has to be postulated and cannot be derived.

(iii) CP-violation and the Number of Quarks. It is clear that the simplest way to produce CP-violation would be to increase the number of quarks [69]. The argument for CP-conservation in the case of the left-handed four-quark model started with four (2 x 2) parameters of a unitary matrix and continued with three (4-1) "absorbed" phases. Generalizing the argument to n doublets of left-handed quarks would give an $n \times n$ unitary matrix A with n^2 real parameters. The total number of quarks is 2n, allowing us to "absorb" (2n-1) phases into the definitions of the quark states. We remain with $n^2-(2n-1)$ real parameters, while an $n \times n$ orthogonal matrix allows only $\frac{1}{2}n(n-1)$ parameters. We are therefore left with an $n \times n$ unitary matrix containing:

$\frac{1}{2}\,n(n-1)$ real rotation angles (generalized Cabibbo angles)

$\frac{1}{2}\,(n-1)(n-2)$ phase parameters (CP violating phases).

For one generation of quarks (n = 1) we have no angles and no phases. For two generations, we obtain one Cabibbo angle and no phases. For three generations, we obtain three angles and one phase parameter, yielding CP-violating effects within a purely left-handed SU(2) x U(1) gauge theory [69]. We discuss this possibility in detail in Sections 4.7 and 4.10.

We do not have a strong prejudice for or against any of the above mechanisms for CP-violation. It is important to realize that almost any extension of the four-quark left-handed model leads to CP violation. At the present time the extension to six quarks appears to be most attractive, due to reasons which are unrelated to CP-violation (see Section 4.5). We therefore prefer the six-quark version of CP-violation over the options of introducing right-handed $c \leftrightarrow s$ currents or complicated Higgs spectra.

3.10 The Mass Spectrum of Second-Generation Fermions and the Cabibbo Angle.

We have seen, so far, that the second-generation fermions behave in all respects like their first-generation predecessors. Their weak, electromagnetic and strong interaction patterns are identical. The only exception is the mass spectrum, which was simple and qualitatively "understandable" for the first-generation fermions, but is totally puzzling in the case of the second generation.

There is no explanation whatsover for the μ-e, c-u and s-d mass differences. While the ν_e-e and u-d differences may well be of electromagnetic origin, the ν_μ-μ and c-s differences are larger by 2-3 orders of magnitude. The ν_e-e and the u-d differences are of essentially comparable order of magnitude and equal signs. The ν_μ-μ and c-s differences are of different orders of magnitude and opposite signs. Except for the presence of the Cabibbo angle which is likely to enter into various mass calculations, we see no reason for the totally different mass patterns of the two generations.

On the level of naive qualitative speculations, the simplest "explanation" could have been the following: There is a new interaction (beyond the usual weak, electromagnetic and QCD interactions) which distinguishes between fermions of the two generations. First-generation fermions do not participate in this interaction (presumably having vanishing values of some new charge which couples to it). Second-generation fermions respond to the "new interaction" and largely acquire their masses through it. Thus, the alleged "new interaction" is responsible for the μ-e mass difference as well as for the mass values of the c and s quarks. Such a speculation is not, apriori, unattractive. After all, something must eventually distinguish between the muon and the electron!

The real difficulty of our naive "new interaction" is, of course, the incredibly accurate measurement [70] of the muon magnetic moment, which agrees with the QED prediction to within 25 parts per billion in g (or 25 parts per million in g-2). Our "new interaction" must be strong enough to account for the muon mass, but weak enough to contribute to $(g-2)_\mu$ below the present experimental uncertainty, and below the contribution of the ordinary weak interactions.

An example for such an artificial interaction (which, however, teaches us nothing new) is the coupling of the Higgs particles to the fermions. This coupling is, by definition, proportional to the fermion mass. It distinguishes between μ and e, c and u, etc. At the same time, the Higgs-particle contribution to g-2 is well below the present level of experiments [71]. The Higgs couplings teach us nothing new, since the fermion masses are introduced into them "by hand". Whether a more meaningful "new interaction" exists we do not know, but it is attractive to assume that in some approximation, all first-generation fermions are massless, while second generation fermions acquire their mass through a mechanism which distinguishes between the two generations.

The assumption of zero "bare mass" for the first-generation fermions leads to an interesting speculation concerning the value of the Cabibbo angle [72]. Assuming that prior to the Cabibbo mixing:

$$m_u^o = m_d^o = 0 \tag{3.58}$$

we may obtain the following mass matrix for the u and c quarks:

$$\begin{pmatrix} 0 & m_{uc} \\ m^*_{cu} & m^o_c \end{pmatrix} \tag{3.59}$$

The unitary matrix needed to diagonalize this mass matrix can be defined by a rotation angle θ_1 which can be expressed in terms of the final mass eigenvalues m_u and m_c:

$$\tan 2\theta_1 = \frac{2\sqrt{m_u m_c}}{m_c - m_u} \tag{3.60}$$

A similar angle, θ_2, "rotates" the "bare" d_o and s_o states into the "physical" d and s:

$$\tan 2\theta_2 = \frac{2\sqrt{m_d m_s}}{m_s - m_d} \qquad (3.61)$$

The Cabibbo angle is, of course, given by:

$$\theta = \theta_2 - \theta_1 = \frac{1}{2}\left\{\arctan \frac{2\sqrt{m_d m_s}}{m_s - m_d} - \arctan \frac{2\sqrt{m_u m_c}}{m_c - m_u}\right\} \qquad (3.62)$$

Assuming:

$$m_u \sim 4 \text{ MeV};\ m_d \sim 7 \text{ MeV};\ m_s \sim 150 \text{ MeV};\ m_c \sim 1500 \text{ MeV} \qquad (3.63)$$

we find:

$$\theta \sim 9^o$$

Compared with the "experimental" value of 13^o (see Section 3.1). The agreement is not bad, in view of the crude assumptions used here.

This calculation of the Cabibbo angle ignores several important effects and involves some unjustified assumptions. We do not consider it to be a solution to the problem of understanding the relation between fermion masses and Cabibbo angle. We have mentioned it here only as an illustration of one possible way of attacking the problem. Other interesting attempts have been suggested by different authors [73].

3.11 Grand Unification and the Second Generation of Fermions

We have indicated in Sections 2.9 and 2.10 that all the motivations for a quark-lepton connection or for a grand unification of strong, electromagnetic and weak interactions already exist at the level of first-generation fermions. The second-generation fermions do not add to these motivations. Models such as the SU(5) and SO(10) schemes (see Section 2.10) relate only quarks and leptons of the same generation. Consequently, each generation of fermions is assigned to a separate representation of the grand unification algebra. In the case of SO(10), the left-handed fermions ν_μ, μ, c, s (and the left-handed antifermions) form a 16-dimensional multiplet, analogous to the one formed by ν_e, e, u, d. In SU(5), the second-generation fermions form an additional set of $10 + \bar{5}$ multiplets. Such grand unification schemes shed no light on the distinction between different generations. In fact, it is clear that in such models the Cabibbo angle (or angles) which represents "generation mixing" cannot be understood within the framework of the grand unification group. It is also apparent that the mass differences between first- and second-generation fermions are not due, in such models, to any of the interactions which are represented by the gauge Bosons of the grand unification algebra.

There are more ambitious models which try to assign all fermions (of both generations) to one large multiplet of a grand unification scheme. The most interesting model in this category is the E(7) model [37].

In E(7), all fundamental fermions are in the "spinor" 56-dimensional representation. E(7) has a maximal subgroup SU(6) x SU(3). SU(6) is the flavor gauge algebra and SU(3) is the usual color gauge group. The 56-multiplet of E(7) decomposes into the following SU(6) x SU(3) multiplets:

$$56 \supset (6,3) + (\bar{6},\bar{3}) + (20,1)\ . \qquad (3.64)$$

Hence, the fundamental fermions are:

(i) Six quarks (color triplets)

(ii) Six antiquarks (color antitriplets)

(iii) Twenty leptons and antileptons (color singlets).

Since the electric charge is an SU(6) generator, we conclude that, in this model, SU(6) is a "simple unification" group (see Section 2.9). It includes an SU(3) sub-group and dictates the charges of the six quarks to be $\frac{2}{3}$, $-\frac{1}{3}$, $-\frac{1}{3}$, $\frac{2}{3}$, $-\frac{1}{3}$, $-\frac{1}{3}$. Hence, the four quarks of the first two generations are supplemented by two additional $Q = -\frac{1}{3}$ quarks. The Weinberg angle is predicted, at the SU(6) level, to obey:

$$\sin^2\theta_W = \frac{3}{4} \qquad (3.65)$$

in clear conflict with experiment. There is no reason to expect the SU(6) gauge Bosons to have very high masses. Consequently, the renormalization effects on $\sin^2\theta_W$ should not be substantial (see Sections 2.9, 2.10).

The leptons and antileptons fall into a 20-dimensional representation of SU(6). Lepton number is not conserved. There are four negatively charged leptons (e^-, μ^-, τ^- and one more), four positively charged leptons (their antiparticles) and twelve neutral leptons. Of the four negatively charged leptons, two must be in SU(2) x U(1) triplets, and two are in doublets.

The E(7) model represents a bold attempt to unite all fermions in one multiplet. Unlike SU(5) or SO(10) it makes a definite prediction about the total number of quarks and leptons. It predicts an unequal number of $Q = 2/3$ and $Q = -1/3$ quarks. All of these predictions can be tested. The main difficulty of the model is, however, its unacceptable value for $\sin^2\theta_W$.

Any model (including E(7)) which introduces fermions of different generations into the same multiplet of a grand unification gauge group must violate natural flavor conservation by neutral currents. If the s and d quarks belong to the same representation of such an algebra, it must have a generator corresponding to an $\bar{s}d$ neutral current. Such a current can be made small by various means, such as assuming a very large mass for the corresponding vector Boson. However, the absence of $|\Delta S| = 1$ and $|\Delta C| = 1$ neutral currents must be introduced explicitly into the model, and it does not follow "naturally".

We believe that the two major difficulties mentioned above (i.e. $\sin^2\theta_W$ and the absence of natural flavor conservation) provide us with strong arguments against such models. However, their explicit predictions concerning the existence and number of various quark- and lepton-flavors will serve as the most conclusive test.

3.12 Summary: Second-Generation Fermions

The second generation of fermions raises only one new fundamental question: Why do these fermions exist, and what distinguishes them from their predecessors?

All weak interactions of second-generation fermions are, so far, consistent with being identical to those of the first generation. There is no indication for right-handed charged currents. All left-handed fermions seem to fit in SU(2) x U(1) doublets. There is no evidence against the hypothesis that the classification of second-generation fermions is identical to that of the first generation.

The mass pattern of the second generation fermions is completely mysterious and the presence of "generation mixing" by the Cabibbo angle is the only obvious connection between the two generations. It is very likely that the Cabibbo angle (or angles) and the fermion masses are intimately related.

The natural conservation of all flavors by the neutral currents emerges as an attractive hypothesis, and it provides an important constraint for model building.

4. Third Generation Fermions: ν_τ, τ^-, t, b

4.1 Introducing the Third Generation of Fermions

Unlike the first two generations of fermions, the third generation is not yet established. We have very strong evidence for the existence of the τ^--lepton, some evidence for the fifth quark (probably b), indirect evidence for a neutral lepton related to τ and no concrete evidence for a sixth quark.

We do not know of any profound reason for the existence of the third generation of fermions (or for the existence of the second generation, for that matter). The discovery of the τ^--lepton (like the discovery of the μ^--lepton) was both surprising and "unwanted" by any convincing theory.

While the first two generations are clearly similar to each other in many respects, the pattern of the third generation is not yet established. There are several possibilities. Some of them are the following:

(i) The third generation of fermions is analogous to the first two generations. It includes two leptons (ν_τ and τ^-) and two quarks (t and b). The left-handed leptons and quarks belong to SU(2) x U(1) doublets with possible Cabibbo-like mixing with earlier generations [74].

(ii) There is no third generation. The fifth and sixth left-handed quarks are associated, respectively, with the first and second generations. Both have $Q = -\frac{1}{3}$ and they are denoted by b and h. Each generation of quarks forms an SU(3)-triplet. The t-quark does not exist. The additional leptons join ν_e, e, ν_μ, μ in an SU(3) octet. Such a situation occurs in practically all "simple-unification" schemes (see Section 2.9), such as SU(3) x SU(3), E(6), E(7), etc. [31, 32, 37].

(iii) The τ-lepton belongs to a third generation which is similar to the first two, but each generation of left-handed leptons contain three leptons: (ν_e, e^-, E^-); (ν_μ, μ^-, M^-); (ν_τ, τ^-, T^-). The fifth and sixth left-handed quarks belong to the first two generations which contain (each) a triplet of left-handed quarks. This is the case in the SU(3) x U(1) model [57] invoked to account for the trimuon events observed in neutrino processes (see Section 5.2).

There are other possibilities which we will not discuss here. All of them can be tested experimentally, by studying the production and decay properties of the new leptons and new quarks.

As a reference point and a convenient theoretical framework, we will use the possibility (i), namely: a third generation of fermions which is as similar as possible to the first two generations. Whenever possible, we will discuss experimental tests of this hypothesis.

4.2 The τ-Lepton: Experimental Facts and Open Problems

The first indications for the existence of the τ-particle were announced [75] in July 1975. In the two years since that time, many of its properties were elucidated. It is now clear that, barring the possibility of a completely new type of particle, the τ appears to be a lepton. Its known properties are briefly summarized here:

(i) The mass of τ^- is around 1.9 GeV [76]. There is some indication of τ-events at the $\psi''(3.77)$ resonance region, hinting that the mass may be somewhat lower [77]. There is no evidence of τ-events at $\psi'(3.68)$, hence: $m(\tau)$ is probably larger than 1.84 GeV. The τ-mass is suspiciously similar to that of the charmed D-meson (1.87 GeV), but all other properties of τ and D are radically different.

(ii) The energy dependence of the production cross section $e^+e^- \to \tau^+\tau^-$ is consistent with the expression computed for a point-like $J = \frac{1}{2}$ particle [78]. Better data are required in order to fully establish this point. The energy dependence for $\tau^+\tau^-$ production is different from the energy dependence for $D\bar{D}$ production.

(iii) The decays:

$$\tau^- \to e^- + \nu + \bar{\nu} \qquad (4.1)$$

$$\tau^- \to \mu^- + \nu + \bar{\nu} \qquad (4.2)$$

are observed at a branching ratio of 15%-20% (each) [79]. This is consistent with theoretical expectations [80]. We have deliberately avoided any labels for the neutrinos, and we return to this question in Section 4.3.

(iv) The momentum spectra of the electrons and muons produced in τ-decay are consistent with the prediction of a pure V-A theory [78]. However, other possibilities such as various combinations of V-A and V+A are not yet excluded. The momentum spectrum of electrons in τ-decay is completely different (much "harder") than the one observed in D-decay.

(v) The $\rho^-\nu$ and $A_1^-\nu$ decay modes have been observed with the following branching ratios [81,82].

$$B(\tau^- \to \rho^- + \nu) \sim 0.24 \pm 0.09 \qquad (4.3)$$

$$B(\tau^- \to A_1 + \nu) \sim 0.11 \pm 0.07 \qquad (4.4)$$

These values are consistent with theoretical expectations [80]. The decay: $\tau^- \to \pi^- + \nu$ has not been observed [81] and there is some doubt as to whether it occurs at the expected branching ratio of 7-10%. We hope that this point will soon be clarified experimentally.

(vi) Assuming that a new neutral lepton ν_τ is emitted in all τ-decays, the following upper limits for its mass are obtained [82]:

$$m(\nu_\tau) < 300 \text{ MeV} \qquad (\text{from } \tau^- \to A_1^- + \nu_\tau) \qquad (4.5)$$

$$m(\nu_\tau) < 550 \text{ MeV} \qquad (\text{from } \tau^- \to e^- + \bar{\nu}_e + \nu_\tau) \ . \qquad (4.6)$$

(vii) The following upper limits have been obtained for τ-decays in which e-number, μ-number or τ-number are not conserved [83]:

$$B(\tau^- \to e^- + \gamma) < 2.6\% \qquad (4.7)$$

$$B(\tau^- \to \mu^- + \gamma) < 1.3\% \qquad (4.8)$$

$$B(\tau^- \to \ell^- + \ell^- + \ell^+) < 0.6\% \qquad (\ell^\mp \equiv e^\mp \text{ or } \mu^\mp) \ . \qquad (4.9)$$

(viii) All properties of τ are consistent with the hypothesis that it is a sequential lepton, namely - a lepton carrying its own conserved (or, effectively coserved; see Section 3.8) quantum number [78].

We will therefore assume that τ is a lepton which belongs to a new SU(2) x U(1) multiplet, and is not associated with e or μ .

4.3 Does τ^- Have its Own Neutral Lepton?

The simplest pattern for the coupling of the τ-lepton to the charged weak current duplicates the couplings of the electron and muon. We assume that τ^- and a new neutral lepton ν_τ form a left-handed SU(2) x U(1) doublet, forming a charged weak current of the form:

$$\bar{\nu}_\tau \gamma_\alpha (1-\gamma_5) \tau^- \qquad (4.10)$$

There is no evidence against this simple hypothesis. However, it is interesting to study whether the existence of a new neutral

lepton is indeed a necessary consequence of the present experimental information on the τ-particle [84].

We could avoid the new neutral lepton by assigning the left-handed τ^- to an SU(2) x U(1) singlet. In the absence of Cabibbo-like mixing between τ^-, e^- and μ^-, a singlet τ^- would be stable. This is, of course, unacceptable. However, there is no apriori argument against τ-μ or τ-e mixing. When such mixing is present we would have two doublets and one singlet:

$$\begin{pmatrix}\nu_e\\ e'\end{pmatrix}_L \qquad \begin{pmatrix}\nu_\mu\\ \mu'\end{pmatrix}_L \qquad (\tau')_L \tag{4.11}$$

where the "weak eigenleptons" e', μ', τ' are given by:

$$\begin{pmatrix}e'\\ \mu'\\ \tau'\end{pmatrix} = B \begin{pmatrix}e\\ \mu\\ \tau\end{pmatrix} \tag{4.12}$$

and B is a unitary 3 x 3 matrix. The decay of τ^- will then proceed through the τ^--component residing in the same doublet with ν_e or ν_μ. The leptonic decays of τ^- would then involve an "ordinary" neutrino (ν_e or ν_μ) and an "ordinary" antineutrino ($\bar{\nu}_e$ or $\bar{\nu}_\mu$). Horn and Ross [84] have studied this possibility and showed that the following partial widths emerge for purely leptonic τ-decays:

$$\Gamma(\tau^- \to \mu^- e^- e^+) = \Gamma(\tau^- \to e^- \mu^- \mu^+) = K(1-4x+8x^2) \tag{4.13}$$

$$\Gamma(\tau^- \to \mu^- \mu^- \mu^+) = \Gamma(\tau^- \to e^- e^- e^+) = 2K(1-4x+6x^2) \tag{4.14}$$

$$\Gamma(\tau^- \to \mu^- \nu_\mu \bar{\nu}_\mu) = \Gamma(\tau^- \to \mu^- \nu_e \bar{\nu}_e) = \Gamma(\tau^- \to e^- \nu_\mu \bar{\nu}_\mu) = \Gamma(\tau^- \to e^- \nu_e \bar{\nu}_e) = K \tag{4.15}$$

$$\Gamma(\tau^- \to e^- \nu_\mu \bar{\nu}_e) = \Gamma(\tau^- \to \mu^- \nu_e \bar{\nu}_\mu) = 4K \tag{4.16}$$

where K is a factor which depends on the mixing angles of the matrix B and on $x=\sin^2\theta_W$. From Equations (4.13)-(4.16) we obtain the following interesting relation:

$$\frac{\Gamma(\tau^- \to \ell^- \ell^- \ell^+)}{\Gamma(\tau^- \to \mu^- \nu\bar{\nu})} = 1 - 4x + \frac{20}{3}x^2 \sim 0.4 \tag{4.17}$$

where $\Gamma(\tau^- \to \ell^- \ell^- \ell^+)$ represents the sum of all possible combinations for $\ell^\mp \equiv e^\mp$ or $\mu^\mp$, and $\Gamma(\tau^- \to \mu^- \nu\bar{\nu})$ represents a sum over all types of neutrinos. We have used $x \sim 0.25 - 0.3$. The observed branching ratio [79] for $\tau^- \to \mu^- \nu\bar{\nu}$ then leads to the prediction:

$$\Gamma(\tau^- \to \ell^- \ell^- \ell^+) \sim 6\% - 8\% \tag{4.18}$$

in gross disagreement with the much smaller experimental upper limit [83]:

$$\Gamma(\tau^- \to \ell^- \ell^- \ell^+) < 0.6\% \tag{4.19}$$

We therefore conclude that the "concocted" model which attempts to avoid a new neutral lepton, fails [84]. Thus, we have indirect evidence that such a lepton exists, and is probably associated with τ^- in the same left-handed doublet:

$$\begin{pmatrix}\nu_\tau\\ \tau^-\end{pmatrix}_L \tag{4.20}$$

We still have two possibilities concerning the mass of ν_τ:

(i) $m(\nu_\tau) < m(\tau^-)$. In this case ν_τ is emitted in all τ-decays and the experimental limit [82]:

$$m(\nu_\tau) < 300 \text{ MeV} \tag{4.21}$$

is valid.

(ii) $m(\nu_\tau) > m(\tau^-)$. In this case we expect Cabibbo-like mixing among the three left-handed doublets: (ν_e, e^-); (ν_μ, μ^-); (ν_τ, τ^-). The τ^- could decay through such mixing effects without emitting a ν_τ. The mass of ν_τ could easily be of the order of 10 GeV [85]. An amusing consequence of this scheme is the transition $\mu^- \to e^- + \gamma$ which proceeds

through the Cabibbo-like mixing of the leptonic doublets. The branching ratio for $\mu^- \to e^- + \gamma$ is then proportional (see Section 3.8) to $[m(\nu_\tau)]^2$ and is of the order of 10^{-9} for $m(\nu_\tau) \sim 20$ GeV [85]. We have no reason to believe that $m(\nu_\tau) > m(\tau^-)$ and we consider it to be a somewhat ugly (but not yet excluded) possibility.

We summarize: we have indirect evidence for the existence of a neutral lepton associated with τ^-. It is probably lighter than 300 MeV, although it may still be heavier than τ^-.

4.4 Models with Six or More Leptons

Assuming that ν_τ exists, we have at least six leptons. There is a wide variety of models based on six or more leptons which are not inconsistent with the available data. We briefly list here several such models. Our list is far from exhaustive.

(i) Left-handed six-lepton SU(2) x U(1) model. This is the simplest scheme involving three left-handed doublets:

$$\begin{pmatrix}\nu_e\\ e^-\end{pmatrix}_L \quad \begin{pmatrix}\nu_\mu\\ \mu^-\end{pmatrix}_L \quad \begin{pmatrix}\nu_\tau\\ \tau^-\end{pmatrix}_L \tag{4.22}$$

All right-handed leptons are in SU(2) x U(1) singlets. This classification contradicts the atomic physics parity violation experiment (see Sections 2.3, 2.5). Each of the three neutral leptons ν_e, ν_μ and ν_τ may or may not be massless. If one or more neutral leptons has a mass, Cabibbo-like mixing is very likely, leading to decays such as $\mu^- \to e^- + \gamma$, $\tau^- \to \mu^- + \gamma$, $\tau^- \to e^- + \gamma$. The rates for these decays are proportional to the mixing angles and to the neutrino mass differences (see Equation (3.52), Section 3.8).

(ii) Vector-like leptonic SU(2) x U(1) model. The only SU(2) x U(1) classification of the right-handed electron, which is consistent with all data (Sections 2.3, 2.5), is in a doublet. Extending this conclusion to all other leptons we end up with a six-lepton vector-like model, having the three left-handed doublets of Equation (4.22) and three right-handed doublets:

$$\begin{pmatrix}N_e\\ e^-\end{pmatrix}_R \quad \begin{pmatrix}N_\mu\\ \mu^-\end{pmatrix}_R \quad \begin{pmatrix}N_\tau\\ \tau^-\end{pmatrix}_R \tag{4.23}$$

Here, at least some of the neutral leptons must be massive in order to avoid conflict with the V-A features of μ-decay, β-decay and hyperon decays. It is clear that in such a model $m(N_e) \neq m(N_\mu) \neq m(N_\tau)$. Consequently, a 3 x 3 matrix of Cabibbo-like angles leads to elaborate mixing effects, as well as to violations of e-number, μ-number and τ-number conservation. It is also possible that some of the right-handed neutral leptons are related to some of the left-handed ones. For instance, if ν_τ is heavy (see Section 4.3), it is entirely possible that $\nu_\tau \equiv N_e$ or $\nu_\tau \equiv N_\mu$. A six-lepton model with massive neutral leptons of different masses will, in principle, exhibit CP-violation effects analogous to those expected in a six-quark model (see Section 3.9 and 4.10).

(iii) More complicated SU(2) x U(1) models. More complex SU(2) x U(1) models may involve larger number of leptons, or the assignment of some right-handed leptons to doublets and others to singlets. Some other schemes propose SU(2) triplets of the type:

$$\begin{pmatrix}E^+\\ \nu_e\\ e^-\end{pmatrix} \tag{4.24}$$

and yet others involve doubly charged leptons. We see no reason to adopt any of these models and will not discuss them any further.

(iv) $SU(2)_L \times SU(2)_R \times U(1)$. In Section 2.6 we discussed the attractive possibility of an $SU(2)_L \times SU(2)_R \times U(1)$ gauge algebra. The full lepton classification of such a model presumably includes the three left-handed doublets of Equation 4.22 in three $(\frac{1}{2}, 0)$ representations of $SU(2)_L \times SU(2)_R \times U(1)$. The corresponding right-handed leptons are in three $(0, \frac{1}{2})$ representations. Note, however, that in the version in which $M_{W_R^\pm} >> M_{W_L^\pm}$ (see Section 2.6) it is entirely possible that the right-handed neutral companion of the electron (or, respectively, μ or τ) is ν_e (or, respectively, ν_μ or ν_τ). In such a case all ν-particles have non-vanishing masses. The dominance of left-handed couplings in μ-decay and β-decay is then guaranteed by the asymmetry of the $W^\pm$ masses rather than by an asymmetric lepton classification.

There is only one piece of experimental data which might motivate us to consider complicated leptonic models, involving eight or more leptons and large gauge groups: the trimuon events observed in neutrino reactions. We return to this issue in Section 5.2.

4.5 Do We Need the t- and b-Quarks?

There is no fundamental theoretical argument which tells us that the number of different types of quarks must be larger than four. However, there are several phenomenological and theoretical considerations which may already necessitate additional quarks. Some of these considerations are:

(i) The observations of the new $\mu^+\mu^-$ resonance $\Upsilon(9.5)$ [86] and its possible excited state $\Upsilon'(10.1)$ [87], are most easily interpreted as bound states of a new type of quark. We discuss the implications of the Υ-particles in Section 4.6. At this point we only state that their existence is, at present, the strongest indication for the presence of a fifth quark.

(ii) The first two generations of fermions exhibit a certain degree of quark-lepton symmetry or, at least, analogy. The existence of the τ-lepton and its probable neutral partner ν_τ, implies that a new doublet of quarks will be needed in order to preserve the same symmetry [74].

(iii) In a pure left-handed SU(2) x U(1) model, the requirement of an equal number of left-handed quark doublets and lepton doublets is not just a question of aesthetics or a pleasant analogy. The divergent parts of the triangle anomaly diagrams [30] are removed [29] only if the (ν_τ, τ^-) doublet is supplemented by a (t,b) left-handed doublet.

(iv) We have seen in Section (3.9) that in a pure left-handed SU(2) x U(1) model, CP violation is naturally introduced at the level of six quarks, while at the four-quark level it can be only induced through the couplings of a sufficiently complicated set of Higgs particles. While there are several different ways of incorporating CP-violation into a gauge theory of the weak interactions, the simplest and most direct appears to be the introduction of six (or more) quarks [69]. We discuss CP-violation in the six-quark model in Section 4.10.

(v) In Section 2.6 we have discussed a left-right symmetric $SU(2)_L \times SU(2)_R \times U(1)$ model. We mentioned two variations of the model: one [19,20] in which $M_{W_L^\pm} << M_{W_R^\pm}$ and one [21] in which $M_{W_L^\pm} = M_{W_R^\pm}$ but the right-handed doublets always connect light fermions to heavy fermions. In this second version, the right-handed

partners of the u and d quarks must be new quarks, presumably b and t, respectively. Note that this requirement is not related to the "y-anomaly". No y-anomaly is expected in such a model, because of the orthogonality of $W_L^{\pm}$ and $W_R^{\pm}$. However, the fifth and sixth quarks are necessary in the second variation of the $SU(2)_L \times SU(2)_R \times U(1)$ model.

Except for the existence and interpretation of the T particles, none of the above arguments is entirely convincing. However, their accumulated weight should certainly lead us to study seriously the various features of the proposed t and b quarks.

4.6 New Mesons with b or t Quarks: The T-Family, B-Mesons and T-Mesons

One of the simplest methods of discovering a new type of quark q is, of course, the observation of its bound $q\bar{q}$ system. The successful description of the ψ-family in terms of the simple "charmonium" model [88] encourages us to speculate on the features of similar systems involving heavier quarks such as b or t. The "standard" work on this subject is the analysis of Eichten and Gottfried [89], which predicts the level structure of Figure 12 for a $q\bar{q}$ system, as a function of the mass of the heavy quark. Eichten and Gottfried used the same potential which proved successful in the case of charmonium and showed that with such a potential the energy differences between the levels shrink as the mass of the quark increases. Furthermore, the number of levels below the threshold for the production of pairs of new mesons, increases as a function of the quark mass.

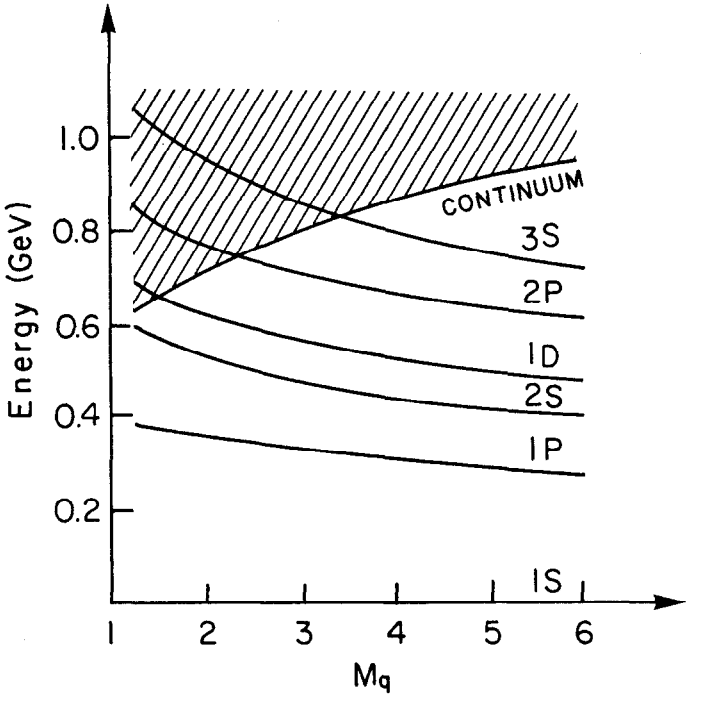

Figure 12: Relative positions of the levels of "quarkonium" as a function of the quark mass [89].

The observation of the T particle in the reaction [86]

$$\begin{array}{l} p + \text{nucleus} \rightarrow T + \text{anything} \\ \qquad\quad \big\lfloor \rightarrow \mu^+ + \mu^- \end{array} \tag{4.25}$$

immediately led to its interpretation as a bound state of a new heavy quark and antiquark with a quark mass around 4-5 GeV. For such a mass value, the Eichten-Gottfried analysis leads to the following predictions [89]:

(i) $m(T') - m(T) \sim 420$ MeV . (4.26)

(ii) From the mass difference quoted in (i), it follows that the decay

$$T' \rightarrow T + \pi + \pi \tag{4.27}$$

is not a dominant decay mode of T' . Consequently, the branching ratios:

$$B' = \frac{\Gamma(T' \rightarrow \mu^+\mu^-)}{\Gamma(T' \rightarrow \text{all})} \quad \text{and} \quad B = \frac{\Gamma(T \rightarrow \mu^+\mu^-)}{\Gamma(T \rightarrow \text{all})} \tag{4.28}$$

are not very different. Assuming that T and T' are $b\bar{b}$ or $t\bar{t}$ bound states, we obtain a rough estimate [90]:

$$\frac{B'}{B} \sim 0.6 \quad (\text{for a b-quark; } Q = -\tfrac{1}{3}) \tag{4.29}$$

$$\frac{B'}{B} \sim 0.4 \quad (\text{for a t-quark; } Q = \tfrac{2}{3}) \tag{4.30}$$

(iii) A third level, T'' is predicted below the "continuum", with

$$m(T'') - m(T') \sim 330 \text{ MeV} \tag{4.31}$$

and

$$B'' = \frac{\Gamma(T'' \rightarrow \mu^+\mu^-)}{\Gamma(T'' \rightarrow \text{all})} \sim 0.7\, B' \quad (\text{for b or t}) . \tag{4.32}$$

(iv) In a hadronic production process, such as $p+p \rightarrow T+\text{anything}$, the expected production rates of T, T' and T'' are comparable to each other. The mass differences are of the order of 5%, and the full mass dependence of the production cross-section is expected to yield effects of the order of, at most, factor of two or three [90]. Since both the production cross-section and the $\mu^+\mu^-$ branching ratios for T, T' and T'' are predicted to be more or less of the same order of magnitude, we expect to see all three resonances as $\mu^+\mu^-$ bumps in pp scattering. We denote:

$$N(T) = \sigma(p+p \rightarrow T+\text{anything}) \cdot \frac{\Gamma(T \rightarrow \mu^+\mu^-)}{\Gamma(T \rightarrow \text{all})} \tag{4.33}$$

A typical estimate then yields [90]:

$$N(T) \cdot N(T') \cdot N(T'') \sim 1:0.3:0.15 \quad (\text{for b-quark; } Q = -\tfrac{1}{3}) \tag{4.34}$$

$$N(T) \cdot N(T') : N(T'') \sim 1:0.12:0.05 \quad (\text{for t-quark; } Q = \tfrac{2}{3}) \tag{4.35}$$

Note that all estimates for the branching ratios B and the resonance signals N depend on the smallness of the decay $T' \rightarrow T+\pi+\pi$. This, in turn, is very sensitive to the T'-T mass difference which is predicted to be 420 MeV.

Experimentally, a double peak structure is observed [87] in the 10 GeV region (Figure 13). However, the mass difference between the two peaks appears to be closer to 600 MeV, and definitely larger than the predicted 420 MeV. This immediately implies that the branching ratio

$$B' = \frac{\Gamma(T' \rightarrow \mu^+\mu^-)}{\Gamma(T' \rightarrow \text{all})} \tag{4.36}$$

is significantly smaller than the predicted value (Equations (4.29), (4.30)). Consequently, the resonance signal N(T') should be substantially smaller than predicted by Equations (4.34), (4.35).

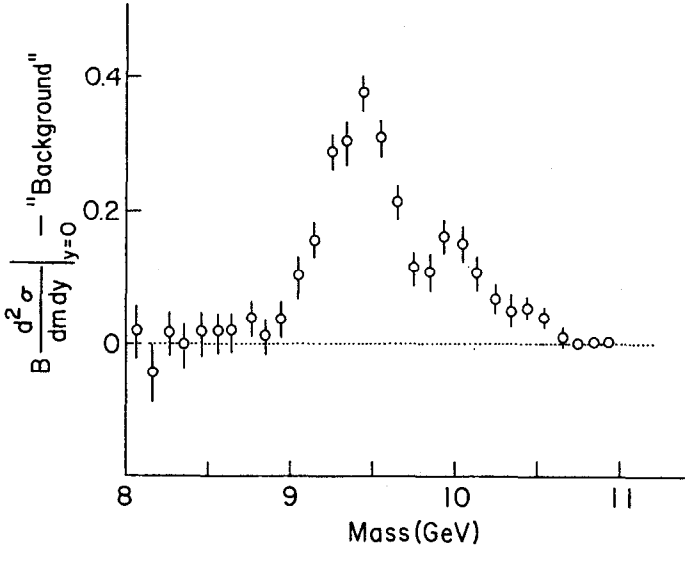

Figure 13: The measured cross section $\left.\frac{d^2\sigma}{dm\,dy}\right|_{y=0}$ for $p+p \to \Upsilon+\text{anything}$ times the branching ratio $B = \frac{\Gamma(\Upsilon \to \mu^+\mu^-)}{\Gamma(\Upsilon \to \text{all})}$, after background subtraction. The two peaks presumably correspond to Υ and Υ' [87].

Experimentally [87]:

$$\frac{N(\Upsilon')}{N(\Upsilon)} \sim \frac{1}{3} \tag{4.37}$$

consistent with Equation (4.33), but totally inconsistent with our entire line of reasoning (because Equation (4.33) was based on a 420 MeV Υ'-Υ mass difference while the data give a 600 MeV difference!)

This puzzling situation may or may not be settled in the near future. However, we still feel fairly confident that the Υ and Υ' represent bound states of (at least one) new heavy quark.

Assuming that we have here only one new quark, is it the bottom quark (b) or the top quark (t)?

(i) Various estimates of the absolute production cross-section favor the b-hypothesis [90],[91]. However, we cannot regard these estimates as conclusive since there are still some important open questions concerning the mechanism of ψ production in hadronic reactions.

(ii) The relative size of the Υ and Υ' signals also tends to favor the b-hypothesis. We have seen in Equations (4.34) and (4.35) that $N(\Upsilon'):N(\Upsilon)$ is expected to be larger for b than for t. If anything, it is too large.

(iii) It is likely that a reliable picture of the Υ-family will emerge only from the observation of these particles in e^+e^- collisions. The production cross-sections for:

$$e^+ + e^- \to \Upsilon,\ \Upsilon',\ \Upsilon'',\ \text{etc.}$$

as well as the widths for radiative decays between $C = -1$ and $C = +1$ states depend on Q^2, the squared charge of the new quark. This should enable us to determine whether we are facing a b-quark or a t-quark.

Note that the properties of "toponium" or "bottomonium" are independent of the weak interaction properties of the new quarks. On the other hand, most of the properties of low-lying mesons containing one new quark are sensitive to the gauge theory assignment of the left- and right-handed b-quark (or t-quark). The most notable exception to this statement are the charges of the new mesons. For instance, the lowest-lying mesons including b-quarks presumably correspond to the isospin doublet:

$$B^0 \equiv (b\bar{d}) \; ; \quad B^- \equiv (b\bar{u})$$

while the lowest-lying mesons with a t-quark are:

$$T^+ \equiv (t\bar{d}) \; ; \quad T^0 \equiv (t\bar{u})$$

The observation of new charged mesons and their decay modes to charmed or strange mesons could determine whether we have a b or a t quark. The B^- and T^+ would decay into charm=+1 or strangeness=-1 systems while $T^-(=\bar{T}^+)$ and $B^+(=\bar{B}^-)$ would decay into charm=-1 or strangeness=+1 systems.

4.7 The Left-handed Six Quark Model

We now proceed to introduce the left-handed SU(2) x U(1) six-quark model [69,92], including the left-handed doublets

$$\begin{pmatrix} u \\ d \end{pmatrix}_L \quad \begin{pmatrix} c \\ s \end{pmatrix}_L \quad \begin{pmatrix} t \\ b \end{pmatrix}_L \tag{4.38}$$

with possible Cabibbo-like mixing, and the right-handed singlets:

$$(u)_R \quad (d)_R \quad (c)_R \quad (s)_R \quad (t)_R \quad (b)_R \tag{4.39}$$

While our discussion centers on the SU(2) x U(1) model, we note that an $SU(2)_L$ x $SU(2)_R$ x U(1) model based on the same six quarks (Section 2.6) would lead to the same predictions for all charged current and flavor-changing neutral current processes. In such a model the left- and right-handed quarks are in the (1/2, 0) and (0, 1/2) doublets, respectively.

The charged quark current of the SU(2) x U(1) model has the form:

$$J^- = (\bar{u}\ \bar{c}\ \bar{t})\ \gamma_\mu\ (1-\gamma_5) A \begin{pmatrix} d \\ s \\ b \end{pmatrix} \tag{4.40}$$

where A is a unitary 3 x 3 matrix. The most general form of the matrix A can be represented by [69]:

$$A = \begin{pmatrix} c_1 & s_1c_3 & s_1s_3 \\ -s_1c_2 & c_1c_2c_3 - s_2s_3e^{i\delta} & c_1c_2s_3 + s_2c_3e^{i\delta} \\ s_1s_2 & -c_1s_2c_3 - c_2s_3e^{i\delta} & -c_1s_2s_3 + c_2c_3e^{i\delta} \end{pmatrix} \tag{4.41}$$

where:

$$c_j \equiv \cos\theta_j; \quad s_j \equiv \sin\theta_j; \quad j = 1,2,3 \; .$$

The three angles $\theta_1, \theta_2, \theta_3$ are Cabibbo-like angles, representing mixing of the three left-handed doublets. The phase angle δ introduces CP-violation (see Sections 3.9, 4.10).

What can we say about the values of the parameters $\theta_1, \theta_2, \theta_3, \delta$? The angle θ_1 is the original Cabibbo angle. The value of $\cos\theta_1$ is directly measured in nucleon β-decay and is found to be

$$\cos\theta_1 = 0.974 \pm 0.002 \tag{4.42}$$

$$\theta_1 = (13.2 \pm 0.5)^0 \tag{4.43}$$

The combination $\sin\theta_1\cos\theta_3$ appears in all strangeness changing semi-leptonic decays. It corresponds to the $\sin\theta$ factor in ordinary Cabibbo theory. We find:

$$\sin\theta_1\cos\theta_3 = 0.229 \pm 0.003 \tag{4.44}$$

yielding:

$$\cos\theta_3 \geq 0.96 \qquad (4.45)$$

or:

$$\theta_3 \leq 16^o \qquad (4.46)$$

We do not have a direct determination of θ_2 . However, we can set a bound on θ_2 using a theoretical estimate of the K_S^o - K_L^o mass difference [90]. We have already mentioned (in Section 3.2) that a successful estimate of the mass of the charmed quark can be obtained by considering the contribution of Figure 7a to the K_S^o - K_L^o mass difference. In a model involving a t-quark in addition to the c-quark, such an estimate should presumably remain valid. It now relates the K_S^o-K_L^o mass difference to a certain function of m_c, m_t and θ_2. The usual expression (Equation 3.23):

$$\Delta M \approx K m_c^2 \cos^2\theta \sin^2\theta$$

is replaced by [90]:

$$\Delta M \approx K\, s_1^2 c_1^2 c_3^2 \left[c_2^4 m_c^2 + s_2^4 m_t^2 + \frac{2 s_2^2 c_2^2 m_t^2 m_c^2}{m_t^2 - m_c^2} \ln\left(\frac{m_t^2}{m_c^2}\right) \right] \qquad (4.47)$$

where K is, again, a factor depending on parameters such as G and M_W but not on the quark masses or Cabibbo angles.

It is clear that for very large values of m_t, equation (4.47) will hold only if $s_2^2 \ll 1$. Crudely speaking, we must have:

$$\tan^2\theta_2 < \frac{m_c}{m_t} \qquad (4.48)$$

If m_t is somewhere in the 5-20 GeV range, we obtain:

$$\theta_2 < 30^o \qquad (4.49)$$

For larger values of m_t we clearly obtain lower values of θ_2 .

We cannot establish an upper bound on the phase angle δ . We will see in Section 4.10 that we can only state that $\sin\delta \neq 0$ and is larger than 5×10^{-3}.

We conclude that all θ-angles in the Cabibbo matrix A are small:

$$\theta_1 \sim 13^o \; ; \quad \theta_2 < 30^o \; ; \quad \theta_3 < 16^o \qquad (4.50)$$

The three doublets:

$$\begin{pmatrix} u \\ d \end{pmatrix}_L \qquad \begin{pmatrix} c \\ s \end{pmatrix}_L \qquad \begin{pmatrix} t \\ b \end{pmatrix}_L \qquad (4.51)$$

are mixed by relatively little amounts, and the <u>main</u> weak transitions will normally connect u to d, c to s, t to b . Transitions proportional to $\sin\theta_i$ (i = 1,2,3) become important only when the main transitions are kinematically forbidden, as is the case in strange particle decays and, possibly in bottom-quark decays (see Section 4.8).

4.8 Weak Production and Weak Decays of b-Quarks in the Left-handed Six Quark Model

Having determined the bounds on the mixing angles θ_1, θ_2 and θ_3, we can now proceed to discuss the production of b-quarks in neutrino reactions and the weak decays of mesons containing b-quarks.

The simplest and most likely mechanism for b-production is the reaction:

$$\bar{\nu} + u \rightarrow \mu^+ + b \; . \qquad (4.52)$$

The production rate is proportional to $\sin^2\theta_1 \cdot \sin^2\theta_3$. Using the known value of θ_1 and the bound on θ_3 (Equation (4.50)) we get:

$$\frac{\sigma(\bar{\nu}+N \rightarrow \mu^+ + b + \text{anything})}{\sigma(\bar{\nu}+N \rightarrow \mu^+ + \text{anything})} < 0.5\% \qquad (4.53)$$

Another mechanism for b-production in $\bar{\nu}N$ scattering involves the c-quarks of the "$q\bar{q}$-ocean" in the target nucleon. The cross-section for:

$$\bar{\nu} + c \rightarrow \mu^+ + b \qquad (4.54)$$

includes the coupling strength of the $c \leftrightarrow b$ transition, which is likely to be significantly larger than the corresponding $u \leftrightarrow b$ transition. However, the production cross section is strongly suppressed by the small parameter which represents the probability of finding a $c\bar{c}$ pair in the nucleon. If the bound $\theta_3 < 16^o$ is more or less saturated, the process (4.52) is expected to dominate. However, if $\theta_3 << 16^o$, *production off a c-quark may become the largest source* of b-quarks. In that case, the production rate will probably be significantly smaller than the 0.5% of Equation (4.53).

The production of b-quarks in neutrino (rather than antineutrino) reactions proceeds only via the "$q\bar{q}$-ocean", and the expected rate is substantially smaller than in $\bar{\nu}N$ reaction.

Assuming that $m_b < m_t$, the dominant weak decay modes of the b-quark are:

$$\begin{aligned} b &\rightarrow c + e^- + \bar{\nu}_e \\ b &\rightarrow c + \mu^- + \bar{\nu} \\ b &\rightarrow c + d + \bar{u} \end{aligned} \qquad (4.55)$$

All important decay modes will include charmed particles [92]. Assuming that the semileptonic branching ratio

$$\frac{\Gamma(b \rightarrow c + \mu^- + \bar{\nu}_\mu)}{(b \rightarrow \text{all})} \qquad (4.56)$$

is of the order of 10%, we conclude that for every event of the type:

$$\bar{\nu} + u \rightarrow \mu^+ + b \qquad (4.57)$$

we will have:

(i) 0.1 events with a $\mu^+\mu^-$ pair

(ii) 0.1 Events with a $\mu^+\mu^+$ pair

(iii) 0.01 events with a $\mu^+\mu^-\mu^+$ triplet

If $\theta_3 \sim \theta_1$, the overall rate of "unusual" multimuon events due to b-production would be:

$$\frac{\sigma(\bar{\nu}+N \rightarrow \mu^+ + \mu^+ + \text{anything})}{\sigma(\bar{\nu}+N \rightarrow \mu^+ + \text{anything})} \sim 5 \times 10^{-4} \qquad (4.58)$$

$$\frac{\sigma(\bar{\nu}+N \rightarrow \mu^+ + \mu^- + \mu^+ + \text{anything})}{\sigma(\bar{\nu}+N \rightarrow \mu^+ + \text{anything})} \sim 5 \times 10^{-5} \qquad (4.59)$$

If $\theta_3 < \theta_1$, the corresponding rates are, of course, lower. At the same time, trimuon events and equal-sign dimuons may come from other sources such as production of $c\bar{c}$ pairs.

If $m_b > m_t$, the dominant weak decay modes of the b quark are:

$$\begin{aligned} b &\rightarrow t + e^- + \bar{\nu}_e \\ b &\rightarrow t + \mu^- + \bar{\nu}_e \\ b &\rightarrow t + d + \bar{u} \end{aligned} \qquad (4.60)$$

In that case, t-decays resemble c-decays (see Section 4.9), and the decays $b \rightarrow t$ will have similar characteristics to the decays $b \rightarrow c$ mentioned above. Consequently, the general features of the experimental signature of b-decays are independent of whether $m_b > m_t$ or $m_b < m_t$.

The lowest lying mesons containing b-quarks are expected to be:

$$B^o \equiv (b\bar{d}) \quad ; \quad B^- \equiv (b\bar{u})$$

Their leading decay modes are, presumably:

$$B^o \rightarrow D^+ + e^- + \bar{\nu}_e \; ; \quad D^+ + \mu^- + \bar{\nu}_e \; ; \quad D + \text{pions} \qquad (4.61)$$

$$B^- \rightarrow D^o + e^- + \bar{\nu}_e \; ; \quad D^o + \mu^- + \bar{\nu}_e \; ; \quad D + \text{pions} \; . \qquad (4.62)$$

If the angles θ_2, θ_3 are sufficiently small, the lifetime of the B^o

meson may be relatively long. In that case, B^0-$\bar{B}^0$ mixing effects may be substantially larger than D^0-$\bar{D}^0$ mixing and CP-violating effects may be stronger than they are in the K^0-$\bar{K}^0$ system [90,93].

If we identify the T as a $b\bar{b}$ state, the mass of the B^0 and B^- mesons is expected to be approximately 5 GeV. The presently available neutrino beams should enable us to produce such mesons, and with improved studies of multimuon events in $\bar{\nu}N$ scattering, we may find further evidence for the existence of the b-quark.

Needless to say, in the left-handed SU(2) x U(1) model no "y-anomaly" is expected in $\bar{\nu}N$ scattering. In the $SU(2)_L$ x $SU(2)_R$ x U(1) model with a $(u,b)_R$ doublet in the (0, 1/2) representation (see Section 2.6) we do not expect right-handed b-production in anti-neutrino experiments, because of the orthogonality of $W_L^{\pm}$ (which couples to the ν_μ or $\bar{\nu}_\mu$ beam) and $W_R^{\pm}$ (which couples to the right-handed b). In such a model, the experimental situation of b-production in neutrino processes is identical to that of the left-handed SU(2) x U(1) model discussed in this section. However, any degree of mixing between $W_L^{\pm}$ and $W_R^{\pm}$ would change this conclusion and would allow for the production of right-handed b-quarks.

4.9 Weak Production and Weak Decays of t-quarks in the Left-Handed Six-Quark Model

We first consider the case $m_t < m_b$. In this case direct production of t-quarks in neutrino reactions will mostly proceed by converting a "valence" d-quark into a t-quark:

$$\nu_\mu + d \to \mu^- + t \qquad (4.63)$$

A second possible mechanism would utilize the strange quark of the "$q\bar{q}$-ocean":

$$\nu_\mu + s \to \mu^- + t \qquad (4.64)$$

$$\bar{\nu}_\mu + \bar{s} \to \mu^+ + \bar{t} \qquad (4.65)$$

The production of a d-quark is favored by the large "valence" to "ocean" probability ratio. The production of an s-quark enjoys a larger "Cabibbo-factor". Both of these mechanisms are, of course, completely analogous to the mechanisms for charm production. For the dominant mechanism we expect that, well above threshold for t-production:

$$\frac{\sigma(\nu_\mu+d \to \mu^-+t)}{\sigma(\nu_\mu+d \to \mu^-+c)} \sim \tan^2\theta_2 \qquad (4.66)$$

Using the crude estimate of Equation (4.48) we then find:

$$\frac{\sigma(\nu_\mu+d \to \mu^-+t)}{\sigma(\nu_\mu+d \to \mu^-+c)} < \frac{m_c}{m_t} \qquad (4.67)$$

For $m_t \sim 5$ GeV and $E_\nu \sim 200$ GeV we would expect at most 1% of all νN events to contain a t-quark.

The decay modes of the t-quark are very similar to those of the c-quark (as long as $m_t < m_b$). The dominant decays involve strange particles:

$$\begin{aligned} t &\to s+e^++\nu_e \\ t &\to s+\mu^++\nu_\mu \\ t &\to s+u+\bar{d} \end{aligned} \qquad (4.68)$$

The lowest lying mesons containing t-quarks are

$$T^+ \equiv (t\bar{d}) \qquad T^0 \equiv (t\bar{u})$$

and their most likely decay modes

$$T \to \bar{K}+e^++\nu_e+\text{pions} \qquad (4.69)$$

$$T \to \bar{K} + \mu^+ + \nu_e + \text{pions} \qquad (4.70)$$

$$T \to \bar{K} + \text{pions} \qquad (4.71)$$

An interesting indirect source of t-quarks (for $m_t < m_b$) is the production of b followed by the $b \to t$ decay. A typical process would be:

$$\bar{\nu}_\mu + u \to \mu^+ + b \quad \hookrightarrow t + \begin{cases} e^- + \bar{\nu}_e \\ \mu^- + \nu_\mu \\ d + \bar{u} \end{cases} \qquad (4.72)$$

If $m_t < m_b$, practically all b-decays will include a t-quark (unless the b-t mass difference is small).

The experimental signature of t-quarks produced in neutrino experiments is very similar to the signature of the charmed quarks. For instance, t-production in νN scattering would lead to $\mu^-\mu^+$ and μ^-e^+ events similar to those generated by c-production. The only different feature which might be observable would be the average transverse momentum of the μ^+ or e^+ relative to the direction of the allegedly exchanged W-Boson. The transverse momentum of the μ^+ in t-decay is likely to be larger than that of the c-generated μ^+. Consequently, a high statistics experiment might detect a two-slope structure in the p_T distribution of the μ^+'s. The second slope will gradually appear only at high energies, above the t-threshold.

All the above remarks relate to the case $m_t < m_b$. However, assuming that the T particle is a $b\bar{b}$ state (see Section 4.6), it is more likely that $m_b < m_t$. In that case, the A matrix of Equation (4.41) together with equation (4.50) predicts that all dominant t-decays will include a b-quark:

$$t \to b + e^+ + \nu_e$$

$$t \to b + \mu^+ + \nu_\mu \qquad (4.73)$$

$$t \to b + u + \bar{d}$$

Since most b-decays involve a charmed quark, t-decays will often exhibit a remarkable cascade, such as:

$$t \to b + \mu^+ + \nu_\mu \quad \hookrightarrow c + \mu^- + \bar{\nu}_\mu \quad \hookrightarrow s + \mu^+ + \nu_\mu \qquad (4.74)$$

Assuming that:

$$\frac{\Gamma(t \to b + \mu^+ + \nu_\mu)}{(t \to \text{all})} \sim \frac{\Gamma(b \to c + \mu^- + \bar{\nu}_\mu)}{(b \to \text{all})} \sim \frac{\Gamma(c \to s + \mu^+ + \bar{\nu}_\mu)}{(c \to \text{all})} \sim 10\% \qquad (4.75)$$

and that, well above the threshold for t-production (see Equations (4.66), (4.67)):

$$\frac{\sigma(\nu + N \to \mu^- + t + \text{anything})}{\sigma(\nu + N \to \mu^- + \text{anything})} \sim 0.5\% \qquad (4.76)$$

we expect the following rates of multimuon events due to t-production:

$$\begin{aligned} R(\mu^-\mu^+) &\sim 10^{-3} \\ R(\mu^-\mu^-) &\sim 5 \times 10^{-4} \\ R(\mu^-\mu^-\mu^+) &\sim 10^{-4} \\ R(\mu^-\mu^+\mu^+) &\sim 5 \times 10^{-5} \\ R(\mu^-\mu^+\mu^-\mu^+) &\sim 5 \times 10^{-6} \end{aligned} \qquad (4.77)$$

Here $R(\mu^- x)$ is defined as:

$$R(\mu^- x) = \frac{\sigma(\nu + N \to \mu^- + t + \text{anything})}{\sigma(\nu + N \to \mu^- + \text{anything})} \cdot \frac{\Gamma(t \to x + \text{anything})}{\Gamma(t \to \text{all})} \qquad (4.78)$$

The rates for all of these multimuon signals are quite small. However, some of the signatures are unique (especially those of $\mu^-\mu^+\mu^+$ and $\mu^-\mu^+\mu^-\mu^+$).

4.10 CP-Violation in the Left-Handed Six-Quark Model

The incorporation of CP-violation into the gauge theory was actually the first motivation for the introduction of the six-quark model [69]. CP-violation is naturally built into the left-handed six-quark model (see Sections 3.9, 4.7). The phase parameter δ is responsible for all CP-violating effects in the quark matrix elements. Thus, the CP-violating amplitudes are proportional to $\sin\delta$.

If we restrict our attention to CP-violating phenomena involving the three "light" quarks u, d and s, we immediately see that all such CP-violating amplitudes are proportional to $\sin\theta_3$. This follows from the structure of the matrix A (Equation (4.41)). The relevant matrix elements of A are A_{22} and A_{32}, in which $e^{i\delta}$ is always multiplied by $\sin\theta_3$. We can further show that all CP-violating amplitudes involving only external u, d, s quarks must vanish in the limit $m_c = m_t$. The proof is simple: if $m_c = m_t$ and if the c and t quarks do not appear in the initial or final state of the considered transition, we may always choose one linear combination of c and t which decouples from both the d and s quarks. Consequently, no interference between amplitudes of different phase is possible. We therefore conclude that all CP violating transitions involving only u, d, s quarks must be proportional to $m_c^2 - m_t^2$.

The overall conclusion of this discussion is that all CP-violating amplitudes among states containing only u, d, s quarks must be proportional to:

$$(m_c^2 - m_t^2)\,\sin\theta_3\,\sin\delta \qquad (4.79)$$

This holds for all CP-violating K-decays as well as for the electric dipole moment of the neutron.

Why is CP-violation a small effect? The present theory does not answer this question. The parameters θ_3 and δ may be extremely small, but they do not have to be small. All we know is: $0 \leq \sin\delta \leq 1$, $0 \leq \sin\theta_3 \leq 0.28$. This is, of course, consistent with, but does not explain, the magnitude of CP-violation.

We now proceed to calculate the parameters of the CP-violating amplitudes in $K^o \to 2\pi$. This was first done by Pakvasa and Sugawara [94] and, independently, by Maiani [95]. The standard formalism starts from the mass matrix of the neutral K-system with matrix elements $M_{k\ell} - \frac{1}{2} i\Gamma_{k\ell}$.

$$M_{k\ell} = M_o + (k|H_w|\ell) + P\sum_x \frac{(k|H_w|x)(x|H_w|\ell)}{M_o - E_x} \qquad (4.80)$$

$$\Gamma_{k\ell} = 2\pi \sum_x (k|H_w|x)(x|H_w|\ell)\;\delta(E_x - M_o) \qquad (4.81)$$

If CP is violated, the M-matrix is not symmetric and its eigenvalues are proportional to

$$(1-\varepsilon)K_o + (1+\varepsilon)\bar{K}_o\;; \quad (1+\varepsilon)K_o - (1-\varepsilon)\bar{K}_o \qquad (4.82)$$

The ε-parameter which characterizes the magnitude of CP-violation in the K_o eigenstates is given by:

$$|\varepsilon| = \frac{\mathrm{Im}\, M_{12}}{\sqrt{\Delta M^2 + \frac{1}{4}\Gamma_S^2}} \qquad (4.83)$$

where $\Delta M = m(K_S) - m(K_L)$ and Γ_S is the width of K_S^o. The violation of CP in $K_L \to 2\pi$ may be due either to the mixture of opposite CP-

values in the K_L - state (characterized by ε) or to CP-violation in the decay amplitude itself. The latter is characterized by the parameter ε' , where:

$$\varepsilon' = \frac{i}{\sqrt{2}} \, e^{i(\delta_2 - \delta_o)} \, \frac{\text{Im } A_2}{A_o} \tag{4.84}$$

δ_2, δ_o are the I = 2 and I = 0 $\pi\pi$ S-wave phase shifts at $\sqrt{s} = M_K$. The amplitudes A_2, A_o are defined by:

$$\langle K^o | (\pi\pi)_{I=0} \rangle = A_o e^{i\delta_o} \tag{4.85}$$

$$\langle K^o | (\pi\pi)_{I=2} \rangle = A_2 e^{i\delta_2} \tag{4.86}$$

The calculation of ε requires a calculation of $\frac{\text{Im } M_{12}}{\Delta M}$. The numerator is given by the diagram in Figure 14, where $x = c,t$. The denominator is given by the same diagram, but is dominated by the $x = u$ term. In the approximation $\cos\theta_1$, $\cos\theta_3 \sim 1$, and defining:

$$\eta = \frac{m_c^2}{m_t^2} \tag{4.87}$$

we obtain [96]:

$$\left| \frac{\text{Im } M_{12}}{M} \right| \sim s_2 c_2 s_3 \sin\delta \left\{ \frac{s_2^2 \left(1 + \frac{\eta \ell n \eta}{1-\eta}\right) + c_2^2 \left(\eta - \frac{\eta \ell n \eta}{1-\eta}\right)}{c_2^4 \eta + s_2^4 - 2 s_2^2 c_2^2 \frac{\eta \ell n \eta}{1-\eta}} \right\} \tag{4.88}$$

for any m_t between 5 GeV and 20 GeV and for any θ_2 obeying the bound of Equation (4.48), we find that the numerical value of the expression in the curly brackets is between 3 and 7. Hence:

$$\left| \frac{\text{Im } M_{12}}{M} \right| \sim 5 s_2 c_2 s_3 \sin\delta \ .$$

Using this expression and the approximate relation $2\Delta M \sim \Gamma_S$, we find

$$|\varepsilon| \sim 3 s_2 c_2 s_3 \sin\delta \tag{4.89}$$

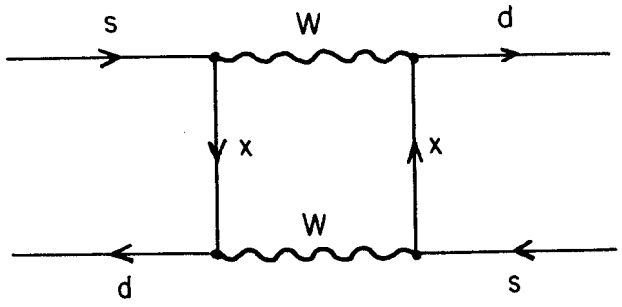

Figure 14: Dominant diagram for calculating $\frac{\text{Im } M_{12}}{\Delta M}$. Contributions for $x = u, c, t$ should be included.

The small observed magnitude of ε is unexplained (but not inconsistent with the theory). In fact, using:

$$|\varepsilon| \sim 2 \times 10^{-3} \tag{4.90}$$

$$s_3 < 0.28 \; ; \quad s_2 < 0.5 \tag{4.91}$$

we obtain from Equation (4.89):

$$\sin\delta > 5 \times 10^{-3} \tag{4.92}$$

At least one of the parameters θ_2, θ_3, δ must be small in order to account for the smallness of ε .

The ε' parameter is experimentally consistent with zero, and is definitely much smaller than ε . This is actually predicted in the left-handed six-quark model [94, 96]. There are two classes of diagrams which contribute to ε' (Figure 15). The diagram of Figure 15 a involves the conversion of a $c\bar{c}$ or $t\bar{t}$ system into $d\bar{d}$. This is strongly suppressed by the Zweig-Iizuka rule. The suppression factor cannot be determined accurately but is probably of the order of 1-10%. The second diagram (Figure 15 b) involves a term of order M_q^2/M_W^2 . For $m_t \lesssim$ 5-20 GeV , this gives us another factor of 1%-10%. The estimates of ε' are given by [94, 96]:

Figure 15a: $$|\varepsilon'| \sim \varepsilon \left|\frac{A_2}{A_0}\right| \cdot 0\left(\frac{m_q^2}{m_W^2}\right) \tag{4.93}$$

Figure 15b: $$|\varepsilon'| \sim \left|\frac{A_2}{A_0}\right| \sin\delta \; s_2 c_2 s_3 \; (\zeta_c - \zeta_t) \tag{4.94}$$

where ζ_c, ζ_t are the $c\bar{c}$ and $t\bar{t}$ Zweig-Iizuka suppression factors, respectively. We therefore conclude that:

$$\left|\frac{\varepsilon'}{\varepsilon}\right| \sim \left|\frac{A_2}{A_0}\right| \quad (1\%\text{-}10\%) \tag{4.95}$$

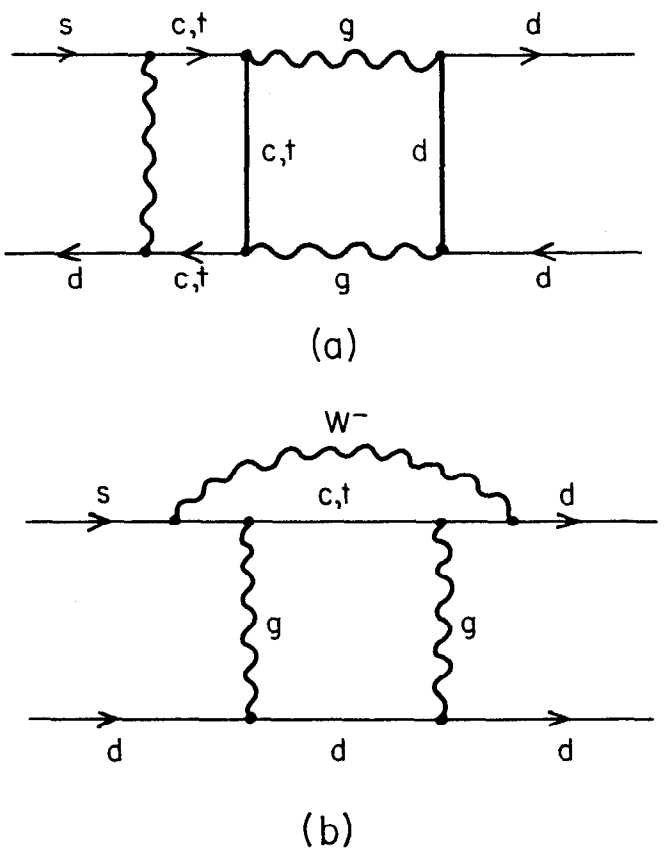

Figure 15: Diagrams contributing to ε' . (a) A mechanism suppressed by the Zweig-Iizuka rule. (b) A mechanism suppressed by m_q^2/m_W^2 .

This prediction is consistent with the experimental situation and represents a nontrivial success of the model.

Predictions of the model for other CP-violating K-decays have been extensively discussed by Ellis et al. [96]. In all interesting cases the predictions of the model are experimentally indistinguishable from the predictions of the superweak theory.

The electric dipole moment of the neutron is due, in the six quark model, to the diagram of Figure 16. It is easy to see that here, again, the CP-violating effect would disappear if either θ_3 or δ would vanish; it would also vanish if $m_c = m_t$ or $m_s = m_b$ (since here the s-quark does not appear in the initial or final state). Maiani [95] and Ellis et al. [96] have discussed this process. The predicted dipole moment is [96]:

$$\left|\frac{D}{e}\right|_n \sim \frac{G\alpha}{\pi^3} \sin\delta \; s_1^2 s_2 c_2 s_3 \frac{(m_t^2-m_c^2)(m_b^2-m_s^2)}{m_W^4} m_u \qquad (4.96)$$

Substituting Equation (4.89) into this expression and assuming $m_c^2 << m_t^2$, $m_s^2 << m_b^2$ we obtain:

$$\left|\frac{D}{e}\right|_n \sim \frac{G\alpha s_1^2 \varepsilon}{3\pi^3} \frac{m_t^2 m_b^2}{m_W^2} m_u \sim 10^{-30} \text{ cm} \qquad (4.97)$$

This prediction is, again, not very different from the predictions of the superweak theory, and is, again, consistent with (but far below) the present experimental limit.

The overall emerging picture is the following: CP violation is naturally incorporated into a gauge theory based on the left-handed SU(2) x U(1) six-quark scheme of Section 4.7. There is no inconsistency with experiment, but the smallness of the ε-parameter is not predicted. The relation $\varepsilon' << \varepsilon$ is a natural consequence of the model and an

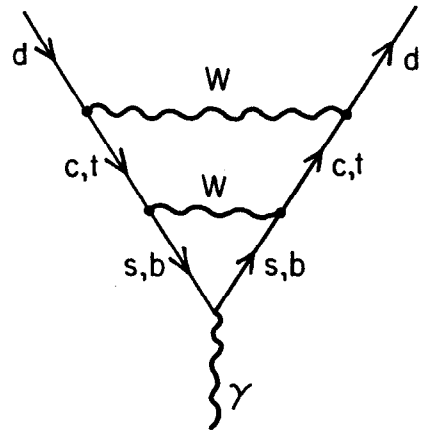

Figure 16: Dominant contribution to the neutron electric dipole in the left-handed six-quark model.

extremely small electric dipole moment for the neutron is predicted. If and when the b- and t-quarks are discovered, it would be extremely interesting to determine θ_2 and θ_3 from the weak production and weak decays of the heavy quarks. This would enable us to express all CP-violating amplitudes in terms of a single parameter δ . At the present time all we know is that, within the left-handed six quark model:

$$\theta_1 \sim 13^\circ \; ; \quad \theta_2 < 30^\circ \; ; \quad \theta_3 < 16^\circ \; ; \quad \delta > 0.3^\circ \qquad (4.98)$$

4.11 Right-Handed Models Involving b- and t-Quarks

The last four Sections (4.7-4.10) were devoted to a discussion of the purely left-handed six quark model. We assumed (Section 4.7) that all right-handed quarks are in SU(2) x U(1) singlets. We noted that the two versions of the $SU(2)_L \times SU(2)_R \times U(1)$ model of Section 2.6 would lead to similar predictions for charged currents, either because $M_{W_L^\pm} \ll M_{W_R^\pm}$ or because of the orthogonality of $W_L^\pm$ and $W_R^\pm$.

We now proceed to discuss the possibility of observable right-handed charged currents involving the six quarks, u, d, c, s, t, b . We continue to use the left-handed assignments of Section 4.7 but consider possible right-handed doublets. Our discussion of charged currents in Sections 3.1 and 3.2 has led us to exclude the following right-handed doublets:

$$(u,d)_R \; ; \quad (u,s)_R \; ; \quad (c,d)_R \; . \qquad (4.99)$$

Consequently, the only possible right-handed doublets are:

$$\begin{array}{l} (t,d)_R \\ (c,s)_R \; ; \quad (t,s)_R \\ (u,b)_R \; ; \quad (c,b)_R \; ; \quad (t,b)_R \; . \end{array} \qquad (4.100)$$

Our analysis of the neutrals currents in Section 2.4 excluded the possibility $I_3(d_R) = -\frac{1}{2}$. This excludes any $(q,d)_R$ doublet, including, of course, $(t,d)_R$. The same analysis indicates that u_R is probably in a singlet, but that conclusion is not yet fully established. Thus, the $(u,b)_R$ doublet is unlikely, but not ruled out.

If the T is a $b\bar{b}$ state, the mass of the b-quark (and the B^-, B^0 mesons) is expected to be around 5 GeV. In this case, a right-handed $(u,b)_R$ doublet would lead to a substantial "y-anomaly" in $\bar{\nu}N$ scattering, and to a significant rise with energy of the ratio

$$\frac{\sigma(\bar{\nu}+N \to \mu^+ + \text{anything})}{\sigma(\nu+N \to \mu^- + \text{anything})} \qquad (4.101)$$

The absence of these effects [13] together with the identification $T = b\bar{b}$ will provide us, if confirmed, with an additional convincing argument against a $(u,b)_R$ doublet.

We have discussed the $(c,s)_R$ doublet in detail in Section 3.3. There is no evidence for it, but no direct evidence against it. However, the natural conservation of charm by neutral currents (see Sections 3.5, 3.6, 3.7) led us to believe that $I_3(c_R) = I_3(u_R)$. This, presumably, indicates that c_R is also in a singlet.

If we accept this conclusion we remain with one and only one possible right-handed SU(2) x U(1) doublet:

$$\begin{pmatrix} t \\ b \end{pmatrix}_R$$

As long as the b- and t-quarks are not discovered we obviously cannot exclude such a doublet. However, we have no reason to expect its existence and the natural conservation of b-number and t-number by neutral currents would not permit it.

Our overall tentative conclusion is that, within SU(2) x U(1), it is unlikely that any right-handed doublets of quarks exist.

Right-handed doublets within various versions of $SU(2)_L \times SU(2)_R \times U(1)$ are, of course, allowed. In the version with $M_{W_L^\pm} \ll M_{W_R^\pm}$, right-handed charged currents are always suppressed, and their detection depends on the value of $M_{W_L^\pm}/M_{W_R^\pm}$. In the version with $M_{W_L^\pm} = M_{W_R^\pm}$, the right-handed doublets can be detected, in principle, through complicated decays such as:

$$b \to s + u + \bar{c} \tag{4.102}$$

or:

$$t \to c + d + \bar{s} \tag{4.103}$$

both proceeding through a $W_R^\pm$. The detection of such decay modes and their identification as being induced by $W_R^\pm$ would be extremely difficult.

4.12 Summary: Third-Generation Fermions

The basic questions of the third generation of fermions are very simple:

(i) Does the third generation exist?

(ii) If so, does it follow a similar pattern to its two predecessors?

(iii) If so, why?

We have almost conclusive evidence for the τ^--lepton and for its sequential character.

We have convincing indirect evidence for the neutral lepton ν_τ, but we are not sure about its mass (less than 300 MeV or more than 2 GeV?).

We have good evidence for a new quark in the existence of T and T' . We have hints that the new quark is the b-quark, but we cannot be certain until it is observed in e^+e^- collisions.

There is no experimental evidence for any additional quarks.

The assumption that third-generation quarks and leptons follow the same pattern of the first and second generation does not contradict any known data. However, there is very little data to support it, at the present time.

5. Summary and Open Problems

5.1 Do We Have a Successful Gauge Theory of Quarks and Leptons?

A surprisingly successful and simple picture of the world of quarks and leptons is obtained within the original example [2] of a gauge theory for the weak and electromagnetic interactions: SU(2) x U(1) .

This picture includes the following ingredients:

(i) The gauge group is SU(2) x U(1).

(ii) We have six quarks and six leptons.

(iii) All left-handed fermions are in SU(2) x U(1) doublets:

$$\begin{pmatrix} u \\ d \end{pmatrix}_L \quad \begin{pmatrix} c \\ s \end{pmatrix}_L \quad \begin{pmatrix} t \\ b \end{pmatrix}_L \quad ; \quad \begin{pmatrix} \nu_e \\ e \end{pmatrix}_L \quad \begin{pmatrix} \nu_\mu \\ \mu \end{pmatrix}_L \quad \begin{pmatrix} \nu_\tau \\ \tau \end{pmatrix}_L \qquad (4.104)$$

where small Cabibbo-like mixing definitely exists for quarks and may exist for leptons.

(iv) All right-handed fermions are in SU(2) x U(1) singlets.

(v) CP-violation is incorporated into the gauge theory.

(vi) The pattern of Higgs particles is minimal: there are two SU(2) x U(1) doublets before symmetry breaking and one remaining physical Higgs particle after symmetry breaking.

(vii) The masses of $W^{\pm}$ and Z and the Weinberg Angle are

$$\sin^2\theta_W \sim 0.25 - 0.3 \qquad (4.105)$$

$$M_{W^{\pm}} \sim 68 \text{ GeV} \qquad (4.106)$$

$$M_Z \sim 81 \text{ GeV} \qquad (4.107)$$

This model is, essentially, the simplest possible gauge theory for the weak and electromagnetic interactions. That such a simple (almost naive!) model works so well, is amazing. It is consistent with almost all established experimental facts including all charged current processes and all neutral current processes involving neutrinos. It is consistent with theoretical prejudices such as the absence of anomalies and "natural" flavor conservation by neutral currents. There are only two problems:

(a) The smallness (or absence) of parity violation in the atomic Bismuth experiments [11] implies that the right-handed electron is not a singlet. It could be in a doublet, but then we run into anomalies and into other theoretical unpleasantness.

(b) There is no clear mechanism for parity violation in the theory. The left-and right-handed fermions transform in an asymmetric way, and the theory does not conserve parity at any stage. This is particularly embarrassing in view of the fact that CP violation is incorporated into the theory in a natural way and is generated by the same spontaneous symmetry breaking mechanism which generates the masses and the Cabibbo angles.

In a well-defined, tightly built model such as the SU(2) x U(1) gauge theory, it would normally be very hard to rectify these two difficulties without losing some of the successes or creating other difficulties. However, the extended $SU(2)_L \times SU(2)_R \times U(1)$ model (Section 2.6) can do precisely what we need:

(i) All right-handed fermions continue to be in singlets of $SU(2)_L$ but are in doublets of $SU(2)_R$. Hence, all left handed fermions are in $(\frac{1}{2}, 0)$ multiplets and all right handed fermions are in $(0, \frac{1}{2})$.

(ii) Parity is conserved by the original Lagrangian of the model, and is spontaneously broken by the usual Higgs mechanism which induces left-right asymmetry.

(iii) All neutral currents conserve parity, but all neutrino induced neutral-current processes obey the predictions of the standard SU(2) x U(1) theory, in agreement with experiment. There is no parity violation in atomic physics (to lowest order in the weak interaction).

(iv) We pay a price in the form of a more complicated spectrum of gauge Bosons and Higgs particles. This was discussed in detail in Section 2.6 and we will not repeat it here.

We believe that the $SU(2)_L \times SU(2)_R \times U(1)$ picture provides an attractive framework for the continued study of gauge theories of the propeties of quarks and leptons. New experimental problems may arise. We discuss several such problems in Section 5.2. Many theoretical problems remain open. We list some of them in Section 5.3.

5.2 Experimental Loose Ends and Open Problems

At the time of this writing there are several experimental "loose ends", concerning the properties of quarks and leptons. At the rate of progress of this field, some of these issues may be resolved and other problems may emerge before this review is published. We feel, however, that a short discussion of these points is both necessary and useful.

(A) Trimuon events. There are several potential sources of events of the type:

$$\nu_\mu + N \to \mu^- + \mu^- + \mu^+ + \text{anything} \qquad (5.1)$$

The sources include: (i) Trivial background due to K and π decays, accompanied by "ordinary" μ-pairs. (ii) A normal charged-current event, accompanied by a low mass $\mu^+\mu^-$-pair produced by a virtual photon or by a vector meson. (iii) Associated charm production followed by $c \to \mu^+$ and $\bar{c} \to \mu^-$ decays. (iv) Production of a b or t quark followed by a cascade of semileptonic quark decays (see Equations (4.59), (4.74), (4.77).

All the above sources are consistent with the overall view of Section 5.1. It is not entirely clear whether the present data [97] on trimuon events in νN scattering (Reaction 5.1) are consistent with the combined contributions of the above mechanisms. It is possible that of the fifteen or so presently observed trimuon events, few are due to each of these mechanisms. At the same time, it is possible that at least some of the observed trimuons are of a different source. A particularly interesting hypothesis which has attracted attention is that some trimuon events are generated by a mechanism in which all three muons are associated with the leptonic vertex and are due to a sequence of decays of a new lepton [98]. Such a new lepton M^- must have a significant charged current coupling to ν_μ. It cannot be accommodated within the simple theories of Section 5.1. Several ways out have been proposed:

(i) An SU(3) x U(1) gauge group in which SU(3) triplets of quarks and leptons appear [57]. In particular, a left-handed triplet including (ν_μ, μ^-, M^-) is assumed. The $\nu_\mu \to M^-$ transition is induced by a charged gauge Boson V^+ which is different from the usual W^+. With the aid of an extra discrete symmetry, the SU(3) x U(1) model can be arranged to agree with all charged and neutral current data as well as with the absence of anomalies and the "natural" conservation of flavors in neutral currents [57]. The SU(3) x U(1) model appears to be the most attractive model which can accommodate the M^- lepton. *However, if such a lepton is not needed by the trimuon events, there is no compelling motivation for pursuing an SU(3) x U(1) scheme.*

(ii) Within SU(2) x U(1), the M^--lepton can be accommodated only at the expense of artificial concoctions involving universal mixing of all fermions [99]. The idea is simple: A significant $\nu_\mu \to M^-$ transition requires that M^- has a large component in the same SU(2) x U(1) doublet as ν_μ. This doublet can have the form:

$$\begin{pmatrix} \nu_\mu \\ \mu^- \cos\alpha + M^- \sin\alpha \end{pmatrix}_L \qquad (5.2)$$

However, the $\nu_\mu \to \mu^-$ transition will now have a strength $G\cos\alpha$, inconsistent with μ-e universality and with the Cabibbo Universality relating μ-decay to β-decay. This can be rectified if all "standard" $I_3 = -\frac{1}{2}$ fermions (e^-, d, s) are mixed with new heavy fermions, with the same universal mixing angle α. We consider this to be an ugly scheme.

(iii) Other models for the M^--lepton involve various versions of $SU(2)_L \times SU(2)_R \times U(1)$ [100], SU(3) x SU(3) [32] or larger groups. We will not discuss these models in detail.

(B) Parity Violating Neutral Currents. At present, there is no experimental proof of parity violation by the neutral current. All neutrino-induced reactions have a left-right asymmetry built into the initial state. Hence, the final state is not parity invariant, but the current may still conserve parity. Within the framework of the left-handed SU(2)x U(1) model, the data tell us that neutral currents must violate parity. On the other hand, in the $SU(2)_L \times SU(2)_R \times U(1)$ model, all neutral currents conserve parity. The best experimental way to probe this issue is to look for parity violation in neutral current processes which do not involve neutrinos. These include atomic and nuclear physics experiments and asymmetry measurements in $e^+e^- \to \mu^+\mu^-$ and e+p → e+anything. All of these experiments may be performed in the near future. Table II (Section 2.6) serves as a guide on this subject. In particular, it is important to improve both the theoretical analysis and the experimental accuracy of the atomic Bismuth experiments in order to find whether their result is, indeed, an order of magnitude below the predictions of the standard SU(2) x U(1) model.

(C) Right-Handed Charged Currents. There is no positive experimental evidence for right-handed charged currents. There are, however, confusing hints. One of them is the "y-anomaly" which was claimed by one experiment and is not seen by others [13]. It would be important to settle this dispute and to rule out a right-handed $u \leftrightarrow b$ transition in $\bar{\nu}_\mu N$ scattering.

The possible existence of a $(c, s)_R$ doublet is still an open question (Section 3.3). Studies of D and F^+ decays as well as the y-distribution of $\bar{\nu}+N \to \mu^-+\mu^+$+anything should help to clarify this question.

(D) τ-Decays. The V,A structure of τ-decays is not fully understood. This must be settled in the near future. The potential problem [81] of not observing $\tau^- \to \pi^-+\nu$ should be carefully studied. We hope to hear soon that the decay has been observed at the expected level. The properties of ν_τ are not known, but their understanding will probably require several years of study.

(E) Heavy $q\bar{q}$ Systems. There are still some important open problems in the Charmonium spectrum and, now, also in the Υ-family. In Charmonium, the X(2.85) and χ(3.45) states are extremely puzzling [101] and seem to defy any sensible classification. In the Υ-family, the relative $\mu^+\mu^-$ branching ratios of Υ and Υ' are incompatible with the Υ-Υ' mass difference (Section 4.6). All of these problems

should be clarified soon. We normally assume that the ψ-family represents one new quark (c-quark) and the T-family represents one additional quark (probably b). It is probable, but not absolutely clear, that only one new quark is involved in each of these families. Only a clarification of the remaining theoretical and experimental "loose ends" in both families will exclude the possibility of having more than one new quark in each family.

(F) Neutrino Masses and Mixing. Finally, the entire question of leptonic Cabibbo-like mixing as well as the possibility of neutrino oscillations depend on whether ν_e, ν_μ and ν_τ are massless. The existence of zero mass particles usually has a profound meaning and it is extremely important to improve on the mass limit of all neutral leptons.

5.3 Theoretical Open Problems

We conclude with a short list of open theoretical problems:

(A) Which is the correct gauge group of the weak and electromagnetic interactions? SU(2) x U(1) was extremely successful but is now in some trouble. $SU(2)_L \times SU(2)_R \times U(1)$ is an attractive, promising alternative which preserves much of the beauty of SU(2) x U(1). Other groups such as SU(3), SU(3) x U(1) and SU(3) x SU(3) have been proposed. A direct experimental study of the correct gauge group must involve the discovery of the charged and neutral gauge Bosons. Their number depends on the group, but their mass pattern depends on the Higgs particles and their vacuum expectation values. The observation of weak phenomena in the next generation of e^+e^- machines (PEP and PETRA) should enable us to have some feeling for the masses of the W and Z Bosons, although it is very unlikely that these masses will be directly accessible at such installations.

(B) Is there any theoretical limit on the number of fundamental fermions? The asymptotic freedom condition dictates [102] that the number of quark flavors must be less than 17. Another argument, based on cosmology considerations, limits the number of massless neutrinos to seven [103]. Assuming that every such neutrino is in a doublet and that the numbers of quark and lepton flavors are the same, we end up with an upper limit of seven or eight "generations" of fermions. These limits are, at present, almost in the domain of science fiction. We do not have any other useful limit on the number of flavors, but any profound understanding of the structure of matter must explain why the number of fundamental building-blocks is what it is.

(C) Perhaps the most difficult open problem is the calculation of masses and angles. All quark and lepton masses, as well as all Cabibbo-like angles, CP-violation parameters and, possibly, parity-violation parameters, are presumably generated by the same mechanism of spontaneous symmetry breaking. We have very little understanding of what determines the values of all of these mass and angle parameters. All attempts to calculate them have essentially failed, so far. The total number of such free parameters is large (of order 20 or more in the case of three generations of fermions), and it is clear that no satisfactory theory can afford to leave them as arbitrary quantities.

(D) The connection between quarks and leptons and the possible grand unification of weak, electromagnetic and strong interactions is another open problem. We discussed it in some detail in Sections 2.8, 2.9, 2.10 and 3.11. A major theoretical breakthrough is clearly needed here. We believe that the next chapter in our pursuit of a deep

understanding of the structure of matter must establish a clear connection between quarks and leptons. Such a connection will be an important step towards a unified picture of the fundamental building-blocks of matter and their interactions.

Acknowledgement

I would like to thank my colleagues at the Weizmann Institute and SLAC for many helpful discussions and remarks. Maurice Jacob has pressed me to write this review for Physics Reports while Fred Gilman and David Leith have provided the opportunity by inviting me to lecture in the 1977 SLAC Summer Institute. To them, and to J. Bjorken and J. Ellis I owe special thanks.

References

[1] For general reviews of gauge theories of weak and electromagnetic interactions see e.g. E.S. Abers and B.W. Lee, Phys. Reports 9, 1 (1973); S. Weinberg, Reviews of Modern Phys. 46, 255 (1974); J.C. Taylor, Gauge Theories of the Weak Interactions, Cambridge University Press (1976).

[2] S. Weinberg, Phys. Rev. Letters 19, 1264 (1967); A. Salam, Proceedings of the 8th Nobel Symposium, Stockholm, 1968.

[3] For a detailed list of references concerning $SU(2)_L \times SU(2)_R \times U(1)$ see our discussion in Section 2.6 and references [18]-[24].

[4] S.L. Adler, Phys. Rev. Letters 14, 1051 (1965); W.I. Weisberger, Phys. Rev. Letters 14, 1047 (1965).

[5] M. Gell-Mann, Phys. Rev. 125, 1067 (1962); Physics 1, 63 (1964).

[6] See e.g. J.D. Bjorken, Proceedings of the SLAC Summer Institute, 1976.

[7] F. Reines, H. Gurr and H. Sobel, Phys. Rev. Letters 37, 315 (1976).

[8] J. Blietschau et al., Nucl. Phys. B114, 189 (1976).

[9] H. Faissner, report to the International Conference on Neutrino Physics and Astrophysics, "Neutrino 77", Elbrus, USSR, June 1977.

[10] For discussions of parity violation in atoms see, e.g., M.A. Bouchiat and C.C. Bouchiat, Phys. Letters 48B, 111 (1974); J. Bernabeu and C. Jarlskog, CERN preprint, TH2206, 1976; M.W.S.M. Brimicombe, C.F. Loving and P.G.H. Sandars, J. Phys. B1, 237 (1976); E.M. Henley and L. Wilets, Phys. Rev. A14, 1411 (1976).

[11] P.E.G. Baird et al., Nature 264, 528 (1976); P.G.H. Sandars, Review talk at the International Symposium on Lepton and Photon Interactions at High Energies, Hamburg, August 1977.

[12] J. Blietschau et al., Nucl. Phys. B118, 218 (1977); A. Benvenuti et al., Phys. Rev. Letters 37, 1039 (1976); B.C. Barish et al., unpublished; K. Tittel, talk presented at the International Symposium on Lepton and Photon Interactions at High Energies, Hamburg, August 1977.

[13] M. Holder et al., Phys. Rev. Letters 39, 433 (1977); B.C. Barish et al., Cal. Tech. preprint, CALT 68-606, June 1977; See, however, A. Benvenuti et al., Phys. Rev. Letters 37, 189 (1976).

[14] See e.g. C.H. Albright, C. Quigg, R.E. Shrock and J. Smith, Phys. Rev. D14, 1780 (1976).

[15] D. Cline et al., Phys. Rev. Letters 37, 252 (1976); 37, 648 (1976).

[16] See e.g. R.N. Cahn and F.J. Gilman, SLAC preprint, August 1977.

[17] A. de Rujula, H. Georgi and S.L. Glashow, Harvard preprint, HUTP-77/A046, July 1977.

[18] For early work related to various versions of $SU(2)_L \times SU(2)_R \times U(1)$ see: S. Weinberg, Phys. Rev. Letters 29, 388 (1972); J.C. Pati and A. Salam, Phys. Rev. D10, 275 (1974); R.N. Mohapatra and J.C. Pati, Phys. Rev. D11, 566 (1975), D11, 2558 (1975).

[19] H. Fritzsch and P. Minkowski, Nucl. Phys. B103, 61 (1976).

[20] R.N. Mohapatra and D.P. Sidhu, Phys. Rev. Letters 38, 667 (1977), and CCNY preprint CCNY-HEP-77/3, May 1977.

[21] A. De Rujula, H. Georgi and S.L. Glashow, Harvard preprint HUTP-77/A002, January 1977.

[22] J.C. Pati, S. Rajpoot and A. Salam, Imperial College preprints, ICTP/76/11 and ICTP/76/15, 1977.

[23] R.N. Mohapatra, F.E. Paige and D.P. Sidhu, Brookhaven preprint, August 1977; H.S. Mani, J.C. Pati and A. Salam, Trieste preprint, IC/77/80, August 1977.

[24] H. Georgi and S. Weinberg, Harvard preprint, HUTP-77/A052, August 1977.

[25] Particle Data Group, Reviews of Modern Physics 48, S1 (1976).

[26] See e.g. M. Gell-Mann, R.J. Oakes and B. Renner, Phys. Rev. 175, 2195 (1968).

[27] S. Weinberg, Phys. Rev. Letters 29, 388 (1972).

[28] H. Georgi, H.R. Quinn and S. Weinberg, Phys. Rev. Letters 33, 451 (1974).

[29] C. Bouchiat, J. Illiopoulos and Ph. Meyer, Phys. Letters 38B, 519 (1972); D. Gross and R. Jackiw, Phys. Rev. D6, 477 (1972).

[30] S.L. Adler, Phys. Rev. 177, 2426 (1969); J.S. Bell and R. Jackiw, Nuovo Cimento 51, 47 (1969).

[31] See e.g. H. Fritzsch and P. Minkowski, Phys. Letters 63B, 99 (1976); D. Horn and G.G. Ross, Cal. Tech. preprint, CALT-68-597, May 1977; See also references [32],[37].

[32] J.D. Bjorken and K. Lane, SLAC preprint, 1977; Y. Achiman, Phys. Letters 70B, 187 (1977).

[33] J.C. Pati and A. Salam, Phys. Rev. D8, 1240 (1973); D10, 275 (1974).

[34] H. Fritzsch and P. Minkowski, Annals of Physics 93, 193 (1975).

[35] M.S. Chanowitz, J. Ellis and M.K. Gaillard, CERN preprint, TH-2312, May 1977.

[36] H. Georgi and S.L. Glashow, Phys. Rev. Letters 32, 438 (1974).

[37] See e.g. F. Gursey and P. Sikivie, Phys. Rev. Letters 36, 775 (1976); P. Ramond, Nuclear Phys. B110, 214 (1976).

[38] C. Jarlskog, CERN report, unpublished.

[39] A. Sirlin, Nuclear Phys. B71, 29 (1974). See also D.H. Wilkinson, Nature 257, 189 (1975).

[40] See e.g. S. Yamada, talk at the International Symposium on Lepton and Photon Interactions at High Energies, Habmburg, August 1977; P. Bosetti et al., Phys. Rev. Letters 38, 1248 (1977); C. Baltay et al., Phys. Rev. Letters 39, 62 (1977).

[41] See e.g. talks by A. Barbaro-Galtieri, G. Knies and S. Yamada at the International Symposium on Lepton and Photon Interactions at High Energies, Hamburg, August 1977.

[42] R. Brandelik et al., Phys. Letters 67B, 363 (1977); J. Burmester et al., Phys. Letters 67B, 367 (1977).

[43] M. Picolo et al., Phys. Letters 70B, 260 (1977).

[44] A. Benvenuti et al., Phys. Rev. Letters 35, 1199 (1975); 35 1249 (1975); M. Holder et al., Phys. Letters 69B, 377 (1977).

[45] See e.g. M.K. Gaillard and B.W. Lee, Phys. Rev. D10, 897 (1974).

[46] S.L. Glashow, J. Illiopoulos and L. Maiani, Phys. Rev. D2, 1285 (1970).

[47] F.A. Wilczek et al., Phys. Rev. D12, 2768 (1975).

[48] E. Golowich and B.B. Holstein, Phys. Rev. Letters 35, 831 (1975).

[49] R. Brandelik et al., DESY preprint, DESY 77/44, July 1977.

[50] K. Sasaki, Phys. Letters 67B, 341 (1977).

[51] A. Ali and T.C. Yang, DESY preprint; F. Bletzacher, H.T. Nieh and A. Soni, Stonybrook preprint; G.L. Kane, Phys. Letters 70B, 227 (1977).

[52] S. Yamada, talk at the International Symposium on Lepton and Photon Interactions at High Energies, Hamburg, August 1977.

[53] H. Fritzsch and P. Minkowski, Cal. Tech. Preprint, CALT-68-532, December 1975, unpublished.

[54] V. Barger and D.V. Nanopoulos, Wisconsin preprint, 1977, unpublished.

[55] H. Harari, unpublished.

[56] S.L. Glashow and S. Weinberg, Phys. Rev. D15, 1958 (1977); E.A. Paschos, Phys. Rev. D15, 1966 (1977).

[57] B.W. Lee and S. Weinberg, Phys. Rev. Letters 38, 1237 (1977); B.W. Lee, R.E. Shrock and S. Weinberg, Fermilab preprint, August 1977. An earlier SU(3)×U(1) model was proposed by G. Segre and J. Weyers, Phys. Letters 65B, 243 (1976). See also M. Barnett and L.N. Chang, SLAC preprint, PUB-1932, 1977.

[58] See e.g. A. de Rujula, H. Georgi and S.L. Glashow, Phys. Rev. Letters 35, 69 (1975); R. Kingsley, Phys. Letters 63B, 329 (1976): R. Kingsley et al., Phys. Rev. D11, 1919 (1975).

[59] G. Goldhaber et al., SLAC-LBL collaboration, unpublished note, 1977.

[60] C. Baltay, Report to the Rencontre de Moriond, Flaine, March 1977.

[61] J.D. Bjorken and S. Weinberg, Phys. Rev. Letters 38, 622 (1977).

[62] See e.g. T.P. Cheng and L. F. Li, talk at the Orbis Scientiae, Coral Gables, January 1977.

[63] V. Gribov and B. Pontecorvo, Phys. Letters 28B, 493 (1969). For a more recent discussion see e.g. H. Fritzsch and P. Minkowski, Phys. Letters 62B, 72 (1976).

[64] T.P. Cheng and Ling-Fong Li, Phys. Rev. Letters 38, 381 (1977).

[65] J.D. Bjorken, K, Lane and S. Weinberg, SLAC preprint, PUB-1925, April 1977.

[66] S. Weinberg, Phys. Rev. Letters 37, 657 (1976).

[67] R.N. Mohapatra, Phys. Rev. D6, 2023 (1972).

[68] See e.g. H. Fritzsch and P. Minkowski, Phys. Letters 68B, 421 (1976).

[69] M. Kobayashi and K. Maskawa, Progress of Theoret. Phys. 49, 652 (1973).

[70] J. Bailey et al.,Phys. Letters 67B, 225 (1977).

[71] R. Jackiw and S. Weinberg, Phys. Rev. D5, 2396 (1972).

[72] H. Fritzsch, CERN preprint, TH-2358, August 1977; See also F. Wilczek and A. A. Zee, Princeton preprint, July 1977.

[73] A. De-Rujula, H. Georgi and S.L. Glashow, Harvard preprint, HUTP-77/A028, June 1977.

[74] H. Harari, Proceedings of the International Symposium on Lepton and Photon Interactions at High Energies, Stanford, August 1975.

[75] M.L. Perl et al., Phys. Rev. Letters 35, 1489 (1975).

[76] See e.g. M.L. Perl et al., Phys. Letters 63B, 117 (1976); J. Burmester et al., DESY preprint 77/24 and reference [78].

[77] SLAC-LBL collaboration, private communication from M.L. Perl.

[78] See e.g. M.L. Perl, talk at the Rencontre de Moriond, Flaine, March 1977 (SLAC-PUB-1923); G. Flugge, DESY preprint 77/35, June 1977.

[79] M.L. Perl, talk at the International Symposium on Lepton and Photon Interactions at High Energies, Hamburg, August 1977, and references therein. See also references [81], [82].

[80] H.B. Thacker and J.J. Sakurai, Phys. Letters 36B, 103 (1971); Y.S. Tsai, Phys. Rev. D4, 2821(1971); C.H. Llewellyn-Smith and J.D. Bjorken, Phys. Rev. D7, 88 (1973).

[81] S. Yamada, Talk at the International Symposium on Lepton and Photon Interactions at High Energies, Hamburg, August 1977.

[82] G. Knies, talk at the International Symposium on Lepton and Photon Interactions at High Energies, Hamburg, August 1977.

[83] SLAC-LBL collaboration, private communication from G.J. Feldman and J.A. Jaros.

[84] D. Horn and G.G. Ross, Phys. Letters 67B, 460 (1977); G. Altarelli, N. Cabibbo, L. Maiani and R. Petronzio, Phys. Letters 67B, 463 (1977). See also, J.F. Donoghue and L. Wolfenstein, Carnegie-Mellon preprint, COO-3066-97, July 1977.

[85] H. Fritzsch, Cal. Tech. preprint, CALT-68-583, January 1977.

[86] S. Herb et al., Phys. Rev. Letters 39, 212 (1977).

[87] W.R. Innes et al., Fermilab-Columbia-Stonybrook preprint, August 1977. See also, L. Lederman, talk presented at the International Symposium on Lepton and Photon Interactions at High Energies, Hamburg, August 1977.

[88] T. Appelquist et al., Phys. Rev. Letters 34, 365 (1975); E. Eichten et al., Phys. Rev. Letters 34, 369 (1975).

[89] E. Eichten and K. Gottfried, Phys. Letters 66B, 286 (1977).

[90] J. Ellis, M.K. Gaillard, D.V. Nanopoulos and S. Rudaz, CERN preprint, TH-2346, July 1977.

[91] C.E. Carlson and R. Suaya, Phys. Rev. Letters 39, 908 (1977); T. Hagiwara, Y. Kazama and E. Takasugi, Fermilab preprint, PUB-77/72-THY, August 1977.

[92] H. Harari, Phys. Letters 57B, 265 (1975); Annals of Physics 94, 391 (1975).

[93] E.A. Paschos, Phys. Rev. Letters 39, 858 (1977).

[94] S. Pakvasa and H. Sugawara, Phys. Rev. D14, 305 (1976).

[95] L. Maiani, Phys. Letters 62B, 183 (1976).

[96] J. Ellis, M.K. Gaillard and D.V. Nanopoulos, Nuclear Phys. B109, 213 (1976).

[97] A. Benvenuti et al., Phys. Rev. Letters 38, 1110 (1977); B.C. Barish et al., Phys. Rev. Letters 38, 577 (1977); D. Reeder, talk at the international Symposium on Lepton and Photon Interactions at High Energies, Hamburg, August 1977.

[98] A. Benvenuti et al., Phys. Rev. Letters 38, 1183 (1977).

[99] See e.g. A De-Rujula, H. Georgi and S.L. Glashow, Harvard preprint, June 1977; V. Barger et al., Wisconsin preprint, COO-598, April 1977.

[100] See e.g. A. Zee, F. Wilczek and S.B. Treiman, Phys. Letters 68B, 369 (1977).

[101] See e.g. M.S. Chanowitz and F.J. Gilman, Phys. Letters 63B, 178 (1976); J.D. Jackson, Proceedings of the SLAC Summer Institute, 1976.

[102] H.D. Politzer, Phys. Rev. Letters 30, 1346 (1973); D.J. Gross and F. Wilczek, Phys. Rev. Letters 30, 1343 (1973).

[103] G. Steigman, D.N. Schramm and J.E. Gunn, Phys. Letters 66B, 202 (1977).

QUARK CONFINEMENT*

S. D. Drell
Stanford Linear Accelerator Center
Stanford University, Stanford, California 94305

LECTURES PRESENTED AT THE SLAC SUMMER INSTITUTE, JULY 1977

These lectures are concerned with the problem of "where are the quarks?" Almost 10 years ago the classic MIT-SLAC experiments on deep inelastic electron scattering[1] revealed the existence of localized bits and pieces of electromagnetic charge and current within the proton. These more elementary parts of the proton--or partons--were inferred from the Bjorken scaling behavior.[2] Furthermore, the subsequent studies with electron, muon, and neutrino beams as well as the spectacular results of electron-positron collisions have strengthened the interpretation of partons as quarks.[3] In fact today there is no persuasive alternative to the physical picture of hadrons as rather loosely bound aggregates of relatively light quarks. However beyond the impressive successes of the quark model in its diverse applications to spectroscopy[4] (both old and charmed), scaling behavior, and quark line counting rules for large p_T processes,[5] there remains a dilemma: Why are individual quarks apparently trapped within the hadron?

As you well know the actual experimental nature and extent of quark trapping or confinement is not completely settled by experiment. Although many searches have failed to find fractionally charged particles to a very low density in matter,[6] LaRue, Fairbank and Hebard[7] have recently reported observation of fractional charges on two superconducting Ni spheres weighing

*Work supported by The Department of Energy.

10^{-4} grams and magnetically levitated between condenser plates. Their response to a periodic electric force is interpreted as evidence of charge 1/3 on the spheres. If supported and confirmed by subsequent experiments this result will imply that quark confinement is not permanent but that quarks may in fact be paroled from their hadronic prisons by sufficiently high energies, perhaps one or more orders of magnitude greater than the hadron mass.

The purer the field theorist, the more unacceptable is this alternative to permanent confinement. In these lectures I won't take sides. I simply want to describe, explain, and analyze some theoretical efforts to understand the novel behavior of quark constituents in the hadron. In contrast to atomic, molecular, and nuclear forces that grow stronger the smaller the distance between the interacting particles, the forces between quarks grow weaker at small distances--that is how we understand Bjorken scaling and the almost-free quark dynamics, or asymptotic freedom, for large momentum transfer processes. On the other hand, these forces grow very strong--perhaps without limit if the confinement is indeed permanent, corresponding to "infra-red slavery"--as the separation increases corresponding to the dynamics of strongly interacting quarks at low momenta. (See Fig. 1.)

Such novel, unconventional physical behavior translates into new and different mathematical behavior in the fundamental underlying theory. This behavior is opposite from what we are familiar with in QED, our only true and tested friend in the theoretical world.

It is well known that in quantum field theories we must renormalize the coupling constants. In quantum electrodynamics the charge is the dimensionless coupling constant; and the renormalized charge e_R is smaller in magnitude than the bare one e_0 introduced in defining the Lagrangian and Hamiltonian of the

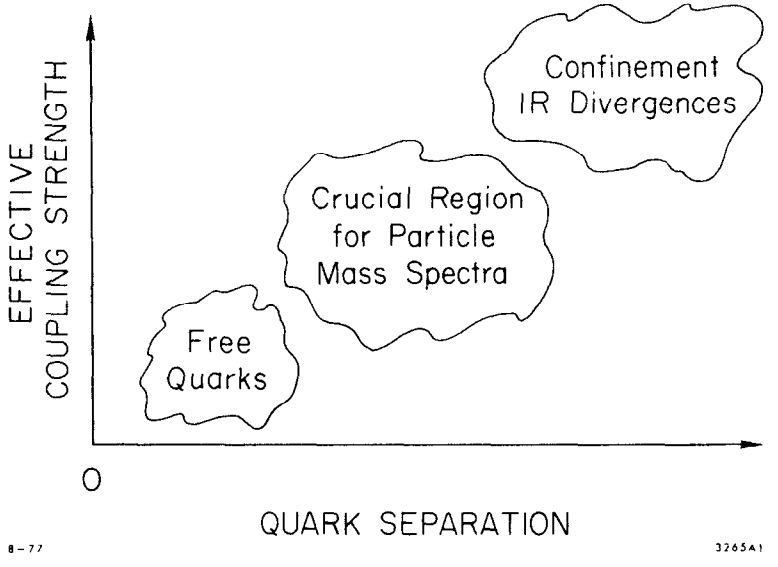

Fig. 1

theory. e_R is the charge of the physical electron dressed by quantum fluctuations. The vacuum, or ground state, of the quantized electromangetic field is bubbling everywhere with virtual electron-positron pairs. Their presence originates in the zero point quantum fluctuations of the electromagnetic field strengths. Since all components of E and B don't commute we cannot set them identically to zero; only their average strength can vanish. The virtual pairs in the vacuum are physically polarized in the neighborhood of an electron by the electrostatic forces.[8] The effect of this polarized cloud of pairs in the vacuum sea is to partially shield and reduce the strength of the electron charge when it is viewed from a distance greater than the range characteristic of the polarization, i.e., the electron compton wavelength

$$R \sim c\Delta t \sim \frac{\hbar}{mc} \quad .$$

Thus the electron charge as seen by a macroscopic applied field, or by a test charge at distances > R, corresponding to scattering with q < mc, is

$$e_R = \int d^3r \left[\rho_0(r) + \rho_p(r)\right]$$

where $\rho_0(r) = e_0\delta^3(r)$ for an electron at the origin; and $\rho_p(r)$ is illustrated in Fig. 2. When however we probe the electron at small distances we see inside the polarization cloud and eventually, for q >> mc, probe the bare charge $e_0 > e_R$. This physical picture is important in assuring us that in QED, the simplest of gauge field theories, the exact force law grows stronger more rapidly than 1/r at smaller distances, and decreases for large r. This is precisely opposite to the desired behavior for explaining confinement and asymptotic freedom; i.e., a charge that grows weaker when probed at small distances but grows stronger at large separation.

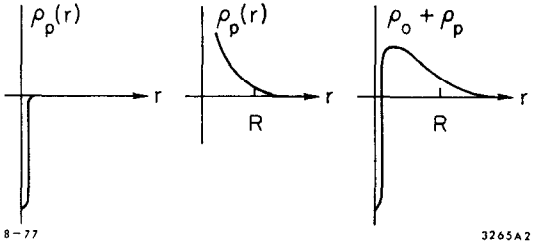

Fig. 2

From the above discussion there is a clue as to how field theory must be changed from QED if we are to construct a theory that incorporates asymptotic freedom. Spurred by the successes of QED as well as by their mathematical beauty we work in the context of gauge theories--such as QED--i.e., theories with space-time dependent symmetry transformations under which the theory is invariant, viz. in QED

$$A_\mu(x) \to A_\mu(x) + \frac{\partial \delta\chi}{\partial x^\mu}$$

$$\psi(x) \to (1 + ie\delta\chi(x))\psi(x) \quad .$$

Evidently we will require a more complex gauge theory than QED for which the gauge group is U(1): i.e., the group of space-time dependent phase transitions on one complex or two real fields, representing a charged particle. The U(1) symmetry leaves the charge residing on the electron. In contrast if the forces are to weaken at short distances the coupling strength must weaken for large q and this can happen only if the polarization cloud can acquire at least some of the charge of the particle itself. This in turn means that the quanta must be able to remove charge from the sources in contrast to the electrically neutral photons of QED. This is a possibility for non-abelian gauge theories[9] when other special requirements are also satisfied. A non-abelian gauge theory is one with internal symmetry transformations that act on the particle labels themselves, such as turning protons into neutrons in the example of SU(2), in addition to depending on space-time coordinates, viz.

$$v_\mu^\alpha \to v_\mu^\alpha + \frac{\partial \delta\chi^\alpha}{\partial x^\mu} - g\varepsilon^{\alpha\beta\gamma}\delta\chi^\beta v_\mu^\gamma$$

$$\psi \to (1 + ig\frac{\tau^\alpha}{2}\delta\chi^\alpha)\psi \quad .$$

It has been shown for example that a renormalizable SU(3) gauge theory of strong interactions formulated with massless gluons that are color octets--this is a renormalizable theory so long as the gluon fields are massless--has the property of asymptotic freedom if there are not too many quarks whose masses are "light" on the scale of momentum transfers exhibiting the weak coupling limiting behavior and hence scaling.[10]

However the fact that the theory includes massless gluons introduces its own difficulties. With non-abelian theories the method for removing infra-red divergences is more complex and delicate than that of Bloch-Nordsieck since the ordering of vertices matters and there is no simple classical current behavior in the soft gluon limit.[11] This very difficulty has been conjectured into a virtue in order to explain quark trapping. The untamed singularities in the infra-red or soft gluon limit are presumed[12] to be the source of an interaction strength that grows beyond bounds as the separation between quarks increases. There is no mathematical proof of this conjecture; what is more quarks may have in fact been observed.[7] So this is a questionable conjecture on all grounds. What is known from the constructive analysis of Cheng, Eichten, and Li[13] is that the requirements of asymptotic freedom and of freedom from IR divergences are mutually incompatible in renormalizable gauge theories. Hence we must have IR divergences if we are to insist on asymptotic freedom and, therefore, it is necessary for us to appeal to confinement as a way of removing the IR difficulty. It is asserted that we cannot radiate massless gluons and consequently we avoid the infinities associated with their massless propagation.

This framework of ideas has aesthetic appeal although lacking hard calculational foundations. The problem we face as theorists is one dating to Year 1 of modern physics--how to solve relativistic field theories without

resorting to weak coupling iterative expansions for implementing the renormalization program. In other words, how can we test our theoretical ideas when we cannot solve our equations. That is today's problem and explains why I must proceed by asking very limited questions in search of modest progress and encouragement; and why I must resort to simple models that to many may appear to be little more than elementary school exercises. We ask:

What do we need, phenomenologically, of a field theory for confinement?

What methods can we bring to bear on field theory for constructing non-perturbative solutions? An iterative procedure starting with quark and gluon degrees of freedom can hardly be expected to give low-lying physical hadronic spectra in a reliable way in a finite number of practicable operations.

We take the following as the starting ingredients of a theory:[14]

1) There are three flavors of light "old" quarks. Massive new quarks (with "charm" and perhaps more varieties) are, by assumption, not essential in the study of confinement.

2) Quarks carry a hidden quantum number "color." Hadrons are always formed of combinations of quarks that are color neutral. The quarks come in three colors and the theory is invariant under SU(3) of color; then the configurations $Q\bar{Q}$ and QQQ are the simplest colorless structures, corresponding to mesons and baryons respectively. Since these colorless--or color singlet--combinations of quarks have the quantum numbers of normal hadrons, the problem of quark confinement becomes that of color confinement.

3) Massless gauge gluons are the quanta carrying the force between quarks. The color quantum number plays the same role that electric charge does in QED; and the colored quarks interact with one another via colored electric and colored magnetic fields. What we are describing here is a non-abelian gauge theory along the lines first introduced by Yang and Mills.[15] In contrast with abelian QED, where the quanta are electrically neutral and do not change the charge of their sources, the gluons are themselves colored. They must remain massless, as in QED, for the theory to be renormalizable in the usual fashion. However in order to maintain local color conservation (i.e. color conservation as a local, not simply a global, symmetry) the gluons must carry off, say, red-blueness upon changing a red to a blue quark. This means that such a theory with SU(3) of color must have 8 gluons corresponding to all $3 \times 3 - 1 = 8$ color combinations, where we have subtracted the combination that is colorless and does not enter the theory. Another new feature of such a non-abelian gauge theory is that, being colored, gluons change the color charge of their sources. As we mentioned earlier such a theory can lead to forces that grow weaker at smaller and smaller distances, becoming asymptotically free at very short ones.

Such an asymptotically free gauge theory--henceforth called QCD--presents itself strongly as appropriate for a fundamental underlying theory of strong interactions if we can explain why we see neither quarks nor massless gluons--namely if we can explain "color confinement"! Furthermore for the theory as stated thus far the confinement must be permanent: no massless gluons are observed. In the highly successful theoretical tradition of turning adversity into achievement, or ∞ to 0, we appeal to the infra-red divergences to trap the quarks and gluons as noted earlier. This is a hope! Color confinement has not been proved for such theories. We are dealing with strong forces

and looking for composite bound states of quarks that form the observed extended hadrons. But we have thus far lacked the mathematical methods for constructing such states from elementary quark and massless gluon constituents. The distance from starting point to physical matter is too great for perturbation theory.

In particular since we must avoid an iterative weak coupling expansion and the actual implementation of the renormalization procedure in terms of a Feynman graph expansion we must do something about the infinities buried in quantum field theory. In principle this can be done by introducing a cut-off and working with a theory that is finite at each stage. If the low-lying states and their excitation energies remain finite at the end in the limit of the cut-off increasing to ∞ we may consider this approach satisfactory. One way to implement a cut-off procedure is to formulate the theory on a finite lattice with a finite number of degrees of freedom--in the same way that we can approximate a continuous string by a weighted one, or vice versa. In fact in their pioneering original paper on field quantization, Heisenberg and Pauli[16] started from a discrete theory in terms of discrete cells in space and proceeded to the continuum limit. We reverse this step with the lattice theory. This procedure, formulated initially by Wilson[17] in the language of path integrals and transcribed to Hamiltonian form by Kogut and Susskind[18] has stimulated a lot of work--a fair amount of it right here at SLAC.[19] Although no definitive solutions of physical gauge theories have been obtained, both physical insight and reliable and straightforward methods have been developed and I will describe them in my second lecture.

A very nice phenomenological approach that is less ambitious on fundamental theoretical grounds on one hand but which has been impressively successful in reproducing known physical properties of low-lying hadronic states on the other is the approach of semi-classical "bag" theories; and in particular the MIT bag model.[20] In this approach the bag is posited by fiat in the form of boundary conditions imposed on a canonical field theory. Alternatively one can proceed by constructing exact solutions of the classical field equations in the interacting field theory that localize the energy in space and that cannot be found by iterative procedures starting from empty space vacua. Such solutions--known as solitons--occur[21] in field theories with degenerate vacua, in which case they are frequently referred to as topological solitons, an example of which is the 't Hooft-Polyakov monopole[22] in three dimensions; they also occur in field theories with conservation laws of charge, isospin, or some appropriate additive quantum number reflecting an internal symmetry, in which case they are referred to as non-topological solitons.[21] A well studied example is that of a charged bose or fermi field interacting with a neutral scalar Higgs field. The SLAC bag model[23] and other similar ones[24] which construct semi-classical extended hadrons from local field theory are of this latter class. Aside from being semi-classical solutions--i.e. solutions obtained by neglecting quantum fluctuations and zero point corrections to a one-particle treatment of the quarks, such approaches also have the presumed drawback of violating the requirements of asymptotic freedom since they contain Higgs scalars explicitly in the Hamiltonian. I view these Higgsons as a phenomenological crutch for constructing low-lying colorless hadrons from QCD. They are useful because field theory has not yet fully demonstrated the ability to predict such hadrons from gluons and quarks alone.

The MIT bag model treats a hadron as a finite region in space to which almost free and light quarks are confined by fiat. This is accomplished formally by modifying the free quark field theory by two assumptions:

1. A constant energy density is added to the Hamiltonian within the hadron, i.e.:

   $T^{\mu\nu} \to T^{\mu\nu} + g^{\mu\nu} B$

   within the bag, or

   $H \to H + B$

   where the volume tension B acts to compress the bag against the outward pressure of the quark gas.

2. A boundary condition is imposed such that the colored fields of quarks and gluons are confined within a finite region of space--i.e., the interior of the hadron:

   $n_\mu (T^{\mu\nu} + g^{\mu\nu} B) = 0$ on the surface

In this initial zeroth order formulation of the MIT bag model, if we treat the surface as that of a spherical static bag, or "cavity," of radius R, the energy of a quark in the bag is

$$E = \frac{c}{R} + B\,\frac{4\pi R^3}{3}$$

where $c \tilde{>} 2$ is a constant characterizing the energy of a massless fermion in a spherical well with infinitely high walls. The minimum gives a ground state energy and bag radius of

$$E_0 = \frac{4}{3}\,\frac{c}{R_0}\,; \qquad R_0 = \left(\frac{c}{4\pi B}\right)^{1/4} \tag{1.1}$$

Adding massless color gauge fields, or gluons, to the bag Hamiltonian, with the assumption that the SU(3) color symmetry is unbroken, leads to the result that all hadronic states have conventional quantum numbers; i.e., they are color singlets. This follows from the boundary conditions for the color gauge fields which require that they vanish on the surface of the bag if the total energy-momentum are conserved within the bag world line--i.e., within the hypertube representing the space-time trajectory of the bag. This is the formal statement of gluon confinement and gives

$$n_\mu \mathscr{F}^{\mu\nu} = 0 \quad \text{on the surface}$$

where n_μ is the space-like normal to the surface. Since by Gauss' law, the total color charge of a bag is given by a volume integral of the divergence of the color electric field, we have

$$Q_{\text{color}} = \int_{\substack{\text{bag}\\ \text{volume}}} d^3r\ \partial_k \mathscr{F}^{k0} = \int_{\substack{\text{bag}\\ \text{surface}}} d\,S\, n_\mu \mathscr{F}^{\mu 0} = 0 \tag{1.2}$$

Hence only color singlet bags can be formed.

With the inclusion of gluons and of interactions between the quarks via gluon exchange the bag model is reminiscent of nuclear shell theory which describes nuclear spectroscopy in terms of nucleons confined within a phenomenological nuclear potential and interacting with one another via a spin-orbit potential that shapes the shell structure. Here the bag is a relativistic representation of the dominant confining forces. There is a residual and relatively weak quark-quark interaction resulting from the exchange of an octet of massless colored gluons and which is expressed via the Yang-Mills mechanism. The quark-quark interaction is required to be weak at short

distances so that Bjorken scaling is not destroyed. It is also required to be weak at large distances, or near zero momentum, if we are to avoid large renormalizations of the impressively successful naive quark model estimates of transitions among low-lying baryonic states. The bag provides the infra-red cutoff so that the quark-gluon interaction is treated iteratively in a weak coupling expansion, only the lowest contribution of which has been analyzed.

In this approximation, the MIT bag model remains a static spherical "cavity" in which quarks and gluons and their first quantized modes of motion satisfy appropriate boundary conditions which insure that only color singlets occur. It is a four-parameter model since in addition to the volume tension B, there is also the quark-gluon coupling constant $\alpha_c = g^2/4\pi$, which characterizes the strength of the quark-quark interaction; the mass of the strange quark, $m_s \neq 0$, which characterizes the breaking of the SU(3) flavor symmetry; and a constant Z_0 that characterizes the volume dependent zero point energy associated with the quantum modes of the bag.

There are four contributions to the energy of a hadron:

(1) The kinetic energy of the quarks confined in the bag; for N quarks in S-orbits within a spherical bag of radius R this is given by

$$E_{kinetic} = \frac{1}{R}\sum_{i=1}^{N} \sqrt{x_i^2(m_iR) + (m_iR)^2} \tag{1.3}$$

where $x_i(m_iR)$ is the wave number of a quark in the static bag as fixed by boundary conditions, and is slowly varying with quark mass, with $x_i(0) \approx 2$. This term gives rise to roughly 3/4 of the mass of a typical hadron.

(2) The bag energy which expresses the fact that the confining potential, or pressure B, has a dynamical origin in an underlying relativistic field theory and thus carries energy; in QCD it is the average gluon field energy within the bag,

$$E_{vol} = B \cdot \left(\frac{4\pi}{3}\right) R^3 \tag{1.4}$$

(3) The zero point energy of all the modes in the static bag, or cavity, enters because it changes with the volume of the cavity. In conventional field theory formulated over all space it is highly divergent but can be discarded as a constant, the same for all processes. Here we simply parametrize the finite part of the zero point energy by

$$E_0 = -Z_0/R \tag{1.5}$$

A divergent contribution proportional to $V = 4\pi/3\ R^3$ is submerged in a renormalization of B, and for simple slab-like and spherical models with spinor and vector field constituents there are no contributions to E_0 proportional to R^2, R, or constant.

(4) There is a contribution to the energy associated with the gluon mediated interactions between the quarks. The bag itself is assumed to be the expression of the strong, long-range confining forces whose energy is given by (1.4). The residual quark-quark interaction is treated perturbatively to lowest order in $\alpha_c = g^2/4\pi$. The two lowest order Born graphs are shown in Fig. 3. Since to this order no gluon self-couplings occur the gluons behave like 8 independent color fields $\vec{E}^a$ and $\vec{B}^a$, a = 1, ... , 8, which must satisfy the boundary conditions for confinement. The assumption made in treating the self energy contributions (Fig. 3b) is that only those parts of it are retained that are required to enable $\vec{E}^{(a)}$ and $\vec{B}^a$ satisfy the required boundary conditions on the bag surface, i.e.,

$$\vec{n} \cdot \vec{E}^a\,(R) = 0 \tag{1.6}$$

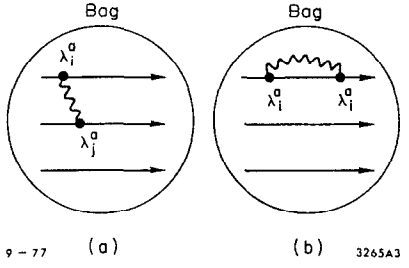

Fig. 3

$$\hat{n} \times \vec{B}^a (R) = 0 \tag{1.7}$$

Otherwise the self energy contributions are assumed to be included in the assigned phenomenological quark masses. The interaction energy from Fig. 3a is static and has the electrostatic and magnetostatic contributions of, respectively,

$$\Delta E_E^{(1)} = \frac{1}{2} g^2 \sum_{i \neq j} \sum_a \int_{bag} d^3 r \, \vec{E}_i^a (r) \cdot \vec{E}_j^a (r) \tag{1.8}$$

$$\Delta E_M^{(1)} = -\frac{1}{2} g^2 \sum_{i \neq j} \sum_a \int_{bag} d^3 r \, \vec{B}_i^a (r) \cdot \vec{B}_j^a (r) \tag{1.9}$$

To this must be added from Fig. 3b the contributions required to turn (1.8) and (1.9) into interaction energies of fields $\vec{E}^a$ and $\vec{B}^a$ for which the boundary conditions (1.6) and (1.7) are satisfied. This is no problem for the $\vec{B}_i^a$ which, as constructed from the quark current distribution by Maxwell's equations, automatically satisfy (1.7), i.e., it follows from

$$\vec{\nabla} \cdot \vec{B}_i^a = 0$$

$$\nabla \times B_i^{(a)} = j_i^a = q_i^+ \vec{\alpha} \lambda^a q_i = \frac{3}{4\pi} (\hat{r} \times \vec{\sigma}_i) \lambda_i^a \frac{\mu_i'(r)}{r^3} \quad ; \quad \hat{r} \equiv \frac{\vec{r}}{r} \tag{1.10}$$

where $\mu_r'(r)$ is the scalar magnetization density for a quark of mass m_i in the lowest cavity eigenstate, that $\vec{B}_i^a$ satisfies (1.7) automatically. However, the $E_i^{(a)}$ do not satisfy the cavity boundary condition (1.6), a deficiency most easily remedied by adding the static electric self-energy from Fig. 3b to (1.8) leading to

$$\Delta E_E = \frac{g^2}{2}\sum_a \int_{bag} d^3r \left(\sum_i \vec{E}_i^a(r)\right)\cdot\left(\sum_j \vec{E}_j^a(r)\right) \tag{1.11}$$

Note that

$$\sum_j \vec{E}_j^a(r) = \sum_j \lambda_j^a \frac{\hat{r}}{4\pi r^2}\int_0^{(r)} d^3r'\ \rho_j\ (r')$$

and if we neglect quark mass differences $\rho_j = \rho$, independent of j. Hence

$$\sum_j \lambda_j^a \left|{}^{\text{color}}_{\text{singlet}}\right\rangle = 0 \tag{1.12}$$

so that the boundary condition (1.6) is satisfied since the color charge density vanishes locally.[25]

With these assumptions--in particular the assumption of zero local color separation in a spherical cavity--the electrostatic interaction energy vanishes, and the final expression for the magnetic interaction simplifies to a spin-spin term

$$\Delta E_M = 8\alpha_c\lambda \sum_{i>j}\left(\vec{\sigma}_i\cdot\vec{\sigma}_j\right)\frac{\mu(m_i,R)\mu(m_j,R)}{R^3}\ I(m_iR,\ m_jR) \tag{1.13}$$

where $\lambda = 1$ for a baryon and $= 2$ for a meson; μ is the quark modes' magnetic moment, and I is a mass dependent constant. This interaction splits the π from the ρ mass, and the N from the Δ in the right direction.

The sum of the four contributions to the hadron energy; i.e., (1.3), plus (1.4), plus (1.5), plus (1.13) evaluated in the appropriate spin and flavor state in the spherical static bag is then variationally minimized with respect to the radius R to determine the hadron mass. The spectrum of the ground state baryon [56] and meson [35] together with static properties of these states are then compared[20] with the predictions based on four adjustable constants in Fig. 4 and Table I.

Fitting the data with these ingredients has been a considerable triumph of this MIT bag approach as seen in the next two figures. Note that these results emerge from a lowest order perturbation calculation of the quark-quark spin dependent interaction for which the expansion parameter is determined to be $\alpha_c = 0.55$.

Buoyed by these results, one can press on further to study low-lying excited hadrons for which one quark is in a P-wave excited state and the remainder are in the ground state. In such a study of $1/2^-$ and $3/2^-$ baryons and of 0^+ and 1^+ mesons there are no additional free parameters since all were determined in the fit to the ground state $1/2^+$ and $3/2^+$ baryons and 0^- and 1^- mesons. In this case the study is limited[26] to quarks in $P_{1/2}$ states in a spherical cavity in order to satisfy the boundary conditions, which for the quark field become on the spherical surface

$$\hat{r}\cdot\nabla(\bar{q}q) = -2B$$

and can therefore not be satisfied locally for distributions, such as $P_{3/2}$ states, that are not spherical. Since the calculations are carried out to lowest order in α_c, the quarks are treated as non-interacting in forming the states.

However, there is a problem. If one makes hadrons out of quarks only in $S_{1/2}$ and $P_{1/2}$ modes, one finds that the resulting baryon spectrum contains states which do not exist in nature. These states turn out to be modes where the center of mass of the quarks moves relative to the surface of the bag--so-called translation modes. Such modes are spurious and result from use of

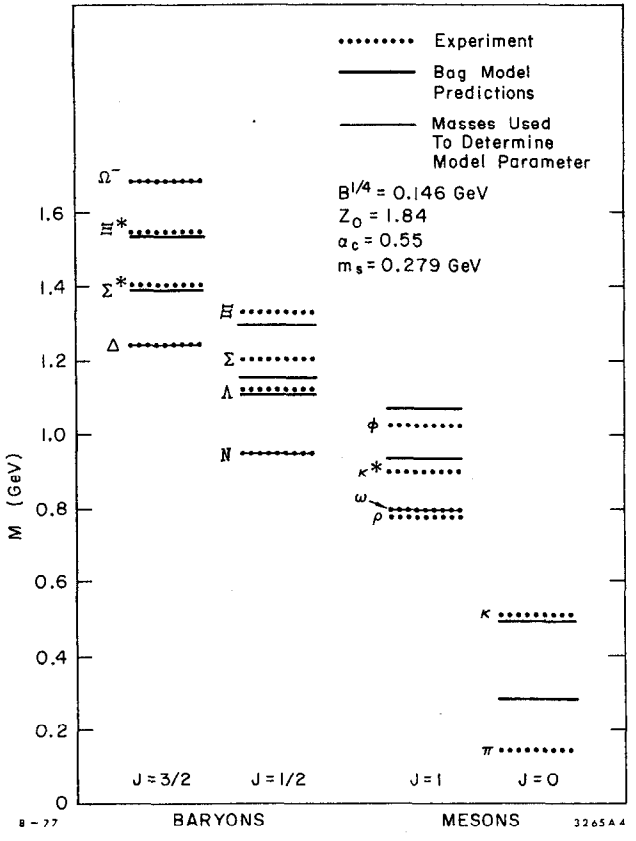

Fig. 4

Table I

		Experiment	MIT Bag
Magnetic Moments	p	2.79	1.9
	n/p	-0.685	-2/3
	Λ/p	-0.240 ± 0.021	-0.255
	Σ^+/p	0.93 ± 0.16	0.97
	Σ^0/p		0.31
	Σ^-/p	-0.53 ± 0.13	-0.36
	Ξ^0/p		-0.56
	Ξ^-/p	-0.69 ± 0.27	-0.23

		Experiment (Cabibbo)	MIT Bag	
			$\Delta s = 0$	$\Delta s = 1$
Axial-Vector Coupling Constant	F	0.41 ± 0.02	0.44	0.47
	D	0.83 ± 0.02	0.65	0.71

		Experiment	MIT Bag
Charge Radii	$\langle r_p^2 \rangle^{1/2}$	0.88 ± 0.03 fm	0.73 fm
	$\langle r_N^2 \rangle^{1/2}$	-0.12 ± 0.01 fm	0 fm

a fixed cavity approximation for the bag. In reality, the quarks may move at will, and the surface of the bag will move to keep them confined: if the quark's center of mass moves, so will the "center" of the bag.

This problem has been discussed by Rebbi.[27] Its resolution involves including $P_{3/2}$ quark modes in the spectroscopy, since the translation modes are eigenstates of orbital angular momentum. However, $P_{3/2}$ modes cannot satisfy the bag boundary condition locally over the surface of the bag. In order to perform the calculations, the boundary condition has to be composed only to achieve a global pressure balance and spherical cavities are used for confinement. The resulting spectrum for the L = 1[70] baryon states of negative parity, built of two quarks in $1S_{1/2}$ cavity eigen modes and the third quark in a linear combination of $1P_{1/2}$ and $1P_{3/2}$ modes is too low as found by deGrand[28] and shown in Fig. 5. Much of the blame for this defect is attributed to the $P_{3/2}$ states whose eigenfrequencies are found to be quite small. Resolution of this difficulty awaits future study that will require going beyond a static spherical cavity approximation.

Next I turn briefly to the problem of deriving bag models from local canonical field theory.[23,24] The fundamental idea is that the vacuum is highly polarized in the presence of quarks. The "bags" themselves are extended, coherent vacuum excitations to which the quarks, which may have an extremely large bare mass, are bound. The mechanism creating the bags in the published models is a scalar Higgs field that develops a non-vanishing expectation value. A non-abelian colored gauge interaction is introduced à la QCD so that the binding to form low mass bag states occurs only when the quarks form color singlet states which are the hadrons. Within the bag the interaction between the quarks is relatively small, i.e., negligible in

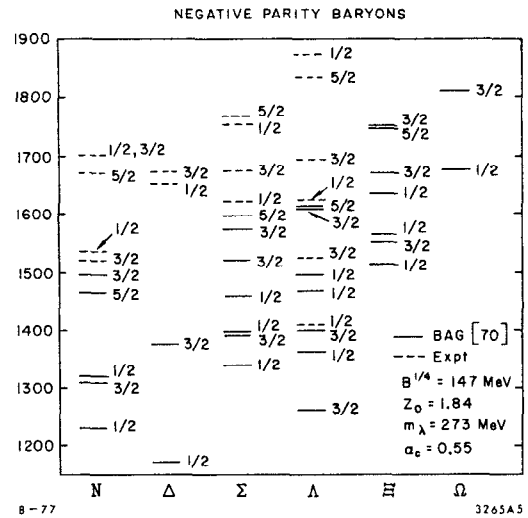

Fig. 5

comparison with the very strong interaction binding the quarks to the bag and forming their wave functions. This gives a picture of hadrons as bound states of two or three almost free quasi-particles from which they derive their SU(3) properties. However there is an energy associated with the size of the bag--or vacuum excitation--containing the quarks which prevents their being separated. In this picture quark trapping may be just an approximate state of affairs at low energy and massive individual colored quarks may be found at higher energies after all.

The mechanism for polarizing the vacuum and forming "bags" is the same one giving rise to the abnormal states in the Lee-Wick theory of uniform nuclear matter.[29] In their example with many particles, a classical treatment with neglect of surface effects is valid. To illustrate this idea, consider the following classical energy expression for a statistical ensemble of N nucleons, each of mass M, plus a scalar field with the self coupling illustrated in Fig. 6.

$$E = \int \rho dV \left[M + g\sigma(x)\right] + \int dV\, U(\sigma)$$

$\rho(x)$ represents the number density of nucleons,

$$N \equiv \int \rho dV$$

and g is a measure of their interaction strength with the field strength σ. The "normal state" of matter is described by setting $\sigma = 0$ so that the field state is at the minimum energy $U(0) = 0$ and the assemblage of nucleons, neglecting surface and kinetic effects (i.e., the height of the fermi surface relative to their mass energy), is

$$E_{normal} = MN = \rho_0 V_0 M$$

in terms of the uniform nucleon density ρ_0 within the volume V_0.

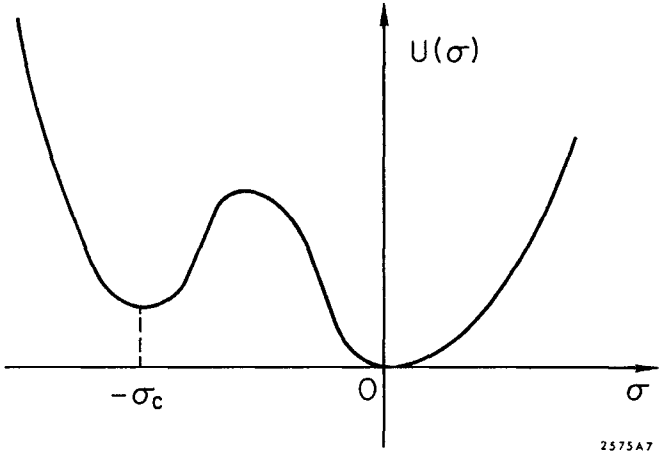

Fig. 6

The "abnormal state" is described by "polarizing the field vacuum" and exciting the field strength $\sigma = -\sigma_c$, the value at the local minimum in Fig. 6 within the volume V_0 of nucleons, i.e.,

$$\begin{aligned} \sigma &= -\sigma_c \qquad \text{inside } V_0 \\ \sigma &= 0 \qquad\quad \text{outside } V_0 \ . \end{aligned} \tag{1.14}$$

The total energy is now given by

$$E_{abnormal} = \rho_0 V_0 (M - g\sigma_c) + U(-\sigma_c)V_0 = E_{normal} + V_0\left[-g\sigma_c\rho_0 + U(-\sigma_c)\right]$$

and evidently at large enough densities ρ_0 the abnormal state (1.14) will be at a lower energy than the normal one.

As these models have been implemented so far the color interaction involving the gluons plays no direct role in the energies and structure of the color singlet states that are the hadrons. This is because the solutions have been constructed by treating the Higgs scalar field and the gauge fields classically and by ignoring the quantum fluctuations in treating the quark in terms of single particle Dirac theory. In particular the single particle energies of quarks trapped in bags vs. free particle quark states are considered but the shift in vacuum energies of the quarks due to the presence of the bag is ignored (i.e. we work in the tree approximation, and normal ordering terms are dropped). The canonical field theory approach to bags shares with the MIT bag model approach the defect that neither is as yet a fully quantized field theory.

Recently T. D. Lee and collaborators[21,24] (R. Friedberg and A. Sirlin) have given a thorough and systematic discussion of these quasiclassical soliton solutions for interacting spinor, scalar, and vector gluon fields. General solutions of the coupled field equations, including the limiting forms reducing to both the MIT and SLAC bag solutions have been described. Friedberg and Lee have also studied the accuracy of the quasiclassical approximation in the two limiting regions where exact answers are known. For fully relativistic theories of interacting spinor-scalar fields in the weak coupling limit the ratio R of exact binding energies to those calculated quasiclassically is

$$R = 1 \qquad \text{when} \quad N \gg 1$$

$$R = 0.77 \qquad \text{when} \quad N = 2$$

where N is the number of fermions bound together. For non-relativistic quark fields, but relativistic scalar fields, they find

$R = 1$ when N is arbitrary and the coupling is strong
or when $N \gg 1$ and the coupling is arbitrary

$R = 0.77$ when $N = 2$ and the coupling is weak.

It remains unknown however how good R is when $N \sim 2$ or 3 as for mesons and baryons, and when the fields are relativistic and the coupling is strong. It is to this question that I now turn. In Appendix A, the quantum corrections are calculated for a special example in 1x - 1t dimension and shown to be large for N = 1 and strong coupling.

QUANTUM FIELD THEORY ON A LATTICE

We shall now formulate quantum field theory on a lattice. Our first reason is to convert quantum field theory to a finite, well defined one without implementing a renormalization program which, in practice, requires an iterative weak coupling expansion in Feynman graphs. Such iterative steps cannot help us in calculating finite physical quantities in the presence of strong interactions. It is a deeper question of whether or not to take the lattice spacing $a \to 0$ in the end, retaining the low lying spectra and long wavelength coherent phenomena that survive this limit. Perhaps there is a fundamental length or structure on a scale that is sufficiently small, $\lesssim$ (few) x 10^{-16} cm, that it has not yet been probed by experiments. This can remain an open question today since we are concerned only with excitations of a few GeV and with structures $\gtrsim 10^{-14}$ cm. Particularly in this lecture I will discuss models leading to coherent "soliton" solutions and phase transitions.

The second reason for going to a lattice is that phase transitions and coherent states have been extensively studied in statistical mechanics and solidstate physics which can provide us with powerful methods and deep insights. The alternative of working in momentum space, as we normally do with Feynman propagators, and simply cutting off the momenta at a $k_{max} \sim 1/a$, the reciprocal of the lattice spacing, is less rich in helpful insights. The question of phase transitions enters naturally into these discussions as shown in Fig. 7. A weak coupling, abelian gauge theory like QED exhibits and describes free electrons and massless quanta. However we seek a strong coupling, non-abelian gauge theory, like QCD, which confines its quarks and vector gluons,

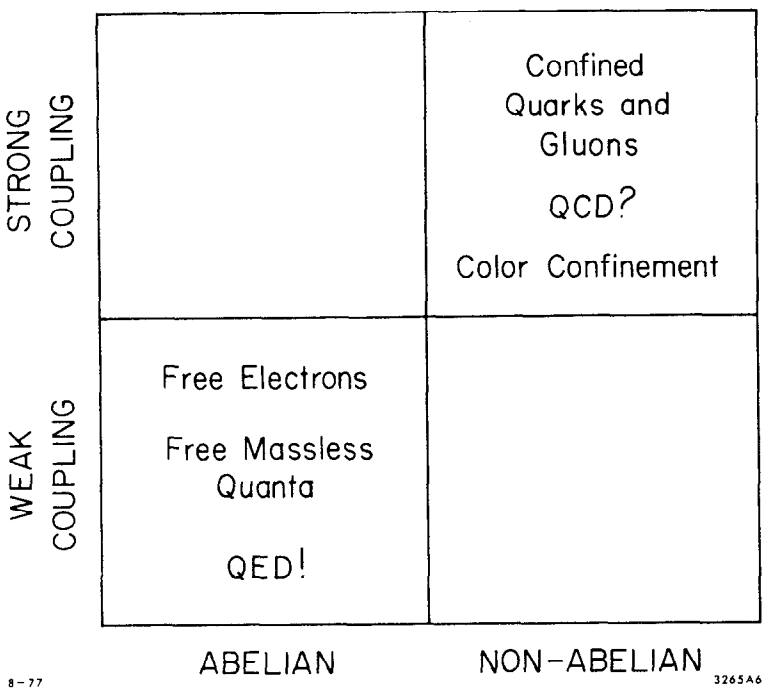

Fig. 7

but which exhibits and describes physical hadrons. Is there a phase transition as we go from weak to strong coupling? or from abelian to non-abelian gauge theories? are both of the above required? or neither, i.e., is there a smooth transition with a typical quark mass characterized by, say,

$$m \sim \left(\frac{1}{a}\right) e^{-1/g^2}$$

$$\sim 10^{-3} \text{ GeV for } g^2 = \frac{1}{137}$$

$$\gg 10 \text{ GeV for } g^2 \gtrsim 1$$

To be useful, the procedure of going onto a lattice should not destroy symmetries of the theory. This means we require internal symmetries such as local gauge invariance and chiral symmetry to remain exact. Those derived from the homogeneity and isotropy of space, i.e., Lorentz and Poincaré invariance, will be lost because there are now only discrete symmetries on the lattice. But we require relativistic results for spectra, say, in the low energy region as well as in the $a \to 0$ limit.

Let us first transcribe the gradient operator and then its gauge invariant form to a discrete lattice. For simplicity in writing I will use the notation of a one-dimensional spatial lattice; its generalization to three dimensions causes no problem. Time will be treated as a continuous variable, since I am constructing a Hamiltonian formalism, although formulations putting time on a discrete lattice have also been developed and give no special difficulties.

The continuum variable x is replaced by a discrete lattice of length L and spacing $a \equiv 1/\Lambda$ defined so that there are $(2N + 1)$ points:

$$L = (2N + 1)a \tag{2.1}$$

With periodic boundary conditions, the allowed momenta on the lattice are

$$k = \frac{2\pi}{L} n \qquad n = 0, \pm 1, \ldots \pm N \tag{2.2}$$

and

$$k_{max} = \frac{2\pi}{L} N. \tag{2.3}$$

The volume integral then becomes simply a sum over lattice points:

$$\int dx \to \frac{1}{\Lambda} \sum_{j=-N}^{N} \tag{2.4}$$

The fields and canonical momenta are defined at discrete lattice points and their fourier expansion includes a finite number of modes up to k_{max}:

$$\psi(x) \to \psi_j = \sum_{k=-k_{max}}^{+k_{max}} e^{ikj/\Lambda} \psi(k)$$

$$\psi_k = \frac{1}{2N + 1} \sum_j \psi_j e^{-ikj/\Lambda} \tag{2.5}$$

The lattice version of the canonical (anti-) commutator relations is

$$\left[\Pi_j, \psi_{j'}\right] = -i\Lambda\delta_{jj'} \tag{2.6}$$

The simplest and most direct definition of the gradient on the lattice is as a difference operator

$$\nabla\psi(x) \to \Lambda\left[\psi_{j+1} - \psi_j\right] \tag{2.7}$$

This gives for the kinetic energy term in the Hamiltonian of a scalar field

$$\frac{1}{2}\int dx (\nabla\psi)^2 \to \frac{L}{2} \sum_k \psi^+(k)\psi(k) \left\{4\Lambda^2 \sin^2 \frac{k}{2\Lambda}\right\} \tag{2.8}$$

which reduces to the usual quadratic in k for $k/2\Lambda \ll 1$, and for all k gives the connection between energy and momentum for a free particle of mass m:

$$E(k) = \sqrt{m^2 + 4\Lambda^2 \sin^2 \frac{k}{2\Lambda}} \tag{2.9}$$

As illustrated this is a very good approximation to the correct dispersion relation for $k/2\Lambda < 1$ and deviates up near the max where $k_{max}/2\Lambda = \pi/2$, giving the familiar band structure of solids (Fig. 8).

There is however a problem[19a,b] in applying (2.7) to a theory of quarks described by spin 1/2 Dirac fields in that (2.8) is replaced by a first derivative expression which when properly hermitized becomes

$$-i\int dx\, \psi^+(x)\alpha\nabla\psi(x) = -\frac{i}{2}\int dx \left\{\psi^+(x)\alpha\nabla\psi(x) - \left[\nabla\psi^+(x)\right]\alpha\psi(x)\right\} \\ \rightarrow L\sum_k \psi^+(k)\alpha\psi(k)\cdot\left\{\Lambda \sin\frac{k}{\Lambda}\right\} \tag{2.10}$$

With this form for momentum given by (2.10) the energy-momentum dispersion relation becomes for a free Dirac particle, instead of (2.9),

$$E_D(k) = \sqrt{m^2 + \Lambda^2 \sin^2 \frac{k}{\Lambda}} \tag{2.11}$$

which has again the correct $k/\Lambda << 1$ limit but which leads to a doubling of states of a given energy as illustrated by Fig. 8.

This difficulty is readily resolved by defining the gradient on the lattice to be the operator multiplying the fourier amplitude by ik and thereby assuring that in both cases of spin 0 and of spin ½ fermions (2.9) and (2.11) are replaced by the correct relativistic relation

$$E(k) = \sqrt{m^2 + k^2} \qquad |k| < k_{max} = \frac{2\pi N}{L}$$

On the lattice this definition reads

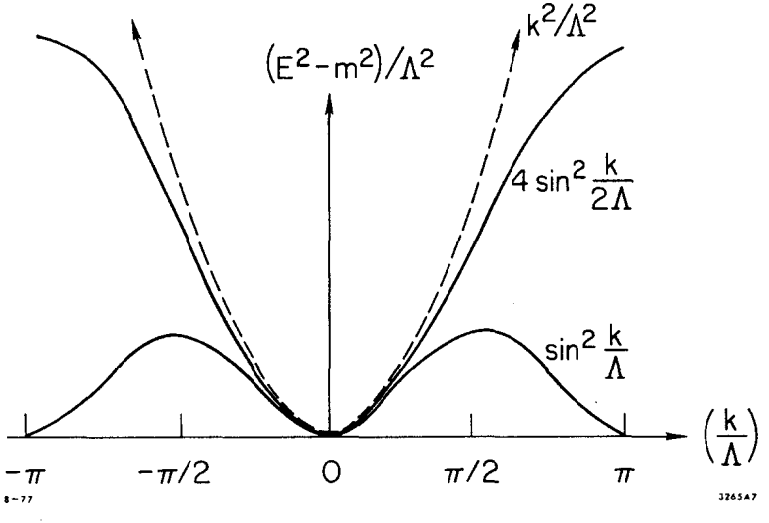

Fig. 8

$$(\nabla\psi)_j \equiv \sum_k ik\, e^{ikj/\Lambda}\, \psi(k)$$

$$= \sum_{j'} \psi_{j'} \left\{ \frac{1}{2N+1} \sum_k e^{ik(j-j')/\Lambda}\, ik \right\} \qquad (2.13)$$

$$\equiv \Lambda \sum_{j'} \psi_{j'} \left[-\delta'(j - j') \right]$$

As defined, for $N \to \infty$

$$\delta'(j - j') = \frac{-(-)^{j-j'}}{(j-j')} \qquad j \neq j'$$

$$= 0 \qquad j = j' \qquad (2.14)$$

and shows that the gradient couples sites all along the lattice. For completeness I record the analogous result in 3 dimensions

$$\delta'(\overrightarrow{j - j'}) = \delta'(j_x - j'_x)\, \delta_{j_y, j'_y}\, \delta_{j_z, j'_z} \qquad (2.15)$$

to show that it remains simple.

Next we must form a gauge invariant derivative - i.e., introduce gauge fields while preserving local gauge invariance on the lattice. In continuum QED, local gauge invariance leads to a differential law of current conservation; i.e., locally at any point the time rate of change of the charge density equals the negative of the divergence of the current density from that point. The formal expression of the underlying local gauge invariance is this: in the Lagrangian or Hamiltonian of the theory there appear only the fields themselves

$$\text{viz.} \quad \frac{1}{4} F_{\mu\nu}\, F^{\mu\nu} \qquad (2.16)$$

or interaction terms formed gauge invariantly

$$\text{viz.} \quad \frac{1}{i} \psi^+(x)\, \vec{\alpha} \cdot \left(\vec{\nabla} - ie\vec{A}(x) \right) \psi(x)$$

which is invariant under

$$\psi(x) \to e^{ie\chi(x)} \psi(x)$$

$$\vec{A} \to \vec{A} + \vec{\nabla}\chi(x) \qquad (2.17)$$

On the lattice we have no local divergence of the current but can speak only of the (color) charge being moved in a discrete step from one lattice site to the next and so on. Indeed by (2.13) and (2.14) the lattice gradient moves a particle along the entire lattice chain (in the direction of the component of the gradient by (2.15)). To preserve local color charge conservation—and the asymptotic freedom idea—evidently the gauge field must be defined on the links joining the lattice sites if we are to avoid discontinuous steps of color charge disappearing from one lattice point and appearing on another one. This is the formulation of K. Wilson and of A. Polyakov,[17] who independently introduced the lattice theory with gauge fields thus defined as the oriented links or strings between nearest neighbor lattice points. In the language of abelian QED the operator representing a gauge field must transform like a field with charge +1 at the starting point of the link and with charge -1 at the final end point. If we start with a quark of charge +1 at lattice point j and wish to move it to the next point j+1, gauge invariance requires that a unit bit of string be created pointing from j to j + 1. This is the operator $U(\ell_{j,\, j+1})$ which transforms like a field with charge +1 at j and -1 at j + 1. This process is illustrated as follows in Fig. 9. The simplest gauge invariant expression expressing this transition is

$$\bar{\psi}_j\, U(\ell_{j,j+1}) \psi_{j+1} \qquad (2.18)$$

Fig. 9

if under the local gauge transformation,

$$\bar{\psi}_j \to \bar{\psi}_j \, e^{-ie\chi(j)}$$
$$\psi_{j+1} \to e^{ie\chi(j+1)}\psi_{j+1} \tag{2.19}$$

we also stipulate

$$U(\ell_{j,j+1}) \to e^{ie\chi(j)} \, U(\ell_{j,j+1}) e^{-ie\chi(j+1)} \tag{2.20}$$

Thus the form of U such that (2.17) carries over to the lattice for nearest neighbor points is

$$U(\ell_{j,j+1}) = e^{ieaA(\ell_{j,j+1})} \tag{2.21}$$

$$\text{with } A(\ell_{j,j+1}) \to A(\ell_{j,j+1}) + \frac{1}{a}\left\{\chi(j) - \chi(j+1)\right\} \tag{2.22}$$

under a gauge transformation. Equation (2.21) is the lattice form of the exponential of a line integral from j to j + 1. To transport charge over a succession of links we write the ordered product

$$U(j_1,j_2) = \prod_{j_1<\ell<j_2} U(\ell) \tag{2.23}$$

and observe that with the convention

$$A(\ell_{1,2}) = -A(\ell_{2,1}) = -A(-\ell_{1,2})$$

we have

$$U(\ell_{1,2}) = U^+(\ell_{2,1}) = U^+(-\ell_{1,2}) \tag{2.24}$$

We can now write the gauge invariant extension of (2.16) to the lattice as

$$\sum_{j_1<j_2} \psi^+_{j_1} \alpha\left\{\frac{i\delta'(j_1-j_2)}{a}\right\} U(j_1,j_2)\psi_{j_2} + \sum_{j_1>j_2} \psi^+_{j_1} \alpha\left\{\frac{i\delta'(j_1-j_2)}{a}\right\} U^+(j_2,j_1)\psi j_2\Bigg] \tag{2.25}$$

and observe that in the continuum limit $a \to 0$, (2.25) reduces[30] to (2.17).

For a non-abelian gauge theory the analogue to (2.21) is

$$U(\vec{\ell}) = e^{ig \sum_{\alpha} \lambda_{\alpha} \vec{A}_{\alpha}(\ell) \cdot \vec{\ell}} \tag{2.26}$$

where the λ_{α} are the c-number matrices belonging to a specific $(N\bar{N})$ representation of the gauge group, par ex. the 8 hermitian generators of SU(3). The ordered product construction of (2.23) applies also in this case. In the lattice formulation the unitary operators (2.21) and (2.26) defined on lattice links (as illustrated in Fig. 9) replace the gauge field $\vec{A}_{\alpha}$ appearing in (2.16) in the continuum theory.

Local gauge invariance requires that new string bits be created for each increased unit of separation of a particle q and anti-particle $\bar{q}$ on the lattice. If each string bit has a finite mass (corresponding to finite field energy) the mass of a gauge invariant state increases without bound as the separation between q and $\bar{q}$ grows; this behavior corresponds to confinement. What we must establish is that the lattice gauge theory we have formulated when applied to weak coupling abelian QED in 3x-1t dimensions does not confine; but does confine for non-abelian QCD and strong coupling.

Nothing like this has been accomplished yet. Calculations so far by Wilson[17] and by Kogut and Susskind and collaborators[18] have been iterative strong coupling treatments and contain approximations that make it impossible to judge the content of the theory independent of the validity of the calculational techniques. The problem at this time is to develop calculational methods that one can trust so that the result of calculating mass spectra in QCD will equally well destroy the theory if they fail to reproduce the observed spectra as they will confirm it if they do! No weaseling out! Wilson's 1975 result from his strong coupling expansion is a nucleon mass of 1720 MeV with a large lattice spacing of $1/5 \times 10^{-13}$ cm. The Padé extension of strong coupling calculations by Kogut, Susskind and collaborators gives a π/N mass ratio of .82 instead of .15 and contains difficulties related to the use of (2.7) for the gradient together with a compensating point splitting prescription to avoid the difficulty in (2.11). These efforts and our local ones[19] are proceeding—it is slow and difficult work. Neither simplifying extreme of very weak or strong coupling approximations is adequate. I wish here to describe the methods we are exploiting and validating by solving simple models with known exact properties against which we can improve our understanding and approximations. We believe the basic problem that must be solved first is that of developing simple, understandable, intuitive techniques of calculation with which to arm oneself before undertaking the assault on the real physics problem.

TRANSVERSE ISING MODEL

The transverse Ising model in 1-space, 1-time dimension describes an array of spins with nearest neighbor interactions in the presence of a constant transverse magnetic field and is an interesting example on which to test methods for two reasons:

1) There are a finite number of states for the spin degree of freedom (up or down) at each lattice site in common with spin 1/2 quark theories (in 1-x dimension there are four states at each site for each color of quark: 0, q, $\bar{q}$ and $q\bar{q}$).

2) The exact solution of this model is known[31] and calculations can be compared with exactly computed critical indices and temperatures of the known phase transition.

The Ising model Hamiltonian represents an approximation to the ϕ^4 field theory in the 1x-1t dimension if we are far into the spontaneously broken symmetry region with strong coupling. To see this we write this theory on the lattice in terms of dimensionless canonical variables, and using the nearest neighbor gradient[32]

$$\frac{1}{\Lambda} H = \sum_{j=-N}^{N} \left[\frac{1}{2} p_j^2 + \lambda_0 \left(x_j^2 - f_0^2 \right)^2 \right] + \sum_{j=-N}^{N-1} \frac{1}{2} \left(x_{j+1} - x_j \right)^2$$

$$x_j \equiv \psi_j \qquad (2.27)$$

$$p_j \equiv \frac{1}{\Lambda} \pi_j \qquad \left[x_j, p_{j'} \right] = i\delta_{jj'},$$

The lowest two eigenlevels of the single-site Schrödinger problem (neglecting the coupling between two neighboring sites j and j + 1 in the gradient term) lie deep in the potential well if the zero point energy is very small compared with the height of the center bump; i.e.,

$$\lambda_0^{\frac{1}{2}} f_0 << \lambda_0 f_0^4 \qquad (2.28)$$

These two low lying levels are, respectively, symmetric and antisymmetric under reflection as shown in Fig. 10. The energy gap between them is proportional to the tunneling between the two minima in the double-bottomed potential $\lambda_0 \left(x_j^2 - f_0^2 \right)^2$ at $\pm f_0$. Since (2.28) means that there is very little tunneling this gap is very small— i.e.,

$$\Delta\varepsilon_{gap} \sim \lambda_0^{\frac{1}{2}} f_0 \, e^{-\lambda_0^{\frac{1}{2}} f_0^3} << \lambda_0^{\frac{1}{2}} f_0 \qquad (2.29)$$

if $\lambda_0^{\frac{1}{2}} f_0^3 >> 1$. When conditions (2.28) and (2.29) are satisfied we can neglect higher excitations at each lattice site. The two states retained correspond to the spin down and up configurations in the Ising model. The gradient term

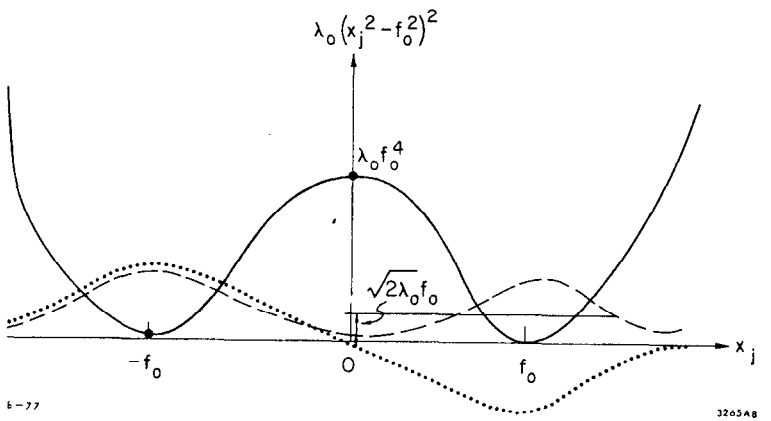

Fig. 10

induces mixing between the symmetric and antisymmetric solutions which is approximately given by

$$\langle \text{sym} \,|x_j|\, \text{antisym}\rangle^2 \approx f_0^2 \equiv \Delta_0 \tag{2.30}$$

When this mixing is comparable to the gap separating the levels—i.e., for

$$\lambda_0^{\frac{1}{2}} f_0 \, e^{-\lambda_0^{\frac{1}{2}} f_0^3} \approx \Delta_0 = f_0^2 \tag{2.31}$$

the gradient term is comparable to the single site terms and we can make neither a weak nor strong coupling limiting approximation. Condition (2.31) requires $f_0^2 << 1$, $\lambda_0 >> 1$, consistent with $\lambda_0^{\frac{1}{2}} f_0^3 >> 1$.

The explicit form of the Hamiltonian in this approximation can be written in terms of Pauli matrices

$$\frac{1}{\Lambda} H = \sum_{j=-N}^{N} \left\{ \frac{1}{2} \varepsilon_0 \, \sigma_z(j) \right\} - \sum_{j=-N}^{N-1} \Delta_0 \, \sigma_x(j) \, \sigma_x(j+1) \tag{2.32}$$

which is just the transverse Ising model. Looking back at (2.27) we see the value of configuration space methods in studying strong coupling problems in field theory. For large λ_0 the character of the solutions is determined by the potential term and so it makes sense to start in a representation or language that diagonalizes this part of the Hamiltonian. This is what we do in configuration space by expressing H as a sum of single site Schrödinger problems, with the "relatively" small gradient term providing the coupling between different sites. Such couplings can be treated iteratively in this limit. The spectrum of eigenstates at each site is identical. The eigenstates of H are then characterized by specifying the different individual levels of excitation populated at each site. Barring additional degeneracies arising for specific values of λ_0 and f_0^2, the first excited state will be $(2N + 1)$-fold degenerate corresponding to having the excited level at any one of the lattice sites. When the gradient terms are included in H, their effect is to lift this degeneracy; they also mix these states in general with the ground state and with the more-highly-excited spectrum. It is when these gradient-induced splittings are small relative to the spacing between the single-site excited states that the site basis is expected to provide a reasonable picture of the true ground state. In contrast for weak couplings, we want to treat the gradient exactly and this we accomplish by working in momentum space in terms of which the gradient is diagonal and a propagator formalism is then useful for iterating the relatively weak potential terms.

Important features of the solution to (2.32) can be learned from studying its limiting behavior for $\varepsilon_0/\Delta_0 \to \infty$ (strong coupling) and $\varepsilon_0/\Delta_0 \to 0$ (weak coupling). In the strong coupling limit, $\varepsilon_0/\Delta_0 \to \infty$, (2.32) describes an assembly of noninteracting spins that all line up with spin down in the nondegenerate ground state

$$|0\rangle = \prod_j \begin{pmatrix} 0 \\ 1 \end{pmatrix}_j \tag{2.33}$$

of energy density (in units of Λ) $E_0\left(\Delta_0/\varepsilon_0 \to 0\right) = -\varepsilon_0/2$. The particle-like excitations lie $+\varepsilon_0$ above the ground state for each site excited to the spinup configuration, $\begin{pmatrix} 1 \\ 0 \end{pmatrix}_j$. In the opposite, or weak coupling extreme, $\varepsilon_0/\Delta_0 \to 0$, the eigenstates

$$|\Rightarrow\rangle_j \equiv \frac{1}{\sqrt{2}} \begin{pmatrix} 1 \\ 1 \end{pmatrix}_j \tag{2.34}$$

and

$$|\Leftarrow\rangle \equiv \frac{1}{\sqrt{2}} \begin{pmatrix} 1 \\ -1 \end{pmatrix}_j \tag{2.35}$$

diagonalize the Hamiltonian. The ground state is doubly degenerate, being formed as a product of states (2.34) at each site, or all states (2.35) at each site. For each "wall" between two adjacent sites, one formed as (2.34) and the other reversed as (2.35), there is an excitation of $+2\Delta_0$ units of energy. In this extreme the excitations are kink-like as illustrated by Fig. 11. These low lying excitations in the weak coupling limit correspond to collective "kink" states rather than single particle excitations.

From a study of the exact H, (2.32), it is known[31] that a second order phase transition occurs between the nondegenerate ground state (2.33) and the degenerate configurations (2.34) and (2.35). The transition occurs when $\varepsilon_0 = 2\Delta_0$. The behavior of the order parameter, or "magnetization," in this model is given by

$$\langle \sigma_x \rangle = \begin{cases} \left[1 - \left(\varepsilon_0/2\Delta_0\right)^2\right]^{1/8} & \text{for } \dfrac{\varepsilon_0}{2\Delta_0} \lesssim 1 \\ 0 & \text{for } \dfrac{\varepsilon_0}{2\Delta_0} > 1 \end{cases} \tag{2.36}$$

It is these exact results that we must reproduce by a simple and direct calculational procedure that lends itself to generalization to 4-dimensional gauge theories. Our approach is as follows:

1) Divide the lattice into small blocks containing several adjacent sites, as illustrated in Fig. 12 for two-site blocks. Within each block diagonalize the two site Hamiltonian; viz. for (2.32)

$$H_{(1)} = \frac{\varepsilon_0}{2}\left[\sigma_z(1) + \sigma_z(2)\right] - \Delta_0\, \sigma_x(1)\, \sigma_x(2) \tag{2.37}$$

which has $2^2 = 4$ eigenstates[33] that can be determined exactly.

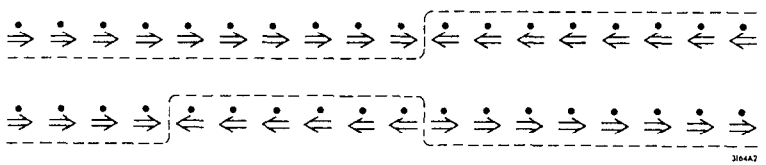

Fig. 11

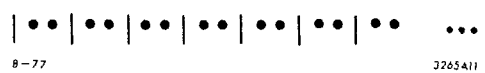

Fig. 12

2) "Thin" the degrees of freedom by a truncation procedure which amounts simply to keeping a suitable subset including the lowest lying of these eigenstates and discarding the higher excitations. This is equivalent to a variational solution using a trial form that spans a subset of the full Hilbert space and constructing an effective truncated Hamiltonian. Our simplest algorithm for (2.37) is simply to keep the two lowest of its four eigenstates. Part of the motivation of our work with this model is to learn by experience the ingredients of accurate algorithms.

3) We then iterate this procedure, including thereby more terms in the gradient that couple different lattice sites by forming neighboring blocks: two neighboring blocks into superblocks in the example in Fig. 13. The two retained eigenstates from the original blocking form a block basis in terms of which to express the Hamiltonian. In this simple example we again find a spin form since there are 2 eigenstates at each block site; but the effective coupling strengths, block spacings, and energy intervals are renormalized.

4) We repeat the same steps successively, continually eliminating the higher excitations. We can think of this procedure as successively eliminating higher momentum states in constructing the series of truncated Hamiltonians to describe the physics of the low momentum states alone.

5) The iterative steps are continued until the successive rescaling leads to a soluble problem, either in the weak or strong coupling regime, for the treatment of the remaining coupling terms

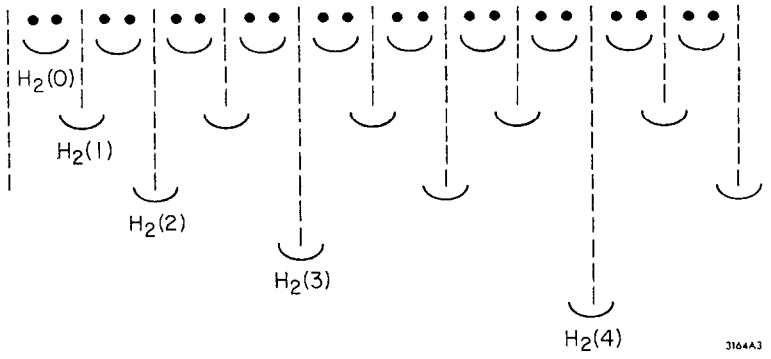

Fig. 13

between different blocks contained in the gradient term.

Applying this procedure to (2.37) we note that within one block of two adjacent sites there are four independent states which we denote by $|\uparrow\uparrow\rangle$, $|\uparrow\downarrow\rangle$, $|\downarrow\uparrow\rangle$, and $|\downarrow\downarrow\rangle$, where $|\uparrow\uparrow\rangle \equiv |\uparrow\rangle_1 |\uparrow\rangle_2$, etc. The problem of diagonalizing the 2-site Hamiltonian reduces simply to one of diagonalizing two 2 x 2 matrices, since $|\downarrow\downarrow\rangle$ mixes only with $|\uparrow\uparrow\rangle$, and $|\downarrow\uparrow\rangle$ with $|\uparrow\downarrow\rangle$. The eigenstates and eigenvalues are simply found and are given in Table II. Step (i) of our general procedure will be to choose this set of four eigenstates as the new orthonormal system which we will use to construct a basis for H. Step (ii), the thinning out procedure, is simply accomplished by retaining only the two lowest energy states in Table II for each box when we add back the terms linking different boxes in (2.37). It is reasonable to expect that the most important part of the true ground state will be in the subspace spanned by these two states in each box. In order to implement this approximation we need only construct the truncated or effective Hamiltonian for this choice of trial states and see if we can solve it.

To compute $H^{(tr)}$ we label each 2-site box by an integer 'p' and divide the Hamiltonian into two parts, H_1 and H_2. H_1 contains only those terms in (2.37) which refer to single boxes and H_2 contains the remaining interaction terms in (2.37) which couple sites in adjacent boxes; i.e.,

$$H_2 = -\Delta_0 \sum_p \sigma_x\,(p,1)\;\sigma_x\,(p+1,0) \tag{2.38}$$

where $\sigma_x(p,\alpha)$ operates on the spin in box p and at site $\alpha = 0, 1$ within each box. In keeping with our approximation of retaining only the two lowest states in each box, the truncated $H_1^{(tr)}$ can be written as a sum of 2 x 2 matrices operating on the two states we keep for each box. In particular

Table II

State	Energy	Energy Relative to Lowest State
$\frac{1}{\sqrt{1+a_0^2}}(\lvert\downarrow\downarrow\rangle+a_0\lvert\uparrow\uparrow\rangle)^* \equiv \lvert\psi_0\rangle$	$-\sqrt{\varepsilon_0^2+\Delta_0^2}$	0
$\frac{1}{\sqrt{2}}(\lvert\uparrow\downarrow\rangle+\lvert\downarrow\uparrow\rangle) \equiv \lvert\psi_1\rangle$	$-\Delta_0$	$\sqrt{\varepsilon_0^2+\Delta_0^2}-\Delta_0$
$\frac{1}{\sqrt{2}}(\lvert\downarrow\uparrow\rangle-\lvert\uparrow\downarrow\rangle)$	$+\Delta_0$	$\sqrt{\varepsilon_0^2+\Delta_0^2}+\Delta_0$
$\frac{1}{\sqrt{1+a_0^2}}(-a_0\lvert\downarrow\downarrow\rangle+\lvert\uparrow\uparrow\rangle)$	$+\sqrt{\varepsilon_0^2+\Delta_0^2}$	$2\sqrt{\varepsilon_0^2+\Delta_0^2}$

$^*a_0 = \left(\sqrt{\varepsilon_0^2+\Delta_0^2}-\varepsilon_0\right)/\Delta_0$.

referring to Table II we see that $H_1^{(tr)}$ can be written as

$$H_1^{(tr)} = \sum_p \begin{pmatrix} -\Delta_0 & 0 \\ 0 & -\sqrt{\varepsilon_0^2+\Delta_0^2} \end{pmatrix}_{(p)}$$

$$= \sum_p \left\{ -\frac{1}{2}\left[\Delta_0 + \sqrt{\varepsilon_0^2+\Delta_0^2}\right]\mathbb{1}_{(p)} + \frac{1}{2}\left[\sqrt{\varepsilon_0^2+\Delta_0^2}-\Delta_0\right]\sigma_z(p)\right\} \tag{2.39}$$

The eigenstates of (2.39) can be written as products over boxes of the two lowest eigenstates in Table II; i.e.,

$$\lvert\Psi_1\rangle = \prod_{\text{boxes } p} \lvert\psi(p)\rangle \tag{2.40}$$

Hence the interaction (2.38) can now be re-expressed in terms of the truncated basis (2.40) by evaluating its matrix elements for flipping one "spin" in each of two adjacent boxes. To compute this we take the matrix element of $\sigma_x(p,1)$ between the states

$$\lvert\psi_0(p)\rangle = \frac{1}{\sqrt{1+a_0^2}}\left\{\lvert\downarrow\downarrow\rangle + a_0\lvert\uparrow\uparrow\rangle\right\} \tag{2.41}$$

and

$$\lvert\psi_1(p)\rangle = \frac{1}{\sqrt{2}}\left\{\lvert\downarrow\uparrow\rangle + \lvert\uparrow\downarrow\rangle\right\} \tag{2.42}$$

The actual computation is quite trivial:

$$\sigma_x(p,1)\lvert\psi_0(p)\rangle = \frac{1}{\sqrt{1+a_0^2}}\left[\lvert\downarrow\uparrow\rangle + a_0\lvert\uparrow\downarrow\rangle\right]_p \tag{2.43}$$

and so

$$\langle\psi_1(p)\rvert\sigma_x(p,1)\lvert\psi_0(p)\rangle = \frac{1+a_0}{\sqrt{2(1+a_0^2)}} \tag{2.44}$$

Similarly

$$\langle\psi_1(p+1)\rvert\sigma_x(p+1,0)\lvert\psi_0(p+1)\rangle = \frac{1+a_0}{\sqrt{2(1+a_0^2)}} \tag{2.45}$$

It follows from this that for 'j' in the p^{th} box, and for both cases $\alpha = 0$ and 1,

$$\sigma_x^{(tr)}(j) = \frac{1+a_0}{\sqrt{2(1+a_0^2)}}\sigma_x(p)$$
$$\sigma_x^{(tr)}(j+1) = \frac{1+a_0}{\sqrt{2(1+a_0^2)}}\sigma_x(p+1) \tag{2.46}$$

We can now rewrite our effective Hamiltonian for the two site box. Since our truncation procedure retained just two states per box we again have a spin form for the truncated Hamiltonian. $H^{(tr)}$ has exactly the same form as the original Hamiltonian but different coefficients:

$$H^{(tr)} = \sum_p \left[C_1 \begin{pmatrix} 1 & 0 \\ 0 & 1 \end{pmatrix}_p + \frac{1}{2}\varepsilon_1 \begin{pmatrix} 1 & 0 \\ 0 & -1 \end{pmatrix}_p - \Delta_1 \begin{pmatrix} 0 & 1 \\ 1 & 0 \end{pmatrix}_p \begin{pmatrix} 0 & 1 \\ 1 & 0 \end{pmatrix}_{p+1} \right] \tag{2.47}$$

where

$$C_1 = -\frac{1}{2}\left(\Delta_0 + \sqrt{\varepsilon_0^2 + \Delta_0^2}\right)$$

$$\varepsilon_1 = \sqrt{\varepsilon_0^2 + \Delta_0^2} - \Delta_0 \tag{2.48}$$

and

$$\Delta_1 = \frac{\Delta_0 (1 + a_0)^2}{2(1 + a_0^2)}$$

At this point we face one of two possibilities. Either the values of ε_1 and Δ_1 are such that we can treat the resulting effective Hamiltonian, $H^{(tr)}(1)$ by perturbation theory for $\varepsilon_1/\Delta_1 > 1$ or $\varepsilon_1/\Delta_1 < 1$; or, we may repeat the same procedure that we just went through, but this time combining neighboring pairs of blocks p in the Hamiltonian $H^{(tr)}$ and thereby including additional interaction terms in a new basis to which we again apply the same state-thinning steps as in (2.38) to (2.47). One readily sees in the comparison of (2.47) with the original (2.37) that each successive restriction of our class of trial wave functions by this procedure leads us to a new effective Hamiltonian of the same <u>form</u> as the original Hamiltonian, and with the coefficients of the effective Hamiltonian given by (2.48) in terms of the coefficients found in the preceding step of the calculation.

The details of this procedure and its systematic improvement with more sophisticated and general, but nevertheless very simple, truncation steps are discussed in Ref. (19c). For these lectures I will simply summarize the more salient features: We define the ratio after n iterations

$$y_n \equiv (\varepsilon/\Delta)_n$$

and study

$$R(y_n) \equiv y_{n+1} - y_n \tag{2.49}$$

in order to see whether with successive iterations this ratio decreases, driving us to the weak coupling or gradient-dominant limit, or whether it increases driving us to the strong coupling limit. R(y) is plotted schematically in Fig. 14. This figure shows that there are three fixed points in our procedure of generating new effective Hamiltonians in successive steps (called a "renormalization group transformation" by Wilson and Kadanoff); namely, at $y = 0$, $y = \infty$, and $y_c = 2.55\ldots$. At fixed points, the ratio $y \equiv \varepsilon/\Delta$ does not change as the iteration process is continued and so H^{tr} changes only by an overall scale. When $R(y) = 0$ we have a fixed point. There is also a fixed point if $y = \infty$ and $R(\infty) > 0$ so that this value cannot be reduced. Whenever $R(y) < 0$ the ratio $(\varepsilon/\Delta) = y$ decreases for that iteration and so the new (ε'/Δ') lies to the left of the y we started with. Since, as shown in Fig. 14, R(y) is negative for all $y < y_c = 2.55$ we see that if we start at any point in this range, successive iterations of our truncation procedure will drive us to a form for the effective Hamiltonian which is the weak coupling perturbation theory limit. On the other hand, for $y > y_c$ successive iterations drive us to $y = \infty$ since, in this case, $R(y) > 0$. This implies $\varepsilon/\Delta \gg 1$ which is the strong coupling limit of the Hamiltonian. Hence those theories described by (2.37) for which the initial $y < y_c$ are theories with a degenerate ground state and spontaneously broken symmetry as described earlier. On the other hand, for $y > y_c$ we have a unique ground state. Clearly y_c is the point at which the nature of the ground state changes, and so y_c is the <u>critical point</u> of this theory.

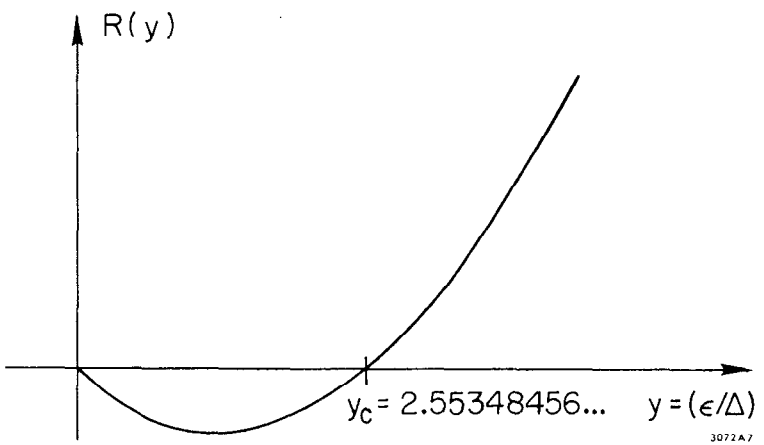

Fig. 14

The result $y_c = 2.55 \ldots$ which is obtained from our simple procedure is not far from the exact transition point $y_c^{exact} = 2$ discussed above (2.36). The fixed points $y = 0$ and $y = \infty$ are the stable fixed points of this renormalization group transformation, and the fixed point at $y = y_c$ is an unstable fixed point. The fact that at $y = y_c$ the Hamiltonian continues to reproduce itself up to a scale factor says that at this critical point the physics going on at different length scales is essentially the same.

One can further discuss the order parameter (2.36) which we find with the above procedure to have a critical index of 0.39 instead of the exact result of 1/8. The simple modification of replacing a_0, as defined in Table II by our truncation procedure, by a variational parameter $a(\epsilon/\Delta)$ determined at the end of the iteration to minimize the energy reduces the calculated value to 1/5. The comparison of the ground state energy density computed this way and the exact energy is shown in Fig. 15. The worst disagreement is 3%. This can be readily reduced further.[34] Discontinuities in the ground state energies are also well reproduced by this procedure as described elsewhere.[19c]

Abstracting from this model we see that study of R(y), which gives the change in the ratio of the single site potential terms in the theory to the gradient terms coupling neighboring sites, teaches a great deal about what we want to learn from the study of gauge theories and confinement. Let us consider such theories with only one coupling constant--i.e., one single site potential term in the theory--which is the strength of the coupling between the quarks and gluons. Then with y defined as above as the ratio of the strength of the single-site coupling to the gradient term, we can plot the general form of the function R(y) = (change of y in finite number of iterations)

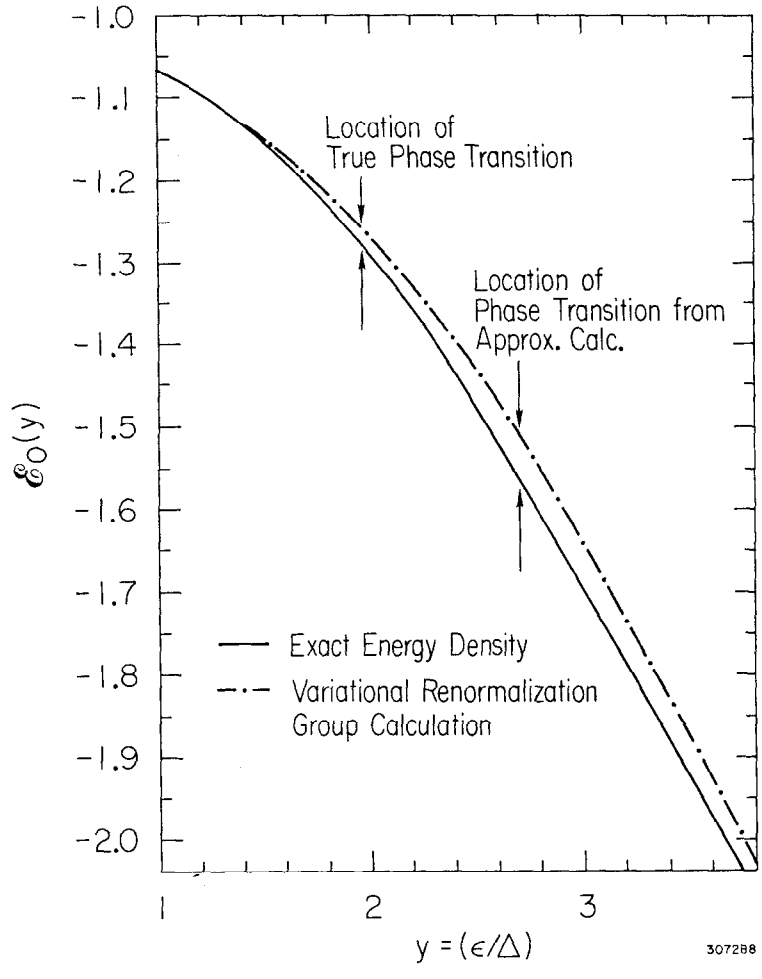

Fig. 15

as in (2.49). A few examples of simple forms for R(y) are given in Figs. 16a-16c and lead to different conclusions about the theories they are assumed to characterize.

In Fig. 16a we see that $R(y) \geq 0$ for all values of $0 \leq y \leq \infty$. If a theory has this form for R(y) we can conclude two things. First, the points $y = 0$ and $y = \infty$ are the only fixed points of the theory. The Hamiltonian at $y = 0$, i.e., zero coupling constant, is a "free field theory," and can presumably be solved exactly. The $y = \infty$ Hamiltonian becomes the single site Schrödinger problem with neglect of the gradient terms. Second, we observe that if we start at some finite value of y successive iterations drive us to larger value of y; i.e., $R(y) > 0$. Eventually after a finite number of iterations our problem can be studied by treating the gradient terms as a perturbation on the single site terms. Hence, in any theory for which $R(y) > 0$ we can conclude that the low energy (or long-wavelength) physics is described by an effectively strong-coupling constant Hamiltonian. It follows from this discussion that the mass gap in such a theory will be given by calculating the gap between the first two eigenstates of the effective single site Schrödinger problem. The gap is thus a function of the effective single site coupling g_∞, where the subscript denotes the many iterations $N \gg 1$ to reach the strong coupling behavior. In general, since the scale of H is set by the cutoff Λ, this means that the lowest mass gap in the theory will be $\approx \Lambda g_\infty$. However, the scale of physical masses should be negligible with respect to the maximum momentum Λ if we are to retain practical Lorentz invariance for the low-lying eigenstates in spite of our cutoff procedure. Therefore we are only interested in theories for which $g_\infty \ll 1$, or in other words, $g_\infty \Lambda$ finite (and perhaps $\lesssim 1$ GeV).

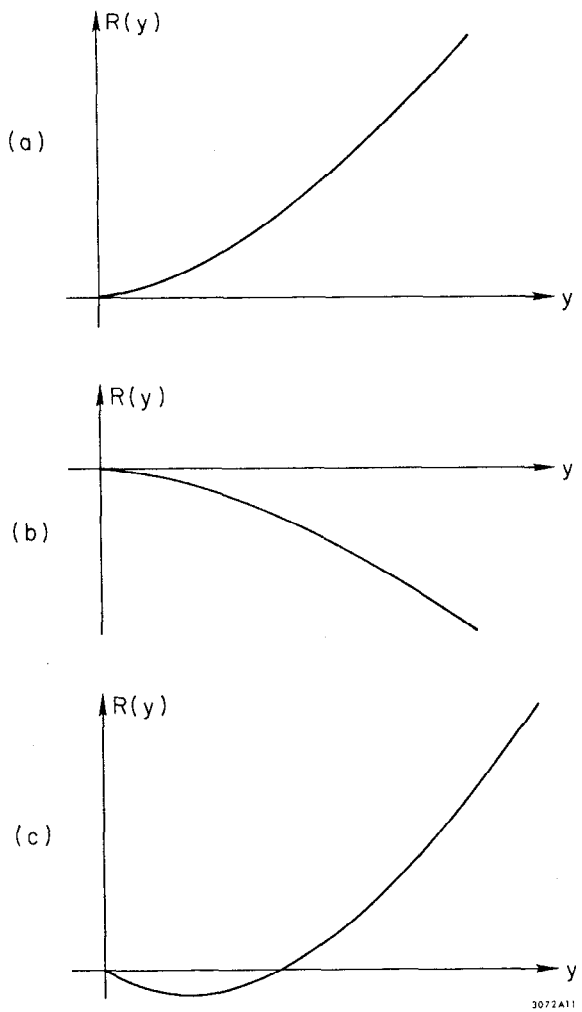

Fig. 16

Generally the Hamiltonian at a fixed point reproduces itself up to a scale factor ρ, and after N iterations the overall scale of H_N is $\Lambda\rho^N$. Since this should be finite ($\tilde{\sim}$ 1 GeV) this suggests that the question of the practical relativistic invariance of a theory for which R(y) behaves as in Fig. 16a can be settled by computing the scale parameter ρ in the y = 0 limit. If we find $\rho < 1$ then we can take the cutoff $\Lambda \to \infty$ and still keep the masses of the lowest states finite if we choose the original bare coupling constant g_0 to tend appropriately to zero as a function of increasing Λ. This is an example of a theory whose short distance behavior is "free" but whose long wavelength behavior is not. Such a theory could describe asymptotically free quarks for high momenta and also give confinement.

If we next look at R(y) for Fig. 16b we come up with the opposite conclusion. If $R(y) < 0$ each successive set of N-iterations will make it smaller. Hence the large wavelength or low energy physics of this theory is given by weak coupling perturbation theory, whereas the single-site or short distance behavior is governed by a strong coupling constant.

Fig. 16c tells us that the two different cases can occur depending upon the starting value for y, i.e., whether $y_0 < y_c$ or $y_0 > y_c$. This is just the form of R(y) calculated for our Ising model in Fig. 14 and one can refer back to the exact solution of this theory[31] to see how an effectively relativistic theory emerges.

The use of the function R(y) to catalogue types of theories has its analogue in the study of the renormalization group equations in momentum space, where one encounters the well known $\beta(g)$ function in terms of which the asymptotic behaviors of field theories are described. Both functions, $\beta(g)$ and R(y), describe the change in coupling constant (g or y) as we change

the scale of distance in the theory. The two functions are complementary to one another in that we have introduced R(y) here in coordinate space, whereas $\beta(g)$ normally appears in the momentum space analysis of the renormalization group equations. In our renormalization group procedure on a lattice we build larger and larger blocks at each state of the calculation so that we are studying the behavior of the theory at lower and lower momenta. When working in momentum space one normally studies the renormalization group equations by scaling up the momenta to higher and higher values at each stage, and correspondingly to smaller and smaller values of the underlying lattice spacing. In our approach Fig. 16a describes a theory which is asymptotically free (high momenta) and Fig. 16b describes one that is infrared stable. The β function has just the complementary behavior as illustrated by Fig. 17 for asymptotically free and infrared stable theories.

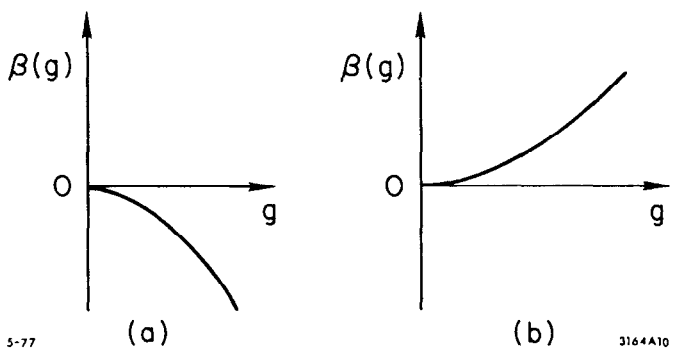

Fig. 17

THIRRING MODEL

The Thirring model[35] of quartically self-coupled fermions, described by the Hamiltonian

$$H = \int dx \left[-\bar{\psi} i \not{\partial} \psi - \frac{1}{2} g \left\{ (\bar{\psi}\psi)^2 - (\bar{\psi} \gamma_5 \psi)^2 \right\} \right] \qquad (2.50)$$

is a more interesting one for applying these methods for several important reasons:

1) It deals with fermions (à la quarks).

2) It is essential to use the definition (2.13) for the lattice gradient which couples distant lattice sites in order to avoid the deficiency in (2.11) of doubling the number of states as illustrated in Fig. 8 and at the same time preserve chiral symmetry.

3) In the continuum Thirring model the wave function renormalization Z_2 vanishes when the strength of the coupling g exceeds a

finite critical value and it is important to reproduce this behavior indicating failure of the multiplicative renormalization procedure and the concomitant loss of the single charged fermion (and generally charged degrees of freedom) from the finite mass spectrum. Failure of such states to propagate is a form of confinement in this model.

Introducing dimensionless field variables $\chi_j = \Lambda^{-\frac{1}{2}}\psi_j$ and a convenient matrix representation that diagonalizes the quartic term in (2.50); viz.

$$\alpha = \gamma_5 = \begin{pmatrix} 1 & 0 \\ 0 & -1 \end{pmatrix} \qquad \gamma_0 = \begin{pmatrix} 0 & 1 \\ 1 & 0 \end{pmatrix}$$

$$\chi_j = \begin{pmatrix} b_j \\ d_j^+ \end{pmatrix} \qquad \left\{b_j, b_{j'}^+\right\} = \left\{d_j, d_{j'}^+\right\} = \delta_{jj'} \tag{2.51}$$

$$\left\{b_j, d_{j'}\right\} = 0 \quad \text{etc.}$$

the Hamiltonian can be written[36]

$$\frac{1}{\Lambda} H = \sum_{j_1, j_2} i\delta'(j_1 - j_2)\left\{b_{j_1}^+ b_{j_2} - d_{j_1}^+ d_{j_2}\right\}$$

$$-g \sum_j \left(n_b(j) + n_d(j) - 1\right)^2 \tag{2.52}$$

where $n_b(j) \equiv b_j^+ b_j$ and $n_d(j) \equiv d_j^+ d_j$ are number operators. This theory possesses two conserved "charges"

$$Q = \sum_j \left(n_b(j) - n_d(j)\right) = \sum_j :\chi_j^+ \chi_j:$$

$$Q_5 = \sum_j \left(n_b(j) + n_d(j) - 1\right) = \sum_j \chi_j^+ \gamma_5 \chi_j \tag{2.53}$$

as well as discrete P, C, and T operations for classifying states. The weak coupling limit g = 0 reduces to free massless fermions, the solution to which is most readily recognized in momentum space which diagonalizes the gradient operator. In fact with

$$b(k) \equiv \frac{1}{\sqrt{2N+1}} \sum_j b_j e^{-ikj/\Lambda}$$

$$d(k) \equiv \frac{1}{\sqrt{2N+1}} \sum_j d_j e^{-ikj/\Lambda} \tag{2.54}$$

we have

$$H(g = 0) = \sum_{k=-\pi\Lambda}^{\pi\Lambda} k\left(b^+(k)b(k) - d^+(k)d(k)\right)$$

$$= \sum_{k=-k_{max}}^{k_{max}} k\left(n_b(k) - n_d(k)\right) \tag{2.55}$$

The lowest eigenstate of (2.55) corresponds to filling all $k < 0$ states with fermions (b-quanta) and all $k > 0$ ones with antifermions (d-quanta), i.e.

$$n_b(k) = \theta(-k)$$

$$n_d(k) = \theta(k) \ .$$

This leads to a doubly degenerate ground state in the neutral $Q = 0$ sector depending on whether the $k = 0$ state is empty ($Q_5 = -1$) or occupied by a pair ($Q_5 = +1$) and to two states of the same energy and with charge $Q = \pm 1$, $Q_5 = 0$ corresponding to a fermion or an antifermion present in the $k = 0$ state. The energy of these four-fold degenerate states is

$$E_0 = -2 \sum_{k=0}^{k_{max}} k$$

In contrast the strong coupling limiting behavior $g \gg 1$ is found simply from the quartic term in (2.52) which can be diagonalized on each site separately. There are only four states at each site corresponding to $n_b(j) = 1, 0$ and $n_d(j) = 1, 0$. These site states, their quantum numbers and eigenenergies are shown in Table III, where $|0\rangle$ is defined by $b_j|0(j)\rangle = d_j|0(j)\rangle = 0$.

We see therefore that at each site the $Q = 0$ states, corresponding to nothing or a bound pair at a site, are degenerate ground states, with the single fermion states of charge $Q = \pm 1$ pushed up in energy by $g\Lambda$. Therefore any neutral state which contains an unbound pair with a fermion and an antifermion split to different lattice sites will lie higher in energy by $2g\Lambda$ for each such split pair. One can of course study how the gradient term splits the $2(2N + 1)$-fold degeneracy of the ground states with $Q = 0$. However it is clear that we are seeing here a form of quark confinement in the strong coupling limit with $g \gg 1$ since the gap to propagating single quark states is $\sim 2g\Lambda \gg \Lambda$, the lattice cutoff.

The perturbation treatment of the gradient term in the strong coupling limit has been given.[19b] It is clear from the form of (2.52) that the gradient moves single fermions or antifermions from one lattice site to another and gives no first order energy shift to the low lying states with $Q = 0$ and $n_b(j) = n_d(j)$. In second order either a fermion and antifermion are both moved from a common initial lattice site to a common final one, as illustrated (Fig. 18a), or the (anti-) fermion is moved away and returns to its initial site (Fig. 18b).

It is not surprising that there exists a spin formalism in the sector of low lying states in which each lattice site is either empty (spin down)

Table III

State	Q	Q_5	$-g\left[n_b(j) + n_d(j) - 1\right]^2$
$\|0\rangle$	0	-1	-g
$\|+\rangle = b^+\|0\rangle$	+1	0	0
$\|-\rangle = d^+\|0\rangle$	-1	0	0
$\|\pm\rangle = b^+d^+\|0\rangle$	0	+1	-g

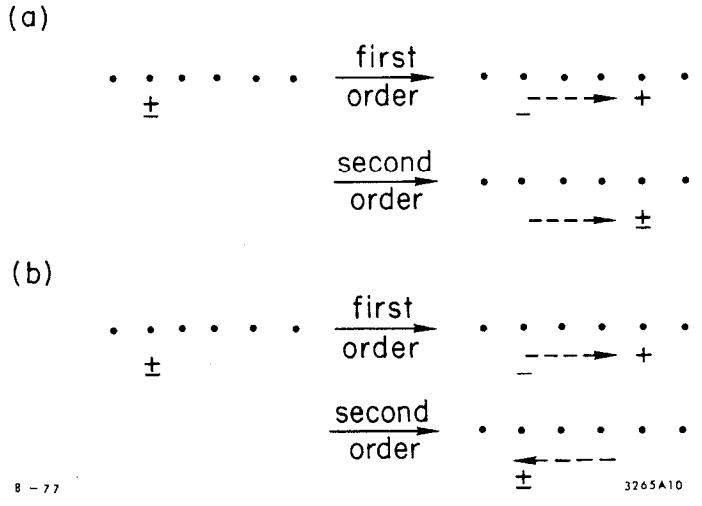

Fig. 18

or occupied by a pair (spin up). In fact the second order treatment of the gradient gives an effective Hamiltonian in order $1/g^2$ that is identical to the Heisenberg antiferromagnetic chain about which a great deal has been known since the work of Bethe[37] in 1931. In particular such a system is known to have a doubly degenerate ground state for a chain with an odd number, $2N + 1$, of lattice sites corresponding to the odd site being either spin up ($S_3 = +\frac{1}{2}$) or down ($S_3 = -\frac{1}{2}$) and to have a low lying excitation spectrum of spin waves that is linear in k, without a mass gap, for an infinitely long chain.

Our interest, as in the Ising model, is mainly in the intermediate coupling region where the Thirring model changes from free fermion to no single fermion propagation. Can we understand what is going on, as learned from the study of the continuum model, by our lattice truncation methods?

Aside from detailed technical issues associated with the fact that fermions give us two eigenstates at each lattice site for both particles and antiparticles and with the use of the gradient operator δ' coupling distant lattice sites, (2.32) for the Ising model and (2.52) are very similar. Therefore so is the formal treatment via the lattice blocking procedure--and not surprisingly the success of these methods as well as the character of the results that are obtained. Already we have noted the strong coupling limiting behavior that charged fermions move high up to mass $\sim g\Lambda$ and fail to propagate. In fact these methods show[19d] that there is a critical coupling strength such that for $g > g_{cr} \gtrsim 1.1$ we are driven to the strong coupling limiting behavior; whereas for $g < g_{cr}$, the Hamiltonian converges to the same fixed form that the free $g = 0$ Hamiltonian iterates to. What happens is that the wave function renormalization constant defined as the amplitude to create a $Q = 1$, $Q_5 = 0$ state at rest from the vacuum, i.e.,

$$\sqrt{Z_2(g)}\begin{pmatrix}1\\0\end{pmatrix} \equiv \langle 0|\chi(k = 0)|+\rangle$$

vanishes for finite $g \geq g_{cr}$ even in the presence of a finite cutoff Λ. When one discusses the continuum Thirring model it is necessary to give singular quantities in the theory well defined meanings. For example Johnson introduced a point splitting prescription

$$j^{\mu}(x) = \tfrac{1}{2}\lim_{\varepsilon \to 0}\left\langle\left[\bar{\psi}(x + \varepsilon), \gamma^{\mu}\psi(x - \varepsilon)\right]\right\rangle$$

to define the current, where the bracket indicates a suitable averaging over directions of ε. This procedure also leads to a wave function renormalization $Z_2(g)$ that vanishes at a finite value of g, similar to the lattice result. In both formulations the theory cannot be multiplicatively renormalized for g greater than some finite critical value g_{cr} and the Schwinger terms are similar.

The picture emerging from this truncation procedure is found to be consistent with the continuum model in that there is a finite critical value g_{cr} such for $g < g_{cr}$ the theory has no mass gap; for $g > g_{cr}$ the cutoff lattice theory cannot be multiplicatively renormalized in the usual fashion. The lattice theory still exists for $g > g_{cr}$; in fact, for this region its behavior seems entirely sensible and is driven to the strong coupling limit which corresponds to a Heisenberg antiferromagnetic chain with nearest neighbor interactions only. This theory possesses a massless excitation spectrum as first found by Bethe. For $g > g_{cr}$, however, the "single particle" operator $\frac{1}{\sqrt{L}}\int dx\, \psi^{+}(x)$ fails to create any finite energy states from the vacuum. In fact, the excitations of unit charge are found to lie an energy $\sim g\Lambda$ above the ground state. This result shows that for a certain region of the parameter g the particles and low-lying excitation spectra found in finite cutoff lattice

theories are not simply related to the fundamental field introduced in the starting Lagrangian and Hamiltonian.

The breakdown of multiplicative renormalization and the concomitant loss of the charged degrees of freedom from the finite mass spectrum is interesting in that it seems to occur in several types of lattice theories for appropriate values of coupling constant. The strong coupling limit of the Schwinger model[38]--i.e., QED in 1x-1t dimensions--is very similar to the Thirring model in that charged fermion states move up to high mass and fail to propagate.[19b] In particular each bit of gauge field adds an energy $\approx g_0\Lambda$, where g_0 is the dimensionless coupling constant and is related by $g_0 \equiv e/\Lambda$ to the dimensional charge e as defined in (2.21) for a 1x-1t dimensional gauge theory. Hence in this extreme limit each lattice site is "neutral." However the results of the blocking procedure with arbitrary coupling strength have not yet been found. Presumably if there is a qualitative difference between non-abelian gauge theories to which we look for an explanation of quark confinement, and these non-gauge models, it will be that for the gauge theories whenever $g \neq 0$ we will lose the simple multiplicative renormalization procedure and, with it, propagating free fermion (quark) states.

This is where our program now stands. Having also shown that the iterative renormalization group techniques that I have been describing in this lecture satisfy Coleman's theorem[39] by not predicting false Goldstone bosons in 1x-1t dimensions,[40] we are finally ready to tackle gauge theories in higher dimensions.

APPENDIX A

In this appendix, we consider the 1x-1t dimensional version of the scalar field Lagrangian used in the SLAC bag model to illustrate the importance of understanding the quantum corrections to the semi-classical analysis. Starting with the Lagrangian ($f^2 > 0$)

$$L = \int dx \left[\frac{1}{2} \left(\frac{\partial \phi(x,t)}{\partial t} \right)^2 - \frac{1}{2} \left(\frac{\partial \phi}{\partial x} \right)^2 - \lambda (\phi^2 - f^2)^2 \right] \tag{A.1}$$

we exhibit the "kink" or soliton state and show that it is a low-mass configuration only in the strong-coupling regime of the theory.[41] Hence when we go beyond the semiclassical tree approximation, we must face the problem of solving a strong coupling quantum field theory.

The Hamiltonian corresponding to (A.1) is

$$H = \int dx \left\{ \frac{1}{2} \pi^2(x,t) + \frac{1}{2} \left(\frac{\partial \phi}{\partial x} \right)^2 + \lambda (\phi^2 - f^2)^2 \right\} \tag{A.2}$$

with $\pi \equiv \dot{\phi}$ the canonical field momentum:

$$\left[\pi(x,t), \phi(x',t) \right] = -i\delta(x - x') \quad .$$

Ignoring the quantum aspects of the theory, we drop the momentum π in (A.2) and treat $\phi(x)$ as a static classical field: $\phi \to g(x) \equiv \phi_{cl}(x)$. Evidently the ground state energy of the positive definite classical Hamiltonian

$$H_{cl} = \int dx \left\{ \frac{1}{2} \left(\frac{dg}{dx} \right)^2 + \lambda (g^2 - f^2)^2 \right\} \tag{A.3}$$

vanishes for a constant field

$$g^{(0)} = \pm f \tag{A.4}$$

Equation (A.4) describes the doubly degenerate ground state. The general solution of (A.3) satisfies the non-linear Euler-Lagrange equation

$$\frac{d^2g}{dx^2} - 4\lambda g(g^2 - f^2) = 0 \tag{A.5}$$

and substituting any solution of (A.5) in (A.3) gives the classical energy E(g). The only time-independent solutions of (A.5) that give a finite value for the energy H_{cl} in addition to (A.4) are the one-parameter family of "kinks"

$$g^{\pm}(x,x_0) = \pm f \tanh\left\{\sqrt{2\lambda}\ f(x - x_0)\right\} \tag{A.6}$$

Substituting (A.6) in (A.3) yields the classical energy

$$E^{kink} = \frac{4}{3}\sqrt{2\lambda}\ f^3 \tag{A.7}$$

We readily demonstrate that the kink describes a stable configuration even though its energy (A.7) lies above the ground state value of $E^0 = 0$ for the constant configuration (A.4) by constructing a conserved "charge" from the current

$$j_\mu(x) = \varepsilon_{\mu\nu}\frac{\partial\phi}{\partial x_\nu}\ ; \qquad \mu,\nu = 0,1$$
$$\varepsilon_{\mu\nu} = -\varepsilon_{\mu\nu}\ ; \qquad \varepsilon_{01} = 1 \tag{A.8}$$

Evidently

$$\partial j_\mu/\partial x_\mu = 0$$

and so

$$Q \equiv \int dx j_0(x) = \int dx\,\frac{\partial\phi}{\partial x} = \phi(\infty) - \phi(-\infty) \tag{A.9}$$

is a time-independent quantity. The conserved "charge" (A.9) vanishes for the vacuum state (A.4) since $g(\infty) = g(-\infty)$; for the kink (A.6), however, $Q^{kink} = \pm 2f \neq 0$. Hence the kink is stable.

The usual way to construct the quantum corrections to the kink is by expanding in a power series of the fluctuations about the classical solution

$$\phi(x,x_0) = g(x) + \phi'(x,x_0) \tag{A.10}$$

However, such an expansion converges, if it indeed converges at all, only in the weak coupling regime, whereas the semi-classical treatment indicates that the strong coupling regime is the one of interest to us. To make this point, introduce (A.10) into (A.2) so as to obtain

$$H = \int dx\left[\left\{\frac{1}{2}\left(\frac{dg}{dx}\right)^2 + \lambda(g^2 - f^2)^2\right\}\right.$$
$$+ \left\{\frac{1}{2}\pi^2 + \frac{1}{2}\left(\frac{\partial\phi'}{\partial x}\right)^2 + \frac{1}{2}\phi'^2\left(4\lambda(3g^2 - f^2)\right)\right\} \tag{A.11}$$
$$\left. + \left\{4\lambda g\phi'^3 + \lambda\phi'^4\right\}\right]:$$

where we have used (A.5) to eliminate the terms linear in ϕ'. The usual weak coupling approach to (A.2) is to expand ϕ about the constant $g = \pm f$ corresponding to the minimum in the classical energy. The quadratic terms in (A.11) lead to normal mode motion for oscillators of mass

$$m_f = \sqrt{8\lambda}\ f\ . \tag{A.12}$$

Since the classical kink energy is given by (A.7), we expect the kink to be a better approximation to the low-lying energy states of the theory than the perturbative result only if

$$E^{kink} \ll m_f \tag{A.13}$$

or

$$f^2 \ll 1. \tag{A.14}$$

The condition (A.13) corresponds to strong coupling according to (A.11) since, for fixed oscillator mass (A.12), it is equivalent to the conditions

$$\lambda \gg m_f^2 \qquad \text{and} \qquad \lambda f \gg m_f^2 \tag{A.15}$$

In this regime the non-linear cubic and quartic corrections in (A.11) will be large and their higher order contributions important.

A systematic application of the standard iterative techniques of renormalizable quantum field theory shows directly the importance of developing a strong coupling approach for this regime of parameters. Returning to (A.11), we already have computed the classical energy difference between a kink solution (A.6) in the Q = 2f sector and the classical ground state energy of the constant g(x) = f in the Q = 0 sector. It is given by (A.7); i.e.,

$$\left[E^{\text{kink}} - E^{0}\right]_{\text{classical}} = \frac{4}{3}\sqrt{2\lambda}\, f^3 \,. \tag{A.16}$$

In order to evaluate the lowest order quantum mechanical energy difference between the "kink" and no kink solutions, we must also include the zero point energies due to quantum fluctuations computed from (A.11). In particular, these vacuum fluctuations are different in the two sectors for different values of g(x) and this difference must be computed for us to know the true excitation energy of the kink state with Q = 2f relative to the Q = 0 ground state.

An equivalent way of describing these corrections is as the sum over the loop corrections to the tree approximation. To lowest order the one loop correction to the zero point energies due to quantum fluctuations is calculated by neglecting the cubic and quartic terms in (A.11). In particular, we must calculate the shift in the sum over the spectrum of zero point energies for small oscillations about the kink solution (A.6) for g(x), relative to the oscillations about the constant g(x) = f. This difference was computed by Dashen, Hasslacher, and Neveu.[41] For the constant solution, the sum over the zero point energies is given formally by

$$\frac{1}{2}\sum_n \omega_n = \frac{1}{2}\sum_k \sqrt{k^2 + 8\lambda f^2} \tag{A.17}$$

which expresses the sum over plane wave solutions with mass $m_f = \sqrt{8\lambda}\, f$ as in (A.12). For the kink solution we expand the field in normal modes

$$\phi'(x,t) = \sum_n \frac{1}{\sqrt{2E_n}}\left(u_n(x,t)\, a_n + u_n^*(x,t)\, a_n^+\right) \tag{A.18}$$

$$\dot{\phi}'(x,t) \equiv \pi = -i\sum\sqrt{\frac{E_n}{2}}\left(u_n a_n - u_n^* a_n^+\right)$$

$$\left[a_n, a_{n'}^+\right] = \delta_{n;n'}$$

with u_n forming a complete basis of solutions to the Schrödinger equation derived from (A.11):

$$\left[\frac{d^2}{dx^2} - 4\lambda\left(3g^2 - f^2\right)\right] u_n = E_n^2\, u_n \,. \tag{A.19}$$

As shown by Dashen, Hasslacher, and Neveu (A.19) can be solved in terms of known functions when g is given by the kink (A.6), and the shift of zero point energy from (A.17) can be evaluated after performing a simple mass renormalization. They found

$$\Delta E^{\text{Q.M.}} = \frac{1}{2}\sum_n \left(E_n - \omega_n\right) = \left(\frac{\sqrt{3}}{6} - \frac{3}{\pi}\right)\sqrt{2\lambda}\, f \tag{A.20}$$

i.e., the kink energy is shifted down by an amount of the order of m_f itself as a result of the quantum excitations being drawn into the potential well at the kink boundary. The moral to be drawn from (A.20) is that the shift in the fluctuation energy in the 1-loop approximation is a very large one, much larger than the classical kink energy itself, which as shown in (A.16) is

smaller by the factor $f^2 << 1$. Evidently then an expansion in fluctuations about the "soliton" solutions of the classical problem does not define a reliable iterative procedure for our purposes and we are faced inescapably with the challenge of strong coupling theory.

As was shown subsequently in a fully quantized variational analysis of this theory,[19a] formulated on a discrete lattice, the results (A.7) plus (A.20) for the kink are, in the limit of low-lying kink energy, just the expansion of an expression

$$E_{kink}^{(QM)} \simeq \frac{4}{3}\sqrt{2\lambda}\, f^3 \left[1 - f_{cr}^2/f^2\right]^{3/2}$$

where $f_{cr}^2 \approx 0.83$.

REFERENCES

1. For a recent review see R. Taylor, Proc. 1975 Int. Symp. Lepton Photon Interactions, Stanford, California.
2. J. D. Bjorken and E. A. Paschos, Phys. Rev. 185, 1975 (1969). R. P. Feynman, Phys. Rev. Lett. 23, 1415 (1969), and in High Energy Collisions (Gordon & Breach, New York, 1969), p. 237.
3. See discussions in Proceedings in Ref. 1.
4. F. Gilman, lectures at this Summer Institute.
5. See SLAC Summer Institute 1976.
6. G. Gallinaro, M. Marinelli, and G. Morpurgo, Phys. Rev. Lett. 38, 1225 (1977).
7. G. La Rue, W. Fairbank, and A. Hebard, Phys. Rev. Lett. 38, 1011 (1977).
8. Cf. J. D. Bjorken and S. D. Drell, Relativistic Quantum Mechanics (McGraw-Hill Co., N.Y., 1974), p. 70.
9. H. Politzer, Phys. Rev. Lett. 30, 1346 (1973). D. Gross and F. Wilczek, Phys. Rev. Lett. 30, 1343 (1973). G.'t Hooft (unpublished).
10. D. Gross and F. Wilczek, Phys. Rev. D8, 3633 (1973); D9, 980 (1974). Sixteen color triplets of fermions are allowed.
11. T. Appelquist and J. Carrazone, Nucl. Phys. B120, 77 (1977).
12. For a recent general review of these ideas see W. Marciano and H. Pagels, Rockefeller U. preprint COO-2232B-130, to be published.
13. T. P. Cheng, E. Eichten, and L.-F. Li, Phys. Rev. D9, 2259 (1974).
14. H. Fritzsch, M. Gell-Mann, and H. Leutwyler, Phys. Lett. 47B, 365 (1973). See Ref. 12.

15. C. N. Yang and R. L. Mills, Phys. Rev. 96, 191 (1954).

16. W. Heisenberg and W. Pauli, Z Physik 56, 1 (1929).

17. K. Wilson, Phys. Rev. D10, 2445 (1974) and Erice Lectures (1975).
R. Balian, J. Drouffe, and C. Itzykson, Phys. Rev. D10, 3376 (1974); D11, 2098, 2104 (1975).

18. J. Kogut and L. Susskind, Phys. Rev. D11, 395 (1975).
J. Kogut, McGill Summer School Lectures (1976).

19. a) S. D. Drell, M. Weinstein, and S. Yankielowicz, Phys. Rev. D14, 487 (1976)
b) D14, 1627 (1976).
c) "Quantum Field Theories on a Lattice: Variational Methods for Arbitrary Coupling Strengths and the Ising Model in a Transverse Magnetic Field," Stanford Linear Accelerator Center preprint SLAC-PUB-1942 (1977), to appear in Phys. Rev.
d) S. D. Drell, B. Svetitsky, and M. Weinstein, "Fermion Field Theory on a Lattice: Variational Analysis of the Thirring Model," Stanford Linear Accelerator Center preprint SLAC-PUB-1999 (to be published).

20. a) A. Chodos, R. Jaffe, K. Johnson, C. Thorn, and V. Weisskopf, Phys. Rev. D9, 3471 (1974).
b) T. de Grand, R. L. Jaffe, K. Johnson, and J. Kiskis, Phys. Rev. D12, 2060 (1975) and many references therein.

21. We use the convention here of R. Friedberg, T. D. Lee, and A. Sirlin, Phys. Rev. D13, 2739 (1976); Nucl. Phys. B115, 1, 32 (1976). See also T. D. Lee and R. Friedberg, Phys. Rev. D15, 1694 (1977).

22. G. 't Hooft, Nucl. Phys. B79, 276 (1974). A. M. Polyakov, JETP Letts 20, 194 (1974).

23. W. Bardeen, M. Chanowitz, S. Drell, M. Weinstein, and T.-M. Yan, Phys. Rev. D11, 1094 (1975).

24. P. Vinciarelli, Nuovo Cimento Lett. 4, 905 (1972).
M. Creutz, Phy. Rev. D10, 1749 (1974).
M. Creutz and K. S. Soh, Phys. Rev. D12, 443 (1975).
R. Friedberg and T. D. Lee, "Fermion-Field Nontopological Solitons II. Models for Hadrons," Columbia University preprint CO-2271-89 (1977), to be published.

25. Including mass differences alters the electrostatic energy by $\lesssim 5$ MeV. This is discussed in Ref. 20b.

26. T. DeGrand and R. Jaffe, Ann. Phys. (N.Y.) 100, 425 (1976).

27. C. Rebbi, Phys. Rev. D12, 1407 (1975); D14, 2362 (1976).

28. T. A. DeGrand, Ann. Phys. (N.Y.) 101, 496 (1976).

29. T. D. Lee and G. C. Wick, Phys. Rev. D9, 2291 (1974).
T. D. Lee and M. Margulies, Phys. Rev. D11, 1591 (1975).

30. Simply use the limiting behavior of $\delta'(\ell_1 - \ell_2)$ as the derivative of a Dirac delta function to confirm this.

31. E. Lieb, T. Schultz, and D. Mattis, Ann. Phys. (N.Y.) 16, 407 (1961).
See E. Lieb and D. Mattis, Mathematical Physics in One Dimension (Academic Press, N.Y., 1966).
Also more recently: P. Pfeuty, Ann. Phys. (N.Y.) 57, 79 (1970) and B. Stoeckly and D. Scalapino, Phys. Rev. B11, 205 (1975).

32. The following discussion of the transverse Ising model is taken from Ref. 19c.

33. For (2.37) one has a 4-degree of freedom problem of two coupled spin Hamiltonians to diagonalize.

34. M. Aelion and M. Weinstein (to be published).

35. W. Thirring, Ann. Phys. (N.Y.) 3, 91 (1958).

K. Johnson, Nuovo Cimento 20, 773 (1961).

G. F. Dell'Antonio, Y. Frishman, and D. Zwanziger, Phys. Rev. D6, 988 (1972).

B. Klaiber, in Lectures in Theoretical Physics, lectures delivered at the Summer Institute for Theoretical Physics, University of Colorado, Boulder, 1967, edited by A. Barut and W. Brittin (Gordon and Breach, New York, 1968), Vol. X, part A.

36. The following discussion of the Thirring model is taken from Refs. 19b and 19d.

37. H. A. Bethe, Z. Phys. 71, 205 (1931).

38. J. Schwinger, Phys. Rev. 128, 2425 (1962).

J. Lowenstein and J. Swieca, Ann. Phys. (N.Y.) 68, 172 (1971).

39. S. Coleman, Math. Phys. 31, 259 (1973).

40. S. D. Drell and M. Weinstein (to be published).

41. R. Dashen, B. Hasslacher, and A. Neveu, Phys. Rev. D10, 4114, 4130 (1974); D11, 3424 (1975). See also Ref. 23.

HADRON SPECTROSCOPY

Frederick J. Gilman

Stanford Linear Accelerator Center
Stanford University, Stanford, California 94305

I. INTRODUCTION: THE QUARK MODEL

Hadron Spectroscopy is a subject which is interesting in its own right. The question of how matter is organized certainly falls within the bounds of the subject matter of physics and is therefore something we as physicists want to understand. With hundreds of hadronic states known to exist we have a substantial problem on our hands. Aside from that, it must be admitted that some people enjoy botany--working out a classification scheme and finding a specimen of some rare species can be a lot of fun.

In past years, another reason often given[1] for studying hadron spectroscopy was that it reflects the symmetries of strong interactions. In other words, a symmetry group of the strong interactions, if realized in the conventional way, results in hadrons falling into mass degenerate multiplets which correspond to irreducible representations of the symmetry group. If the symmetry was only approximate, there could be breaking of the mass degeneracy, but still recognizable multiplets.

However, much of our present interest in hadron spectroscopy stems from another source, the evidence for hadronic substructure. Hadron spectroscopy, plus a great deal of other evidence points toward such a substructure, and in particular to a quark basis for hadronic matter. By interpreting hadron spectroscopy we can deduce some of the properties of the quarks.

Furthermore, in the absence of free quarks, it is through hadron spectroscopy that we can learn about the dynamics of hadron constituents, and in particular about the quark-quark forces. Included in this is the nature of quark confinement and the kind of force law involved, as well as finer details such as the "residual forces" responsible for mass splittings, the relativistic or non-relativistic character of the situation, etc.

In the following lectures we shall pursue the subject of hadron spectroscopy from what has now become the conventional, quark model point of view. Much of the discussion of the "new" particles will be found in the lectures of M. Perl[2] which complement these.

We start by outlining the basic components of the picture of hadron spectroscopy we will use. This is widely, but not universally, shared by most particle physicists.

Quarks

Having already cited quarks as the building blocks of hadrons, let us review the evidence briefly:

(1) Deep Inelastic eN, μN, νN, and $\bar{\nu}$N Scattering.

The magnitude of the cross section, scaling behavior, and the relationship of structure functions observed in deep inelastic scattering indicate that the nucleon has point, spin 1/2 constituents with which the weak or electromagnetic current interacts.[3] Further, the amount of scattering depends on whether the target is a neutron or proton and on the spin orientation of the proton,[4] so that the constituents which are related to the nucleons isospin or spin are also what is "seen" by the weak or electromagnetic currents.

(2) Electron-Positron Annihilation

The ratio R of the cross section for $e^+e^- \to$ hadrons to that for $e^+e^- \to \mu^+\mu^-$ is a (different) constant both below and above charm threshold, as it should be if the basic process were production of a pair of point particles, followed by their eventual materialization as hadrons.[5] In fact, the part of R due to charmed meson production at SPEAR agrees with what is expected from the basic process of production of a pair of charmed quarks.[6] Furthermore, the observation of back-to-back jets at SPEAR yields the additional information that their angular distribution is characteristic of production of a pair of spin 1/2 particles.[5]

(3) Hadron Spectroscopy.

With a few possible exceptions,[7] the hundreds of hadrons we now know are understood as quark-anti-quark bound states (mesons) or three quark bound states (baryons). An enormous simplification has taken place and is part of the standard "lore". Now one often forgets that something as basic as the ordering of spins and parities of states $(0^-,1^-$ as lowest mass mesons and $1/2^+$, $3/2^+$ as lowest mass baryons is trivially understood in the quark model but is otherwise quite mysterious.

(4) Weak and Electromagnetic Current Matrix Elements.

The quark model gives us a quantitative understanding of both the magnetic moments and magnetic transition moments between the ground state baryons, as we will see in detail later. When formulated in the general framework of the transformation from current to constituent quarks,[8] one can discuss the photon transition amplitudes from the nucleon to excited nucleon resonances. When a few reduced matrix elements are fixed in terms of known amplitudes, one gets correct predictions for the signs and magnitudes of a fair number of other amplitudes.[1] Further, if one is willing to use PCAC to relate matrix elements of the axial-vector current to pion amplitudes, then a similar theory of pionic transitions ensues. Again the signs and magnitudes of many amplitudes are correctly given. It would seem very unlikely that all this is an accident.

(5) *High Transverse Momentum Phenomena*

It seems very plausible that high transverse momentum hadron production in hadron-hadron collisions has its origin in "hard scattering" of constituents of the hadrons.[9] When compared to (1)-(4) above the connection to quarks is much less direct, and certainly not unique. But the similarities to hadron production in deep inelastic scattering and electron-positron annihilation, especially the production of jets in each case, are quite striking. Although it is much harder to get precision information on quarks in this case, this is an important area of research exactly because it may give us information on quark dynamics in a different setting.[10]

Color

Quarks are thought to carry a strong interaction charge called color. There are three such colors, which we take as red, yellow, and blue. Present experimental evidence for the need for color comes from three sources:

(1) The rate for $\pi^0 \to \gamma\gamma$. The amplitude for $\pi^0 \to \gamma\gamma$, when related to that for $\partial_\mu A_\mu \to \gamma\gamma$ by PCAC, has a magnitude and sign given by the triangle graph (with a closed fermion loop) anomaly[11] in the coupling of two vector currents to an axial-vector current. Without color, one gets the wrong rate. With it, the amplitude is increased by a factor of three and the rate by a factor 9. It then agrees with experiment.[12]

(2) The ratio $R = \sigma(e^+e^- \to \text{hadrons})/\sigma(e^+e^- \to \mu^+\mu^-)$. Color increases the predicted cross section (on the basis of the quark model) by a factor of three. This is needed to get even rough agreement with experiment both below and above charm threshold.[5]

(3) The Baryon Wave Function. The wave function for fermions should be totally antisymmetric. If the three quarks in a baryon are a singlet with respect to color (see below), the color part of the wave function is antisymmetric. Thus the remainder (spin, space and quark type or flavor) must be symmetric. This is indeed the case from the experimental spectrum and in particular is true for the ground state which has a symmetrical spatial wave function combined with one symmetrical in spin and flavor.

Each of these experimental pieces of evidence for color needs some theoretical analysis to deduce the appropriateness of the concept of color, but they only involve "counting" the color quantum numbers. There are other, non-experimental, reasons for color, which have a much less solid basis in concrete facts. They all involve using color as a non-Abelian charge in a gauge field theory context. Nevertheless, they are important and have much to do with the overwhelming acceptance of the idea that colored quarks and gluons are the basis of all strong interactions.

(1) *Quantum Chromodynamics (QCD)*.

The theory of quarks coupled via the color "charge" to gauge vector bosons (gluons) is often referred to as QCD. The color gauge group is SU(3) and there is an octet of gluons. It is a non-trivial point that QCD is the only known field theory (and a non-Abelian gauge theory at that) which has a change of being the correct one for strong interactions.

(2) Asymptotic Freedom

Under certain conditions a non-Abelian gauge theory like QCD has the property of asymptotic freedom:[13] the effective coupling constant vanishes logarithmically at small distances, i.e. at large four-momentum squared. This allows one to "understand" the scaling behavior (characteristic of free field theory) observed in deep inelastic scattering. Even more, the theory predicts that scaling is not exact and the (small) predicted logarithmic breaking is consistent with what is seen in recent experiments.[3]

(3) Infrared Slavery

The increase in the coupling constant as one goes to larger distances inspires the hope that the color forces become infinite for very large separations and quarks (and other objects with color) are confined. Up to now this has not been shown rigorously, but there are some suggestive model calculations of how it might come about.[14]

(4) Okubo-Zweig-Iizuka[15] Rule Violation

Certain strong interaction decays where none of the final hadrons contain the quarks of the initial hadron, are very much suppressed in rate. This is particularly well exemplified in the case of the "new" particles. A theory of these processes involving intermediate gluons leads to a systematics of the mass and spin-parity dependence of the degree of suppression.[16]

(5) Spin-Dependent Quark-Quark Forces

Such forces result in hadron states with the same quark content but different relative spin orientations being split in mass. From the experimental observations it seems that the force between quark and quark in a baryon must have the same sign as between quark and antiquark in a meson. Exchange of a neutral vector meson without color does not yield such a result, but exchange of gluons coupled to color does if within color singlet mesons and baryons. While single gluon exchange does not have to be the origin of all such forces, it still is to be desired that the lowest order effect have at least the right sign.

(6) Dynamical Gluons

Sum rules for deep inelastic scattering indicate that quarks do not carry all the momentum or energy of the nucleon.[3] If the remainder is assigned to the gluons they should manifest themselves in a variety of ways by interacting with quarks and other gluons to produce hadrons in hadron-hadron collisions, to produce gluon jets in e^+e^- collisions, etc.[17]

Confinement

As we have already indicated above in our discussion of "infrared slavery," color is central to another aspect of quarks, that of confinement. We will take as a principle, perhaps derivable at a later time from QCD, that color is confined, i.e. only color singlet states can be seen. Then both quarks and gluons are not found among the asymptotic states of the theory. Bound states which are colorless can be and are seen: they are the hadrons.

The form of the effective color confining potential is not known for sure. Some arguments[14] in QCD and the string model suggest that the effective potential is linear, $V(r) = kr$, so that the force, $-dV/dr = -k$ is a constant. It then takes infinite energy to move a quark infinitely far away, as expected for a confining potential. Estimates of the constant, k, principally from fitting charmonium spectroscopy[18] suggest that $k \approx 0.2$ GeV^2 = 17 metric tons $\times$ (the acceleration of gravity).

Flavor

In addition to carrying color, quarks are distinguished from one another by their "flavor." At present we know of four flavors for quarks: up, down, strange, and charm. A fifth flavor (at least) is strongly suspected on the basis of the recently discovered Υ enhancement[19] at $\sim$ 9.5 GeV in the muon pair spectrum produced in proton-nucleon collisions. A particle data group type summary of the quark flavors is given in Table I.

The masses given in Table I of course cannot have the usual meaning since we do not see the quarks as free particles. They are so-called "constituent masses" and occur as parameters with the dimensions of mass in certain equations. They are different than current quark masses which occur in other equations. Any meaning to be attached to them is only within these equations, if then.

TABLE I

Quark Flavors à la the Particle Data Group

Quark	J^P	Mass (MeV)	Q/e	Baryon No.	Strangeness	Charm
u	$1/2^+$	~350	2/3	1/3	0	0
d	$1/2^+$	~350	-1/3	1/3	0	0
s	$1/2^+$	~500	-1/3	1/3	-1	0
c	$1/2^+$	~1650	2/3	1/3	0	1
?	$1/2^+$	~5000	?	1/3	0	0

The values of Q/e are most easily obtained by noting that baryons contain three quarks. Then the Δ^{++}, Δ^+, Δ^o, Δ^- charge states of the 3-3 resonance yield the u and d quark charges, while the Σ^{*+}, Σ^{*o}, Σ^{*-} or Ω^- force the charge on the s quark to be -1/3. In the case of the charmed quark, the best present evidence for Q/e = 2/3 comes from the charges of the D^o and D^+, the (non-strange) mesons containing a charmed quark. That it is a charmed quark and not antiquark in the D^o and D^+ follows from assuming that $c \to s$ in weak decays (so that the states with a charmed quark decay into final hadrons with strangeness -1).

There is other confirmatory evidence for all these charge assignments, such as the size of the change in R in e^+e^- annihilation on crossing the appropriate threshold, the size of the electromagnetic coupling of the vector mesons, etc.

We now review briefly the states composed of quarks which we do observe, the hadrons. The simplest possible hadrons are made of a quark and an antiquark forming a meson, or three quarks, forming a baryon. All other combinations of one, two, or three quarks and/or antiquarks have a net color (are not singlets under color SU(3)) and are forbidden by the principle of color confinement.

Mesons

In the case of mesons it is simple to see that the color wave function

$$\left(\bar{q}_{1R}\, q_{2R} + \bar{q}_{1B} q_{2B} + \bar{q}_{1Y} q_{2Y}\right)\Big/\sqrt{3}$$

is a normalized color singlet for any antiquark ($\bar{q}_1$) -quark (q_2) bound state.

The quark and antiquark spin may be combined to form a total quark spin, S, which is either 0 or 1. When coupled with the relative internal orbital angular momentum, L, we can form a total meson angular momentum, $\vec{J} = \vec{L} + \vec{S}$.

To complete the meson wave function we can choose any of the four (or more ?) flavors (u, d, s, c) for the quark and any of the four flavors for the antiquark. Thus there are 16 possible flavor possibilities for <u>each</u> value of L, S, and J. A meson wave function in the quark model then can be written in factorized form as

$$\Psi_{\text{color}}\,(\text{singlet}) \times \Psi_{\text{flavor}} \times \left[\Psi_{\text{spin}}\,(S=0,1) \times \Psi_{\text{orbital}}\,(L=0,1,\ldots)\right]_{\text{total } J} .$$

Since the quark and antiquark have opposite intrinsic parity, the overall parity of such a mesonic system is $P = (-1)^{L+1}$. For charge self-conjugate meson states, i.e. composed of $\bar{u}u$, $\bar{d}d$, $\bar{s}s$, $\bar{c}c$ or a linear combination, the charge conjugation quantum number is $C = (-1)^{L+(S+1)+1} = (-1)^{L+S}$. Thus the L = O, charge self-conjugate mesons, with S = O and 1 have $J^{PC} = O^{-+}$ and 1^{--}, respectively.

Baryons

For baryons the situation is a little more complicated. The normalized color singlet state with quarks $q_1 q_2 q_3$ is

$$\frac{1}{\sqrt{3!}} \begin{vmatrix} q_{1R} & q_{2R} & q_{3R} \\ q_{1B} & q_{2B} & q_{3B} \\ q_{1Y} & q_{2Y} & q_{3Y} \end{vmatrix}$$

as is easily seen by noting that a transformation induced by an element of the color SU(3) group multiplies the matrix in the determinant above by another matrix of determinant unity.

The total quark spin, S, may be 1/2 or 3/2. This is to be combined with the net internal orbital angular momentum L, to form the total baryon angular momentum, $\vec{J} = \vec{L} + \vec{S}$. The internal orbital angular momentum can be constructed in several ways, but most simply one may take $\vec{\ell}_{12}$ as the orbital angular momentum between quarks 1 and 2 and add to it $\vec{\ell}_3$, the orbital angular momentum of the third quark relative to the center of mass of the first two, to form $\vec{L} = \vec{\ell}_{12} + \vec{\ell}_3$.

The flavor wave function is also a bit more complicated than for mesons because not all flavor states are allowed for a given L and S due to Fermi statistics. With a color singlet wave function which is antisymmetric, the remainder of the baryon wave function must be symmetric. We will discuss the detailed implications of this later.

The parity of a baryon state defined as above is $P = (-1)^{\ell_{12} + \ell_3}$. In particular, the ground state, with all relative orbital angular momenta zero, has positive parity.

Exotics

The meson and baryon states we have discussed so far are the conventional ones of the quark model and involve the minimum number of quarks and/or antiquarks which can form a color singlet. We might well define a manifest exotic as a state with quantum numbers such that it cannot be made out of quark-antiquark in the case of a meson and three quarks in the case of a baryon.

Traditionally, one breaks up exotics into two categories. Exotics of the first kind, or "flavor exotics," are states in SU(2), SU(3),... representations not found when hadrons are formed as described above. Examples include doubly charged mesons, a baryon with positive strangeness, a meson with two units of charm, etc.

Exotics of the second kind are sometimes called "CP exotics." These are specifically mesons with parity $P = (-1)^J$ which have CP = -1 or a meson with $J^{PC}=0^{--}$. Neither of these can be formed from a quark and antiquark. A particular example of such an exotic is a vector meson with even charge conjugation.

In models which have a mechanism for forming exotic states, very often there are hadrons which do not have manifestly exotic quantum numbers themselves, but which have a quark content such that they have exotic relatives. These states are sometimes called "crypto-exotics." It is convenient to extend our definition of an exotic to include them. From here on an exotic is a meson which is not a quark-antiquark state or a baryon which is not three quarks. To use this definition we of course imply that we can tell what quarks are inside a given hadron!

There are many examples of predictions of such exotic states:

(1) $q\bar{q}q\bar{q}$ mesons and $qqq\ q\bar{q}$ baryons as in bag model calculations;[20]

(2) $(c\bar{q})(\bar{c}q)$ bound states of two charmed mesons to form "molecular" charmonium;[21]

(3) Baryonium;[22]

(4) Mesons composed of $\bar{q}q$ in a color octet state coupled to a gluon;[23]

(5) Quarkless states composed of gluons alone or "glueballs;"[24]

(6) States where the energy-momentum and perhaps spin are carried by fields other than the quarks, such as a neutral "soul;"[25]

(7) String excitations in a model of quark binding through a field theoretic string. String excitations may also be coupled to the quark orbital angular momentum to produce a fairly complicated spectroscopy.[26]

In fact, it is difficult to avoid exotic states with any real dynamics in a field theoretic framework. For no matter whether we confine quarks with gluons, with strings, or with some other fields, in a true field theory the binding field will have dynamical degrees of freedom of its own. Then, in addition to the quarks, there will be other fields which carry energy and momentum--which have their own spectrum of excitations and can "slosh" around inside the hadron relative to the quarks. The coupling of these excitations to the quark excitations in general gives rise to extra, sometimes manifestly exotic, states in the hadronic spectrum in addition to the ones usually expected. It is thus not a question so much of whether exotic states exist at all: almost any theory of hadrons worthy of the name predicts them at some mass. The important question is quantitative: at what mass and with exactly what quantum numbers do they occur?

II. RADIAL AND ORBITAL EXCITATIONS: THE "OLD" MESONS

As indicated in the previous section any flavor of quark can be combined with any flavor of antiquark to form a possible flavor state for a meson. With four flavors of quarks the possible states are then:

$\bar{u}u$	$\bar{u}d$	$\bar{u}s$	$\bar{u}c$
$\bar{d}u$	$\bar{d}d$	$\bar{d}s$	$\bar{d}c$
$\bar{s}u$	$\bar{s}d$	$\bar{s}s$	$\bar{s}c$
$\bar{c}u$	$\bar{c}d$	$\bar{c}s$	$\bar{c}c$

These sixteen flavor possibilities are available, indeed they are compulsory for each value of L, S, and J. With a fifth quark, there are 25 such states; with a sixth, 36.

If the u and d quarks are degenerate in mass and have the same strong interactions, e.g. through gluon exchanges, then there is an SU(2) symmetry of strong interactions, usually called isotopic spin invariance. Similarly, to the extent that the u, d, and s quarks may be regarded as degenerate and have the same strong interactions one has SU(3) symmetry. The 16 states shown above may be split up into multiplets corresponding to irreducible representations of these symmetry groups as shown in Table II.

TABLE II

SU(2) and SU(3) Multiplets for Mesons

Quark Flavor State			Isospin (SU(2) Representation)	SU(3) Representation
$\bar{d}u$	$(\bar{u}u - \bar{d}d)/\sqrt{2}$	$\bar{u}d$	1	8
$\bar{s}u$	$\bar{s}d$		1/2	
	$\bar{d}s$	$\bar{u}s$	1/2	
	$(\bar{u}u + \bar{d}d - 2\bar{s}s)/\sqrt{6}$		0	
$\bar{d}c$	$\bar{u}c$		1/2	$\bar{3}$
$\bar{s}c$			0	
	$\bar{c}u$	$\bar{c}d$	1/2	3
		$\bar{c}s$	0	
	$(\bar{u}u + \bar{d}d + \bar{s}s)/\sqrt{3}$		0	1
	$\bar{c}c$		0	1

In the limit where all four quarks are degenerate, one would have an SU(4) flavor symmetry. The SU(3) 8, $\bar{3}$, 3, and the combination of singlets, $(\bar{u}u + \bar{d}d + \bar{s}s - 3\bar{c}c)/\sqrt{12}$ then form a 15 dimensional representation of SU(4), with the orthogonal state, $(\bar{u}u + \bar{d}d + \bar{s}s + \bar{c}c)/\sqrt{4}$, remaining as a singlet of SU(4).

One might ask why one now bothers to study the "old" meson spectroscopy since charmonium (the set of $\bar{c}c$ states) serves as such a clear example of the meson ground state and excited levels, and "when you've seen one quark flavor combination, you've seen them all." The answer, first of all, is that is is precisely by comparing the ground state and excited levels for different flavors, that we learn that they are very similar. Secondly, there are differences in the detailed level structure and these reflect critically on the dynamics between quarks. Thirdly, certain L, S states are much more accessible and hence better studied, for the "old" mesons (e.g., high orbital angular momentum excitations), while other types of states are clearer experimentally for charmonium or charm.

For the L = 0 ground state there are sixteen $J^P = 0^-$ (S = 0) and sixteen 1^- (S = 1) flavor combinations. It now appears that all these mesons have been found experimentally. They are discussed in the lectures of M. Perl.[2] We proceed then to discuss the radial and orbital excitations, particularly of the "old" mesons.

We define a meson radial excitation as a state which has all the same quantum numbers, including internal quark L and S, as another $\bar{q}_1 q_2$ state at lower mass. The idea as well as the name for such states is borrowed from non-relativistic potential theory. There, in a potential of sufficient strength, one finds a series of such levels, each successive radial excitation having another node in its radial wave function. Familiar examples of such a situation occur for the Coulomb, harmonic oscillator and linear potentials.

Suppose such a higher mass pseudoscalar or vector meson is discovered; is it necessarily a radial excitation of the ground state? For a $J^P = 0^-$ state the answer is yes; one can only make a pseudoscalar out of a quark and antiquark if L = S = 0. Thus all quantum numbers including L and S are the same as that for the ground state pseudoscalar. For a $J^P = 1^-$ state, this is not necessarily so. Both internal L = 0, S = 1 and L = 2, S = 1 can result in $J^P = 1^-$ states and only the first case meets our definition of a radial excitation of the ground state. Furthermore, the closeness in mass of L = 0 radial excitations and L = 2 states in linear and harmonic potentials makes mixing between the corresponding $J^P = 1^-$ states very likely.

Barring such complete mixing, how can we tell the L = 0 from L = 2 vector mesons? First, if a pseudoscalar partner is found nearby in mass, we know it must be a radial excitation, and hence also the vector meson. Second, if we have enough confidence in our knowledge of the potential binding the quark and antiquark together, then we can calculate the mass predicted for a given state and expect experiment to agree. Along the same lines, if we know experimentally the mass of expected nearby states, it may be possible to associate a new state with L = 0 or L = 2 depending on its mass. Third, in a nonrelativistic picture $\Gamma(V^0 \to e^+e^-) \propto |f(r = 0)|^2$, the square of the spatial wave function at the origin. This vanishes for L = 2 in the nonrelativistic approximation. For charmed quarks at least, even after relativistic corrections, the L = 2 vector mesons should have a very much smaller leptonic width than those with L = 0. Last, in a theory of pionic decays based on the quark model, the relative signs of various vector meson decay amplitudes are different depending on whether L = 0 or 2. For example, the amplitudes for $\rho' \to \pi\omega$ vs. $\rho' \to \pi\pi$ have a different relative sign[27] if the ρ' is a quark-antiquark state with L = 2 rather than L = 0. Similar

considerations led to the establishment[28] of a $J^P = 3/2$, $I = 3/2$ pion-nucleon resonance at ~1700 MeV as a radial excitation of the $\Delta(1232)$ rather than an $L = 2$ baryon state.

The most persuasive evidence for a sequence of mesonic radial excitations comes from charmonium. There we have[29] the $\psi \equiv \psi$ (3095) and its radial excitation $\psi' \equiv \psi(3684)$. The new state,[30] $\psi(3772)$, on the basis of its leptonic width and agreement with potential model calculations is most likely an $L = 2$ level, though with some mixture of the $L = 0$ radial excitation, ψ'. The mass region between ~4 and ~4.2 GeV contains several bumps, with one very likely another radial excitation of the ψ. The $\psi(4414)$ fits fairly well as yet a third radial excitation. There is every reason to expect still higher mass radially excited states, but they become very difficult to distinguish from background because of the increasing total width and smaller coupling to e^+e^-.

With some recent additions to the list of known states, the evidence for radial excitations in the "old" meson spectrum is fairly convincing by itself. The only established[12] mesonic radial excitation for quite some time was the $\rho'(1600)$. In the last year or so it has been joined by a K'(1400), which was found[31] in an isobar analysis of the $K\pi\pi$ final state produced in K^- p collisions at 13 GeV/c. It is a $J^P = 0^-$ state decaying to $K(\pi\pi)_{S\text{-wave}}$, so, as noted before, it must be a radial excitation of the ground state K(495). It has a possible partner in the $K^{*\prime}$(1650), a vector meson found in some $K\pi$ phase shift solutions from the same experiment.[32] The situation in the later case is very similar to that for $\pi\pi$ phase shifts, where some solutions show the $\rho'(1600)$ rather distinctly.

The last few months have seen a population explosion among vector mesons composed of "old" quarks. The initial result from Orsay[33] was an indication of a resonance decaying to 5π near 1780 MeV. This has been followed by evidence for a relatively narrow bump at ~1820 MeV from Frascati.[34] Even more recent data indicates that the region from 1500 to 2000 MeV may be quite complicated with as many as half a dozen (or even more!) vector meson states found in that region.[35] Inasmuch as we do expect both $L = 0$ radial excitations and $L = 2$ vector mesons composed of $\bar{u}u$, $\bar{d}d$, and $\bar{s}s$ in that mass region, such a complicated situation is not totally unexpected. At still higher mass there are indications of a bump in inclusive K^* production in e^+e^- annihilation[36] near 2100 MeV ($a\,\phi''$?) and also a bump in diffractive six pion photoproduction mass spectra[37] ($a\,\rho''$?) around 2200 MeV.

The situation for the mass spectrum of established ground state mesons, and their radial excitations with non-zero isospin is summarized in Fig. 1. Note the apparent regularity: $M_\rho^2 - M_\pi^2 \approx M_{K^*}^2 - M_K^2 \approx M_{D^*}^2 - M_D^2 \approx M_{K^{*\prime}}^2 - M_{K'}^2$. This is not true for the corresponding states composed of $(\bar{u}u + \bar{d}d)/\sqrt{2}$, $\bar{s}s$, or $\bar{c}c$ quarks (with isospin zero). Even so, Fig. 1 does suggest that there should be a π' in the 1300 to 1400 MeV mass range. Further, it is of considerable interest to see if $L = 2$ vector mesons lie nearby those radial excitations with $L = 0$, as seems to be the case with $\psi(3684)$ and $\psi(3772)$. Although much remains to be sorted out, nevertheless, both charmonium and the "old" meson spectroscopy emphatically indicate that a sequence of radial excitations does exist in the meson spectrum.

The other clear set of excitations in the meson spectrum is that corresponding to non-zero orbital angular momentum between the quarks. The only orbitally excited states explored experimentally with even moderate thoroughness are those with $L = 1$. We recall from Section I that the quark model rules say that for each quark flavor combination we have an $L = 1$, $S = 0$ state with $J^{PC} = 1^{+-}$ and $L = 1$, $S = 1$ states with $J^{PC} = 0^{++}$, 1^{++}, and 2^{++}.

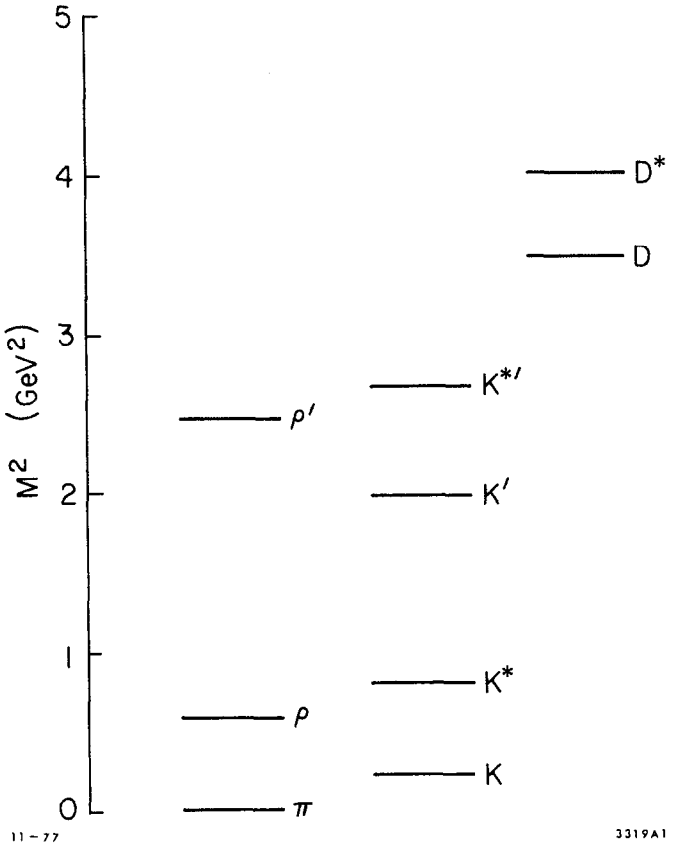

Fig. 1 Meson ground states and radical excitations with non-zero isospin.

The most spectacular examples of the L = 1, S = 1 states are the $X(3414)$, $\chi(3508)$, and $X(3552)$ levels of the charmonium ($\bar{c}c$) system.[2,38] The L = 1, S = 0 charmonium state has odd charge conjugation and will be difficult to find experimentally--so we shouldn't worry that it isn't an established state. In fact, we have every reason on the basis of charmonium to expect that the L = 1 meson states will be found in all possible quark flavor combinations.

For the $J^P = 2+$ states, this expectation is already fulfilled for the u, d, and s flavors. All the needed states are established, and we have the "ideal" or "magic" mixing situation shown in Table III.

TABLE III

$J^P = 2^+$ Mesons Composed of u, d, and s Quarks

Quark Flavor State	Observed Meson[12]
$\bar{d}u$, $(\bar{u}u - \bar{d}d)/\sqrt{2}$, $\bar{u}d$	$A_2(1310)$
$(\bar{u}u + \bar{d}d)/\sqrt{2}$	$f(1270)$
$\bar{s}u$ $\bar{s}d$	$K^*(1420)$
$\bar{d}s$ $\bar{u}s$	$\bar{K}^*(1420)$
$\bar{s}s$	$f'(1515)$ [c]

The $J^P = 1^+$ states of u, d and s quarks are a traditional area of experimental confusion. However, in the last year or so the situation is beginning to clarify. The biggest single advance has been the evidence[39,40,41] for two Q mesons, $Q_1(\sim 1300)$ and $Q_2(\sim 1400)$, which are axial-vector states containing a strange quark and a u or d quark. The observed states are actually mixtures[40] of the S = 0 and S = 1 quark model states. The B(1235) meson is an established[12] candidate for the isospin one axial-vector state composed of u and d quarks with

quark spin S = 0. The D(1285) (not to be confused with the charmed mesons) is the only established[12] isospin zero meson which likely has $J^P = 1^+$ (and from its positive charge conjugation would correspond to S = 1).

Along with the Q mesons, the traditional problem child of the axial-vector mesons is the A_1. Even here some real progress is being made.[41] Although earlier analyses of diffractive three pion production were never able to show evidence for a real resonance at the peak mass of ~1100 MeV, more recent theoretical work[42] with multichannel analyses do indicate resonance behavior, although perhaps at a higher mass (even possibly 1400 to 1500 MeV). At the same time, more direct experimental indications of a resonance decaying to $\pi\rho$ at ~1100 MeV come from several different experiments performed at CERN.[41] It seems unlikely that the uncertainty with regard to the A_1 will persist very much longer. With, in addition, the new evidence[43] for the heavy lepton decay $\tau \rightarrow A_1 \nu_\tau$, the establishment of a suitable isovector meson to match the L = 1, S = 1 axial-vector state of the quark model seems finally to be within sight.

While the situation for 1^+ states composed of u, d, and s quarks is considerably improved, that for the $J^P = 0^+$ states is more confusing than ever. The δ(970) seems healthy enough[12] as a candidate for the I = 1 state composed of u and d quarks. However, the s-wave Kπ phase shift rises slowly and passes through 90° near 1250 MeV. If defined as a strange, $J^P = 0^+$ resonance,[12] it must be very broad (~450 MeV), and furthermore, the drop in elasticity and phase motion at higher mass (~1400 MeV) is then suggestive of another resonance in the same channel.[40] The isospin zero s-wave ππ phase shift does much the same thing: it passes slowly through 90° near 700 MeV [ε(700)??], exhibits a clear resonance which also couples to $K\bar{K}$ [S* (990)] , and very likely shows another resonance, the ε'(1200), as a broad state. Discarding the ε(700), the latter state's width is ~600 MeV; otherwise it is narrow (~200 MeV).

The possibility that there are too many I = 0 and/or strange 0^+ states to fit the quark model is a big headache. Down through the ages, various explanations of this (e.g. dilatons,[44] glueballs,[45] cryptoexotics[7]) have been entertained which allow some or all of the observed 0^+ states to be other than $\bar{q}q$ L = 1 levels. On the other hand, if we throw out the ε(700) (and a higher mass K* besides κ(1250) we have a "peculiar" SU(3) octet plus singlet[46] with respect to quark model mass formulas. It is difficult to be optimistic that this situation will be resolved soon. It is fortunate that we have the χ states, the full set of 2+ states composed of u, d, and s quarks, and the improving situation with 1^+ mesons to bolster our confidence that all the L = 1 levels will be found eventually in all quark flavor combinations.

At the next level of orbital excitation, L = 2, we expect S = 0 ($J^{PC} = 2^{-+}$) and S = 1 ($J^{PC} = 1^{--}$, 2^{--}, 3^{--}) states. Of these only the 3^- states are in good shape: the g(1690), ω*(1675) and K*(1780) are all established[12] to have $J^P = 3^-$. The "ideal" or "magic" mixing pattern seems evident also, and we expect an $\bar{s}s$ (φ-like) state with $J^P = 3^-$ at 1850 to 1950 MeV. Other candidates for L = 2 levels, like the A_3 ($J^P = 2^-$) and L ($J^P = 2^-$) remain to be firmly established,[12] but enough has been found to give us assurance that all the L = 2 levels must exist for all quark flavor combinations.

When we get to L = 3, the only established state[12] is the h(2040), which fits as the L = 3, S = 1 isoscalar state composed of u and d quarks with $J^P = 4^+$. There are, however, some signs of a 4^+ K* state[40] near 2100 MeV and also of the corresponding I = 1 non-strange state.[41]

At still higher mass, there are bumps[12] in the $\bar{p}p$ total cross section at ~2190 and ~2360 MeV. Recent results[47] from $\bar{p}p \rightarrow \pi^-\pi^+$ using both differential cross section and polarization measurements strongly suggest broad

resonances at 2150, 2310, and 2480 MeV with $J^{PC} = 3^{--}$, 4^{++}, and 5^{--} respectively. This later result matches fairly well with an earlier fit[48] to angular distributions for $\bar{\pi}\, p \to \bar{p}p\, p$ assuming one pion exchange, which suggested a sequence of resonances in the same mass range.

Thus it is suggestive, at the very least, that many, broad, states occur at high masses. There seem to be narrower states as well,[49] although these may have another origin. Certainly, looking at the Regge plot of spin versus mass squared in Fig. 2, there is no sign that even the conventional states on the leading trajectory do not continue without interruption well into the 2 GeV mass region. The major outstanding question is the existence and nature of other, non-$\bar{q}q$ states in the meson spectrum.

III. BARYONS

As already discussed in Section I the overall color singlet nature of the three quarks in a baryon results in a color part of the wave function which is completely antisymmetric. According to Fermi-Dirac statistics the remainder of the wave function must be symmetric.

For the ground state, with all quarks in relative s-waves and L = 0, we have a symmetric spatial wave function. If the total quark spin is S = 3/2, then the spin wave function is symmetric and the only remaining quantity, flavor, also must have a symmetric wave function. With four quark flavors from which to choose, there are 20 possible symmetric three quark flavor states. These are shown in Table IV, together with the corresponding observed baryon, if known.

In the case of total quark spin S = 1/2, it may be shown that the spin wave function is of "mixed symmetry." With a symmetric ground state spatial wave function, Fermi-Dirac statistics now demands a mixed symmetry flavor wave function. With four quarks, it turns out there are again 20 such quark flavor states. It is purely an accident that the number of flavor states is the same

TABLE IV

S = 3/2 Baryon Ground States

Quark Flavor States				Observed States[12,50]
uuu	uud	udd	ddd	$\Delta^{++,+,o,-}(1232)$
	uus	uds	dds	$\Sigma^{*+,o,-}(1385)$
		uss	dss	$\Xi^{*o,-}(1530)$
			sss	$\Omega^{-}(1670)$
uuc	udc	ddc		Σ_c^* or $C_1^{*++,+,o}(2500?)$[51]
	usc	dsc		$S^{*+,o}$ (?)
		ssc		T^{*o} (?)
ucc	dcc			X_u^{*++}, X_d^{*++} (?)
	scc			X_s^{*+} (?)
ccc				Θ^{++} (?)

as for a symmetric flavor wave function: as we will see below, this is not true when there are other than four quark flavors. The appropriate mixed symmetry states composed of u, d, s, and c quarks, together with their experimental counterparts, are shown in Table V.

It is instructive for some of the things to follow to exhibit the explicit quark model wave functions as they depend on spin and flavor. We denote by $u\uparrow$ an "up" quark with spin component $S_z = +1/2$, $u\downarrow$ an "up" quark with spin component

TABLE V

S = 1/2 Baryon Ground States

Quark Flavor States				Observed States[12,50]
	uud	udd		$N^{+,o}(940)$
	uus	{ud}s	dds	$\Sigma^{+,o,-}(1190)$
		[ud]s		$\Lambda(1115)$
		uss	dss	$\Xi^{o,-}(1320)$
uuc	{ud}c	ddc		Σ_c or $C_1^{++,+,o}(2426?)$[52]
	{us}c	{ds}c		$S^{+,o}$ (?)
		ssc		T^{o} (?)
	[us]c	[ds]c		$A^{+,o}$(?)
	[ud]c			Λ_c or $C_o^{+}(2260)$[51]
ucc	dcc			X_u^{++} , X_d^{+} (?)
	scc			X_s^{+} (?)
	{ } = symmetrized, in flavor			[ ] = antisymmetrized in flavor

$S_z = -1/2$, etc. Then the wave function for a Δ^{++} with $J_z = 3/2$ is simply, $u\uparrow u\uparrow u\uparrow$, while that for a Δ^{+} with $J_z = 3/2$ is, $(1/\sqrt{3})$ $(u\uparrow u\uparrow d\uparrow + u\uparrow d\uparrow u\uparrow + d\uparrow u\uparrow u\uparrow)$. In the case of a Δ^{+} with $J_z = +1/2$, we must have complete symmetry in both spin and flavor, so the normalized wave function is:

$(1/\sqrt{9})(u\uparrow u\uparrow d\downarrow + u\uparrow d\downarrow u\uparrow + d\downarrow u\uparrow u\uparrow + u\uparrow u\downarrow d\uparrow + u\uparrow d\uparrow u\downarrow + d\uparrow u\uparrow u\downarrow + u\downarrow u\uparrow d\uparrow$

$+ u\downarrow d\uparrow u\uparrow + d\uparrow u\downarrow u\uparrow)$.

For the nucleon, say a proton with $J_z = 1/2$, one may construct the wave function in several ways. The simplest, perhaps, is to start with u and d quarks having $S = S_z = 0$. This is antisymmetric in spin, so we antisymmetrize in flavor also to obtain something symmetrical under overall interchange of the two quarks:

$$(u\uparrow d\downarrow - d\uparrow u\downarrow - u\downarrow d\uparrow + d\downarrow u\uparrow)/2.$$

If we now add a third quark, $u\uparrow$ and completely symmetrize it with the first two, we get on normalizing the result:

$(1/\sqrt{18})$ $(2u\uparrow u\uparrow d\downarrow + 2u\uparrow d\downarrow u\uparrow + 2d\downarrow u\uparrow u\uparrow - u\uparrow d\uparrow u\downarrow - d\uparrow u\uparrow u\downarrow - d\uparrow u\downarrow u\uparrow$

$- u\uparrow u\downarrow d\uparrow - u\downarrow u\uparrow d\uparrow - u\downarrow d\uparrow u\uparrow)$.

To get the neutron wave function with $J_z = 1/2$ we need only make the interchange $u \longleftrightarrow d$. The other $L = 0$ baryon wave functions are constructed analogously, and can be obtained straightforwardly.

As a first use of these wave functions let us consider the static electromagnetic properties of baryons. We picture these as arising from those of the constituent quarks. We have been doing this all along for the charge:

$$Q\ (\text{hadron}) = \sum_i Q_i\ (\text{quark}). \qquad (1)$$

Now we do the same for the magnetic moments. In other words, we assume that

$$\vec{\mu}\ (\text{hadron}) = \sum_i \vec{\mu}_i\ (\text{quarks}). \qquad (2)$$

We define the magnetic moment for a particle of spin J as

$$\mu = \langle J_z = J \left| \mu_z \right| J_z = J \rangle . \qquad (3)$$

This coincides with the usual definition for J = 1/2, 1, etc. With our previous assumption we have

$$\mu = \langle J_z = J \left| \sum_i \frac{eQ_i}{2m_i} \sigma_z^{(i)} \right| J_z = J \rangle \quad . \tag{4}$$

At this point the "quark masses," m_i, appearing in Eq. (4) are not defined and need not be directly related to the masses discussed in Section I. Setting $m_u = m_d$, we calculate the values of the baryon magnetic moments shown in Table VI, with the aid of the explicit wave functions developed above. There are also two transition moments that are experimentally accessible and calcuable in the same way. These are $\mu_{\Sigma\Lambda}$ and $\mu_{\Delta p}$, which are $-1/\sqrt{3}$ and $2\sqrt{2}/3$, respectively in the units of Table VI.

The comparison of these theoretical values with experiment is shown in Table VII. We fix $\mu_p = 2.79$ and calculate all other moments. In the column labeled $m_u/m_s = 1$, SU(3) symmetry is assumed. The value $m_u/m_s = 0.7$ corresponds to the constituent quark masses given in Table I and agrees somewhat better with experiment. The overall agreement with experiment is certainly very adequate, if not close to spectacular.

Radial excitations of the baryon ground state, as for meson radial excitations, differ only in having a different radial wave function and should have the same spin and flavor states available as the ground state. For S = 3/2 we then have a symmetric flavor wave function, while for S = 1/2 one of mixed symmetry. The number of possible baryon (three quark) flavor states as a function of the number of different quark flavors is given in Table VIII. Also shown is the number of flavor states times the number of S_z states available for the entire ground state or its radial excitation. We often refer to the set of these states by their total spin (S_z) and flavor multiplicity, e.g. for three quarks (u, d, s) it is the "56", made up of an SU(3) octet with S = 1/2 and a decuplet with S = 3/2.

TABLE VI

Baryon Magnetic Moments in the Quark Model

State	μ (units of $e/2m_u$)
Δ^{++}	2
Δ^{+}	1
Δ^{o}	0
Δ^{-}	-1
Σ^{*+}	$4/3 - 1/3\ (m_u/m_s)$
Σ^{*o}	$1/3 - 1/3\ (m_u/m_s)$
Σ^{*-}	$2/3 - 1/3\ (m_u/m_s)$
Ξ^{*o}	$2/3 - 2/3\ (m_u/m_s)$
Ξ^{*-}	$-1/3 - 2/3\ (m_u/m_s)$
Ω^{-}	$-(m_u/m_s)$
p	1
n	-2/3
Σ^{+}	$8/9 + (1/9)\ (m_u/m_s)$
Σ^{o}	$2/9 + (1/9)\ (m_u/m_s)$
Σ^{-}	$-4/9 + (1/9)\ (m_u/m_s)$
Λ^{o}	$-1/3\ (m_u/m_s)$
Ξ^{o}	$-2/9 - 4/9\ (m_u/m_s)$
Ξ^{-}	$1/9 - 4/9\ (m_u/m_s)$

TABLE VII

Comparison of Theory and Experiment for Baryon Magnetic Moments

Magnetic Moment	Theory $m_u/m_s = 1$	Theory $m_u/m_s = 0.7$	Experiment[12] (Nucleon Magnetons)
μ_p	2.79 (input)	2.79 (input)	2.79
μ_n	-1.86	-1.86	-1.91
μ_{Σ^+}	2.79	2.70	$2.62 \pm .41$
μ_{Σ^0}	.73	.84	
μ_{Σ^-}	-.93	-1.02	$-1.48 \pm .37$
μ_Λ	-.93	-.65	$-.67 \pm .06$
μ_{Ξ^0}	-1.86	-1.49	
μ_{Ξ^-}	-.93	-.56	$-1.85 \pm .75$
$\mu_{\Sigma\Lambda}$	-1.61	-1.61	$\pm\left(1.82^{+.25}_{-.18}\right)$[53]
$\mu_{\Delta p}$	2.63	2.63	2.6 to 3.4[54]

TABLE VIII

Multiplicity of the Baryon Ground State or its Radial Excitations

N = No. of Quark Flavors	No. of Baryon Flavor States S = 1/2	No. of Baryon Flavor States S = 3/2	No. of Spin Times Flavor States
1	0	1	4
2	2	4	20
3	8	10	56
4	20	20	120
5	40	35	220
6	70	56	364

Besides the ground state or its radial excitations, we will of course have the same accounting of baryon spin and flavor states whenever the quark spatial wave function is symmetric. For then the flavor times spin wave function is required to be symmetric, and we have exactly the same arguments on the available spin and flavor states that led us to Table VIII, for the ground state or its radial excitations.

For baryon orbital excitations one can in principle have quark spatial wave functions which are symmetrical, antisymmetrical, or of mixed symmetry. The lowest orbital excitation, that with L = 1, turns out to have a spatial wave function with mixed symmetry among the three quarks. For the case of quark spin S = 3/2 (a symmetric spin wave function), this forces a mixed symmetry flavor wave function. However, when S = 1/2 (mixed symmetry spin wave function) the overall Fermi-Dirac statistics can be satisfied with either a

symmetrical, mixed symmetry, or antisymmetrical flavor wave function. The situation with regard to the multiplicity of baryon flavor states in this case is shown in Table IX.

TABLE IX

Multiplicity of the Baryon Orbital Excitations with Mixed Symmetry Spatial Wave Functions

	No. of Baryon Flavor States				No. of Spin Times
	S = 3/2	S = 1/2			
N = No. of Quark Flavors	Mixed	Antisym.	Mixed	Sym.	Flavor States
1	0	0	0	1	2
2	2	0	2	4	20
3	8	1	8	10	70
4	20	4	20	20	168
5	40	10	40	35	330
6	70	20	70	56	572

Again, such an array of spin and flavor states will arise any time the three quark spatial wave function is of mixed symmetry. The set of these spin and flavor states is then often referred to by their total spin times flavor multiplicity, e.g. for three quarks one has the "70", composed of an S = 3/2 SU(3) octet and an S = 1/2 SU(3) singlet, octet, and decuplet.

Aside from the observed charmed baryons, which are candidates for being members of the L = 0 ground state, only states composed of u, d and s quarks are known for baryons. Therefore, in discussing the observations of radially and orbitally excited baryonic levels,[55] we consider only states composed of three quarks. As indicated above, we refer to the multiplets of given L by their spin (S_z) times flavor multiplicity.

The first excited baryon level above the ground state is a 56, L = 0 multiplet, i.e. a radial excitation of the 56, L = 0 ground state. Its most familiar non-strange member is the Roper resonance, N*(1470). The radially excited counterpart of the 3-3 resonance is the $\Delta^*(1690)$.

At slightly higher mass, on average, is a set of negative parity states which form a 70, L = 1 orbital excitation. All seven of the non-strange resonances needed to fill this multiplet are known to exist with the right spins and isospins—no more and no less than the expected states.

Above the 70, L = 1 there is another possible radial excitation of the ground state 56, L = 0. However, most of the evidence for this is based on the N*(1780) with $J^P = \frac{1}{2}^+$ and confirmation of the whole multiplet awaits evidence for some of the other states.

In the same mass range there is a further established multiplet, a 56, L = 2. Most, if not all of the six non-strange states sitting in this multiplet are found experimentally, including the long established N*(1688) with $J^P = \frac{5}{2}^+$ and the $\Delta^*(1950)$ with $J^P = \frac{7}{2}^+$.

In the 2 GeV mass region there is fairly good evidence for a 70, L = 3 set of states. In particular the established N*(2190) and N*(2140) with $J^P = \frac{7}{2}^-$ and $\frac{9}{2}^-$ respectively, rather uniquely fit into just such a multiplet.

At still higher mass there are the established $J^P = \frac{9}{2}^+$ N*(2220) and the $\frac{11}{2}^+$ $\Delta^*(2420)$. Even though essentially all the other states remain to be found, these two levels are very likely the first members of a 56, L = 4 multiplet.

Thus we see a fairly extensive sequence of radial and orbital excitations in the baryon spectrum, just as in the case of the meson spectrum. A few more multiplets are quite possible in the mass range discussed up to now (e.g. a 56, L = 2 radial excitation and a 70, L = 1 radial excitation).

The established multiplets so far all have the property that L even corresponds to a flavor times spin multiplicity of 56 while those with L odd have a multiplicity of 70. While this is trivial for the ground state, or first orbital excitation, it is entirely non-trivial that we do not see, say, 70, L = 0 and 70, L = 2 multiplets below 2 GeV. (These are expected in a harmonic oscillator potential to be degenerate with the 56, L = 2). The full significance of this for the quark-quark force remains to be seen. In fact, there are recent suggestions that the empirical connection of 56's and 70's with L even and odd, respectively, may break down: this is based on a $5/2^-$ Δ^* near 1960 MeV which would seem to fit best in a 56, L = 1 multiplet.[56]

At still higher mass spins and parities are unknown, but there are N* bumps at 2650 and 3030 MeV and Δ^*'s at 2850 and 3230 MeV. If one draws the leading Δ^* Regge trajectory (Fig. 3) it has a slope very much like that for the mesons (Fig. 2). Further, if we take the $\Delta^*(2850)$ and $\Delta^*(3230)$ as the next two states on the leading trajectory with $J^P = 15/2^+$ and $19/2^+$, respectively, then we have 5 states, all seemingly on a linear trajectory. As with the mesons, we have no reason to doubt that the baryon spectrum continues on to much higher masses, albeit with broader, low elasticity states, making it almost impossible to isolate individual levels and their quantum numbers.

IV. HADRON MASSES

As in our treatment of all other aspects of spectroscopy in these lectures, we discuss the subject of hadron masses within a picture of hadrons as composed of quarks. More particularly, we will work in a constituent or "atomic" model with quarks bound by an effective potential due to the action of colored gluons.[58,59]

In such a picture, hadron masses come from four sources:

(1) Quark masses;

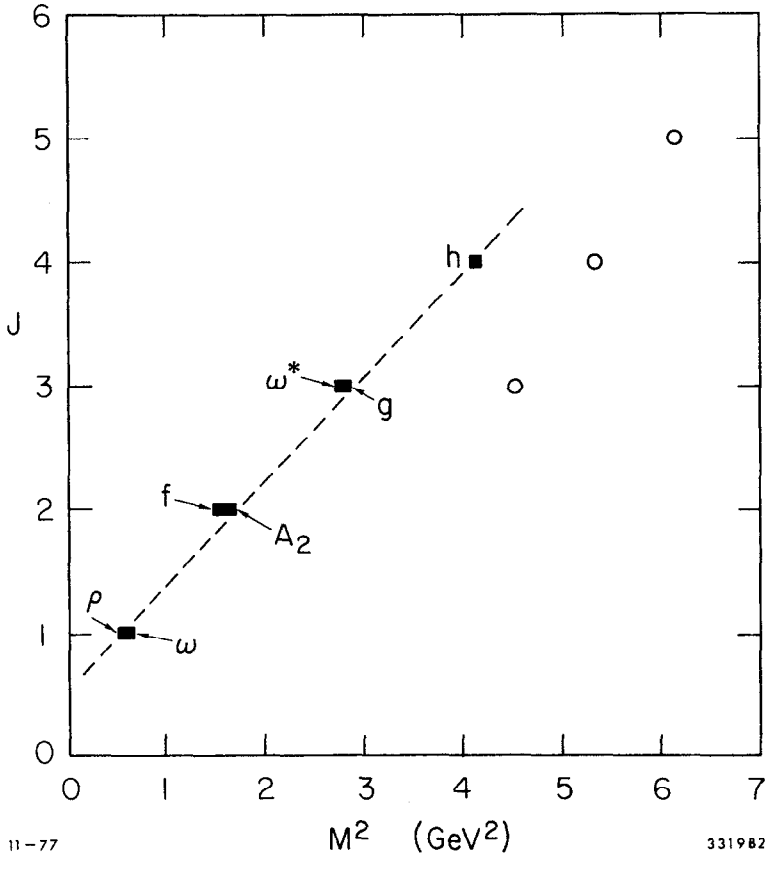

Fig. 2 Leading Regge trajectory for mesons (solid squares) and states established in Reference 47 (open circles).

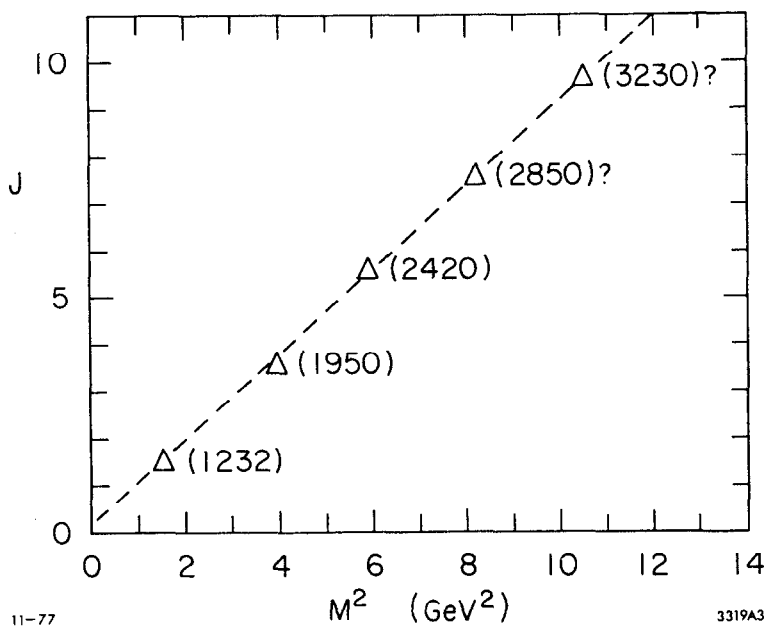

Fig. 3 Leading isospin 3/2 baryon Regge trajectory.

(2) The primary level of excitation of the potential, in other words the kinetic and potential energy of the quarks;

(3) The residual interactions between quarks of a spin-spin, spin-orbit or tensor force character, which split the principal levels of the potential;

(4) The gluons which carry energy (or mass) by themselves and also provide diagonal and off-diagonal elements to the meson mass matrix due to transitions of the form $\bar{q}_1 q_1 \longleftrightarrow$ gluons $\longleftrightarrow \bar{q}_2 q_2$.

The division among categories (1) through (4) is somewhat arbitrary. For example, sources (2) and (3) may be thought of as coming from the same basic origin, the exchange of gluons between quarks. If we could solve QCD the quark-quark interaction should emerge in toto from theory and give us (2) and (3) in one swoop.

Further, different values of the quark mass could well result in making (2), (3) and/or (4) different for various quark flavors. Thus effects from (1) could, for example, actually manifest themselves as mass splittings through a difference of forces of type (3).

The effect of the gluon energy, source (4), is usually assumed to be the same for all baryons with given L. On the other hand, mesons, $\bar{q}_i q_j$ with $i \neq j$, are distinguished from those with $i = j$ for given L, S, and J by the gluon annihilation and creation terms noted in (4).

Let us then examine where various masses and mass differences arise from in terms of sources (1) through (4).

Masses of Orbital and Radial Excitations Relative to the Ground State

Almost by definition these come from source (2), the level of excitation of the overall binding potential. Examples are the mass splitting between the L = 0 and L = 1 mesons or L = 0 and L = 1 baryons. The ω - f, ρ - A_2, K* - K**(1420),

ϕ - f' and ψ-χ (3552) mass differences,[12] which are each ~450 MeV, are all of the type: 1^- (L = 0) - 2^+ (L = 1). From this pattern[57] we expect that the 2^+ D** is at M_{D^*} + 450 MeV ≈ 2450 MeV and the 2^+ F** at M_{F^*} ≈ 2600 MeV.

If we measure the L = 0 to L = 1 mass splitting for baryons by that between states with symmetric spin wave functions (or between those with mixed symmetry spin wave functions), we also find a value of ~450 MeV. As for the meson examples given above, this mass splitting seems to be independent of quark flavor.

Splitting of States with Given L and S, Different J

This arises from spin-orbit forces or tensor forces which fall into category (3). In atomic physics this is called fine structure. For mesons, such forces give different masses to the δ, A_1, and A_2, or the χ_0, χ_1, and χ_2. These mass differences are all in the range 100 to 200 MeV for mesons, but somehow turn out to be very much smaller for baryons, e.g. the near degeneracy of the $1/2^-$, $3/2^-$ and $5/2^-$ N*'s with L = 1 and S = 3/2.

If the spin-orbit force arose from an "effective vector" exchange between the quark and antiquark in a meson and the effective potential is attractive, then it is possible to show that the mass splitting is proportional to $\vec{L} \cdot \vec{S}$ with a positive coefficient. Since

$$\vec{L} \cdot \vec{S} = \frac{J(J+1) - L(L+1) - S(S+1)}{2} \quad ,$$

the L = 1, S = 1 meson states would be 0^+, 1^+, and 2^+ in order of increasing mass. This is just the case for χ_0, χ_1, and χ_2. In principle the tensor force could have ruined this ordering, but at least for charmonium it turns out to have a smaller, but non-zero, coefficient.[59]

There is no proof that the quark-quark force has to have an "effective vector" form. Of course, this would result automatically if one gluon exchange dominated. But in the case of charmonium this gives rise to mass splittings[58] which are too small by an order of magnitude. There is no reason to expect that one gluon exchange is the dominate source of the spin-orbit force for any of the other mesons either.

Splitting of States With the Same L, Different S

These again have a source (3) origin, but are of the spin-spin variety. Such terms result in the N - Δ, Σ-Σ^*, etc. mass difference for baryons and the π - ρ , K - K*, D - D*, etc. splittings among mesons. They also split the B relative to the A_2, A_1, and δ.

If the interaction between quarks has an effective vector character, then in a non-relativistic situation the spin-spin interaction contribution to the mass from quarks i and j has the form:

$$\Delta M_{s\text{-}s} \propto \frac{1}{m_i m_j} \vec{S}_i \cdot \vec{S}_j \vec{\nabla}^2 V(r_{ij}) \quad , \qquad (5)$$

where V(r) is the effective potential in configuration space. With a single vector particle being exchanged, the proportionality constant in Eq. (5) has opposite signs for the case of two quarks (in a baryon) or a quark and antiquark (in a meson). However, if colored gluons are exchanged in color singlet hadrons, it turns out that the sign of the proportionality constant in Eq. (5) is the same for mesons and baryons.[58,59,60] Furthermore, the sign is such (positive) that with $\nabla^2 V(r)$ positive (as it is expected to be) the system with parallel quark spins has a higher energy than that with antiparallel spins. So if we accept the sign and general form of the spin-spin interaction that comes from colored gluon exchange, we predict that the ρ is heavier than the π, the K* heavier than the K,

and Δ heavier than the nucleon. While just one gluon exchange is unlikely to dominate completely in all these cases where mass splittings are a few hundred MeV, the experimentally observed sign in mesons and baryons seems to indicate that gluon exchange has something to do with at least the qualitative nature of these splittings.

Because of the explicit quark masses in the non-relativistic form of ΔM_{s-s}, even states with the same quark flavors but different relative quark spin orientations have different masses. This may well be the origin of the mass difference between the Λ and Σ.[58,60]

To see this, assume that

$$\Delta M_{s-s} = c \sum_{i>j} \frac{\vec{s}_i \cdot \vec{s}_j}{m_i m_j} \tag{6}$$

where c is a positive constant for the L = 0 baryons. In the Σ, the u and d quarks are in a symmetrical (I = 1) flavor state and hence a symmetrical (S = 1) spin state. The total spin of all three quarks is 1/2. This leads to

$$\vec{s}_u \cdot \vec{s}_d = \frac{1}{4} \quad , \tag{7a}$$

$$\vec{s}_u \cdot \vec{s}_s = \vec{s}_d \cdot \vec{s}_s = -\frac{1}{2} \tag{7b}$$

Hence,

$$\Delta M_{s-s}(\Sigma^o) = c\left[\frac{1}{m_u m_d}\left(\frac{1}{4}\right) + \frac{1}{m_u m_s}\left(-\frac{1}{2}\right) + \frac{1}{m_d m_s}\left(-\frac{1}{2}\right)\right]$$

$$= \frac{c}{4m_u^2} - \frac{c}{m_u m_s} \quad , \tag{8}$$

on taking $m_u = m_d$. For the Λ, the u and d quarks are in antisymmetrical flavor (I = 0) and spin = 0) states. Then for the Λ^o,

$$\vec{s}_u \cdot \vec{s}_d = -3/4, \tag{9a}$$

and

$$\vec{s}_d \cdot \vec{s}_s = \vec{s}_u \cdot \vec{s}_s = 0, \tag{9b}$$

so that

$$\Delta M_{s-s}(\Lambda) = -\frac{3c}{4m_u^2} \quad . \tag{10}$$

Combining (8) and (10), we have

$$M(\Sigma^o) - M(\Lambda^o) = \frac{c}{m_u^2} - \frac{c}{m_u m_s}$$

$$= \frac{c}{m_u^2}\left(1 - \frac{m_u}{m_s}\right) . \tag{11}$$

Since the strange quark is heavier than the up (or down) quark, we have $M_{\Sigma o} > M_{\Lambda o}$ in agreement with experiment.

It is interesting to note that the Λ_c and Σ_c would be split in mass by the same mechanism. With the charmed quark replacing the strange one,

$$M(\Sigma_c) - M(\Lambda_c) = \frac{c}{m_u^2}\left(1 - \frac{m_u}{m_c}\right) \quad . \tag{12}$$

Since $m_c > m_s$, this mass difference should be even larger than that between the Σ and Λ. If we identify the Σ_c with the BNL neutrino induced $\Lambda 4\pi$ system[52] at 2426 MeV and consider the Λ_c to be at 2260 MeV,[57] then this prediction is correct!

Splitting of States with Different Flavor

Such mass differences arise directly from source (1), but as we just saw they can arise indirectly from (3)[(or (2)]. The splitting of different flavor states with the same L, S, J and all other quantum numbers, allows us to estimate constituent quark mass differences. For example, we take

$$m_s - m_u \approx M(\Omega^-) - M(\Xi^*) \approx M(\Xi^*) - M(\Sigma^*)$$

$$\approx M(\Sigma^*) - M(\Delta) \approx 150 \text{ MeV} \qquad (13)$$

Similarly,

$$m_c - m_s \approx M(\Sigma_c^*) - M(\Sigma^*) \approx 1150 \text{ MeV} \qquad (14)$$

Essentially the same mass differences are obtainable by considering the ground state vector mesons, i.e. $2(m_c - m_s) \approx M(\psi) - M(\phi)$ and $2(m_s - m_u) = M(\phi) - M(\rho)$.

To get an absolute quark mass scale we must fix one of these masses. One way to do this is from charmonium, where calculations indicate $M_c \approx 1650$ MeV. Another way is to take $M_u \approx M_d$ to be $M_N/3$ or $M_\rho/2$, A third method is to take the expressions in terms of quark masses for the baryon magnetic moments in Section III very seriously. All these methods give the same answer:

$$m_u \approx m_d \approx 350 \text{ MeV}$$

$$m_s \approx 500 \text{ MeV}$$

$$m_c \approx 1650 \text{ MeV}. \qquad (15)$$

These "constituent quark masses" were already given in Table I. We repeat the caveat given there: These are not real masses, but only parameters with the dimensions of mass that appear in certain equations discussed above. Other equations give other values, e.g. current quark masses.

In addition to quark masses, gluons (source (4)) can also give hadrons composed of different flavors different masses. In particular, consider the contributions to the meson mass illustrated in Fig. (4). For mesons with net flavor (i.e., $i \neq j$), the second diagram makes no contribution to the mass matrix, for the gluons do not carry flavor. But for mesons with no net flavor ($i = j$), the second diagram contributes. Suppose it has the same value for all i and k, i.e. is flavor independent. Then for mesons with no net flavor we have two extreme situations.

If the first diagram due to the quark masses dominates the mass matrix, then the I = 0 eigenstates are $(\bar{u}u + \bar{d}d)/\sqrt{2}$, $\bar{s}s$, and $\bar{c}c$. We have the situation of "magic mixing" at the SU(3) level. The vector mesons $(\rho), \omega, \phi, \psi$ are a good example, as are the $J^P = 2^+$ and 3^- mesons.

On the other hand, if the second diagram due to annihilation into gluons dominates the mass matrix for N quark flavors, then its eigenstates are the $SU(N)_{flavor}$ singlet and non-singlet (s). For example, with u, d, and s quarks, the I = 0 eigenstates would be the SU(3) singlet and octet states, $(\bar{u}u + \bar{d}d + \bar{s}s)/\sqrt{3}$ and $(\bar{u}u + \bar{d}d - 2\bar{s}s)/\sqrt{6}$, respectively. The "old" pseudoscalar mesons are closer to, but not exactly in, this situation.

Furthermore, our assumption of the flavor independence of the second diagram is only approximate. Asymptotic freedom suggests that more gluons or higher mass of the meson makes the second diagram smaller.[16] Analysis of the situation with charmonium suggests a fairly big flavor dependence.[61] It will be interesting to test these ideas on the $\bar{s}s$ mesons in the L = 1 and L = 2 levels to see if the expected dependence on mass and gluon number is found experimentally.

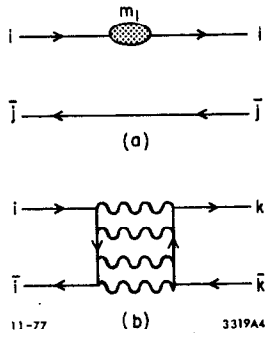

Fig. 4 (a) Meson mass matrix contribution due to quark mass.

(b) Meson mass matrix contribution due to gluon annihilation.

"Electromagnetic" Mass Differences

A particular example of some importance of the ideas we have been discussing is hadron electromagnetic mass differences. These have their origin in two physically distinct sources. First is the difference in mass of the u and d quarks. This is a source of type (1), which also has indirect effects of type (3). Second, there is explicit photon exchange between quarks, a manifest electromagnetic process.

By an accident (??) of nature the u - d mass difference and the effects due to photon exchange are of the same order, namely several MeV. Thus both are usually treated at the same time as "electromagnetic" mass differences.

These mass differences are characterized by several unique features. First, we can surely treat the splittings to lowest order in the perturbation. Further, we have a known interaction: one photon exchange in lowest order leads to a Coulomb interaction and to a magnetic dipole interaction. The first is proportional to the product of the charges, $Q_i Q_j$, of the quarks involved, while the second is proportional to the product of their charges and the dot product of their spins, $Q_i Q_j \vec{s}_i \cdot \vec{s}_j$. For the L = 0 baryons composed of u, d, and s, these quantities and the quark masses, summed over the appropriate flavors, are given in Table X.

We shall now assume that the mass of a state is determined by

$$M = M_o + \sum_{i=1}^{3} m_i + c_1 \sum_{i>j} Q_i Q_j + c_2 \sum_{i>j} Q_i Q_j \vec{s}_i \cdot \vec{s}_j \quad . \tag{16}$$

Here M_o depends on sources (2), (3) and (4) and consequently is different for each L, S, J, etc. All the "electromagnetic" effects are assumed to be in the last three terms: the difference in u - d quark masses in Σm_i, and the Coulomb and magnetic interactions in the last two terms, with c_1 and c_2 constants for a

given excitation of the overall binding potential. We neglect a possible dependence of c_2 on the mass of the quarks involved (at least for u, d, s). Also neglected at this simplified level are indirect effects of type (3), e.g. differences in the spin-spin interaction (buried in M_o) arising from strong interaction gluon exchange because different mass quarks (u and d) are involved. These more indirect effects, which are not necessarily negligible, can be taken into account in a more sophisticated calculation.[62]

If we apply Eq. (16) to the L = 0 baryons,[58] then there are three parameters (m_u m_d, c_1, and c_2) that enter mass differences, while there are four independent octet baryon mass differences. There is, therefore, one relation:[63]

$$M(p) - M(n) + M(\Xi^o) - M(\Xi^-) = M(\Sigma^+) - M(\Sigma^-). \qquad (17)$$

Experimentally, the left- and right- hand sides are -7.69 ± 0.6 MeV and -7.98 ± 0.08 MeV, respectively.

The three remaining independent mass differences may be solved for $m_u - m_d$, c_1, and c_2:

$$m_u - m_d = -1.9 \text{ MeV}, \qquad (18a)$$

$$c_1 = 3.6 \text{ MeV}, \qquad (18b)$$

$$c_2 = -7.2 \text{ MeV}. \qquad (18c)$$

Looking back at Table X, we find that the proton-neutron mass difference of -1.3 MeV arises as -1.9 MeV, + 1.2 MeV, and -0.6 MeV from the $m_u - m_d$, Coulomb, and magnetic terms respectively. The correct experimental sign is due to $m_u - m_d$! In general, all three terms give comparable contributions to baryon mass differences. The magnetic term is <u>not</u> negligible.

TABLE X

"Electromagnetic" Terms Contributing to Ground State Baryon Masses

State	$\sum_i m_i$	$\sum_{i>j} Q_iQ_j$	$\sum_{i>j} Q_iQ_j \vec{s}_i \cdot \vec{s}_j$
p	$2m_u + m_d$	0	1/3
n	$m_u + 2m_d$	-1/3	1/4
Σ^+	$2m_u + m_s$	0	1/3
Σ^o	$m_u + m_d + m_s$	-1/3	0
Σ^-	$2m_d + m_s$	1/3	-1/12
Ξ^o	$m_u + 2m_s$	-1/3	1/4
Ξ^-	$m_d + 2m_s$	1/3	-1/12
Λ	$m_u + m_d + m_s$	-1/3	1/6
Δ^{++}	$3m_u$	4/3	1/3
Δ^+	$2m_u + m_d$	0	0
Δ^o	$m_u + 2m_d$	-1/3	-1/12
Δ^-	$3m_d$	1/3	1/12
Σ^{*+}	$2m_u + m_s$	0	0
Σ^{*o}	$m_u + m_d + m_s$	-1/3	-1/12
Σ^{*-}	$2m_d + m_s$	1/3	+1/12
Ξ^{*o}	$m_u + 2m_s$	-1/3	-1/12
Ξ^{*-}	$m_d + 2m_s$	1/3	+1/12
Ω^-	$3m_s$	1/3	+1/12

For the ground state decuplet one may now deduce the relations:[58]

$$M(\Delta^{++}) - M(\Delta^{+}) = M(p) - M(n) + M(\Sigma^{+}) + M(\Sigma^{-}) - 2M(\Sigma^{o}), \tag{19a}$$

$$M(\Delta^{+}) - M(\Delta^{o}) = M(\Sigma^{*+}) - M(\Sigma^{*o}) = M(p) - M(n), \tag{19b}$$

$$M(\Delta^{o}) - M(\Delta^{-}) = M(\Sigma^{*o}) - M(\Sigma^{*-}) = M(\Xi^{*o}) - M(\Xi^{*-}) \tag{19c}$$

$$= M(p) - M(n) - M(\Sigma^{+}) - M(\Sigma^{-}) + 2M(\Sigma^{o}).$$

Only the last of these is testable now with some sensitivity:
$M(\Xi^{*o}) - M(\Xi^{*-}) = -3.3 \pm 0.6$ MeV and $M(p) - M(n) - [M(\Sigma^{+}) + M(\Sigma^{-}) - 2M(\Sigma^{o})]$ $= -3.07 \pm 0.10$ MeV, in good agreement. Adding (19b) and (19c) we obtain

$$M(\Sigma^{*+}) - M(\Sigma^{*-}) = 2M(p) - 2M(n) \tag{20}$$
$$- M(\Sigma^{+}) - M(\Sigma^{-}) + 2M(\Sigma^{o}).$$

The left- and right- hand sides of this later relation are -4.1 ± 1.5 MeV and -4.36 ± 0.10 MeV, so it is consistent with experiment within rather large errors.

This striking success for predicting ground state baryon electromagnetic mass differences on the basis of Eq. (16) is not repeated for mesons. If we stick to u, d, and s quarks there are only two independent mass differences: $M(\pi^{+}) - M(\pi^{o})$ and $M(K^{+}) - M(K^{o})$. Since $Q_i Q_j$ and $Q_i Q_j \vec{S}_i \cdot \vec{S}_j$ are proportional for mesons of given total quark spin (like pseudoscalars), there are also only two independent parameters (say $m_u - m_d$ and c_1). Therefore we do not get mass formulas like Eqs. (17), (18), (19), and (20) in this case.

While there is no relation, we can still invert the equations relating the two mass differences to the two parameters. Since the pion must be a deeply bound, relativistic system there is no reason for Eq. (16), linear in $\sum_i m_i$ to be valid. Indeed if we push blindly ahead we find $m_u - m_d \approx -7.1$ MeV, which very much disagrees with the value derived from the baryons.

It appears that to describe the meson electromagnetic mass differences we need to go beyond our simplified formula, Eq. (16). Some success[62] has been reported, including values for the D and D* electromagnetic mass differences in agreement with experiment, by taking into account the difference in the strong spin-spin interaction due to $m_u - m_d$.

REFERENCES

1. This and other aspects of hadron spectroscopy not discussed here are found in F. J. Gilman, Proceedings of the Summer Institute on Particle Physics, 1974, M. Zipf, ed., SLAC Report No. 179, Vol. 1, p. 307.

2. M. Perl, these proceedings.

3. See the reviews of deep inelastic scattering by F. J. Gilman, Proceedings of the XVII International Conference on High Energy Physics, J. R. Smith, ed. (Rutherford Laboratory, Chilton, Didsot, 1974), p. IV-149 and by C. H. Llewellyn-Smith, Proceedings of the 1975 International Symposium on Lepton and Photon Interactions at High Energies, W. T. Kirk, ed. (Stanford Linear Accelerator Center, Stanford, 1975), p. 709.

4. M. J. Alguard et al., Phys. Rev. Letters 37, 1261 (1976).

5. R. F. Schwitters, Proceedings of the 1975 International Symposium on Lepton and Photon Interactions at High Energy, W. T. Kirk, ed. (Stanford Linear Accelerator Center, Stanford, 1975, p. 5. Also V. Luth, topical conference in these proceedings.

6. G. Feldman, topical conference in these proceedings.

7. For a review of some aspects of exotics, see R. Jaffe, topical conference in these proceedings.

8. H. J. Melosh, Phys. Rev. D9, 1095 (1974).

9. See the discussion of J. D. Bjorken, Proceedings of the Summer Institute on Particle Physics, 1975, M. Zipf, ed., SLAC Report No. 191, p. 85.

10. R. Blankenbecker, S. Brodsky and D. Sivers, Phys. Reports 23C (1976); S. D. Ellis and R. Stroynowski, Rev. Mod. Phys. 49, 753 (1977).

11. S. L. Adler, Phys. Rev. 177, 2426 (1969); J. S. Bell and R. Jackiw, Nuovo Cim. 51, 47 (1969).

12. Particle Data Group, Rev. Mod. Phys. 48, 51 (1976).

13. G. 't Hooft, unpublished. D. J. Gross and F. Wilczek, Phys. Rev. Letters 30, 1343 (1973); H. D. Politzer, Phys. Rev. Letters 30, 1346 (1973).

14. A review of quark confinement in QCD is given by L. Susskind, invited talk at the 1977 International Symposium on Lepton and Photon Interactions at High Energies, Hamburg, Germany, August 25-31, 1977.

15. S. Okubo, Physics Letters 5, 165 (1963); G. Zweig, unpublished. J. Iizuka, Supplement to Progress Theor. Physics 37-38, 21 (1966).

16. T. Appelquist and H. D. Politzer, Phys. Rev. Letters 34, 43 (1975); A. De Rujula and S. L. Glashow, Phys. Rev. Letters 34, 46 (1975).

17. See, for example, J. Ellis et al., Nucl. Phys. B111, 253 (1976). Also T. deGrand et al., SLAC-PUB-1950, 1977 (unpublished) and references therein.

18. E. Eichten et al., Phys. Rev. Letters 34, 369 (1975).

19. S. W. Herb et al., Phys. Rev. Letters 39, 252 (1977); W. R. Innes et al., Phys. Rev. Letters 39, 1240 (1977).

20. R. Jaffe, Phys. Rev. D15, 267 and 281 (1977); R. Jaffe, MIT preprint MIT-CTP-657, 1977 (unpublished). See also Reference 7.

21. L. B. Okun and M. B. Voloshin, JETP Letters 23, 333 (1976); A. De Rujula et al., Phys. Rev. Letters 38, 317 (1977). See also M. Bander et al., Phys. Rev. Letters 36, 695 (1976); C. Rosenzwug, Phys. Rev. Letters 36, 697 (1976); Y. Iwasaki, Prog. Theor. Phys. 54, 492 (1975).

22. J. Rosner, Phys. Rev. Letters 21, 950 (1968) and the review and references in Reference 44.

23. D. Horn and J. Mandula, Caltech preprint CALT-68-575, 1977 (unpublished).

24. H. Fritzsch and M. Gell-Mann, Proceedings of the XVI International Conference on High Energy Physics, J. D. Jackson and A. Roberts, eds. (National Accelerator Laboratory, Batavia, 1972), Vol. 2, p. 135; J. Kogut et al., Nucl. Phys. B114, 199 (1976); D. Robson, University of Liverpool preprint, 1977 (unpublished).

25. A neutral fermion "soul" for baryons was more popular before the advent of color when the spin-statistics theorem for quarks was otherwise in question. Related effects on the spectroscopy occur from the motion of a "bag" relative to the quarks; see A. Chodos et al., Phys. Rev. D9, 3471 (1974) and W. Bardeen et al., Phys. Rev. D11, 1094 (1975). Also, T. A. DeGrand and R. L. Jaffe, ref. 60.

26. See R. Giles and S.-H. Tye, SLAC preprint SLAC-PUB-1907, 1977 (unpublished).

27. F. J. Gilman, Experimental Meson Spectroscopy-1974, D. Garelick, ed. (American Institute of Physics, New York, 1974), AIP Conference Proceedings No. 21, p. 369.

28. R. Cashmore et al., Nucl. Phys. B92, 37 (1975).

29. Throughout these lectures we use the notation of putting a particles mass in MeV in parentheses after its name.

30. P. A. Rapidis et al., Phys. Rev. Letters 39, 526 (1977).

31. G. Brandenburg et al., Phys. Rev. Letters 36, 1239 (1976). See also Reference 40.

32. P. Estabrooks et al., SLAC preprint, SLAC-PUB-1886, 1977 (unpublished).

33. G. Cosme et al., Phys. Letters 67B, 231 (1977). See also Reference 35.

34. B. Esposito et al., Phys. Letters 68B, 389 (1977); C. Bacci et al., Phys. Letters 68B, 393 (1977); G. Barbiellini et al., Phys. Letters 68B, 397 (1977). See also Reference 35.

35. F. Laplanche and C. Bemporad, invited talks at the 1977 International Symposium on Lepton and Photon Interactions at High Energies, Hamburg, Germany, August 25-31, 1977.

36. B. Esposito et al., Frascati preprint LNF-76/64-P, 1977 (unpublished). See also Reference 35.

37. See B. Knapp, Particles and Fields '76, H. Gordon and R. Peierls, eds. (Brookhaven National Laboratory, Upton, New York, 1977), p. A13.

38. See the review of charmonium in G. J. Feldman and M. L. Perl, Phys. Rep., to be published and SLAC-PUB-1972, 1977 (unpublished).

39. G. Brandenburg et al., Phys. Rev. Letters 36, 703 and 706 (1976); H. Otter et al., Nucl. Phys. B106, 77 (1976). See also R. K. Carnegie et al., Phys. Letters 63B, 235 (1976).

40. D. W. G. S. Leith, invited talk at the V. International Conference on Experimental Meson Spectroscopy, Boston, April 28-30, 1977 and SLAC-PUB-1908, 1977 (unpublished). T. Lasinski, topical conference in these proceedings.

41. R. Hemingway, tpoical conference in these proceedings and references therein.

42. J. L. Basdevant and E. Berger, Argonne preprint ANL-HEP-PR77-02, 1977 (unpublished); R. Aaron and R. S. Longacre, Phys. Rev. Letters 38, 1509 (1977).

43. G. Knies and M. L. Perl, invited talks presented at the 1977 International Symposium on Lepton and Photon Interactions at High Energies, Hamburg, Germany, August 25-31, 1977. J. Jaros, private communication.

44. See J. Rosner, Phys. Reports 11C, 189 (1974).

45. H. Fritzsch and M. Gell-Mann, Reference 24.

46. D. Morgan, Phys. Letters 51B, 71 (1974).

47. A. A. Carter et al., Phys. Letters 67B, 117 (1977) and references therein to previous work.

48. B. Hyams et al., Nucl. Phys. B73, 202 (1974).

49. See the review in D. Treille, topical conference in these proceedings.

50. We employ the notation, (Co, C1, S, T, ...) of M. K. Gaillard et al., Rev. Mod. Phys. 47, 277 (1975) or B. W. Lee et al., Phys. Rev. D15, 157 (1977) for charmed baryon states; but use as well Λ_c, Σ_c and Σ_c^*, where these indicate the states with the quark content of a Λ, Σ, and Σ^*, respectively, with the s quark replaced by a c quark.

51. B. Knapp et al., Phys. Rev. Letters 37, 882 (1976).

52. E. G. Cazzoli et al., Phys. Rev. Letters 34, 1125 (1975).

53. F. Dydak et al., Nucl. Phys. B118, 1 (1977).

54. A recent discussion of values for $\mu_{\Delta p}$ is found in F. J. Gilman and I. Karliner, Phys. Rev. D10, 2194 (1974).

55. The present state of baryon spectroscopy is reviewed by K. Lanius, Proceedings of the XVII International Conference on High Energy Physics, (JINR, Dubna, 1976), Vol. I, p. C45.

56. R. E. Cutkosky and R. E. Hendrick, Carnegie-Mellon University preprints COO-3066-81 and COO-3066-99, 1977 (unpublished).

57. The charmed particle masses discussed here are from work done with S. Meshkov (unpublished).

58. A. De Rujula et al., Phys. Rev. D12, 147 (1975).

59. A review, particularly of work on charmonium masses is found in J. D. Jackson, Proceedings of the Summer Institute on Particle Physics, 1976, M. Zipf, ed., SLAC Report No. 198, p. 147.

60. The effect of the "color magnetic" interaction in hadron spectroscopy was first calculated in the MIT bag model by T. DeGrand et al., Phys. Rev. D12, 2060 (1975). See also T. A. DeGrand and R. L. Jaffe, Ann. Phys. (N.Y.) 100, 425 (1976) and T. A. DeGrand, Ann. Phys. (N.Y.) 101, 496 (1976).

61. See, for example, the recent discussion of pseudoscalar mesons by H. Fritzsch and J. D. Jackson, Phys. Letters 66B, 365 (1977) and references therein.

62. See L.-H. Chan, Phys. Rev. D15, 2478 (1977), and L.-H. Chan, Louisianna State University preprint, 1977 (unpublished).

63. S. Coleman and S. L. Glashow, Phys. Rev. Letters 6, 423 (1961).

LECTURES ON THE QUARK MODEL, ORDINARY MESONS, CHARMED MESONS, AND HEAVY LEPTONS*

Martin L. Perl
Stanford Linear Accelerator Center
Stanford, California 94305

*Work supported by the Department of Energy.

LECTURES ON THE QUARK MODEL, ORDINARY MESONS, CHARMED MESONS, AND HEAVY LEPTONS

Martin L. Perl
Stanford Linear Accelerator Center

1. INTRODUCTION

These lectures have two connected themes. First the quark model is used to discuss the masses, internal quantum numbers, and weak decays of the ordinary mesons and charmed mesons. In this discussion the quarks are treated as elementary particles; and this view is particularly valuable in discussing the weak decays of the mesons. About 3/4 of the lectures are devoted to these topics.

The last 1/4 of the lectures is devoted to the theory of, and evidence for, a new charged lepton produced in e^+e^- annihilation. In developing the theory of the decay modes, and in comparing the heavy lepton with the singly charmed meson we make extensive use of the connections between the weak decays of quarks and the weak decays of leptons.

2. THE QUARK MODEL FOR MESONS

I will use the fractionally charged quark model, Table I, to:

a. explain the internal quantum of the mesons such as spin, charge, parity....;

b. discuss the weak decays of mesons, particularly of the charmed mesons;

c. understand the general mass spectrum of the mesons.

Some general references are:

R.H. Dalitz in High Energy Physics (Gordon and Breach, 1965).

R.H. Dalitz in Meson Spectrocopy (Benjamin, 1968).

J.D. Jackson in Proc. of SLAC Summer Inst. on Particle Physics - 1976 (SLAC-198).

TABLE I

The fractionally charged quarks with spin 1/2 and baryon number 1/3

Name	u	d	s	c
Old Name	p	n	λ	s'
I	1/2	1/2	0	0
Iz	1/2	-1/2	0	0
Q	+2/3	-1/3	-1/3	+2/3
S (strangeness)	0	0	-1	0
C (charm)	0	0	0	1

We assume a meson consists of one quark, q_i, and one antiquark, $\bar{q}_j$, bound together by a non-relativistic potential $V(q_i, \bar{q}_j)$. No one really understands why this non-relativistic model works so well considering that the forces between the quarks are strong. A meson then has a mass

$$M = m_i + m_j + V(q_i, \bar{q}_j) \qquad (1)$$

if its quark content is a single type of quark and a single type of antiquark. Here m_i, m_j are the masses of quark i and antiquark j.

In general a meson may have mixed quark content such as the $\pi^o = (u\bar{u} - d\bar{d})/\sqrt{2}$. Therefore define a diagonal quark mass operator $M + \bar{M}$ where

$$\begin{aligned} \langle u|M|u\rangle &= \langle \bar{u}|\bar{M}|\bar{u}\rangle = m_u \\ \langle d|M|d\rangle &= \langle \bar{d}|\bar{M}|\bar{d}\rangle = m_d \end{aligned} \qquad (2)$$

and so forth. Let $\chi(q, \bar{q})$ be the quark content wave function; for example π^o has $\chi = (u\bar{u} - d\bar{d})/\sqrt{2}$. Then the meson mass is given by

$$M = \langle \chi|M + \bar{M}|\chi\rangle + V(q, \bar{q}) \qquad (3)$$

For example

$$M_{\pi^o} = \langle u\bar{u} - d\bar{d}|M + \bar{M}|u\bar{u} - d\bar{d}\rangle/2 + V$$
$$= (m_u + m_u + m_d + m_d)/2 + V \qquad (4)$$
$$= m_u + m_d + V$$

In this model the spin and parity are calculated using LS coupling as follows

L = orbited angular momentum between q_i and $\bar{q}_j$

S = total spin of q_i and $\bar{q}_j$ = 0 or 1

J = total angular momentum.

Therefore

If S = 0, then J = L ;

if S = 1 and L = 0, then J = 1 ; (5)

if S = 1 and L > 0, then J = L - 1, L, L + 1 .

we use atomic spectroscopy notation:

$$n^{2S+1}L_J \qquad (6)$$

where n is the radial excitation quantum number and L is written S, P, D, F....for L = 0, 1, 2, 3... Since q_i, $\bar{q}_j$ are a fermion-anti-fermion pair the parity is given by

$$P = -(-1)^L \qquad (7)$$

To get a feeling for the energy degeneracy of a state $n^{2S+1}L_J$ as a function of n, S, L, and J we consider two potentials:

a. the attractive coulomblike (hydrogen atomlike) potential

$$V(r) = -A/r \quad , \quad A > 0 \qquad (8a)$$

b. the attractive harmonic oscillator potential

$$V(r) = \tfrac{1}{2}Kr^2 \quad , \quad K > 0 \qquad (8b)$$

The degeneracies are shown schematically in Fig. 1.

However the potential used most commonly for $(q_i, \bar{q}_j)$ is the attractive linear potential

$$V(r) = Br \quad , \quad B > 0 \qquad (9)$$

The calculation of the S state energy levels for a linear potential is discussed in App. 1. Figure 2 compares the energy level spacings for the S states for the three potentials when the spacing is the same between the two lowest level for all the potentials.

3. THE GROUND STATES OF ORDINARY MESONS

A. The Psudeoscalar Mesons: The ground state pseudoscalar mesons have

$$L = 0, \; S = 0, \; J = 0, \; P = -1 \qquad (10)$$

hence they are in the $^1S_0$ state. Their quark content and some properties are given in Table II

TABLE II

Name	Mass (MeV/c^2)	I	I_z	Y	Quark Content
K^+	494	½	½	1	$u\bar{s}$
K^o	498	½	-½	1	$d\bar{s}$
$\bar{K}^o$	498	½	½	-1	$s\bar{d}$
K^-	494	½	-½	-1	$s\bar{u}$
π^+	140	1	1	0	$u\bar{d}$
π^o	135	1	0	0	$(u\bar{u} - d\bar{d})/\sqrt{2}$
π^-	140	1	-1	0	$d\bar{u}$
η	549	0	0	0	$(u\bar{u} + d\bar{d} - 2s\bar{s})/\sqrt{6}$
η'	958	0	0	0	$(u\bar{u} + d\bar{d} + s\bar{s}(/\sqrt{3}$

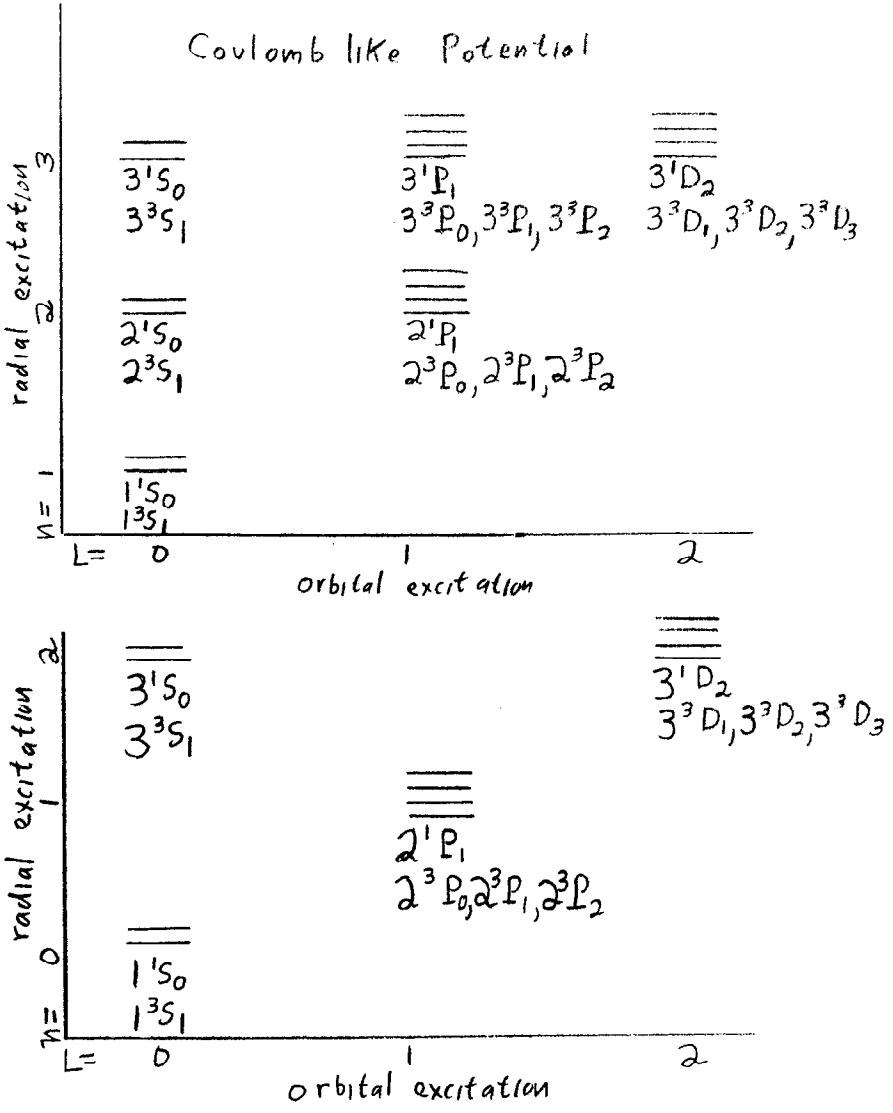

Fig. 1

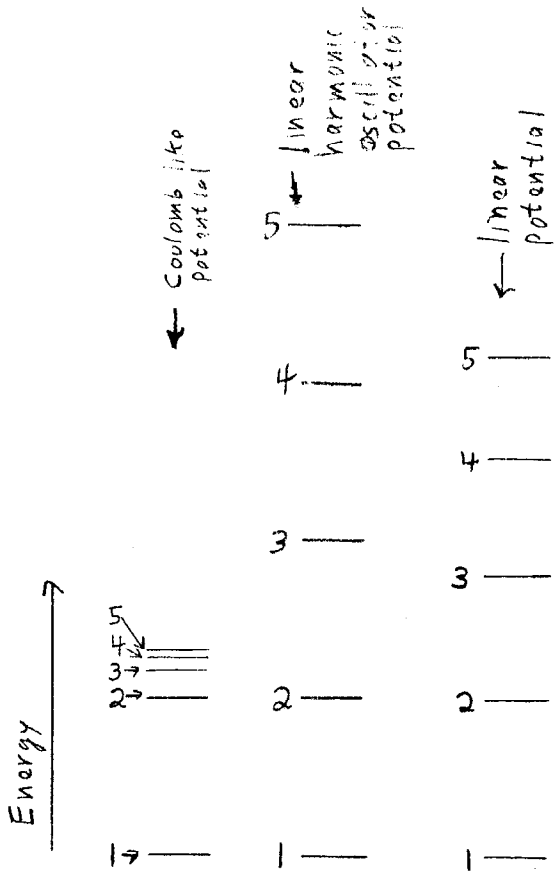

Fig. 2. Comparison of S state energy levels. The numbers are the radial quantum number n

We see how beautifully the quark model explains all the internal quantum number of these mesons. The quark content of the K and π mesons is straightforward, but as the parenthesis indicate the η, η' quark content is not straightforward. Here we have given the SU(3) quark wave functions. $(u\bar{u} + d\bar{d} + s\bar{s})/\sqrt{6}$ is an SU(3) singlet and $(u\bar{u} + d\bar{d} - s\bar{s})/\sqrt{6}$ is an $I_z = 0$ state which is orthogonal to it and to the π^o. I will return to the η, η' quark content question after discussing the masses.

To begin the discussion of the masses we use Eq. 3 with the extreme simplification:

$$V(q_i, \bar{q}_j) = -E_b \tag{11}$$

where E_b is a binding energy independent of the quark content and the SU(3) multiplet. Also assume

$$m_u = m_d = m \tag{12}$$

and let

$$m_s - m = \delta \tag{13}$$

Then
$$M_K = 2m + \delta - E_b \ , \qquad M_\pi = 2m - E_b \ , \tag{14}$$

hence

$$\delta = m_s - m = M_K - M_\pi = 363 \text{ MeV}/c^2 \tag{15}$$

Using Eq. 15

$$M(u\bar{u} + d\bar{d} - 2s\bar{s}) - M_K = \delta/3 = +121 \text{ MeV}/c^2$$
$$M(u\bar{u} + d\bar{d} + s\bar{s}) - M_K = -\delta/3 = -121 \text{ MeV}/c^2 \tag{17}$$

But

$$M_\eta - M_K = +51 \text{ MeV}/c^2 \ , \qquad M_{\eta'} - M_K = +460 \text{ MeV}/c^2 \ , \tag{17}$$

hence this simplest model does not fit M_η or $M_{\eta'}$.

We can obviously fit $M_{\eta'}$ by settting $\chi(\eta') = (u\bar{u} + d\bar{d} + s\bar{s})/\sqrt{3}$ and allowing E_b to depend on the SU(3) multiplet. Then

$$E_b(8) \neq E_b(1) \tag{18}$$

and we can adjust $E_b(1)$ to give $M_{\eta'}$. But we still cannot fit well M_π, M_K, and M_η simultaneously. In his lectures F. Gilman discusses more sophisticated models for the masses, however fitting these pseudoscalar masses with the simple quark model remains a problem. (We shall see in the next section that the vector meson masses can be easily fit.)

Finally we note that there is no clear experimental proof for setting

$$\chi(\eta') = (u\bar{u} + d\bar{d} + s\bar{s})/\sqrt{3}$$
$$\chi(\eta) = (u\bar{u} + d\bar{d} - 2s\bar{s})/\sqrt{6} \tag{19}$$

beyond the arguments that then we can fit $M_{\eta'}$ by adjusting $E_b(1)$.

B. The Vector Mesons: For the vector mesons

$$L = 0, \ S = 1, \ J = 1, \ P = -1 \tag{20}$$

hence they are in the $^3S_1$ state. Their quark content and some properties are given in Table III

TABLE III

Name	Mass (MeV/c^2)	I	I_z	Y	Quark Content
K^{*+}	892	½	½	1	$u\bar{s}$
K^{*o}	892	½	-½	1	$d\bar{s}$
$\bar{K}^{*o}$	892	½	½	-1	$s\bar{d}$
K^{*-}	892	½	-½	-1	$s\bar{u}$
ρ^+	770	1	1	0	$u\bar{d}$
ρ^o	770	1	0	0	$(u\bar{u} - d\bar{d})/\sqrt{2}$
ρ^-	770	1	-1	0	$\bar{d}u$
ω	783	0	0	0	$(u\bar{u} + d\bar{d})/\sqrt{2}$
ϕ	1019	0	0	0	$s\bar{s}$

Here the quark content of the ϕ has been made $s\bar{s}$ to explain ϕ properties such as $\phi \to K^+K^-$ being the dominant decay mode. We then set $\chi(\omega) = (u\bar{u} + d\bar{d})/\sqrt{2}$ to give a quark wave function orthogonal to the π^o and ϕ. These are <u>not</u> the SU(3) multiplet quark contents for the I = 0 states.

We now repeat the simple mass calculation of the previous section using $E_b(8) = E_b(1) = E_b$. Then

$$\delta = m_s - m = M_{K^*} - M_\rho = 122 \text{ MeV}/c^2 \qquad (21)$$

Then the theory predicts

$$\begin{aligned} M_\omega - M_\rho &= 0 \\ M_\phi - M_\rho &= 2\delta = 244 \text{ MeV}/c^2 \end{aligned} \qquad (22)$$

This is in good agreement with the measurements:

$$\begin{aligned} M_\omega - M_\rho &= 13 \text{ MeV}/c^2 \\ M_\phi - M_\rho &= 249 \text{ MeV}/c^2 \end{aligned} \qquad (23)$$

Thus the simplest quark model mass calculation works here.

4. A LOOK AHEAD ON CHARMED MESON MASSES

Lets be very, very simple by using the mass values from the last section and assuming

$$E_b = 0! \qquad (24)$$

Then

$$m = M_\rho/2 = 385 \text{ MeV}/c^2 \qquad (25a)$$

$$m_s = M_{K^*} - M_\rho = 507 \text{ MeV}/c^2 \qquad (25b)$$

Following Eq. 25a we get the mass of the charm quark, m_c,

$$m_c = M_{\psi/2} = 1547 \text{ MeV}/c^2 \qquad (26)$$

Then we predict the mass of the D or D* meson should be

$$M_D \text{ or } M_{D^*} \sim m + m_c = 1932 \text{ MeV}/c^2 \qquad (27)$$

The measurements are

$$\begin{aligned} M_{D^o} &= 1863 \text{ MeV}/c^2 \ , \\ M_{D^{*o}} &= 2006 \text{ MeV}/c^2 \ , \end{aligned} \qquad (28)$$

which means that Eq. 27 is a surprisingly good estimate considering the extreme simplicity of the theory.

5. WEAK DECAYS VIA THE QUARK MODEL

We are going to study next the use of the quark model for the weak decays of the hadrons. We do this for two reasons:

a. The quark model provides a simple way to systematize the weak decays of the hadrons.

b. The understanding of the properties of the charmed mesons depends upon a clear picture of their weak decays.

In this section we compare non-quark and quark models for a simple weak decay mode — the leptonic decay of a pseudoscalar.

$$P^+ \to \ell^+ + \nu_\ell \qquad (29)$$

where ℓ is a lepton and ν_ℓ is its associated neutrino. Examples are:

$$\begin{aligned} \pi^+ &\to \mu^+ + \nu_\mu \\ \pi^+ &\to e^+ + \nu_e \\ K^+ &\to \mu^+ + \nu_\mu \\ D^+ &\to \mu^+ + \nu_\mu \end{aligned} \qquad (30)$$

Some references for notation and method of calculation are M.L. Perl,

High Energy Hadron Physics (Wiley, 1974); and J. Bjorken and S. Drell, Relativistic Quantum Mechanics (McGraw-Hill, 1964).

A. Non-quark Model Calculation of $P^+ \to \ell^+ + \nu_\ell$

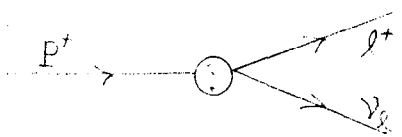

M = P mass, m = ℓ mass, P = P four-momentum, p = ℓ four-momentum, k = ν_ℓ four-momentum.

$$\text{Decay width} = \Gamma = \frac{(2\pi)^4}{2M}\int \frac{d^3p\,d^3k\,|T|^2}{(2\pi)^6 2p_o 2k_o}\,\delta^4(P_f - P_i) \tag{31}$$

$$|T|^2 = \sum_{\text{spins}} |M|^2$$

$$M = \frac{fG}{\sqrt{2}}\,P^\mu U_\ell(p)\gamma_\mu(1-\gamma_5)U_\nu(k) \tag{32}$$

$$G = 1.02 \times 10^{-5}/M^2_{\text{proton}}$$

f = constant which takes account of unknown vertex (in units of mass) (33)

Then in rest frame of P

$$|T|^2 = 2f^2G^2m^2[M^2 - m^2] \tag{34a}$$

$$\int \frac{d^3p\,d^3k}{2p_o 2k_o}\,\delta^4(P) = \pi k_o/M \tag{34b}$$

Finally we get the classic result

$$\Gamma = \frac{f^2G^2Mm^2}{8\pi}\left(1 - \frac{m^2}{M^2}\right)^2 \tag{35}$$

For a pion $\tau_\pi = 1/\Gamma_\pi = 2.6 \times 10^{-8}$ sec. Therefore

$$f_\pi = .92\,M_\pi = 129 \text{ MeV} \tag{36}$$

In Sec. 5C we shall see that the quark model provides an understanding of why $f_\pi \tilde{\approx} M_\pi$.

B. Quark Model Calculation of $\pi^+ \to \ell^+ + \nu_\ell$

We use a bound state calculation. Some references are J.J.J. Kokkadee, The Quark Model (Benjamin, 1964), R. Van Royan and V. Weisskopf, Nuovo Cimento 50, 617 (1967).

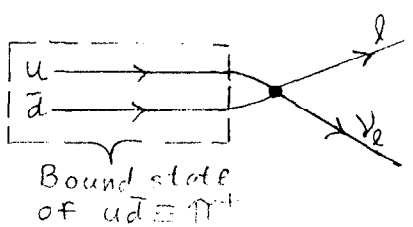

Let V_{rel} = relative velocity of u and $\bar{d}$ quarks. Then for a bound state

$$\Gamma_{V_{rel}\to 0} = |\psi(0)|^2\,\sigma(u + \bar{d} \to \ell + \nu_\ell) \tag{37}$$

where $\psi(\underset{\sim}{r})$ is the $u\bar{d}$ spatial wave function with normalization

$$\int d^3r\,|\psi(\underset{\sim}{r})|^2 = 1 \tag{38}$$

For $V_{rel} \to 0$ we calculate $\sigma(u + \bar{d} \to \ell + \nu_\ell)$ in the extreme non-relativistic limit

$$\sigma(u + \bar{d} \to \ell + \nu_\ell) = \frac{(2\pi)^4}{4m_q^2 V_{rel}}\int \frac{d^3k\,d^3p\,|T'|^2}{(2\pi)^6 2k_o 2p_o}\,\delta^4(P_f - P_i) \tag{39}$$

$$|T'|^2 = \sum_{\text{spins}} |M'|^2$$

$$M' = \frac{G}{\sqrt{2}}\,\bar{U}_u(p_u)\gamma^\mu U_{\bar{d}}(p_{\bar{d}})U_\ell(p)\gamma_\mu(1-\gamma_5)U_\nu(k) \tag{40}$$

Here m_q is the quark mass and p_u, $p_{\bar{d}}$, p, k are the four-momenta of the u, $\bar{d}$, ℓ and ν_ℓ respectively. Then in the rest frame of the π

$$|T'|^2 = 16\, G^3 m_q^2 (M^2 - m^2) \tag{41}$$

The reader should compare Eqs. 40 and 41 to Eqs. 34a and 32 respectively. Finally using $M \approx 2m_q$

$$\sigma(u + \bar{d} \to \ell + \nu_\ell) = \frac{1}{V_{rel}} \left(\frac{G^2 m^2}{2\pi}\right) \left(1 - \frac{m^2}{M^2}\right)^2 \tag{42}$$

and

$$\Gamma_\pi = |\psi_\pi(0)|^2 \frac{G^2}{2\pi}\, m^2 (1 - \frac{m^2}{M^2})^2 \tag{43}$$

Comparing Eq. 43 with Eq. 35

$$f_\pi = 2|\psi(0)|/\sqrt{M_\pi} \tag{44}$$

C. Quark Model Interpretation of f_π: If we use

$$\psi_\pi(\bar{r}) = \frac{1}{2\pi} \frac{1}{R^{3/2}} e^{-r/R_\pi} \tag{45}$$

Then $\psi_\pi(0) = (2\pi R_\pi^{3/2})^{-1}$ and

$$f_\pi = 1/(\pi M_\pi^{1/2} R_\pi^{3/2}) \tag{46}$$

Finally using the crude approximation $R_\pi \sim 1/M_\pi$

$$f_\pi \sim M_\pi/\pi \tag{47}$$

which should be compared to $f_\pi = .92\, M_\pi$ in Eq. 36.

Thus:

a. we have obtained the correct order of magnitude for f_π

b. the calculation can obviously be improved by changing ψ_π or R_π.

c. in general f_π is related to the $u\bar{d}$ wave function.

D. Generalization for Other Pseudoscalar Mesons: If we use the crude idea that all ordinary pseudoscalar mesons have the same radius R then from Eq. 46

$$f_K^2/f_\pi^2 = M_\pi/M_K \tag{48}$$

and we predict

$$\frac{\Gamma(K^+ \to \mu^+ \nu_\mu)}{\Gamma(\pi^+ \to \mu^+ \nu_\mu)} \text{ should equal } \frac{\left(1 - \frac{m_\mu^2}{M_\mu^2}\right)}{\left(1 - \frac{m_\mu^2}{M_\pi^2}\right)^2} \tag{49}$$

But this is wrong because $K^+ \to \mu^+ \nu_\mu$ involves a strangeness changing current and hence the Cabibbo angle — the subject of the next section.

6. STRANGENESS CHANGING DECAYS AND THE CABIBBO ANGLE

The weak decay calculations which we have been doing generalize into a current-current interaction:

$$M_{weak} = \frac{G}{\sqrt{2}} J^\mu J_\mu^\dagger \tag{50}$$

where J is a weak current. For example, in Eq. 32 $J = fP^\mu$ is the current changing the meson into the vacuum. (For the rest of this section we suppress the momentum and spin structure of J.)

J is divided as follows:

$$J = J_\ell + J_h \tag{51}$$

where J_ℓ is the lepton part of J and J_h is the hadron part. In all of our calculations J_ℓ is taken to have a V-A structure as in $\bar{U}_\ell \gamma_\mu (1 - \gamma_5) U_\nu$. But the V, A structure is not fixed in J_h. There we write

$$J_h = J_h^V + J_h^A \tag{52}$$

and

$$J_h^V = J_h^V(\Delta S = 0) + J_h^V(\Delta S = 1)$$
$$J_h^A = J_h^A(\Delta S = 0) + J_h^A(\Delta S = 1) \qquad (53)$$

Now consider $\Gamma(K^+ \to \mu^+\nu_\mu)/\Gamma(\pi^+ \to \mu^+\nu_\mu)$. Experiment gives 1.33 for this ratio, but Eq. 49 gives 5.2. This and other studies of K decays say that the $J_h(\Delta S = 1)$ current is suppressed. (A very useful references is S. Wojcicki, Proc. of SLAC Summer Inst. on Particle Physics - 1976 (SLAC-198).

The Cabibbo theory uses SU(3) to connect the $\Delta S = 0$ and $\Delta S = 1$ currents and leads to:

$$J_h^V = \sin\theta_V J'^V_h(\Delta S = 0) + \cos\theta_V J'^V_h(\Delta S = 1)$$
$$J'_A = \sin\theta_A J'_h{}^A(\Delta S = 0) + \cos\theta_A J'^A_h(\Delta S = 1) \qquad (54)$$

θ_V and θ_A are Cabbibo angles.

We avoid the use of SU(3) by going to the quark model and assuming

$$\theta_V = \theta_A = \theta_C \approx 0.25 \text{ rad} \qquad (55)$$

Just as we can indicate the particle content of the charged lepton current by

$$J_\ell(\text{charged}) = J^C_\ell = \bar{\nu}_e e + \bar{\nu}_\mu \mu \quad ; \qquad (56)$$

so the charged quark current is

$$J^C_q = \underset{\Delta S=0}{\cos\theta_C \bar{u}d} + \underset{\Delta S=1}{\sin\theta_C \bar{u}s} \qquad (57)$$

ASIDE: Returning for a moment to $\Gamma(K^+ \to \mu^+\nu_\mu)/\Gamma(\pi^+ \to \mu^+\nu_\mu)$ we would now predict for this ratio

$$\left(\frac{\sin\theta_C}{\cos\theta_C}\right)^2 \frac{\left(1 - \frac{m_\mu^2}{M_K^2}\right)^2}{\left(1 - \frac{m_\mu^2}{M_\pi^2}\right)^2}$$

which is too small. Therefore Eqs. 48 and 49 are wrong. SU(3) symmetry gives

$$f_\pi = f_K \qquad (58)$$

Therefore

$$\frac{\Gamma(K^+ \to \mu^+ \nu_\mu}{\Gamma(\pi^+ \to \mu^+ \nu_\mu)} = \tan^2\theta_C \left(\frac{M_K}{M_\pi}\right) \frac{\left(1 - \left(\frac{m_\mu}{M_K}\right)^2\right)^2}{\left(1 - \left(\frac{m_\mu}{M_\pi}\right)^2\right)^2} = 1.15 \qquad (59)$$

which is quite close to the experimental value of 1.33.

7. NEUTRAL CURRENTS AND THE CHARM QUARK

There will also be neutral currents

$$J^N_\ell = \bar{\nu}_e\nu_e + \bar{\nu}_e\nu_\mu - \bar{e}e - \bar{\mu}\mu \qquad (60)$$

$$J^N_q = \bar{u}u + (\cos\theta_C\bar{d} + \sin\theta_C\bar{s})(\cos\theta_C d + \sin\theta_C s) \qquad (61)$$

But Eq. 61 has strangeness changing neutral current terms, such as $\sin\theta_C \cos\theta_C \bar{s}d$, which are not observed in experiments. This was one reason for introducing the charm quark which has the structure in J^N_q

$$J^N_q = (-\sin\theta_C\bar{d} + \cos\theta_C\bar{s})(-\sin\theta_C d + \cos\theta_C s) \qquad (62)$$

The sum of Eqs. 61 and 62 is

$$J^N_q = \bar{u}u + \bar{d}d + \bar{s}s + \bar{c}c \qquad (63)$$

and this has no strangeness changing neutral current.

We put all this together by defining the doublets

$$\begin{pmatrix}\nu_e\\ e^-\end{pmatrix},\begin{pmatrix}\nu_\mu\\ \mu^-\end{pmatrix}\ ,\ \begin{pmatrix}u\\ d'\end{pmatrix},\begin{pmatrix}c\\ s'\end{pmatrix} \tag{64}$$

where

$$\begin{aligned} d' &= +d\cos\theta_C + s\sin\theta_C \\ s' &= -d\sin\theta_C + s\cos\theta_C \end{aligned} \tag{65}$$

Then for the doublet $\begin{pmatrix}\alpha\\ \beta\end{pmatrix}$ the charged current contribution is

$$J^C = \bar{\alpha}\beta \quad ; \tag{66}$$

and the neutral current contribution is

$$J^N = \bar{\alpha}\alpha - \bar{\beta}\beta \tag{67}$$

Explicitly

$$J^C_\ell = \bar{\nu}_e e^- + \bar{\nu}_\mu \bar{\mu} \tag{68a}$$

$$J^C_q = \cos\theta_C(\bar{u}d + \bar{c}s) + \sin\theta_C(\bar{u}s - \bar{c}d) \tag{68b}$$

$$J^N_\ell = \bar{\nu}_e\nu_e + \bar{\nu}_\mu\nu_\mu - \bar{e}^-e^- - \bar{\mu}^-\mu^- \tag{68c}$$

$$J^N_q = \bar{u}u + \bar{c}c - \bar{d}d - \bar{s}s \tag{68d}$$

It is now easy to represent pictorially the decays of the s quark (Fig. 3) and the c quark (Fig. 4). In these figures the Cabibbo factor in the amplitude is given under the diagram; and for clarity we use the still hypothetical W intermediate boson.

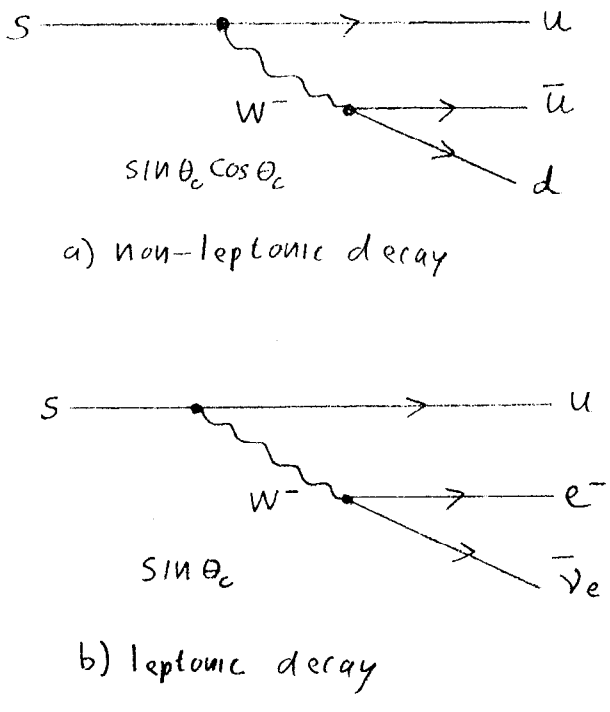

Fig. 3

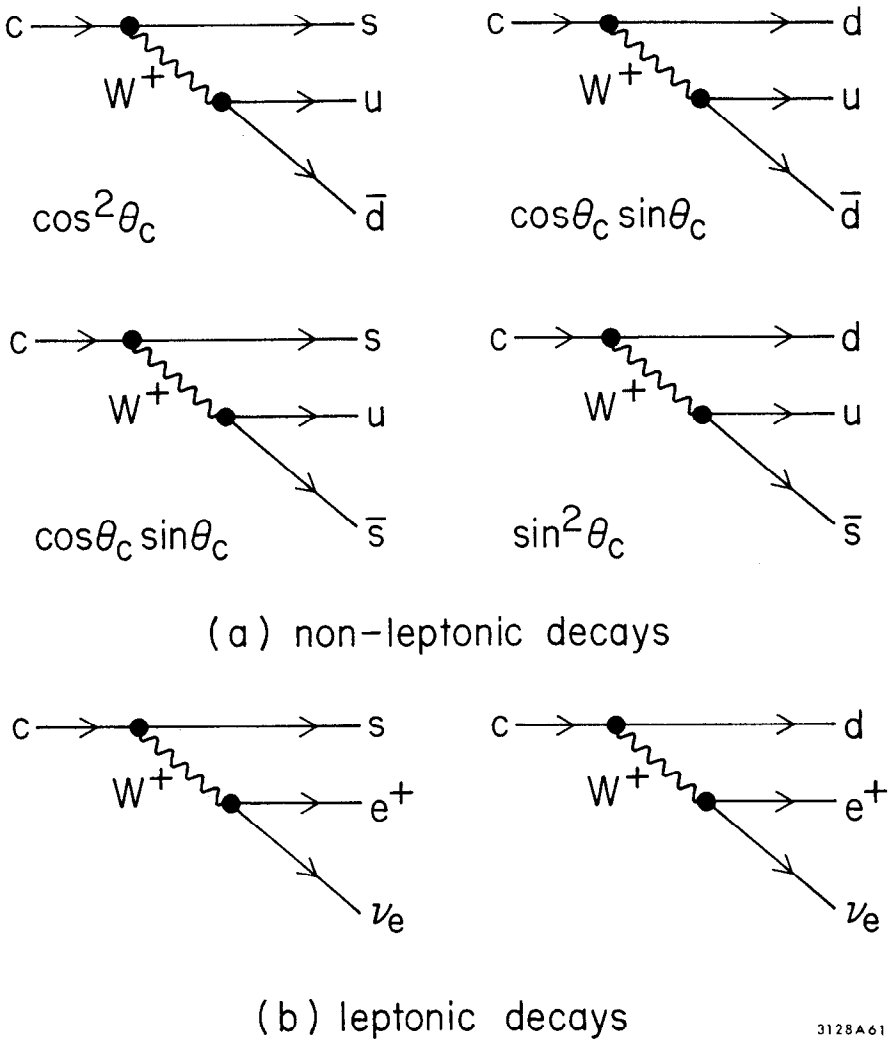

Fig. 4

8. SINGLY CHARMED MESONS

A comprehensive review of the properties of the singly charmed D mesons has been given by G.J. Feldman at this conference. Therefore I will limit this written version of my lectures to a discussion of the quark model picture of these mesons, and I will only give some illustrative data.

A. Internal Quantum Numbers and Quark Content of Singly Charmed Mesons:

The quark model predictions are given in Table IV

TABLE IV

Name	D		F
Charm	+1		+1
Strangeness	0		+1
I	1/2		0
I_z	+1/2	-1/2	0
Quark content	$c\bar{d}$	$c\bar{u}$	$c\bar{s}$
Pseudoscalar name	D^+	D^o	F^+
Vector name	D^{*+}	D^{*o}	F^{*+}

a. As reviewed by Feldman at this conference the D and D* have been found and studied. All measurements on the D's are consistent with the above table and with $J^P(D) = 0^-$, $J^P(D^*) = 1^-$

b. Evidence for the existence of the F meson was presented at this conference by W. De Boer and the reader is referred to his paper.

B. Theory of the $D^{+,o}$ Decay Modes: We expect the D to decay weakly

into decay modes which predominantly contain (Fig. 3)

$$\begin{aligned} c &\to s + u + \bar{d} \\ c &\to s + e^+ + \nu_e \\ c &\to s + \mu^+ + \nu_\mu \end{aligned} \qquad (69)$$

These modes should dominate by the factor

$$\left(\frac{\cos\theta_s}{\sin\theta_c}\right)^2 \approx \frac{1}{\sin^2\theta_C} \approx 16 \qquad (70)$$

over the next strongest modes. For example we expect

$$\frac{\Gamma(D^o \to K^-\pi^+)}{\Gamma(D^o \to \pi^-\pi^+)} \approx \frac{\Gamma(D^o \to K^-\pi^+)}{\Gamma(D^o \to K^-K^+)} \approx 16 \qquad (71)$$

The decay modes which have been seen, Table V, taken from Feldman's paper at this conference, are in very nice agreement with these quark model predictions. Incidently most of the D's decay modes contain one or more π^o's and are very difficult to find in present detectors.

TABLE V

$\sigma \cdot B$ in nb for various D decay modes at three values of $E_{c.m.}$

		$E_{c.m.}$ (GeV) 3.774	4.028	4.414
D	$\bar{K}^+\pi^-$	0.27 ± 0.05	0.57 ± 0.11	0.30 ± 0.09
	$\bar{K}^o\pi^+\pi^-$+c.c.	0.44 ± 0.11	1.09 ± 0.30	0.91 ± 0.34
	$\bar{K}^+\pi^-\pi^+\pi^-$	0.34 ± 0.09	0.83 ± 0.27	0.91 ± 0.39
	$\pi^+\pi^-$	---	<0.04	---
	K^+K^-	---	<0.04	---
TOTAL D^o OBSERVED MODES		1.05 ± 0.15	2.49 ± 0.42	2.12 ± 0.53
D^+	$\bar{K}^o\pi^+$+c.c.	0.15 ± 0.05	< 0.18	---
	$\bar{K}^+\pi^-\pi^+$	0.34 ± 0.05	0.40 ± 0.10	0.33 ± 0.12
	$\pi^-\pi^+\pi^-$	---	< 0.03	---

C. Theory of the F^+ Decay Modes: The expected hadronic decay modes are shown in Fig. 5. For leptonic decays just replace $(u, \bar{d})$ by $(\nu_e, e$ or (ν_μ, μ)

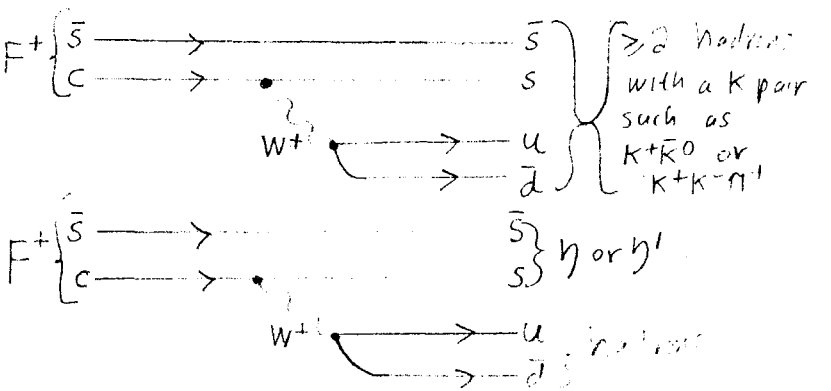

As described by De Boer at this conference the $F^+ \to \eta^o$ + anything and $F^+ \to \eta^o + \pi^+$ decay modes of the F have been seen. No one has found any decay modes containing K pairs.

D. Masses of the D-D^* System and D* Decay Modes

The masses of the D-D* system are

$$\begin{aligned} M_{D^o} &= 1863.3 \pm 0.9 \text{ MeV/c}^2 \\ M_{D^-}^{+} &= 1868.4 \pm 0.9 \text{ MeV/c}^2 \\ M_{D^{*o}} &= 2006. \pm 1.5 \text{ MeV/c}^2 \\ M_{D^{*\pm}} &= 2008.6 \pm 1.0 \text{ MeV/c}^2 \end{aligned} \qquad (72)$$

The decay of a D^* to D requires no change in the strange or charm quark content, hence this decay can proceed through the strong or electromagnetic interactions. The strong decay of course requires sufficient mass difference between the D^* and D for a π to be produced. Figure 6 summarizes the mass differences situation in terms of Q values; only the $D^{*o} \to D^+$ decay has insufficient mass difference to produce a π.

9. THE ENERGY LEVELS OF CHARMONIUM

We now have extensive information on the charmonium family of particles: ψ/J, ψ', $\psi(3772)$, and χ states. In this written version of my lectures I will only discuss the energy level scheme because an extensive review has just been done by G.J. Feldman and myself which will appear in Phys. Reports. (This review was also issued as SLAC-PUB-1972).

A. Theory of Charmonium Energy Levels

We consider the $c\bar{c}$ system and use the quark model described in Sec. 2. We have states $n^{2s+1}L_J$ where n is the radial excitation quantum number, s is the total spin (0 or 1), L is the orbital angular momentum, and J is the total angular momentum. We expect the mass spectrum in Fig. 7 with the following considerations

a. The rate of mass increase with radial excitation depends upon the type of potential as discussed in Sec. 3.

b. The effect on the mass of the orbital excitation (increase in L) depends upon the potential V. Some examples are given in c., d., e.

c. For an attractive coulomb potential, $V_{coul.} = -$ constant/r, and spin zero particles, E(n, L) is degenerate in L.

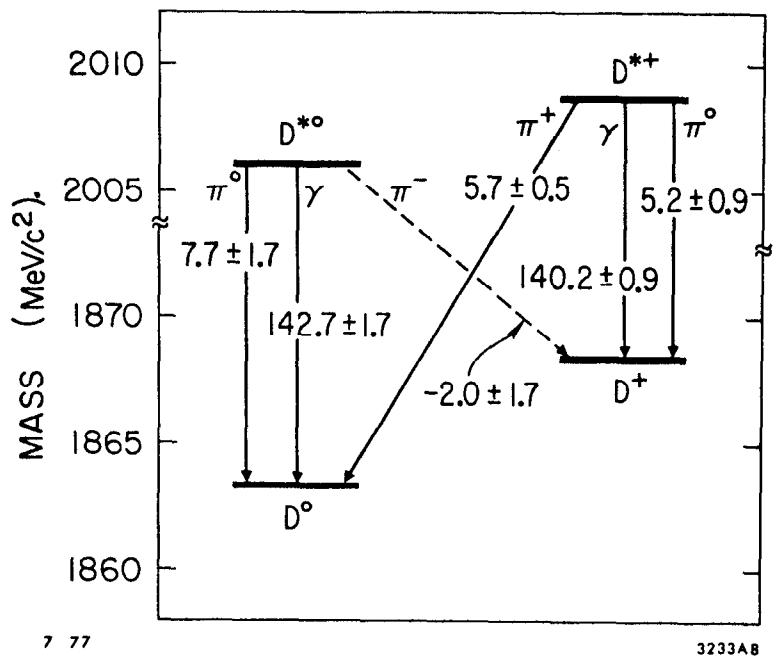

FIG. 6. Q values for D^* → D transitions.

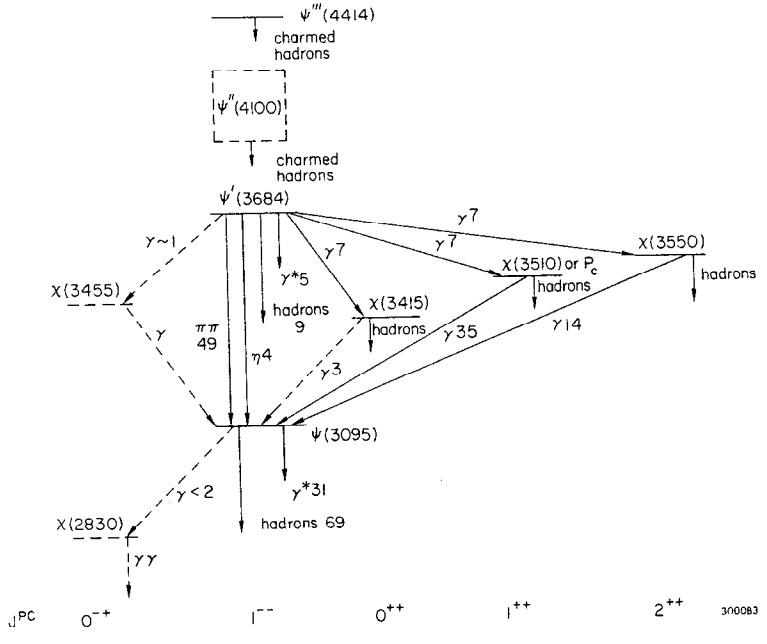

Fig. 7

d. If V is attractive and its r dependence is steeper than 1/r, E(n, L) increases.

e. If there is a spin-orbit coupling,

$$V_{\text{spin-orbit}} = f(r)\ \vec{J}\cdot\vec{L} \quad , \tag{73}$$

then E(n, L, J) will depend on L and J.

f. If there is an $\vec{s}_1\cdot\vec{s}_2$ interaction between quarks q_1 and q_2; then for the same n and L, E(n, L, J) will depend on $\vec{J} = \vec{s}_1 + \vec{s}_2$.

B. Identified Charmonium Energy Levels: Figure 7 shows the charmonium states which have been found, and the conventional association of them with $n^{2s+1}L_J$ states. For the justification see G.J. Feldman and M.L. Perl, Phys. Report (to be published). I have not listed the possible charmonium states associated with the peaks in $\sigma(e^+ + e^- \to \text{hadrons})$ at 3.95, 4.1, or 4.4 GeV because the structure and nature of these peaks is obscure at present. For eaxmple the 4.1 is probably split into 2 peaks, and the SLAC-LBL collaboration has never felt sufficiently sure of the nature of the 3.95 peak to discuss it in detail in a publication.

10. THEORY OF LEPTONIC AND SEMI-LEPTONIC DECAYS OF THE D MESONS

We now turn to a discussion of the theory of the leptonic and semi-elptonic decays of the singly charmed D mesons. In the next section we will then compare this theory with the theory of the decays of the heavy lepton. We are then prepared to describe our present experimental knowledge of the semi-leptonic decays of the D mesons in Sec. 12. And to conclude these lectures we present in Sec. 13 the evidence for, and properties of, the proposed τ heavy lepton. These four sections are

connected not only thru the underlying weak decay theory; but also thru the detailed experimental work which has been necessary to separate semi-leptonic decays of the D from the decays of the τ.

A. Leptonic Decays: The purely leptonic decay calculation

$$D^+ \to e^+ + \nu_e \quad , \quad D^+ \to \mu^+ + \nu_\mu \tag{74}$$

is the same as the calculation for $\pi^+ \to \ell^+ + \nu_\ell$ (Sec. 5), but now the amplitude has a $\sin\theta_C$ factor

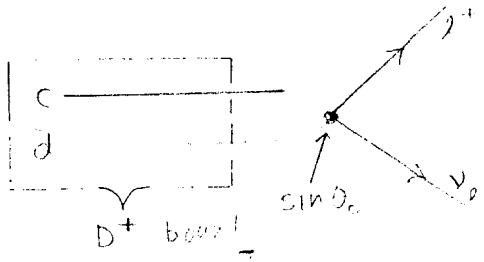

We obtain

$$\Gamma(D^+ \to \ell^+\nu_\ell) = \sin^2\theta_C \frac{f_o^2 G^2 M_D m_\ell^2}{8\pi}\left(1 - \frac{m_\ell^2}{M_D^2}\right)^2 \tag{75}$$

B. Semi-leptonic Decays — Exclusive Channels:

The simplest exclusive channels for calculation are:

$$D^+ \to \ell^+ + \nu_\ell + \pi^o \quad , \quad D^o \to \ell^+ + \nu_\ell + \pi^- \tag{76}$$

$$D^+ \to \ell^+ + \nu_\ell + K^o \quad , \quad D^o \to \ell^+ + \nu_\ell + K^- \tag{77}$$

But the decay modes in Eq. 76 will be suppressed by a $\sin^2\theta_C$ factor relative to the decay modes in Eq. 77; therefore we will only consider:

$$D^{+,o} \to \ell^+ + \nu_\ell + K^{o,-} \tag{78}$$

We don't use the quark model here

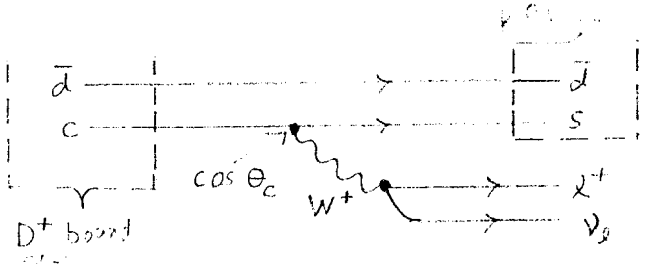

because the process

$$\bar{d} + s \to K^o \text{ bound state}$$

is hard to calculate. We will use

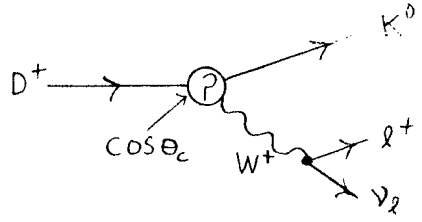

where particles D^+, K^o, ℓ^+, ν_ℓ have four-momenta P, K, p, k and masses M, m, 0, 0 respectively. Then

$$\Gamma = \frac{(2\pi)^4}{2M}\int \frac{d^3K d^3p d^3k}{8(2\pi)^9 k K_o p_o k_o} |T|^2 F^2(q^2)\delta^4(P_f - P_i) \tag{79}$$

where $q^2 = (P - K)^2$ and

$$F(q^2) = \text{transition form factor for } D \to K \tag{80}$$

In Eq. 79

$$|T|^2 = \sum_{\text{spins}} |M|^2 \cos^2 \theta_C \tag{81}$$

$$M = \frac{G}{\sqrt{2}} P^{\nu} \bar{U}_{\ell}(p) \gamma_{\mu}(1 - \gamma_5) U_{\nu}(k) \tag{82}$$

Since $\cos \theta_C \approx 1$ we shall neglect it.

In the rest frame of the D

$$|T|^2 = 8M^2[2p_o k_o - p \cdot k]$$

and

$$\Gamma = \frac{G^2 M}{32\pi^3} \int dp_o dK_o [4p_o k_o - q^2] F^2(q^2) \tag{83}$$

or

$$\frac{d\Gamma}{dp_o dK_o} = \frac{G^3 M}{32\pi^3} [4p_o k_o - q^2] F^2(q^2) \tag{84}$$

Remember p_o = ℓ energy and K_o = K energy in the D rest frame.

The kinematic limits on K_o are

$$K_{o,\,\max} = \frac{M^2 + m^2}{2M} \xrightarrow{m \to 0} \frac{M}{2} \tag{85a}$$

$$K_{o,\,\min} = \frac{(M - 2p_o)^2 + m^2}{2(M - 2p_o)} \xrightarrow{m \to 0} \frac{M}{2} - p_o \tag{85b}$$

where M is the D mass and m is the K mass.

Since we don't know much about $F(q^2)$ we write

$$\int dK_o [4p_o k_o - q^2] F(q^2) = \langle F(q^2) \rangle \int dK_o [4p_o k_o - q^2]$$

$$= \langle F(q^2) \rangle \frac{4p_o^2 (p_{max} - p_o)^2}{M - 2p_o} \tag{86}$$

where

$$p_{max} = \frac{M^2 - m^2}{2M}$$

Finally we obtain the lepton energy spectrum

$$\frac{d\Gamma}{dp_o} = \frac{G^2 M \langle F^2(q^2) \rangle}{8\pi^3} \frac{p_o^2 (p_{max} - p_o)^2}{M - 2p_o} \tag{87}$$

It is useful to define

$$y = \frac{p_o}{p_{max}} \quad , \quad 0 < y < 1 \quad ; \tag{88}$$

Then Eq. 87 becomes

$$\frac{d\Gamma}{dy} = \frac{6^2 M p_{max}^4 \langle F^2(q^2) \rangle}{16\pi^3} \frac{y^2 (1 - y)^2}{c - y} \tag{89}$$

where

$$c = \frac{M}{2p_{max}} = \frac{M^2}{M^2 - m^2}$$

To see how $d\Gamma/dy$ behaves it is a useful approximation to ignore m^2 with respect to M^2, then

$$\frac{dM}{dy} = \frac{G^2 M_D^5 \langle F^2(q^2) \rangle}{192\pi^3} [y^2 (1 - y)] \tag{90}$$

where we have explicitly indicated the D mass. Figure 8 shows this function normalized so that $(d\Gamma/dy)_{max} = 1$

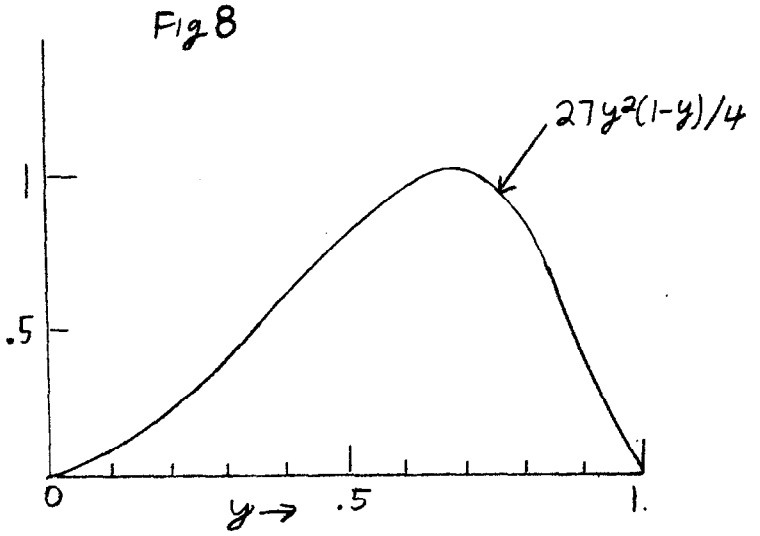

The total decay rate is

$$\Gamma(D^{o,+} \to \ell^+ \nu_\ell K^{-,o}) = \frac{G^2 M_D^5}{192\pi^3} \frac{\langle F^2(q^2)\rangle}{12} \qquad (91)$$

Comparing this to the leptonic decay rate, Eq. 75, we obtain

$$\frac{\text{pure leptonic decay rate}}{\text{semi leptonic decay rate}} \sim \frac{m_\ell^2 M_\pi^2 \sin^2\theta_c}{M_D^4} \sim 10^{-4} \text{ to } 10^{-6}; \qquad (92)$$

where we have set $\langle F^2(q^2)\rangle \sim 1$ and $f_D \sim M_\pi$. Hence the pure leptonic decay rate of the D is negligible compared to the semi-leptonic decay rate.

C. Inclusive Semi-leptonic Decays of the D and the Total Decay Rate:

The inclusive semi-leptonic decay rate is given by the quark model diagram in Fig. 9

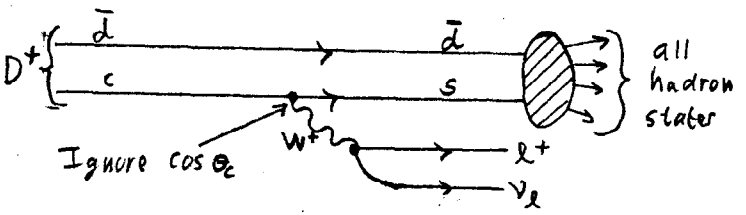

Fig. 9

for

$$D^+ \to \ell^+ + \nu_\ell + (\text{hadrons})^o \qquad (93)$$

The quark decay

$$c \to s + \ell^+ + \nu_\ell \qquad (94)$$

is just like

$$\mu^+ \to \bar{\nu}_\mu + e^+ + \nu_e$$

$$\tau^+ \to \bar{\nu}_\tau + \mu^+ + \nu_\mu \qquad (95)$$

$$\tau^+ \to \bar{\nu}_\tau + e^+ + \nu_e$$

As we show in the next section, all these weak decays have

$$\Gamma = \frac{G^2 M^5}{192\pi^3} \qquad (96)$$

where M is themass of the initial particle and all the final particles have zero mass.

To calculate $\Gamma(D^+ \to \ell^+ \nu_\ell (\text{hadrons})^o)$ we treat the c quark as free in the D; and we let the probability for

$$s + \bar{d} \to \text{hadrons}$$

be 1. Then using Eq. 96,

$$\Gamma(D^+ \to \ell^+ \nu_\ell (\text{hadrons})^\circ) = \frac{G^2 M_D^5}{192\pi^3}\left(\frac{m_c}{M_b}\right)^5 \qquad (97)$$

where m_c is the c quark mass.

We cannot make a present comparison of this to Eq. 91 for the exclusive decay $D^+ \to \ell^+ \nu_\ell K^\circ$ because our models are too crude. All we really know is the $G^2 M_D^5/(192\pi^3)$ factor.

To calculate the total decay rate compare Fig. 10 for

$$\Gamma(D^+ \to \text{hadrons}) \qquad (98)$$

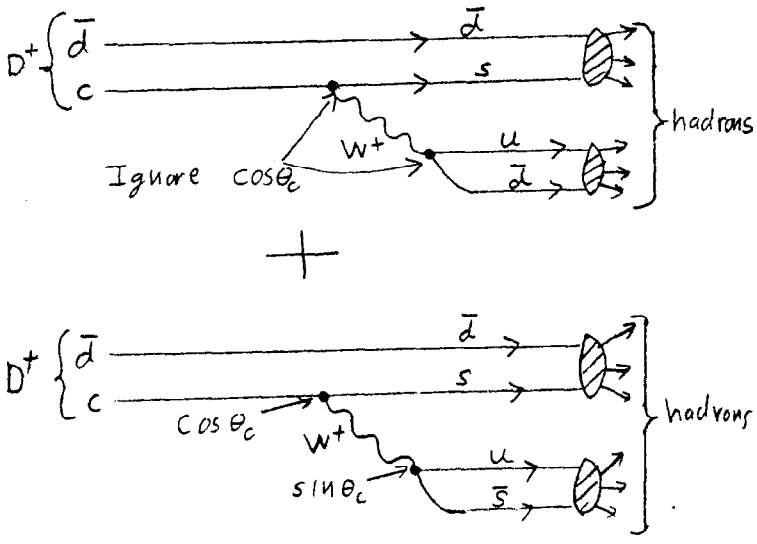

Fig. 10

with Fig. 9. We do the following:

a) ignore the second diagram,

b) do $c \to s + u + \bar{d}$ as we did $c \to s + \ell + \nu_\ell$,

c) let the probability for $u + \bar{d} \to$ hadrons be 1.

Then

$$\Gamma(D^+ \to \text{hadrons}) = \frac{G^2 M_D^5}{192\pi^3}\left(\frac{m_c}{M_D}\right)^5 \times 3 \qquad (99)$$

where the factor 3 is for the three colors for the quarks. Then we predict the relative decay rates in Table VI.

TABLE VI

DECAY MODE	RELATIVE RATE	FRACTIONAL RATE IN %
$D^+ \to e^+ + \nu_e + (\text{hadrons})^\circ$	1	20
$D^+ \to \mu^+ + \nu_\mu + (\text{hadrons})^\circ$	1	20
$D^+ \to (\text{hadrons})^+$	3	60
TOTAL	5	100%

Measurements on the inclusive lepton decay modes yield about 10% for either the e or μ mode separately (Sec. 12), which is in fair agreement with our calculations considering the crudeness of our models. Finally

$$\text{D lifetime} \approx \left[\frac{5G^2 m_c^5}{192\pi^3}\right]^{-1} \approx \frac{1}{5}\left(\frac{m_\mu}{m_c}\right)^5 (\mu \text{ lifetime})$$

$$\approx 7 \times 10^{-13} \text{ sec} \qquad (100)$$

Some references on the decay modes of the D mesons are:

A. Ali and T.C. Yang, Phys. Lett. 65B, 275(1976);

I. Hinchliffe and C.H. Llwellyn Smith, Nuc. Phys. B114, 45(1976).

M.K. Gaillard et al., Rev. Mod. Phys. 47, 277(1975).

J. Ellis et al., Nucl. Phys. B100, 313(1975).

Figure 11 from Hinchliffe and Llewellyn Smith shows some detailed calculations on various exclusive semi-leptonic decay charmed of the D; it should be compared with Fig. 8

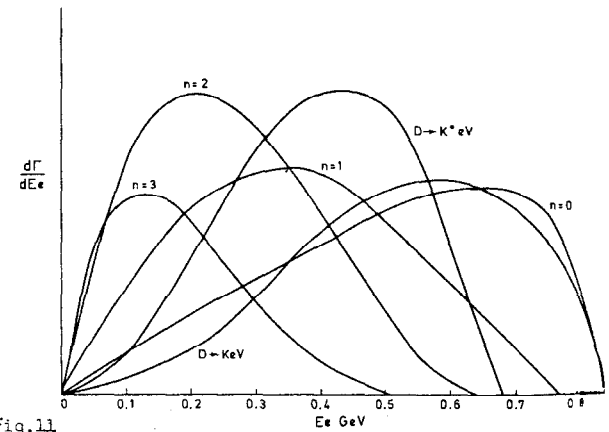

Fig.11 Electron spectrum $d\Gamma/dE_e$ for the decay modes, $D \to Ke\nu\,(n\pi)$ (with constant matrix elements), labelled by $n = 0, 1, 2, 3$ on figure, $D \to Ke\nu$ and $D \to K^*e\nu$. The relative scale of the curves has no meaning.

11. THEORY OF THE DECAYS OF CHARGED LETPONS

In Sec. 13 there is a brief discussion of various types of leptons -- sequential, paraleptons, and ortholeptons. The calcuations done here apply to these types; except for the decay modes $E^- \to \bar{\nu}_e + \bar{\nu}_e + e^-$ and $M^- \to \bar{\nu}_\mu + \bar{\nu}_\mu$ where E^- and M^- are parleptons. For illustrative purposes I will use the sequential type with lepton τ and associated neutrino ν_τ.

A. Purely Leptonic Decays: The purely leptonic modes are

$$\tau^- \to \nu_\tau + e^- + \bar{\nu}_e$$
$$\tau^- \to \nu_\tau + \mu^- + \bar{\nu}_e \qquad (101)$$

which occur thru the diagram:

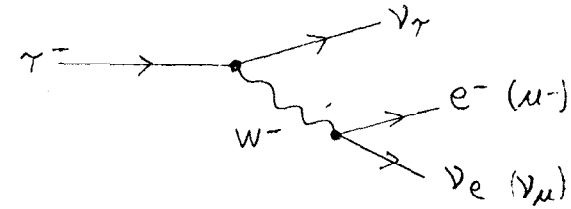

For the τ, ν_τ, e, ν_e the four-momenta are P, K, p, k and the masses are m, 0, 0, 0. I will do both V-A and V+A coupling

$$\Gamma = \frac{(2\pi)^4}{2m}\int \frac{d^3K d^3p d^3k}{(2\pi)^9 8K_o p_o k_o}\,|T|^2\delta^4(P_f - P_i) \qquad (102)$$

where

$$|T|^2 = \tfrac{1}{2}\sum_{spins}|M|^2$$

$$M = \frac{G}{\sqrt{2}}\bar{U}_{\nu_\tau}(K)\gamma^\mu(1+\lambda\gamma_5)U_\tau(P)$$
$$X\,\bar{U}_e(p)\gamma_\mu(1-\gamma_5)U_{\nu_e}(k) \qquad (103)$$

In Eq. 103:

$$\lambda = +1 \text{ for V+A coupling of } \tau \text{ to } \nu_\tau$$
$$\lambda = -1 \text{ for V-A coupling of } \tau \text{ to } \nu_\tau \qquad (104)$$

Then after much calculation

$$\sum_{\text{spins}} |M|^2 = 32\, G^2 [(1-\lambda)^2 k\cdot PK\cdot p + (1+\lambda)^2 k\cdot Kp\cdot P] \qquad (105)$$

(V-A term; V+A term)

First we do V-A; that is $\lambda = -1$. In the rest frame of the τ

$$\Gamma = \frac{G^2}{(2\pi)^5} \int \frac{K\cdot p d^3K d^3p}{K_o p_o} \delta(E_f - E_i)$$

After more manipulation

$$\Gamma = \frac{G^2}{(2\pi)^5} \left(\frac{8\pi^2 m}{3}\right) \int p_o^2 (3m - 4p_o) dp_o \qquad (106)$$

$$\frac{d\Gamma}{dp_o} = \frac{G^2 m}{12\pi^3}\, p_o^2\, (3m - 4p_o) \qquad (107)$$

Here p_o is the energy of the lepton in the τ rest frame. It is convenient to define

$$y = 2p_o/m \quad , \quad 0 \leq y \leq 1 \qquad (108)$$

Then

$$\frac{d\Gamma}{dy} = \frac{G^2 m^5}{96\pi^3}\, y^2 (3 - 2y), \text{ for V-A} \qquad (109)$$

Also

$$\Gamma = \frac{G^2 m^5}{192\pi^3} \qquad (110)$$

which is the classic result we have already used.

For V+A coupling

$$\frac{d\Gamma}{dy} = \frac{G^2 m}{16\pi^3}\, y^2 (1 - y) \quad , \quad \text{for V+A} \qquad (111)$$

and

$$\Gamma = \frac{G^2 m^5}{192\pi^3} \qquad (112)$$

as before.

Figure 12 compares the V-A to V+A y spectrum in the rest frame of the τ. We note that V-A gives a harder spectrum; and this is used in Sec. 13 to show that V-A fits the τ data better than V+A.

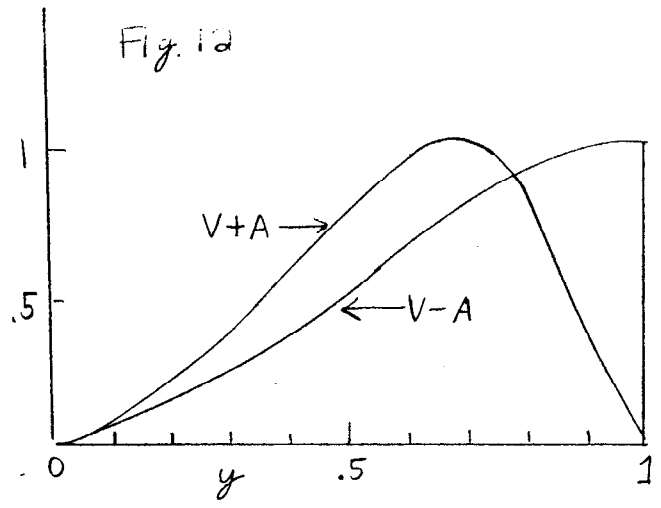

Incidently, it is easy to calculate the spectrum for pure V coupling by setting $\lambda = 0$. Then

$$\frac{d\Gamma}{dy} = \frac{G^2 m^5}{96\pi^3} y\,[4.5 - 4y] \text{ for pure V} \qquad (113)$$

The same result is obtained for pure A coupling.

B. $\tau^- \to \nu_\tau + \pi^-$ Decay Mode: The

$$\tau^- \to \nu_\tau + \pi^- \qquad (114)$$

is calculated just as we calculated $\pi^- \to \mu^- + \bar{\nu}_\mu$ in Sec. 5A. In the diagram

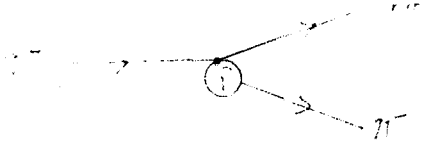

the τ, ν_τ, π^- have four-momenta p, k, P and masses m, o, o respectively. Then

$$\Gamma = \frac{(2\pi)^4}{2m}\int \frac{d^3k d^3P}{(2\pi)^6 4k_o P_o} |T|^2 \delta^4(P_f - P_i) \qquad (115)$$

$$|T|^2 = \tfrac{1}{2} \sum_{\text{spins}} |M|^2 \qquad (116)$$

$$M = \frac{fG}{\sqrt{2}} P^\mu \bar{U}_\tau(p)\gamma_\mu(1 - \gamma_5)U_{\nu_\tau}(k) \qquad (117)$$

where we have assumed V-A coupling. In the rest frame of the τ

$$|T|^2 = 2f^2G^2m[2P\cdot kp_o] = f^2G^2m^4 \qquad (118)$$

This leads to

$$\Gamma(\tau^- \to \nu_\tau \pi^-) = \frac{f^2G^2m^3}{16\pi}\,I \qquad (119)$$

Conventional theory assumes $f = f_\pi = .92\ m_\pi$

C. Other Decay Modes and the Charged Lepton Lifetime: The calculation of the decay rates for other decay modes:

$$\begin{aligned} &\tau^- \to \nu_\tau + \rho^- \\ &\tau^- \to \nu_\tau + A^- \\ &\tau^- \to \nu_\tau + \pi^- + \pi^+ + \pi^- \end{aligned} \qquad (120)$$

are more complicated. The basic references are:

H.B. Thacker and J.J. Sakurai, Phys. Lett. 36B, 103(1971);

Y.S. Tsai, Phys. Rev. D4, 2821(1971).

Expected decay modes for a conventional, sequential, V-A, charged lepton with 1.9 GeV/c^2 are given in Table VII. Table VII exhibits the important results that for a mass 1.9 GeV/c^2 charged lepton most of the decay modes will give only one charged particle -- an e, μ, or hadron.

Figures 13 and 14 give the predicted branching ratios and lifetimes for a conventional, sequential, V-A, charged lepton.

12. MEASUREMENTS ON SEMI-LEPTONIC DECAYS OF D MESONS

At this conference comprehensive reports on data on the semi-leptonic decays of D mesons have been presented by W. De Boer, R. Madaras, and J. Kirz.

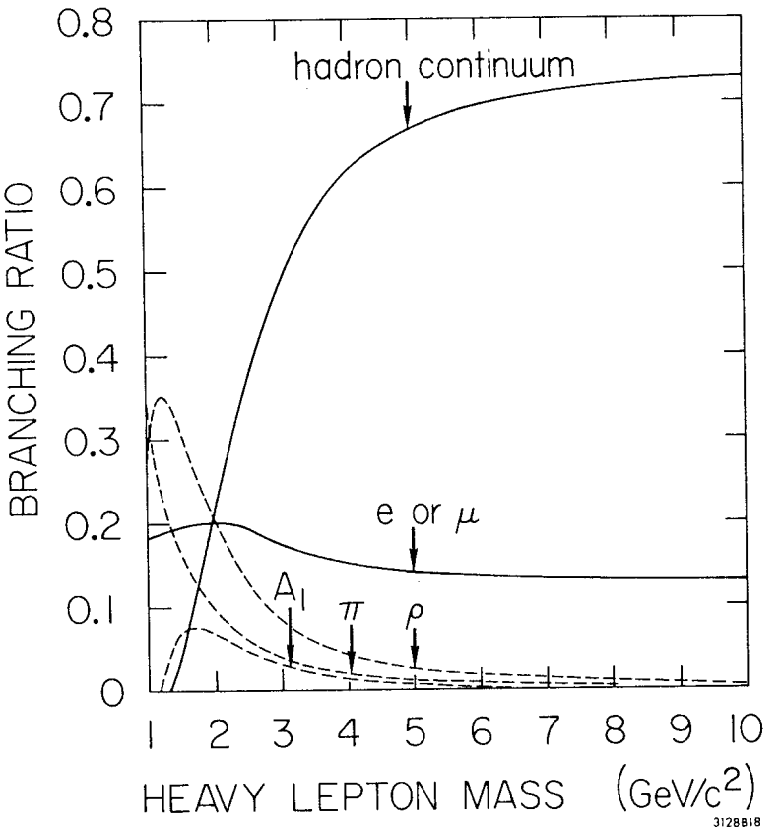
BRANCHING RATIO
0.8
0.7
0.6
0.5
0.4
0.3
0.2
0.1
0
hadron continuum
e or μ
A1
π
ρ
1 2 3 4 5 6 7 8 9 10
HEAVY LEPTON MASS (GeV/c²)
3128B18

Fig.13

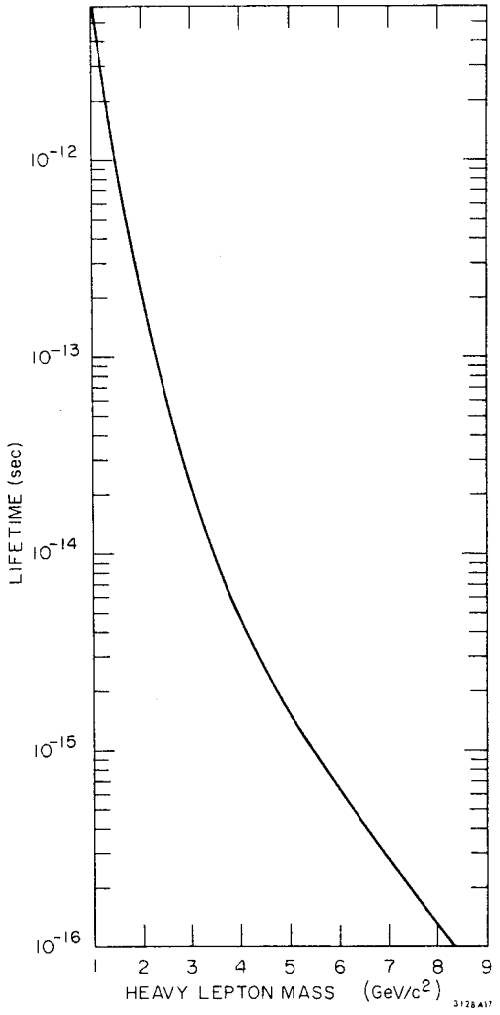
LIFETIME (sec)
10⁻¹²
10⁻¹³
10⁻¹⁴
10⁻¹⁵
10⁻¹⁶
1 2 3 4 5 6 7 8 9
HEAVY LEPTON MASS (GeV/c²)
3128A17

Fig.14

TABLE VIII

Predicted branching ratios for a τ^- sequential charged heavy lepton with a mass 1.9 GeV/c, an associated neutrino mass of 0.0, and V-A coupling. The hadron continuum branching ratio assumes a threshold at 1.2 Ge V for production of $\bar{u}d$ quark pairs whose final state interaction leads to the hadron continuum.

decay mode	branching ratio	number of charged particles in final state
$\nu_\tau e^- \bar{\nu}_e$	.20	1
$\nu_\tau \mu^- \bar{\nu}_\mu$	.20	1
$\nu_\tau \pi^-$	.11	1
$\nu_\tau K^-$	.01	1
$\nu_\tau \rho^-$	.22	1
$\nu_\tau K^{*-}$	.01	1
$\nu_\tau A_1^-$	.07	1, 3
ν_τ (hadron continuum)$^-$	.18	1, 3, 5

13. EVIDENCE FOR, AND PROPERTIES OF, THE PROPOSED τ CHARGED LEPTON

In this written version of these lectures I am inserting for this section a review on the τ charged lepton which I presented at the 1977 International Symposium on Lepton and Photon Interactions at High Energies (Hamburg, 1977).

Appendix I : The Linear Potential

For S states the radial part of the Schrödinger equation is :

$$\frac{-\hbar^2}{2m}\frac{d^2U}{dr^2} + V(r)U = EU \qquad (1)$$

where the entire radial wave function is

$$R(r) = U(r)/r$$

Inserting the linear potential $V(r) = Br$

$$\frac{d^2U}{dr^2} + \frac{2m}{\hbar^2}(E - Br)\,U = 0 \qquad (2)$$

At $r = 0$ we require $U(0) = 0$ to make $R(0)$ finite. Equation 2 reduces to the Airy Equation

$$\frac{d^2U}{dz^2} - zU = 0 \qquad (3)$$

by setting

$$z = -\left(\frac{2m}{\hbar^2 B^2}\right)^{1/3}(E - Br) \qquad (4)$$

To get $U(0) = 0$ we look up the zero of U in Eq. 3, $U(z_1) = 0$, $U(z_2 = 0)$, $U(z_3 = 0)$ .... and set

$$E_1 = -\left(\frac{\hbar^2 B^2}{2m}\right)^{1/3} z_1$$

$$E_2 = -\left(\frac{\hbar^2 B^2}{2m}\right)^{1/3} z_2 \qquad (5)$$

. .

. .

specifically

$$z_1 = -2.34$$

$$z_2 = -4.09$$

$$z_3 = -5.52$$

$$z_4 = -6.79$$

$$z_5 = -7.94$$

$$\begin{array}{cc} \cdot & \cdot \\ \cdot & \cdot \\ \cdot & \cdot \end{array}$$

SLAC-PUB-2022
October 1977
(T/E)

REVIEW OF HEAVY LEPTON PRODUCTION IN e^+e^- ANNIHILATION*

Martin L. Perl

Stanford Linear Accelerator Center
Stanford University, Stanford, California 94305

ABSTRACT

The existing data on $e^{\pm}\mu^{\mp}$, $e^{\pm}x^{\mp}$, $\mu^{\pm}x^{\mp}$, and related events produced in e^+e^- annihilation are reviewed. All data are consistent with the existence of a new charged lepton, $\tau^{\pm}$, of mass $1.9 \pm .1$ GeV/c^2.

(Invited talk presented at the 1977 International Symposium on Lepton and Photon Interactions at High Energies, Hamburg, Germany, August 25-31, 1977.)

*Work supported by the Department of Energy.

I. INTRODUCTION

Since the discovery[1,2] of anomalous $e^{\pm}\mu^{\mp}$ events at SPEAR two and one half years ago, there has been a steady increase in the data on these events and the related two-charged prong $e^{\pm}x^{\mp}$ and $\mu^{\pm}x^{\mp}$ events. All such data which has been published, or has been presented at this or previous conferences, agree on the following points.

a. Anomalous two-charged prong leptonic events ($e^{\pm}\mu^{\mp}$, $e^{\pm}x^{\mp}$, $\mu^{\pm}x^{\mp}$, e^+e^-, $\mu^+\mu^-$) are produced in e^+e^- annihilation.
b. Most of these events do not come from the decays of charmed particles.
c. The behavior of these events is consistent with the hypothesis that a new charged lepton, τ, exists with a mass of 1.9 ± 0.1 GeV/c^2.

Points a and b have been thoroughly discussed by the individual speakers using their own data; and so with respect to these points I will only summarize their data and conclusions. In this paper I will put more emphasis on point c, the consistency of the data with the τ hypothesis; and on using the τ hypothesis to deduce a variety of properties of the τ.

I will try to give a complete set of experimental references in this paper. I will give very few theoretical references because I have given complete lists of older theoretical references in two review articles;[3,4] and T. F. Walsh[5] will provide an up-to-date theoretical summary.

An excellent and recent experimental review[6] of the heavy lepton in e^+e^- annihilation was given by G. Flugge at the 1977 Experimental Meson Spectroscopy Conference; and I gave an earlier review[7] at the XII Rencontre de Moriond.

II. SUMMARY OF THEORY

A. Sequential Lepton Model

In discussing the evidence for the τ I shall distinguish several possible types of leptons. First there is the sequential type:

Charged lepton	Associated neutrinos
$e^{\pm}$	$\nu_e, \bar{\nu}_e$
$\mu^{\pm}$	$\nu_\mu, \bar{\nu}_\mu$
$\tau^{\pm}$	$\nu_\tau, \bar{\nu}_\tau$
.	.
.	.
.	.

(1)

in which the τ^- and its associated neutrino, ν_τ, have a unique lepton number which is conserved in all interactions. This is a simple way to prevent the electromagnetic decays $\tau^- \to e^-\nu_\tau, \mu^-\nu_\tau$. The purely leptonic decay modes are

$$\tau^- \to \nu_\tau + e^- + \bar{\nu}_e$$
$$\tau^- \to \nu_\tau + \mu^- + \bar{\nu}_\mu \qquad (2)$$

Depending on the τ mass, m_τ, and the nature of the coupling there will also be semileptonic decay modes containing hadrons[8,9] such as:

$$\tau^- \to \nu_\tau + \pi^- \quad (3)$$

$$\to \nu_\tau + \rho^- \quad (4)$$

$$\to \nu_\tau + \pi^- + \pi^+ + \pi^- \quad (5)$$

B. Paralepton Model

Another simple way to suppress the electromagnetic decay of the τ is to assume it is a paralepton[10] where the τ has the lepton number of the oppositely charged e or μ.[11] Specifically:

$$E^- \text{ has the same lepton number as } e^+$$

$$M^- \text{ has the same lepton number as } \mu^+$$

C. Ortholepton Model

In principle the τ could have the same lepton number as the same sign e or μ. We then call it an ortholepton.[10] Specifically:

$$e^{*-} \text{ has the same lepton number as } e^- \quad (7)$$

$$\mu^{*-} \text{ has the same lepton number as } \mu^-$$

Then the $e\gamma e^*$ or $\mu\gamma\mu^*$ coupling must be strongly suppressed to make the electromagnetic decay rate small compared to the weak decay rate, as is required by the data (see 10c). I shall not discuss other models.[3,5,11,12]

III. SIGNATURES FOR NEW CHARGED LEPTONS PRODUCED IN e^+e^- ANNIHILATION

A. $e^\pm\mu^\mp$ Events

The cleanest signature for new charged lepton production is

$$e^+ + e^- \to \tau^+ + \tau^- \quad (8)$$
$$\quad\quad \downarrow \quad\quad\quad \downarrow$$
$$\quad \bar{\nu}_\tau e^+ \nu_e \quad \nu_\tau \mu^- \bar{\nu}_\mu$$

Such events must have:

i. an $e^\pm\mu^\mp$ or $e^-\mu^+$
ii. no other charged particles
iii. no photons
iv. missing energy
v. a "hard" heavy lepton momentum spectra for the e and μ as shown in Fig. 1.

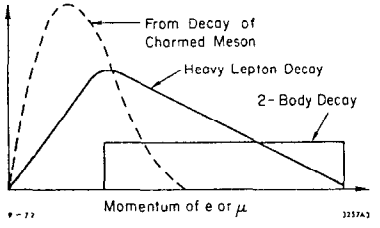

Fig. 1 Schematic comparison of the momentum spectrum for a lepton from a heavy lepton decay compared to the lepton spectrum from a charmed particle semileptonic decay or from a two-body decay.

B. $e^\pm x^\mp$, $\mu^\pm x^\mp$ Events

The decay of a τ with a mass of 1.9 GeV/c^2 is expected to yield only one charged particle (an e, μ, or hadron) a large fraction of the time; perhaps as much as 85% of the time. This leads to a two-charged prong event with or without photons:

$$e^+ + e^- \to \tau^+ + \tau^- \quad (9)$$
$$\quad\quad \downarrow \quad\quad\quad \downarrow$$
$$\quad \bar{\nu}_\tau e^+ \nu_e \quad \nu_\tau x^- + \geq 0\,\gamma\text{'s}$$

where x is an e, μ, or charged hadron.

IV. $e^\pm\mu^\mp$ DATA

Table I lists the $e\mu$ data reported previously or at this conference; and Figs. 2-4 show the lepton momentum spectra. All the sets of $e\mu$ events in Table I have the following properties:

a. Their production cross section and properties are consistent with their sole source being the pair production of a mass 1.9 ± 0.1 GeV/c^2 charged lepton.
b. No other explanation for these events has been put forth which fits their production cross section and properties.

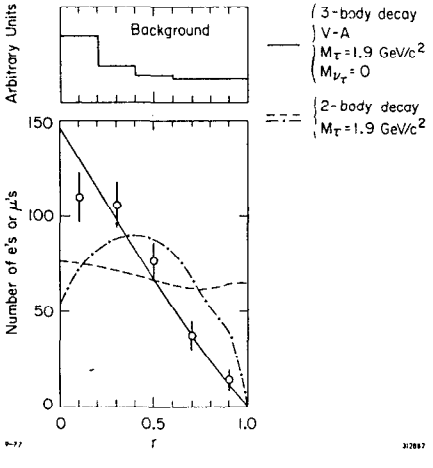

Fig. 2 The momentum spectrum for $e\mu$ events, with $3.8 \leq E_{c.m.} \leq 7.8$ GeV, from the SLAC-LBL Magnetic Detector Collaboration[7,15] corrected for background. Here $r = (p - 0.65)/(p_{max} - 0.65)$ where p is the e or μ momenta in GeV/c. The solid theoretical curve is for the 3-body leptonic decay of a mass 1.9 GeV/c^2 τ; the dashed theoretical curve is for the 2-body decay of an unpolarized boson; and the dash-dotted theoretical curve is for the 2-body decay of a boson produced only in the helicity = 0 state.

TABLE I

Data on eμ events. In addition to the lower limits on p_e and p_μ all these sets of p_μ events have acoplanarity requirements such as 10^o or 20^o. The references should be consulted for details on the event selection criterion.

Experimental group or detector	$E_{c.m.}$ range (GeV)	Lower limits on p_e p_μ (GeV/c)	Total number of eμ events	Number of background events	Comment	Ref.
M. Bernardini et al.	1.2 to 3.0				Early search at ADONE, lepton mass ≥ 1.0 GeV/c^2	13
S. Orioto et al.	2.6 to 3.0				Early search at ADONE, lepton mass ≥ 1.15 GeV/c^2	14
SLAC-LBL magnetic detector	3.8 to 7.8	0.65 0.65	190	46	First evidence. Used to determine m_τ, m_{ν_τ}, τ-ν_τ coupling.	1,2, 15, 16
PLUTO Group	3.6 to 5.0	0.3 1.0	23	1.9	Very clean. Strong argument against charm.	6,17, 18, 19
LBL-SLAC lead glass wall	3.7 to 7.4	0.4 0.65	22	0.4	Very clean. Low p_e cutoff.	20, 21
DASP Group	4.0 to 5.2	0.15	11	0.7	Good γ detection. Good hadron identification.	22

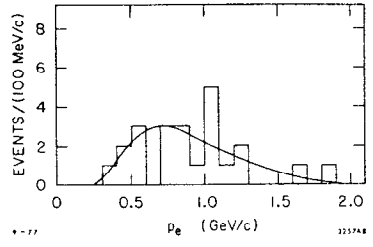

Fig. 3 The electron momentum spectrum for eμ events with $4.0 \leq E_{c.m.} \leq 5.0$ GeV from the PLUTO Group[6,17,19], compared with the theoretical curve for the 3-body leptonic decay of a mass 1.9 GeV/c^2 τ.

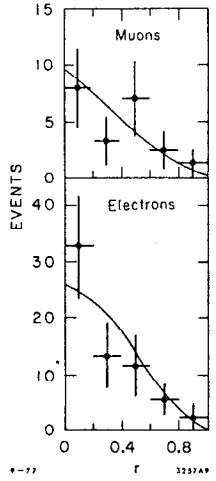

Fig. 4 The muon and electron spectra for eμ events with $4.0 \leq E_{c.m.} \leq 7.4$ GeV from the LBL-SLAC Lead Glass Wall Experiment[20,21]; compared with the theoretical curve for the 3-body leptonic decay of a mass 1.9 GeV/c^2 τ. Here $r = (p-p_{cut})/(p_{max}-p_{cut})$ where $p_{cut} = 0.65$ GeV, for the muons and 0.40 GeV/c for the electrons.

In Figs. 2 and 4

$$r = (p - p_{cut})/(p_{max} - p_{cut}) \tag{10}$$

is a variable used to consolidate the lepton momentum spectra from different $E_{c.m.}$ energies. Here p is the momentum of the e or μ in GeV/c; p_{max} is its maximum value which depends on $E_{c.m.}$ and m_τ; and p_{cut} is the low momentum cutoff used in the selection of the eμ events.

V. $\mu^\pm x^\mp$ DATA

These two-charged prong events have the form

$$e^+ + e^- \rightarrow \mu^\pm + x^\mp + \geq 0 \text{ photons; } x = e \text{ or hadron} \tag{11}$$

Note that unlike the eμ events, photons are allowed in these events to allow contributions from decay modes like $\tau^- \rightarrow \rho + \nu_\tau \rightarrow \pi^- + \gamma + \gamma + \nu_\tau$. In these events $\mu^\pm\mu^\mp$ pairs we excluded either by direct identification of the x as a μ or by μ pair background subtraction. The $\mu^\pm x^\mp$ data reported previously and at this conference is summarized in Table II.

Figures 5 and 6 show the SLAC-LBL magnetic detector data.[25] Note in Fig. 5 that the 2-prong events have a considerably larger production cross section than any other single multiplicity. This is also true for other μx and ex data and is one of the basic reasons why the 2-prong μx and ex events require a lepton source explanation. Figure 7 shows the beaufitul data of the PLUTO Group.[26]

TABLE II

Data on $\mu^{\pm}x^{\mp}$ events (Eq. (11)) as described in the references. These sets of events have acoplanarity cuts.

Experimental group or detector	$E_{c.m.}$ range (GeV)	Lower limits on p_μ p_x (GeV/c)	Number μx events above background	Comments	Ref.
Maryland-Princeton-Pavia	4.8	1.0 ~0.1		First evidence. Small statistics.	23,24
SLAC-LBL magnetic detector	4.0 to 7.8	1.0 0.2	103 ± 18 above $E_{c.m.}$=5.8 GeV	Strong signal above 5.8 GeV. Clearly different from $\mu+>2$ charged particle events.	25
PLUTO Group	4.0 to 5.0	0.7 ~0.1	~230	Strong signal in 3 $E_{c.m.}$ ranges in 4-5 GeV regions.	6, 17,19 26
DASP Group	4.0 to 5.2	0.7 ~0.1	≈12	Can be directly compared to ex events.	22
Maryland-Princeton-Pavia	7	1.15 ~0.1	8^{+4}_{-3}	Good charged prong detection.	27,28

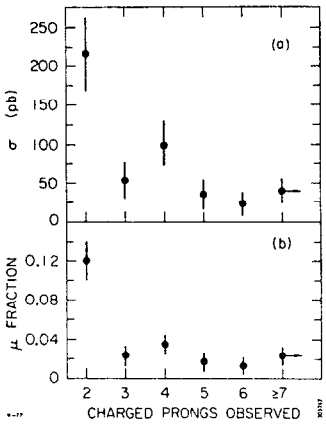

Fig. 5 (a) Anomalous muon production cross section and (b) ratio of anomalous muons to candidates versus the number of observed charged prongs in the $E_{c.m.}$ range 5.8 to 7.8 GeV from the SLAC-LBL Magnetic Detector Collaboration.[25]

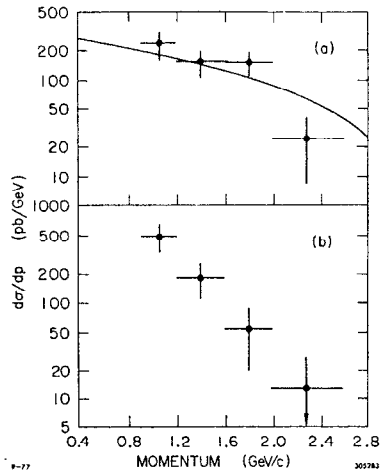

Fig. 6 Differential cross section for anomalous muon production versus momentum for (a) two-prong events and (b) multiprong events in the $E_{c.m.}$ range 5.8 to 7.8 GeV from the SLAC-LBL Magnetic Detector Collaboration.[25] The solid curve represents the expected cross section from the decays of a mass 1.9 GeV/c^2 τ.

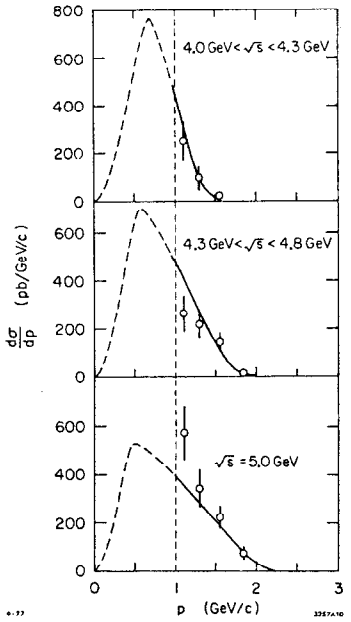

Fig. 7 The muon spectrum for μx events from the PLUTO Group[6,17,19] compared to the theoretical curve for the 3-body leptonic decay of a mass 1.9 GeV/c^2.

VI. $e^{\pm}x^{\mp}$ DATA

These events are of the form

$$e^+ + e^- \rightarrow e^{\pm} + x^{\mp} + \geq 0 \text{ photons} \quad x = \mu \text{ or hadron} \qquad (12)$$

and are listed in Table III.

Figures 8 and 9 show the preliminary momentum spectrum of the e in the ex event from the DASP[21] and DELCO[30] group respectively. Both spectra are consistent with that expected from a 1.9 ± 0.1 GeV/c^2 charged lepton.

TABLE III

Data on $e^{\pm}x^{\mp}$ events. See references for the acoplanarity cut.

Experimental group or detector	$E_{c.m.}$ range (GeV)	Lower limits on p_e p_x (GeV/c)	Number of ex events above background	Comments	Ref.
LBL-SLAC lead glass wall	3.7 to 7.4	0.4 0.65	70	See hadronic decay modes of τ.	20,21
DASP Group	4.0 to 5.2	.2 .2	60	See hadronic decay modes of τ. K/π ratio = 0.07 $\pm$ 0.06 compared to 0.24 $\pm$ 0.05 for ≥ 3 charged prong e events	22,29
DELCO	3.7 to 7.4	.1 .3	230	Very, very clean e selection with large solid angle	30

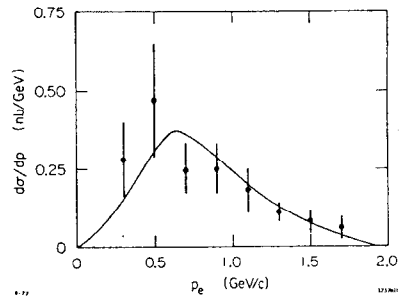

Fig. 8 The electron spectrum for ex events from the DASP Group (Refs. 22, 29) compared to the theoretical curve for the 3-body leptonic decay of a mass 1.9 GeV/c^2 τ.

VII. e^+e^- AND $\mu^+\mu^-$ DATA

If the τ hypothesis is correct one should observe noncoplanar events of the form

$$e^+ + e^- \rightarrow e^+ + e^- + \text{missing energy}$$
$$e^+ + e^- \rightarrow \mu^+ + \mu^- + \text{missing energy} \qquad (13)$$

which are not from QED processes. It is difficult to isolate such anomalous events because of contamination from QED processes such as

$$e^+ + e^- \rightarrow \mu^+ + \mu^- + \gamma$$
$$e^+ + e^- \rightarrow \mu^+ + \mu^- + \gamma + \gamma \qquad (14)$$
$$e^+ + e^- \rightarrow \mu^+ + \mu^- + e^+ + e^-$$

in which only the $\mu^+\mu^-$ pair is detected. Two results have been reported.

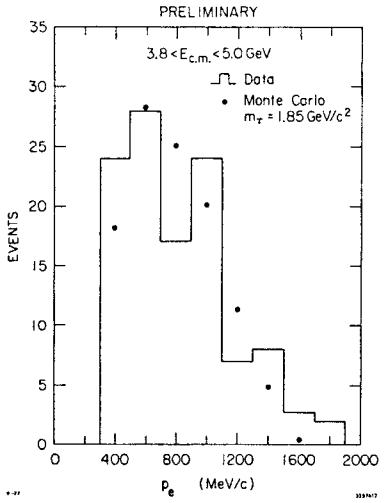

Fig. 9 Preliminary data from the DELCO Group[30] on the electron spectrum for ex events, compared to a theoretical Monte Carlo calculation for the 3-body leptonic decay of a mass 1.85 GeV/c^2 τ.

e^+e^- and $\mu^+\mu^-$ pairs in SLAC-LBL magnetic detector data[31]—e^+e^- and $\mu^+\mu^-$ pairs were selected requiring $p_e > 0.65$ GeV/c, $p_\mu > 0.65$ GeV/c and $\theta_{copl} > 20^o$. After corrections (which are large) for QED processes and for hadronic backgrounds, the following ratios of number of events is found.

$$\frac{\text{Number } ee}{\text{Number } e\mu} = 0.52 \pm .10 \pm \begin{matrix} .16 \\ .19 \end{matrix} \qquad (15)$$

$$\frac{\text{Number } \mu\mu}{\text{Number } e\mu} = 0.63 \pm .10 \pm .19$$

Here the first error is one standard deviation in the statistical error; and the second error is the limits on the systematic errors added in quadrature.

$\mu^+\mu^-$ pairs in Colorado-Pennsylvania-Wisconsin "Iron Ball" experiment at SPEAR[32,28]—Using $p_\mu > 1.2$ GeV/c and $\theta_{copl} > 10^o$ this experiment finds 25 $\mu^+\mu^-$ events. The expected background from QED processes and hadronic contamination is 14 events, leaving 11 anomalous $\mu^+\mu^-$ events. The authors report[32] that this number is consistent with that expected from the τ.

VIII. WHY THESE ANOMALOUS TWO-CHARGED PRONG EVENTS ARE NOT FROM CHARMED PARTICLE DECAYS

There are two reasons why there is a natural tendency to try to explain these anomalous two-prong events as due to the semileptonic decays of a pair of charmed particles. First the $e\mu$ events were found just as the hunt for singly charmed mesons began. Second as shown in Section IX.A the τ mass lies within 100 MeV/c^2 of the D meson masses. Nevertheless it has been shown repeatedly that almost all of $e\mu$ events and most of the ex and μx events require a non-charm explanation. The best way to see why this is so is to read the papers of each experimental group to see why they each came to this conclusion using their own data. Here I will summarize the reasons for this conclusion.

A. Summary of Why Anomalous Two-Prong Events are not From Charm

i. Very few or no $\geq$ three-charged prong $e^{\pm}\mu^{\mp}$ events have been found compared to the number of two-charged prong, 0 photons $e^{\pm}\mu^{\mp}$ events.[15,17,19] Since charm will produce more $\geq$ three-charged prong $e\mu$ events than two-charged prong $e\mu$ events, particularly at high $E_{c.m.}$ energy, the two-charged prong, 0 photon, $e\mu$ events cannot come from charm.

ii. The momentum spectra of the e or μ in $e\mu$, ex and μx events is too hard for charm (the charm e or μ spectra is now known experimentally[19,21,22,30]).

iii. The ratio of eK to eπ events is too small for charm.[22,33]

iv. The production cross sections for $e\mu$, ex, and μx events are all compatible with the point particle production of a mass 1.9 ± 0.1 lepton.[6,7,19,21,22,30] These production cross sections do not follow the ups and downs of the charm production cross section. A recent example is the production cross section for ex events presented by the DELCO Group[30] at this conference. There is a sharp dip in the ≥ 3 prong e events (the signature for charm events) at about 4.28 GeV/c. But there is no dip in the 2-prong e events (the signature for τ events) at this point. At the $\psi(3772)$ there is a peak in the raw number of 2-prong e events, but according to Kirkby[30] about half of these events are from charm because the e and x momentum go down to the hundred MeV/c range. Once this correction is made, there is no peak in the 2-prong e event at $\psi(3772)$.

In the next section I will show in more detail the production cross section for $e\mu$ events including new data at $\psi(3772)$.

B. New Data on $e\mu$ Production Cross Sections

The LBL-SLAC lead glass wall experiment[20,21] found 8 $e^{\mp}\mu^{\pm}$ events ($p_e > 0.65$ GeV/c, $p_\mu > 0.65$ GeV/c, $\theta_{copl} > 20^o$, no other charged tracks, 0 photons) at $E_{c.m.} = 3.772$ GeV, which is the peak of the ψ''. One of these events had its e in the lead glass wall. There are three types of backgrounds:

a. background from hadronic events = 2.3 events
b. background from joint semileptonic decays of a $D\bar{D}$ pair ≤ 0.2 events
c. background from the semileptonic decay of a D and the misidentification of a hadron $\lesssim 1.9$ events.

There may be some double counting between a and c because a study of ≥ 3-prong $e^{\pm}\mu^{\mp}$ events at ψ'' finds 65 events with a calculated background of 64; and this background of 64 events is calculated using the same method as the 2.3 events in a. The small statistics and the presence of the ψ'' make it impossible to prove we have heavy lepton $e\mu$ events at the ψ''. The observed $e\mu$ production cross section is $5.4 \begin{smallmatrix} +2.8 \\ -4.7 \end{smallmatrix}$ where the lower error takes into account the uncertainty as to how to do the backgrounds.

To display this result in comparison with earlier $e\mu$ data we define

$$R_{e\mu,\text{observed}} = \sigma_{e\mu,\text{observed}}/\sigma_{ee\to\mu\mu} \tag{16}$$

Note that $R_{e\mu,\text{observed}}$ is corrected for background contamination but is not corrected for acceptance or triggering efficiency. Figure 10 shows $R_{e\mu,\text{observed}}$. The points at the $\psi(3772)$ is consistent with a monotonic rise in $R_{e\mu,\text{observed}}$ and shows no effect of the peak in R (Fig. 11) at that resonance. Comparing Fig. 10a with Fig. 11, we also see no peak in $R_{e\mu,\text{observed}}$ at the 4.1 or 4.4 peaks in R. Thus $R_{e\mu,\text{observed}}$ does not follow charm production as reflected in the variations in R.

In Fig. 12 we define

$$R_\tau = R_{e\mu,\text{observed}}/(2B_e\, B_\mu\, A_{e\mu}) \tag{17}$$

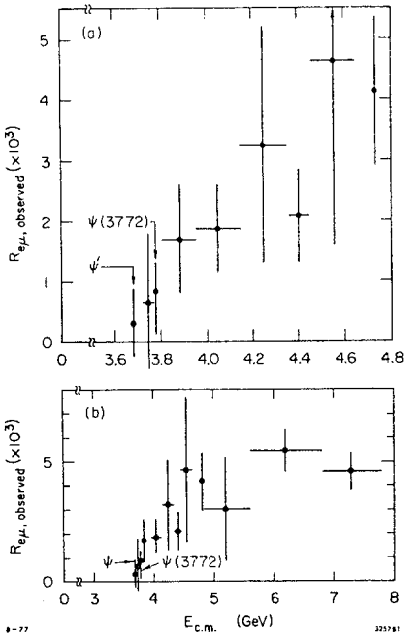

Fig. 10 $R_{e\mu,\text{observed}}$ for (a) $3.6 \leq E_{c.m.} \leq 4.8$ GeV and (b) $3.6 \leq E_{c.m.} \leq 7.8$ GeV.

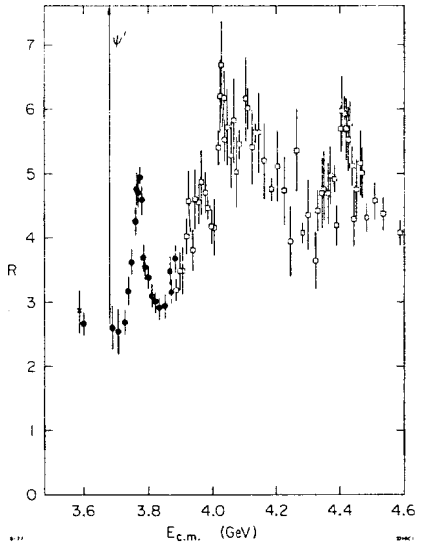

Fig. 11 R for $3.6 \leq E_{c.m.} \leq 4.6$ GeV.

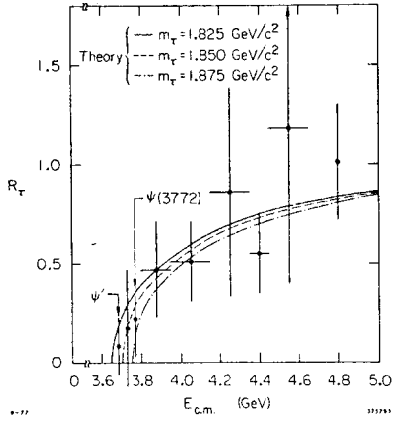

Fig. 12 R_τ compared to theoretical R_τ curves for various τ masses.

where the branching ratios to e and μ are taken to be[16] $B_e = B_\mu = .186$ and $A_{e\mu}$ is the product of the acceptance, the trigger efficiency, and various particle loss corrections. From Fig. 12 we see that if we take R_τ at the $\psi(3772)$ as being its nonzero value, the τ mass lies in the range of 1800 to 1875 MeV/c^2. In any case we see that R_τ is a monotonic function of $E_{c.m.}$ as it must be for the heavy lepton.

IV. PROPERTIES OF THE τ

A. τ Mass

Table IV gives those m_τ values which have been reported. I have not included information where data is said to be consistent with a certain m_τ but no error on that m_τ is given.

TABLE IV

Measurements of m_τ assuming V-A coupling and $m_{\nu_\tau} = 0.0$.

Experiment	Data Used	Method	τ Mass (GeV/c^2)	Comment	Ref.
SLAC-LBL magnetic detector	$e\mu$	$p_\perp$	1.91 ± .05	Statistical error	7,16
		$\cos\theta_{coll}$	1.85 ± .10	Statistical error	
		r	1.88 ± .06	Statistical error	
		composite	1.90 ± .10	Statistical and systematic error	
PLUTO Group	μx	$\sigma_{\mu x}$	1.93 ± .05		19
LBL-SLAC lead glass wall	$e\mu$'s at 3.772	p_e, p_μ	1.800 to 1.875	If $e\mu$'s at 3.772 are from τ	this paper
LBL-SLAC lead glass wall	ex at 3.772	σ_{ex}	1.800 to 1.875	If ex's at 3.772 are from τ	21

B. ν_τ Mass

Two upper limits have been set on m_{ν_τ}. Using $e\mu$ events[7,16]: $m_{\nu_\tau} \leq 0.6$ GeV/c^2 with 95% CL. Using μx events[19]: $m_{\nu_\tau} \leq 0.54$ GeV/c^2 with 95% CL.

C. τ-ν_τ Coupling

Using Fig. 13 we find[7,16] that V+A coupling has a χ^2 probability of less than 0.1% to fit the r distribution (Eq. (10)) of the $e\mu$ events. V-A coupling has a 60% χ^2 probability. If we ignore the r=.1 point the χ^2 probability for V+A is 5%. An additional argument against V+A coupling is that one cannot obtain a consistent m_τ value as shown in Table V.

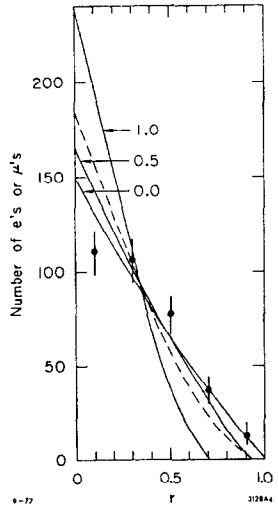

Fig. 13 r for all $e\mu$ events from the SLAC-LBL Magnetic Detector Collaboration. r is defined in the caption of Fig. 2.

TABLE V

m_τ for V+A coupling and $m_{\nu_\tau} = 0.0$.

Method	$p_\perp$	$\cos\theta_{coll}$	r
Mass (GeV/c^2)	2.12 ± .05	1.95 ± .10	Upper limit is 1.76 with 95% CL.

Using μx events, the PLUTO Group also finds[6,19] the V-A coupling is favored over V+A coupling. Neither experiment is able to say anything about coupling intermediate between V+A and V-A such as pure V or pure A.

X. DECAY MODES OF T

A. Purely Leptonic Decay Modes

Table VI gives the existing data on the purely leptonic decay rates: B_e for $\tau^- \to e^- \nu_\tau \bar{\nu}_e$ and B_μ for $\tau^- \to \mu^- \nu_\tau \bar{\nu}_\mu$.

We note that these purely leptonic branching ratios are in agreement within the errors. This is a very pleasing result considering the wide variety of methods and the difficulty of working with these small signals. These measurements are also in agreement with the theoretical calculations for a $m_\tau = 1.9$ GeV/c, $m_{\nu_\tau} = 0.0$, V-A coupling, sequential charged lepton, and Table VII.

B. Semileptonic Decay Modes

Table VIII gives the existing information on semileptonic decay modes of the τ. Comparing this table with Table VII we see that several of the predicted decay semileptonic modes of the τ have been seen, and within errors they have the expectant branching ratios. The $\tau^- \to \pi^- + \nu_\tau$ has not been seen; using $B_e = .2$, the DASP Group finds[22] a preliminary result $B_\pi = .02 \pm .025$. If further experiments confirm this relatively low value of B_π then the present theory of the nature of the τ lepton will have to be revised. For example: the τ might not have V-A coupling to the conventional weak currents.

Since this is the first presentation of the "A_1" + ν_τ decay mode by the SLAC-LBL Collaborators;[35] I will show some preliminary graphs. (Incidently the notation "A_1" is used because the expected spin (1^+) of the A_1 has not been tested and

TABLE VI

The measured fractional decay rates B_e and B_μ. V-A coupling, $m_\tau = 1.9$ GeV/c and $m_{\nu_\tau} = 0.0$ was used to calculate acceptances.

Experimental group or detector	Data Used	B_e or B_μ	Comment	Ref.
SLAC-LBL magnetic detector	$e\mu$	$0.186 \pm .010 \pm .028$	Assume $B_e = B_\mu$. First error is statistical, second is systematic.	7,16
SLAC-LBL magnetic detector	μx	$0.175 \pm .027 \pm .030$	Assume $B_x = 0.85$. First error is statistical, second is systematic.	7,16
PLUTO Group	μx	$B_\mu = 0.14 \pm .034$		19
PLUTO Group	$\mu x, e\mu$	$B_e = 0.16 \pm .06$		19
LBL-SLAC lead glass wall	$e\mu$	$0.224 \pm .032 \pm .044$	Assume $B_e = B_\mu$. First error is statistical, second is systematic.	20,21
DASP Group	$e\mu$	$0.20 \pm .03$	Assume $B_e = B_\mu$.	22
DELCO Group	ex	0.15	No error given.	30
Iron Ball	$\mu\mu$	$0.22 \, {}^{+.07}_{-.08}$		32
Maryland-Princeton-Pavia	μx	$0.20 \pm .10$		27

TABLE VII

Predicted branching ratios for a τ^- sequential charged heavy lepton with a mass 1.9 GeV/c^2, an associated neutrino mass of 0.0, and V-A coupling. The predictions are based on Refs. 8 and 9 as discussed in Ref. 34. The hadron continuum branching ratio assumes a threshold at 1.2 GeV for production of $\bar{u}d$ quark pairs whose final state interaction leads to the hadron continuum. From the third column it is predicted that 85% of the decays of the τ will contain only one charged particle.

Decay mode	Branching ratio	Number of charged particles in final states
$\nu_\tau \bar{e}^- \bar{\nu}_e$	.20	1
$\nu_\tau \nu^- \bar{\nu}_\mu$	.20	1
$\nu_\tau \pi^-$	.11	1
$\nu_\tau K^-$	.01	1
$\nu_\tau \rho^-$	.22	1
$\nu_\tau K^{*-}$	.01	1
$\nu_\tau A_1^-$	.07	1,3
ν_τ (hadron continuum)$^-$	.18	1,3,5

TABLE VIII

Observed semileptonic decay modes of the τ. V-A coupling, $m_\tau = 1.9$ GeV/c^2 and $m_{\nu_\tau} = 0.0$ was used to calculate acceptances. Here h means hadron.

Experimental group or detector	Decay mode (for τ^-)	Branching ratio	Ref.
LBL-SLAC lead glass wall	$h^- + \nu_\tau + \geq 0\ \gamma$'s	0.45 ± 0.19	20,21
DASP Group	$\rho^- + \nu_\tau$	$0.24 \pm .09$	22
DASP Group	$\pi^- + \nu_\tau$	$B_e B_\pi = 0.004 \pm .005$	22
PLUTO Group	"A_1"$^- + \nu_\tau$	$0.11 \pm .04 \pm .03$ for "A_1" $\rightarrow$ all	19
LBL-SLAC lead glass wall and SLAC-LBL magnetic detector	"A_1"$^- + \nu_\tau$		35

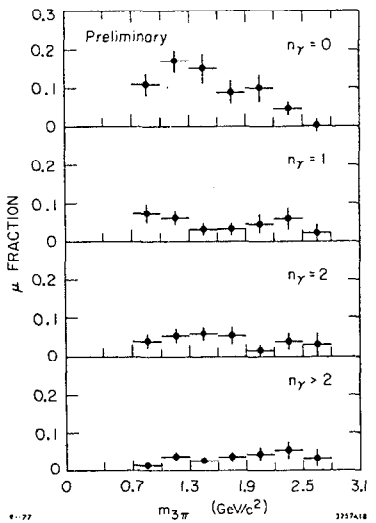

Fig. 14 μ/μ candidates versus invariant mass of remaining three prongs in 4-prong events.

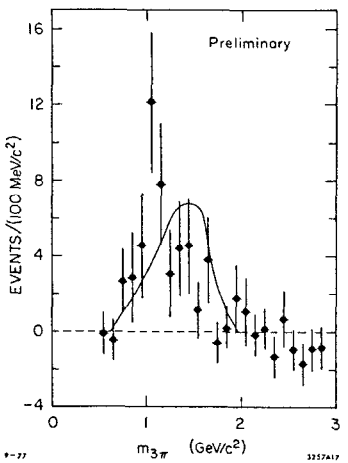

Fig. 15 3-particle invariant mass distribution opposite muons corrected for hadron misidentification. The curve gives the mass distribution expected from non-resonant production ($\tau \rightarrow \nu\pi\rho$), corrected for acceptance effects, and normalized to the data in the range $.7 < m_{3\pi} < 1.8$.

and because the evidence from hadronic experiments on the A_1 is confusing. The SLAC-LBL analysis which was carried out by J. Jaros selects events using the following criteria

i. $E_{c.m.} > 6$ GeV
ii. 4-charged prongs with total charge 0
iii. one of the prongs must be identified as a muon by the muon tower or mini-muon tower of the magnetic detector
iv. $p_\mu > 0.9$ GeV/c.

Figure 14 shows the ratio μ/μ candidates versus the mass of the 3π system. (The non-μ particles are assumed to be pions.) Only the 0 photon data shows a ratio greater than the ~0.05 expected from π decay, K decay, and punchthru. Figure 15 shows the 3π mass spectra of the 0 photon events corrected for background. The peak in the 1.-1.2 GeV/c² region is too narrow to come from the nonresonant $\tau \rightarrow \quad \nu_\tau + \pi + \rho$ decay mode. Figure 16 shows that the μ in these events have "hard" spectrum required for the τ.

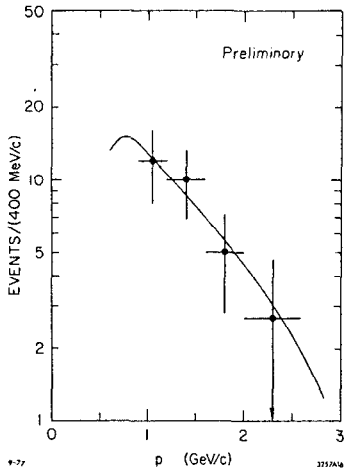

Fig. 16 Muon spectrum opposite tri-pions with $1.0 < m_{3\pi} < 1.3$. The curve is the Monte Carlo prediction for $m_\tau = 1.85$, $m_{\nu_\tau} = 0$, V-A, $E_B = 3.5$, normalized to the data.

C. Upper Limits on Rare Decay Modes

TABLE IX

Upper limits on rare decay modes of the τ using V-A coupling, $m_\tau = 1.9$ GeV/c², $m_{\nu_\tau} = 0.0$ for acceptance calculations.

Experimental group or detector	Mode	Upper limit on branching ratio	C. L.	Ref.
PLUTO Group	$\tau^- \rightarrow$ (3 charged particles)$^-$	0.01	95%	6
PLUTO Group	$\tau^- \rightarrow$ (3 charged leptons)$^-$	0.01	95%	6
SLAC-LBL magnetic detector	$\tau^- \rightarrow$ (3 charged leptons)$^-$	0.006	90%	36
SLAC-LBL magnetic detector	$\tau^- \rightarrow \rho^- + \pi^0$	0.024	90%	37
PLUTO Group	$\tau^- \rightarrow e^- + \gamma$ $\tau^- \rightarrow \mu^- + \gamma$	0.12	90%	6
LBL-SLAC lead glass wall	$\tau^- \rightarrow e^- + \gamma$	0.026	90%	38
LBL-SLAC lead glass wall	$\tau^- \rightarrow \mu^- + \gamma$	0.013	90%	38

XI. CONCLUSIONS

a. All data on anomalous $e\mu$, ex, μx, ee and $\mu\mu$ events produced in e^+e^- annihilation is consistent with the existence of a mass 1.9 ± 0.1 GeV/c^2 charged lepton, the τ.

b. This data cannot be explained as coming from charmed particle decays.

c. Many of the expected decay modes of the τ have been seen. A very important problem is the existence of the $\tau^- \rightarrow \nu_\tau \pi^-$ decay mode.

d. There has not been the space to discuss it here, but ν_μ experiments[6,7] say that the τ cannot be a muon-related ortholepton or paralepton with conventional coupling strengths. The results in Eq. (15) say that the τ is not an electron-related paralepton[7,31] using the theoretical work of Ali and Yang.[40] The τ may be a sequential lepton or an electron-related ortholepton.

REFERENCES

(1) M. L. Perl in Proceedings of the Summer Institute on Particle Physics (SLAC, Stanford, California, 1975).
(2) M. L. Perl et al., Phys. Rev. Lett. 35 (1975) 1489.
(3) G. J. Feldman and M. L. Perl, Phys. Reports (to be published); also issued as a SLAC preprint.
(4) M. L. Perl and P. Rapidis, Stanford Linear Accelerator Center preprint SLAC-PUB-1496(1974)(unpublished).
(5) T. F. Walsh, this conference.
(6) G. Flügge in Proceedings of the 1977 Experimental Meson Spectroscopy Conference (Northeastern University, Boston, 1977); also issued as DESY 77/35.
(7) M. L. Perl in Proceedings of the XII Rencontre de Moriond, Flaine, 1977, edited by Tran Thanh Van (R. M. I. E. M., Orsay).
(8) H. B. Thacher and J. J. Sakurai, Phys. Lett. 36B (1971) 103.
(9) Y. S. Tsai, Phys. Rev. D 4 (1971) 2821.
(10) C. H. Llewellyn Smith, Oxford University preprint 33/76 (1976), submitted to Proc. Roy. Soc.
(11) J. D. Bjorken and C. H. Llewellyn Smith, Phys. Rev. D 7 (1973) 88.
(12) S. Weinberg, this conference.
(13) M. Bernardini et al., Nuovo Cimento 17 (1973) 383.
(14) S. Orioto et al., Phys. Lett. 48B (1974) 165.
(15) M. L. Perl et al., Phys. Lett. 63B (1976) 466.
(16) M. L. Perl et al., Stanford Linear Accelerator Center preprint SLAC-PUB-1997 (1977), submitted to Phys. Lett.
(17) H. Meyer in Proceedings of the Orbis Scientiae, Coral Gables, 1977.
(18) J. Burmester et al., DESY 77/25.
(19) G. Knies, this conference.
(20) A. Barbaro-Galtieri et al., Lawrence Berkeley Laboratory preprint 6458.
(21) A. Barbaro-Galtieri, this conference.
(22) S. Yamada, this conference.
(23) M. Cavalli-Sforza et al., Phys. Rev. Lett. 36 (1976) 588.
(24) G. Snow, Phys. Rev. Lett. 36 (1976) 766.
(25) G. J. Feldman et al., Phys. Rev. Lett. 38 (1976) 177.
(26) J. Burmester et al., DESY 77/24.
(27) D. H. Badtke et al., this conference.
(28) H. Sadrozinski, this conference.
(29) R. Brandelis et al., DESY 77/36.
(30) J. Kirkby, this conference.
(31) F. B. Heile et al., to be published.
(32) U. Camerini et al., this conference.
(33) R. Brandeli et al., DESY 77/36.
(34) G. J. Feldman in Proceedings of the 1976 Summer Institute on Particle Physics (SLAC, Stanford, California, 1976); also issued as SLAC-PUB-1852 (1976).
(35) J. Jaros et al., to be published.
(36) G. J. Feldman, private communication.
(37) H. K. Nguyen, private communication.
(38) J. Jaros, private communication.
(39) M. Murtagh, this conference.
(40) A. Ali and T. C. Yang, Phys. Rev. D 14 (1976) 3052.

QUARKS AND PARTICLE PRODUCTION *

K.C. Moffeit

Stanford Linear Accelerator Center

* Work supported by the U.S. Energy Research and Development Administration.

1. INTRODUCTION

Early evidence for the quark structure of hadrons was indirect. The symmetries found in hadron spectroscopy showed that particles could be explained by the appropriate grouping of three quarks. Our present and early enthusiasm for the quark model is derived from these early successes. Fred Gilman and Marty Perl have made a detailed review in these proceedings of the spectroscopy of particles composed of quarks. Quark model predictions for particle production in terms of sum rules and scattering amplitudes have also been made. The earliest of these was the recognition that the pion composed of two-quarks and the proton (three quarks) should have the ratios of their total cross sections on protons equal to two-thirds which is approximately the case.

Inelastic lepton-nucleon scattering at large momentum transfer provided a direct means of probing small distance nucleon structure. The early results from SLAC showed a large cross section at high momentum transfer suggesting (in analogy the Rutherford alpha-scattering experiment) that the scattering took place from fundamental point-like constituents within the nucleon. These data were soon interpreted in terms of the quark-parton model whose important feature suggested by Feynman is its emphasis on the infinite-momentum frame.[1] In this frame the proper motion of the constituents of the proton is slowed down by the relativistic time dilation, and the proton charge distribution is Lorentz-contracted as well. Then for violent enough collisions the incident lepton scatters instantaneously and incoherently from the individual constituents of the proton as viewed in the diagrams of Fig. 1.

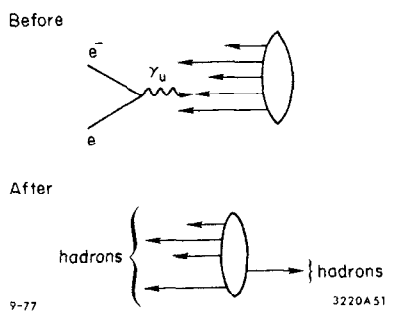

1. Diagram for inelastic electron scattering from the constituents of the proton.

Bjorken[2] extended this simple picture to observe that the fundamental reaction is that of elastic scattering of the electron on the parton and predicted that the structure function νW_2 was only a function of $x = Q^2/2M\nu$. The scaling variable x gives the fraction of momentum carried by the struck parton. The structure function measures the momentum distribution of the partons within the proton. The approximate scaling[3] seen in Fig. 2 has a spread in νW_2 of about 30% with Q^2 and ν each varying by an order of magnitude.

Since this exciting time in the late sixties and early seventies data from neutrino scattering, hadronic final states in ℓp collisions, e^+e^- annihilation, large p_T in hadron collisions, and jet formation are now available. It is the goal of these lectures to look at the production process in these different reactions in terms of the underlying quark-parton dynamics.

We will assume the partons are the familiar u, d, s quarks and their anti-particle counterparts. The charm quark c will be included; however, for most of what I say it is not important. The quantum number assignments are given in Table I.

TABLE I: Quantum number assignments for the up-u, down-d, strange-s, and charm-c quarks.

	u	d	s	c
Charge	2/3	-1/3	-1/3	2/3
Baryon #	1/3	1/3	1/3	1/3
Strangeness	0	0	1	0
Charm	0	0	0	1
Spin	1/2	1/2	1/2	1/2

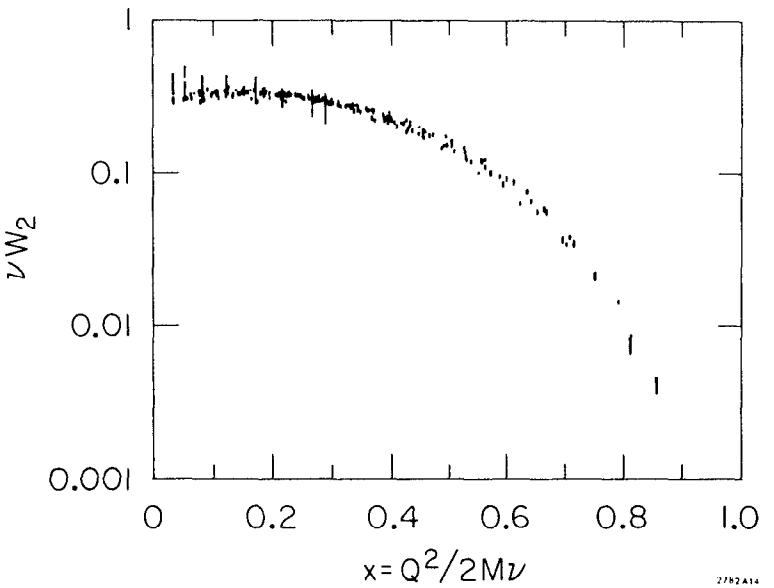

2. Values of νW_2 for the proton with $Q^2 > 1$ GeV^2 and $W > 2$ GeV. SLAC data except for large vertical bars below $x = 0.3$ are obtained from muon data taken at Fermilab. Figure from Ref. 3

The quark-parton model has the proton made up of three valence quarks (u, u, d) and a "sea" of $q\bar{q}$ pairs.

We will begin with a discussion of the spin of the quarks and show how the experiments in electroproduction and e^+e^- collisions support their spin 1/2 character. The next section will deal with the quark momentum distribution functions within the nucleons. We will review how these are obtained from electroproduction and neutrino scattering. We will see that the leading hadrons produced in ep and νp collisions reflect these quark momentum distributions. In Section IV we investigate inclusive hadron distributions produced in different reactions and compare their average multiplicity, average transverse momentum, and Feynman scaling of the final state hadrons. In the last section we will look at exclusive states in terms of the predictions of the additive quark model which assumes that only a single quark-quark scattering occurs for peripheral hadron interactions.

I. SPIN OF THE PARTONS

A. Electroproduction

The measurement in electroproduction of the ratio of the scattering by longitudinal (σ_S) and transverse (σ_T) photons can be interpreted in terms of the spin of the partons. For spin 1/2 partons helicity will be conserved in the scattering process and a parton whose direction is reversed will have to absorb a unit of angular momentum in order to maintain the same helicity, and hence only contribute to σ_T. Similarly, a spin 0 parton would contribute only to σ_S. The longitudinal and transverse components of the flux of virtual photons in ep scattering can be adjusted at a particular point in the Q^2 and ν plane. For large incident electron energy we mainly have transverse photons. However, if the incident electron has just enough energy to reach the Q^2,ν point then we have a large longitudinal photon flux. The SLAC-MIT[4] groups have measured the ratio of the longitudinal to transverse cross sections $R = \sigma_L/\sigma_T$. In Figure 3, their measurements of R are shown for different x values as a function of Q^2. R_p is small as expected for spin 1/2 quarks. For simple models with spin 1/2 constituents, R_p should vanish as $1/Q^2$. The results are consistent with either a limiting behavior or with R_p = constant.[3]

The measurements with polarized electrons on polarized protons yield further information on the spin structure of the quarks. These measurements were carried out at SLAC using the PEGGY polarized electron source developed by Yale[5]. Longitudinally polarized electrons provide a flux of elliptically polarized virtual photons and the polarized target gives a target of polarized quarks. Only when the spins are antiparallel can the spin 1/2 quark absorb the unit of angular momentum. Naively, only one of the quarks contributes to the scattering when the virtual photon and target polarizations are aligned ($\sigma_{3/2}$) and two contribute when the polarizations are opposite ($\sigma_{1/2}$). The measurement of the asymmetry parameter

$$A = \frac{\sigma_{1/2} - \sigma_{3/2}}{\sigma_{1/2} + \sigma_{3/2}} \qquad (1)$$

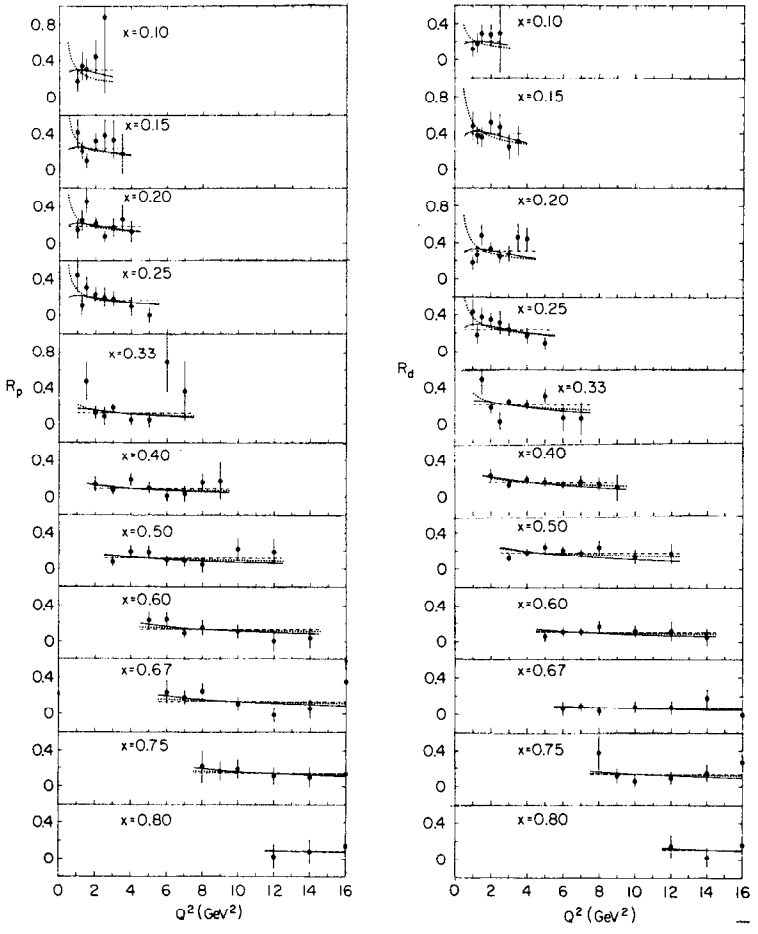

3. Value of $R_p = \sigma_L/\sigma_T$ for ep scattering. Reference 4.

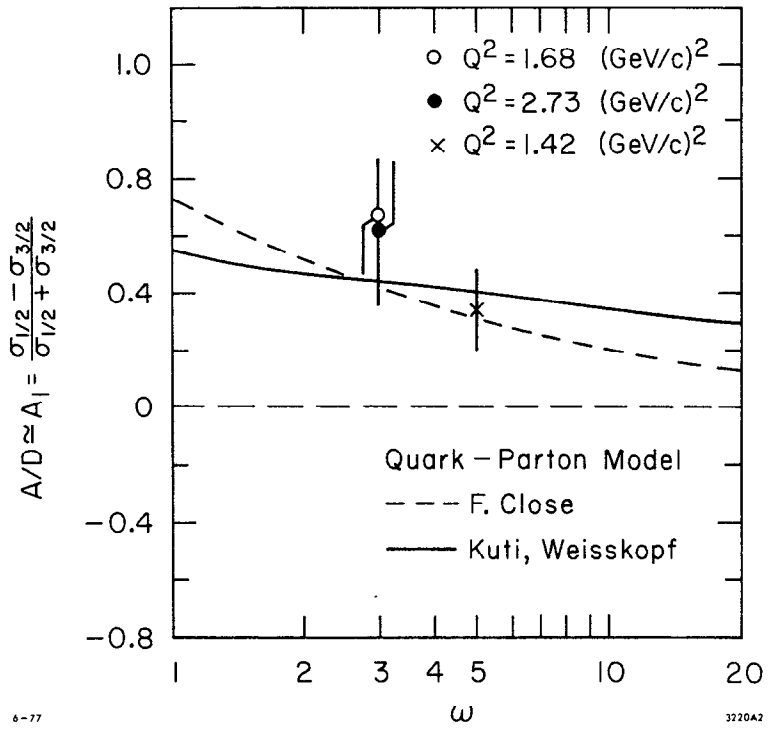

4. Virtual photon-proton asymmetry A_1. Data of Ref. 5. Curves are theoretical prediction for quark-parton models with spin-1/2 constituents.

is shown in Figure 4 along with the predictions from the quark-parton models of Kuti-Weisskopf and Close[6]. Obviously, our naive calculation of A = (2-1)/(2+1) = 1/3 is only a crude approximation. The data are consistent with either model. The asymmetries are positive and large, in agreement with predictions of quark-parton models of the proton having spin-1/2 constituents.

B. e^+e^- Collisions

The quark model for e^+e^- collisions assumes a single photon coupling to quark anti-quark pairs or lepton pairs (see Figure 5). The strength depends on the square of the charge. The final state hadrons result from the fragmentation of the quarks (see diagram b of Figure 5). This simple picture predicts scaling of the total cross section, i.e., the energy dependence for $e^+e^- \to$ hadrons is the same as that for $e^+e^- \to \mu^+\mu^-$. If the spin of the quark is 1/2 as is the muon then the ratio of the cross sections is the sum of the squares of the charges of the quarks,

$$R = \frac{\sigma(e^+e^- \to \text{hadrons})}{\sigma(e^+e^- \to \mu^+\mu^-)} = \sum_i Q_i^2 \qquad (2)$$

The SPEAR measurements[7] of R are shown in Figure 6. R is approximately constant at $R \tilde{\sim} 2.5$ for $E_{cm} < 3.7$ GeV. As E_{cm} increases R rises with a structure occurring in the 4 GeV region. Above 4.5 GeV R is again constant at a value of $R \tilde{\sim} 5$. The increase of R near 4 GeV suggest a threshold for production of new particles. This result came before the discovery of the J/ψ and ψ'. With the discovery of these narrow states and charmed mesons we are confident that the step in R is due to the coupling of the photon to charm anti-charm

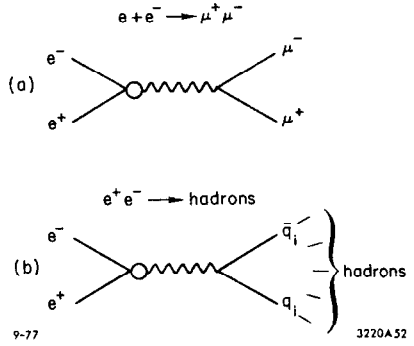

5. Diagrams for $e^+e^- \to \mu^+\mu^-$ and the quark model diagram for $e^+e^- \to$ hadrons through an intermediate $q\bar{q}$ pair.

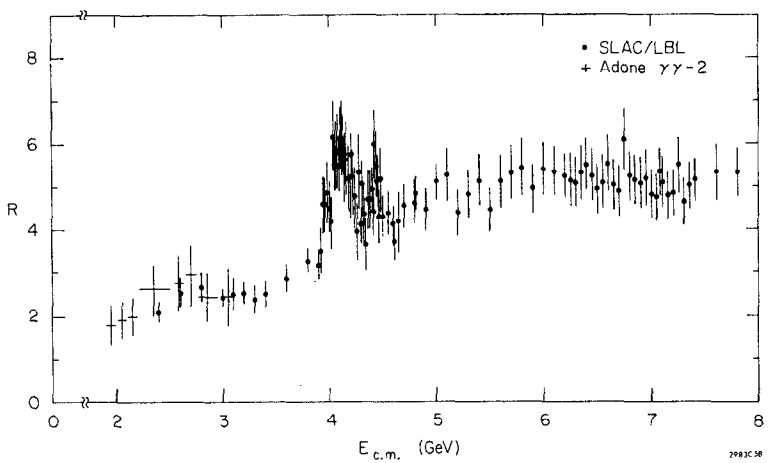

6. e^+e^- → hadrons: Ratio of cross sections for e^+e^- → hadrons to $e^+e^- \rightarrow \mu^+\mu^-$. Figure from Ref. 7.

quark states.

The magnitude of R gives us additional information about the quarks. A naive calculation below charm threshold gives

$$R = \frac{\Sigma Q_i^2}{Q_\mu^2} = \frac{\frac{4}{9} + \frac{1}{9} + \frac{1}{9}}{1} = \frac{2}{3}$$

compared to the measured value of about 2.5. In terms of the quark model for hadron production, either there must be more quark pairs or the charge assignments of the quarks are wrong. As discussed by F. Gilman in these proceedings, a solution is to add a new quantum number, color, to the traditional quark. We then obtain R = 2 for three triplets of fractionally charged quarks. The opening of charm threshold ($Q_c = \frac{2}{3}$) would yield R = $3\frac{1}{3}$ as compared to the measured value R ~ 5 (see Figure 6). An additional contribution to R is from the heavy lepton discovered by the SPEAR group[8] also with a threshold near E = 4 GeV. At the higher energy the heavy lepton pair production will contribute one unit to R and because of its decay will be included in the measurement of e^+e^- → hadrons. We expect from the quark model with color plus heavy lepton production a value R = $4\frac{1}{3}$ compared to the SPEAR measurement of R of 5 to 5.5. The recent measurement from DESY by the PLUTO group shows R between 4 and 5, as reported by W. DeBoer[9] in these proceedings. The systematic uncertainty of these measurements is 10 to 20% and are in agreement with the value R = $4\frac{1}{3}$.

C. Jet Structure in e^+e^- Annihilation

Jet structure has long been recognized as a natural prediction of the quark-parton model and has been investigated in lepton production[10], large p_T reactions[11], and e^+e^- collisions[12]. Because the initial state is simple, e^+e^- annihilation should have unambiguous jet structure. Here the quark anti-quark pair are initially produced back-to-back. The quarks fragment to hadrons with limited transverse momentum with respect to the original quark direction. At high enough beam energy the hadrons have longitudinal momentum larger than the $\langle p_T \rangle \sim 350$ MeV and jets are seen. At SPEAR energies the jet structure has been observed but since the CMS energy is not large enough their existence is determined by a statistical analysis[12].

In order to determine how jet-like an event is we find the direction for each hadronic event which minimizes the sum of the squares of the transverse momenta of the detected tracks. We then calculate a quantity called sphericity

$$S = \frac{3\left(\sum_i P_{\perp i}^2\right)_{\min}}{2\sum_i \vec{P}_i^{\,2}} \qquad (3)$$

For events with tracks distributed isotropically (looking like a balloon) sphericity will be near one, for events with limited transverse momentum (jet-like events) S approaches zero. The observed sphericity distributions[12] for three cm energies are shown in Figure 7. The curves give comparisons to jet model and phase-space model calculations. At $E_{cm} = 3$ GeV very little difference between the two

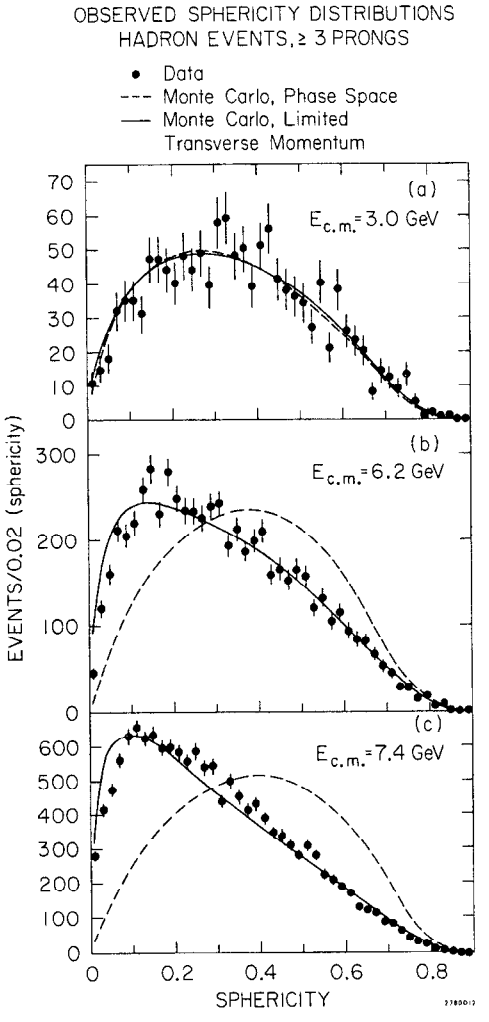

7. Observed sphericity distributions for $e^+e^- \to$ hadrons. SPEAR data from Ref. 12.

models occur, however, by 2.6 GeV the data clearly are only compatible with the limited transverse momentum model and is evidence for jet structure in e^+e^- hadron production.

The jet direction angular distribution reflects the angular distribution of the initial quark production. The most general angular distribution is

$$\frac{d\sigma}{dr} \propto 1 + \alpha \cos^2\theta + \alpha \mathbb{P}^2 \sin^2\theta \cos 2\phi \qquad (4)$$

where $\mathbb{P}$ is the transverse polarization of the beam. For spin 1/2 particles (e.g. $e^+e^- \to \mu^+\mu^-$) alpha is 1 and for spin 0 particles *alpha is -1. It is very difficult to determine the spin character* from the theta dependence alone since the SPEAR detector measures the theta dependence about $\cos\theta = 0$. Here the difference between $1 + \cos^2\theta$ and $\sin^2\theta$ is small. Fortunately, the beams at SPEAR become transversely polarized due to synchrotron radiation. The SPEAR magnetic detector has full angular coverage in phi hence the $\cos 2\phi$ dependence can be investigated. From $e^+e^- \to \mu^+\mu^-$ the SPEAR analysis finds $\langle |P^2 \rangle = 0.47 \pm 0.05$ at $E_{cm} = 7.4$ GeV. At 6.2 GeV $\langle P^2 \rangle = 0$ as expected due to a depolarizing resonance of the storage ring. The phi distributions of the jet axis are shown in Figure 8 for the hadronic events. The jet axis was determined by minimizing the transverse momenta as discussed above. The data at 6.2 GeV are isotropic as expected since the polarization is zero. At 7.4 GeV we see an asymmetry with maxima and minima at the same values of ϕ as found in $e^+e^- \to \mu^+\mu^-$.

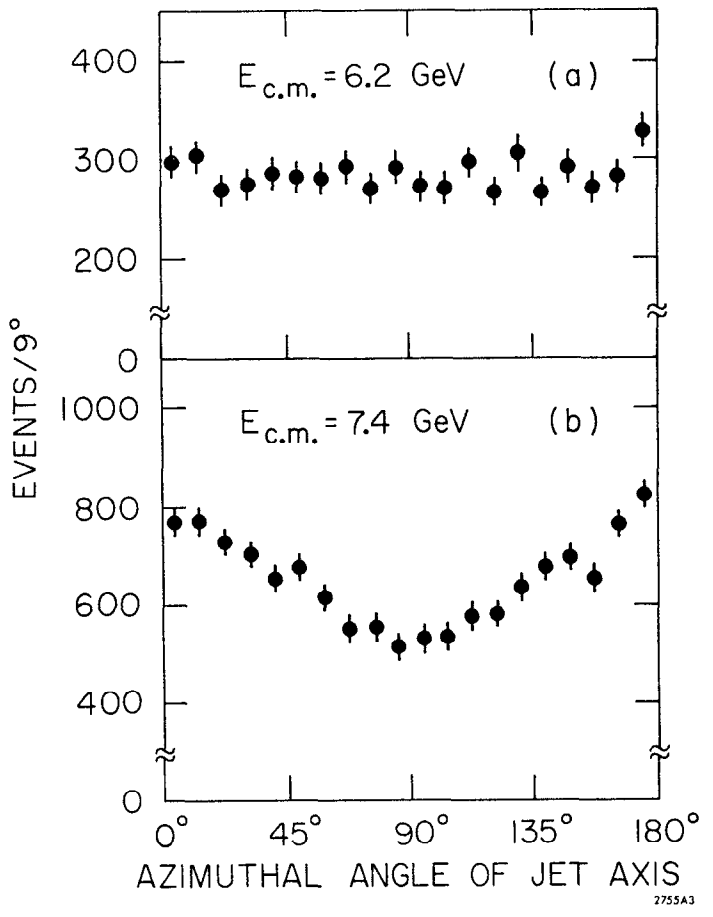

8. $e^+e^- \to$ hadrons: Azimuthal angular dependence of the jet axis. SPEAR data from Ref. 12.

The measured value of α in Equation 4 will be less than the true value of α because of the incomplete acceptance of the detector, the loss of neutral particles, and the method of reconstructing the jet axis. A Monte Carlo was performed treating the generated tracks as the detector would. This jet model calculation gives $\alpha = 0.97 \pm 0.14$ for the produced jet axis angular distribution. This means that the jet axis angular distribution is consistent with that for a pair of spin 1/2 particles. In the framework of the quark-parton model, the quarks must have spin 1/2 rather than spin zero.

II. QUARK MOMENTUM DISTRIBUTION FUNCTION

Complete knowledge of the deep inelastic structure functions for electron and neutrino scattering off protons and neutrons is sufficient to obtain the momentum distribution function of the quarks in a proton[1, 14]. In this section, we will look at a few examples of how we obtain the quark distributions.

As our first example, the measurement of $\nu W_2^{ep}(x)$ and $\nu W_2^{en}(x)$ near $x = 1$ gives the relative strength of the d(x) and u(x) distribution functions where u(x) means the number of u-type quarks with fraction momentum between x and x + dx. Neglecting the contributions from the "sea" quarks we have:

$$\nu W_2^{ep}(x) = \frac{4}{9} x u^p(x) + \frac{1}{9} x d^p(x)$$
$$\nu W_2^{ep}(x) = \frac{4}{9} x u^n(x) + \frac{1}{9} x d^u(x). \qquad (5)$$

By isospin symmetry the number of d-type quarks in the neutron is the same as the number of u-type quarks in the proton. Therefore we assume

$$u(x) = u^p(x) = d^n(x) \qquad (6)$$
$$d(x) = d^p(x) = u^n(x)$$

The ratio

$$R = \frac{\nu W_2^{ep}(x)}{\nu W_2^{en}(x)} = \frac{\frac{4}{9} x u(x) + \frac{1}{9} x d(x)}{\frac{1}{9} x u(x) + \frac{4}{9} x d(x)} = \frac{1 + 4\frac{d(x)}{u(x)}}{4 + \frac{d(x)}{u(x)}} \qquad (7)$$

gives the relative strength of d(x) and u(x). R can have a value between 1/4 and 4. Since we have neglected the contributions from the "sea" quarks, Equation 7 should not be valid near $x = 0$. The measurements of R are shown in Figure 9. At the largest x the ratio approaches 0.25 suggesting that $d(x)/u(x) \to 0$ as $x \to 1$. Farrar *et al.*[16] solve for d(x)/u(x) in Equation 7 in terms of R and use the data of Figure 9 to obtain the x-dependence of d/u. Figure 10 shows that d(x)/u(x) tend to fall as $1 - x$ for $x > 0.4$. The systematics in the data do not rule out $d(x)/u(x) \lesssim 0.2$ near $x = 1$.

In neutrino scattering the V-A coupling in charged current interaction is much more selective than in electroproduction. As we heard in H. Harari's lectures, the Cabbibo theory of hadronic interactions contain two isospin doublets:

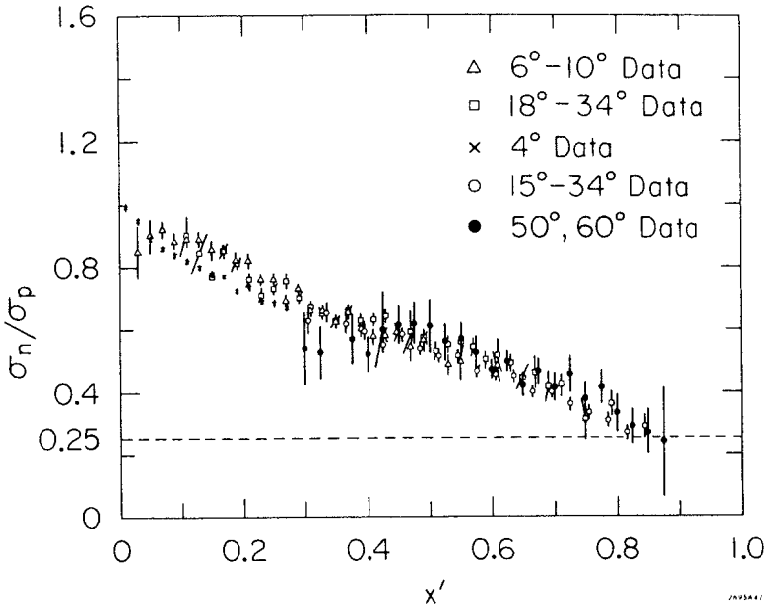

9. Ratio of the electroproduction cross sections on neutrons and prctons. Figure from Ref. 15.

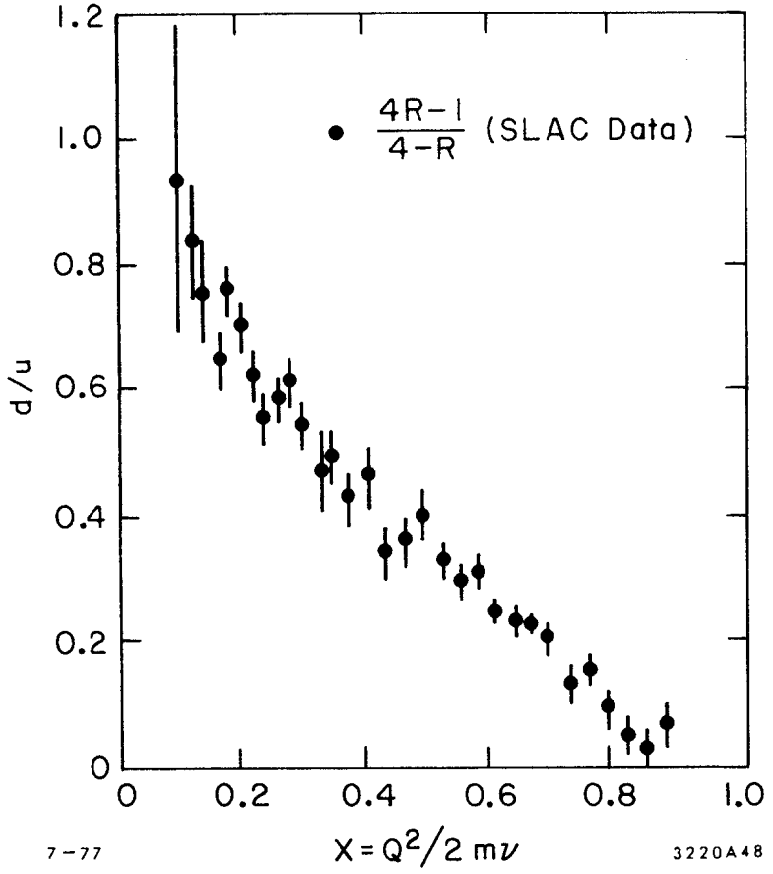

10. d(x)/u(x) from the electroproduction data of Figure 9.

$$\begin{vmatrix} u \\ d' \end{vmatrix} \quad \text{and} \quad \begin{vmatrix} c \\ s' \end{vmatrix} \tag{8}$$

where $d' = d\cos\theta_c + s\sin\theta_c$ and $s' = -d\sin\theta_c + s\cos\theta_c$. Weak decays occur within a doublet. The relative strength of the coupling is proportional to $\cos^2\theta_c \sim 0.95$ or $\sin^2\theta_c \sim 0.05$. Table II gives a list of allowed neutrino and anti-neutrino reactions. The Cabbibo favored reactions are given first and the valence quark scattering is given on the left.

The column labelled f(y) gives the expected distribution in $y = \frac{E_\nu - E_\mu}{E_\nu}$. This comes from the V-A nature of the coupling. If we look at the neutrino-quark scattering in the center of mass both 0° and 180° are allowed by conserving helicity and angular momentum.

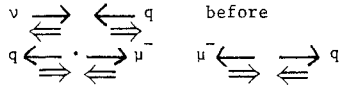

However, the antineutrino-quark scattering at 180° is forbidden by angular momentum conservation, since it is impossible to both conserve the angular momentum and maintain the proper helicity of the two scattered particles.

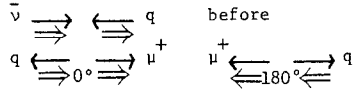

Table II: Allowed neutrino and antineutrino reactions on quarks.

	Valence		Sea	
favored $\cos^2\theta_c$	$\nu+d\to\mu^-+u$	$\frac{f(y)}{\text{flat}}$	$\nu+s\to\mu^-+c$	$\frac{f(y)}{\text{flat}}$
			$\nu+\bar{u}\to\mu^-+\bar{d}$	$(1-y)^2$
			$\nu+\bar{c}\to\mu^-+\bar{s}$	$(1-y)^2$
	$\bar{\nu}+u\to\mu^+d$	$(1-y)^2$	$\nu+c\to\mu^++s$	$(1-y)^2$
			$\bar{\nu}+\bar{d}\to\mu^++\bar{u}$	flat
			$\bar{\nu}+\bar{s}\to\mu^++\bar{c}$	flat
disfavored $\sin^2\theta_c$	$\nu+d\to\mu^-+c$	flat	$\nu+s\to\mu^-+u$	flat
			$\nu+\bar{u}\to\mu^-+\bar{s}$	$(1-y)^2$
			$\nu+\bar{c}\to\mu^-+\bar{d}$	$(1-y)^2$
	$\bar{\nu}+u\to\mu^++s$	$(1-y)^2$	$\bar{\nu}+c\to\mu^++d$	$(1-y)^2$
			$\bar{\nu}+\bar{d}\to\mu^++\bar{c}$	flat
			$\bar{\nu}+\bar{s}\to\mu^++\bar{u}$	flat

In terms of the scaling variable $y = \frac{E_\nu - E_\mu}{E_\nu}$ the neutrino distribution from quarks will be flat and the antineutrino one will follow $(1-y)^2$. In Table II the column labelled f(y) gives the distribution for the given reactions. Note that antineutrino scattering from the sea antiquarks gives a flat distribution in y. It is just this property that allows us to measure the antiquark contribution to the structure function in deep inelastic neutrino scattering.

From Table II we see that the main contribution in νp scattering is from the d-quark and in $\bar{\nu}p$ scattering is from the u-type quark.

Therefore, the ratio

$$\frac{\left.\frac{d^2\sigma}{dxdy}\right|^{\nu p}}{\left.\frac{d^2\sigma}{dxdy}\right|^{\bar{\nu} p}} = \frac{d(x)}{(1-y)^2 u(x)} \qquad (10)$$

Farrer et al.[16] extract d(x)/u(x) after integrating over y and accounting for the relative normalization of the cross section using the x-distribution from the 15' HBC. The comparison of d(x)/u(x) from electroproduction and neutrino interactions is shown in Figure 11. The neutrino data are in good agreement with the electron scattering experiments.

The neutrino and antineutrino scattering experiments are very important to the determination of the "sea" quark distribution functions. The valence quark contribution to antineutrino scattering has a $(1-y)^2$ distribution while the contributions from the antiquarks are flat in y. Therefore near y = 1 only the antiquarks contribute in antineutrino scattering. This is seen clearly in the 15' HBC data shown in Figure 12[17]. A fit to the data gives a value for the antiquark component as 0.12 ± 0.05.

In a similar way the Gargamelle experiment[18] has determined the quark and antiquark distribution functions as a function of x'. As seen in Figure 13, the major contribution comes from the quarks; however, a significant but smaller antiquark contribution is present at small x. We also see that neglecting the "sea" quark contribution above x = 0.2 is reasonable.

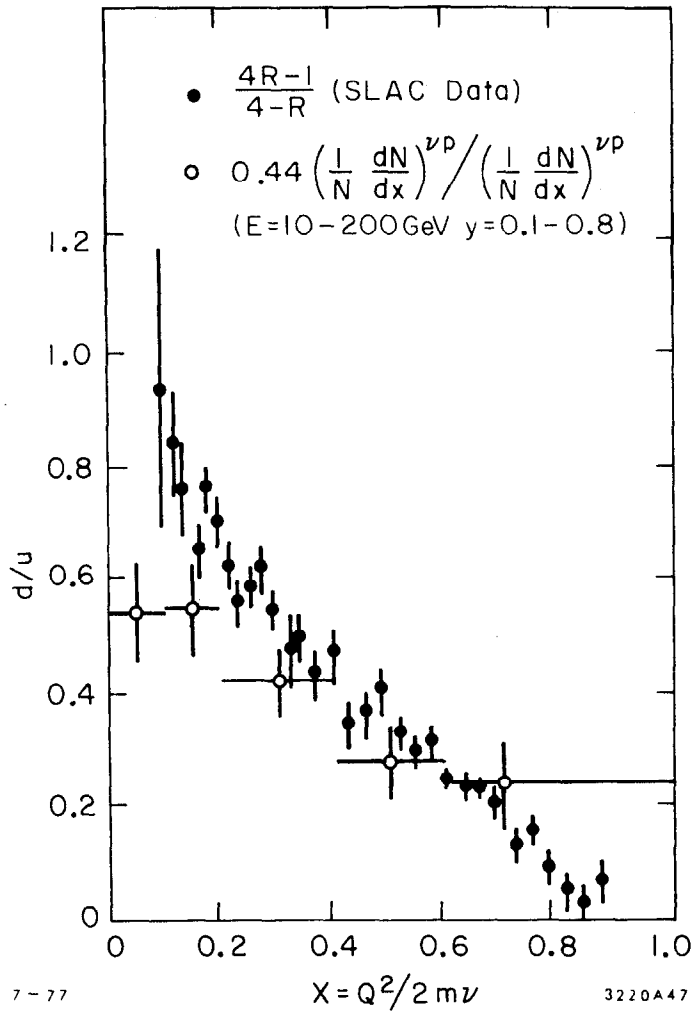

11. Data on the ratio d(x)/u(x) from neutrino and antineutrino experiments on hydrogen (open circles). Data from electron scattering experiments on hydrogen and deuterium is shown for comparison (black dots).

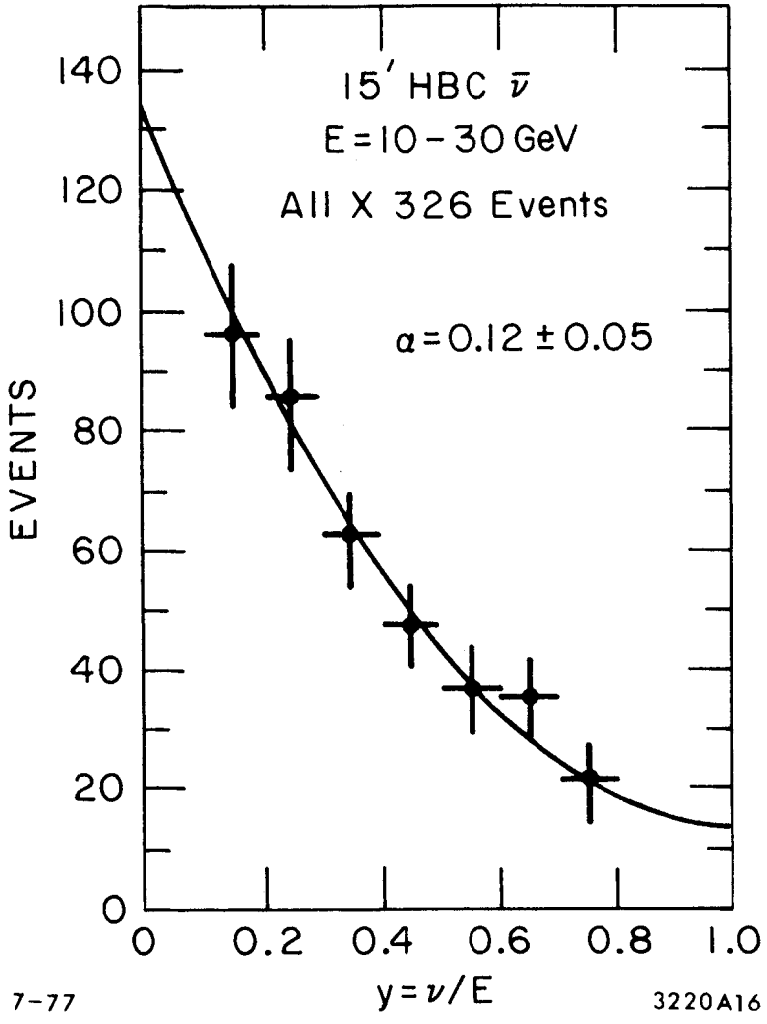

12. The y-distribution in the 10-30 GeV energy range for antineutrinos from an experiment in the Fermilab 15' HBC. Ref. 17.

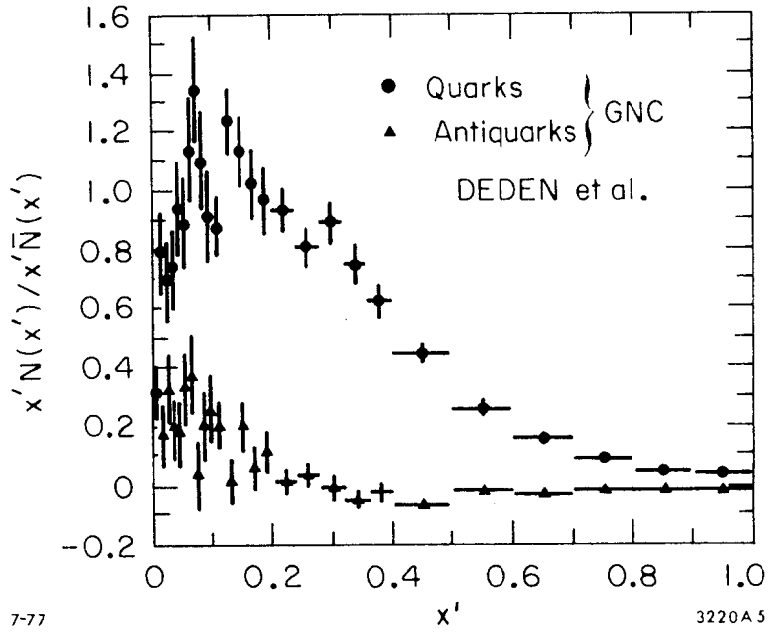

13. Quark and antiquark momentum distributions data of Ref. 18.

An example of the quark distribution functions obtained from the electroproduction and neutrino scattering data is shown in Figure 14 as determined by Field and Feynman[19]. Figure 15 shows the comparison to the neutrino scattering data and the electroproduction data using the distribution functions of Figure 14.

III. QUANTUM NUMBER RETENTION

Neutrino scattering on protons occurs as a result of the d-type quarks yielding a u-type quark in the virtual W^+ direction (see diagram of Figure 16). One of the most interesting questions concerning quark jets is whether the quark quantum numbers are retained in the quark fragmentation region. In the above example of neutrino scattering we expect a positive charge excess for the target and W^+ fragmentation regions with the target region excess twice that of the W^+ region (see Figure 16).

The results of the University of Michigan HBC experiment[21] are shown in Figure 17. The open circles show the positive charge excess and show an asymmetry of the type expected.

Other evidence for quantum number retention is seen in the electroproduction results of Martin et al.[22] (Figures 18 and 19). They observe an excess of π^+ over π^- which increases with increasing x. The x-dependence of the π^+/π^- ratios agrees well with model calculations using quark distribution functions like those of Figure 14[23]. The u-type quark is dominate at large x giving the excess positive charge as seen in Figure 18. The increase of the K^+/π^+ ratio can be

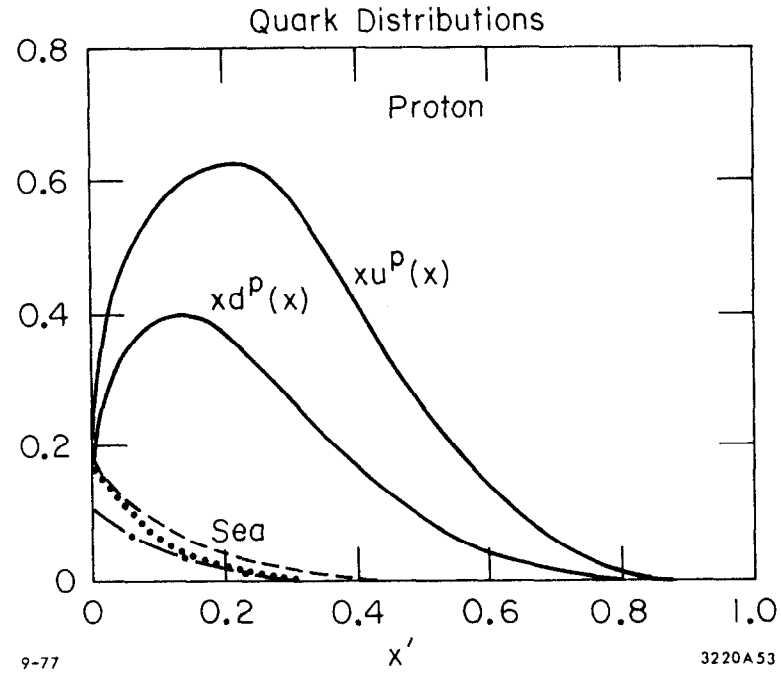

14. Quark distributions within the proton. Figure from Ref. 19.

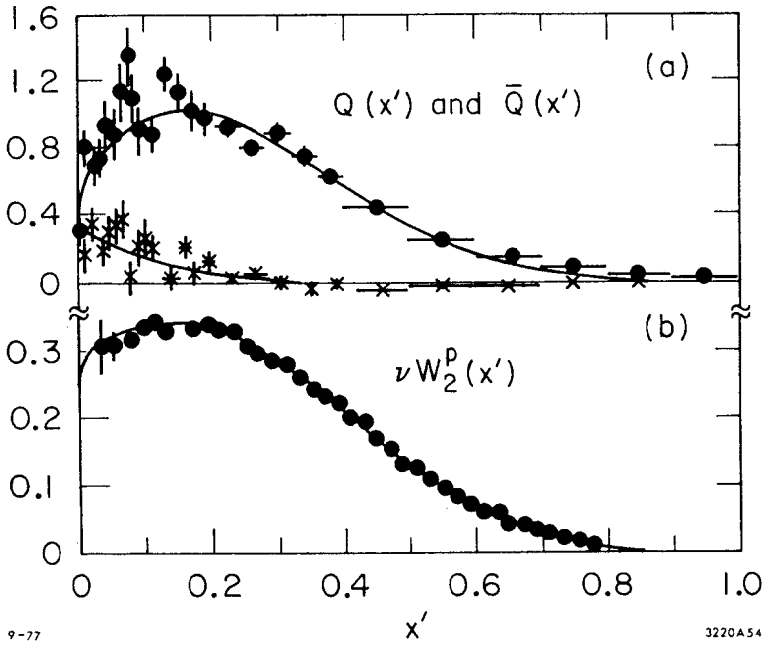

15. Comparison of the quark distribution functions with the data that was used to help determine them. (a) Momentum carried by the quarks, Q(x) and antiquarks $\bar{Q}(x)$. Data are from the Gargamelle neutrino experiment (Ref. 18). (b) Fit to $\nu W_2^{ep}(x')$. Data from Ref. 20.

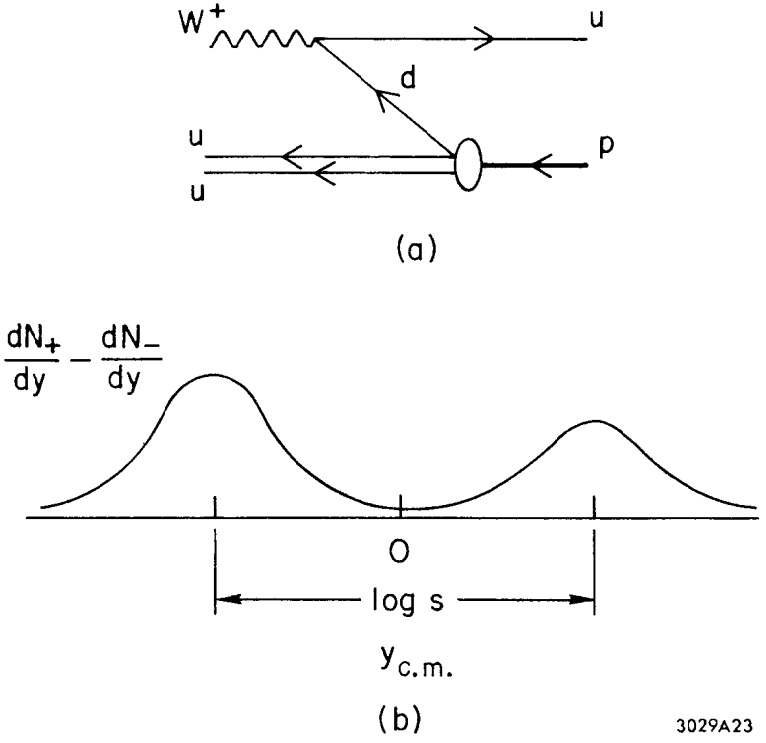

16. (a) Diagram for $\nu p \to \mu^- X$ scattering in the $W^+ p$ c.m. (b) Expected distribution in rapidity of the hadronic charge density for $\nu p \to \mu^- x$ in the $W^+ p$ c.m.

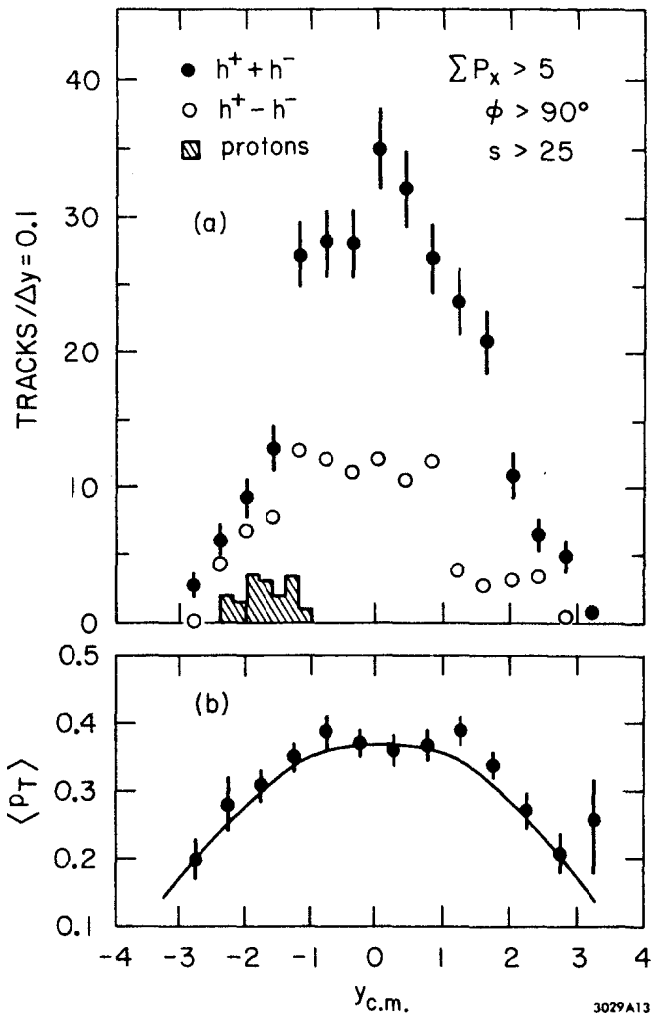

17. Distributions $(dN_+ \pm dN_-)/dy$ of charged particles observed in $\nu p \to \mu^- x$ in the $W^+ p$ c.m. Figure from Ref. 21.

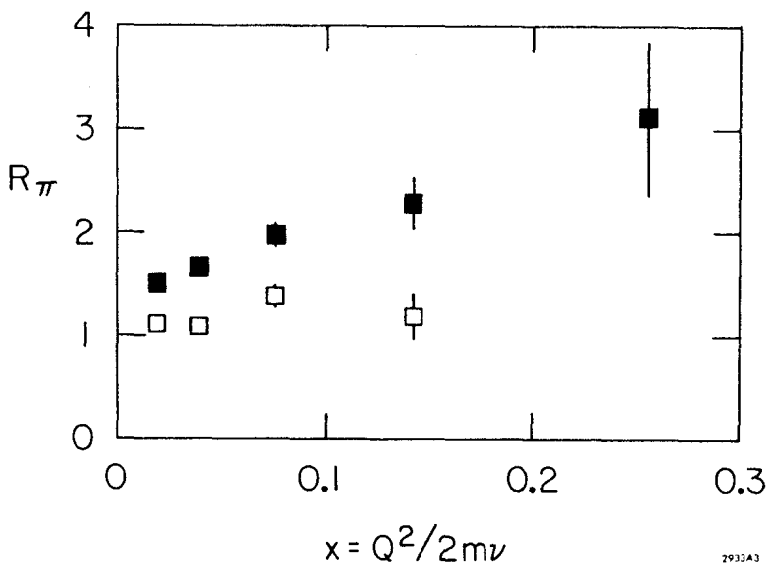

18. Charge ratios (+/-) for pions as a function of the scaling variable $X = \frac{Q^2}{2m\nu}$. Here the filled squares are for the proton target results, and open symbols are for a neutron target. Data from Ref. 22.

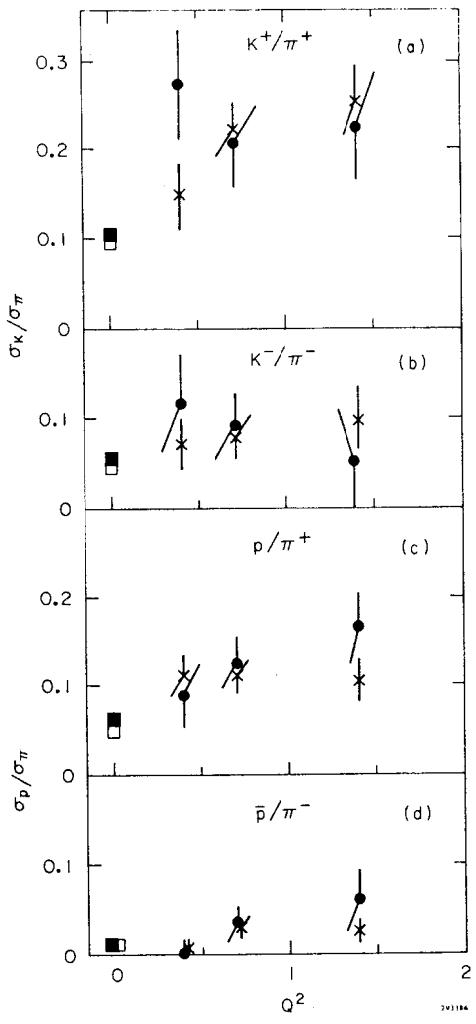

19. Production ratios for proton target and deuteron target (crosses). Figure from Ref. 22.

understood by the struck u-type quark combining with the $\bar{d}$ or $\bar{s}$ quarks from $d\bar{d}$ and $s\bar{s}$ pairs as the u-quark fragments into hadrons.

IV. HADRONS FROM QUARKS

The most striking indication of the underlying quark structure of hadronic matter is jet production in e^+e^- annihilation. Earlier, we reviewed the SPEAR evidence for jet production and also observed the spin 1/2 character of the jets. We are fairly certain that quark-jets are produced in other reactions as well. In Figure 20, diagrams for jet production in other scattering processes are given. For example, in $\ell p \to \ell' x$, the scattered quark will define a jet direction along with the spectator quarks of the proton. In high p_T events from hadron-hadron collisions, the production may proceed via quark-quark[19] or quark-hadron scattering[24]. The scattered quarks and the spectator quarks define jet directions.

In this section, we will look at the properties of the hadron inclusive distributions. If the picture is as simple as that of a parent quark fragmenting into hadrons, the inclusive hadron distributions from different processes should be similar.

A. Multiplicities

The universal nature of charged multiplicities in hadron interactions have long been known. Comparison to μp, νp, γp and e^+e^- shows that this property holds even for these reactions. That is, the average charged multiplicity is the same no matter whether the jets are defined by the incident hadron, virtual photon, W^+, or $q\bar{q}$ direction in e^+e^-

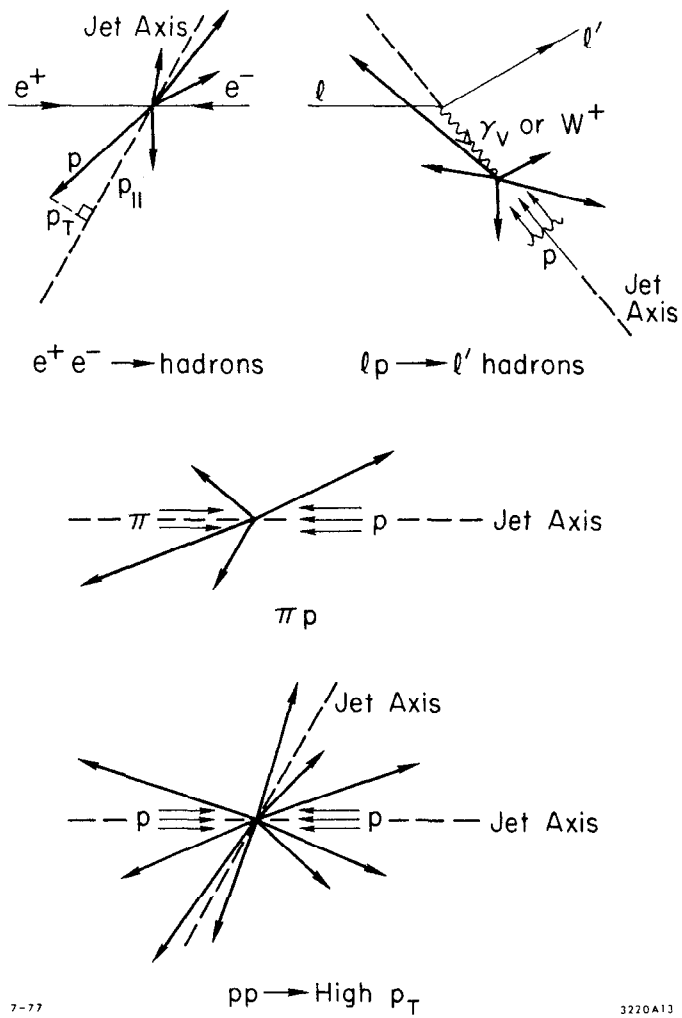

20. Diagrams for the indicated reactions showing hadrons produced with respect to jet-axis, defined by the scattered quark directions.

collisions. The experimental data has been reviewed by Albini et al.[25]. A phenomenological fit was performed to the proton-proton multiplicity over the available energy range. The best χ^2 fit is

$$\langle n_{ch} \rangle_{pp \to x} = 2.50 + 0.28 \ln E_a + 0.55 \ln^2 E_a \qquad (12)$$

where $E_a \equiv \sqrt{s} - M_{BM} - M_T$ is the available energy for particle production. Figure 21 shows the mean charged multiplicity in pp collisions versus the available energy $E_a = \sqrt{s} - 2Mp$; the curve is the best fit, Equation 12. Figure 21 shows the same parameterization also fits meson-proton collisions. What is more remarkable is that the "universal curve" fits the $\langle n_{ch} \rangle$ recoiling against slow protons in the reaction hp → px. The e^+e^- and ℓp → ℓ'x charged multiplicities follow the same parameterization; however, the νp are somewhat larger than the pp behavior. In the νp plot the dashed line gives the "universal" behavior.

Recently, the multiplicity has been measured in 200 GeV/c pp collision with large transverse momentum jets[26]. The average charged multiplicity was found to be about 15 in these events as opposed to 8 for normal events. The extra multiplicity may be due to quarks scattering at large angles fragmenting into hadrons.

We might expect the $\langle n_{ch} \rangle$ of large p_T jets to behave in the "universal" way. The ISR data[27] is shown in Figure 22 as a function of the p_T of the trigger pion. Here the average multiplicity is that recoiling against p_T. The curve of Figure 22 shows the behavior of

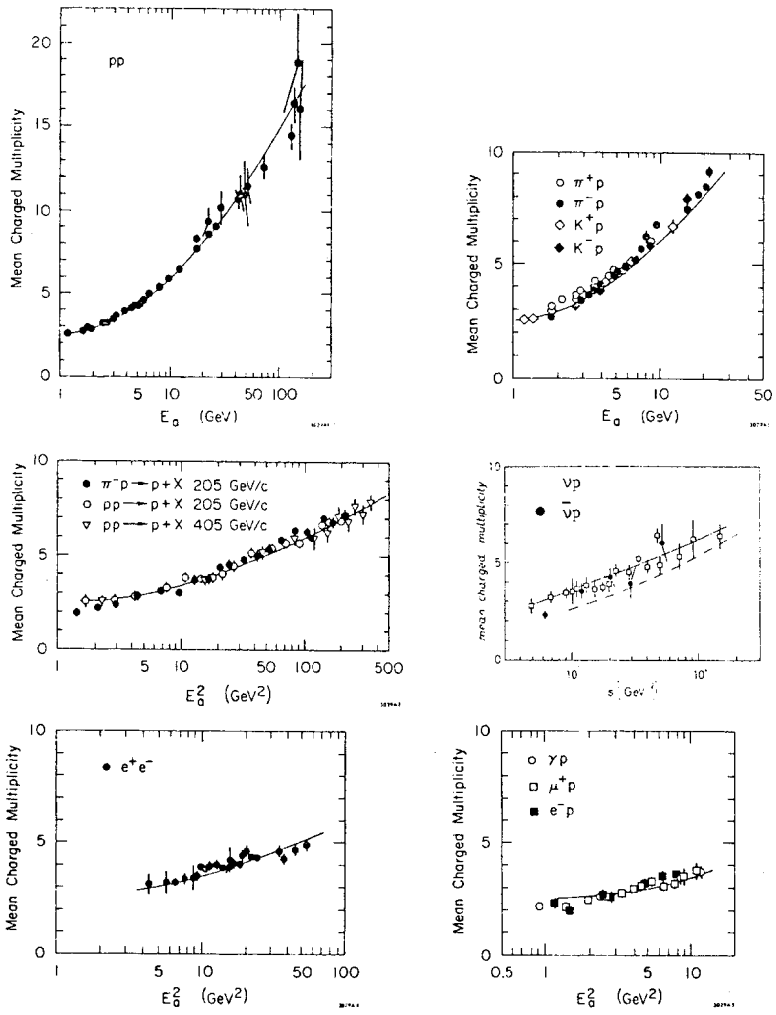

21. Mean charged multiplicity as a function of the available energy for particle production for the indicated reactions. Curves are the best χ^2 fit to the pp data.

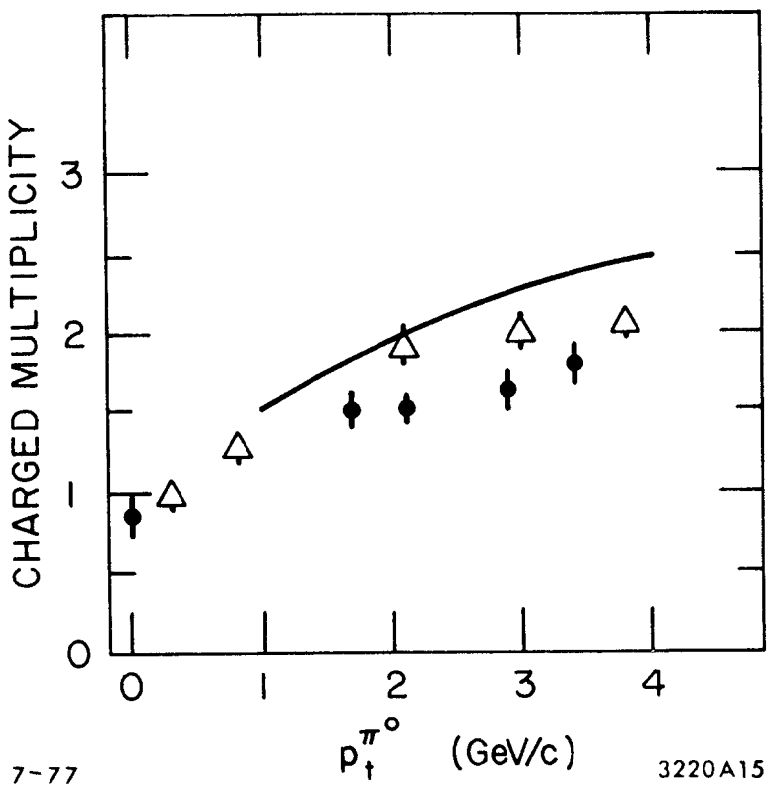

22. Mean charged multiplicity versus p_T of the trigger pion. Curve gives $\frac{1}{2}\langle n \rangle_{ch}$ for e^+e^- collisions at $E_{BM} = p_T$. Figure from Ref. 27.

$1/2 \langle n_{ch} \rangle$ in e^+e^- collisions. The factor 1/2 is taken since only away side jet multiplicity is counted.

B. Transverse Momentum Distribution

The limiting of transverse momentum relative to the beam direction in inclusive hadron production is familiar to us. The e^+e^- production of jets suggests this to be a fundamental characteristic of the hadron fragments from quarks. If this is the case then the transverse momentum distribution should be independent of how the jet is produced. We should obtain comparable average transverse momentum with respect to the jet axis in e^+e^-, νp, ℓp, pp, and large p_T jets in hadron collisions. However, we may expect differences which arise mainly from our inability to define the exact jet direction because we do not detect all final state particles and uncertainties in the initial quark direction due to its transverse momentum within the hadron.

This latter effect is illustrated in Figure 23. We assume the jet direction in ep collisions is along the virtual photon direction in the $\gamma_v p$ cms system. However, the quarks within the proton may have internal transverse momentum $\vec{k}_T$ with respect to the proton direction. The fragmenting hadrons have the characteristic $\vec{h}_T$ transverse momentum distribution with respect to the parent quark direction. Therefore, the measured p_T distribution will be a function of $\vec{h}_T$ and $\vec{k}_T$. If $\vec{k}_T$ is large compared to $\vec{h}_T$ then the internal motion within the proton in ep, νp, and $pp \rightarrow$ high p_T events will effect the transverse momentum distributions of the hadrons.

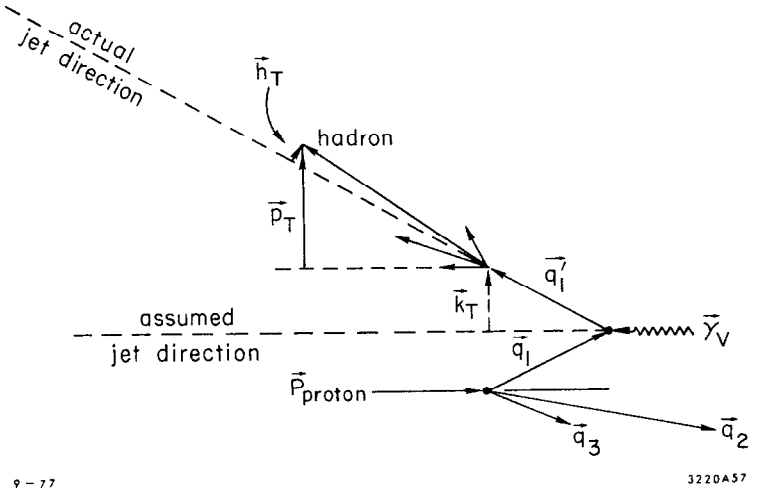

23. Diagram for scattering on quarks with internal transverse momentum $\vec{k}_T$. The final state hadrons have transverse momentum $\vec{h}_T$ with respect to the parent quark direction. Experiments measure $\vec{p}_T$.

Before looking at the $\langle p_T \rangle$ distribution in proton reactions, let us first look at $e^+e^- \to$ hadrons. The hadrons produced in jets in e^+e^- collisions only have $\vec{h}_T$. The observed p_T distribution with respect to the jet axis is shown in Figure 24 for the 7.4 GeV SPEAR data[12]. The Monte Carlo calculation with limited transverse momentum reproduces the data if the hadrons have a mean $\langle \vec{h}_T \rangle$ with respect to the jet-axis in the range of 325 to 360 MeV/c[12].

Instead of using the W^+ direction in the W^+ proton CMS, the neutrino on proton data of Chapman et al.[28] are analyzed with respect to the direction of the total detected hadronic system. This means that the transverse momentum distributions should be similar to that measured in e^+e^- annihilation. They obtain an average p_T of $\sim$350 MeV with little or no Q^2 dependence for $0 < Q^2 < 60$ GeV^2.

The electroproduction data are shown in Figures 25 and 26[29]. The data are analyzed with respect to the virtual photon direction and yield an average p_T increasing with Q^2. In Figure 26 the slope of the exponential p_T^2 fall-off is plotted ($\langle p_T^2 \rangle = A^{-1}$). In photoproduction at $Q^2 = 0$ the hadron component is dominant. As Q^2 increases the virtual proton becomes more point like and the hard scattering process on the quarks become more important. At large Q^2 the $\langle p_T^2 \rangle$ presumably reflects both the contributions from $\vec{h}_T$ and $\vec{k}_T$. Such a large value of $\langle p_T^2 \rangle \sim 1$ GeV^2 seen in Figure 26 means that $\vec{k}_T$ must dominate the transverse momentum distribution at large Q^2.

It has been suggested[30, 31] that for a given Q^2 the $\vec{k}_T$ dependence of the hadron's transverse momentum should be scaled by the fraction of

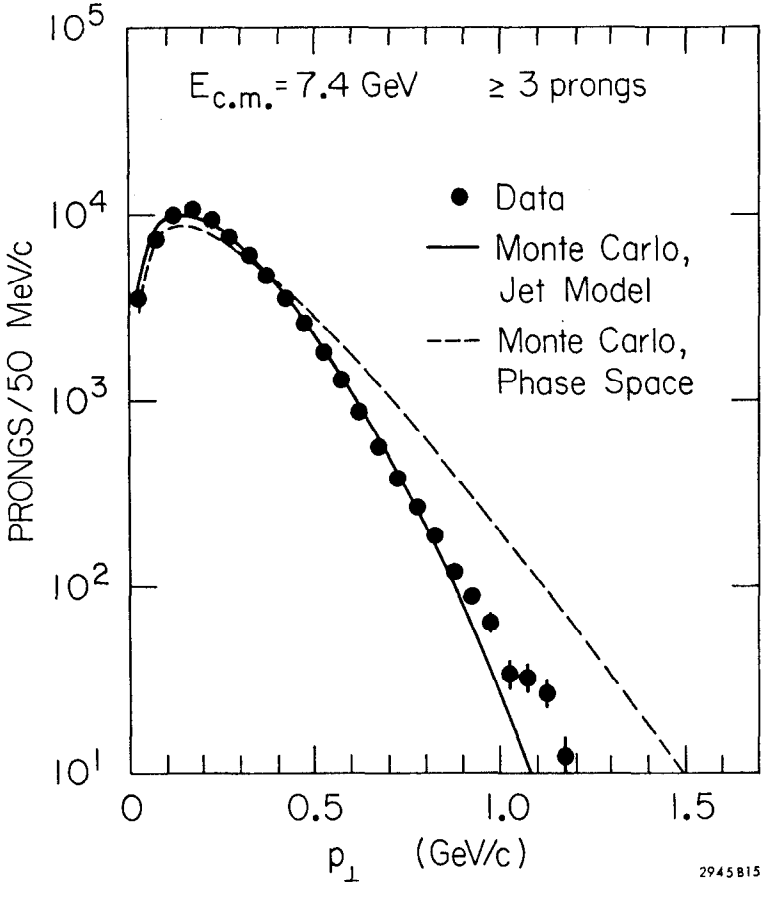

24. $e^+e^- \to$ hadron; transverse momentum distribution of hadrons with respect to jet-axis. Figure from Ref. 12.

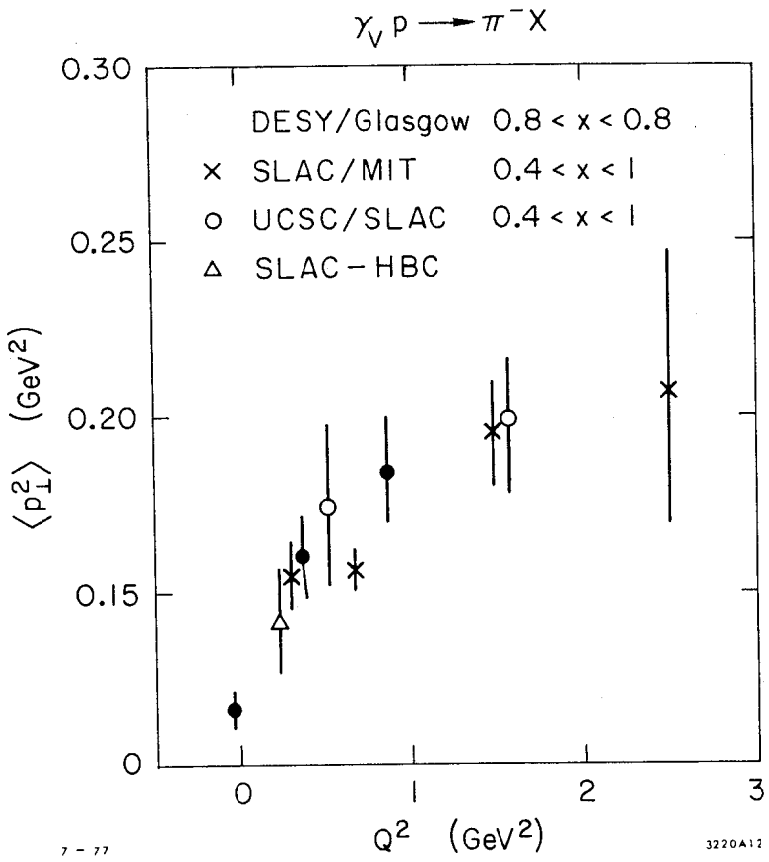

25. $\gamma_V p \to \pi^- x$: $\langle p_\perp^2 \rangle$ versus Q^2. Figure from Ref. 29.

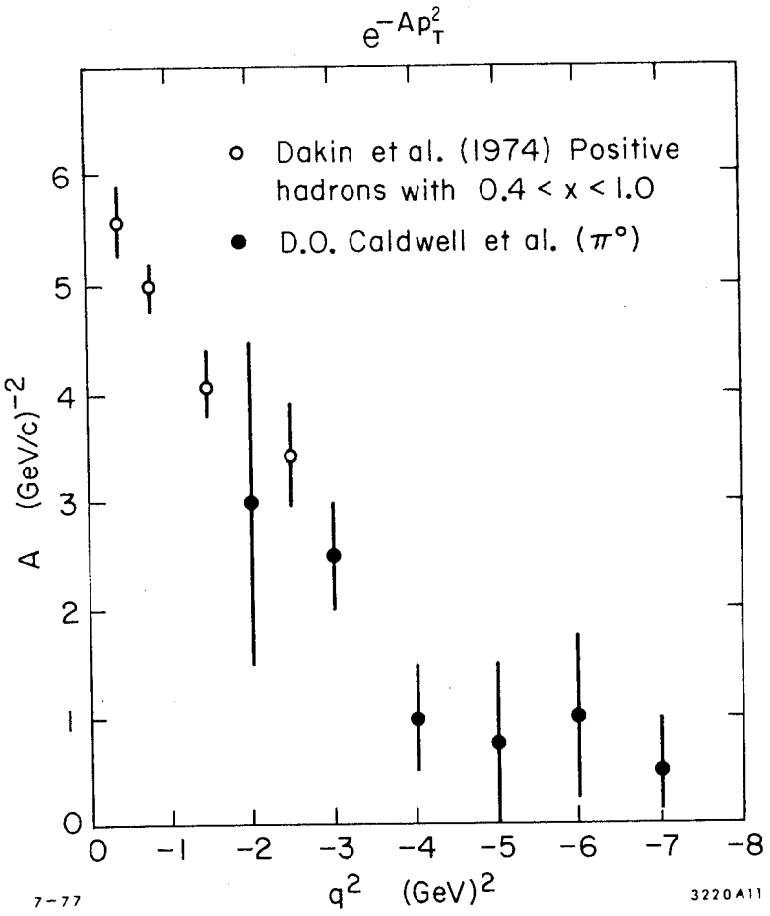

26. $\gamma_V p \to h^+ x$ and $\gamma_V p \to \pi^\circ x$: exponential slope dependence of $p_\perp^2$ distribution. Note that $\langle p_\perp^2 \rangle = \frac{1}{A}$. Figure from Ref. 29.

momentum the hadron has of the parent quark,* $z = \frac{E_{had}}{E_{max}}$,

$$p_T^2 = h_T^2 + z^2 k_T^2 \qquad (13)$$

The average value of p_T is given in Figure 27 as a function of z. Near z = 0 the average value of p_T should be $\langle h_T \rangle$ if Equation 13 is valid. The data of Figure 27 is in remarkable agreement with the e^+e^- results. Up to z-values of 0.5, Equation 13 seems to describe the data. However, above this value the $\langle p_T \rangle$ levels off or perhaps falls near z = 1. M. Gronan and Y. Farni[30] obtain from the μp data with z < 0.5

$\langle h_T \rangle$ = ∿350 MeV

$\langle k_T \rangle$ = 900 ± 150 MeV

Again, as in ep → eπ°x, we find a large value of $\vec{k}_T$. However, we do not understand the behavior above z = 0.5.

In high p_T events from pp collisions, it is convenient to use the hadron transverse momentum with respect to the trigger plane, P_{out}, as defined in Figure 28. The reason for this is that it is difficult to determine the jet-direction. The trigger particle is assumed to approximately define the jet plane on the opposite side. The P_{out} distribution for particles with energy greater than one-half the jet energy is shown in Figure 29[11]. The $\langle P_{out} \rangle$ = 530 ± 20 MeV/c is large and does not depend on the momentum of the jet as seen in Figure 30. P_{out} does depend on the fraction momentum the hadron has in a way similar to that found in ep collisions as seen in Figure 31 where the z_E

* z is the Feynman scaling variable (normally called x) and is used to distinguish it from $x = \frac{Q^2}{2m\nu}$

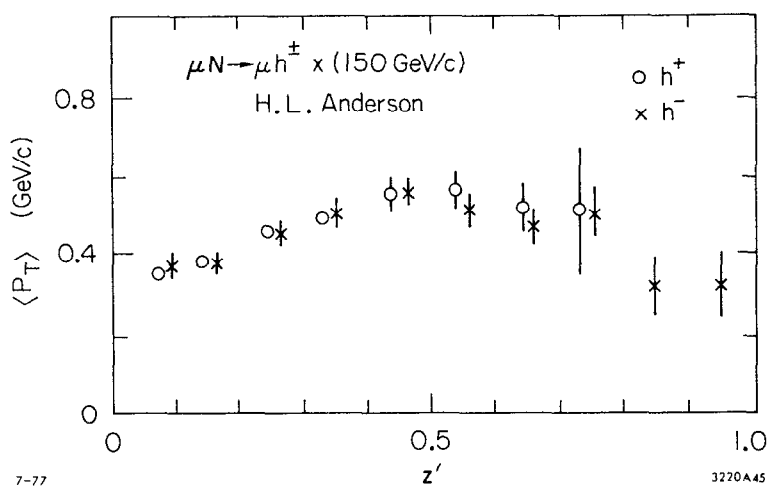

27. Average value of transverse momentum for the reaction μN → μ $h^{\pm}$ x. Data of Ref. 32.

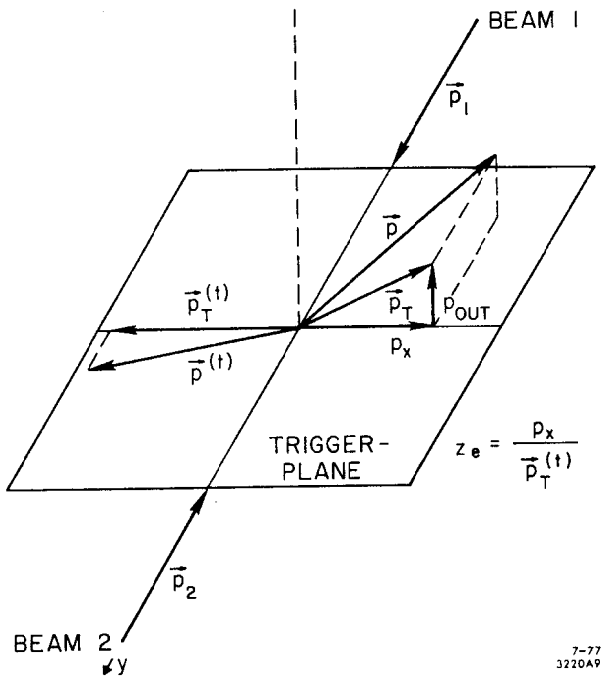

28. Definition of p_{out} and z_E in high p_T events.

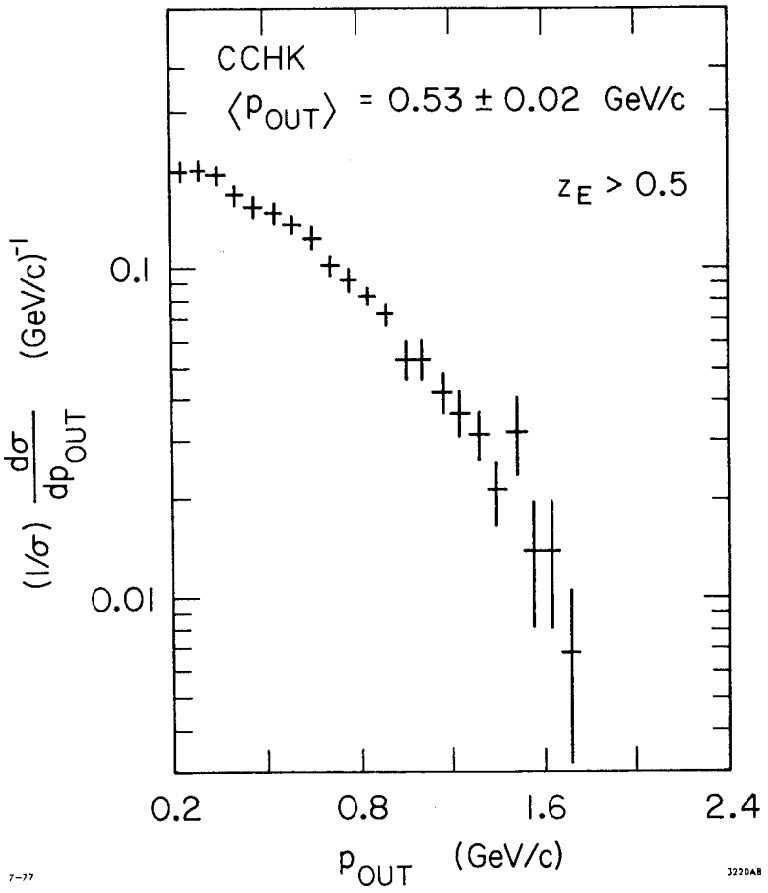

29. Distribution in p_{out} of away secondaries with $z_E > 0.5$. Data of Ref. 11.

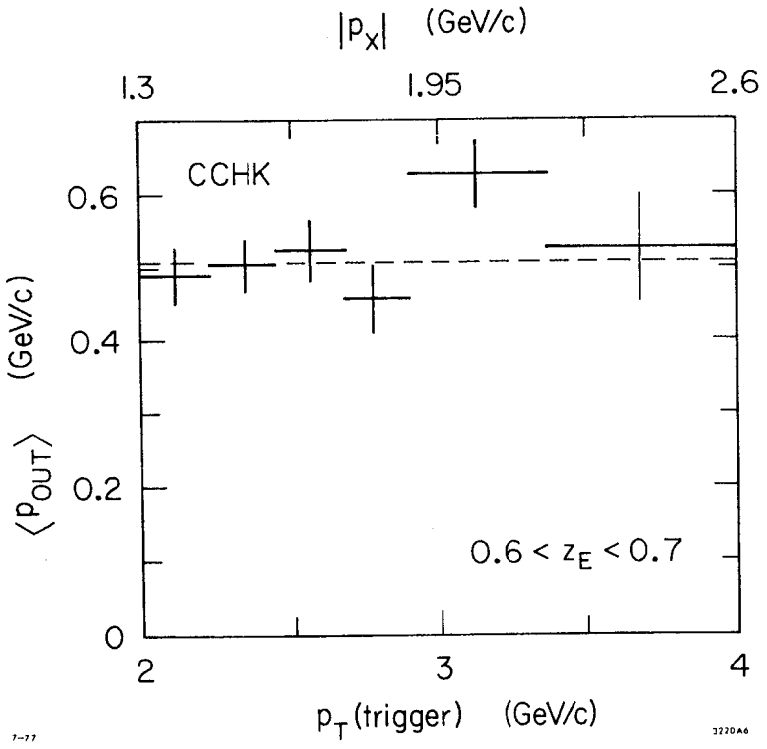

30. Dependence of $\langle p_{out} \rangle$ on the transverse momentum of the trigger, for fixed z_E. Data of Ref. 11.

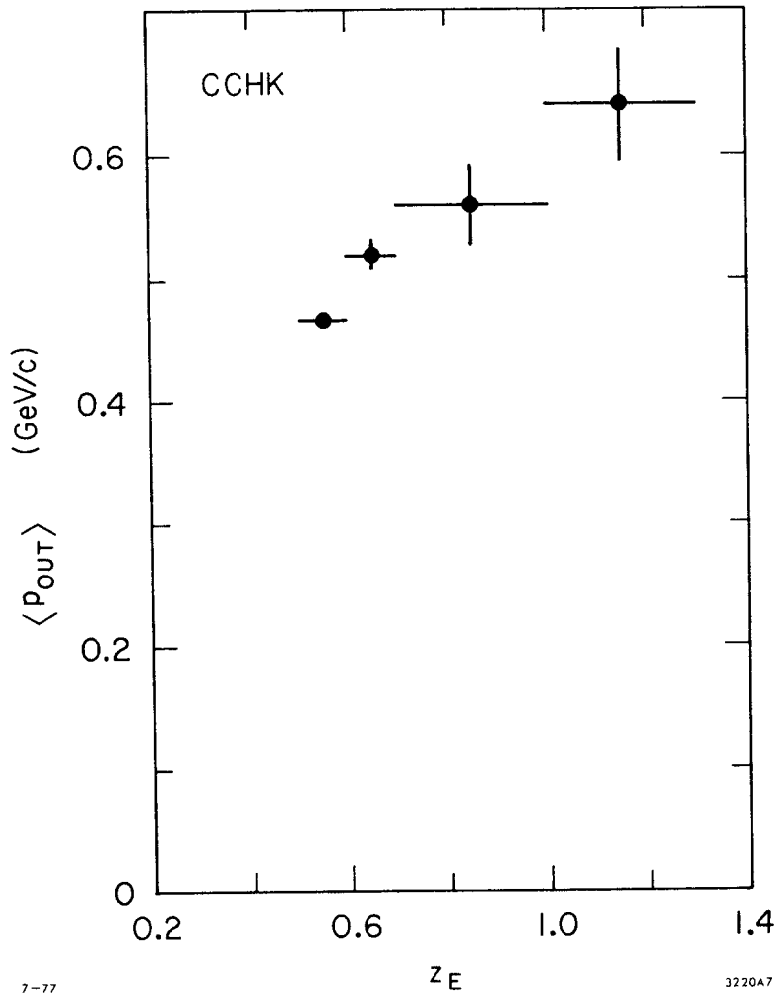

31. Dependence of $\langle p_{out} \rangle$ on z_E. Data of Ref. 11.

dependence of $\langle P_{out} \rangle$ is given. The definition of z_E can be obtained from Figure 28 and is an approximation to z since the p_T of the trigger particle is assumed to be the p_{max} in the opposite side jet. In the framework of a picture with jets originating from partons, one expects the following approximate dependence of $\langle P_{out}^2 \rangle$ on z_E :

$$\langle P_{out}^2 \rangle = \frac{1}{2} \langle h_T^2 \rangle + \frac{1}{2} z_E^2 \langle h_T'^2 \rangle + z_E^2 \langle k_T^2 \rangle \qquad (14)$$

where $\vec{h}_T'$ is the transverse momentum of the trigger hadron with respect to its parent quark direction. The factors 1/2 enter because P_{out} is measured instead of p_T. Assuming $\langle h_T'^2 \rangle = \langle h_T^2 \rangle = 0.167$ GeV^2 then $\langle k_T^2 \rangle \sim 0.49$ GeV^2. It is interesting that large average transverse momenta are again observed. Additional factors may be present besides a transverse component of the quarks within the proton. For example, among the particles with $z_E > 0.5$ there may still be some which do not come from the fragmentation of the scattered partons.

These large transverse momentum distributions indicate an unexpectedly large internal transverse momentum of the constituents within the hadrons. Large $\langle p_T \rangle$ have also been observed in high mass lepton pairs produced in hadron collisions. A discussion of how the internal transverse momentum reveals itself in peripheral hadronic scattering has been made by E.M. Levin and M.G. Ryskin[33].

C. Scaling of Hadrons from Quarks

Feynman scaling implies that the distribution of hadrons from a particular quark flavor depends only on the fraction of energy taken by the hadron. This means that the $z = E_{hadron}/E_{jet}$ distribution for π^+'s produced from the u-type quark in νp scattering, e^+e^- annihilation, and high p_T jet events should be the same. A more familiar test of Feynman scaling is to look at the energy dependence of the hadrons produced in a particular reaction.

Scaling in e^+e^- interactions has $sd\sigma/dz$ independent of the e^+e^- cm energy. Here s accounts for the energy dependence of the flux of $q\bar{q}$ pairs. We know that exact scaling will not hold at SPEAR energies, because passing through charm threshold gives more $q\bar{q}$ pairs and the average multiplicity rises slowly with energy[7]. However, the SPEAR data[12] do show approximate scaling for $z > 0.2$ as seen in Figures 33 and 34. Recently, the DASP experiment[34] has measured separately the pion and kaon distributions. Their data shown in Figure 35 have little energy dependence for both the pions and kaons; however, the energy range tested only goes out to $E_{cm} = 5$ GeV.

Hadron scaling has also been investigated in jets recoiling against high p_T triggers in pp collisions. The ISR data[11] from the split field magnet is shown in Figure 36. The definition of z_E is given in Figure 28 and is an approximation to the actual z-value. Here p_T (trigger) approximates the recoiling jet momentum. The lack of scaling even for z_E near 1 can be due to several factors:

a) Spectator hadrons are included

b) Approximations used in obtained z_E

c) Transverse momentum k_T of the quarks.

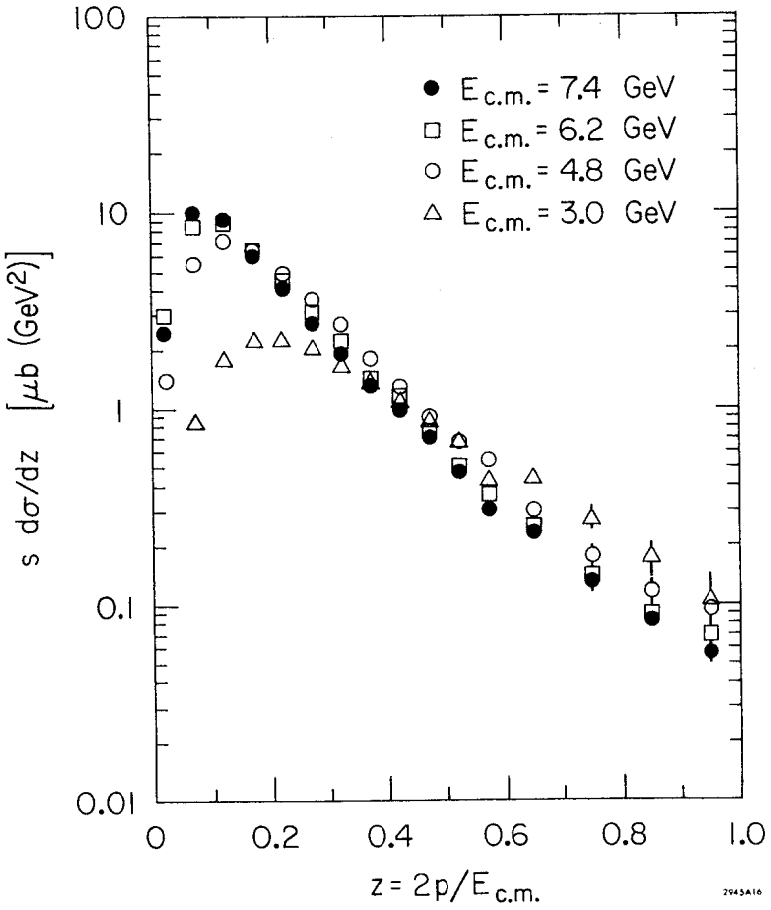

33. The z-dependence of sdσ/dz for the SPEAR data.

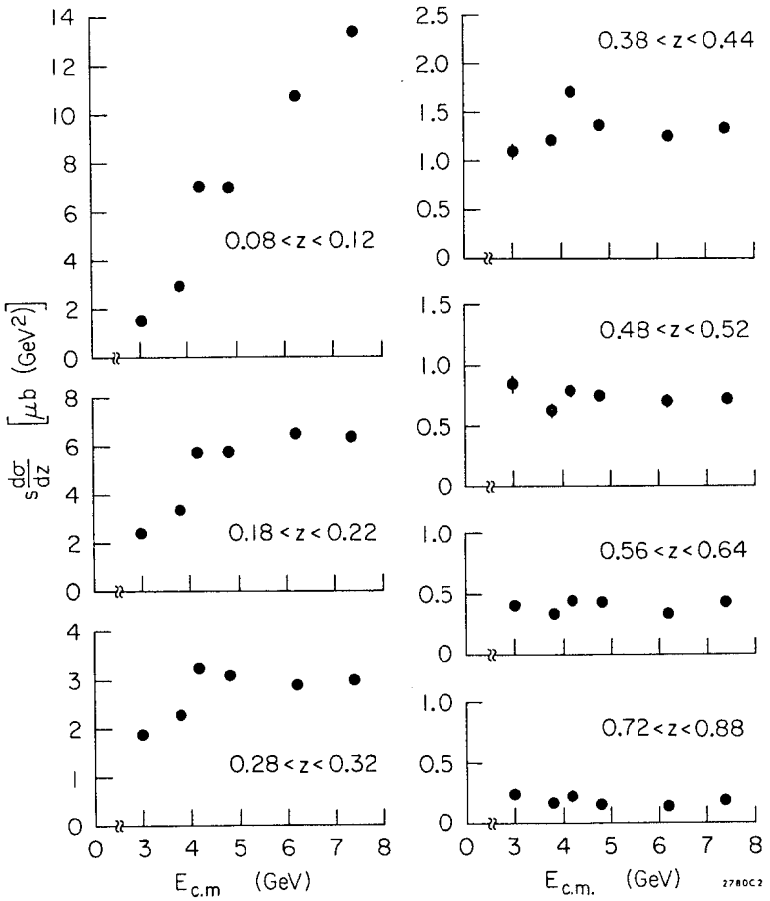

34. Energy dependence of sdσ/dz for different z intervals. SPEAR data.

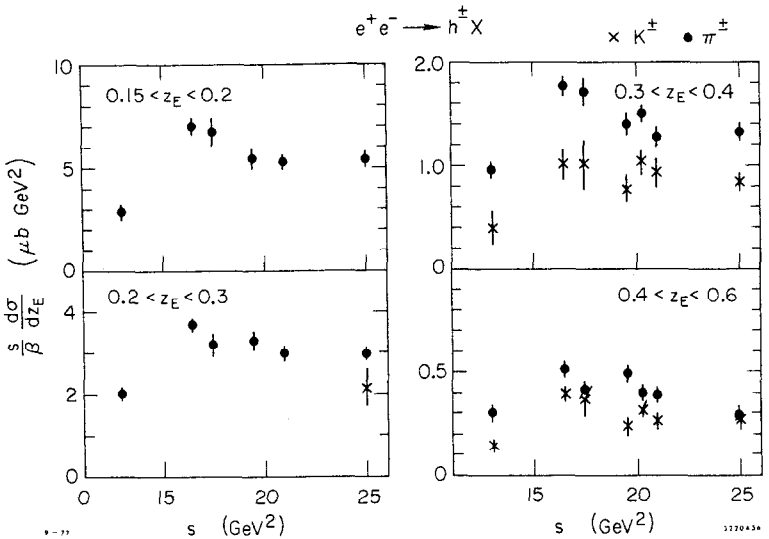

35. Energy dependence of $\frac{sd\sigma}{\beta dz}$ for different z interval for the pions and kaons separately. DASP data from Ref. 34.

The effect of these contributions to the non-scaling behavior seen in Figure 36 has been determined by the authors of Reference 11. They performed a Monte Carlo calculation assuming quark-quark scattering and fragmentation into hadrons. Details of the calculation can be found in Reference 11. The comparison of the Monte Carlo to the data is shown in Figure 37 where the p_T dependence of the cross section for $z_E > 0.5$ is plotted. The spectator contribution shown separately falls off rapidly with p_T. A contributuion to the p_T dependence also comes from the $\vec{k}_T$ distribution of the quarks within the hadrons. These Monte Carlo calculations indicate that scaling, if there, will only be observed at higher p_T.

We have seen indications in the data that lead us to believe that the quark-parton interpretations of hadron production have some merit. One of the most interesting questions is the nature of the basic scattering process yielding the high p_T jets. The constituent interchange model[24] has the basic scattering mechanism as quark-meson scattering. This model gives very impressive agreement to the transverse momentum dependence and energy dependence to various reactions. The interpretation put forward by others[19, 31, 35] has quark-quark scattering as the basic scattering mechanism. In order to obtain a faster fall-off with p_T than the $\frac{1}{p_T^4}$ dependence expected for a point-like scattering process, the s and t dependence of the quark-quark scattering process is adjusted to yield the expected p_T behavior[19]. Detailed Monte Carlo calculations and higher p_T data should help resolve this question.

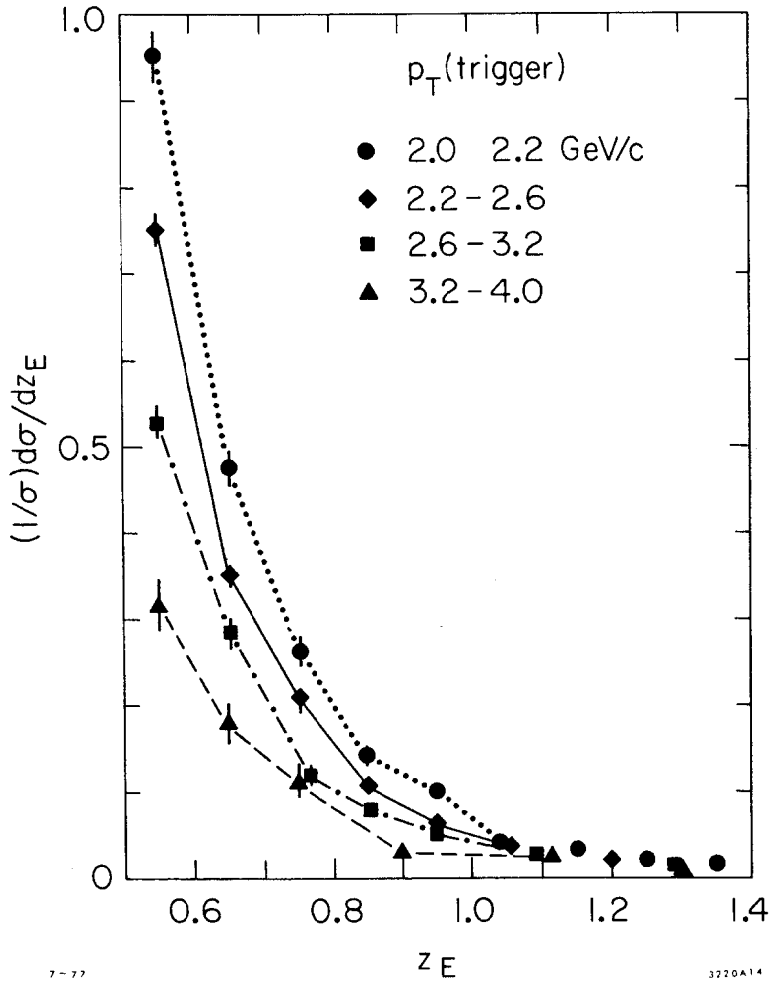

36. The z-dependence of the cross section for hadrons recoiling against a high p_T-trigger. Figure from Ref. 11. p_T and z_E defined in Figure 28.

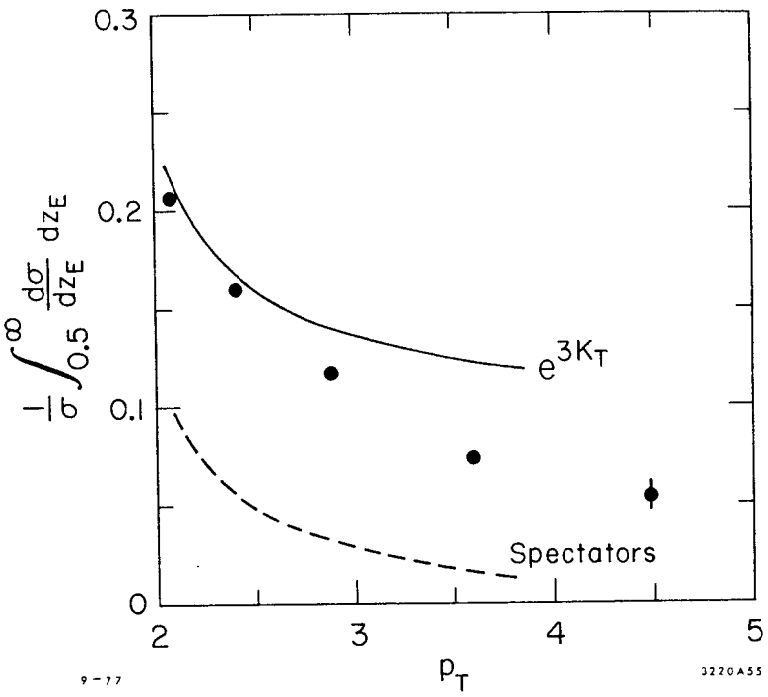

37. p_T dependence of cross sections for hadrons with $z_E > 0.5$. Figure from Ref. 11.

V. SOFT SCATTERING OF QUARKS IN PERIPHERAL HADRON INTERACTIONS

A. Cross Section

The additive Quark Model assumes that peripheral interactions occur by a single quark-quark scattering process. Only in the single scattering process does quantum number exchange take place.

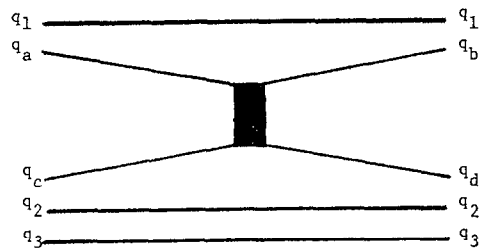

The spectator quarks recombine with the scattered quarks to form the final state hadrons. A single scattering process means baryon exchanges are not allowed and the small u-channel cross sections support this.

The OZI rule[36] is a direct consequence of this limitation. The well-known reaction $\pi^- p \to \phi n$ is forbidden by this rule as well as $\pi^- p \to \psi n$. The $\phi(\psi)$ is mainly a state of $s\bar{s}(c\bar{c})$ quarks. In order for the reaction to take place two scattering processes would be required. The strong suppression of $\pi^- p \to \phi n$ can be seen in Figure 38 where the allowed reactions $\pi^- p \to \rho n$ and $\pi^+ n \to \omega p$ show a similar energy dependence but are a factor 100 or more larger in cross section. The reaction $\pi^- p \to \phi n$ can proceed through a small admixture of nonstrange quarks in the ϕ, as given by the ω-ϕ mixing angle.

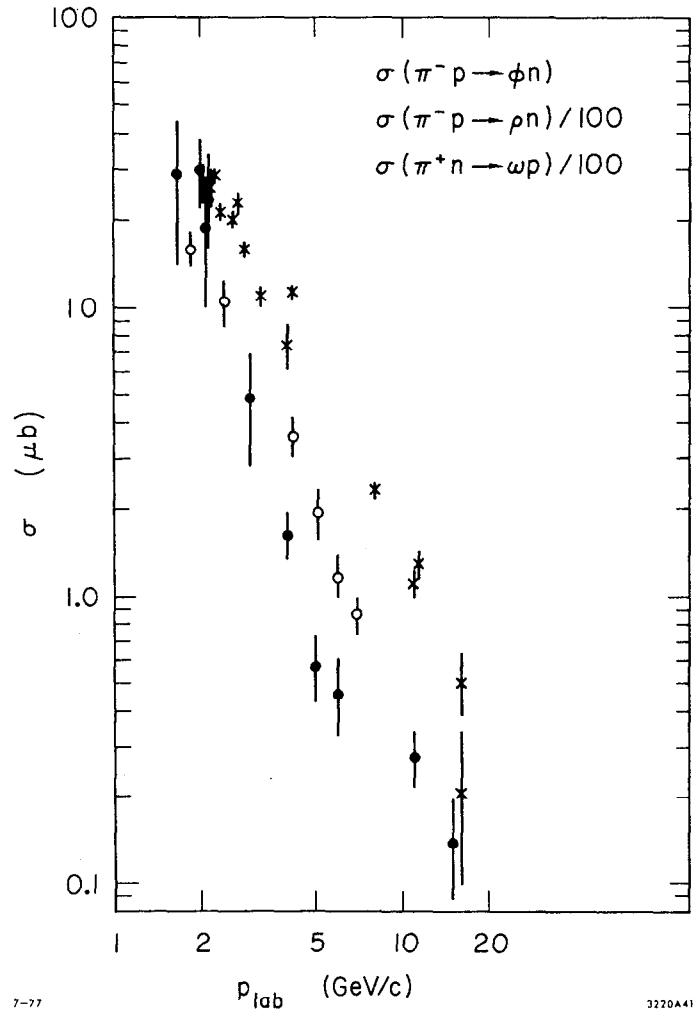

38. Energy dependence of the cross section for the OZI allowed reactions $\pi^- p \to \rho n$ and $\pi^+ n \to \omega p$ compared to the forbidden process $\pi^- p \to \phi n$. The allowed reaction cross sections are divided by 100.

If all the ϕ production proceeded via the ω-ϕ mixing then we would expect the production mechanism to be similar in both reactions. The data of the Argonne effective-mass spectrometer[37] for $\pi^- p \to \phi n$ are found to have a shallower t-dependence than the ω-data. The flatter t-distribution and a sharper energy dependence below 5 GeV may indicate a double scattering process of the quarks, s-channel N^* production or a small $s\bar{s}$ content of the pion.

A test of the OZI selection rule in ϕ production was studied by V. Blobel et al.[38] in pp collisions at 24 GeV/c. The inclusive ϕ cross section is found to be 158 ± 35 μb compared to 3490 ± 420 μb for inclusive ρ° production (only a factor 20 times smaller). Phi production is allowed by the Zweig rule if accompanied by strange particles; however, no tendency is observed for the final states to contain visible strange particles in conjunction with the ϕ. However, the suppression mechanism may not be valid near Feynman x = 0 because of a finite $s\bar{s}$ content of the protons.

B. Spin Dependence

The predictions of the additive quark model for the correlations between the charge properties and spin configurations in peripheral collisions have been successfully tested in a number of reactions. The constraint that only one quark in each hadron interacts places requirements on the allowed spin states of the final hadrons. One can also identify the quark-quark amplitudes in different reactions, then obtain relations between these reactions.

As an example, the reaction

$$\begin{array}{l} K^- p \to \pi^- Y^{*+}(1385) \\ 0^- \ \frac{1}{2}^+ \to 0^- \ \frac{3}{2}^+ \end{array} \qquad (15)$$

in general can have four independent amplitudes. If the quark model relations are satisfied only one amplitude remains. To see this we show in the diagram below the scattering process $K^- p \to \pi^- Y^*$.

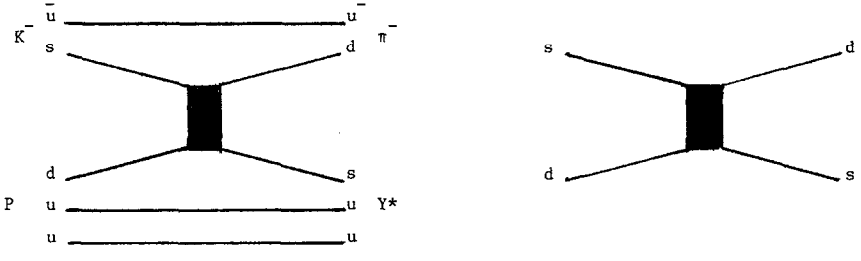

Here we see that the scattering process is sd → ds of spin 1/2 particles. We choose the axis of spin quantization in the direction normal to the quark-quark scattering plane. The spin projection on this axis is called the transversity. The transversity of a single spin 1/2 quark can only change by zero or one unit. Therefore, scattering transitions in the transversity basis are those with no transversity flip or double flip, one for each quark. A single flip would not conserve transversity. Since only the s-quark scatters and the final state must be a 0^- meson, the double flip amplitudes are ruled out, hence only no-flip amplitudes

are allowed. The quark model predicts for the $\Sigma(1385)$

$$T_{\frac{3}{2}-\frac{1}{2}} = T_{-\frac{3}{2}\frac{1}{2}} = 0 \qquad (16)$$

$$T_{\frac{1}{2}\frac{1}{2}} = T_{-\frac{1}{2}-\frac{1}{2}}$$

The reaction $K^-p \to \pi^-\Sigma^+(1385)$ has been measured by the Amsterdam-CERN-Nijmegen-Oxford collaboration at 4.2 GeV/c[39] and their transversity amplitudes are shown in Figure 39 as a function of t'. Except at $t' \sim 0$ the data are in good agreement with the additive quark model predictions of Equation 16. The non-zero double-flip amplitude at small t may result from double scattering contribution where the spectator quarks scatter elastically. A hint of the violation mechanism is obtained by studying the forbidden process $K^-p \to \pi^+Y^{*-}$ which requires double scattering. From Figure 40 we see that the dominating amplitude $T_{\frac{3}{2}-\frac{1}{2}}$ for this exotic process agrees roughly with the $T_{\frac{3}{2}-\frac{1}{2}}$ amplitude of $K^-p \to \pi^-Y^{*+}$, both in size and t behavior.

Since the energy dependence of the exotic reaction $K^-p \to \pi^+Y^{*-}$ *is much larger than that of the allowed reaction we might expect the double scattering process to be negligible at higher energies. The* $K^-p \to \pi^-Y^{*+}$ reaction and the charge exchange reaction $\pi^+p \to K^+Y^{*+}$ *are being studied in high statistics (150 and 275 events/μb) exposures* of the SLAC Hybrid Facility[40]. Their density matrix elements in the *transversity frame are given in Figure 41 for* $\pi^+p \to K^+Y^*$. *Only about*

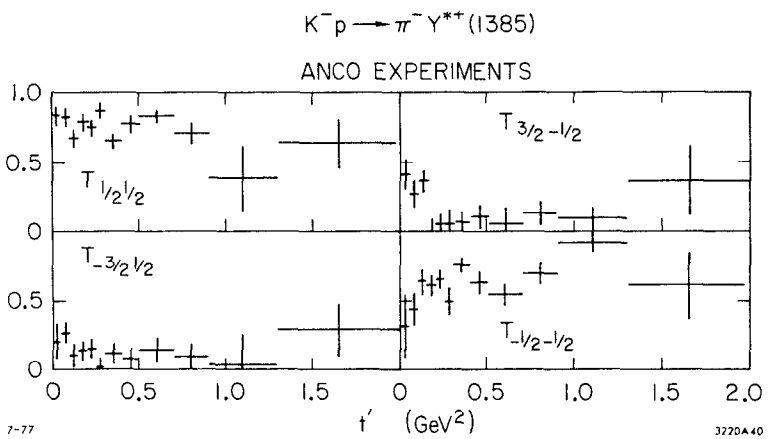

39. t-dependence of transversity amplitudes at 4.2 GeV. Figure from Ref. 39.

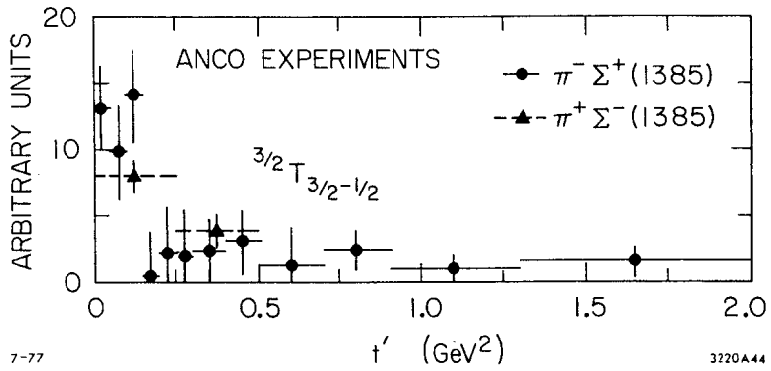

40. t-dependence of the $T_{3/2\ -\ 1/2}$ amplitude for the indicated reactions.

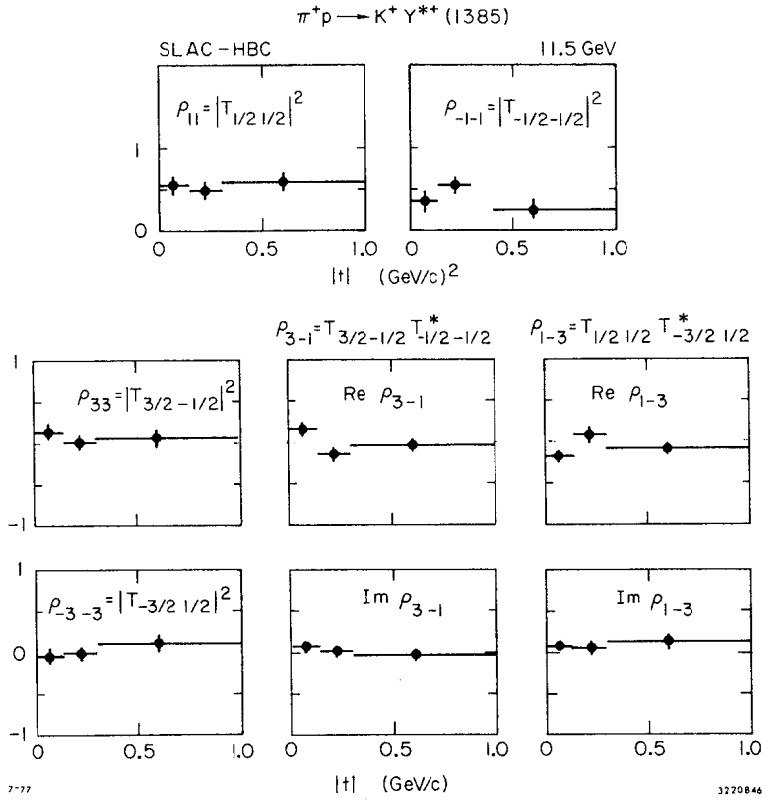

41. t-dependence of transversity amplitudes at 11.6 GeV $\pi^+ p \rightarrow K^+ Y^{*+}$. Data of Ref. 40.

40% of the final statistics were available for these preliminary results. The figure gives the relationship between the density matrix elements and the transversity amplitudes. In most cases good agreement with the expected behavior of the additive quark model is seen. However, the low t behavior in the double flip amplitudes still shows non-zero behavior consistent with the magnitude seen in the 4.2 GeV K^-p data.

The so-called class B relations relate the quark-quark amplitudes in different reactions. For example, we compare the two reactions

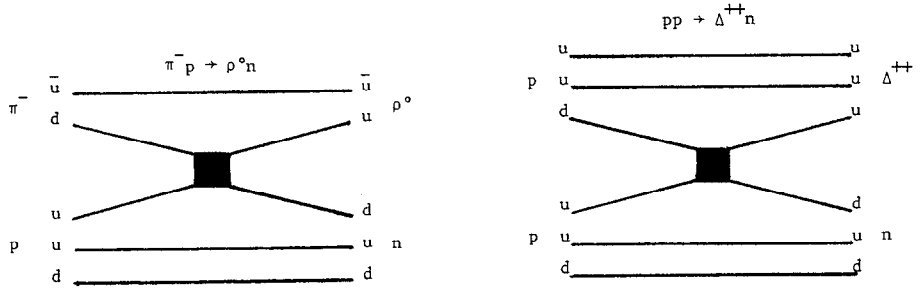

In both reactions the basic process is $du \to ud$ and therefore the amplitudes for the ρ° can be related to those of the Δ^{++}, in particular

$$\langle Y_2^U \rangle_\Delta = \frac{1}{2} \langle Y_2^M \rangle \qquad (17)$$

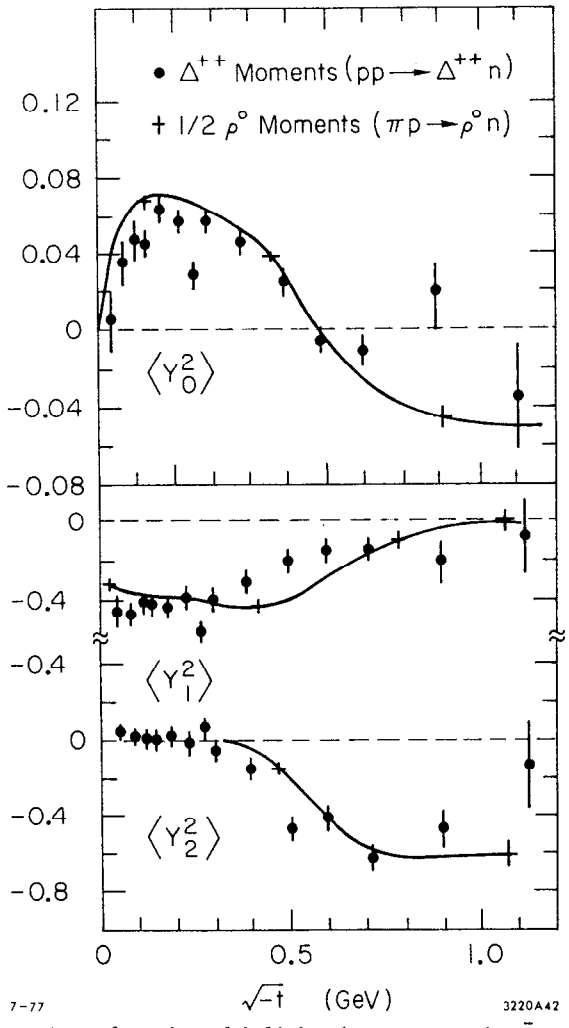

42. Comparison of ρ t-channel helicity decay moments in $\pi^- p \to \rho^\circ n$ and Δ^{++} t channel helicity moments in $pp \to \Delta^{++} n$ at 17 GeV/c [41] as function of $\sqrt{-t}$. The ρ-moments are represented by the solid lines. Quark model Class B relations predict $\langle Y_M^2 \rangle_\Delta = \frac{1}{2} \langle Y_M^2 \rangle_\rho$.

The two reactions have been measured by the CERN-Munich-UCLA collaboration at 17 GeV/c[41]. Figure 42 shows the Λ decay moments together with ρ moments divided by 0.2 as a function of t. Due to the much higher statistics the ρ moments are represented by curves. The agreement is surprisingly good. Whereas many of the predictions like those of our first example ($K^- p \to \pi^- Y^{*+}$) can be obtained by other models (duality, SU(3) and exchange degeneracy, Stodolsky-Sakurai), the class B relates meson properties with baryon properties, which is typical for the additive quark model[42].

CONCLUSIONS

One of the most exciting questions in physics today concerns the underlying quark structure of hadronic matter. Deep inelastic scattering and jet production hint that we are studying basic quark processes. We have found many similarities in diverse reactions. In some cases, we don't quite understand the data as in the non-scaling behavior found in high-p_T events. However, on the whole the results are encouraging.

ACKNOWLEDGEMENTS

I wish to thank J. Bouchez and J.T. Carroll for many helpful discussions. My special thanks to Margaret Kendall for the typing of this paper.

REFERENCES

1. R.P. Feynman, Photon-Hadron Interactions, W.A. Benjamin, Reading, Mass., 1972.
2. J.D. Bjorken, Physical Review 179 (1969) 1547; J.D. Bjorken and E.A. Paschos, Physical Review 185 (1969) 1975.
3. R.E. Taylor, Proceedings of the 1975 International Symposium on Lepton and Photon Interactions at High Energies.
4. E. M. Riordan et al., SLAC-Pub-1634.
5. M.J. Alguard et al., Phys. Rev. Lett. 57 (1976) 1261: N. Sasao, Ph.D. Thesis, Yale University (1977).
6. J. Kuti and V.F. Weisskopf, Phys. Rev. D4 (1971) 3418; F. Close, Nucl. Phys. B80 (1974) 269.
7. R.F. Schwitters, XVIII International Conf. on High Energy Physics, Tbilisi, USSR (1976).
8. M.L. Perl et al., Phys. Rev. Lett. 35 (1975) 1489; Phys. Lett. 63B (1976) 466.
9. W. DeBoer, These Proceedings.
10. M. Della Negra, SLAC-Pub-1242.
11. M. Della Negra et al., CERN/EP/Phys. 77-10.
12. G. Hanson et al., Phys. Rev. Lett. 35 (1975) 1609; G. Hanson, XVII International Conference on High Energy Physics, Tbilisi, USSR (1976).
13. No reference.

14. G .R. Farrar, Nuclear Physics B77 (1974) 429.

15. W.B. Atwood, Electron Scattering Off Hydrogen and Deuterium at 50° and 60° (Ph.D. Thesis), SLAC Report-185, June 1975.

16. G.R. Farrar, P. Schreiner, and W.G. Scott, Fermilab-Pub-77/45-Exp. 7100.180 (1977).

17. B.C. Barish, CALT-68-602 (1977).
M. Derrick et al., ANL-HEP-CP-76-37 (1976).
M. Derrick, ANC-HEP-CP-76-42 (1976).

18. H. Deden et al., Nuclear Physics B85 (1975) 269.

19. R.D. Field and R.P. Feynman, Phys. Rev. D15 (1977) 2590.

20. A. Bodek et al., Phys. Rev. Letters 30 (1973) 1087.

21. J. VanderVelde, presented at the 4 th International Winter Meeting on Fundamental Physics, La Baqueira, Spain (1976).

22. J.F. Martin et al., Phys. Lett. 65B (1976) 483.

23. J.T. Dakin and G.J. Feldman, Phys. Rev. D8 (1973) 2862.

24. R. Blankenbecler, S.J. Brodsky, and J.F. Gunion, Phys. Letters 39B (1972) 649; Phys. Rev. D6 (1972) 2652; Phys. Letters 42B (1973) 461; Phys. Rev. D8 (1973) 287; Phys. Rev. D12 (1975) 3469, SLAC-PUB-1806 (1976).

25. E. Albini et al., Il Nuovo Cimento 32A (1976) 101.

26. C. Bromberg et al., Phys. Rev. Lett. 38 (1977) 1447.

27. M. Della Negra, CERN/EP/PHYS 76-52.

28. J.W. Chapman et al., Phys. Rev. D14 (1976) 5.

29. G. Wolf, Proceedings of the 1975 International Symposium on Lepton and Photon Interaction at High Energies and references therein.

30. M. Gronan, W.S. Laru, T.F. Walsh, and Y. Zarmi, Nucl. Phys. B104 (1976) 307; M. Gronan and Y. Zarmi, Technion-Ph-77-30.

31. G.C. Fox, CALT-68-573.

32. H.L. Anderson et al., Phys. Rev. Letters 36 (1976) 1422.

33. E.M. Levin, M.G. Ryskin, XVIII International Conference on High Energy Physics, Tbilisi (1976).

34. R. Brandelik et al., Phys. Letters 67B (1977) 358.

35. R. Field, CALT-68-593; R. Feynman, R. Field, and G. Fox, CALT-68-595.

36. S. Okubo, Phys. Letters 5 (1963) 165; G. Zweig, CERN preprint TH-412 (1964); J. Iizuka, K. Okada and O. Shito, Prog. Theor. Phys. 35 (1966) 1061; J. Iizuka, Suppl. of Prog. Theor. Phys. 37-38 (1966) 21.

37. D.S. Ayres et al., Phys. Rev. Letters 32 (1974) 1463.

38. V. Blobel et al., Physics Letters 59B (1975) 88.

39. Amsterdam-CERN-Nijmegen-Oxford Collaboration, CERN/EP/Phys 76-23.

40. SLAC-Group BC; private communication.

41. G. Grayer, B. Hyams, C. Jones, P. Weilhammer, W. Hoogland, T. Meyer, R. Poster, P. Schlein, W. Blum, H. Dietl, W. Koch, E. Lorenz, W. Manner, J. Meissburger and V. Stierlin, contribution to the XVI Internat. Conf. on High Energy Physics, Batavia (September 1972); G. Grayer, B. Hyams, C. Jones, P. Weilhammer, W. Blum, H. Dietl, W. Koch, E. Lorenz, G. Lutjens, W. Manner, J. Meissburger, W. Ochs and V. Stierlin, Nucl. Phys. B50 (1972) 29.

42. F. Wagner, MPI-PAE/PTH 19/76.

SLAC-PUB-2050
November 1977
(TE)

GENERAL CHARACTERISTICS OF HADRON PRODUCTION AT SPEAR*

V. Lüth

Stanford Linear Accelerator Center
Stanford University, Stanford, California 94305

I. INTRODUCTION

The very first and preliminary data on the production of hadrons by e^+e^- annihilation were presented at the Kiev Conference five years ago[1] causing great excitement. These first results from ADONE at Frascati were confirmed and the hadronic nature of the final states was proven in the years following. In Figure 1 the most recent update of the measurements at ADONE[2-5] are plotted along with other low energy data from Orsay[6] and Novosibirsk.[7] The quantity R, the ratio of the total hadron production to muon pair production is evaluated as a function of the c.m. energy $E_{c.m.}$ In spite of large errors and inconsistencies between various measurements, they clearly show that hadron production is substantial, i.e., it is comparable or greater than μ-pair production.

*Work supported by the Department of Energy. (Presented at the SLAC Summer Institute, Stanford, CA, July 11-22, 1977.)

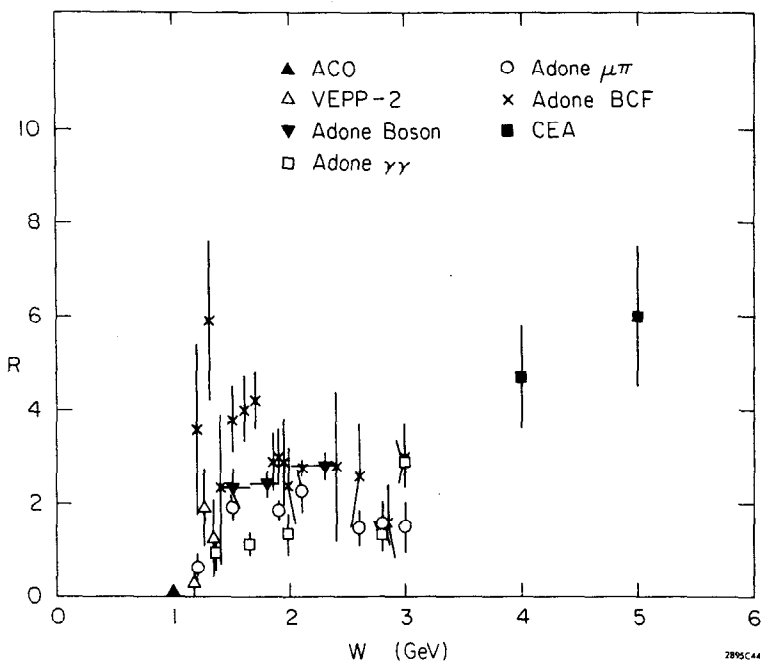

Fig. 1 Results on multihadron production by e^+e^- annihilation as a function of c.m. energy $E_{c.m.}$. Data from Frascati (ADONE),[2-5] Orsay (ACO),[6] Novosibirsk,[7] and Cambridge (CEA).[8]

By far the most serious problems these pioneering experiments at Frascati had to face came from the small solid angle of the detectors. They typically covered no more than 20% of 4π and were placed at interaction regions nearly as long as the detectors. With two charged particles required for triggering this lead to a total acceptance of 10% or less, introducing large systematic uncertainties.

The second generation results from the non-magnetic detector BOLD at CEA,[8] a device with much larger solid angle, was at first met with considerable skepticism. Low beam intensities limited these measurements to two energies, $E_{c.m.} = 4$ GeV and $E_{c.m.} = 5$ GeV. The results, indicating a significantly higher value of R have been confirmed by more recent data from SPEAR[9] and DORIS.[10,11]

In this report we shall discuss what we have learned about hadron production at SPEAR since the discovery of the two narrow resonances, ψ (3095)[12,13] and ψ (3684).[14] To a large extent, this will be an update of Roy Schwitter's presentation at the Photon-Lepton Symposium two years ago at Stanford.[15] In particular, we shall address ourselves to difficulties related to the model dependence of the detector efficiency and effects of the heavy lepton production. We shall include recent results on inclusive production of kaons, protons and Λ hyperons and their implications for charm particle production.

II. PARTON MODEL

Accepting the traditional concept that the electron does not directly couple to hadrons, the production of hadrons by e^+e^- annihilation proceeds dominantly via the exchange of a single, time-like photon between the lepton and the hadron system. Higher order photon exchange

processes generally produce particles at small angles to the beams. Since present detectors do not cover this angular range these processes are of limited importance to hadron production at present energies.

If we restrict ourselves to the one-photon photon exchange as the main process for hadron production by e^+e^- annihilation (Fig. 2a), we see that the annihilation itself is well understood in terms of a point-like lepton-hadron vertex, whereas all ignorance is hidden by the cross hatched region of the photon-hadron vertex. We know, however, that the hadron system must have the quantum numbers of the photon, i.e., $J^{PC} = 1^{--}$ and all additive quantum numbers are equal to zero. A comparison with the diagram for muon pair production in Fig. 2b illustrates that the quantity of more direct interest than the total hadronic cross section, σ_{had}, is R the ratio of hadron to muon pair production,

$$R = \frac{\sigma_{had}}{\sigma_{\mu\mu}} \text{ with } \sigma_{\mu\mu} = \frac{4}{3}\frac{\pi\alpha^2}{s} \quad .$$

Here s is the square of the mass of the virtual photon and α the fine structure constant.

One of the most fundamental theoretical concepts for high energy particle physics is that of scaling. It says that σ_{had} should vary like $1/s$ for large s or stated differently, the ratio R is expected to approach a constant value; "large" generally means large compared to any mass or energy involved. The simplest argument to predict scaling is one of dimensional analysis. It says that at high energies the only unit of length is $s^{-1/2}$, thus a cross section must behave like s^{-1}.

A far more appealing picture that arrives at the same answer is the parton model.[16] Measurements of deep inelastic electron-nucleon

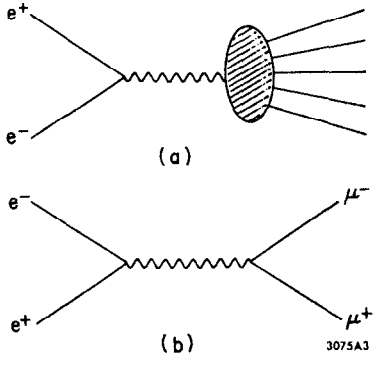

Fig. 2. Feynman diagrams for one-photon exchange (a) $e^+e^- \to$ hadrons; (b) $e^+e^- \to \mu^+\mu^-$.

scattering led to the hypothesis that hadrons are built out of constituents, the partons, which have point-like coupling to the electromagnetic current. Thus, photon-hadron interactions are basically photon-parton interactions and consequently hadron production in e^+e^- annihilation proceeds via the formation of pairs of parton-antiparton. If partons have spin 1/2 then the cross section for producing the free $q_i\bar{q}_i$ pair is the same as for producing a $\mu^+\mu^-$ pair, except for the difference in electric charge Q_i,

$$(e^+e^- \to q_i\bar{q}_i) = Q_i^2 \, \sigma_{\mu\mu}$$

Assuming further that the $q_i\bar{q}_i$ pairs convert to hadrons with probability one, the hadronic cross section equals the sum of the individual parton pair cross section, and

$$R = \frac{\sigma_{had}}{\sigma_{\mu\mu}} = \sum_i Q_i^2 .$$

Given a fixed number of partons having specified charges Q_i, R is constant, and hadron production is said to exhibit scaling. Wherever a threshold for the production of higher mass constituents is reached, there should be an upward step in R proportional to Q_i^2 of the new parton. The value of R at any given energy provides information about the number and properties of the partons produced. Clearly, the existence of partons is purely hypothetical, but they help to explain a great deal of data.

If one associates partons with quarks of spin 1/2, available in 3 colors, then one obtains

$$R_{uds} = 3 \left((2/3)^2 + (1/3)^2 + (1/3)^2 \right) = 2;$$

and above charm threshold

$$R_{udsc} = 10/3.$$

Another consequence of this particular model of hadron production is the jet-like structure of the final states that arises due to limited transverse momenta of the hadrons relative to the parton direction of motion. The angular distribution of the jet-axis has been found to agree with the $1 + \cos^2\theta$ distribution expected for spin 1/2 parton-antiparton pair.[17]

Furthermore, the inclusive momentum spectra are expected to exhibit scaling at high energy. In complete analogy to deep inelastic ep scattering the most general form of the differential cross section can be written as a function of two structure functions W_o and W_1,

$$\frac{d^2\sigma}{dx d\Omega} = \frac{\alpha^2\beta}{4\pi} = [W_1(x,s) \; (1 + \cos^2\theta) + W_o(x,s) \; \sin^2\theta]$$

where

$$x = 2E_h/E_{c.m.}; \; \beta = P_h/E_h$$

and P_h, E_h are respectively the momentum and energy of the hadron. If at sufficiently high energy W_o and W_1 become independent of x, $d\sigma/dx$ will decrease like 1/s (Bjorken scaling) and the ratio R will be constant.

III. THE MAGNETIC DETECTOR AT SPEAR

The solenoidal magentic detector built and operated by the SLAC-LBL collaboration is shown in Fig. 3. It provides a nearly uniform field of 4 kG over a volume 3-m long and 3 m in diameter. A particle produced in the interaction region first traverses the 150 μm steel vacuum pipe,

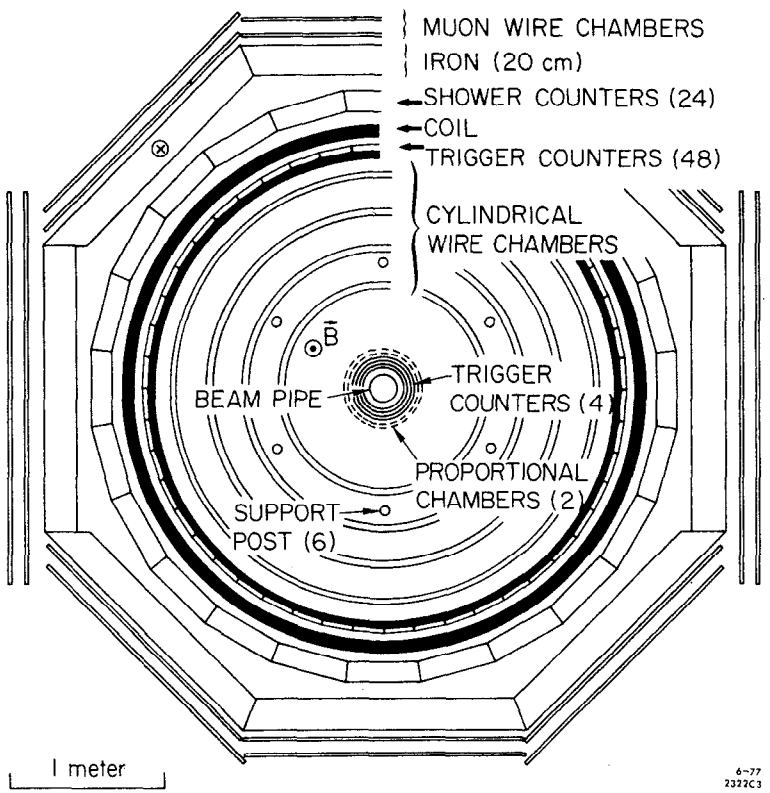

Fig. 3. End view of the SLAC-LBL magnetic detector.

then a pair of cylindrical scintillation counters and two proportional wire chambers that form an element of the trigger system. Continuing outwards, the particle passes through 4 sets of magnetostrictive spark chambers, a trigger hodoscope that provides time-of-flight measurements, the one radiation length coil, and array of shower counters. Most hadrons are absorbed in the 20 cm thick iron yoke and will not reach a set of spark chambers outside that aids muon identification. The momentum analysis (resolution $\Delta p/p \approx 0.015\ p$) and particle identification of the detector extend over 65% of 4π; the azimuthal acceptance is complete, and the subtended polar angle ranges for 50° to 130°. The hardware trigger requires at least two charged particles each firing a trigger counter and an associated shower counter in coincidence with the beams. This requirement, which restricts the data sample to events with at least two particles with momenta above 200 MeV/c, and the limited solid angle of the apparatus are largely responsible for the uncertainties in the cross section data.

The data analysis distinguishes two general categories of events, lepton pairs

$$\begin{matrix} e^+e^- \to e^+e^- \\ e^+e^- \to \mu^+\mu^- \end{matrix} ,$$

and hadronic final states,

$$e^+e^- \to \text{hadrons}.$$

A hadronic event is required to have three or more tracks forming a vertex within the luminous region of the machine. Two-prong events are also included in the hadronic event sample provided the tracks are

acoplanar with the beams by at least 20° and have momenta exceeding 300 MeV/c.

IV. TOTAL CROSS SECTION

The major aim of the SLAC-LBL experiment was to obtain an accurate measurement of the total hadronic cross section σ_{had} over as wide a range in energy as the storage ring would allow. σ_{had} is given by

$$\sigma_{had} = \frac{\Sigma M_i}{\bar{\varepsilon} \int \mathscr{L} dt} , \qquad (1)$$

where M_i is the number of events observed with i charged tracks, $\bar{\varepsilon}$ the average efficiency of all events and $\int \mathscr{L} dt$ is the integrated luminosity as monitored by Bhabha scattering events in the same detector. The important factors limiting the precision of σ_{had} are (a) the statistical error of the event sample, (b) the level of background in the data, (c) the systematic error in the luminosity monitoring, and (d) the systematic errors in the evaluation of the detection efficiency. As we shall see, the last point is the most serious.

The raw number of detected events in the hadronic event class is first corrected for various sources of background. Beam-gas interactions are estimated from event rates just outside the interaction region. Beam-gas backgrounds amount typically to 6% of the total. Cosmic-ray background is suppressed to a negligibly low level by the TOF system. Contaminations due to electrodynamic final states arising from two-photon processes and radiative e^+e^- or $\mu^+\mu^-$ production are calculated to be of the order of a few percent. A correction is made to the two-prong events. Evidence for non-hadronic multibody final states originating from the production and decay of a pair of heavy leptons[18] will be presented below. Such events should not be included in the hadronic cross section measurement. The average detection efficient $\bar{\varepsilon}$ is defined as the ratio of the number of events observed to the number of produced events, i.e.,

$$\bar{\varepsilon} = \sum_i M_i / \sum_j N_j , \qquad (2)$$

where N_j is the number of events produced with j charged particles. Observed and produced multiplicities are related by

$$M_i = \sum_j \varepsilon_{ij} N_j , \qquad (3)$$

where ε_{ij} is the efficiency for detecting an event with i prongs, when it was produced with j charged particles. The matrix elements ε_{ij} are computed by a Monte Carlo simulation of the experiment. Known properties of the detector, such as solid angle, trigger biases, cuts in the data analysis, and a plausible model of the final states are necessary ingredients of such calculations. Given the coefficients ε_{ij}, Eq. (3) is inverted by a maximum likelihood fit to obtain the produced multiplicity distribution N_j, and thereby $\bar{\varepsilon}$.

Three different models of multihadron production have been used to check the sensitivity of $\bar{\varepsilon}$ to the choice of the model and to compare with the data. All pion final states are simulated by a two-jet model, in which the jet axis has a $1 + \cos^2\theta$ angular distribution and particles are emitted from each jet with transverse momenta limited by a matrix element of the form

$$|M|^2 = e^{-\sum p_{\perp i}^2 / 2b^2}$$

The total multiplicity and the charged multiplicity as well as the transverse momentum cut-off b and the orientation of the jet axis have been adjusted to agree with the data.[17] The production and decay of a pair of heavy leptons of mass 1.9 GeV is simulated in accordance with its predicted properties.[19] The third model reproduces the associated production of D and D^* mesons near threshold. All parameters like the masses, relative production rates and branching ratios have been chosen to agree with the data at 4.03 GeV.[20]

In the following we shall compare in some detail the observed and the Monte Carlo simulated distributions. The results are shown on an arbitrary scale with statistical errors only. In Figure 4 the momentum spectra are presented for selected c.m. energies, separately for 2-prongs and multiprongs. The normalization of the τ-pair Monte Carlo is absolute, the sum of all model calculations are normalized to the total number of events. At 4.03 GeV the pion model is normalized to fit the data for $x < 0.6$. Below charm threshold at 3 GeV the all pion jet model fits the data reasonably well, whereas the same model shows a strong disagreement with the data at 7.4 GeV, particularly for two-prong events. The difference can, to a large extent, be accounted for by the expected contribution from $\tau^+\tau^-$ production. The remaining excess in the data at very small x can be explained by a contamination from two-photon processes that has not been subtracted in these plots. At 4.03 GeV the difference between the sum of pion and heavy lepton production is limited to $x < 0.5$ and can be well understood in terms of charm production near threshold. The discrepancy between the data and the jet model calculation can also be observed in the angular correlation of two prong events. The jet

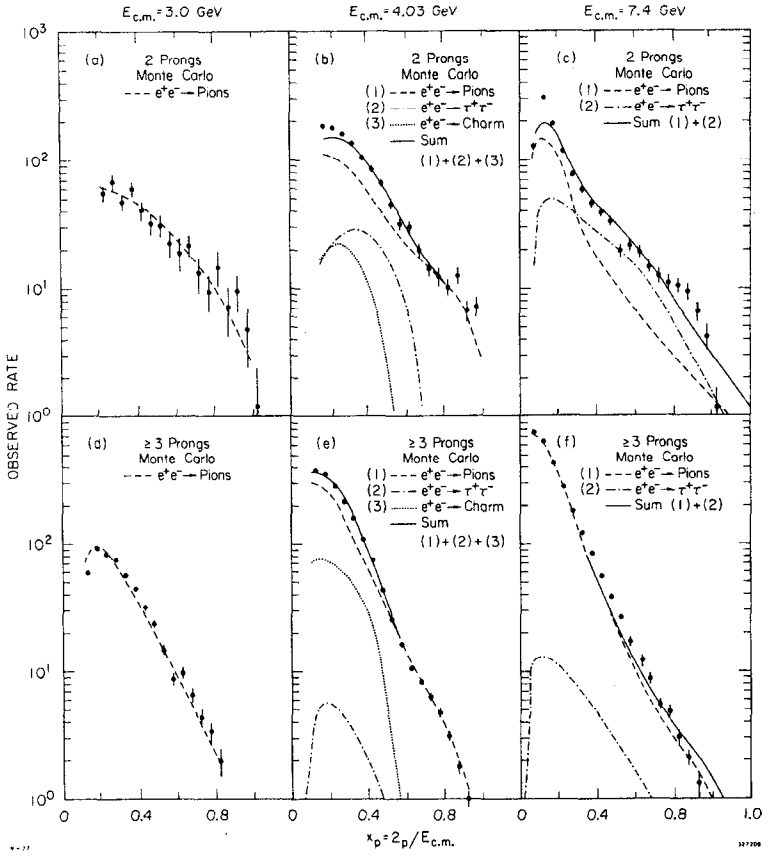

Fig. 4. Observed x distributions for charged particles at various energies. The data are compared to different Monte Carlo simulations. The errors are purely statistical.

model fails to reproduce the pronounced backward peak in the collinearity angle, while this enhancement is present in the heavy lepton simulation (Fig. 5) and can make up for this discrepancy. In conclusion, the high energy data indicate the presence of dynamics that cannot be described by a jet model for hadron production. The fact that the jet model simulation used here does not take into account the production of kaons, nucleons and other heavier particles may account for some differences between data and model, but it can hardly explain this large a discrepancy. If we accept the existence of such a heavy lepton, we should subtract this non-hadronic contribution from our data. In the following we shall take a double route by presenting the results with and without this subtraction. As a consequence we obtain two different multiplicity distributions and two different efficiency curves. If we include all events remaining in the hadronic category after subtraction of beam-gas and two-photon backgrounds, the average detection efficiency rises from roughly 35% at 3 GeV to 63% above 6 GeV (Figure 6a). The subtraction of events expected from $\tau^+\tau^-$ production predominantly affects the two-prong events and raises $\bar{\epsilon}$ to more than 70% at high energy (Fig. 6b).

A complete, though preliminary, result on measurements of the hadronic cross section σ_{had} over the whole c.m. energy range of the SPEAR machine was first presented two years ago at Stanford.[15] Since then many aspects of the analysis have been improved and detailed studies of the detection efficiency have been performed. A present day update of the results is given in Fig. 7 in terms of $R = \sigma_{had}/\sigma_{\mu\mu}$. The difference to the earlier publication is fairly small, and the situation reminds me

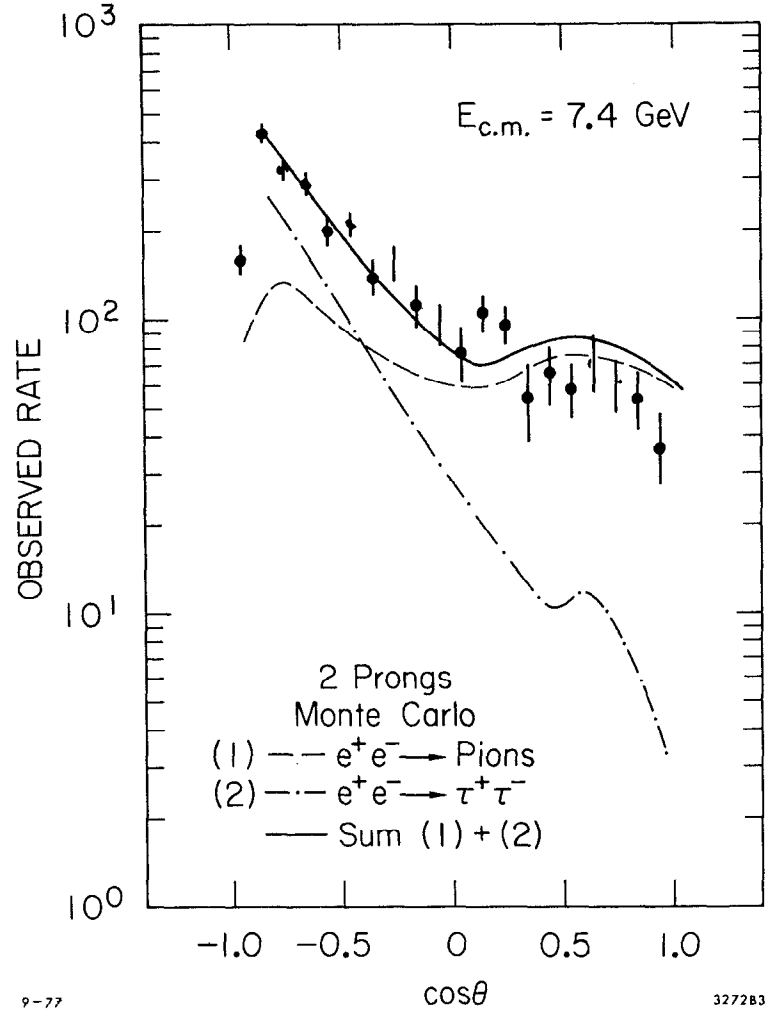

Fig. 5. Comparison of the collinearity angle in two-prong events at 7.4 GeV in data and model.

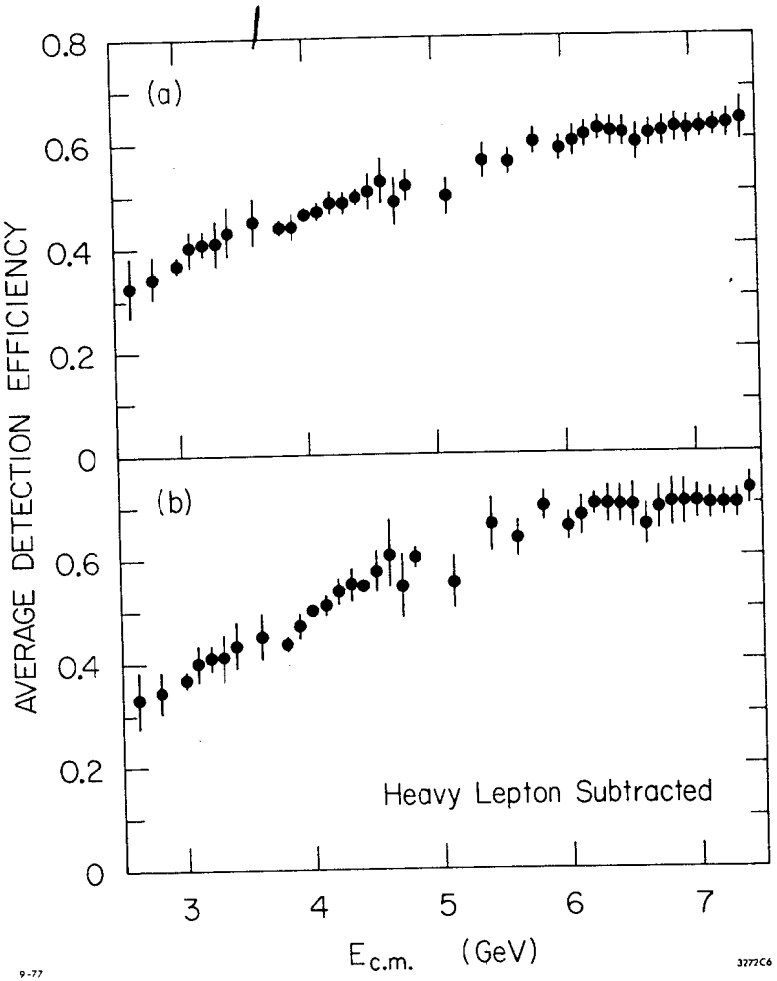

Fig. 6. Average detection efficiency for hadronic events as a function of the c.m. energy : (a) all two and multi-prong events; (b) heavy lepton events subtracted.

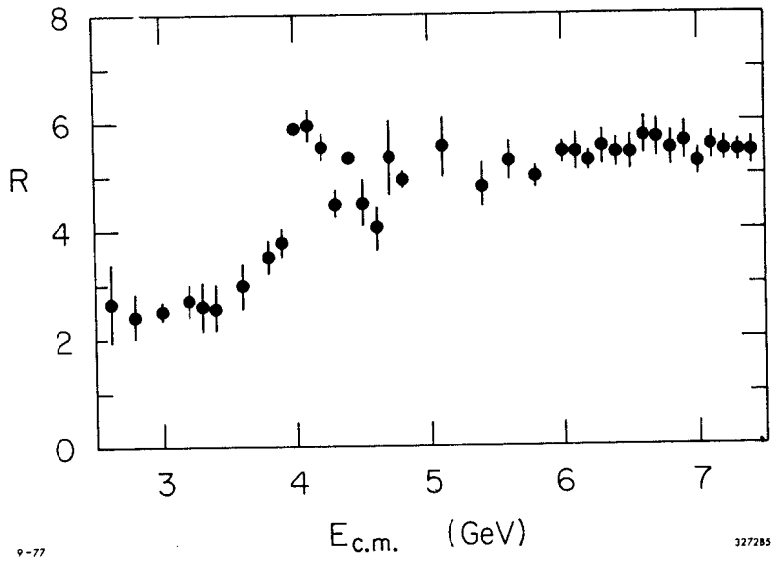

Fig. 7. The ratio of hadron to μ-pair production cross sections versus c.m. energy.

of advertisements of a German automobile company, that were published year after year showing a long list of improvements and changes of the new model, though to a casual observer the car looks still the same after more than 20 years. R is approximately constant below 3.5 GeV with a value around 2.6. Above 6 GeV, R is approximately constant with a value around 5.5. In between, there is a rather complex structure with peaks at 4.03 GeV and 4.41 GeV that are related to charm production thresholds.[20,21] Details are not mapped out here due to somewhat coarser binning in energy. Radiative corrections have been applied to the data to remove the tails of the narrow ψ resonances. The errors include statistical and systematic point-to-point errors. There is an overall uncertainty of ± 10% in the normalization and there could be an additional variation of up to 10% from the lowest to the highest energy due to incorrect modeling in the Monte Carlo.

In Figure 8 the ratio R is presented for the heavy lepton subtracted data, indicating a plateau of R = 4.5 above 6 GeV, exactly one unit of R less than before the subtraction. Most of the rise in R near 4 GeV is observed in the multi-prong data, while the two-prong events show a very small increase relative to μ-pairs. The data are in general agreement with the quark-parton model; though quantitatively there may be some problems since we observe $\Delta R = 1.9$, while we expect only $\Delta R = 4/3$. Likewise the model predicts R = 2 in the low energy region where we observe R = 2.6. If we take this measurement at face value and assume that the predictions of the simple model are uniformly too low by 30%, then we would predict a value of R = 4.3 above threshold for charmed particles and find good

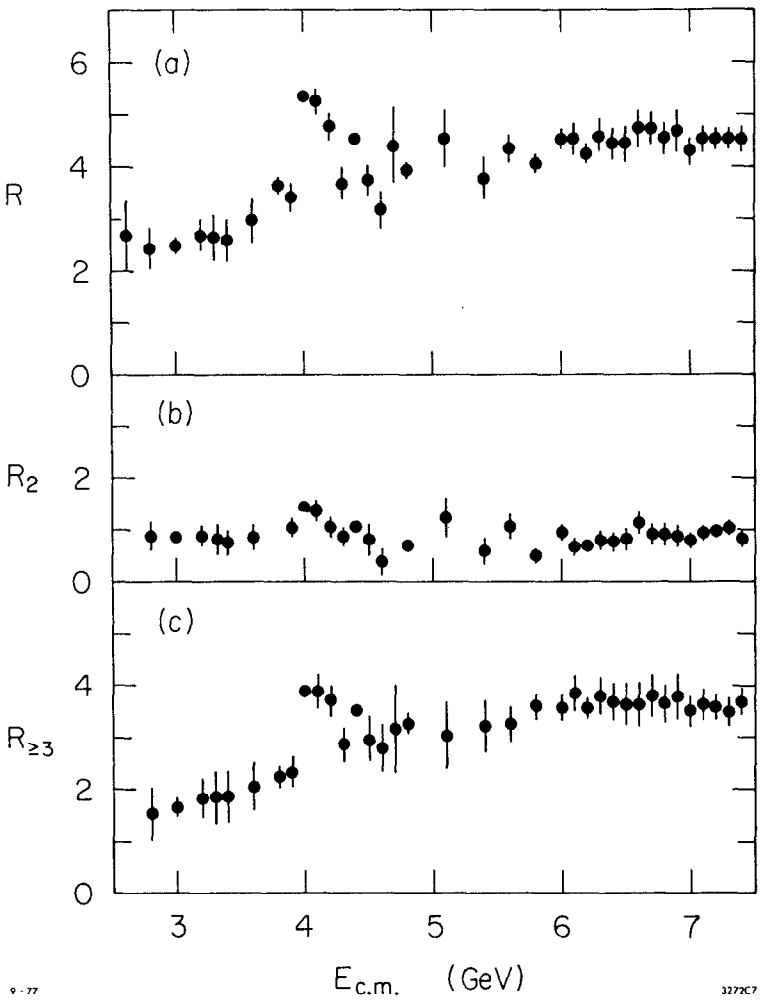

Fig. 8 The ratio R for the heavy lepton subtracted data; (a) all events, (b) two-prongs only, (c) multi-prongs only. The errors are statistical only.

agreement with the data. In any case, the present uncertainties are too large to draw any decisive conclusion with respect to the quark model.

The data presented here are in good agreement with measurement at DORIS[22,23] below 5 GeV, though our results seem to indicate a somewhat larger value of R. In this comparison, one should take into account that there is very little overlap between the two experiments at the higher energies.

V. CHARGED MULTIPLICITY

The charged multiplicity distribution of the hadronic final states are obtained from the observed distributions as a by-product of the Monte Carlo analysis that is used to determine $\bar{\varepsilon}$. The energy dependence of the charged multiplicity for all events in the hadronic category (Figure 9) is consistent with the logarithmic rise of the form

$$\langle n \rangle_{ch} = a + b \ln E_{c.m.},$$

where a = 2.3 and b = 1.3. A similar parametrization fits multiplicity growth in hadron-hadron interactions.[24] A logarithmic rise of $\langle n \rangle_{ch}$ is a consequence of the limitation in transverse momenta of the produced particles and is expected to set in when their average longitudinal momentum clearly exceeds their average transverse momentum. There is little evidence for a break in the distribution around 4 GeV, though the errors are large and the quality of the fit is fair. If we subtract the expected multiplicity distribution for the heavy leptons events from the observed data, the average produced multiplicity exhibits a step by roughly 0.7 between 4 GeV and 5 GeV. From this we derive an average charged multiplicity of 6.6 for charmed particle production around 7 GeV. This result

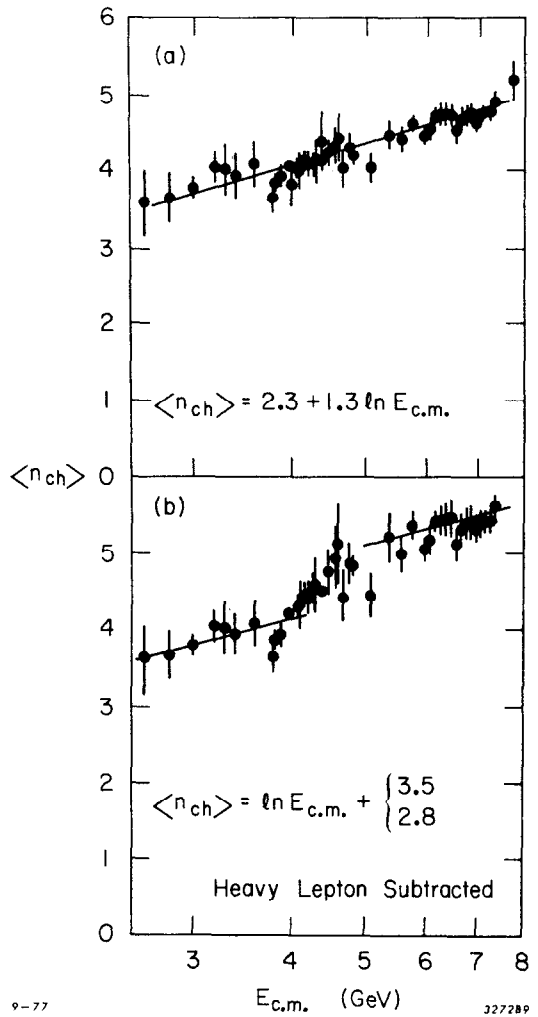

Fig. 9. Average charged multiplicity vs c.m. energy (a) for all events, (b) for heavy lepton subtracted events.

is supported by a direct measurement of $\langle n \rangle_{ch}$ for events containing charmed mesons.[25] Thus the smooth rise observed for all events including the heavy lepton can be understood as being the result of a mixture of two new processes, one with low the other with high multiplicity. This has been well confirmed by the study of inclusive lepton spectra.[18]

Examples of charged multiplicity distributions at several c.m. energies are given in Figure 10, with and without the subtraction of the heavy lepton contribution. The unsubtracted data show a surprisingly large fraction of two-prongs, whereas the subtracted distributions resemble the familiar Poisson shape at all energies.

A comparison between multiplicity data from $p\bar{p}$ annihilation[26] and pp interactions[27] and e^+e^- annihilation may provide some insight in the dynamics of hadron production. In Figure 11 the average multiplicity of negative particles is plotted versus energy for the three interactions. The annihilation data show a much higher multiplicity than pp collisions. This is at least partially explained by the fact that there is more energy available in annihilation than in non-annihilation processes. The annihilation data seem to suggest a similar asymptotic rate of increase (i.e. coupling constant) as the hadron-hadron interactions. At low energy the $p\bar{p}$ and e^+e^- data agree well, but the e^+e^- data exhibit a considerably slower rise with energy.

The multiplicity distributions of the annihilation processes are much narrower than those of the pp interactions, indicating that the correlations between the produced particles are different. In order to compare the widths of the multiplicity distributions of various processes,

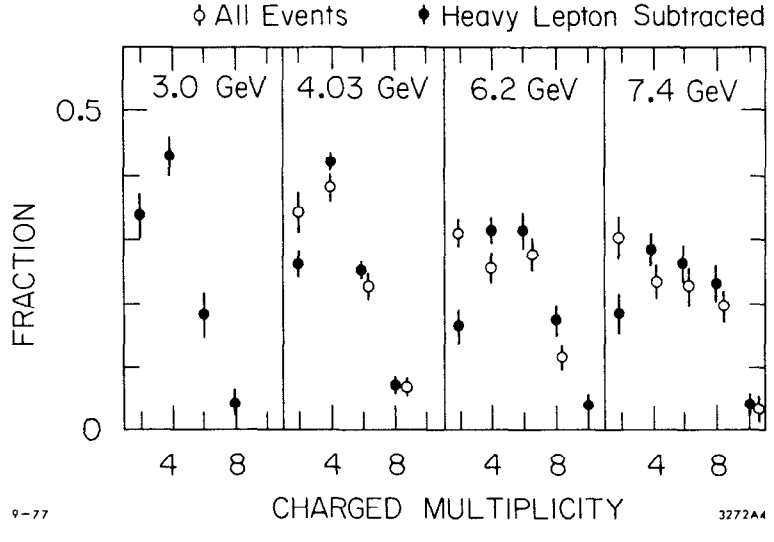

Fig. 10. Charged multiplicity distributions for selected c.m. energies before and after subtraction of the heavy lepton contribution.

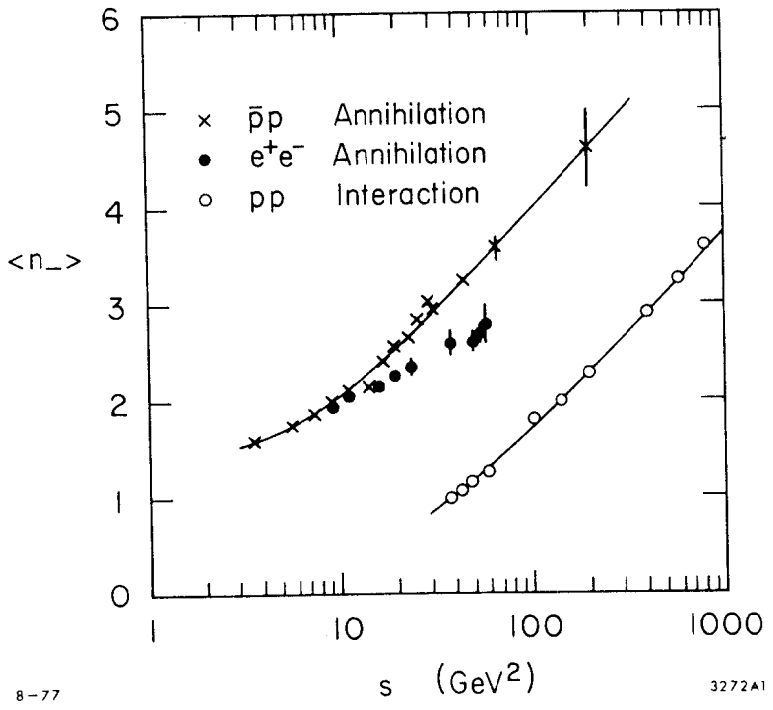

Fig. 11. Average multiplicity of negative particles produced in $p\bar{p}$ [26] and e^+e^- annihilation and pp [27] interactions as a function of c.m. energy. The lines help to guide the eye.

the variable f_2^{--} is plotted versus $\langle n_- \rangle$ in Figure 12, where the correlation integral is defined as

$$f_2^{--} = \langle n_-(n_--1) \rangle - \langle n_- \rangle^2 = \sigma^2 - \langle n_- \rangle .$$

The $\bar{p}p$ data can be parameterized up to about 60 GeV by a linear function of the form

$$f_2^{--} = a + b \langle n_- \rangle$$

with $b = -0.6$. It has been shown [28] that this linear fit with negative values of f_2^{--} for low energy annihilation can be understood in terms of a single cluster or fireball formation, i.e., a Poisson-like total multiplicity with no correlation between particles. The large positive values of f_2^{--} for pp scattering are seen as a consequence of multiple cluster or resonance formation and long-range correlations due to inelastic diffraction and non-diffractive production. Each cluster has its own negative value of f_2^{--} but averaging over several clusters gives a positive f_2^{--}. As one reaches sufficiently high energy one might expect to see f_2^{--} for annihilations to deviate from its linear function and turn to positive values. The recent $\bar{p}p$ data at 100 GeV/c are suggestive of an onset of this type of behavior. The e^+e^- annihilation data indicate a similar deviation from the single cluster behavior in an energy range where jet-like correlations have been observed.

VI. INCLUSIVE MOMENTUM SPECTRA

Single charged particle momentum distributions have been studied at SPEAR for large samples of multihadron final states recorded at different

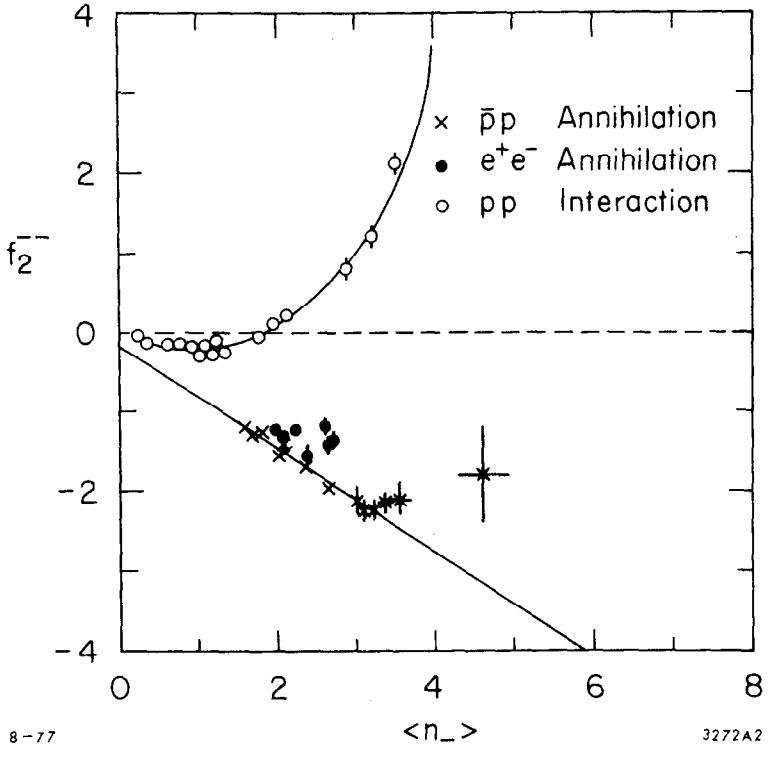

Fig. 12. The correlation integral f_2^{--} vs $\langle n_- \rangle$ for $p\bar{p}$, e^+e^- and pp collisions.

c.m. energies. The data are presented in terms of the scaling variable x defined as

$$x = 2p/E_{c.m.}.$$

This particular definition has been chosen because in general the momentum of the particle, not its energy is measured. The results are presented for the quantity $s\, d\sigma/dx$ which is expected to scale at high energies. The integral of this function can be written as

$$\int s\, d\sigma/dx = \langle n \rangle_{ch} \cdot s \cdot \sigma_{had} \quad .$$

The area under $s\, d\sigma/dx$ must increase with s, because both the mean charged multiplicity and $s \cdot \sigma_{had}$ increase.

The efficiency for the detection of a single charged particle has been evaluated by Monte Carlo, the result is shown in Figure 13 for two extreme energies. ε varies smoothly as a function of x, with a sharp decrease below 150 MeV. The uncertainties in ε could be as large as 20% for the lowest and highest values of x, varying smoothly with x. These uncerrainties are mostly caused by uncertainties in particle tracking and the model calculations. The data are presented in Figure 14 with purely statistical errors. The spectra for all energies rise sharply at small x, peak below x = 0.2, and then fall with increasing x. The area under the curve grows significantly as expected from the sum rule, but almost all of the increase is in the low x region. Above x = 0.2, the spectra are independent of energy for $E_{c.m.}$ greater than 4 GeV. For $x \geq 0.5$ the

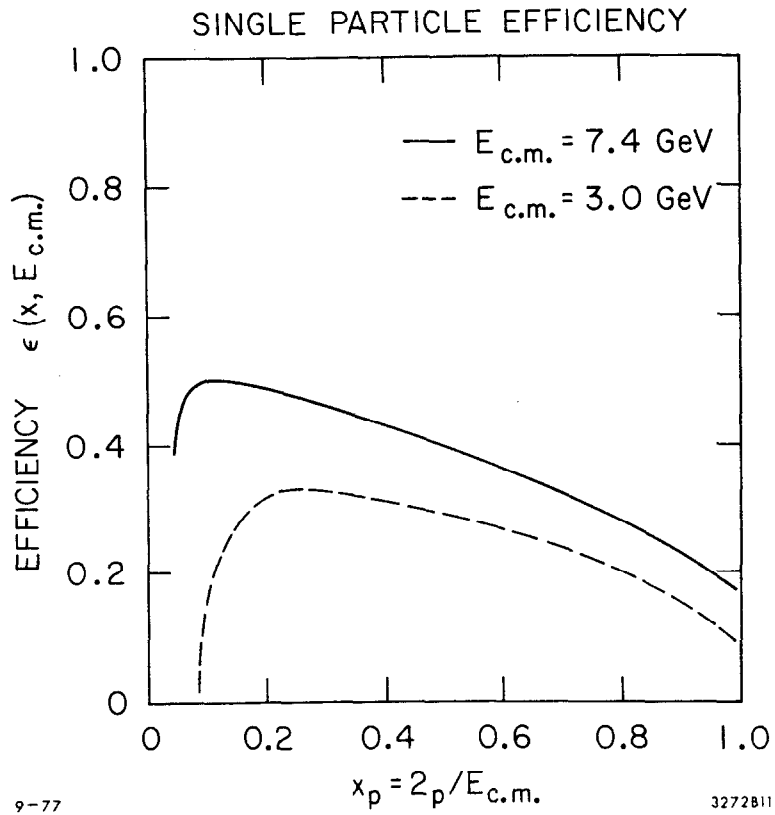

Fig. 13. Single particle efficiencey $\epsilon(x, E_{c.m.})$ for 3.0 GeV and 7.4 GeV c.m. energy.

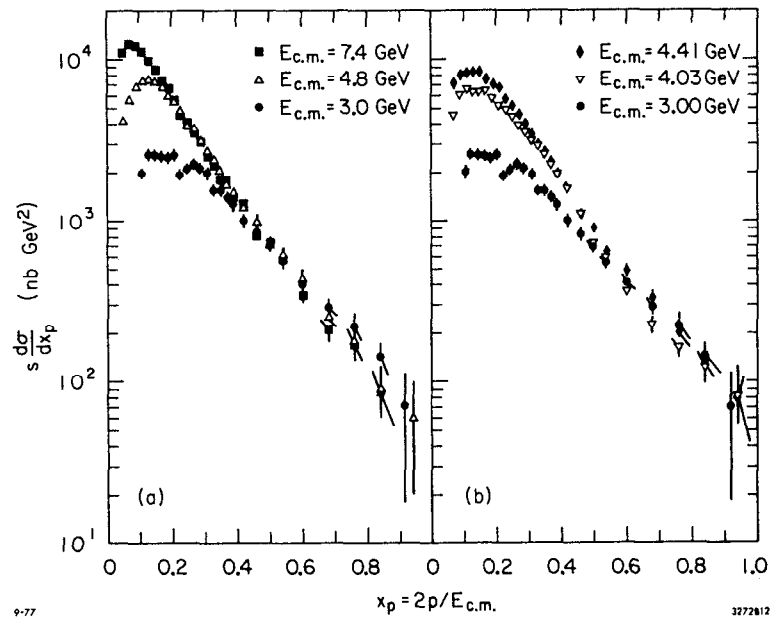

Fig. 14. Test of scaling in inclusive momentum spectra of charged particles, s dσ/dx for various c.m. energies.

data scale to within 20% over the entire energy range. This is rather remarkable considering that the ratio R changes dramatically around 4 GeV. On the other hand, we know that the pair production of charmed particles near threshold is confined to small values of x. At higher energies the spectra for the decay products of charmed particles seem to be not too dissimilar from all other particles produced. The cross sections presented here are somewhat larger than those of the DASP experiment at DORIS.[29] The same trend was observed in the total cross section data and are most likely related to differences in the overall detection efficiency and normalization.

VII. INCLUSIVE K° AND Λ° PRODUCTION

The SLAC-LBL collaborations have recently reported measurements of the production of neutral K mesons[30] as well as Λ hyperons and protons.[31] These measurements are important in their own right, but are of particular interest in e^+e^- annihilation as a probe for thresholds for the production of pairs of charmed particles. The lowest-mass particles carrying the quantum number charm should decay weakly to states of non-zero strangeness. The thresholds for the pair production of charmed mesons should therefore cause a rise in K meson production, whereas charmed baryons should give an increase in the production of Λ hyperons and protons.

1. Inclusive K° Production

The study is based on large data samples of multiprong events recorded between 3.0 GeV and 7.6 GeV c.m. energy. Neutral kaons are identified by their decay $K_S \to \pi^+\pi^-$. Cuts on the reconstructed decay vertex and the effective mass of the pion pair are applied to suppress background from pions produced directly. For a 20 MeV/c^2 wide interval centered on the K° mass the signal to background ratio amounts to roughly 5.0. The observed width of 18 MeV/c^2 (FWHM) agrees well with the estimated resolution of the detector. The purity of the K_S sample is obtained at the expense of a rather low detection efficiency. ε is essentially zero below 100 MeV/c, it rises smoothly and reaches a maximum of roughly 25% at 1 GeV/c momentum. A cut at 200 MeV/c is applied to the data, the loss of low momentum K_S has been estimated by extrapolation of the invariant spectrum to zero momentum. The correction amounts to 4% or less.

The results in terms of a comparison of the inclusive kaon production to total hadron production and to muon pair production are given in Fig. 15. The errors indicated include statistical errors added in quadrature to systematic uncertainties. These systematic errors are estimates of the point-to-point fluctuations which arise from the background subtraction and corrections for losses due to cuts. The errors are consistent with the reproducibility of the results under various other selection criteria. Not included is the 15-20% uncertainty in absolute normalization, mainly due to our lack of knowledge about the multiplicity and dynamics of final states containing neutral kaons.

We assume an equal number of K_S and K_L and define $f_K = 2\sigma_{K_S}/\sigma_{had}$ and $R_K = 2\sigma_{K_S}/\sigma_{\mu\mu}$. Above 4 GeV, where most of the data have been recorded, there is roughly one K_S for every four hadronic final states. The ratio R_K is roughly constant at a value of 2.2 for energies above 4 GeV, except at 4.028 GeV and 4.415 GeV where we observe significant deviations from this average. Below 3.8 GeV, R_K is smaller by more than a factor of two, though the statistics are very limited.

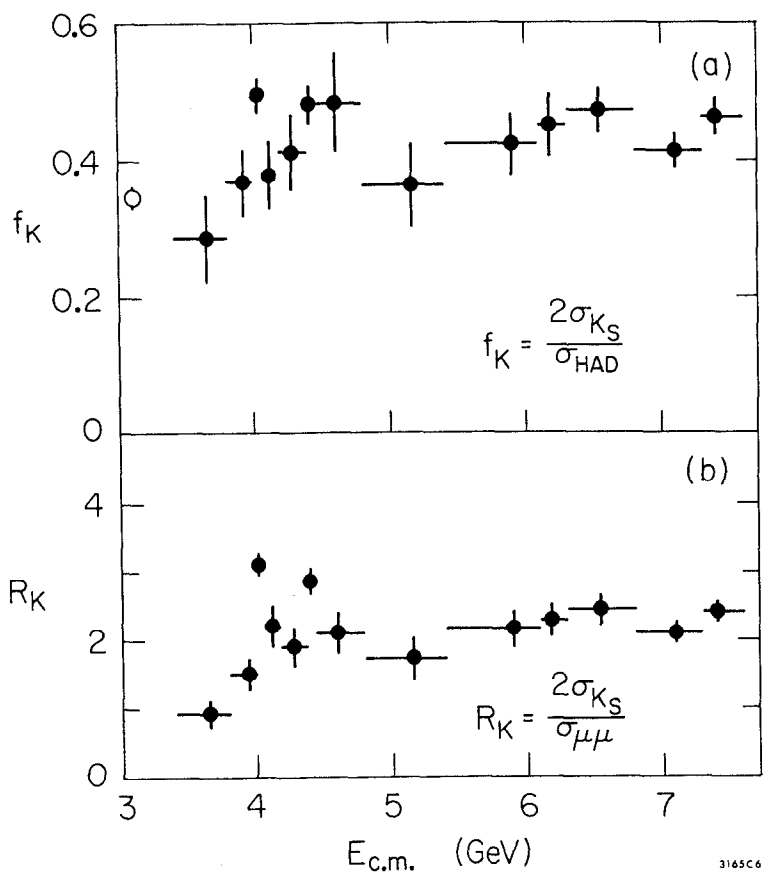

Fig. 15. Inclusive production of neutral kaons as a function of c.m. energy; (a) ratio of kaon to total hadron production, (b) ratio of kaon to μ-pair production. Errors include systematic uncertainties. The data point at 3.1 GeV refers to the $\psi(3095)$ resonance.

A difference between the data recorded at the center of the peaks at 4.028 GeV and 4.415 GeV and the data in the high energy plateau can also be found in the inclusive energy distributions. In Fig. 16 the data are presented in terms of the scaling variable $x_E = 2E_K/E_{c.m.}$, where E_K denotes the kaon energy. Again, the K_S rates have been doubled to obtain the neutral kaon cross sections. Beyond x = 0.6 the spectra agree for all c.m. energies. At low x, however, the 4.028 GeV and 4.415 GeV data are strongly enhanced compared to the data sampled below 4 GeV and above 6 GeV. A similar behavior has been found for charged pions and kaons.[15,29,32]

Assuming that the production of charged kaons is equal to neutral kaons, we have used the neutral kaon spectra to correct the spectra of all charged particles for their kaon content and thereby obtain the charged pion spectra. In Figure 17 the inclusive energy spectrum for charged pion is compared to the inclusive K° spectrum in the high energy data. The two spectra are different by roughly a factor five but follow the same slope.

In summary, the inclusive neutral kaon production has roughly the same energy dependence as the total hadronic cross section. The rate R_K rises just below 4 GeV, peaks at 4.028 GeV and 4.415 GeV and reaches a plateau above 5 GeV. The observation of similar enhancements in the number of kaons per hadronic event supports the hypothesis that the rise and the structure in total hadron cross section is due to the threshold for associated production of charmed mesons that decay preferentially to final states of non-zero strangeness. The kaon excess occurs for x <0.6, as expected for a decay product of pair produced charmed mesons near

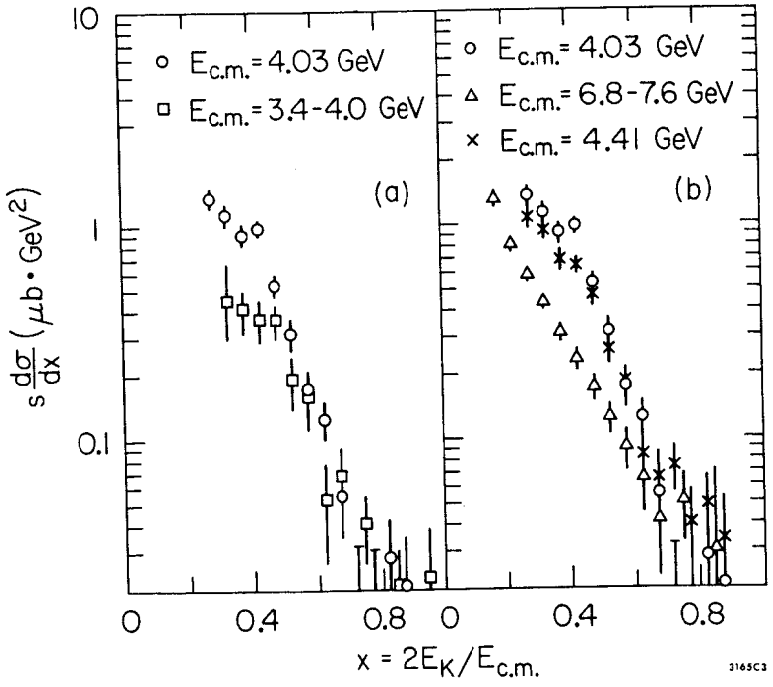

Fig. 16. Inclusive spectra for neutral K mesons as a function of $x = 2E_K/E_{c.m.}$ at various c.m. energies, where E_K denotes the kaon energy and $s = E_{c.m.}^2$. σ refers to twice the K_S cross section. Errors are statistical only.

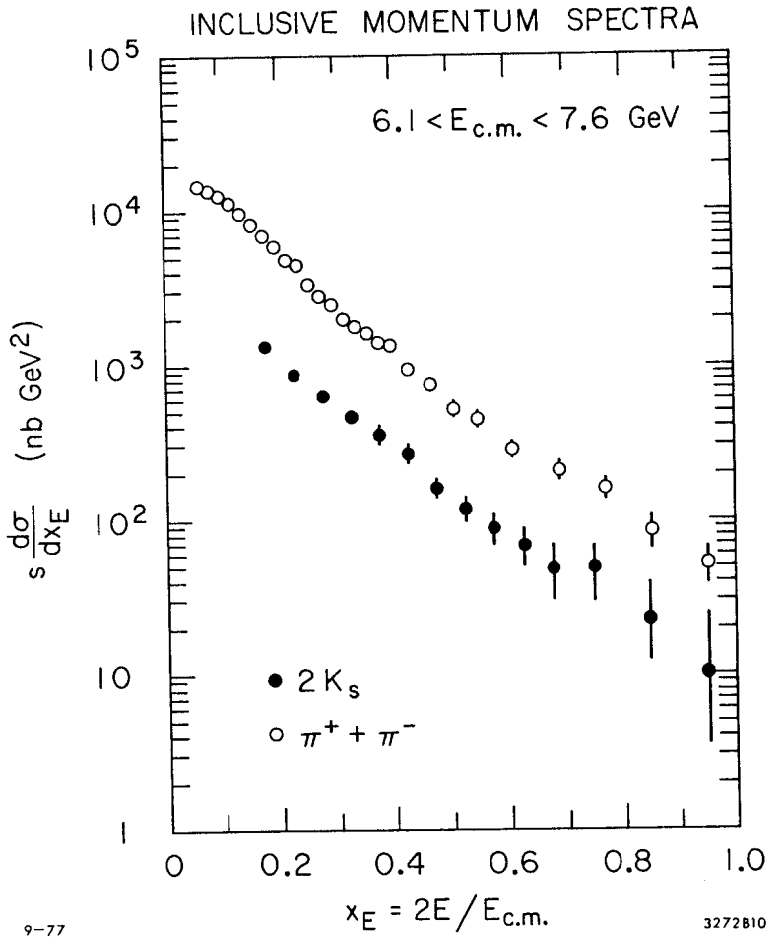

Fig. 17. Comparison of inclusive momentum spectra of charged pions and neutral kaons above 6.1 GeV c.m. energy.

threshold. This interpretation of the enhanced kaon rates has been confimed by the observation of exclusive decays of the D^0 and D^+ mesons.[34,35]

The results presented here are in general agreement with measurements at DESY on inclusive $K^{\pm}$[32] and K_S production,[33] below 5 GeV. Neither DESY group, however, has observed the enhanced kaon yield at the 4.415 GeV structure. This may be due to the fact that their data were not taken at the peak of this resonance, but spread over a much wider range in energy.

2. Inclusive Baryon Production

Protons and antiprotons are identified with the help of the time-of-flight system. This system consists of 48 scintillation counters arranged in a cylindrical array immediately outside the spark chambers at a radius of 1.5 m from the beam axis. Both ends are viewed by photomultipliers and pulse height and delay times of the signals are measured. As time reference the beam collision time is used which is derived from a pick-up electrode. The system is calibrated with Bhabha scattering events. The rms resolution of the system is 0.35 ns, which allows an unambiguous identification of protons and antiprotons up to 1 GeV/c. For higher momenta the following prodecure has been designed to correct for the limited resolution of the TOF system. Using a Monte Carlo simulation of the detector we compute as a function of momentum a matrix of misidentification probabilities ε_{ij}, where the indices i, j stand for π, k, p. The first index corresponds to the measured mass of a particle, the second gives the true ID of a particle. The diagonal element ε_{ii} of this 3 x 3 matrix give the probability that a particle is correctly identified, while the off-diagonal elements ε_{ij} give the misidentification probabilities. For low momenta ε_{ij} becomes a unit matrix, whereas for higher momenta the off-diagonal terms become more important. An inversion of these matrices allows us to evaluate the produced spectra of π, k, and p from the observed spectra. This technique deteriorates at momenta above 2 GeV/c where the particle assignment becomes almost random. We therefore estimate the particle yields in this region by extrapolation of the invariant spectra. The above analysis has been carried out for negative particles only, as to avoid background from beam-gas interactions in the proton yields. Λ and $\bar{\Lambda}$ hyperons are identified by their two-body decay. The vertex reconstruction is identical to the K_S decay. In addition, we require that one of the prongs must have a TOF probability of more than 1% for being a p or $\bar{p}$. We have found a sample of almost 1000 Λ and $\bar{\Lambda}$ decays in 350,000 events.

The efficiencies for events containing Λ hyperons or nucleons have been studied with the help of a Monte Carlo program. The lack of knowledge of the production mechanism and the dynamics of final states containing baryons introduces an overall uncertainty of roughly 25%. The detection efficiency for events containing antiprotons ranges from circa 33% at 3.7 GeV to 50% at 7.4 GeV. The Λ efficiency is calculated to be roughly a factor of three smaller.

The results are presented in Figure 18 in terms of $R_p = 2\sigma_p^-/\sigma_{\mu\mu}$, the ratio of the inclusive charged nucleon to the μ-pair cross section, and $R_\Lambda = (\sigma_\Lambda + \sigma_{\bar{\Lambda}})/\sigma_{\mu\mu}$, the ratio of the inclusive Λ hyperons production to $\sigma_{\mu\mu}$. R_p shows a rapid rise from roughly 0.3 below 4.4 GeV to 0.6 above 5 GeV c.m. energy. R_Λ appears to have a similar increase, though statistical and systematic errors are much worse. R_Λ is about 10-15% of R_p at all energies. The observation of a rise in R_p around 4.4 GeV, well above

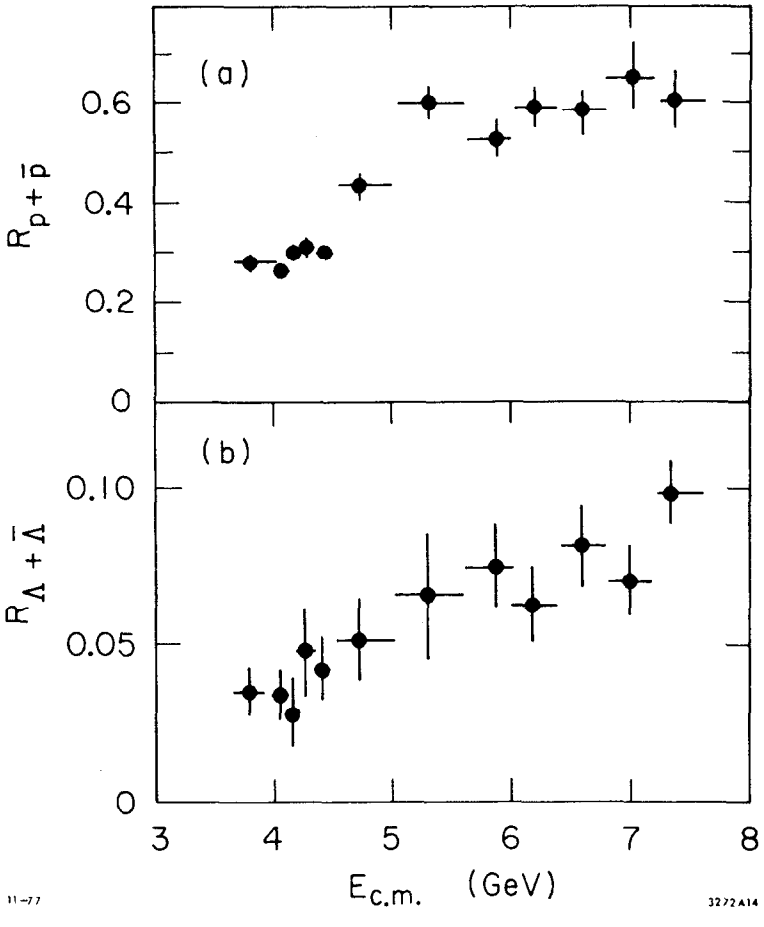

Fig. 18. Inclusive production of baryons as a function of c.m. energy; (a) ratio of charged nucleon to μ-pair production, (b) Λ hyperon to μ-pair production. The errors include statistical and point-to-point systematic uncertainties.

the threshold for charmed mesons near 4 GeV, suggests a baryon threshold near 4.4 GeV. Indeed, candidates for singly charmed, nonstrange baryons have been observed in photoproduction[36] and neutrino interactions.[37]

The most direct evidence for the production of charmed baryons in e^+e^- annihilation would be the observation of peaks in invariant mass distributions of decay products of such baryons. No such peak has been observed, the acceptance of the magnetic detector for the expected decay modes is, however, very low. Therefore, the lack of direct evidence for charmed baryons is still consistent with expected production rates.

If the increase in inclusive baryon cross sections around 4.4 GeV is due to the onset of charmed baryon production the small value of R relative to R_p indicates that their weak decays lead preferentially to nucleons and $\Sigma^{\pm}$ hyperons and not Λ or Σ^0. The easiest explanation for this observation would be a dominant decay of charmed baryons to nucleon, kaon and pions.

VII. SUMMARY

Hadron production by e^+e^- annihilation has developed into an extremely rich and interesting field. The results of the SLAC-LBL experiment at SPEAR can be summarized as follows:

1. Aside from the very narrow resonances ψ (3095) ψ (3684) the variable R, the ratio of hadron to μ-pair production, is approximately constant at a value of 2.6 below 3.5 GeV, and at a value of 4.5 above 6 GeV. These two scaling regions are connected by a region of complicated structure due to charm threshold and resonance formation.

2. Momentum spectra and angular distributions for low multiplicity events clearly deviate from the jet-model predictions and thereby support the existence of a sequential heavy lepton. $\tau^+\tau^-$ production has therefore been subtracted from the hadronic data.
3. The mean charged multiplicity increases logarithmically with energy and after subtraction of the heavy lepton contamination shows a step of 0.7 around 4 GeV.
4. Single particle inclusive spectra exhibit Bjorken scaling for $x > 0.6$ over the energy range from 3.0 GeV to 7.6 GeV.
5. Kaon production follows the rise of the total cross section and shows similar structure near 4 GeV as expected for the charmed meson threshold. Inclusive baryon production suggests a threshold for charmed baryon pair production between 4.5 GeV and 5 GeV.

In *summary, general features of hadron production* e^+e^- *annihilation* are well described by the parton model. The regions of constant R, scaling of inclusive spectra and slow multiplicity rise are direct consequences of the parton picture. The size of the step in R between 3.5 GeV and 5.5 GeV is roughly one standard deviation larger than expected. This could either be explained by quark-gluon interactions that are ignored in the simplest model or be the result of measurement errors. We are looking forward to the second generation experiment at SPEAR that is expected to provide us with a more satisfactory answer.

Acknowledgements

The results presented here are based on the work of the SLAC-LBL collaboration (SP-17) that includes the following members:

G. S. Abrams, M. S. Alam, A. M. Boyarski, M. Breidenbach, W. C. Carithers, W. Chinowsky, S. C. Cooper, J. M. Dorfan, G. J. Feldman, D. Fryberger, G. Goldhaber, G. Hanson, J. Jaros, A. D. Johnson, J. A. Kadyk, R. R. Larsen, D. Lüke, H. L. Lynch, R. J. Madaras, H. K. Nguyen, J. M. Paterson, M. L. Perl, I. Peruzzi, M. Piccolo, F. M. Pierre, T. P. Pun, P. Rapidis, B. Richter, R. H. Schindler, R. F. Schwitters, J. Siegrist, W. Tanenbaum, G. H. Trilling and J. E. Wiss.

Much of the analysis of the unpublished data on total cross section and inclusive spectra was done by J. Siegrist and R. F. Schwitters, S. Cooper and W. Chinowsky. I am very grateful for their help in the preparation of this talk.

REFERENCES

1. R. Wilson, Proc. Int. Conf. High Energy Physics; Kiev, USSR (1972).

2. B. Bartoli et al., Phys. Rev. D6, 2374 (1972).

3. C. Bacci et al., Phys. Lett. B44, 533 (1973).

4. F. Ceradini et al., Phys. Lett. B47, 80 (1973).

5. M. Bernardini et al., Phys. Lett. B51, 200 (1974).

6. G. Cosme et al., Phys. Lett. B40, 685 (1972).

7. L. M. Kudadze et al., Phys. Lett. B42, 515 (1972).

8. A. Litke et al., Phys. Rev. Lett. 30, 1189 (1973); G. Tarnopolsky et al., Phys. Rev. Lett. 32, 432 (1974).

9. J.-E. Augustin et al., Phys. Rev. Lett. 34, 764 (1974); J. Siegrist et al., Phys. Rev. Lett. 36, 700 (1976).

10. J. Burmester et al., Phys. Lett. 66B, 395 (1977).

11. W. de Boer, talk presented at this conference.

12. J.-E. Augustin et al., Phys. Rev. Lett. 33, 1406 (1974).

13. J. J. Aubert et al., Phys. Rev. Lett. 33, 1404 (1974).

14. G. S. Abrams et al., Phys. Rev. Lett. 33, 1433 (1974).

15. R. F. Schwitters, Proc. 1975 Int. Symposium on Lepton-Photon Interactions at High Energies, Stanford 1975, p. 5.

16. S. D. Drell, T. M. Yan, Phys. Rev. 187, 2159 (1969) ibid, D1, 1617 (1970).

17. G. Hanson et al., Phys. Rev. Lett. 35, 1609 (1975).

18. M. L. Perl et al., Phys. Rev. Lett. 35, 1489 (1975).
M. L. Perl et al., Phys. Lett. 63B, 466 (1976).
J. Burmester et al., Phys. Lett. 68B, 297 (1976).
J. Burmester et al., Phys. Lett. 68B, 301 (1976).
R. Brandelik et al., Phys. Lett. 70B, 125 (1977).
G. Feldman et al., Phys. Rev. Lett. 38, 177 (1976).
J. Jaros et al., submitted to Phys. Rev. Lett.
M. L. Perl, Invited talk at the Lepton-Photon Symposium, Hamburg (1977), SLAC-PUB-2022 (1977).

19. Y. S. Tsai, Phys. Rev. D4, 2821 (1971).

20. M. Piccolo et al., Phys. Lett. 70B, 260 (1977).
G. Goldhaber et al., Phys. Lett. 69B, 503 (1977).

21. J. Siegrist et al., Phys. Rev. Lett. 36, 700 (1976).

22. J. Burmester et al., Phys. Lett. 66B, 395 (1976).

23. W. de Boer, talk presented at this conference.

24. J. Whitmore, Phys. Reports 10C, 273 (1974).

25. G. Feldman, talk presented at this conference; SLAC-PUB 2000 (1977).

26. J. G. Rushbrook et al., Phys. Lett. 59B, 303 (1975).

27. C. Bromberg et al., Phys. Rev. D9, 1863 (1974).
C. Bromberg et al., Nuclear Phys. B107, 82 (1976).

28. H. Miettinen, Symposium on $\bar{N}N$ Interactions, CERN 74-18 (1974).

29. R. Brandelik et al., Phys. Lett. 67B, 358 (1977).

30. V. Luth et al., Phys. Lett. 70B, 120 (1977).

31. M. Piccolo et al., submitted to Phys. Rev. Lett. (1977); SLAC-PUB-2023.

32. R. Brandelik et al., Phys. Lett. 67B, 363 (1977).

33. J. Burmester et al., Phys. Lett. 67B, 367 (1977).

34. G. Goldhaber et al., Phys. Rev. Lett. 37, 255 (1976).

35. I. Peruzzi et al., Phys. Rev. Lett. 37, 569 (1976).

36. B. Knapp et al., Phys. Rev. Lett. 37, 882 (1976).

37. E. G. Cazzoli et al., Phys. Rev. Lett. 34, 1125 (1975).

Properties of the D Mesons*

G.J. Feldman

Stanford Linear Accelerator Center
Stanford University, Stanford, California

I. Introduction

The purpose of this talk is to review what we have learned from the study of non-leptonic decays of D mesons.[1] The relevant world data come from two experiments which were performed using the same detector, the SLAC-LBL magnetic detector at SPEAR.[2] SLAC experiment SP17 ran on the magnetic detector through July 1976; experiment SP26 ran from October 1976 through June 1977. The SP17 data which we shall use are published[3] or have been submitted for publication.[4,5] However, with one exception,[6] the SP26 data are unpublished and preliminary.[7]

In section II, we shall review briefly the measurements of the $\psi(3772)$ since it will play a major role in the determination of D meson properties. Section III will discuss the accurate determination of D masses and their consequences. Inclusive measurements and tagged events will be the subjects of sections IV and V, respectively. The distinction between inclusive measurements and tagged events is that in the former one detects a D decay and ignores the remainder of the event, while in the latter, one detects a D decay and studies the remainder of the event.

Due to a lack of time, we shall not be able to cover a number of important topics on which we have experimental information. These include D and D* spins,[8] D^0-$\overline{D^0}$ mixing,[3,4] and ρ and K* formation in D decays.[5,9]

---

*Work supported by the Energy Research and Development Administration.

II. $\psi(3772)$

Figure 1 shows the ratio R of the total cross section for hadron production to the cross section for the production of μ pairs in the energy region 3.6 to 4.6 GeV. The closed circles represent recent SP26 data[6] and show a clear resonance near 3.77 GeV, just above the threshold for the production of D meson pairs. The crossed point[10] and the open squares[11] represent older SP17 data. It is interesting to note that there are sharp rises in R just after each of the D and D* thresholds: $D\bar{D}$ at 3.727 GeV, $D\bar{D}^*$ at 3.869 GeV, and $D^*\bar{D}^*$ at 4.012 GeV.

The question most often asked upon showing someone Figure 1 is "How was it missed before?" The answer is twofold. First, Figure 1 has been corrected for radiative effects in the initial state. The data before these corrections are shown in Fig. 2a, and these data correspond to what we actually observe. The $\psi(3772)$ (or ψ'') is partially obscured by the ψ' radiative tail, and is thus harder to see in a cross section scan. The second part of the answer is simply that insufficient data were collected in this energy region. Evidence for the ψ'' at the two standard deviation level was actually obtained over a year ago.[12]

The next most often asked question is "Into what does it decay?" A partial answer is provided by Fig. 3 which shows the cross section times branching fraction ($\sigma \cdot B$) for the D decay into $K^{\mp}\pi^{\pm}$. It is clear that $D\bar{D}$ is one of the resonant channels. Through section IV we will assume that $D\bar{D}$ is the only substantial decay made of the ψ''. The rationale is that the ψ' and ψ'' differ in mass by only 88 MeV/c^2 and thus should have similar decay modes to channels which are open to both states. However, the total ψ'' width is two orders of magnitude larger than the ψ' width. The simplest explanation for the difference in widths is to

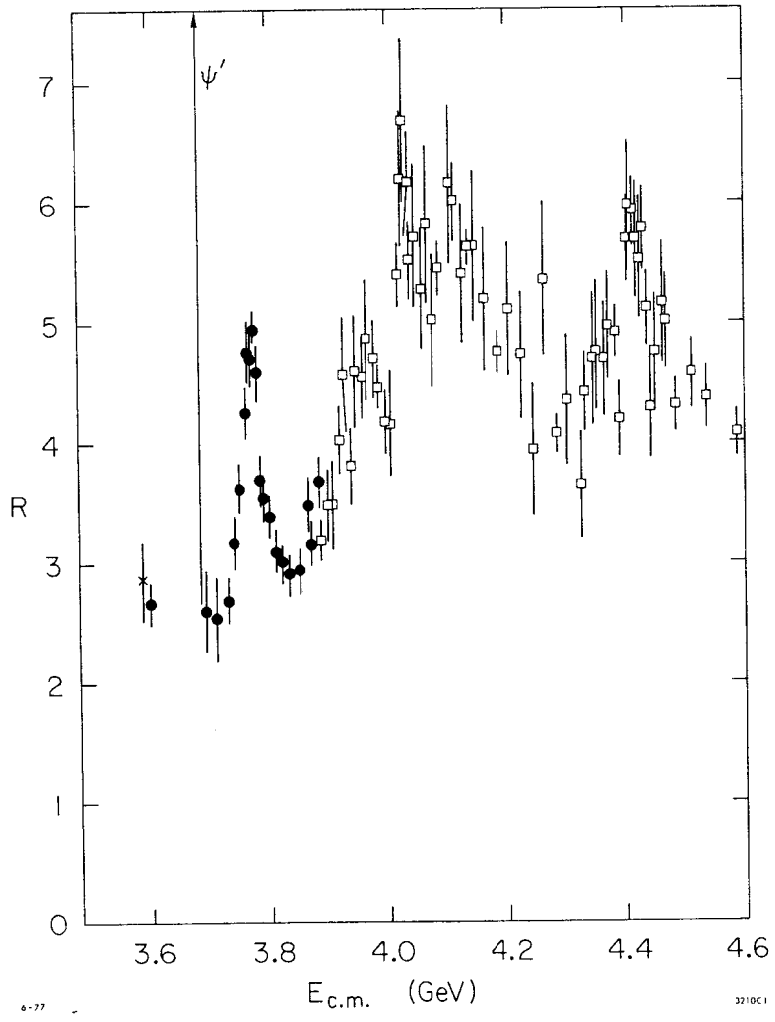

FIG. 1. R vs. $E_{c.m.}$

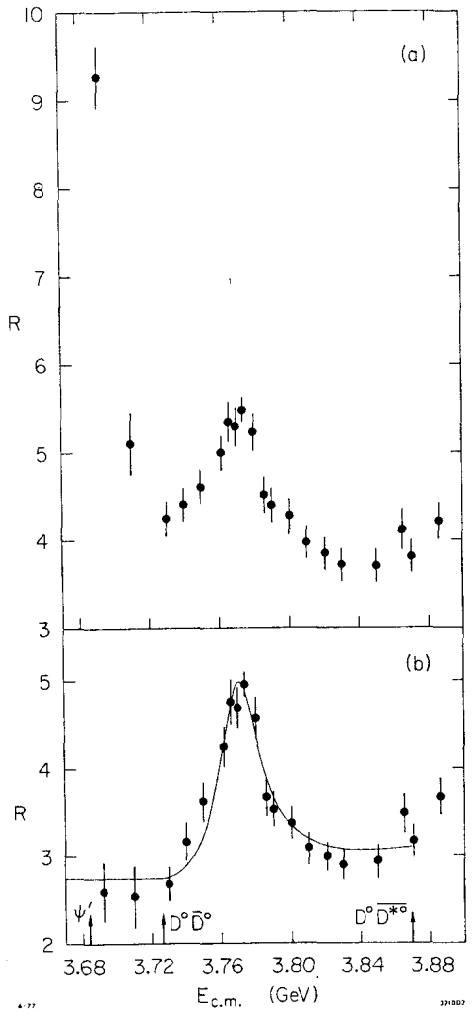

FIG. 2. R vs. $E_{c.m.}$ (a) before and (b) after corrections for radiative effects. The curve is a p-wave Breit-Wigner shape described in the text.

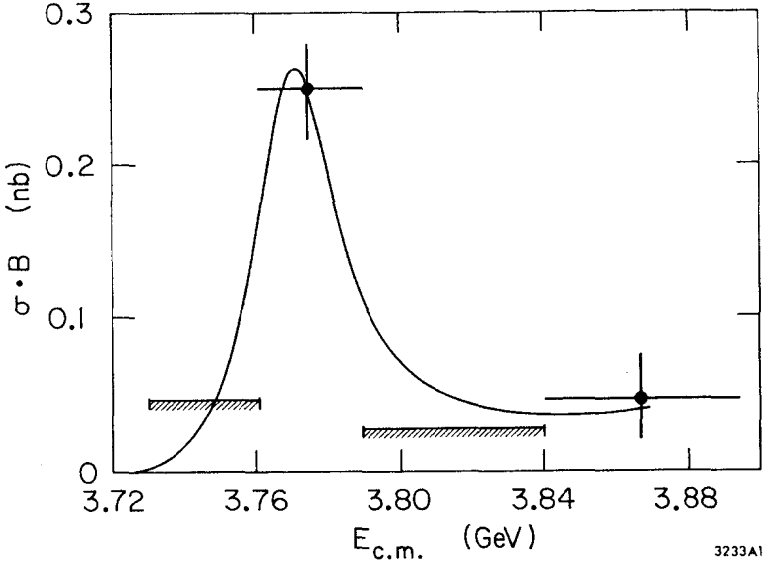

FIG. 3. $\sigma \cdot B$ for $D^0 \to K^{\mp}\pi^{\pm}$ vs. $E_{c.m.}$ The curve is the ψ'' line shape and charmed particle background parameterization shown in Fig. 2.

attribute most of the ψ'' width to the $D\bar{D}$ channel, which is accessible to it, but not to the ψ'. This is a dramatic example of the Okubo-Zweig-Iizuka rule. In section V, we will show that the measured $\psi'' \to D\bar{D}$ branching fraction is consistent with this assumption.

To fit the ψ'' line shape we use the Breit-Wigner form

$$R = \frac{3\pi}{\sigma_{\mu\mu} m^2} \frac{\Gamma_{ee}\Gamma(E)}{(E_{c.m.} - m)^2 + \Gamma^2(E)/4} \quad . \qquad (1)$$

To account for the proximity of the $D\bar{D}$ threshold, we give the width Γ an energy dependence

$$\Gamma(E) \propto \frac{p_o^3}{1 + (rp_o)^2} + \frac{p_+^3}{1 + (rp_+)^2} \quad , \qquad (2)$$

where p_o and p_+ represent the momenta of a D^o and a D^+ respectively, from D pair production, and r represents an interaction radius.[13] In writing Eq. 2 we have assumed that, except for phase space, decays to $D^o\bar{D}^o$ and D^+D^- are equally likely. This is equivalent to assuming that the ψ'' has a definite isospin, either 0 or 1. Although this assumption is not crucial here, it will become important in section IV.

We have obtained acceptable fits for all values of r greater than 1 fm. Figure 2b shows a fit for r = 3 fm. It is interesting to note that fits with energy independent widths give considerably better χ^2's than the one shown in Fig. 2b. This is due to the inability of the p-wave fits to accomodate the high values of R on the leading edge. This effect is not significant in the present data, but warrants watching.

The results of the fits to the ψ'' and the other isolated ψ resonances are given in Table I.[6,11,14,15] This Table differs from the original papers in not including the 0.13% uncertainty in the absolute SPEAR energy callibration. Thus the ψ is defined to have mass 3095 MeV/c^2 and all other mass measurements are technically measurements of the ratio of a given mass to the ψ mass. This convention is necessary to give meaning to the D mass measurements which will be presented in the next section and which have a precision of better than one part in 10^3.

TABLE I

Resonance parameters for the isolated ψ resonances. Γ is the full width, Γ_{ee} is the partial width to electron pairs, and B_{ee} is the branching fraction to electron pairs. See the text for an explanation of the errors on the mass.

State	Mass (MeV/c^2)	Γ (MeV/c^2)	Γ_{ee} (keV/c^2)	B_{ee}
ψ	3095	0.069 ± 0.015	4.8 ± 0.6	0.0069 ± 0.009
ψ'	3684 ± 1	0.228 ± 0.056	2.1 ± 0.3	$(9.3 \pm 1.6) \times 10^{-3}$
ψ''	3772 ± 3	28 ± 5	0.37 ± 0.09	$(1.3 \pm 0.2) \times 10^{-5}$
$\psi(4414)$	4414 ± 5	33 ± 10	0.44 ± 0.14	$(1.3 \pm 0.3) \times 10^{-5}$

III. Masses

A. D^o and D^+ Masses

To calculate a mass one uses the formula

$$m = (E^2 - p^2)^{\frac{1}{2}} \quad . \qquad (3)$$

The advantage of studying $e^+e^- \to D\bar{D}$ is that the energy E must equal E_b, the energy of one of the incident beams. E_b has an rms spread, due to quantum fluctuations in synchrotron radiation, of only about 1 MeV,[16] and its central value can be monitored to high precision.[17] For $D\bar{D}$ production near threshold, as in ψ'' decays, we have the additional advantage that

p^2 is small, about 0.08 $(GeV/c)^2$. Thus any error in p is demagnified in its effect on the determination of the mass. The final result is that we measure masses in ψ'' decays with an rms resolution of about 3 MeV/c^2, which is a factor of 5 to 10 better than they can be measured at higher energies.

Charged kaons are identified by time-of-flight measurements[18] and neutral kaons are identified by measurement of the dipion mass and the consistency of the dipion vertex with the assumed kaon decay.[19] For each particle combination we first require that the measured energy agree with E_b to within 50 MeV and then calculate the mass from Eq. 3 with $E = E_b$. The results, given in Fig. 4 in 4 MeV/c^2 wide bins, show clear signals in five modes including the previously unreported mode $D^- \to K_s^0 \pi^-$. Figure 5 shows the D^+ and D^0 mass spectra for the sum of all observed modes in 2 MeV/c^2 bins. The mass difference of about 5 MeV/c^2 between the D^+ and D^0 is clearly visible. Fits to the mass spectra give

$$M_{D^0} = 1863.3 \pm 0.9 \text{ MeV}/c^2 \qquad (4)$$

and

$$M_{D^+} = 1868.4 \pm 0.9 \text{ MeV}/c^2 \ . \qquad (5)$$

The errors are dominated by systematic uncertainties such as the absolute momentum calibration and the stability of E_b monitoring. The D^+-D^0 mass difference is determined to be 5.1 ± 0.8 MeV/c^2; it is known more precisely than either D mass because several systematic errors cancel in the mass difference. The theoretical estimate of this mass difference has been widely discussed with estimates ranging from 2 to 15 MeV/c^2.[20]

B. D^{*o} Mass

To obtain the D^{*o} mass we employ the same trick with $D^{*o}\overline{D^{*o}}$ production at 4.028 GeV with the following differences:[4]

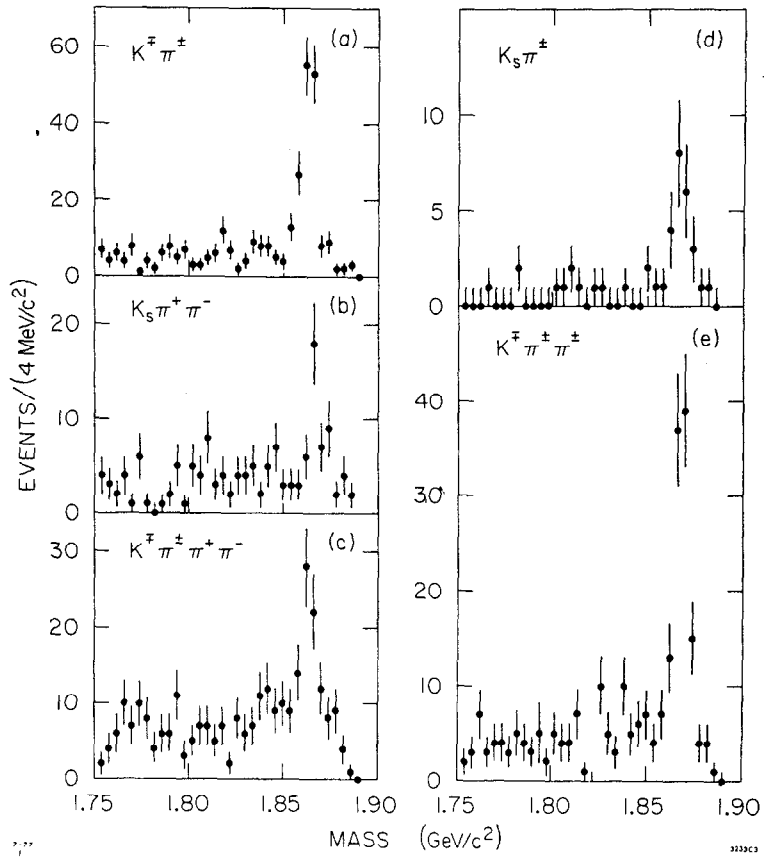

FIG. 4. Invariant mass spectra for various D decay modes at the ψ''.

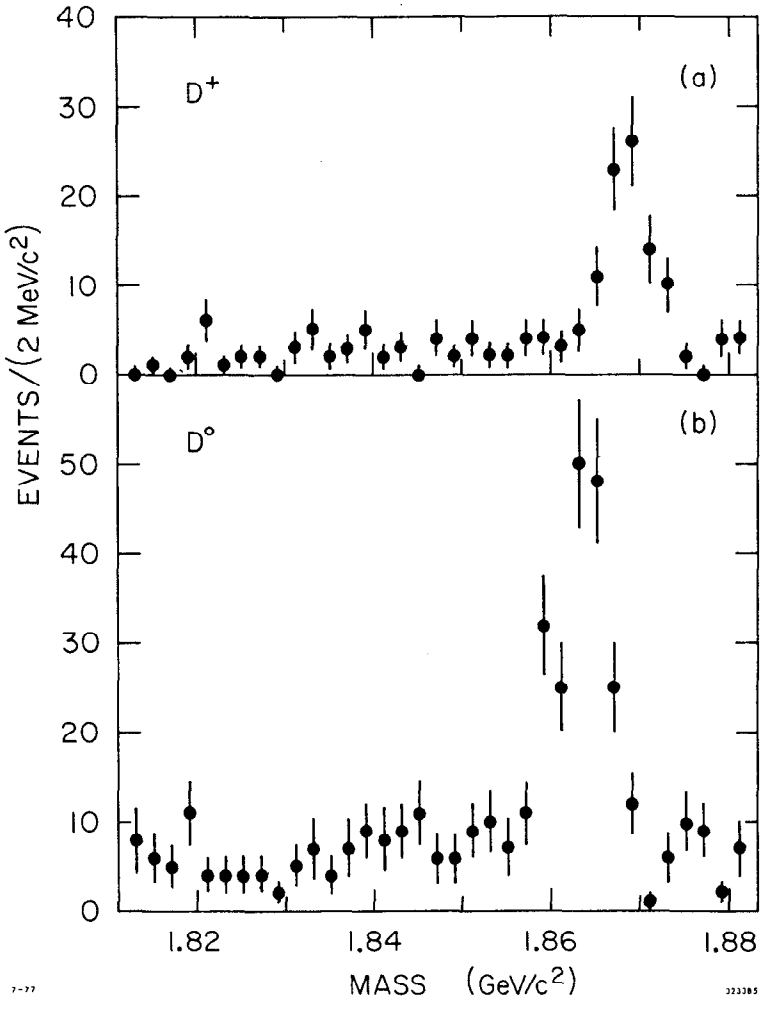

FIG. 5. Invariant mass spectra for the sum of all observed (a) D^+ and (b) D^0 decay modes.

a) We observe the D^0 from $D^{*0} \to D^0\pi^0$ decay. Since the Q value of the reaction is small, the D^0 carries off most of the D^{*0} momentum. Thus the detection of the D^0 rather than the D^{*0} causes no real problem.

b) There is contamination from $D^{*+} \to D^0\pi^+$ and $D^{*0} \to D^0\gamma$ decays. Figure 6a shows the contributions to the D^0 momentum spectrum. The problem here is to determine the center of peak B $[D^{*0} \to D^0\pi^0]$ in the presence of peaks A $[D^{*+} \to D^0\pi^+]$ and C $[D^{*0} \to D^0\gamma]$.

The data and a fit to the data are shown in Fig. 6b. The D^{*0} mass is determined to be 2006 ± 1.5 MeV/c^2. The uncertainty is larger here than it was for the D^0 or D^+ because of the difficulty of extracting the signal and because the fit is not perfect.

C. D^{*+} Mass

There are insufficient statistics to enable us to observe $D^{*+}D^{*-}$ production at 4.028 GeV (see Fig. 6c), so another method is used to obtain the D^{*+} mass: We observe the $D^{*+} \to D^0\pi^+$ decay directly.[3] Since the Q value is small the π^+ momentum will be only m_π/m_{D^*} ($\approx 7\%$) of the D^* momentum. It is thus necessary to use high momentum D^*'s from high energy data ($\langle E_{c.m.} \rangle = 6.8$ GeV) to obtain pions with enough momentum to be visible in the magnetic detector.

The kinematics in this case are not as transparent as they were in the previous cases, but the essential point is that the Q value determines the kinematics and even a crude measurement of the Q value translates into a very precise measurement of the D^{*+} mass. Figure 7 shows the D^{*+}-D^0 mass difference in 1 MeV/c^2 bins. The Q value is determined to be 5.7 ± 0.5 MeV which, when combined with the D^0 mass, yields a D^{*+} mass of 2008.6 ± 1.0 MeV/c^2.

D. Mass Differences and Q Values

We previously gave the mass difference

$$\delta \equiv m_{D^+} - m_{D^0} = 5.1 \pm 0.8 \text{ MeV}/c^2 \quad . \qquad (6)$$

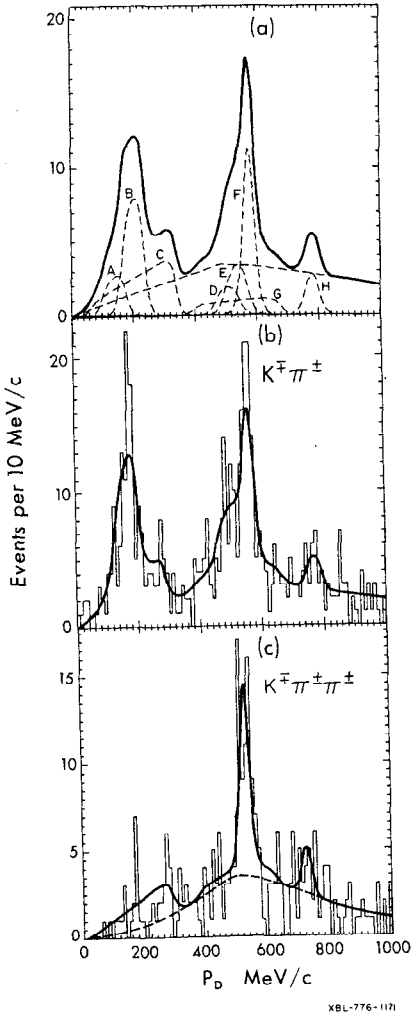

FIG. 6. D momentum spectra at 4.028 GeV for (b) $D^o \to K^{\mp}\pi^{\pm}$ and (c) $D^{\pm} \to K^{\mp}\pi^{\pm}\pi^{\pm}$. The solid curves represent an isospin contrained fit to the data. (a) shows the various contributions to the fit in (b). A,B, and C are contributions from $D^*\overline{D}^*$ production with A: $D^{*+} \to D^o\pi^+$, B: $D^{*o} \to D\pi o$ and C: $D^{*o} \to D^o\gamma$. See Ref. 4 for remainder of key.

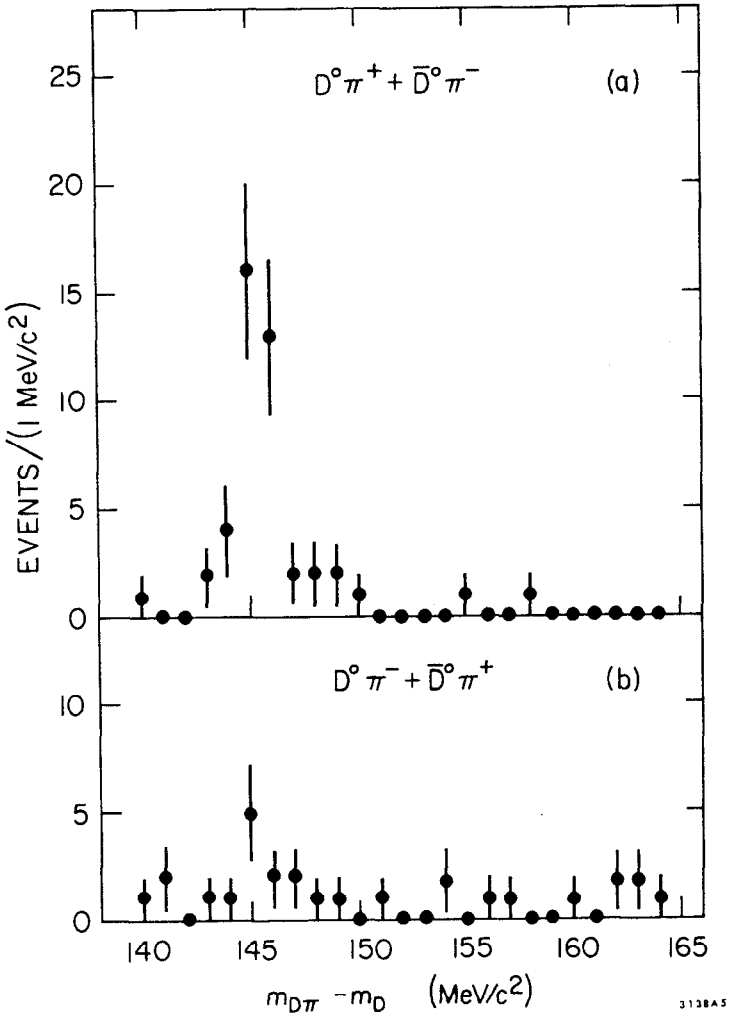

FIG. 7. $D\pi$ - D mass difference spectra for (a) $D^o\pi^+$ and $\overline{D}^o\pi^-$ combinations and (b) $\overline{D}^o\pi^+$ and $D^o\pi^-$ combinations.

We can now add

$$\delta^* \equiv m_{D^{*+}} - m_{D^{*o}} = 2.6 \pm 1.8 \text{ MeV/c}^2 \qquad (7)$$

and

$$\delta - \delta^* = 2.5 \pm 2.4 \text{ MeV/c}^2 \qquad (8)$$

The quantity $\delta - \delta^*$ is an electromagnetic hyperfine splitting for which theoretical estimates vary between 0 and 3 MeV/c^2.[20] The error given in Eq. 8 is somewhat larger than would be naively expected from Eqs. 6 and 7 because of correlations in the errors.

The Q values for $D^* \to D\pi$ and $D^* \to D\gamma$ are given in Fig. 8. The decay $D^{*o} \to D^+\pi^-$ appears to be kinematically forbidden in the limit of zero D^{*o} width. Even allowing for finite D^* width, it cannot be an important decay mode.

E. D^* Branching Fractions

The D^{*o} branching fractions have been determined from the D^o momentum spectrum at 4.028 GeV by fitting the relative contribution of curves B and and C in Fig. 7a.[4] The result is $B(D^{*o} \to D^o\gamma) = 0.45 \pm 0.15$.[21] The D^{*+} branching fractions were not well determined from the 4.028 GeV data due to insufficient statistics, but we can now calculate them using the $D^* \to D\pi$ Q values and a few reasonable assumptions.

The inputs are:

a) D and D^* masses, and

b) $B(D^{*o} \to D^o\gamma)$.

The assumptions are:

a) Isospin conservation in $D^* \to D\pi$ decays,

b) $\Gamma(D^* \to D\pi)$ is proportional to p^3 where p is the D momentum in the D^* rest frame, and

c) the quark model prediciton for $\Gamma(D^* \to D\gamma)$:[22]

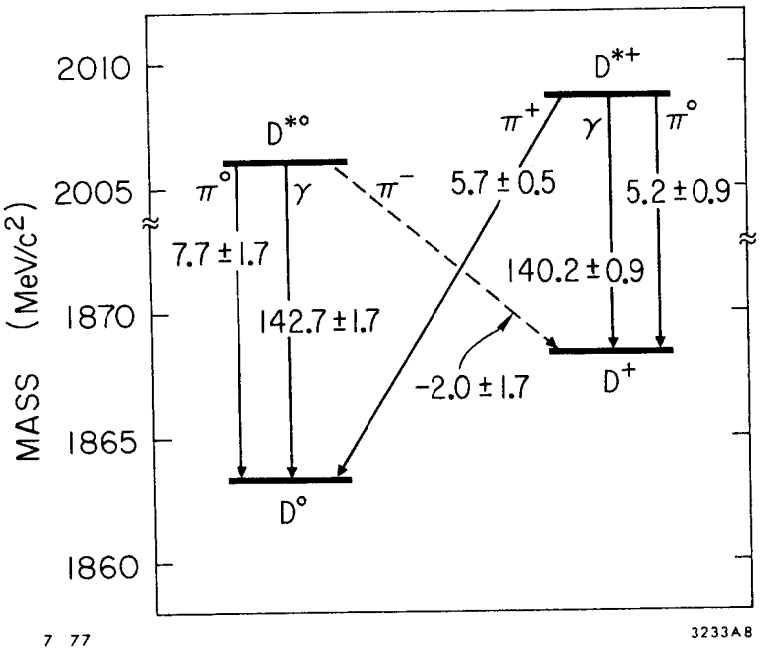

FIG. 8. Q values for $D^* \to D$ transitions.

$$\frac{\Gamma(D^{*+} \to D^{+}\gamma)}{\Gamma(D^{*o} \to D^{o}\gamma)} = \frac{(\mu_c - \mu_{\bar{d}})^2}{(\mu_c - \mu_{\bar{u}})^2} \quad , \tag{9a}$$

where μ is a quark magnetic moment which we assume is inversely proportional to the quark mass. Thus,

$$\frac{\Gamma(D^{*+} \to D^{+}\gamma)}{\Gamma(D^{*o} \to D^{o}\gamma)} = \left(\frac{2\frac{m_u}{m_c} - 1}{2\frac{m_u}{m_c} + 2} \right)^2 \tag{9b}$$

taking $m_d = m_u$. The quark masses are not real masses and cannot be determined with any real accuracy. We will thus take two extreme cases to test the sensitivity of this assumption: $m_u/m_c = m_\rho/m_\psi$ and $m_u/m_c = 0$. We obtain

$$\frac{\Gamma(D^{*+} \to D^{+}\gamma)}{\Gamma(D^{*o} \to D^{o}\gamma)} = \begin{cases} 1/25 \text{ for } \frac{m_u}{m_c} = \frac{m_\rho}{m_\psi} \\ \\ 1/4 \text{ for } \frac{m_u}{m_c} = 0 \ . \end{cases} \tag{9c}$$

The results are given in Table II. Independent of the details of assumption (c), $B(D^{*+} \to D^{+}\gamma)$ is small, and $B(D^{*+} \to D^{o}\pi^{+})$ is about twice as large as $B(D^{*+} \to D^{+}\pi^{o})$. By accident, the total D^{*o} width is about equal to the D^{*+} width. The best experimental information on D^{*} widths comes from Fig. 7 from which we can deduce that $\Gamma_{D^{*+}} < 2.0$ MeV/c^2 at the 90% confidence level.[3]

TABLE

D^{*} branching fractions and w
of the input data and the assumpt

	D^{*o}
$B(D^{*} \to D\pi^{\pm})$	0
$B(D^{*} \to D\pi^{o})$	0.55 ± 0.15
$B(D^{*} \to D\gamma)$	0.45 ± 0.15
$\Gamma(D^{*o})/\Gamma(D^{*+})$	---

IV. Inclusive Measurements

A. Relative Branching Fractions

The cross section times branching have been determined at $E_{c.m.} = 3.774$, the ψ'' (i.e. 3.774 GeV) are shown in F GeV are shown in Fig. 9.[5] The results D^{o} branching fractions from 3.774 GeV data from 4.414 are not in as good agr there are higher backgrounds at 4.414 difficult to extract the signal. No c decays has been seen at any energy. T for $E_{c.m.} = 4.028$ GeV which are consis suppression.

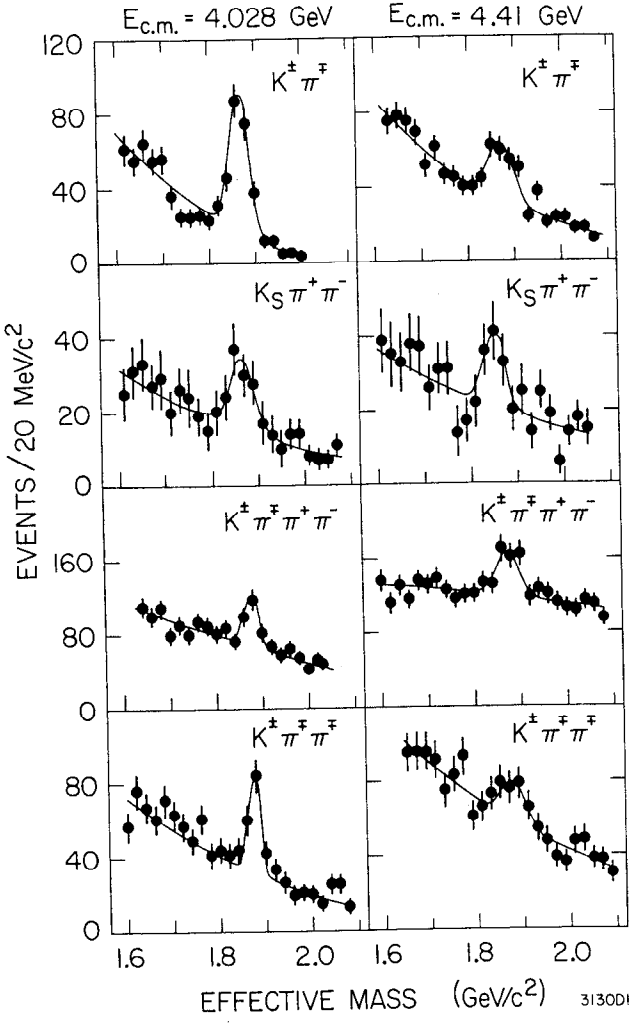

FIG. 9. Invariant mass spectra for various D decay modes at 4.028 and 4.414 GeV.

TABLE III

$\sigma \cdot B$ in nb for various D decay modes at three values of $E_{c.m.}$

Mode		$E_{c.m.}$ (GeV) 3.774	4.028	4.414
D^o	$K^+\pi^-$	0.27 ± 0.05	0.57 ± 0.11	0.30 ± 0.09
	$\bar{K}^o\pi^+\pi^-$ + c.c.	0.44 ± 0.11	1.09 ± 0.30	0.91 ± 0.34
	$K^+\pi^-\pi^+\pi^-$	0.34 ± 0.09	0.83 ± 0.27	0.91 ± 0.39
	$\pi^+\pi^-$	---	< 0.04	---
	K^+K^-	---	< 0.04	---
Total D^o observed modes		1.05 ± 0.15	2.49 ± 0.42	2.12 ± 0.53
D^+	$\bar{K}^o\pi^+$ + c.c.	0.15 ± 0.05	< 0.18	---
	$K^+\pi^-\pi^+$	0.34 ± 0.05	0.40 ± 0.10	0.33 ± 0.12
	$\pi^+\pi^-\pi^+$	---	< 0.03	---

B. Absolute Branching Fractions

In the ψ'' we have for the first time a situation in which charm production is sufficiently simple that we can use measurements of the total cross section and of $\sigma \cdot B$ for D decay modes to calculate absolute branching fractions.

The inputs are

a) $\sigma \cdot B$ measurements at the ψ'' given in section IV.A, and

b) the total cross section measurements in the vicinity of the ψ'' given in section II.

The assumptions are

a) The ψ'' is a state of definite isospin, either 0 or 1. This assumption gives equal partial widths to $D^o\bar{D}^o$ and D^+D^- except for phase

space factors.

b) The phase space factors are given by Eq. 2. The value of r is not known, but as r varies from 0 to infinity, the fraction of $D^0\overline{D^0}$ changes from 0.59 to 0.53. We can thus take this fraction to be 0.56 ± 0.03. The error due to the uncertainty in r is small compared to other systematic errors.

c) $D\bar{D}$ is the only substantial decay mode of the ψ''. The rationale for this assumption was discussed in section II.

The results are given in Table IV. The $\bar{K}^0\pi^+$ decay mode of the D^+ is comparable in size to the $D^0 \to K^-\pi^+$ decay mode. This decay does not appear to be suppressed as was suggested from the analogue of octet enhancement in strangeness changing decays.[23]

TABLE IV

D branching fractions. See the text for a discussion of the input data and the assumption which were used.

Mode		Branching fraction (%)
D^0	$K^-\pi^+$	2.2 ± 0.6
	$\overline{K^0}\pi^+\pi^-$	3.5 ± 1.1
	$K^-\pi^+\pi^-\pi^+$	2.7 ± 0.9
D^+	$\overline{K^0}\pi^+$	1.5 ± 0.6
	$K^-\pi^+\pi^+$	3.5 ± 0.9

C. Comparison to the Statistical Model

It is instructive to compare the absolute branching fractions given in Table IV to the predictions of a statistical model. This model, due to Rosner,[24] uses a Poisson multiplicity distribution and, within each multiplicity, equal contributions from each isospin amplitude. There is no real theoretical justification for this model and one should probably view its predictions with a certain degree of skepticism. Nevertheless, it can serve as a crude guide to the reasonableness of our measurements.

The statistical model predicitons are given in terms of the ratio of a given state to the sum of all states of the form $K + n\pi$. Therefore we will define $f_{Kn\pi}$ to be the ratio

$$f_{Kn\pi} = \frac{\Sigma B(D \to K + n\pi)}{B(D \to \text{all})} \quad . \tag{10}$$

In addition to $K + n\pi$, "all" will include $K\eta + n\pi$, semi-leptonic decays, and Cabbibo suppressed decays. In Table V we list the prediction times $f_{Kn\pi}$ divided by the measurement. We expect this quantity to be unity, but it appears that this will be true only if $f_{Kn\pi}$ is about 0.35. This value seems low as we would expect a value of 0.6 or higher if the semileptonic branching fractions are of the order of 0.2 for the sum of electronic and muonic modes.[1] We may have here the start of a D branching ratio crisis, but I think we should reserve judgement until some modes involving π^0's are measured.

TABLE V

Comparison of the absolute D branching fractions from Table IV with the statistical model of Ref. 24. See text for the definition of $f_{Kn\pi}$.

mode		prediction/measurement
D^0	$K^-\pi^+$	$(2.7 \pm 0.7)\ f_{Kn\pi}$
	$\overline{K^0}\pi^+\pi^-$	$(3.4 \pm 1.1)\ f_{Kn\pi}$
	$K^-\pi^+\pi^-\pi^+$	$(2.6 \pm 0.9)\ f_{Kn\pi}$
D^+	$\overline{K^0}\pi^+$	$(8.7 \pm 3.5)\ f_{Kn\pi}$
	$K^-\pi^+\pi^+$	$(2.9 \pm 0.7)\ f_{Kn\pi}$

D. Charm Production at 4.028 and 4.414 GeV

With the absolute branching fractions from Table IV we are now in a position to calculate the amount of charm production at two of the prominent peaks in the 4 GeV region.

The inputs are

a) $\sigma \cdot B$ from Table III,[5] and

b) B from Table IV.

There are no additional assumptions to those already used in constructing Table IV.

We define $R_D = \sigma_D/(2\sigma_{\mu\mu})$. The factor of 2 in the denominator takes into account the fact that charmed particles are produced in pairs, so that R_D can be directly compared to the total hadronic R. In particular, we compare it to

$$R_{new} \equiv R - R_{old} - R_\tau \qquad (11)$$

where R is taken from measurements of the total hadronic cross section,[11] R_{old} (2.6) is taken from measurements of the total hadronic cross section below charm threshold,[6] and R_τ is the theoretical expression for the production of a 1.9 GeV/c^2 mass lepton.

$$R_\tau = \tfrac{1}{2}\beta(3 - \beta^2) \quad . \qquad (12)$$

If D's and τ's are the only new particles being produced then R_{new} should equal R_D. If the production of F's, charmed baryons, or even other new particles are sizable, then R_{new} will be larger than R_D.

The results are given in Table VI. R_{D^0} is calculated from all observed D^0 modes and also from just the better-measured $K^-\pi^+$ mode. At 4.028 GeV these two measurements are consistent and R_{new} is consistent with being equal to R_D. At 4.414 GeV the two measurements differ somewhat, but nevertheless it is clear that whatever else may be happening at 4.414 GeV, most of the excess cross section is going into D production.[25]

We shall return to a discussion of $R_{D^\pm}/R_D$ in section IV.F.

TABLE VI

Charm production at 4.028 and 4.414 GeV. See text for definitions and a discussion of the input data and assumptions which were used.

	4.028 GeV		4.414 GeV	
	all D^0 modes	$K^-\pi^+$ only	all D^0 modes	$K^-\pi^+$ only
R_{D^0}	2.8 ± 0.7	2.4 ± 0.9	2.8 ± 0.9	1.5 ± 0.6
$R_{D^\pm}$	1.1 ± 0.4	1.1 ± 0.4	1.1 ± 0.5	1.1 ± 0.5
R_D	3.9 ± 0.8	3.5 ± 0.9	3.9 ± 1.0	2.6 ± 0.8
R_{new}	3.4 ± 1.1	3.4 ± 1.1	2.7 ± 1.1	2.7 ± 1.1
$R_{D^\pm}/R_D$	0.28 ± 0.09	0.31 ± 0.10	0.28 ± 0.11	0.42 ± 0.14

E. Charm Production at High Energy

The calculation of charm production in the high energy continuum is not as straight forward as it was at 4.028 and 4.414 GeV because

a) There are no measurements of D^+ production in this region, and

b) The best measurements of D^0 production are somewhat incomplete and indirect.

However, there is just enough information to justify a crude calculation.

The inputs are

a) $\sigma_{D^{*\pm}} \cdot B(D^{*+} \to D^0\pi^+) \cdot B(D^0 \to K^-\pi^+) = 13 \pm 4$ pb,[3]

b) $(25 \pm 9)\%$ of D^0 production comes from D^{*+} production,[3] and

c) $B(D^0 \to K^-\pi^+)$ from Table IV.

Due to the techniques employed in Ref. 3, inputs (a) and (b) refer only to D^0's with momenta greater than 1.5 GeV/c. We shall thus only be able

to calculate a lower limit on R_D, although there is likely to be only a small amount of low momentum D production.

The assumptions are

a) Equal production of charged and neutral D^*'s, and

b) Except for D^* decay, equal production of charged and neutral D's.

The results for $\langle E_{c.m.} \rangle = 6.8$ GeV are

$$R_D \geq 0.9^{+0.7}_{-0.5}, \quad (13a)$$

$$R_{new} = 1.7 \pm 0.8, \text{ and} \quad (13b)$$

$$R_{D^-}/R_D = 0.33 \pm 0.08 . \quad (13c)$$

These results are consistent with $R_{new} = R_D$, but also allow for a reasonable amount of F and charmed baryon production.

F. Alternate Calculation of R_{D^-}/R_D at 4.028 GeV

In section IV.D. we calcualted R_{D^-}/R_D using relative and absolute branching ratios as inputs. We can check the consistency of our measurements by calculating this quantity at 4.028 GeV by an almost orthogonal technique.

The inputs are

a) D^* branching fractions from Table II, and

b) The relative $D^{*o}\overline{D^{*o}}$, $D^{*o}\overline{D^o}$, and $D^o\overline{D^o}$ production rates.[4]

The assumptions are

a) The $\psi(4030)$ is a state of definite isospin, either 0 or 1, so that there is equal production of charged and neutral D's and D^*'s, except for phase space factors. This assumption is somewhat questionable; it has been suggested that the $\psi(4030)$ may have mixed isospin.[26]

b) The phase space factor for $D^*\overline{D^*}$ production is proportional to $p^3_{D^*}$.

The result is

$$R_{D^-}/R_D = 0.25 \pm 0.15 , \quad (14)$$

which is consistent with the determinations of 0.28 ± 0.09 and 0.31 ± 0.10 from Table VI.

It is clear from these measurements that the fraction of charged D produciton at 4.028 GeV is significantly smaller than that at 3.774 GeV where we have assumed $R_{D^-}/R_D = 0.44 \pm 0.03$. In the near future one should be able to combine this result with inclusive lepton production at 4.028 and 3.774 GeV to calculate the ratio of D^+ to D^o semileptonic branching fractions. Since semileptonic decays are $\Delta I = 0$ transitions, this ratio is the inverse of the ratio of D^+ to D^o lifetimes.[27]

V. *Tagged Events*

With the discovery of the ψ'', it becomes possible for the first time to "tag" charmed particle decays. For example, if we detect a D^o decay into $K^-\pi^+$ in a ψ'' decay, then we are also looking, essentially without bias, at a $\overline{D^o}$ decay where the $\overline{D^o}$ has a momentum of 300 MeV/c in a known direction.

A. Decays With All Charged Particles

In section IV.B. we determined absolute D branching fractions by employing some very reasonable assumptions about the nature of ψ''. We can now check these assumptions by using tagged events to measure D branching fractions.

We use the five decay modes shown in Fig. 4 as the tagging decays and look for events in which all or all but one of the decay products of the other D are detected. There are 194 tagging D^o decays and 82 tagging D^- decays.

We find eight cases of $K^{\mp}\pi^{\pm}$ or $K^{\mp}\pi^{\pm}\pi^{+}\pi^{-}$ decay opposite the tagging decays. These eight cases come from six events because in two cases both halves of the event tag each other, and such events must be counted twice. Correcting for detection and triggering efficiencies, these events give

$$B(D^{o} \to K^{-}\pi^{+} \text{ or } K^{-}\pi^{+}\pi^{-}\pi^{+}) = (6.2 \pm 2.7)\% \qquad (15)$$

which is consistent with the value of $(4.9 \pm 1.1)\%$ from Table IV.

There are two cases of a $K^{\mp}\pi^{\pm}\pi^{\pm}$ decay opposite from a tagging $D^{\mp}$ decay, each from a separate event. These two events give

$$B(D^{+} \to K^{-}\pi^{+}\pi^{+}) = (3.4 \pm 2.4)\% \ , \qquad (16)$$

which is in clearly fortuitous agreement with the value of $(3.5 \pm 0.9)\%$ from Table IV.

We can now turn these results around and use them to calculate ψ'' branching fractions without the aid of any assumptions.

The inputs are

a) $\sigma \cdot B$ for D decays at the ψ'' (Table III),

b) B for D decays from the tagged events (Eqs. 15 and 16), and

c) ψ'' total cross section measurements.[6]

The results are given in Table VII along with the values which were assumed in section IV.B. The measurements are consistent with the assumed values.

Table VII

ψ'' branching fractions in per cent. See the text for a discussion of the input data.

	B measured	B (assumed in Sec. IV.B.)
$\psi'' \to D^{o}\bar{D}^{o}$	44 ± 22	56 ± 3
$\psi'' \to D^{+}D^{-}$	44 ± 33	44 ± 3
$\psi'' \to D\bar{D}$	88 ± 40	100

B. Decays With One Missing Neutral

We can also look for events with a charged kaon, another charged particle, and a missing, near zero-mass, neutral particle opposite a tagging D^{o} decay. These decays could be $D^{o} \to K^{\mp}\pi^{\pm}\pi^{o}$, $D^{o} \to K^{\mp}e^{\pm}\nu$, or $D^{o} \to K^{\mp}\mu^{\pm}\nu$ modes, which we shall designate as $D_{\pi 3}$, D_{e3}, and $D_{\mu 3}$ for short. There are ten cases of these events, which leads to

$$B(D_{\pi 3}) + B(D_{e3}) + B(D_{\mu 3}) = (11.7 \pm 4.1)\% \ . \qquad (17)$$

Unfortunately it is quite difficult to distinguish between, $D_{\pi 3}$ and $D_{\ell 3}$ decays in the magnetic detector because

a) the leptons often have low momentum and are not discriminated from pions, and

b) low energy π^{o}'s are difficult to detect.

Figure 10 is a computer reconstruction of the one event, out of these 10 events, most likely to be a $D_{\ell 3}$ decay. One is viewing the magnetic detector along the beam. The short closed boxes represent trigger counters and the long open boxes represent shower counters which have fired. Tracks labeled with the subscript 1 are from the tagging decay while those labeled 2 are from the other D decay. The tagging decay here is $D^{o} \to K^{-}\pi^{+}\pi^{-}\pi^{+}$. Note that the 250 MeV/c π^{+} in the upper right hand corner backscatters and eventually reaches the trigger counter to the right of the K^{-}. Although the computer does not track the backscatter the full distance, the trigger counter in question fires 15 nsec late which is consistent with this hypothesis. There are two charged particles left in the event. The positvely charged particle is unambiguiously identified as a kaon by time-of-flight and the 650 MeV/c negatively charged particle is identified as a muon by the firing of a spark chamber located behind the flux return. There is about a 12% probability that a pion of this momentum would penetrate

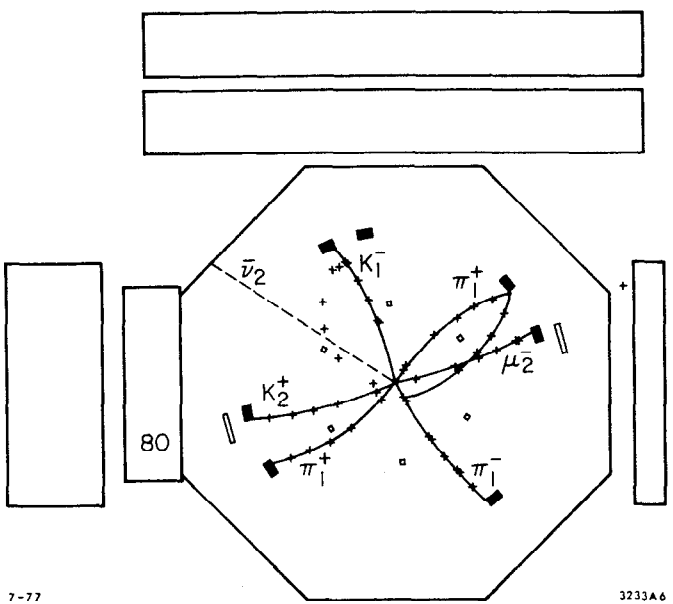

FIG. 10. An event which is interpreted as

$\psi'' \rightarrow D^0 \overline{D^0}$

$\overline{D^0} \rightarrow K^+ \mu^- \bar{\nu}$

$D^0 \rightarrow K^- \pi^+ \pi^- \pi^+$

See text for discussion.

the flux return and be misidentified as a muon. There is approximately 500 MeV/c of missing momentum in the direction indicated by "$\bar{\nu}_2$". The missing energy in the event is consistent with being equal to the missing momentum and within errors one cannot determine from missing mass whether the missing neutral is a neutrino or π^0. If we assume that the missing neutral is a π^0, then in the worst case at least one of the decay photons must be in the active area of the shower counters and deposit at least 200 MeV of energy. The probability of the shower counters failing to fire on a 200 MeV photon is between 10 and 20%. Thus, everything else being equal, this event is 50 to 100 times more likely to be a $D_{\mu 3}$ decay than a $D_{\pi 3}$ decay. I have selected this event for a detailed discussion not so much to convince you that it is a $D_{\ell 3}$ decay as to demonstrate the difficulty of distinguishing these decays in our present detector.

C. Charged Multiplicity in D Decays

To determine the charged multiplicities in D decays, we count the charged particles opposite a tagging decay and use a Monte Carlo calculation of efficiencies to unfold the true distributions from the observed distributions.[28] In this preliminary analysis we have used only the $\bar{K}^{\mp}\pi^{\pm}$ and $\bar{K}^{\mp}\pi^{\mp}\pi^{\pm}$ modes as tagging decays. Backgrounds, which are typically about 10%, have been explicitly subtracted from the data. No attempt has been made to identify neutral kaons so that a K_s decaying to two charged pions will count as two charged particles.

The raw data are displayed in the top portion of Fig. 11 and the unfolded data are displayed in the bottom portion. D^0's decay primarily to two charged particles, while D^+'s decay to roughly equal numbers of one and three charged particles. The mean charged multiplicities are

$$\langle n_c \rangle_{D^0} = 2.3 \pm 0.2 \qquad (18a)$$

$$\langle n_c \rangle_{D^+} = 2.3 \pm 0.3 \ . \qquad (18b)$$

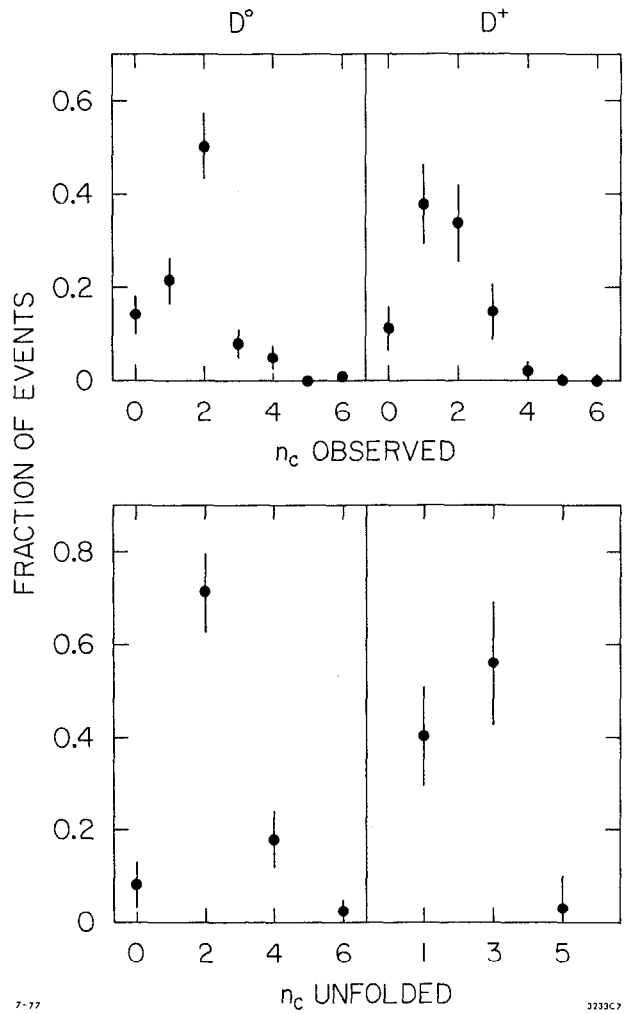

FIG. 11. Observed and true (unfolded) charged multiplicities for D decays.

The statistical model assumed somewhat higher charged multiplicities, typically about 2.7.

D. Two-prong $D\bar{D}$ Decays

Events in which only two charged particles are produced are of special interest experimentally because

a) there is background in two-prong events from QED processes,

b) they have a much lower detection efficiency in the magnetic detector and most other detectors, and

c) $\tau^+\tau^-$ decays occur primarily in two-prong events.

We can calculate the fraction of $D\bar{D}$ decays that go into two charged particles directly from the data in Fig. 11:

$$D^0\bar{D}^0 : 2f_0f_2 = (11 \pm 7)\% \qquad (19a)$$

$$D^+D^- : f_1^2 = (17 \pm 8)\% . \qquad (19b)$$

Here f_n represents the fraction of decays to n charged particles. The fractions of two charged particle events given by Eq. 19 are not vastly different from the overall fraction of two prong events. We thus expect to see the same type of variation with energy in the two prong cross section as in the multiprong cross section.

Semileptonic decays of D's and leptonic decays of τ's are often separated experimentally by multiplicity: the D's are presumed to decay primarily into events with four or more charged particles while τ's are presumed to decay primarily into events with two charged particles.[29] It is thus important to measure the extent to which semileptonic D decays can occur in two-charged-prong events. We do not presently have enough information to determine this but we can set upper limits by assuming that semileptonic decays always occur in the lowest possible charged mutliplicities.

For $D^o\overline{D^o}$ decays the lowest charged multiplicity is clearly two, therefore

$$D^o\overline{D^o} \text{ 2-prong lepton fraction} < f_o$$
$$< 13\% \text{ at } 1\sigma \text{ c.}\ell. \qquad (20a)$$

For D^+D^- decays one might expect that the upper limit is just f_1. However we can obtain a better limit if we assume that Cabbibo suppressed decays are unimportant. Then the simplest semileptonic decay is $D^+ \to K^o\ell^+\nu$. The $\overline{K^o}$ looks like zero prongs two-thirds of the time and like two prongs one-third of the time. Therefore

$$D^+D^- \text{ 2-prong lepton fraction} < 0.66\, f_1$$
$$< 34\% \text{ at } 1\sigma \text{ c.}\ell. \qquad (20b)$$

E. Neutral and Charged Kaon Production in D^+ Decays

If we assume that Cabbibo suppressed decays are unimportant and if $f_1 > 0.33$, then D^+'s must decay to neutral kaons more often than they decay to charged kaons. The proof is straightforward: D^+'s decay to K^-'s, so to conserve charge a D^+ decay to a charged kaon must contain at least three charged particles. A D^+ decay to a neutral kaon will appear to be a three-or-more charged particle decay at least one-third of the time because the kaon will decay into $\pi^+\pi^-$. Therefore, if D^+'s decayed equally to neutral and charged kaons, at least two-thirds of decays would have three-or-more charged particles and $f_1 < 0.33$.

From Fig. 11, $f_1 = (41 \pm 11)\%$, so it is likely that the condition $f_1 > 0.33$ is met, but it is not conclusive.

It is often assumed that overall there should be equal numbers of charged and neutral kaons from charmed particle decays. This need not be the case and, in fact, is not even true in the statistical model.[24] The predictions of this model are shown in Table VIII. The symmetry in the semileptonic decays is a consequence of the fact that these decays are $\Delta I = 0$ transitions. It is clear that if there are equal numbers of neutral and charged D's produced then in this model overall there would be more neutral kaons than charged kaons in their decays.

Table VIII

Fraction of neutral and charged kaons in D decays according to the statistical model (Ref. 24).

	$\overline{K^o}$	K^-
D^o nonleptonic	0.54	0.46
D^+ nonleptonic	0.68	0.32
D^o semileptonic	0.38	0.62
D^+ semileptonic	0.62	0.38

VI. Epilogue: A Beautiful Event

If you study Fig. 11 carefully, you will notice that in the raw charged mutliplicity for tagged D^o decays the number of five-prong events is zero, but not the number of six-prong events. In fact, exactly one decay with six charged particles was detected. When we examined this event, we were amazed to discover that there was, within errors, no missing momentum or energy. This event, which is shown in Fig. 12, is

$$e^+e^- \to \psi'' \to D^o\,\overline{D^o} \qquad (21)$$
$$\qquad\qquad\quad \to K_S\pi^+\pi^-\pi^+\pi^-$$
$$\qquad\qquad\quad \to K^-\pi^+ .$$

If one were so foolhardy as to calculate a branching fraction for $D^o \to \overline{K^o}\pi^+\pi^-\pi^+\pi^-$ from this single event, one would obtain the clearly absurd value of about 25%. We were thus very lucky to be able to see this beautiful decay.

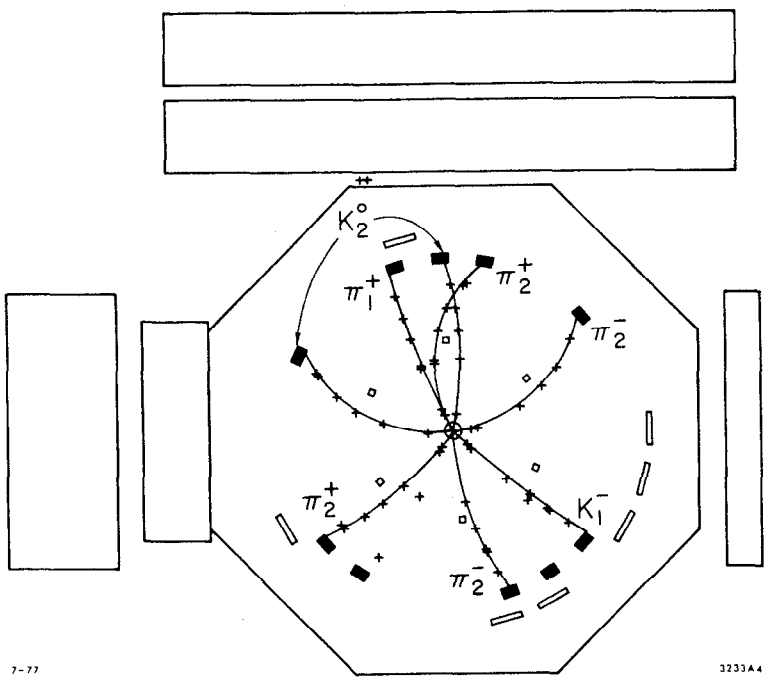

FIG. 12. An event which is interpreted as

$$\psi'' \rightarrow D^o \bar{D}^o$$
$$\hookrightarrow K_s \pi^+\pi^-\pi^+\pi^-$$
$$\hookrightarrow K^-\pi^+ .$$

The extra trigger and shower counters have presumably been fired by secondary interactions. The time-of-flight information from the extra trigger counters indicates that they were not fired by prompt particles.

References

1. Semi-leptonic decays are discussed by W. De Boer, R.J. Madaras, and J. Kirz in these proceedings.

2. J.-E. Augustin et al., Phys. Rev. Lett. 34, 233(1975); G.J. Feldman and M.L. Perl, Phys. Rep. 19C, 233(1975), Appendix A; F. Vannucci et al., Phys. Rev. D15, 1814(1977); A. Barbaro-Galtieri et al., SLAC report number SLAC-PUB-1976 (1977).

3. G.J. Feldman et al., Phys. Rev. Lett. 38, 1313(1977).

4. G. Goldhaber et al., SLAC report number SLAC-PUB-1973 (1977).

5. M. Piccolo et al., SLAC report number SLAC-PUB-1978 (1977).

6. P.A. Rapidis et al., SLAC report number SLAC-PUB-1959 (1977).

7. Members of the SP26 collaboration are A. Barbaro-Galtieri, J.M. Dorfan, R. Ely, G.J. Feldman, J.M. Feller, A. Fong, B. Gobbi, G. Hanson, J.A. Jaros, B.P. Kwan, P. Lecomte, A.M. Litke, D. Lüke, R.J. Madaras, J.F. Martin, T.S. Mast, D.H. Miller, S.I. Parker, M.L. Perl, I. Peruzzi, M. Piccolo, T.P. Pun, P.A. Rapidis, M.T. Ronan, R.R. Ross, B. Sadoulet, D.L. Scharre, T.G. Trippe, V. Vuillemin, and D.E. Yount. Much of the analysis of the unpublished SP26 data presented here is work of I. Peruzzi and M. Piccolo.

8. H.K. Nguyen et al., Phys. Rev. Lett. 39, 262(1977) and unpublished SP26 data.

9. J.E. Wiss et al., Phys. Rev. Lett. 37, 1531(1976).

10. J.-E. Augustin et al. Phys. Rev. Lett. 34, 764(1975).

11. J. Siegrist et al., Phys. Rev. Lett. 36, 700(1976).

12. H.L. Lynch in Proceedings of the International Conference on the Production of Particles with New Quantum Numbers, University of Wisconsin, Madison, Wisconsin, April 22-24, 1976, p. 20.

13. J.D. Jackson, Nuovo Cimento 34, 1645(1964); A. Barbaro-Galtieri in Advance in Particle Physics, edited by R.L. Cool and R.L. Marshak (Wiley, New York), Vol. II, 1968.

14. A.M. Boyarski et al., Phys. Rev. Lett. 34, 1357(1975).

15. V. Lüth et al., Phys. Rev. Lett. 35 1124(1975).

16. P.B. Wilson et al., SLAC report number SLAC-PUB-1894 (1977).

17. In our error analysis, we have assigned the error due to the long-term drift in E_b determination to be 0.5 MeV. This is probably conservative.

18. G. Goldhaber et al., Phys. Rev. Lett. 37, 255(1976); I. Peruzzi et al., Phys. Rev. Lett. 37, 569(1976).

19. V. Lüth et al., SLAC report number SLAC-PUB-1947 (1977).

20. D.B. Lichtenberg, Phys. Rev. D 12, 3760(1975); A. De Rújula, H. Georgi, and S.L. Glashow, Phys. Rev. Lett. 37, 398(1976); K. Lane and S. Weinberg, Phys. Rev. Lett. 37 717(1976); S. Ono, Phys. Rev. Lett. 37, 655(1976); W. Celmaster, Phys. Rev. Lett. 37, 1042(1976); H. Fritzsch, Phys. Lett. 63B, 419(1976); J. Dabaul and M. Krammer, Phys. Lett. 64B, 341(1976); N.G. Deshande et al., Phys. Rev. Lett. 37, 1305(1976); J.S. Guillen, Lett. al Nuovo Cimento 18, 218(1977); D.H. Boal and A.C.D. Wright, University of Alberta report (1976); L.H. Chan, Louisiana State University report (1976); D.C. Peasleee, Phys. Rev. D15, 3495(1977); and N.F. Nasrallah and K. Schilcher, Universität Mainz report NZ-TH 76/15 (1976).

21. The value is from the "normal fit" of Ref. 4. The "isospin constrained fit" gave an erroneous value for $B(D^{o*} \to D^{o}\gamma)$ because the D^{+} mass was fit to be 1873 MeV/c^2. This forbade the decay $D^{*+} \to D^{+}\pi^{o}$ and forced all $D^{*+} \to D^{+}$ decays into the mode $D^{*+} \to D^{+}\gamma$, which in turn forced too high a value of $B(D^{o*} \to D^{o}\gamma)$ through the constraint conditions.

22. See F.J. Gilman in these proceedings for a discussion of the validity of these models for ordinary quarks.

23. G. Altarelli, N. Cabibbo, L. Maiani, Nucl. Phys. B88, 285(1975); R.L. Kingsley, S.B. Treiman, F. Wilczek, and A. Zee, Phys. Rev. D11, 1919(1975); M.B. Einhorn and C. Quigg, Phys. Rev. D12, 2015(1975).

24. J.L. Rosner, Invited talk at Orbis Scientiae, Jan. 17-21, 1977, Coral Gables, Fla., (Institute for Advanced Study report COO-2220-120).

25. See W. De Boer in these proceedings for a discussion of the evidence for F production at 4.4 GeV.

26. A. De Rújula, H. Georgi, and S.L. Glashow, Phys. Rev. Lett. 317(1977). M. Bander, University of California at Irvine report UCI 77-32 (1977).

27. A. Pais and S.B. Treiman, Phys. Rev. D15, 2529(1977).

28. See V. Lüth in these proceedings for a discussion of how this is done for total charged multiplicities.

29. See M.L. Perl in these proceedings.

Recent Results from DORIS

W. de Boer

Max-Planck-Institut

für Physik und Astrophysik,

8 München 40, Germany

Contents

1. Introduction

At last year's Summer Institute there were good reasons to believe that the rich structure in the total cross section in e^+e^- annihilation was due to the production of charmed quarks. Evidence for the charm interpretation of this structure included the following observations:

a. The existence and small widths of the J/ψ and ψ' and the intermediate P_c/χ states. References can be found in recent reviews on e^+e^--annihilation above 2 GeV, Ref. 1-3.
b. Discovery of the D-mesons, as narrow peaks in the $K\pi$ invariant mass spectra [4].
c. Discovery of the semileptonic decays of the new hadrons [5].

During last year some of the 'missing' pieces were found, namely a strong increase in the inclusive kaon production [6, 7] and discovery of the F-mesons [8].

A few observations could not be explained by the charm theory, namely the observation of many dilepton ($e\mu$) events at center of mass energies above 4 GeV [9] and the large value of R in that region [10, 11]. M. Perl interpreted the $e\mu$ events as decay products of a new heavy lepton [1,12].

In this report I will discuss data, obtained at the e^+e^- storage ring DORIS during last year. The two interaction regions were mainly occupied by the experiments DASP, PLUTO and DESY-Heidelberg, who obtained data on

1. Charmonium spectroscopy
2. The total hadronic cross section between 3.6 and 5.2 GeV
3. Anomalous lepton production resulting from the weak decays of charmed hadrons and heavy leptons
4. F-meson production.

2. Detectors

Before discussing the data, I will briefly describe the detectors. Fig. 1 shows a cross section of the PLUTO detector built by groups from DESY and the Universities of Hamburg, Siegen and Wuppertal. The superconducting solenoid (1.4 m diameter, 1.05 m length) produces a 2 T magnetic field parallel to the beam axis. Inside the solenoid there are 14 cylindrical proportional wire chambers (PWC's) interleaved with two cylindrical lead converters, whose radii and thicknesses are 37.5 cm, 0.4 RL and 59.4 cm, 0.72 RL, respectively. Electron and photon detection is achieved over 56 % of 4π by counting the number of tracks in the PWC's behind the lead converters. The probability to misidentify a hadron as an electron was measured to be 3.5 ± 0.7 %. The electron detection efficiency rises from 20 % at 0.3 GeV/c to 80 % above 0.7 GeV/c. Muon identification is achieved in 43 % of 4π by PWC's behind a 68 cm thick iron absorber. The hadron absorber causes a momentum cutoff at $p_\mu = 1.0$ GeV/c. The measured hadron punchthrough and decay is 2.8 ± 0.7 %. The detector is triggered by hardwired logic combinations of PWC wires. It requires at least two tracks with a minimum transverse momentum of 0.24 GeV/c. The solid angle, subtended by the trigger, is 86 % of 4π.

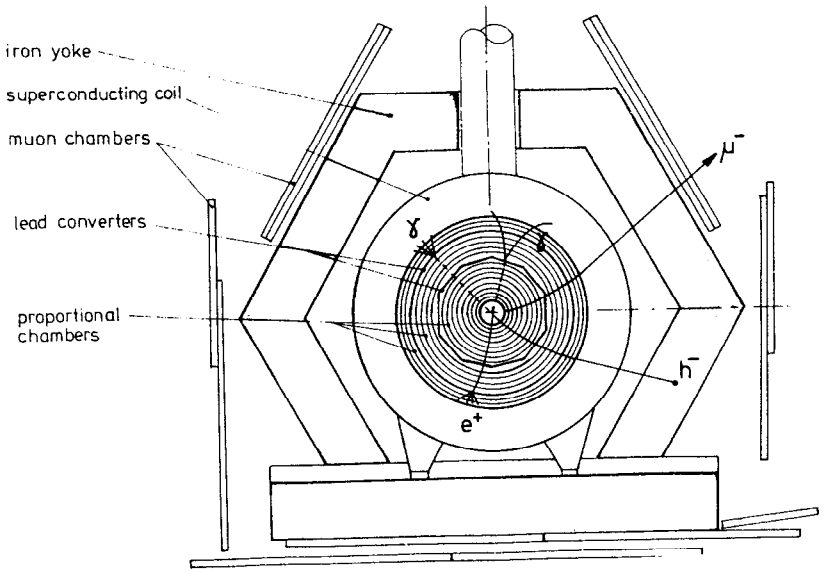

Fig. 1 View of the PLUTO detector along the beam axis

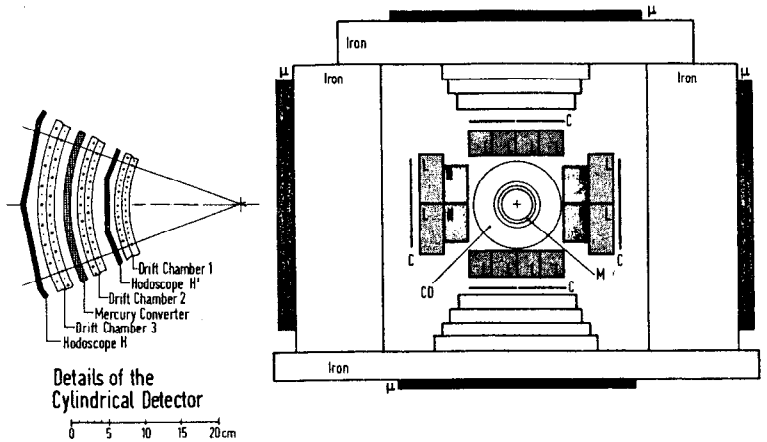

Fig. 2 View of the DESY-HD detector along the beam axis.
N = NaI, L = lead glass, C = counter

A nonmagnetic detector, DESY-HDB (DESY, Univ. Heidelberg), is shown in Fig. 2. The beam pipe is surrounded by cylindrical drift chambers, followed by NaI- and lead glass counters, cosmic ray counters, an iron shield, and muon chambers. A two radiation length thick mercury cylinder in front of the last drift chamber acts as a photon converter. Solid angles covered for detection of muons, electrons or photons, and charged particles are 0.32, 0.45 and 0.95 x 4π, respectively. Energy resolutions are 11 % FWHM for NaI and 30 % FWHM for lead glass, both at 1 GeV.

A cross section of the double arm spectrometer DASP (TH Aachen, DESY, Univ. Hamburg, Max Planck Institute München, Univ. Tokyo) is shown in Fig. 3. Full particle separation between e, μ, p, K and π up to 1.5 GeV/c is achieved in the two magnetic spectrometer arms by means of time of flight measurement, a threshold Čerenkov counter, which for momenta below 2.4 GeV/c fires on electrons only, a shower counter, and a hadron absorber with muon counters after 40 and 60 cm of iron. Forty cm of iron corresponds to a muon momentum cutoff of 0.7 GeV/c. The geometrical solid angle accepted by the two spectrometer arms is 7.2 % of 4π. Particles are traced by means of a set of proportional wire chambers before the magnet and a set of large spark chambers behind the magnet. A nonmagnetic detector has been mounted around the beam pipe. It covers 70 % of 4π. This inner detector is well suited for electron and photon detection by means of a lead scintillator sandwich interleaved with proportional tube chambers. The angular resolution of the shower counter is 0.03 rad and the energy resolution is 14 %/ $\sqrt{E}$. The photon detection efficiency

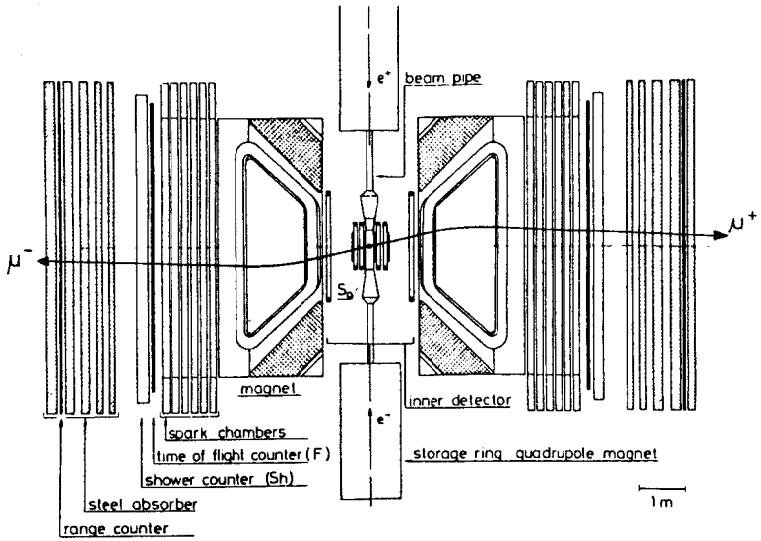

Fig. 3 a Top view of the Double Arm Spectrometer DASP

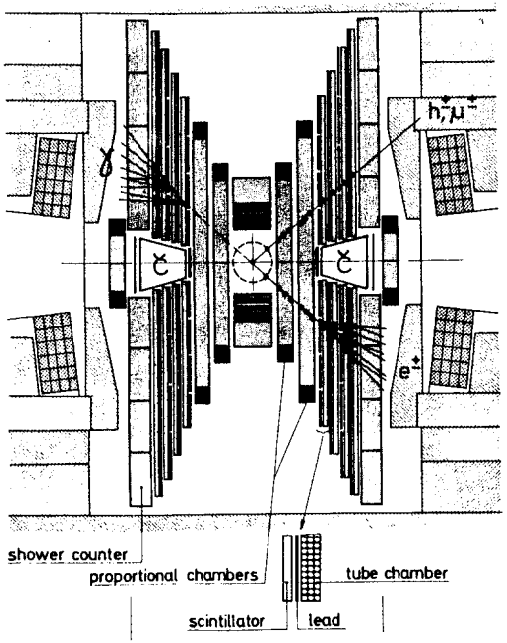

Fig. 3 b View of the inner detector of DASP

is 50 % at 0.05 GeV rising to 80 % at 0.1 GeV and 95 % above 0.3 GeV. The probability to misidentify a charged hadron as an electron is about 2 % for the inner detector and less than 1 % for the outer spectrometer arms. The probability to misidentify a hadron as a muon in the outer detector is 0.04 ± 0.01 for $p_\mu > 0.9$ GeV/c and varies from 0.025 to 0.065 between 0.7 and 0.9 GeV/c. The spectrometer is triggered on a single charged particle, the inner detector on at least 3 particles (charged or neutral) or a minimum deposited energy.

3. Charmonium spectroscopy

Some new results on the J/ψ and ψ' decays have been collected in Tables 1 and 2 [13, 14]. Here we will only discuss the new results on the X(2820), which has been observed in the radiative decays of the $J/\psi \to 3\gamma$.

The new DASP data on this state are shown in Fig. 4. Here we plotted the high mass solution of the two independent invariant mass combinations of the three photons. One sees a narrow peak around 2.8 GeV/c^2 superimposed on a smoothly varying background. The large background (solid and dashed in lines in Fig. 4) comes from the QED process $e^+e^- \to \gamma\gamma\gamma$ and from kinematic reflections of η and η' production. Around 2.8 GeV we observed 41 events instead of the expected background of 19 events. The excess of events (5 sd) was fitted with a Gaussian with a central value of 2.82 ± 0.03 GeV. The width $\sigma_{M(X)} = 0.04 \pm 0.01$ GeV is consistent with the experimental resolution. The same analysis was done at $E_{cm} = 3.6$ GeV. There the data were found to be consistent

Table 1

List of branching ratios $J/\psi \to f$

channel f	BR x 10^3	Γ(eV)	detector
$\gamma\pi^0$	0.073±0.047	5.0±3.2	DASP
$\gamma\eta$	0.80 ±0.18	55 ±12	DASP
	1.3 ±0.4	91 ±28	DESY-HD
$\gamma\eta'$	2.2 ±1.7	152 ±117	DASP
	2.4 ±0.7	165 ±48	DESY-HD
γX	0.12 ±0.05	8.3±3.5	DASP
$\gamma\gamma\gamma$	< 0.078	< 5.1	DASP
$\rho\pi$	10.0 ±2.0	690 ±138	DESY-HD
$\omega\pi^+\pi^-$	7.8 ±1.6	543 ±100	PLUTO
ωf	4.0 ±1.4	276 ±96	PLUTO
$B^\pm\pi^\mp$	2.8 ±0.7	193 ±47	PLUTO

Table 2

List of upper limits $\psi' \to f$

channel f	BR($\psi' \to \gamma h$)xBR($h \to f$)	detector
$\gamma\eta \to \gamma\gamma\gamma$	< 1.6 x 10^{-4}	DASP
$\gamma\eta' \to \gamma\gamma\gamma$	< 1.2 x 10^{-4}	DASP
$\gamma X(2.8) \to \gamma\gamma\gamma$	< 3.4 x 10^{-4}	DASP
$\rho\pi \to \gamma\gamma\pi\pi$	< 10 x 10^{-4}	DESY-HD
$\gamma\chi(3.41) \to \gamma\gamma\gamma$	< 4.0 x 10^{-4}	DASP
$\gamma\chi(3.45) \to \gamma\gamma\gamma$	< 3.1 x 10^{-4}	DASP
$\gamma P_c(3.51) \to \gamma\gamma\gamma$	< 2.6 x 10^{-4}	DASP
$\gamma\chi(3.55) \to \gamma\gamma\gamma$	< 2.0 x 10^{-4}	DASP

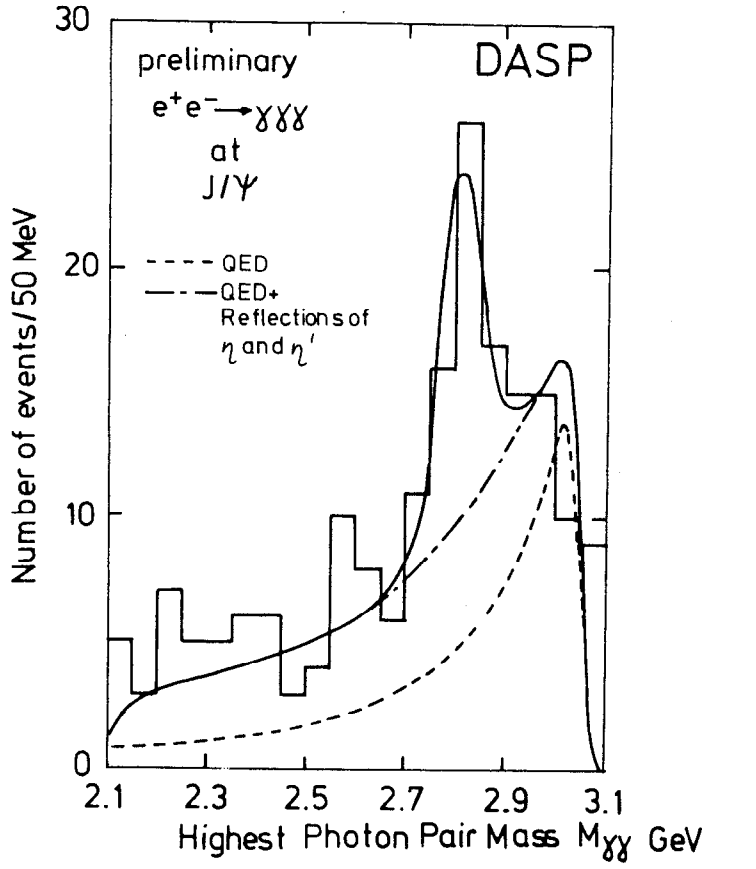

Fig. 4 Invariant $\gamma\gamma$ mass spectrum of $\psi \to \gamma\gamma\gamma$ (high mass solution)

with QED background. An upper limit of the branching ratio Br($\psi' \to X(2820)$) is given in Table 2. The X(2820) has even C-parity and spin J $\neq$ 1. Therefore in principle, this state can be associated with the lowest $^1S_0$ level in the charmonium scheme.

4. The total hadronic cross section

Measurement of the production of hadrons in e^+e^- annihilation has been a rich source of information on the structure of hadrons (see reviews, mentioned in Refs. 1-3). The importance of the total cross section stems from the simplicity of the initial state: the electron and positron annihilate into a virtual photon, which decays into hadrons. Therefore the initial state has well defined quantum numbers and energy. This makes a theoretical interpretation much easier. For example, the quark model predicts in the continuum region (away from resonance production) $R = \sigma_{had}/\sigma_{\mu\mu} = \sum_{n=1}^{N} Q_n^2$. Here R is the ratio of the total hadronic cross section and the muon pair production cross section. The sum is taken over the charges Q_n of all quarks N with a mass below threshold for hadron production at a given center of mass energy. In the SU(3) model with colour R=2 and in the SU(4) model with colour R = 3 1/3. Fig. 6 shows the value of R at center of mass energies between 3.6 and 5.2 GeV as measured by PLUTO. The shaded areas indicate the theoretical expectations for the contributions from charmed quarks ($c\bar{c}$),

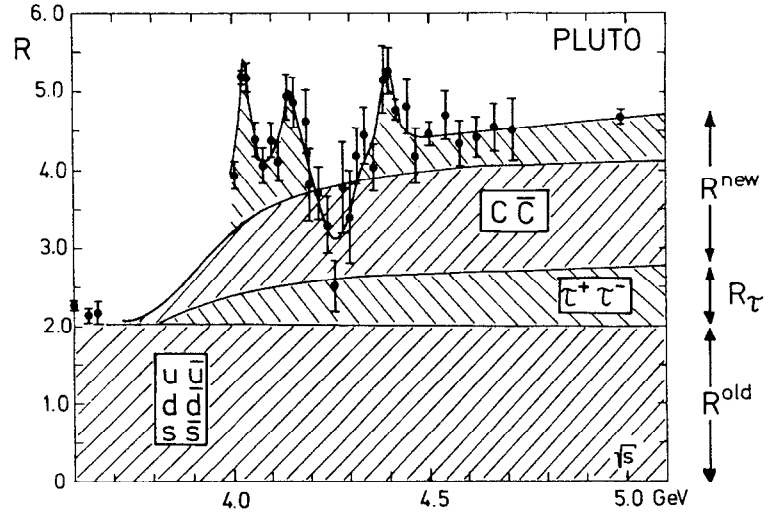

Fig. 5 Total hadronic cross section in units of $R = \sigma_{had}/\sigma_{\mu\mu}$

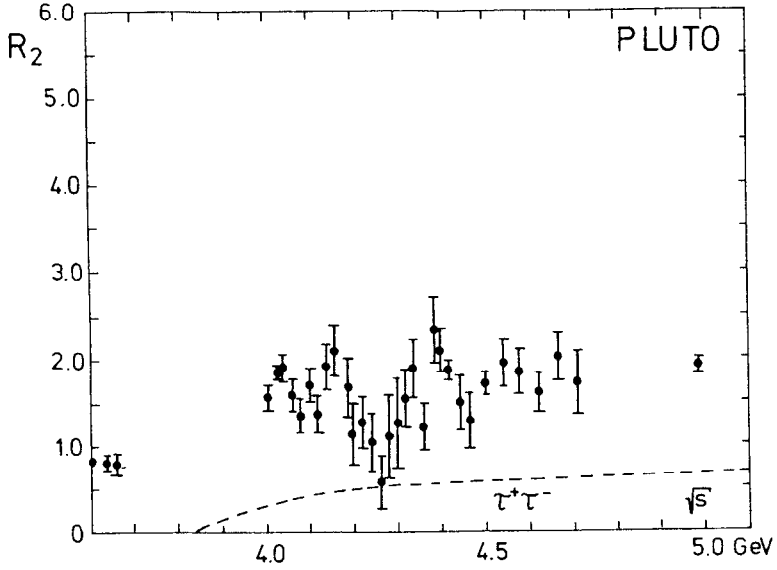

Fig. 6 Total hadronic cross section for twoprongs only. The dashed line is the contribution from a heavy lepton

a heavy lepton ($\tau\ \bar{\tau}$), and the "old" quarks. These data are slightly different from previously published data [11], because of refined radiative corrections and the simulation of jet structure in the Monte Carlo program. The large solid angle of the PLUTO detector (94 % of 4π for detecting charged particles) yields a high detection efficiency: 90 % for multiprongs and 40 % for twoprongs. This brings systematic errors from the Monte Carlo simulation down to 7 %. The total systematic errors, which are not included in the figure, are quoted to be 12 %.

The value of R at E_{cm} = 3.6 GeV is close to the value expected for three quarks, while at E_{cm} = 5 GeV the value of R (4.7 $\pm$ 0.5) disagrees with the value of R expected from the charm model (R = 3.33). However, if the contribution from a heavy lepton is added, the expected value of R (4.2) is not far from the measured value. The PLUTO data shows a similar structure as the SLAC-LBL data, shown at this Conference [15]. However, the latter data are systematically higher by about 15 to 25 %. This is within the quoted systematic errors of 12 % for PLUTO and 15 % for SLAC-LBL.

Fig. 7 shows the twoprong hadronic cross section in units of R. It reproduces the structure observed in the multiprongs, which indicates a rather large charm contribution to the twoprongs. If one subtracts from the twoprongs the contribution expected for a heavy lepton (dotted line in Fig. 7), one finds an increase in R_{2pr} of 0.6 units between 3.6 and 4.03 GeV. At this Conference the branching ratios for D's going into twoprongs was reported to be 13 $\pm$ 8 %, if one takes into account a production ratio $D^{\pm}$: D^{o} = 1 : 4 [16]. One then expects an increase in R_{2pr} of 0.4 $\pm$ 0.2 in reasonable agreement with the observed increase.

5. Inclusive hadron production

5.1 Inclusive kaon production

In the charm model charmed mesons decay preferentially to strange mesons: about 95 % of the decays of D-mesons are expected to contain kaons [17]. Therefore, if the increase in R around 4 GeV is due to charm production, one expects an increase in the kaon yield equal to almost twice the charm cross section, since charmed particles are produced in pairs. Figs. 7 and 8 show the inclusive yield for charged kaons (K^{+} + K^{-}), as measured by DASP [6], and the K^{o}_{S} yield as measured by PLUTO [7]. The sharp rise around 4.03 GeV coincides with the sharp rise of R at that energy. Further evidence for the charm interpretation of the rise in the kaon yield comes from the momentum spectra. Just above charm threshold the increase occurs for $x_E < 0.5$ [6, 7]. This one expects for the decay products from a pair of heavy particles produced almost at rest, for which the kaon momentum is limited to values below half the mass of the heavy particle. At higher center of mass energies the momenta are smeared towards higher values due to the higher momenta of the parent particles [6, 7].

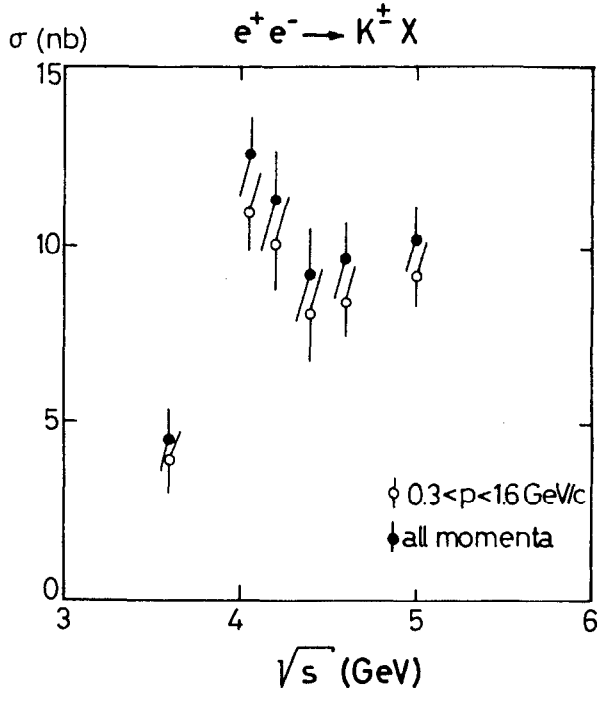

Fig. 7 Inclusive charged kaon production versus E_{cm} (DASP)

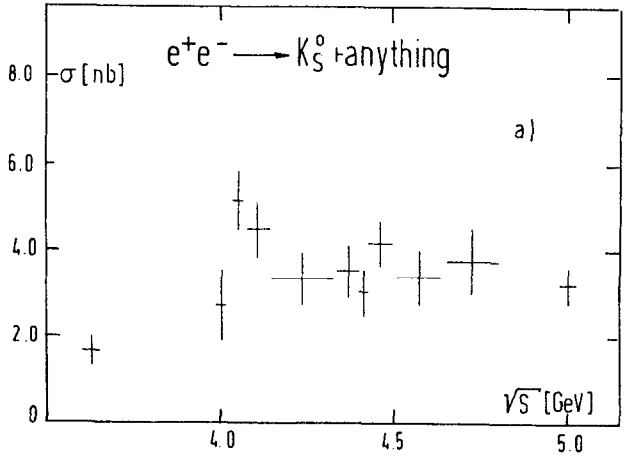

Fig. 8 Inclusive K^0_S production versus E_{cm}, PLUTO

From a comparison of Figs. 7 and 8 one finds that $\sigma(K^+ + K^-) \approx 2\,\sigma(K^0_S)$. This is not an a priori requirement of the theory, since the ratio of charged to neutral kaons depends on several factors, like the specific decay modes of the charmed hadrons and the relative amount of $D^\pm$ and D^0 production [18].

As will be discussed in section 6.3, charmed particles have an appreciable semileptonic branching ratio. Therefore, a large fraction of the final states of a pair of charmed hadrons will have both kaons and leptons. The result of a search for Ke correlations by PLUTO is shown in Fig. 9 [19]. The sharp peak at 4.03 GeV is another clear indication that both, the increase in R at this energy and the increase in the fraction of events with kaons, are due to charm production.

5.2 Inclusive hadron spectra

One of the reasons for studying inclusive hadron production in e^+e^- annihilation is to test scale invariance, which predicts that the shape of the hadron energy spectra is independent of s and that the cross sections vary as $1/s$ [20].

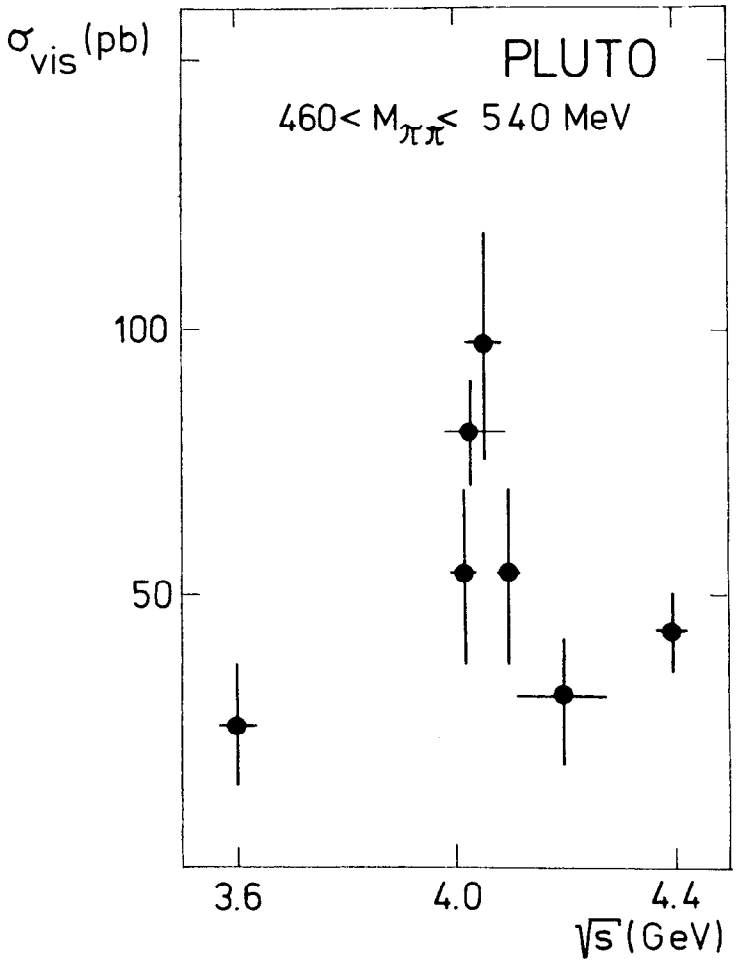

Fig. 9 Cross section $\sigma(e^+e^- \to K^o_S + e + X)$ versus $\sqrt{s}$.

Fig. 10a shows the inclusive pion energy spectra at s = 13 and 25 GeV^2, as function of $x_E = 2\,E_h/\sqrt{s}$, where E_h represents the hadron energy [21]. For $x_E > 0.3$ the spectra are roughly scale invariant. The line in Fig. 10a represents an exponential $\exp(-bx_E)$ with a slope b of 8.8. The increase at low x_E can be accounted for by the fact that charm production has started between s = 13 and 25 GeV^2. Other hadrons (K, $\bar{p}$) show cross sections, which fall roughly on the same exponential line [21].

The PLUTO inclusive hadron spectra are shown in Fig. 10b [22]. Since particle identification was not possible, they used $x_p = 2\,p_h/\sqrt{s}$ instead of x_E. Both variables are only identical if $p_h \gg m_h$. The PLUTO data agrees with the DASP data at all x_p. However, both datasets disagree with the SLAC-LBL data [23] for $x_p > 0.5$, as shown in Fig. 10c.

5.3 Inclusive antiproton yield

In neutrino reactions and photoproduction experiments there is evidence for charmed baryon production, from which one would expect a substantial increase in the antiproton yield for $E_{cm} \geq 4.5$ GeV. [24] Fig. 4 shows the antiproton cross section as function of $\sqrt{s}$, as measured by DASP. There is no evidence for a strong increase above 4.5 GeV. From the difference $R_{\bar{p}}$ (> 5 GeV) - $R_{\bar{p}}$ (4-4.5 GeV) = 0.05 ± 0.04 we estimate $\sigma_{B\bar{B}+X} = 0.4 \pm 0.3$ nb, assuming the branching ratio $\bar{B} \to \bar{p} + X$ to be 0.5.

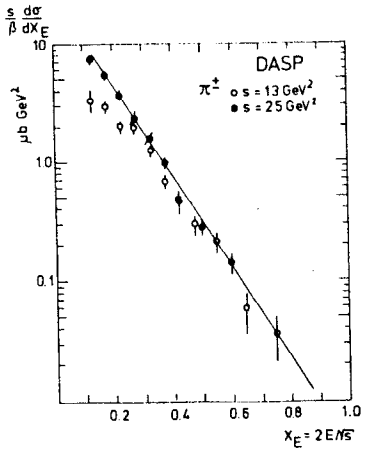

Fig. 10 a

Fig. 10

Energy spectra of charged pions at s = 13 and 25 GeV^2, DASP (a) and momentum spectra of charged hadrons, b) PLUTO c) DASP, SLAC, LBL

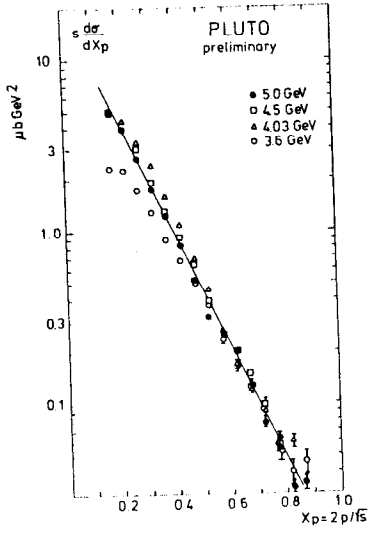

Fig. 10 b

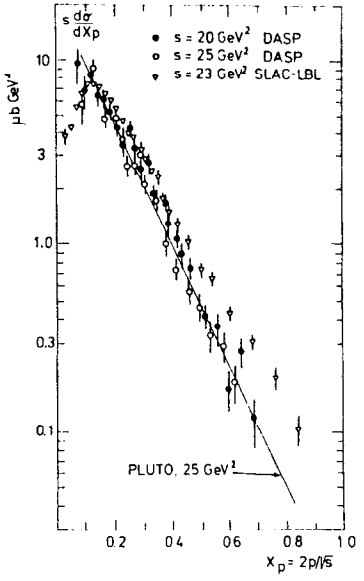

Fig. 10 c

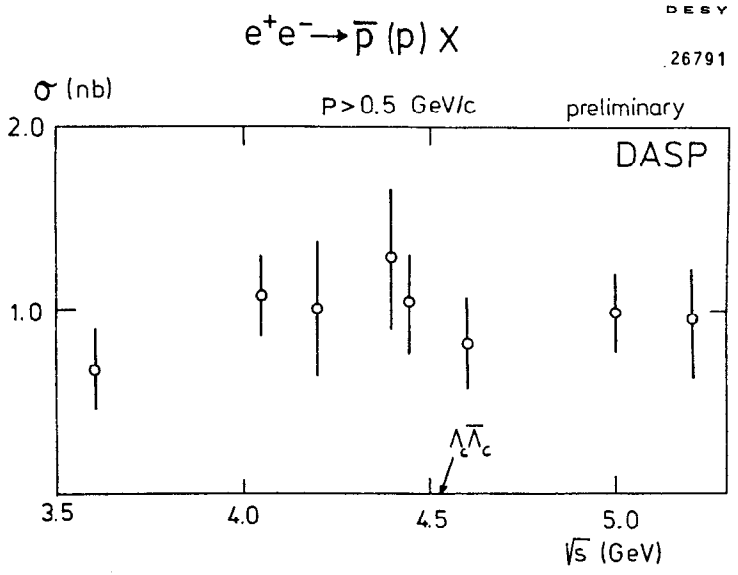

Fig. 11 Inclusive antiproton cross section versus $\sqrt{s}$.

6. Anomalous lepton production

6.1 Sources of anomalous leptons

By anomalous leptons we mean leptons, which can't be explained by the "old" particles. Here we will concentrate on the weak decays of heavy leptons and charmed mesons. Both particles can be produced at the same center of mass energy in e^+e^- annihilation, and both can lead to final states containing leptons plus hadrons. Characteristic features for the decays of these particles can be derived from the relevant quark diagrams, shown in Fig. 12. The decay of a charmed meson is represented as the decay of a charmed quark into a strange quark and an intermediate boson, which decays into a lepton neutrino pair. This gives rise to at least one charged lepton plus a strange meson in the final state. Taking into account that charmed mesons are produced in pairs, one expects an averaged charged multiplicity of 4 to 5 or even higher far above threshold, where the charmed particles can be produced in conjunction with other hadrons. For the leptonic decay of a heavy lepton one expects in most cases only one charged particle, coming from the decay of the intermediate W-boson. More quantitative estimates [25] predict that 85 % of the decays of a heavy lepton contain only one charged particle. Further features by which one can separate experimentally heavy lepton production and charm production, are:

1) The energy dependence of the production cross section (pointlike for heavy leptons, damped by form factors for hadrons).

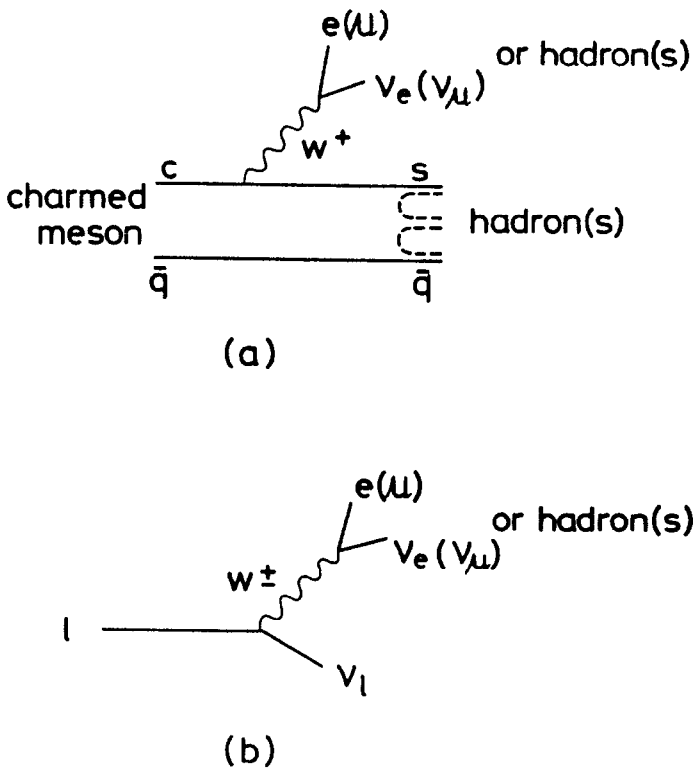

Fig. 12 Quark diagrams for
a) semileptonic decay of a charmed meson and
b) leptonic decay of a heavy lepton.

2) Very few kaons come from heavy lepton decays.

3) The pure leptonic decay mode is about 40 % for a heavy lepton and negligible for charmed hadrons, because the simple-minded quark diagram of Fig. 12 predicts hadrons in the final state. Therefore the semi-leptonic decay mode will be much more important.

4) The lepton spectra from a heavy lepton decay [26] extend to higher momenta than the lepton spectra from charmed particle decays [27].

6.2 Anomalous eμ events

Anomalous eμ events were first found by the SLAC-LBL collaboration [9]. They have now observed 190 eμ events in the energy range $3.8 \leq E_{cm} \leq 7.8$ GeV with a background due to misidentified hadrons of 46 events. These events are unlikely to come from semileptonic decays of hadrons, since the possible contribution from $e^+e^- \to e^\pm \mu^+ +$ unseen hadrons was estimated to be less than 39 % (90 % CL). The undetected hadrons could arise from charged hadrons or photons escaping the detector or neutral particles, like K_L^o or n arising from the semileptonic decays of charmed hadrons.

PLUTO was the first experiment to confirm anomalous eμ events [28]. Based on an integrated luminosity of about 5700 nb^{-1}, taken at center of mass energies between 3.6 and 5.2 GeV, they observed 23 eμ events [28] with a background of 2 events. DASP observed 11 eμ events with a background of 1 ± 0.5 events in the same energy range.

In the DASP detector the muon was identified in the magnetic spectrometer, while the electron was identified in the shower counter of the inner detector. The small background, as compared to the SLAC-LBL data, is due to the better lepton identification. This makes it possible to confirm the heavy lepton also in inclusive lepton spectra, as will be discussed below. A more extensive discussion on the properties of eμ events can be found in recent reviews on heavy leptons [29].

6.3 Anomalous electron production

DASP has studied the reaction $e^+e^- \to e^\pm + X$ [5, 30]. The detector was triggered on a single particle passing through the spectrometer, thus eliminating any experimental bias on the system X. An electron event was defined as follows:

1) A particle with a momentum above 0.2 GeV/c fired the threshold Čerenkov counter.

2) That particle produced a pulseheight in the shower counter consistent with the energy of a showering particle.

3) At least one additional particle was observed in the inner detector, which did not cause a shower. This requirement reduces QED background to less than 5 %. Candidates of the type $e^+e^- \to e^+e^-\gamma$, which accidentally passed the criteria, were removed by a kinematical fit.

The following sources of remaining background were considered:

1. Dalitz decays of π_o (K) or pair conversions of photons. 2. Hadrons mislabeled as electrons. 3. Beam gas interactions. 4. Compton scattering. 5. Semi-leptonic decays of pions and kaons. 6. $e^+e^- \to e^+e^-$ + hadrons. 7. Cascade decay through an intermediate state.

After various cuts on time of flight, interaction volume and pulse height in scintillators and shower counters are made, an estimated background of 11.5 ± 2.1 % for twoprongs and 15 ± 5 % for multiprongs remains. This estimated background was verified from data taken below threshold (3.6 GeV).

In analyzing the topology of the anomalous electron events, we found that the most populous channel was the twoprong no photon class (37 events, see Table 3). Furthermore, the averaged photon multiplicity in the twoprong class, is very low: $\bar{n}_\gamma = 0.5 \pm 0.2$. For the multiprongs (182 events) the averaged charged and photon multiplicities are 5.6 ± 0.3 and 1.9 ± 0.3, respectively. These values were corrected for the limited detection efficiencies (0.73 ± 0.05 for charged particles, 0.70 ± 0.05 for photons). From a Monte Carlo study we estimated that 17 % of the twoprong no photon events can come from higher multiplicity events in which some tracks went undetected. Therefore there exists a genuine two prong no photon class of events.

As mentioned in Section 6.1, charmed particles decay mostly into high multiplicity final states. Detailed estimates, given in Ref. 5, lead to the conclusion that not more than

Table 3

Multiplicity distributions: The number of inclusive electron events are given with N_{ch} charged tracks (including the electron) and N_γ photons observed. The electron momentum is $p_e > 0.2$ GeV/c.

(a) $E_{cm} = 3.99 - 4.52$ GeV

N_γ \ N_{ch}	2	3	4	5	6	7	8	9	10
0	21	9	13	6	3	2			
1	6	5	9	8	5	2	1		
2	4	7	8	6	2		1		
3		2	1	2	2				
4		1	2	2	1	1			
5				1	1				
6		1			1				
7	1	1							

(b) $E_{cm} = 4.52 - 5.2$ GeV

N_γ \ N_{ch}	2	3	4	5	6	7	8	9	10
0	16	9	9	6	1	2		1	1
1	9	7	2	1	5	2			
2	3	1	3	3	2	2	1		
3			1	3	1	1			
4		2		1					
5		1	2	1	1		1		
6			1			1			
7			1						

12 % of the twoprong no photon events can be attributed to decays of charmed hadrons. Therefore the remaining twoprong no photon events can only be understood if one assumes that a new weakly decaying particle different from the charmed particles is produced. The mass of this particle has to be above 1.8 GeV, since no anomalous electron events were found at E_{cm} = 3.6 GeV. Of course the heavy lepton is a good candidate for such a particle.

Before comparing the twoprongs with the heavy lepton hypothesis, we will concentrate on the multiprongs defined as events with three or more charged particles and any number of photons. These multiprongs are mainly due to charm decays. An upper limit of the contribution of a heavy lepton to the multiprong class was calculated to be 12 % from the measured branching ratio of a heavy lepton into multiprongs (see section 6.4) and the assumption that all our twoprongs arise from heavy lepton decays. As mentioned before, the contribution from charm to the twoprongs is less than 12 %. Therefore the two sources for the anomalous electron events are well separated by a cut on the charged multiplicity.

An independent check that the source for the twoprongs is different from the source for the multiprongs comes from the averaged number of kaons in each class: 0.90 $\pm$ 0.18 charged kaons/event for the multiprongs and 0.07 $\pm$ 0.06 charged kaons/event for the twoprongs [30]. The first value is in excellent agreement with the charm hypothesis, while the second value agrees with the value expected for a heavy lepton [25]. The values mentioned above were determined from twoprong and multiprong events with an identified hadron (π, K, $\bar{p}$) in one of the DASP spectrometer arms and an electron in the inner detector,

The electron spectrum for the multiprongs is shown in Fig. 13: (a) at threshold and (b) at all energies. The background from multihadrons and a heavy lepton, shown as the solid and dotted lines in Fig. 13 b was subtracted. The spectrum is rather soft: 85 % of the events have an electron momentum below 0.8 GeV/c. Such a soft spectrum was expected from charm decays, since even the decay modes with the lowest multiplicity $D \to e\nu K$ or $e\nu K^*$ give such a soft spectrum (see Fig. 13a) [27].

The cross section for the multiprongs is plotted in Fig. 14a as function of energy. The background and the contribution from a heavy lepton have been subtracted and radiative corrections were made. Fig. 14b shows the semileptonic branching ratio, defined as $\sigma(e^+e^- \to e^\pm \geq 2 \text{ prongs})/2\,\sigma(\text{charm})$. Here σ(charm) has been obtained from the increase in the total hadronic cross section above 4 GeV, after subtraction of the contribution from a heavy lepton. We used the PLUTO data on the total cross section. The average semileptonic branching ratio is 0.11 $\pm$ 0.03. This error comes mainly from the systematic error in σ(charm). An independent determination of the branching ratio is obtained from the fraction of events where a second electron was seen (27 events with an estimated background of 14 $\pm$ 2). This leads to an averaged semileptonic branching

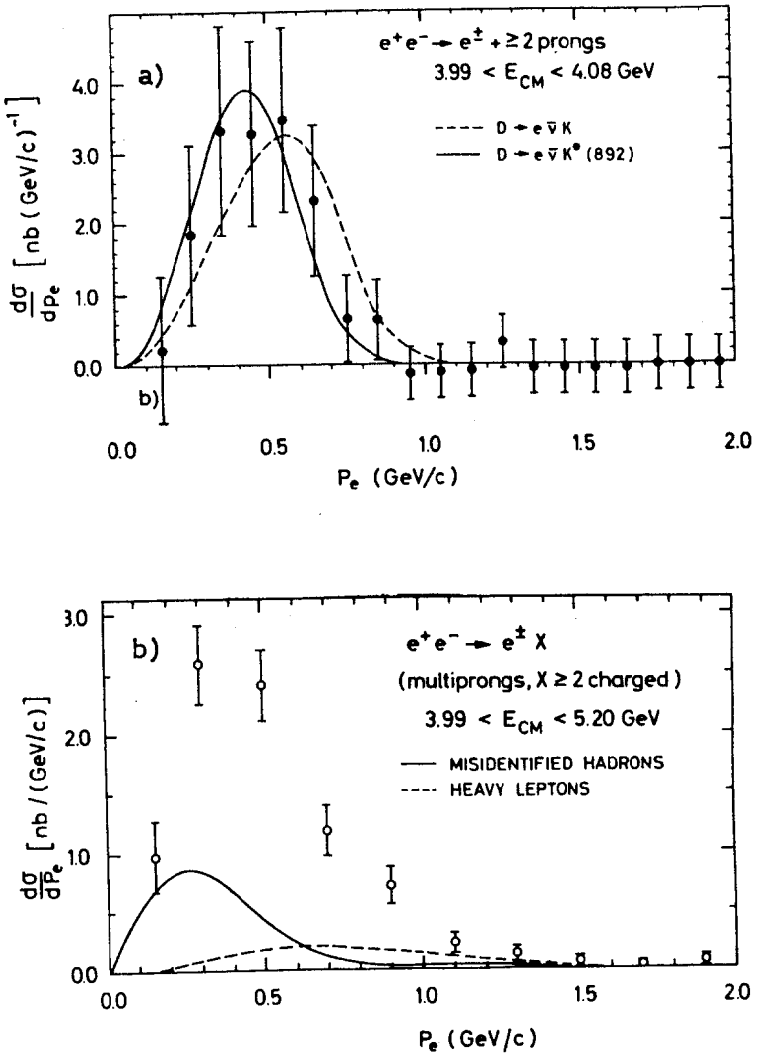

Fig. 13
Inclusive electron spectrum of multiprongs
a) at threshold b) all energies, DASP

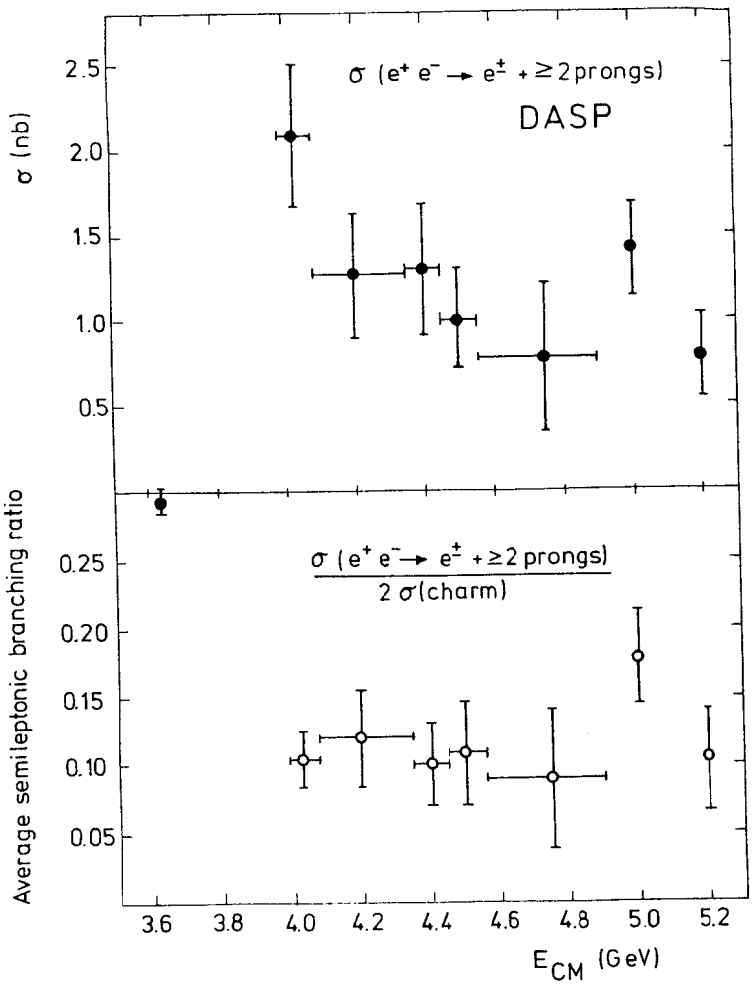

Fig. 14 Inclusive electron cross section (a) and semileptonic branching ratio (b) versus $\sqrt{s}$ for multiprongs ($N_{CH}>2$), DASP

ratio of 0.16 ± 0.06 in agreement with the previous value. Note that the latter value does not depend on σ (charm).

We now discuss the twoprong no photon events, thus excluding events with photons. The twoprong cross section as function of $\sqrt{s}$ is shown in Fig. 15. Here we included all twoprong data with a lepton (e or μ). The total number of observed twoprong events is listed in Table 4. The number of μX is lower than the number of eX events, because of the different momentum cutoffs (0.7 GeV/c for muons, 0.2 GeV/c for electrons).

The data in Fig. 15 were obtained after subtraction of the background given in Table 4 and the feed down from higher multiplicity events. The contribution of charm going into twoprong no photon events was estimated to be small. The energy dependence of the data agrees with the prediction from a heavy lepton (spin 1/2, V-A, $m_\tau = 1.9, m_{\nu_\tau} = 0$ GeV/c^2), shown as the solid line in Fig. 15. Also the lepton momentum spectra agree with this hypothesis, as shown in Fig. 16. The data below 0.7 GeV/c has been corrected for the muon momentum cutoff by assuming eμ universality.

Note the difference between the spectra of the multiprongs (Fig. 13) and twoprongs, which extend up to 1 GeV/c and 2 GeV/c, respectively. This indicates again the different origin of twoprongs and multiprongs.

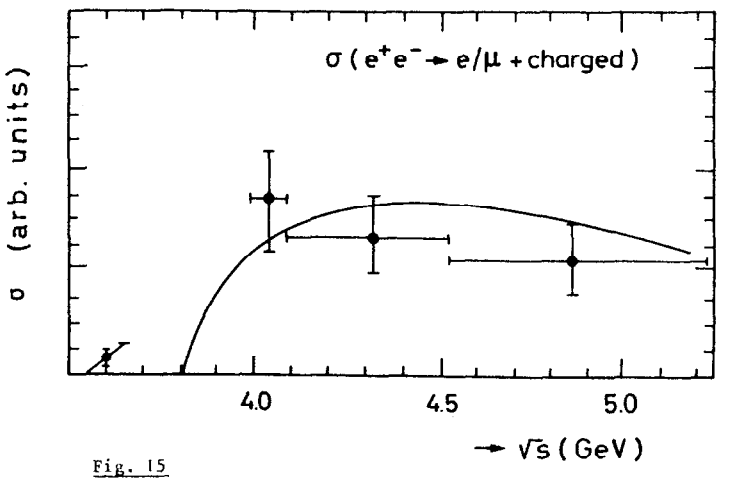

Fig. 15
Energy dependence of twoprong no photon events (eμ + μC + eC) and expectation from a 1.9 GeV heavy lepton (solid curve, V-A assumed).

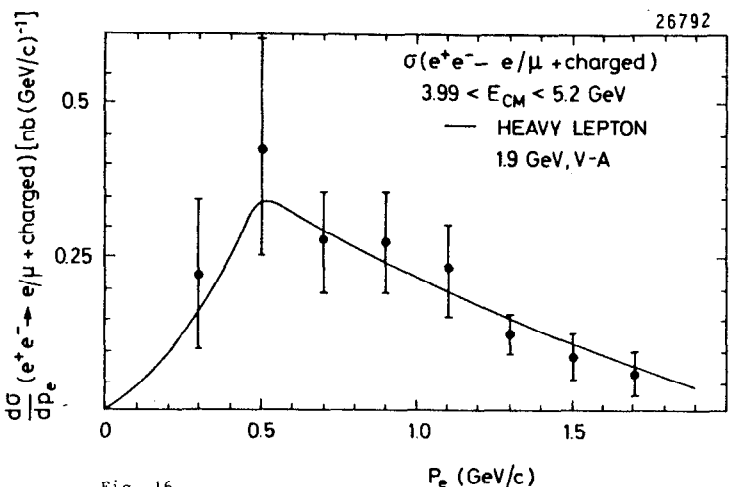

Fig. 16
Inclusive lepton spectra of twoprong no photon events DASP.

Table 4 Number of observed twoprong no photon events for $4.0 \leq \sqrt{s} <$ 5.2 GeV, DASP.

Event signature	Number of events	Background (multihadrons, QED) (events)	Feeddown from multiprongs (events)
eμ	11	0.7 ± 0.3	0.1 ± 0.1
e + 1ch + 0γ	37	5.6 ± 1.4	6.7 + 2
μ + 1ch + 0γ	14	2 ± 0.5	1 ± 0.3

Table 5 Fits to inclusive muon spectra, PLUTO

spin	decay	m_{ν_τ}	m_τ	BR(1) BR(μ)	χ^2 / DF
0	$\sim K_{13}$	0	1.67 ± 0.08	1.35 ± 0.29	6.5/9
1/2	V-A	0.5	1.72 ± 0.09	$.130 \pm 0.017$	22.5/9
1/2	V+A	0	1.79 ± 0.07	$.136 \pm 0.019$	15.1/9
1/2	V-A	0	1.91 ± 0.03	$.109 \pm 0.012$	10.3/9

Table 6 eμ - and μμ - events and backgrounds, for $4.0 < \sqrt{s} < 5.0$ GeV, PLUTO

event signature	number of events	background	visible cross section
$e^\pm \mu^\mp$	23	2	33 pb
$\mu^+ \mu^-$	6	0	8 pb
$e^\pm \mu^\pm$	0	0	0 pb
$e^\pm \mu^\mp$ + n γ	4	2	5 pb
$e^\pm \mu^\mp$ + ≥ 1 pr	7	8	0

From the ratio of twoprongs with electrons to twoprongs with muons one finds $B(e)/B(\mu) = 0.8 \pm 0.3$. This ratio is consistent with one. Therefore we assumed $B(e) = B(\mu)$ and then found from the eμ-events $B(e) = B(\mu) = 0.20 \pm 0.03$.

6.4 Anomalous muon production

Both PLUTO and DASP have studied inclusive muon production. Here we will restrict ourselves to the PLUTO data [31], since the DASP muon data has been shown together with the electron data. The PLUTO detector is very suitable for muon detection, because of its compact, thick iron yoke, which gives a short decay path for pions and kaons and little punch through ($P_{h \to \mu} = 2.8 \pm 0.7$ %, see section 2). The disadvantage is a rather high momentum cutoff of 1 GeV/c, which makes it difficult to observe the semileptonic decays of charmed particles (compare Fig. 13). A muon event is defined by a particle with $|\cos\theta| < 0.75$ penetrating the iron absorber and at least one other track with $|\cos\theta| < 0.87$ having a momentum above 0.2 GeV/c. Background from $e^+e^- \to \mu^+\mu^-$ was removed by requiring an acoplanarity of at least 10°, while contributions from $e^+e^- \to \mu^+\mu^-\gamma$ could be removed by a cut in the missing mass squared [31]. After subtraction of a small remaining background from $e^+e^- \to \mu^+\mu^-\gamma\gamma$ and misidentified hadrons, 215 twoprong and 108 multiprong events remained. The momentum spectrum of the twoprongs is shown in Fig. 17 for three energy intervals. The sharp slope of the spectra excludes a twobody decay, for which a flat spectrum is expected. A second important feature is the

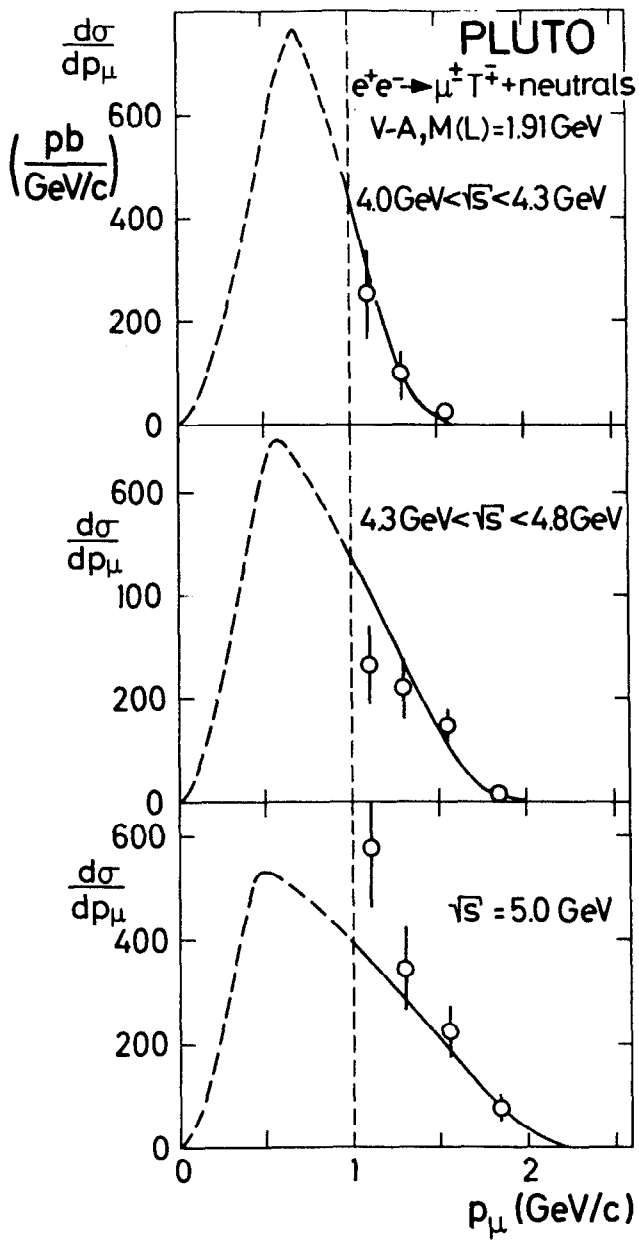

Fig. 17 Inclusive muon spectra of twoprongs, PLUTO

shifting of the spectra towards higher momenta at higher center of mass energies. This is characteristic for the decay from a pair of fixed mass particles due to the Lorentz boost. The Lorentz boost is also evident from the coplanarity distribution of the twoprongs, shown in Fig. 18 for the three energy intervals. A clear shrinking of this distributions at the higher energies is seen.

The spectra of Fig. 17 have been fitted to the heavy lepton hypothesis by varying spin, coupling and the masses m_τ and $m_{\nu\tau}$. The results are presented in Table 5. The spin zero assignment is ruled out (higgs boson ?), even though the χ^2 is smallest, because the resulting branching ratio B(μ) 100 %. This is ruled out by the relative number of eμ and μμ events (see Table 6). The large χ^2 of the next fit with $m_{\nu\tau} = 0.5$ GeV/c^2 excludes the assumption that a new baryon is observed, which decays into n + μ + ν. Among the last two fits the V-A coupling is favoured, although the V+A coupling cannot be ruled out. The last fit is represented by the solid lines in Fig. 17. The resulting mass is 1.91 ± 0.03 GeV/c^2. Fig. 19 shows the muon momentum spectrum of the multiprongs at $\sqrt{s}$ = 5 GeV. The solid line represents a fit to the data at all energies with the parameters for a heavy lepton of the last line of Table 5. A comparison of the multiprongs and the twoprongs yields B(1) = 0.7 ± 0.1, B(≥ 2) = 0.3 ± 0.1, and B(μ) = 0.15 ± 0.03. From the eμ events one then finds: B(e) = 0.14 ± 0.04. Fig. 20 shows the agreement between the electron spectrum of the eμ events and the prediction for a heavy lepton with the parameters of the last line of Table 5, taking into account the decreasing

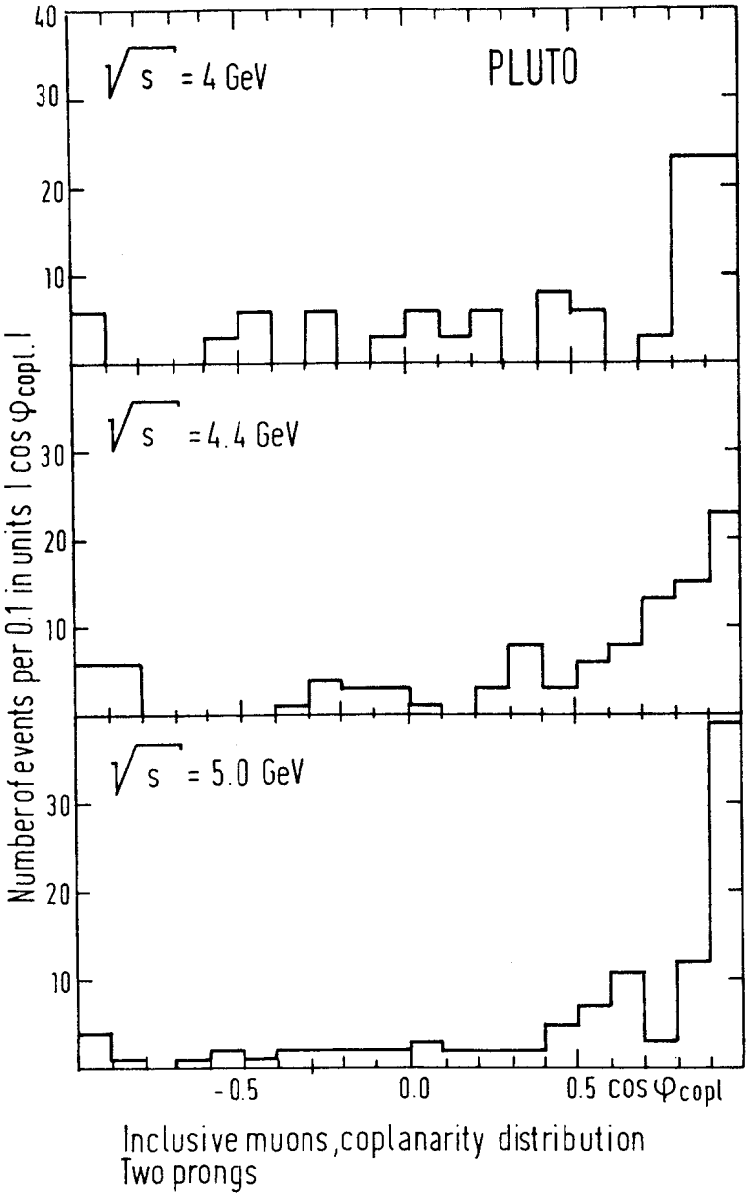

Fig. 18 Coplanarity distribution of inclusive muon twoprong events

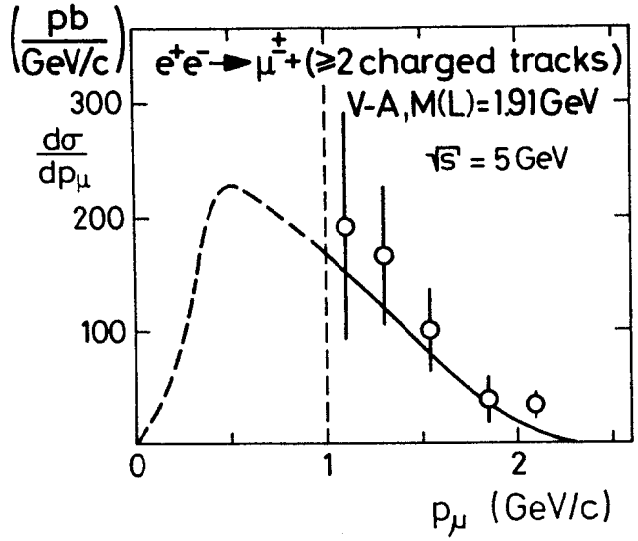

Fig. 19 Inclusive muon spectra of multiprongs, PLUTO

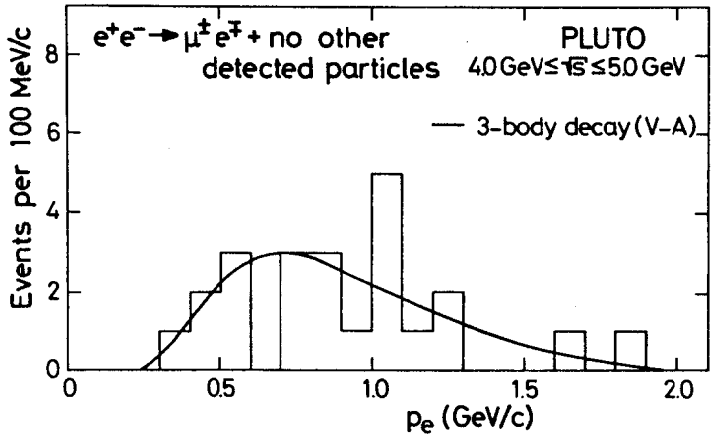

Fig. 20 Electron spectrum of eμ events, PLUTO

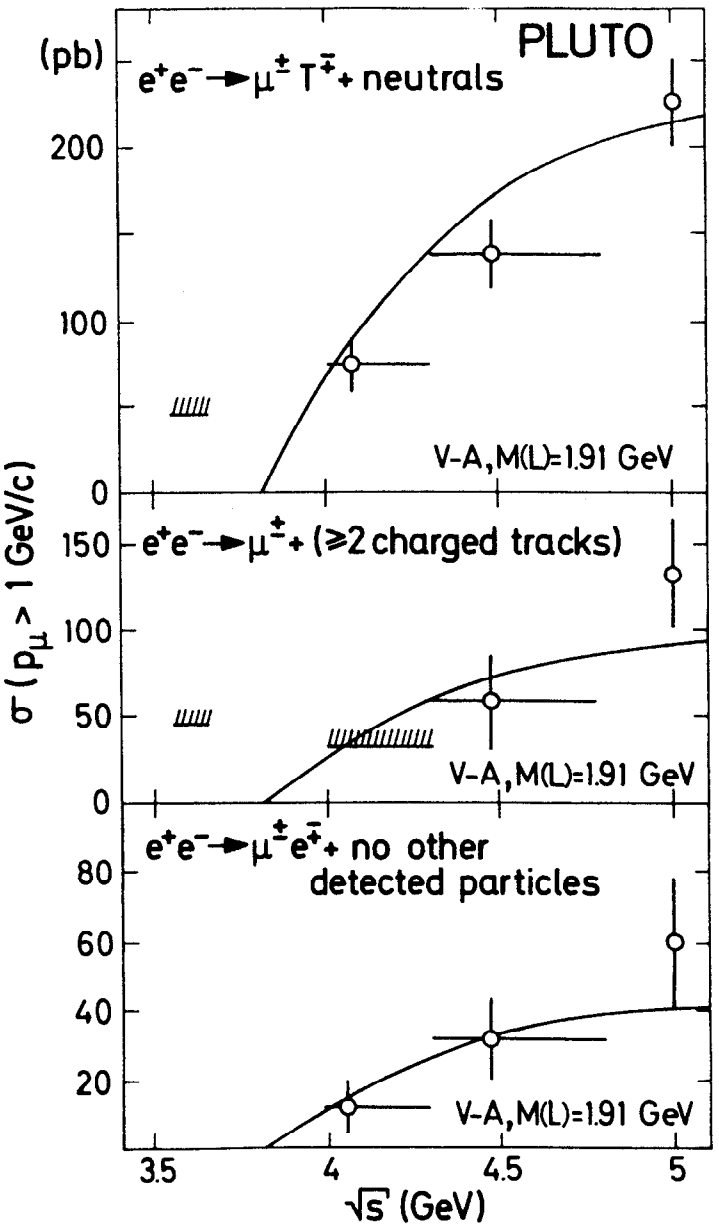

Fig. 21 Inclusive muon cross sections versus $\sqrt{s}$ for twoprongs, multiprongs and ue events. The curves are expectations from τ decay.

electron detection efficiency at low momenta (solid curve). The cross sections for the various event classes are shown in Fig. 21 as function of center of mass energy. They all show the same threshold behaviour and agree with the heavy lepton hypothesis, represented by the solid lines.

7. F-meson production

The charm model [17] predicts, besides the existence of ψ's ($c\bar{c}$ quark pairs) and D-mesons ($c\bar{u}$ or $c\bar{d}$ quark pairs), the existence of F-mesons, made out of a charmed quark and a strange quark ($c\bar{s}$ or $\bar{c}s$ quark pairs). The F-mesons form two isosinglets with charges + 1 and - 1. The lowest mass F-meson should have a weak decay predominantly into an $s\bar{s}$ system, leading to final states containing $K\bar{K}$, ϕ, η or η'. The strong decay of the first excited state $F^* \to F\pi$ is forbidden by isospin conservation and the decay $F^* \to F\pi\pi$ is likely to be forbidden by energy conservation. As will be shown below, the difference between the F^* and F mass is indeed less than 2 pion masses. Therefore the main decay mode of the F^* will be the electromagnetic decay $F^* \to \gamma F$. In case of $D^+ \to \gamma D$ such an electromagnetic decay can be observed as an enhanced low energy photon production, as shown in Fig. 22: the fraction of events with a photon with energy below 0.2 GeV/c (called γ_{low}) is clearly larger at 4.03 GeV than at other energies. At 4.03 GeV D^* production is known to be copious [4, 16]. There is also an enhancement around 4.4 GeV, which could be due to F^* production.

DASP searched for F production by measuring inclusive η

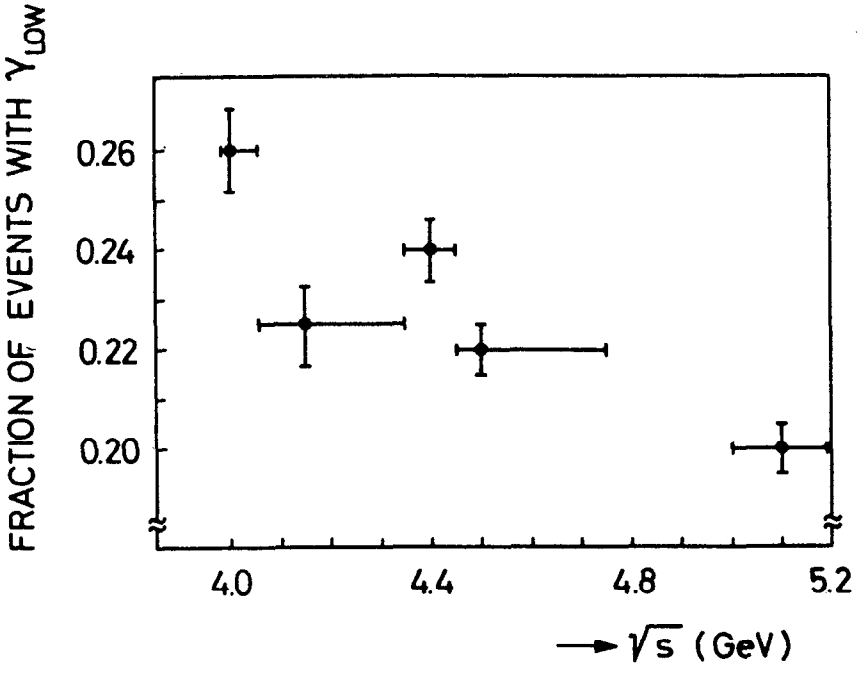

Fig. 22 Fraction of events with a low energy photon versus $\sqrt{s}$.

production in conjunction with a low energy gamma. η's can be detected in the DASP inner detector via its 2γ decay mode. Because η is a frequent byproduct of η' a search for η includes a search for η'. From the energy resolution ($14\%/\sqrt{E}$) and the angular resolution (0.03 radians) of the shower counter one finds an invariant η mass resolution of about 80 MeV.

Fig. 23 shows the invariant mass spectra of all $\gamma\gamma$ combinations for events required to have more than one charged track coming from the interaction point, one photon with $E_\gamma < 0.14$ GeV, and more than one photon with $E_\gamma > 0.1$ GeV. The total momentum of the $\gamma\gamma$ combination was required to be between 0.3 and 1.2 GeV/c. Beam gas background was further reduced by requiring that at least 0.1 GeV be deposited in the forward and backward hemisphere with respect to the beam axis. The solid lines in Fig. 23 represent the background, obtained by reconstructing invariant masses from uncorrelated photon pairs belonging to different events with the same number of photons. This background was normalized to $\gamma\gamma$ combinations with $m_{\gamma\gamma} > 0.7$ GeV/c^2. However, the 'renormalization' was always less than 15 %, since the spectra for the uncorrelated photons were obtained from the same event sample as the spectra for the correlated photons.

At all energies one sees an enhancement at the π_o mass in Fig. 23 with no further significant peaks. However, as shown in Fig. 24a, a significant enhancement around the η mass has been observed at $E_{cm} = 4.4$ GeV. The signal (104 events) with

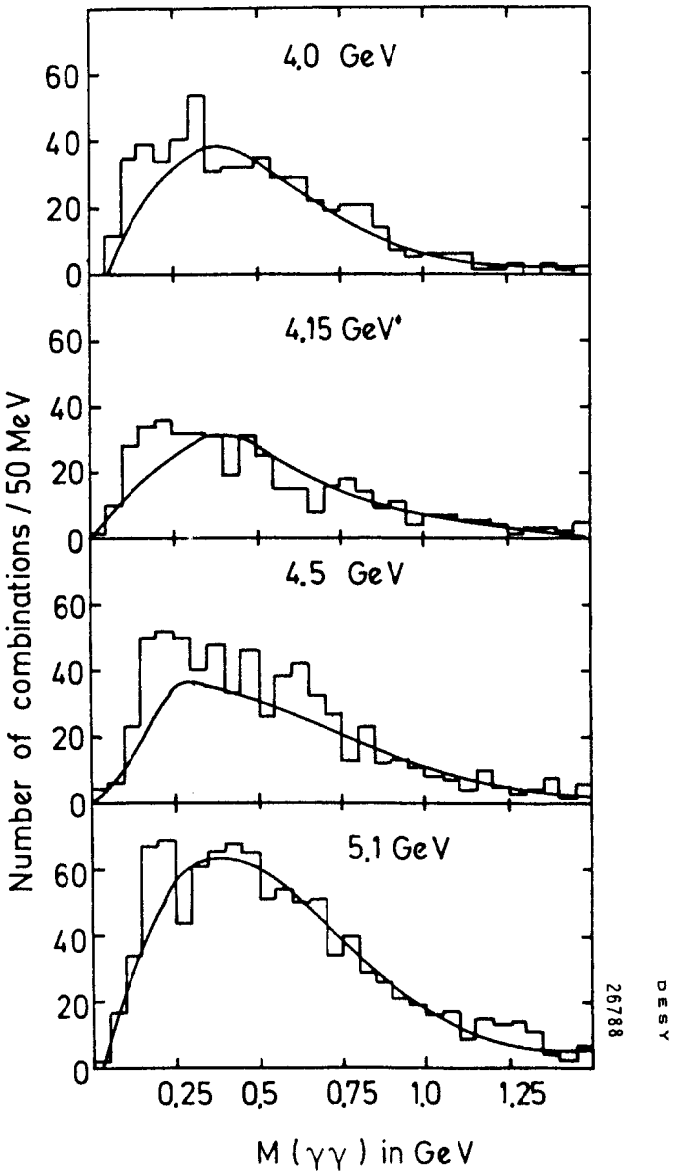

Fig. 23 Invariant γγ mass spectra at various center of mass energies.

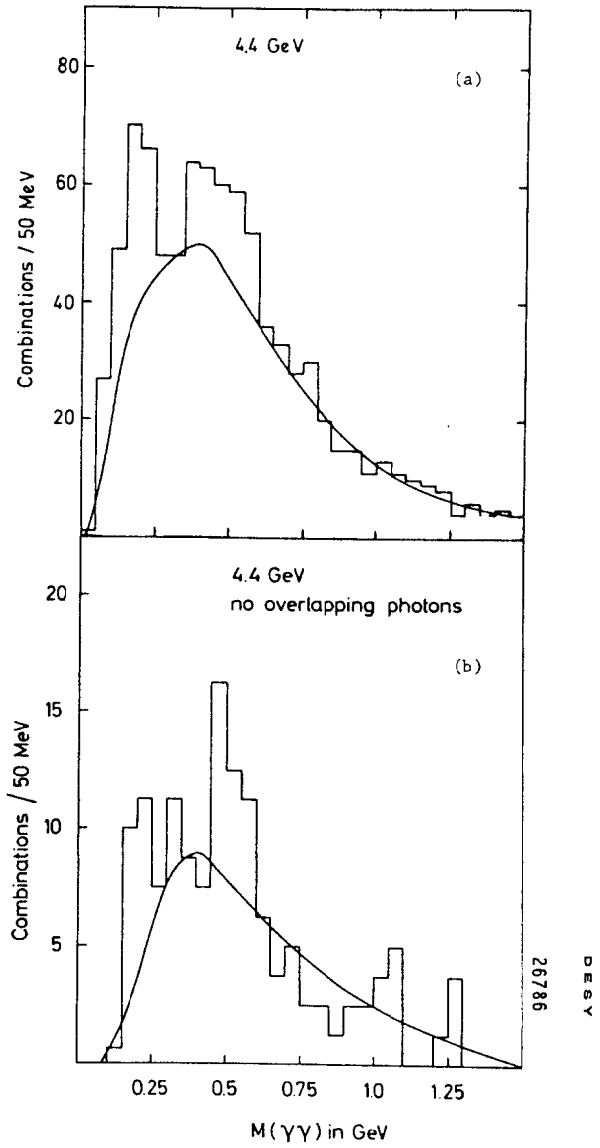

Fig. 24 Invariant γγ mass spectra at $\sqrt{s}$ = 4.4 GeV (a) all data (b) only events, in which there is no overlap between photons and other tracks in the same scintillator of the shower counter.

$0.45 \leq m_{\gamma\gamma} < 0.65$ GeV is more than five standard deviations above background (180 events). An improvement in the signal to background ratio can be obtained by excluding events in which the photons overlap with other particles in the scintillators of the shower counter, thus degrading the energy measurement. The $\gamma\gamma$ mass spectrum for the "clean" events is shown in Fig. 24b.

To test if the excess of low energy photons (γ_{low}) is correlated with η production, we plotted in Fig. 25 the fraction of events with γ_{low} versus $M_{\gamma\gamma}$. As expected from Fig. 22, this ratio is seen to be higher at 4.0 GeV, but independent of $M_{\gamma\gamma}$. However, at 4.4 GeV there is a clear enhancement at the η mass. The curve at 4.4 GeV represents a Gaussian with a width and peak value expected for the η superimposed on a background obtained from a smooth curve through the average ratios at 4.15 and 4.5 GeV.

Fig. 26 shows the visible cross section $e^+e^- \to \gamma_{low} + \eta + X$ as function of center of mass energy. The open cirles were obtained from the excess of events in Fig. 24a. An independent estimate of the background was obtained from the assumption that all events not having a low energy photon are a measure of the background [8]. The results are represented by the black points in Fig. 26. The two methods give the same results, thus showing also that η's are predominantly produced in conjunction with a low energy photon.

In order to determine the mass of the F meson, we searched for the simple two body decay of the F into $\pi\eta$ [8]. The pion

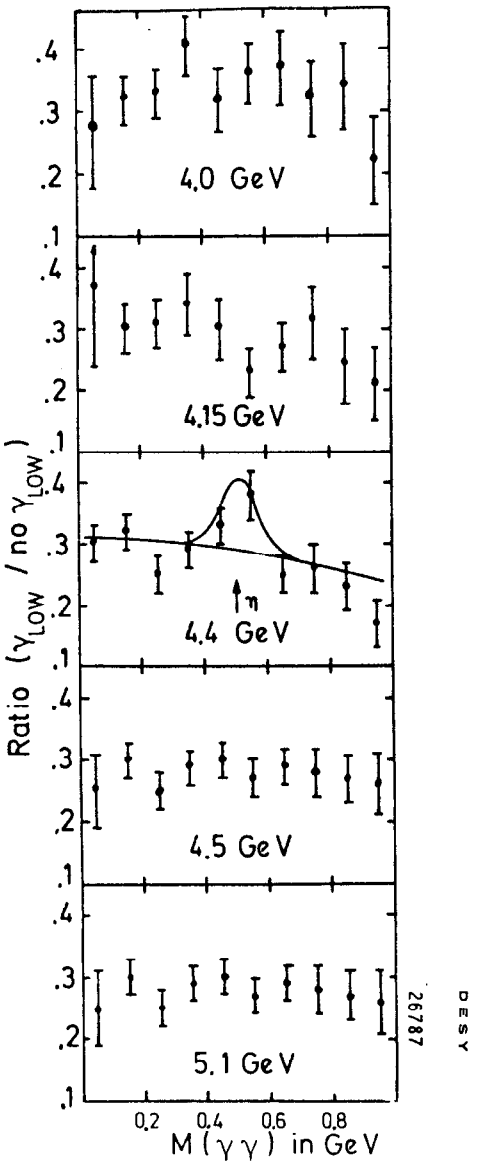

Fig. 25 Ratio of events with γ_{low} and events without γ_{low} versus $M_{\gamma\gamma}$.

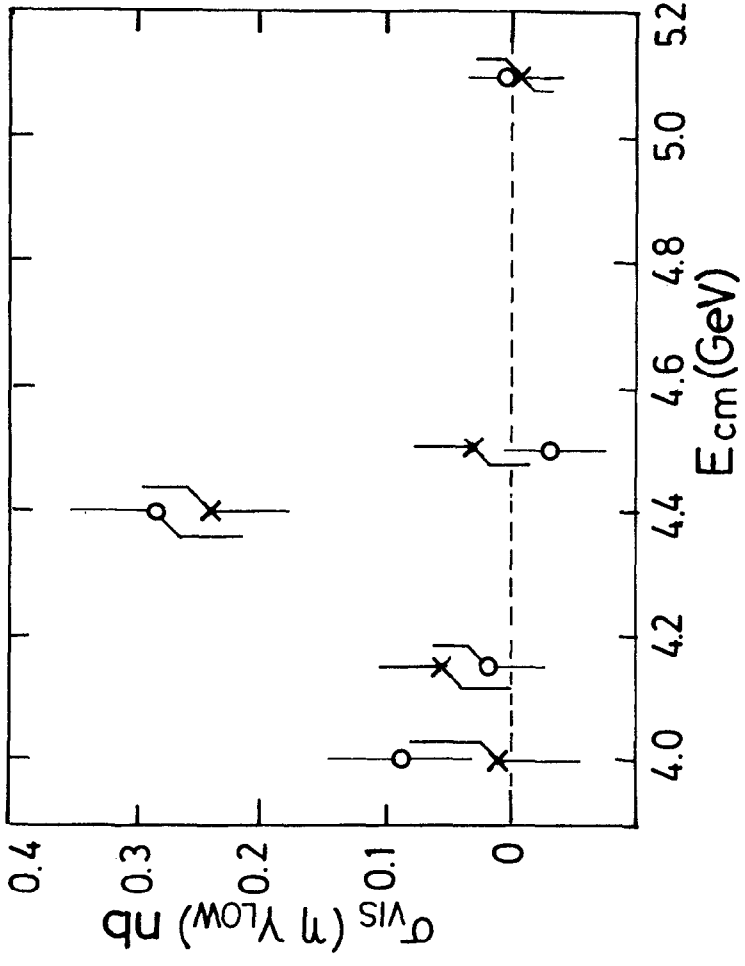

Fig. 26 Cross section for $e^+e^- \to \gamma + \eta + X$ (O = background from uncorrelated γγ pairs) (X = background from events without low energy photon)

was required to be in one of the spectrometer arms, thus determining fully its position and momentum. The events had to fulfil the following selection criteria: the pion momentum is above 0.6 GeV/c, there are at least two photons with energies above 0.1 GeV forming a γγ invariant mass in the η mass region, and there is at least one more photon with an energy below 0.2 GeV.

A total of 35 events satisfied these selection criteria. The events were fitted to the reactions

$$e^+e^- \to FF^* \to (\pi\gamma\gamma)\ (\gamma_{low})\ (X) \qquad (1)$$

$$e^+e^- \to F^*F^* \to (\gamma_{low})\ (\pi\gamma\gamma)\ (X') \qquad (2)$$

There are two constraints to these reactions, namely $M_{\gamma\gamma} = M_\eta$ and $M_X = M_{\pi\eta}$ for (1) or $M_{X'} = M_{\pi\eta} + M_{\gamma_{low}}$ for (2). For (2) this constraint only works if one selects the right γ_{low}. The recoil masses M_X or $M_{X'}$ can be calculated since the initial state and the remaining four vectors in the final state are known.

There were 15 events, which gave a fit to hypothesis (1) with a $\chi^2 < 8$. We made two additional cuts, namely a cut on the difference between the fitted πη mass and the measured πη mass. Three events are lost by this cut as shown in Fig. 27a. Furthermore we required $|M_{\pi\eta} - M_{recoil}| < 0.2$ GeV/c^2, since we required in the analysis that the energy of the low energy photon was less than 0.2 GeV. Four events are lost by this cut, as shown in Fig. 27b, where we plotted $M_{recoil} - M_{\pi\eta}$ versus $M_{\pi\eta}$ for two energy intervals. For the remaining 8 events at 4.4 GeV we

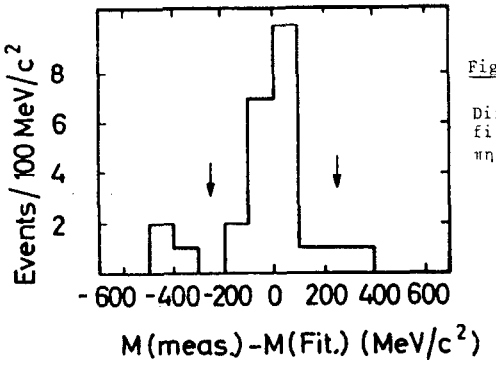

Fig. 27a

Difference between fitted and measured $\pi\eta$ mass.

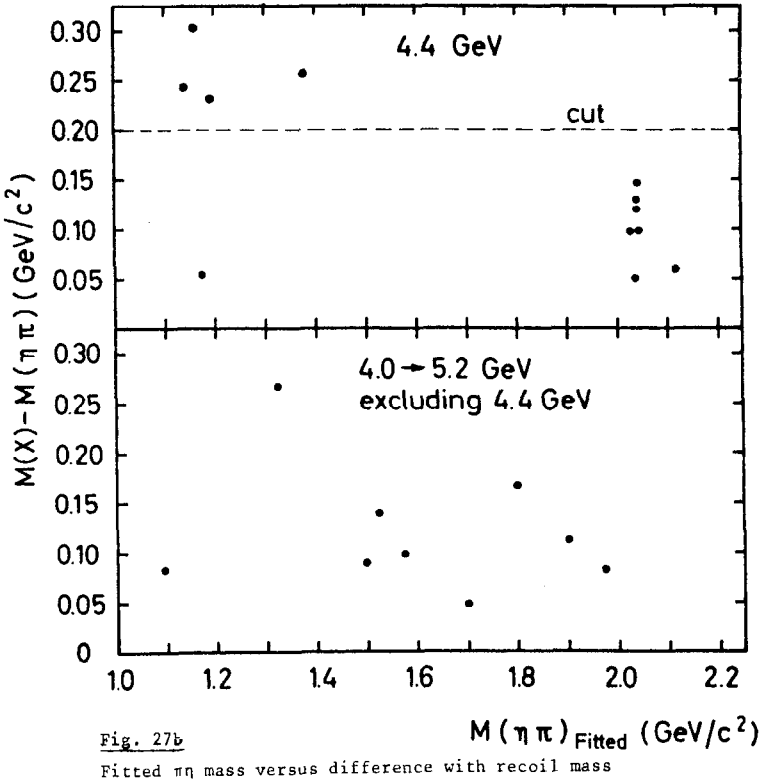

Fig. 27b

Fitted $\pi\eta$ mass versus difference with recoil mass

plotted M_{recoil} versus $M_{\pi\eta}$ in Fig. 28. There is a clear cluster of seven events at $M_{\pi\eta} = 2.04$ GeV/c^2, indicating that these events are indeed coming from reaction (1) or (2). The fact that there are no events in the neighbourhood of this cluster shows that the background is negligible. This can also be seen from Fig. 27b: a similar luminosity was taken at the energies 4.03, 4.4, 4.5, 5.0 and 5.2 GeV, but one sees only a cluster at $E_{cm} = 4.4$ GeV.

We therefore conclude that we see a real signal for $F\bar{F}^*$ or $F^*\bar{F}^*$ production. The latter possibility cannot be ruled out, since most of the events gave also a good χ^2, when fitted to the second hypothesis (2). This fit shifts the $\pi\eta$ mass by about 0.06 GeV. For the averaged value between the two fits, we find

$$M_{\pi\eta} = M_F = 2.03 \pm 0.06 \text{ GeV/}c^2$$

and $M_{recoil} = M_{F^*} = 2.14 \pm 0.06$ GeV/c^2

From $E(\gamma_{low})$ one finds directly $M_{F^*} - M_F = 0.12 \pm 0.04$ GeV/c^2.

Summarizing the results on the F-meson, we find a significant production of η with a low energy photon only near 4.4 GeV. The η production is predominantly accompanied by a low energy photon. The total η production cross section is a substantial fraction of the $\psi(4413)$ cross section, indicating that $F\bar{F}^*$ or $F^*\bar{F}^*$ may be major decay modes.

Analysing events containing η, π and a low energy photon in the final state and fitting these events to either

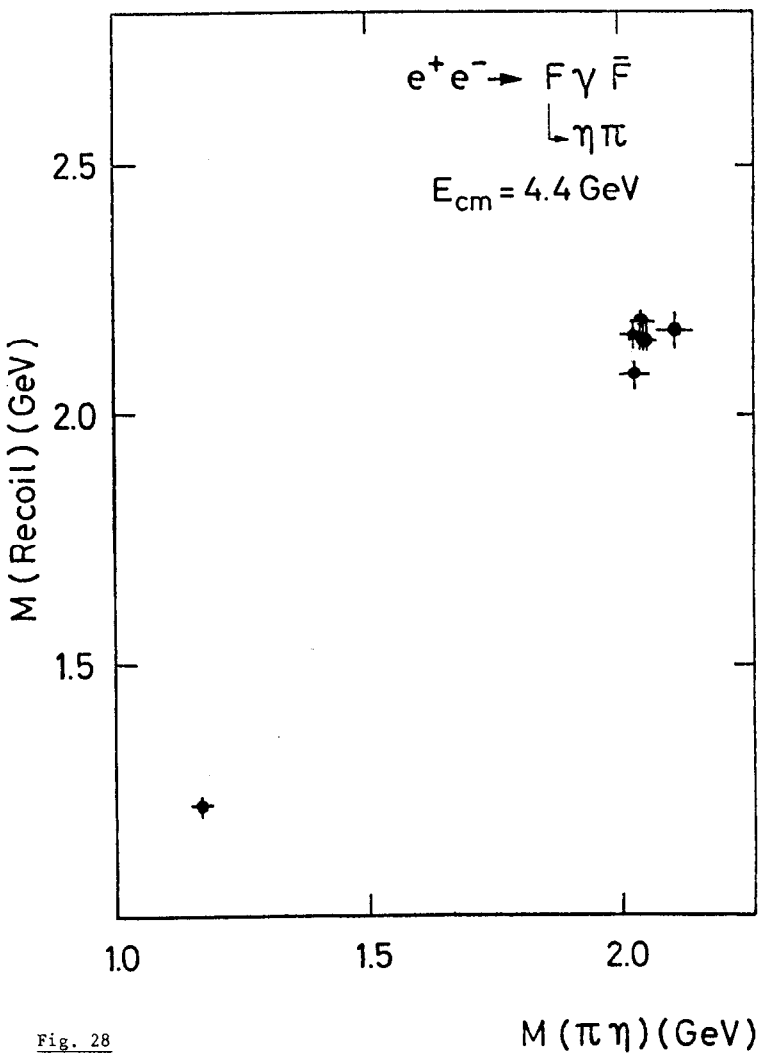

Fig. 28
Fitted πη mass versus recoil mass, DASP.

$e^+e^- \to F\bar{F}^*$ or $F^*\bar{F}^*$ we find 7 events which give the same F and F^* mass values, $m_F = 2.03 \pm 0.06$ GeV and $m_{F^*} = 2.14 \pm 0.06$ GeV. From the energy distribution of the low energy photon alone we find $m_{F^*} - m_F = 0.12 \pm 0.04$ GeV.

ACKNOWLEDGEMENTS

I wish to express my sincere thanks to all who contributed to this report.

References

1) G. J. Feldman and M. L. Perl, Physics Reports 19C, 234 (1975), and SLAC-PUB-1972(1977), to be published in Physics Reports

2) R. F. Schwitters and K. Strauch, Ann. Rev. Nucl. Sci. 26, 89(1976)

3) B. H. Wiik and G. Wolf, DESY Report DESY 77/01(1977)

4) SLAC-LBL Coll., G. Goldhaber et al., Phys. Rev. Letters 37, 255(1976)

5) DASP Coll., W. Braunschweig et al., Phys. Lett. 63B, 466 (1976), DASP Coll., R. Brandelik et al., DESY 77/41, to be published in Phys.Lett.

6) PLUTO Coll., J. Burmester et al., Phys. Lett. 67B, 367 (1977)

7) DASP Coll., R. Brandelik et al., Phys. Lett. 67B, 363(1977)

8) DASP Coll., R. Brandelik et al., DESY 77/44, submitted to Phys. Lett.

9) SLAC-LBL Coll., M. Perl et al., Phys. Rev. Lett. 35, 1489 (1975), 63B, 466(1976)

10) SLAC-LBL Coll., J. Siegrist et al., Phys. Rev. Lett. 36, 700(1976)

11) PLUTO Coll., J. Burmester et al., Phys. Lett. 66B, 395 (1977)

12) M. L. Perl and R. Rapidis, SLAC-PUB-1496(1974)

13) DASP Coll., W. Braunschweig et al., Phys. Lett. 67B, 243 (1977)

14) DESY-HD Coll., W. Bartel et al., Phys. Lett. 64B, 483 (1976) and Phys. Lett. 66B, 489(1977)

15) V. Lüth, this Conference

16) G. Feldman, this Conference

17) S. L. Glashow, J. Iliopoulos and L. Maiani, Phys. Rev. D2, 1285(1970), a review on charm is given by M. K. Gaillard, B. W. Lee and J. L. Rosner, Rev. Mod. Phys. 47, 277(1975)

18) J. L. Rosner, Proceedings of the Orbis Scientiae, Coral Gables, (Jan. 1977), J. L. Rosner and C. Quigg, Fermilab-PUB-77/60-THY(1977)

19) PLUTO Coll., J. Burmester et al., Phys. Lett. 64B, 369 (1976)

20) S. D. Drell, D. Levy and T. M. Yan, Phys. Rev. 187, 2159 (1969), D1 1035, 1617, 2402(1970)

21) DASP Coll., R. Brandelik et al., Phys. Lett. 67B, 358 (1977)

22) PLUTO Coll., U. Timm, Invited talk at the EPS European Conf. on Particle Physics, Budapest (Aug. 1977)

23) G. G. Hanson, Talk given at the XVIIIth Int. Conf. on High Energy Physics, Tiblisi, USSR(1976); SLAC-PUB-1814(1976). See also Ref. 15.

24) E. G. Cazzoli et al., Phys. Rev. Lett. 34, 1125(1975), B. Knapp et al., Phys. Rev. Lett. 37, 882(1976)

25) Y. S. Tsai, Phys. Rev. D4, 2821(1971), H. B. Thacker and J. J. Sakurai, Phys. Lett. 36B, 103(1971)

26) K. Fujikawa and N. Kawamoto, Phys. Rev. D14, 59(1976)

27) A. Ali and T. C. Yang, Phys. Lett. 65B, 275(1976)

28) PLUTO Coll., J. Burmester et al., 68B, 297(1977)

29) M. Perl, Proc. of the XII Rencontre de Moriond, Flaine (March 1977) to be published, SLAC-PUB-1923 (Apr. 1977)

G. Flügge, Proc. of the Vth International conf. on Experimental Meson Spectroscopy, Northeastern Univ., Boston, Massachusetts, (Apr. 1977)

30) DASP Coll., R. Brandelik et al., Phys.Lett. 70B, 125 (1977)

31) PLUTO Coll., M. Meyer, Proceedings of the Orbis Scientiae, Coral Gables (Jan. 1977) and DESY 77/19, PLUTO Coll., J. Burmester et al., Phys. Lett. 68B, 301(1977)

Initial Results from DELCO at SPEAR

Janos Kirz

W.W. Hanson Laboratories of Physics
Stanford University
Stanford, California 94305

and

State University of New York at Stony Brook†
Stony Brook, New York 11794

I. Introduction

DELCO is the new experiment at SPEAR. It was installed just five months ago in the East Pit, and this is the first report on the experiment.

It is well known that it takes at least a year before a major new experiment is debugged, understood, the software developed, and the data analyzed. It is therefore premature to talk about results, and I should entertain you with details of the hardware and the analysis. You, in turn - if this does not interest you greatly, should have the pleasant choice between a nap and another cup of coffee. But wait:

In an effort not to lose you all at the outset, I promise to go beyond nuts and bolts, premature or not, and spend the second half of my time showing you our first results.

What I have to say today is the result of a great deal of sweat and blood on the part of all the people who designed, built, tested, installed, and ran the experiment. I should introduce at least the following:

SLAC/STANFORD

Aaron Baumgarten
Alain Diamant-Berger
Len Birkwood
Roger Coombes
Martin Faessler
Anne Hall
Jasper Kirkby*
Janos Kirz
John Liu
Dale Ouimette
Dan Porat
Karol Porzuczek
Cliff Rasmussen
Mel Schwartz
Stan Wojcicki
Crt Zupancic

U.C. IRVINE

Ronnie Burns
Paul Condon
Paul Cowell

U.C.L.A.

Walt Bacino
Chuck Buchanan
Miro Chronoviat
Tom Ferguson
John Hauptman
Larry Nodulman
Bill Slater
Harold Ticho

* Spokesman

II. Apparatus

DELCO stands for "Direct Electron Counter". The basic objective of the experiment is to detect leptonic or semileptonic decays of new particles, by identifying electrons (or positrons) among the particles produced in hadronic annihilations. And because the measurement of R has been such an important tool for finding new physics, DELCO provides an independent measurement of it, and of the contribution made to R by events with electrons. The heart of the detector (Figs. 1,2) is an atmospheric threshold Cerenkov counter[1], filled with ethane, which detects electrons over 60% of the total solid angle. (Compare DASP: 7%, Lead Glass Wall:6%). But DELCO is really a rather general detector capable of studying most aspects of e^+e^- interactions: The interaction region is at the center of a cylindrical multiwire proportional chamber. This chamber consists of 6 layers with a total of nearly 4000 wires, with 2 mm spacing. Mechanical

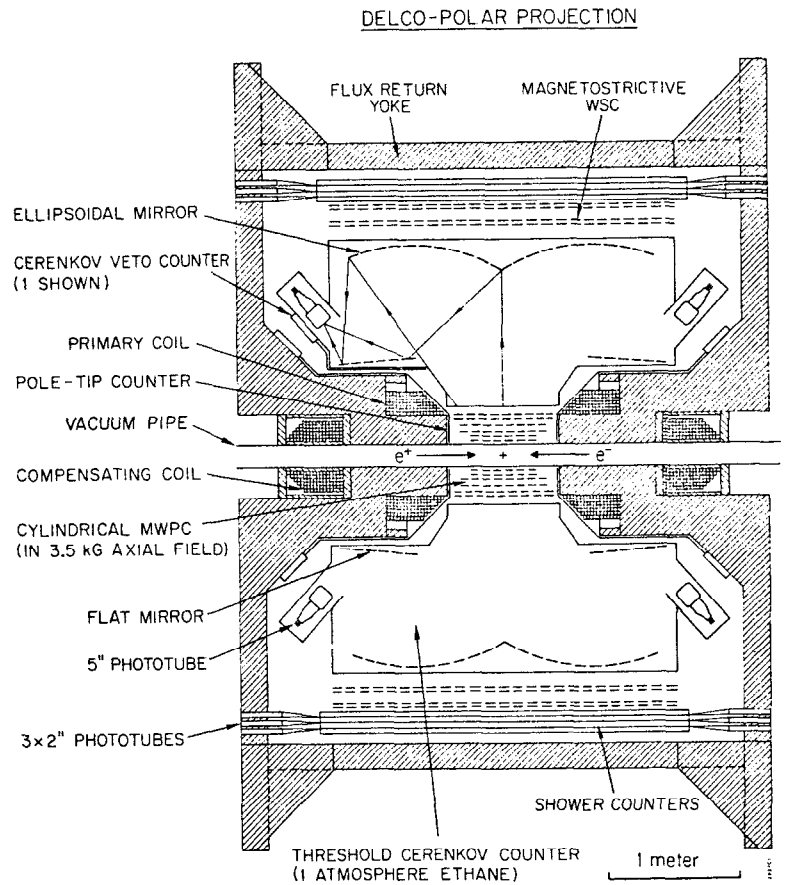

Figure 1

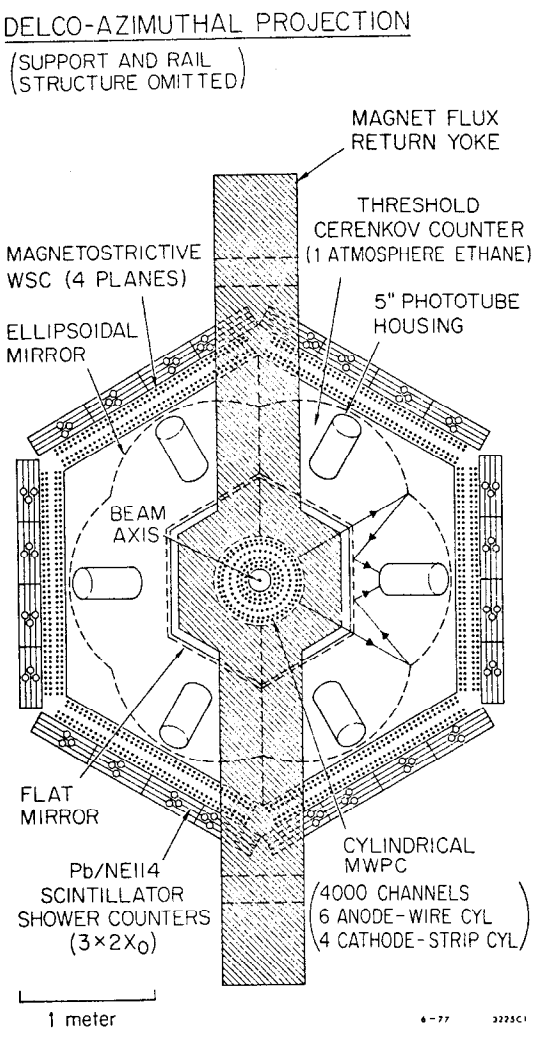

Figure 2

support is provided by low density (29mg/cm^3) styrofoam. The innermost layer is at a radius of 10 cm, the outermost one at 30 cm. In addition to azimuth information, provided by the wires, polar angle measurements are obtained from four cathode (high voltage) planes, which are subdivided into 1 cm wide strips oriented at $\pm 45^o$ with respect to the wires.

This chamber sits in an axial magnetic field of about 3.5 kg generated by a specially designed magnet which leaves most of the space around the interaction region open for particle detection. The beams pass through holes in the polepieces. The return yoke is outside the outermost detectors. The total field integral provides an average azimuthal bend of 50 MeV/c.

Outside the proportional chamber the detector has hexagonal symmetry. Particles traverse the Cerenkov counter, then two magnetostrictive spark chambers, and finally a shower counter. Each sextant of the Cerenkov counter is further subdivided into two cells by a plane perpendicular to the beam direction. The average Cerenkov radiator traversed is 1 meter. The light in each of the 12 Cerenkov cells is focused by an ellipsoidal mirror (via a plane mirror) on a 5" RCA 4522 photomultiplier, coated with PTP wave shifter. In the absence of magnetic bending, all Cerenkov light reaches the photocathode, generating 12 photoelectrons on average for a β=1 particle. One nice feature of the ellipsoid is that all optical paths are isochronous, therefore we can impose stringent timing cuts on Cerenkov signals. (Fig. 3).

In fact, only the light which originates at one focus (the interaction point) is collected at the other focus (the photocathode). The spread due to the finite angle of Cerenkov emission just about fills the area of the 5" photocathode. The bending of low momentum particles in the magnetic field however moves the effective light source away from the

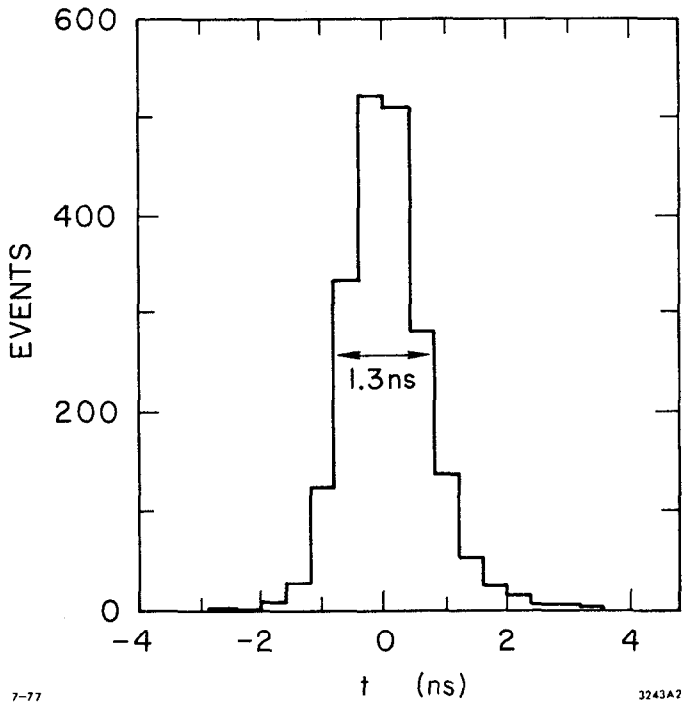

Figure 3 - Distribution of Cerenkov pulse times for $e^+e^-\to e^+e^-$ events compared to the expected time based on the beam-crossing signal.

focus, and this leads to a gradual decrease in the efficiency of the counter below 350 MeV/c.[1] To reduce γ-ray conversions and multiple scattering, the total amount of material seen by the interaction products is kept small: 3.5% of a radiation length for particles perpendicular to the beam direction, made up as follows:

	thickness	g/cm^2	$\%l_r$
Vacuum pipe (stainless steel)	0.015cm	0.12	0.86
MWPC (styrofoam), etc.	20 cm	0.85	2.4
Cerenkov window + ethane	80 cm	0.10	0.2

At this point we reach the mirrors, which are 1.5m x 1.5m objects, constructed by replication of a male mold with a polyester resin/flexcore hexel/polyester resin sandwich.

Outside the Cerenkov counter the spark chambers (with magnetostrictive readout) give 2 pairs of orthogonal coordinate measurements. These are used, together with the MWPC information to determine angles and momenta. The resolution attainable is $\Delta P/P \approx 13\%\ P\ (GeV/c), \Delta\phi = \pm 5$ mr, $\Delta\theta = \pm 4$ mr at 1 GeV/c. But most of what I will show you today is based on rough, preliminary alignment, calibration, etc., so on average today our resolution is considerably poorer.

For the data collected so far, the outermost elements of the detector are the shower counters. These are rather massive items, as they contain 3 layers of lead, each 2 radiation lengths thick, followed by 3/8" thick scintillators (NE 114).

Each shower counter module is divided into 4 strips. If this plane, covering 1/6 of a hexagonal structure (60° in ϕ) were part of a cylinder, each strip would correspond to 15° in ϕ. A measurement of the coordinate along the beam direction (z) is provided by the time difference between the pulses from the two ends of the first scintillator layer. The

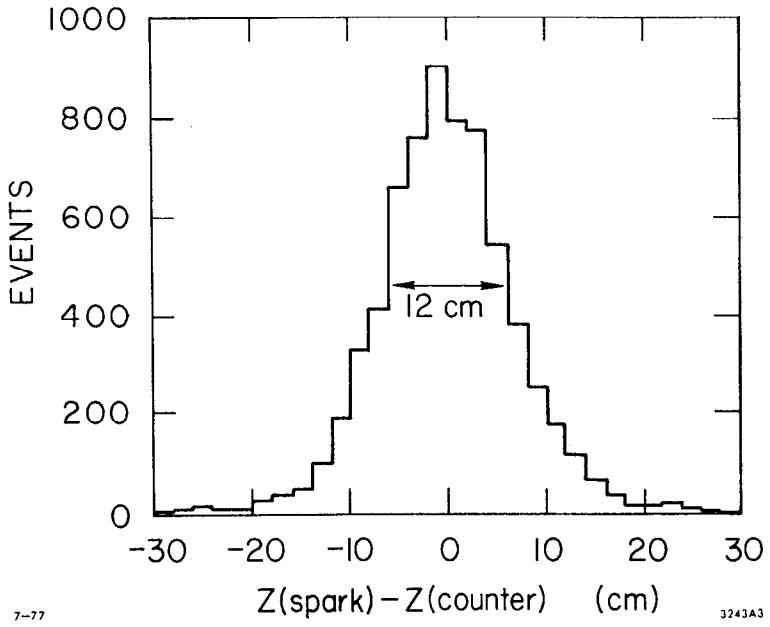

Figure 4 - Difference between the coordinates at the first layer of the shower counter, as predicted by the spark chambers, and as measured by timing in the counter.

resolution is 12 cm F.W.H.M. as illustrated in Fig. 4 where we compare this measurement with what the spark chambers predict. The scintillator in the other 2 layers is cut in the middle, so each sextant contains 8 logical cells, for a total of 48 for the apparatus.

The trigger requires signals from at least two layers of at least 2 cells in separate sextants in time coincidence with beam crossing. Timing information from the shower counters is used to remove cosmic rays from the sample. It will also be used for $\pi/K/p$ separation as the analysis progresses. The timing resolution achieved so far is shown in Fig. 5. In addition the shower counters help in separating hadrons from electrons, and are efficient detectors of γ-rays. In Fig. 6 you see the summed pulse heights from the three layers for electrons from Bhabha events and from muons. Evidently these are the easiest to separate, but the separation is quite clean. The situation is more difficult for lower momentum particles, but we also have more information at our disposal in the distribution of this pulse height among the three layers. In our analysis so far the shower counters are only used to confirm (or deny) the electron identification provided by the Cerenkov counters.

To reduce openings at the two ends of the apparatus, a set of eight pie shaped scintillation counters were installed on the polefaces of the magnet. Time and pulse height information was recorded from these, and from the 12 additional counters which guard the photomultipliers of the Cerenkov counter from direct hits.

Having described the apparatus as it was used this last spring, I should mention what is being added to it for the next run: to better identify muons, a 110 ton lead wall is being installed behind two of the sextants. This will allow some separation of $e-\mu$ type events from $e-\pi$, etc., a task we can not accomplish with the present setup.

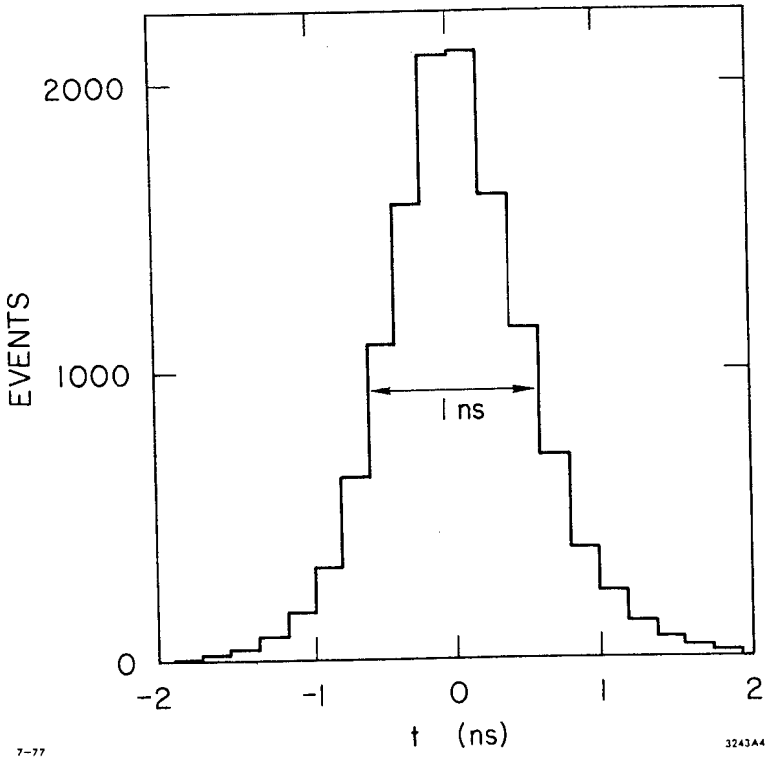

Figure 5 - Distribution of shower counter times for $e^+e^- \rightarrow e^+e^-$ events compared to the expected time based on the beam-crossing signal.

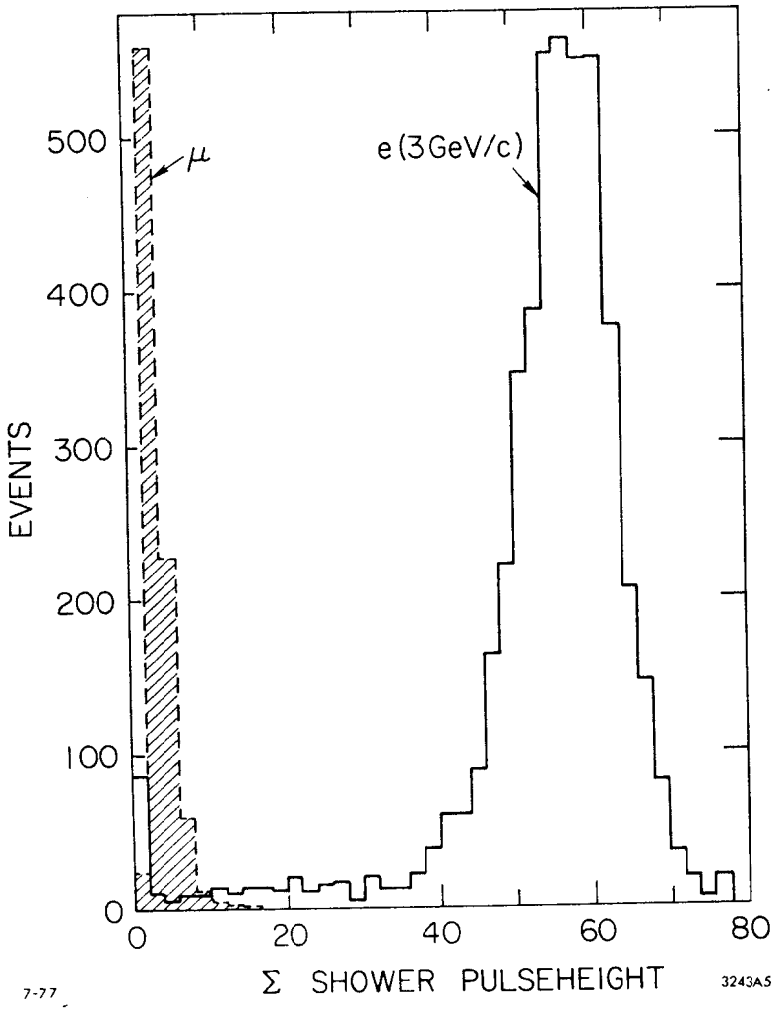

Figure 6 - Sum of the pulse heights from all three layers of the shower counters for 3 GeV/c electrons and for muons. The unit on the abscissa corresponds to the pulse height from a minimum ionizing particle traversing a single layer of the shower counter.

III. Trigger

We already mentioned that at least two shower counter hits in separate sextants in time (±20ns) with the beam crossing were required for the trigger. In addition any one of three requirements had to be satisfied:

1) At least one charged track through planes 1 + 2 of the MWPC. This was detected using a set of fast coincidence circuits

2) At least a third shower counter hit in a third sextant, or

3) The total pulse height in all showers had to be much larger than what a single cosmic ray deposits.

Each of these three requirements excludes the large bulk of cosmic rays in a different way: the first one restricts the effective area of the detector to the MWPC. The second requires a topology more complex than that of single cosmic ray, while the third discriminates by pulse height. Nevertheless, typically 85% of our triggers are due to cosmic rays. The overall trigger rate however is only about 0.7 Hz.

The efficiency of the trigger to detect various types of events is as follows:

a) Bhabhas. Large angle elastic scattering is used to determine the luminosity. We detect them in the range $-.62 < \cos\theta < .62$. We demand that they be coplanar with the beam and collinear within 8°, and for this preliminary analysis we estimate that radiative losses outside these cuts amount to 15± 7%.

b) Hadronic events. Because we are dealing here with a variety of topologies, and because they depend on the physics we want to study (but do not yet know in detail) we can not determine the triggering efficiency exactly. But because both γ rays and charged particles can participate in the trigger, the efficiency is high (85±10%), and an approximate method will suffice:

We construct a very simple model in which a mixture of charged particles is produced in an isotropic, uncorrelated manner, and is accompanied by a number of γ-rays. We calculate what observed event distribution a given mixture will produce, given the geometry of the apparatus and the trigger requirements. We then adjust the mixture of 2, 4, 6,... prongs, and the associated γ's to match the observed prong and γ-ray distribution. Finally we vary the input parameters within the broadest range consistent with the data to estimate the error. The result is really quite insensitive to most of our assumptions. The detection efficiency for events with 4 or more charged prongs is generally over 90%, and they form the bulk of the data. The source of our uncertainty lies with the two-prongs, because possible angular correlations between the charged prongs, as well as the distribution of the associated γ-rays can have a strong effect on the result.

IV. The Data

The data collected during the spring cycle are shown in Table 1. They consist of a scan from the ψ′ to 4.8 GeV, a high energy scan up to 7.2 GeV, and larger chunks in the region around 3.77 GeV, 4.03 GeV, 4.25 GeV, and calibration runs below charm threshold.

After track finding, events are classified first as e^+e^- interactions or undesirables (cosmics, etc.), on the basis of timing and vertex location. The e^+e^- interactions are then further classified as

1) hadronic
2) Bhabha ($e^+e^- \to e^+e^-$)
3) $e^+e^- \to \mu^+\mu^-$
4) other q.e.d. ($\to e^+e^-\gamma$, $e^+e^-e^+e^-$)
   $\to \gamma\gamma$, etc.
5) none of the above (at least as far as the programs see it).

The subclass of the hadronic events which appear to include an electron (e^+ or e^-) is of course of primary interest to us. These fall into two groups: two prong topologies, of which one appears to be an electron, and multiprongs. Because the background processes are different, these two groups are treated separately: Background for the multiprong topology with electrons comes primarily from e^+e^- pairs in Dalitz decays of π^o, η, ω, etc., or from the conversions of γ-rays produced in the decays of these particles. Most of these pairs are easily identified because of the small opening angle. However, especially when the pair is highly asymmetric, and one of the two particles carries most of the momentum, the other one may be too soft to be recognized by the programs. Therefore all candidates, where the program could not find a pair (there are 3386 of these) have been looked at individually, and 2317 appear to be genuine, as best we can determine. Events of this class were first reported by the DASP group (28 events a year ago,[2] 192 earlier today.[3]) Results from the Lead Glass Wall are presented at this conference.[4] Both DASP and Pluto[5] observed hadronic events with electrons and K-s.

Additional background for the two prongs come primarily from various qed processes, where one of the prongs escapes identification as an electron. The study of this sample is in progress, but we have no results to report so far, other than the observation that we indeed see such events.

V. Results.

A. Measurements of R.

Based on the observed number of hadrons and Bhabha events, and the detection efficiencies discussed above, we calculate the parameter R (hadronic annihilations/ $e^+e^- \to \mu^+\mu^-$) as a function of energy. The results are shown in Fig. 7. Our overall uncertainty in scale is 20%, and there may be weakly energy-dependent effects of up to this level, but the

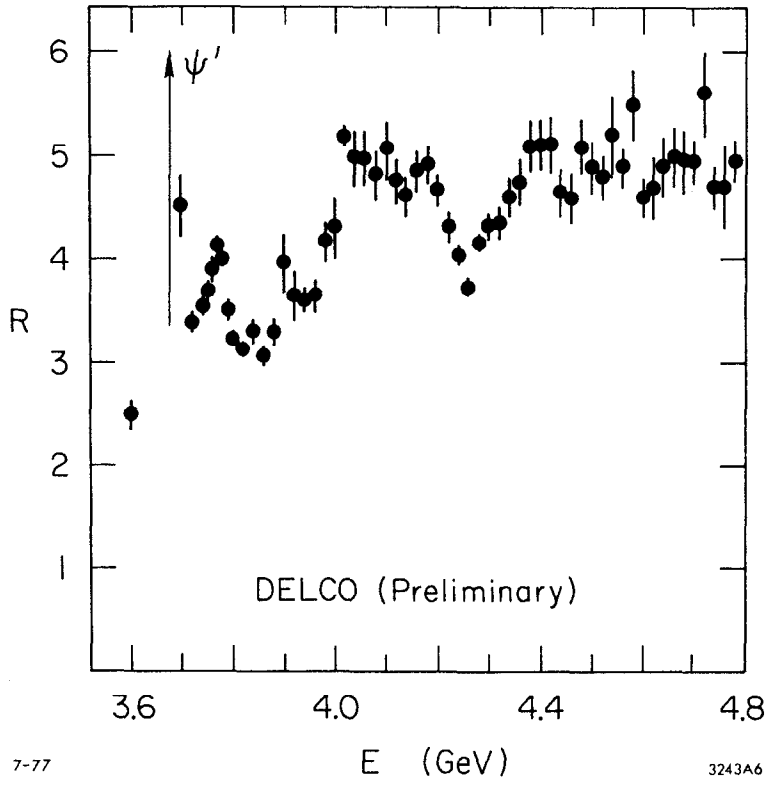

Figure 7 – The parameter R. No corrections have been applied for radiative tails of lower energy resonances.

point-to-point uncertainties are smaller than the statistical errors shown in the figure.

The general features of this plot are in good agreement with published results from Mark I[6] and from Pluto,[7] where these measurements overlap. There is an unmistakable peak near 3.77 GeV, shown in more detail in Fig. 8. These data were taken at the same time, and use the same energy calibration as the data by Rapidis et al.,[6] the mass scales are therefore not independent! To determine the resonance parameters we first subtract the radiative tails of lower energy states (the ψ' contribution is the dominant among these), then fit the remainder to a Breit-Wigner form plus a background term. The radiative effects are handled according to the Jackson and Scharre recipes.[8]

We tried several forms for the background (linear, p wave), and for the resonance (s and p wave), but the results are rather insensitive to the form used. We find

$$M = 3770 \pm 6 \text{ MeV}$$
$$\Gamma = 24 \pm 5 \text{ MeV}$$

consistent with Rapidis et al.[6] The partial width to e^+e^- pairs is 180 ± 120 eV. (Fig. [9]).

Identification with the $^3D_1$ state of $c\bar{c}$, is a natural one, especially in view of the fact that the parameters agree with the prediction made by Eichten et al.[9] better than they have a right to.

Since the resonance lies about 45 MeV above $D^0\bar{D}^0$, and 35 MeV above D^+D^- threshold, it seems likely that it decays predominantly into a mixture of these channels.

B. Measurement of R_e

Let us examine now the energy dependence of the multiprong hadronic events with an e^+ or e^-. The general features are apparent in Fig. 10,

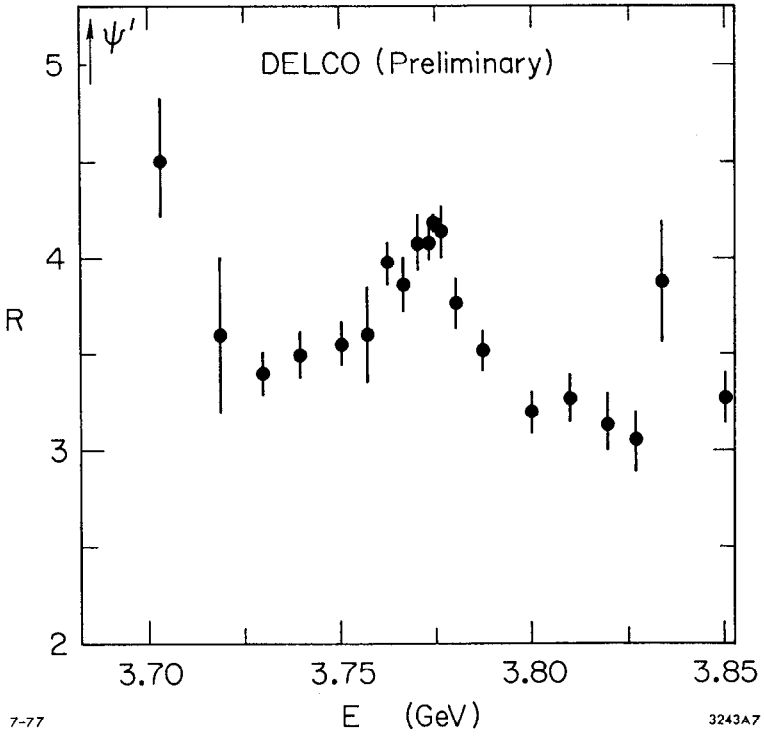

Figure 8 - The data of Figure 7 on an expanded scale around the 3.77 GeV region.

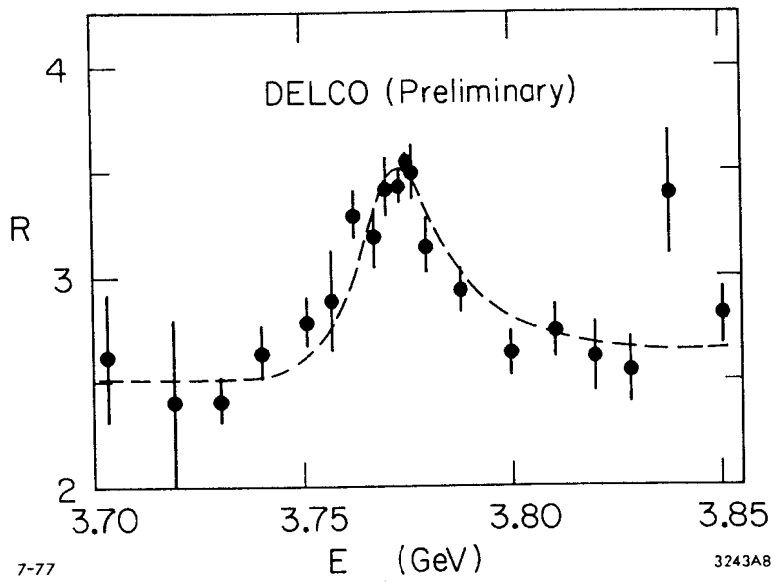

Figure 9 - The data of Figure 8 after subtraction of the radiative tails of lower lying resonances (the ψ' has the largest effect). The dashed curve is a p-wave Breit-Wigner fit.

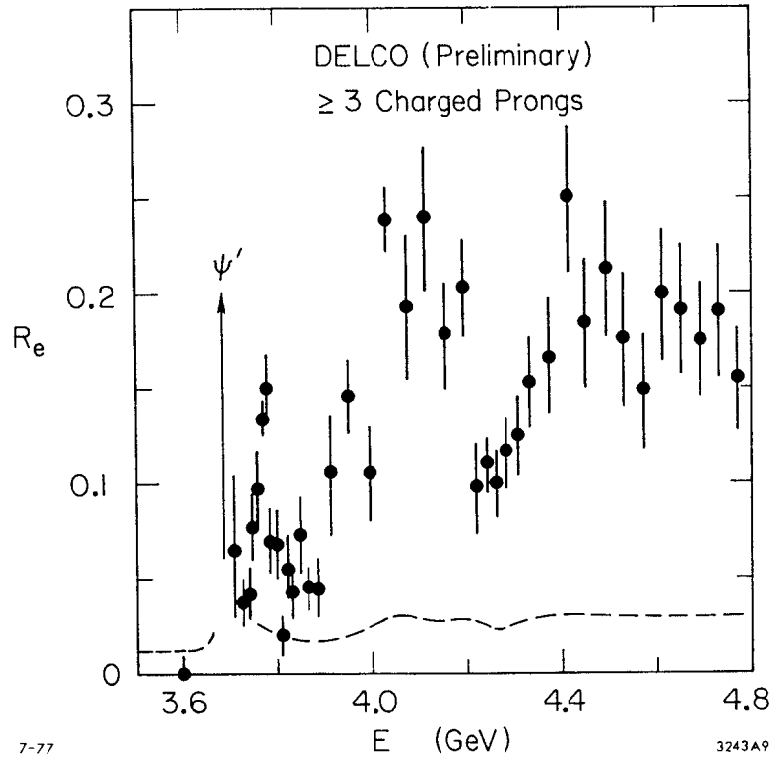

Figure 10 - The parameter R_e, based on events with 3 or more charged prongs only, where one of the prongs is an electron (e^+ or e^-). No correction for detection efficiency has been applied. The dashed curve indicates the expected background.

where the contribution to R by these events is shown before any adjustment for electron detection efficiency.

The value at 3.6 GeV, below the ψ' is low, and corresponds to 0.3% of the hadronic events. One would expect the real signal to be even lower here. We accept this rate as our background level. It corresponds to a hadron rejection by the Cerenkov counter of better than 1000:1.

At the ψ' there is a large signal due to the $\psi' \to e^+e^-\pi^+\pi^-$ decay. Above the ψ' there is a clear peak which coincides with the peak in R. (Note that the increase above the "background" here is at least a factor of 5, while in the overall hadronic sample it is about 1/3!).

Above the peak the value almost returns to the level found at 3.6 GeV, then rises to a level where about 4% of the hadronic events appear to contain an e^+ or e^-. There is however, a prominent dip in this distribution between 4.2 and 4.3 GeV.

C. Hadronic events with electrons at 3.77 GeV; $D \to e + X$.

The mass and width of the peak in R_e at 3.77 GeV agree with the parameters determined in the fit to R. (Fig. 11) If we assume that this resonance decays mainly into $D\bar{D}$, then the peak in R_e must be due to the decay $D \to e^{\pm}+X$. (The momentum spectrum of the electrons does not peak near 1.55 GeV/c as it should if an $e^+e^-\pi^+\pi^-$ decay were important).

To obtain the semileptonic branching ratio of the mixture of charged and neutral D particles, we measure the area under the peak in the R_e plot, and subtract the remaining background. The background consists of events from the radiative tail of the ψ' (this we extrapolate from values below the peak), and of the type of events remaining at 3.6 GeV (we assume that these constitute a fixed fraction of the hadronic events). We find that 12% of the events in the hadronic peak contain an e^+ or e^-!
The branching ratio then is

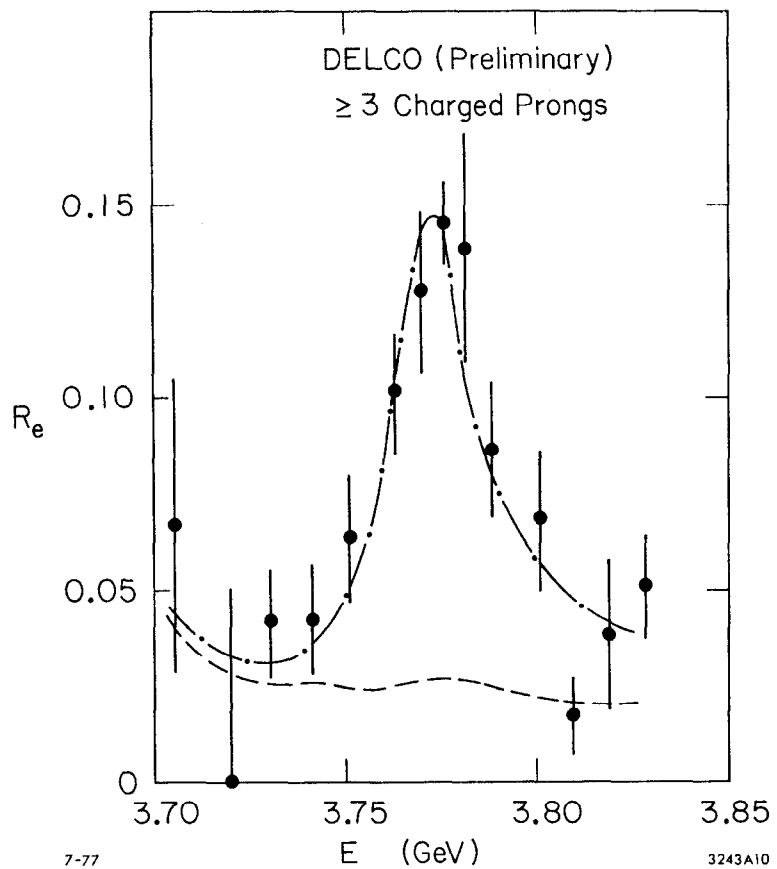

Figure 11 - The data of Figure 10 on an expanded scale around the 3.77 GeV region. The dashed curve indicates the expected background. The dot-dashed curve is a fit to the data with the mass and width found for R.

Table I

DATA COLLECTED DURING SPRING 1977*

(Data Restricted to Last 12 Weeks)

E_{TOTAL} [GeV]	events / pb	Number of events		
		$e^+e^- \to e^+e^-$	hadrons	hadrte$^{\pm}$ †
< 3.65	∿ 0.1	4,748	42,385	375
ψ' ±.02	∿ 0.1	4,294	12,987	194
3.70-3.87	2.0	71,794	37,989	1146
4.03	0.2	10,028	7,153	305
4.27±.05	0. 6	19,538	11,014	357
rest of scan 3.87-4.82	1.5	46,119	28,775	10 62
scan above 4.8	1.2	13,353	12,788	491
TOTAL	5.7	169,874	153,091	3930

* approximate preliminary values

† before hand-scan

$$\frac{D \to e + X}{D \to all} \geq 6 \pm 1\%$$

Note that events with only 2 charged prongs are not included here, and we did not correct for losses in event identification, hence the $\geq$ sign.

VI. Conclusions

1) DELCO is working well, both as a large solid angle detector of electrons, and as a general purpose detector to study e^+e^- physics at SPEAR.

2) The analysis is far enough along to show the well known features of hadronic annihilations, and the new resonance at 3.77 GeV.

3) Observation of a peak in hadronic events with an $e^{\pm}$ at 3.77 GeV allows the determination of the branching ratio of the decay $\frac{D \to e + X}{D \to all}$

4) The analysis has just begun... More results will be forthcoming from data at hand, and from data to be taken starting in November.

5) Physics at SPEAR, as the trail in the High Sierra is full of beauty, with peaks to conquer which ever way one turns, and probably more yet just beyond the horizon.

VII. Acknowledgements

I wish to thank my collaborators: The work reported here is the fruit of their labors, the errors are mine. They, and especially my hosts here at Stanford made this sabbatical year most rewarding and enjoyable.

I am most grateful to Mrs. Margaret Ledford for her help in preparing this manuscript, and for her help throughout the past year.

Footnotes and References

† Permanent address

1) For further information on the Cerenkov counter, see W. E. Slater et al. UCLA Preprint # (to be submitted to Nuclear Instruments and Methods).

2) W. Braunschweig et al. Phys. Letters 63B, 471 (1976).

3) W. DeBoer, DORIS Results on Charm and Heavy Leptons (presented at this Conference).

4) R. Madaras, Anomalous Electron Production in the Lead Glass Wall Experiment at SPEAR (presented at this conference).

5) J. Burmester et al. Phys. Letters 64B, 369 (1976).

6) J. Siegrist et al. Phys. Rev. Letters 36, 700 (1976) P. A. Rapidis et al. Observation of a Resonance in e^+e^- Annihilation Just Above Charm Threshold. (SLAC-PUB-1959, June 1977. Submitted to Phys. Rev. Letters).

7) J. Burmester et al. Phys. Letters 66B, 395 (1977) for the latest results see ref. 3.

8) J. D. Jackson and D. L. Scharre, Nucl. Instruments and Methods 128, 13 (1975).

9) E. Eichten et al. Phys. Rev. Letters 34, 369 (1975); ibid 36, 500 (1976).

ANOMALOUS ELECTRON PRODUCTION IN THE LEAD-GLASS WALL EXPERIMENT AT SPEAR

Ronald J. Madaras
Lawrence Berkeley Laboratory
University of California
Berkeley, California 94720

I. INTRODUCTION

In this talk I will present the latest results of the Lead-Glass Wall Collaboration[1] on anomalous electron production[2] in electron-positron annihilations at SPEAR at center-of-mass energies from 3.77 to 7.4 GeV. This experiment, having SLAC number SP-26, ran at SPEAR from October 1976 through June 1977. The data were collected with the SLAC-LBL Mark I magnetic detector,[3] which was modified by the addition of a lead-glass detector for improved electron and photon identification.

Anomalous electrons in electron-positron annihilations can come from at least two possible sources:

1. Heavy lepton production and decay: For example,

$$e^+e^- \to \tau^+ + \tau^- \qquad (1)$$
$$\tau^+ \to e^+\nu_e\bar{\nu}_\tau \qquad \tau^- \to \mu^-\bar{\nu}_\mu\nu_\tau,\ \pi^-\nu_\tau,\ \rho^-\nu_\tau,\ \vdots$$

Evidence for the heavy lepton, τ, was first found by M. L. Perl[4,5] in 1975, and has been confirmed by further experiments at SPEAR[6-9] and at DORIS.[10-13] The predicted branching ratios for various decay modes of the heavy lepton can be found in Table I.[14] It is seen that the heavy lepton decays into a single charged particle about 85% of the time, so that most of the events of type (1) above will have only two charged particles in the final state.

Table I. Predicted branching ratios for a τ^- charged lepton of mass 1.9 GeV/c^2, an associated neutrino mass of 0.0, and V-A weak interaction coupling.[14]

Decay mode	Branching ratio	Number of charged particles in final state
$e^- \bar{\nu}_e \nu_\tau$	0.20	1
$\mu^- \bar{\nu}_\mu \nu_\tau$	0.20	1
$\pi^- \nu_\tau$	0.11	1
$K^- \nu_\tau$	0.01	1
$\rho^- \nu_\tau$	0.22	1
$K^{*-} \nu_\tau$	0.01	1
$A_1^- \nu_\tau$	0.07	1, 3
(hadron continuum)$^- \nu_\tau$	0.18	1, 3, 5

2. Charmed particle production and decay: For example,

$$e^+e^- \to D + \bar{D} + n \cdot \text{hadrons} \quad (n \geq 0) \qquad (2)$$

$D \to eK\nu,\ eK^*\nu,\ \ldots$; $\bar{D} \to K\pi,\ K\pi\pi,\ \ldots$

It is expected that most of the events of this type will have four or more charged particles in the final state. For example, at the $\psi(3772)$[15] where $D\bar{D}$ with no other hadrons is produced, about 90% of the events of type (2) will contain four or more charged particles. At higher center-of-mass energies, where D^*D^* or $D^*D^*\pi\pi$ are produced, the percentage is higher. Of course, even when four particles are produced, fewer might be detected because the detector doesn't cover the full 4π sr solid angle.

Thus in our analysis, we have divided up the anomalous electron events into two classes:

Two-prong events of the type $e^+ + e^- \to e^\pm + \mu^\mp + n \cdot \gamma$ or $e^\pm + h^\mp + n \cdot \gamma$, with $n \geq 0$ ($h \equiv$ hadron). Two, and only two, charged particles are detected.

Multiprong events of the type $e^+ + e^- \to e^\pm +$ (≥ 2 charged particles) $+ n \cdot \gamma$, with $n \geq 0$. Here at least three charged particles are detected.

We analyze these two classes of events separately in order to separate the charm and heavy lepton signals, as we have seen above that heavy lepton events of type (1) will mainly be two-prong events and that charm events of type (2) will mainly be multiprong events.

In Section II of this talk I will describe the lead-glass detector, and in Section III I will discuss the details of the identification of electrons using this detector. In Section IV I will discuss the results of the analysis of the two-prong events, and give our values for the branching ratios $B(\tau \to e\, \nu_e \nu_\tau)$ and $B(\tau \to h + \text{neutrals})$. In Section V I will discuss the results of the analysis of the multiprong events, and give both the semi-leptonic branching ratio of the charmed D meson into electrons and the semi-leptonic branching ratio of "charmed particles" into electrons for various electron-positron center-of-mass energies.

II. LEAD-GLASS WALL DETECTOR

In order to improve the identification of electrons, we have replaced one octant of the magnet return yoke of the SLAC-LBL Mark I magnetic detector with two layers of lead-glass counters interspersed with magnetostrictive spark chambers. These are shown schematically in Figure 1, and in more detail in Figure 2. The shower counters which were in that octant have been replaced by 1.9 cm-thick scintillation counters. The lead-glass system consists of:

1. a 2 x 26 array of lead-glass "active converters" (AC), 3.3 X_o deep, having dimensions 10 x 11 x 90 cm, followed by:

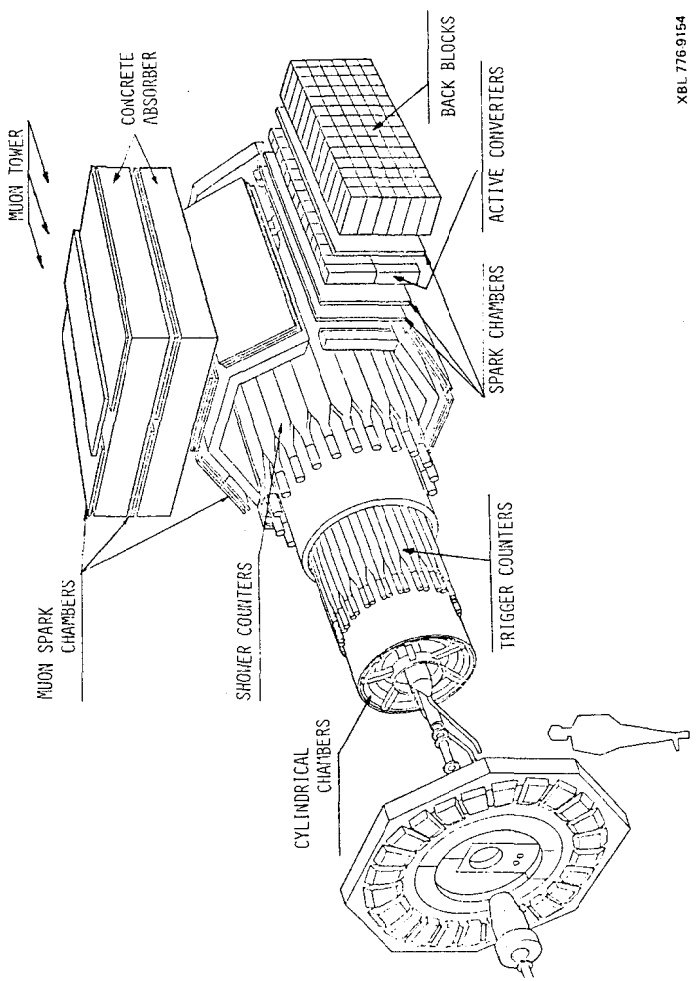

Fig. 1 Exploded view of the SLAC-LBL Mark I magnetic detector with the addition of the Lead-Glass Wall Detector.

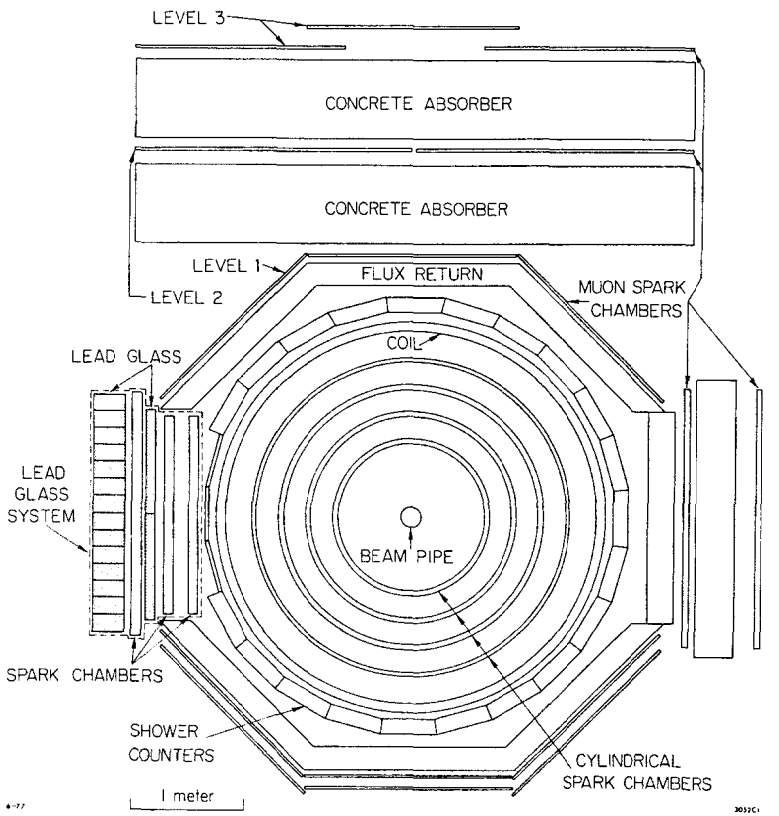

Fig. 2 The SLAC-LBL Mark I magnetic detector with the addition of the Lead-Glass Wall Detector, in a view along the beam line. The two proportional chambers around the beam pipe and the trigger counters are not shown.

2. a 14 x 19 array of lead-glass "back-block counters" (BB), 10.5 X_o deep, having dimensions 15 x 15 x 32 cm, and

3. a set of three magnetostrictive spark chambers.

Each active converter (back block) lead-glass counter was viewed through a lucite lightguide by an EMI 3.5" 9531 R (5" 9618 R) photomultiplier tube. The anode signal from each counter was sent to an ADC in a LBL Large-Scale Digitizer System,[16] and the dynode signals of the counters were summed in rows and used for triggering. Both lead-glass arrays were kept in closed boxes where temperatures were kept constant. The lead-glass system covered polar angles $60° < \theta < 120°$ and azimuthal angles $-20° < \phi < 20°$, and thus covered ~ 6% of 4π sr solid angle.[17]

The lead-glass counters were initially calibrated to an accuracy of ~ 10% by using several radioactive sources. These sources were small thallium doped NaI scintillation crystals diffused with Americium-241, and they themselves were calibrated with several lead-glass counters in an electron beam at SLAC. The final calibration of the gains of all the lead-glass counters was done using electrons of known energy from Bhabha scattering events obtained during the data taking at SPEAR. With this method, the calibration constants of the counters are obtained by minimizing the square of the energy resolution of the counters for the Bhabha events, with the constraint that the average energy deposited in the lead-glass is equal to the actual energy of the Bhabhas. This final calibration has an accuracy of about 5%. The response of the lead-glass system (LGW) to a set of high-energy Bhabha electrons (which were not used in the above calibration) is shown in Figure 3. The energy resolution of the whole system is given by $\sigma/E = 9\%/\sqrt{E}$ (E in GeV). This resolution is degraded from the intrinsic resolution of the counters of $5\%/\sqrt{E}$ due to the presence of the 1 X_o aluminum coil of the Mark I magnet which is before the lead-glass system (see Figure 2).

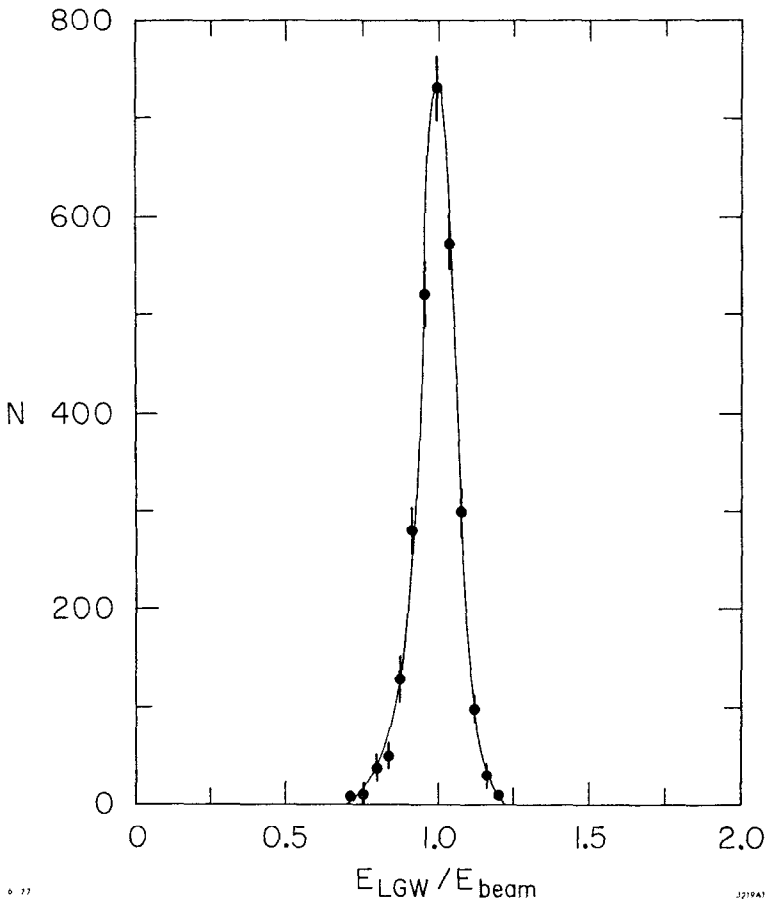

Fig. 3 Distribution of the total energy, E_{LGW}, measured in the whole lead-glass wall (back blocks and active converters) for electrons from Bhabha scattering ($e^+e^- \to e^+e^-$). E_{BEAM} is 3.2-3.7 GeV. The energy resolution is $\sigma_{E_{LGW}}/E_{LGW} = 5.1\%$.

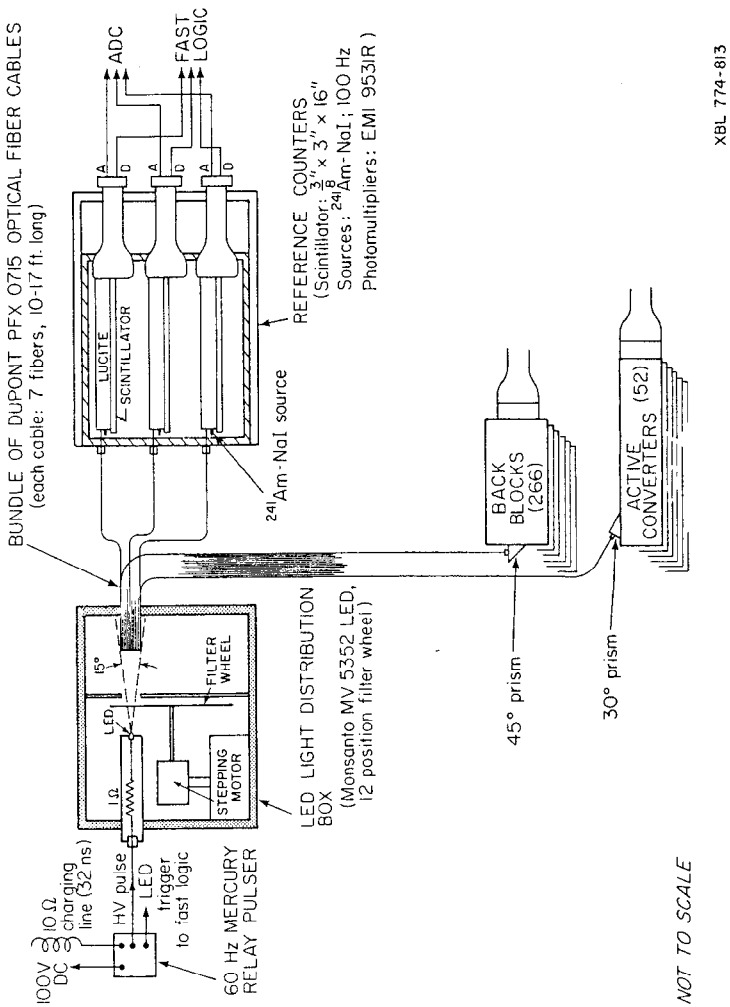

Fig. 4 A schematic diagram of the LED monitoring system for the lead-glass counters.

In order to keep the energy resolution of the whole system of lead-glass counters constant over the ten-month life of the experiment, one has to accurately monitor the gains of each of the 318 counters during this time. This has been successfully achieved with an LED monitoring system[18] which has tracked the gains of the lead-glass counters throughout the experiment with a precision of 1-2%. This system is shown schematically in Figure 4. The light source is a single high-intensity yellow LED, and the light is transmitted to each of the counters via low-attenuation plastic optical fibers. The LED light is monitored using a reference scintillation counter, whose gain is known from frequent ^{241}Am-NaI source and cosmic ray measurements.

III. ELECTRON IDENTIFICATION USING THE LEAD GLASS WALL DETECTOR

A. Cuts. The identification of a particle that enters the Lead-Glass Wall (LGW) is based on its time-of-flight and on the energy deposited in each of the two layers of lead-glass counters. To identify a particle as an electron candidate we require:

1. The particle's momentum, as measured in the Mark I detector, is greater than 300 MeV/c for multiprong events and 400 MeV/c for two-prong events.

2. The measured time-of-flight of the particle agrees with that expected for an electron within two standard deviations (0.8 ns). This reduces the background from misidentification of kaons and protons.

3. The particle is within the fiducial volume of lead-glass.

4. No other charged or neutral particles in the LGW are nearby.

5. The energy deposited in the lead-glass back blocks (E_{BB}) is greater than 10% of the momentum of the particle. (This requirement only exists for the multiprong events.)

6. The energy deposited in the lead-glass active converters (E_{AC}) is substantially greater than the 80 MeV expected for a noninteracting particle:

2-prong events: $E_{AC} > 150$ MeV

multiprong events: $E_{AC} >$ Max (150, 250 · p)
where p is the particle momentum in GeV/c

7. The total energy deposited in the LGW ($E_{LGW} = E_{AC} + E_{BB}$) is approximately equal to the momentum of the particle:

2-prong events: $1.50 > E_{LGW}/p > 0.65$

multiprong events: $1.50 > E_{LGW}/p >$ Min[0.80, 0.65+0.15·(p-0.4)]
(p in Gev/c)

The requirements on the energies deposited in the lead-glass are more severe for the multiprong events than for the two-prong events, because the hadron background is a much larger fraction of the anomalous electron signal for the multiprong events than for the two-prong events.

B. Detection Efficiency. The LGW electron identification efficiency (ε) for the above cuts on the energy deposited in the lead-glass counters is measured using electrons from the reactions $e^+e^- \to e^+e^-\gamma$ and $e^+e^-e^+e^-$. These events are found by requiring two (and only two) oppositely charged coplanar particles which have most of the missing momentum going along the beam direction. In addition, we require that there are no photons detected and that the particle outside the LGW is determined to be an electron by the Mark I detector. The detection efficiency for the electron in the LGW is measured to be:

2-prong event LGW cuts: ε = 75% (p_e = 400 MeV/c) to 98% (p_e>1.0 GeV/c), with $\bar{\varepsilon}$ = 89%.

multiprong event LGW cuts: ε = 55% (p_e = 300 MeV/c) to 90% (p_e>1.0 GeV/c). with $\bar{\varepsilon} \sim 75\%$

The detection efficiency is smaller for the LGW energy cuts appropriate for the multiprong events than for the two-prong events, becuase the cuts are more severe for the multiprong events (see Section III A.).

C. Backgrounds. Important backgrounds to the anomalous electron signal are:

(a) misidentification of hadrons which interact in the magnet coil or active converters so as to satisfy the above requirements on the energy deposited in the lead-glass,

(b) pion and kaon decay,

(c) photon conversions in the beampipe, pipe counters or MWPC (total of 0.052 X_o), or Dalitz decays of π^o's and η's, where both the electron and positron are detected by the Mark I detector.

(d) asymmetric electron-positron pairs from photon conversions or Dalitz decays where one member of the pair is unobserved because its momentum is below the threshold for efficient detection in Mark I (~ 100 MeV/c).

The background due to (c) is eliminated by rejecting electron candidates that have a small opening angle with a particle of opposite electric charge.

We determine the background due to (a), (b) and (d) at various center-of-mass energies in three steps:

i) First, at a center-of-mass energy where we think there is no anomalous electron production, we measure the fraction of particles in the LGW that pass all our cuts defining an electron. This we assume is our basic background rate from (a), (b) and (d). We choose to do this at the ψ(3095), as it is below threshold for charm and heavy lepton production. Using multihadronic events there, we find that 1.4% of all the particles in the LGW which have a momentum of 300 MeV/c are identified as electrons. This fraction decreases with momentum to 0.4% per particle at 1.0 GeV/c.

ii) Second, we assume that the background per particle in the LGW due to (a) and (b) does not change as we go from the ψ(3095) to the highest

center-of-mass energy of 7.4 GeV. This assumption is not crucial for (b), as the background due to this source is estimated to be $\lesssim$ 0.05% per particle.

iii) Third, we determine the additional background rate from asymmetric photon conversions or Dalitz decays (i.e. source (d)) that we might have when we go to higher center-of-mass energies. This background rate can increase with the center-of-mass energy due to increases in the number and energy of the photons and π^0's which are responsible for the background. This additional background rate was determined by measuring at several center-of-mass energies the converted e^+e^- pairs where both particles are detected, and then extrapolating with a Monte Carlo program to the case where only one particle is detected. The results are below:

Momentum (GeV/c)	Background rate due to (a), (b) and (d) as measured at ψ(3095). (% per particle in LGW)	Additional background rate due to (d). (% per particle in LGW) 3.772 (GeV)	4.15 (GeV)	4.4-5.7 (GeV)	6.4-7.4 (GeV)
0.3	1.4%	0.1	0.1	0.2	0.4
0.5	1.0	0.1	0.1	0.1	0.3
0.7	0.7	0.05	0.1	0.1	0.1
$\geq$1.0	0.4	0	0	0	0.05

As is seen, this additional background rate ranges from 0 to 0.4% per particle, with the maximum occuring for p = 0.3 GeV/c, $E_{c.m.}$ = 7.4 GeV. The increase is largest for the lowest momenta.

The average value of the total background rate due to (a), (b) and (d) is 1.1% per particle. This value is averaged over the background momentum spectrum, and is essentially the same for the four center-of-mass energy regions because the hardening of the momentum spectrum in each region compensates for the increase of the background rate in each region.

All of the above values for the background rates were obtained using the lead-glass wall energy cuts appropriate for the multiprong events (see Section III. A.). Using the looser LGW cuts appropriate for the two-prong events, one finds that the background is at most 2.0% per particle, for all momenta and center-of-mass energies.

IV. TWO-PRONG EVENTS

A. Event Sample. We recall from Section I that the "two-prong" events are of the type:

$$e^+ + e^- \to e^\pm + \mu^\mp + n \cdot \gamma$$
$$\text{or } e^\pm + h^\mp + n \cdot \gamma$$

with $n \geq 0$

h = a hadron

Two, and only two, oppositely charged particles are detected. One of them, the electron, is always identified in the lead-glass wall. The other particle is identified most of the time in the Mark I magnetic detector on the basis of information from lead-scintillator shower counters and magnetostrictive spark chambers following the 20-cm-thick iron flux return of the magnet.[19] The detection efficiencies, ε, and misidentification probabilities $P_{i \to j}$ (i.e. the probability that a particle of type i is identified as type j) for the particles identified in the Mark I detector are measured with eeγ events, $\mu\mu\gamma$ events and hadronic events with $\geq$ 5 charged particles. They are:

$$P_{e \to h} = 0.095 \pm 0.020 \qquad \varepsilon_e = 0.89 \pm 0.02$$
$$P_{e \to \mu} = 0.01 \pm 0.01 \qquad \varepsilon_h = 0.58 \pm 0.05$$
$$P_{\mu \to h} = 0.03 \pm 0.01 \qquad \varepsilon_\mu = 0.94 \pm 0.02$$
$$P_{h \to \mu} = 0.18 \pm 0.01$$

I will present here the results of the two-prong event analysis for data taken in three different center-of-mass energy ranges:[20]

$E_{c.m.}$ range (GeV)	Average $E_{c.m.}$ (GeV)	$\int$ Ldt (pb^{-1})
4.1-4.2	4.15	1.0
4.4-5.7	4.9	2.7
6.4-7.4	6.9	5.5

The two-prong event analysis has not yet been completed for the data taken at the $\psi(3772)$.

The two-prong events are selected using the following data cuts:

1) The momentum of the particle in the lead-glass wall is > 400 MeV/c.

2) The particle in the lead-glass wall is identified as an electron using the criteria discussed in Section III.A. for two-prong events.

3) The other particle is oppositely charged, and its momentum is > 650 MeV/c to insure good identification in the Mark I detector.

4) The two charged particles are acoplanar about the incident beams by at least 20°.

5) The square of the missing mass recoiling against the two charged particles is > 0.8, 1.1 or 1.5 GeV^2, for the center-of-mass energy ranges 4.1-4.2, 4.4-5.7, and 6.4-7.4 GeV.

The last two criteria are used to reduce the background from the QED reactions: $e^+e^- \to e^+e^-$, $e^+e^-\gamma$ and $e^+e^-e^+e^-$.

For the combined data from all three center-of-mass energy regions, the number of two-prong events which pass the above cuts is listed in Table II.[6]

Table II. Two-prong events, for the combined data from $E_{c.m.}$ = 4.1-4.2, 4.4-5.7, and 6.4-7.4 GeV. See the above text for the event selection criteria. The first particle listed is always detected in the LGW (here a hadron, h, in the LGW is any particle not identified as an electron). N_γ is the detected number of γ rays associated with the events.

	Observed events		Background		Corrected events	
	$N_\gamma = 0$	$N_\gamma > 0$	$N_\gamma = 0$	$N_\gamma > 0$	$N_\gamma = 0$	$N_\gamma > 0$
eμ	21	8	0.4	1.4	21.6±6.4	3.7±4.5
eh	12	19	3.0	9.1	20.5±9.6	24.2±12.9
ee	23	71			32.1±6.9	100±14
hh	38	122			66±13	213±30

In Table II, the anomalous electron events are in the categories eμ and eh, with or without photons. The background for these events due to misidentification of ee and hh events is listed in columns 3 and 4. The last two columns list the number of anomalous electron events after corrections for the background, the misidentifications among the anomalous events themselves, and the particle detection efficiencies.

It is seen from the last two columns in Table II that there is a significant signal for the anomalous eμ(N_γ=0) and eh($N_\gamma \geq 0$) events. I will now assume that these anomalous two-prong events come from the production and decay of a heavy lepton according to the processes shown in reaction (1) in Section I, and I will show that our data are consistent with this assumption.[21]

B. eμ (N_γ = 0) events. Assuming the eμ events arise from the process:

$$e^+e^- \to \tau^+ + \tau^-, \quad \tau^+ \to e^+\nu_e\bar{\nu}_\tau, \quad \tau^- \to \mu^-\bar{\nu}_\mu\nu_\tau$$

the number of corrected eμ events with $N_\gamma = 0$ is given by:

$$N_{e\mu} = \int Ldt\ \sigma(e^+e^- \to \tau^+\tau^-)\ 2\ B_e\ B_\mu\ A_{e\mu}$$

where: $\int Ldt$ = integrated luminosity

$$\sigma(e^+e^- \to \tau^+\tau^-) = \frac{21.71}{E^2_{beam}}\ \frac{\beta}{2}\ (3-\beta^2)\ \text{nb, where } \beta = \frac{v_\tau}{c}$$

$B_e(B_\mu)$ is the branching ratio for $\tau \to e\ \nu_e\ \nu_\tau(\mu\ \nu_\mu\ \nu_\tau)$

$A_{e\mu}$ is the acceptance of the apparatus for eμ events.[21]

Assuming $B_e = B_\mu$, we can calculate B_e from our data. The results are given in Table III for the three energy regions.

Table III. Measured branching ratios[22] $B_e(\tau \to e\ \nu_e\ \nu_\tau)$ and $B_h(\tau \to$ single charged hadron + neutrals). The branching ratios have been calculated assuming $B_e = B_\mu$, V-A coupling, a point production cross section for the τ, m(τ)=1.9 GeV, and $m(\nu_\tau) = 0.0$. Only statistical errors are shown.

$E_{c.m.}$ range (GeV)	$B_e(\tau \to e\ \nu_e\ \nu_\tau)$ (%)	$B_h(\tau \to$ single charged hadrons + neutrals), (%)
4.1 - 4.2	20.5 ± 8.2	36 ± 41
4.4 - 5.7	19.6 ± 5.2	48 ± 28
6.4 - 7.4	23.2 ± 4.4	43 ± 25
All three ranges combined	21.6 ± 3.1	43 ± 16

The three values of B_e are in good agreement, showing that the energy dependence of eμ production is consistent with the heavy lepton hypothesis. Combining the data and including an estimated 20% systematic error, we obtain:[22]

$$\boxed{B_e(\tau \to e\ \nu_e\ \nu_\tau) = (21.6 \pm 5.3)\%}$$

This is in good agreement with previous measurements[4,8-11] and with the theoretical expectation of 20%.[23]

C. eh ($N_\gamma \geq 0$) events

Assuming the eh events arise from the process:

$$e^+\ e^- \to \tau^+ \ (\to e^+\ \nu_e\ \bar{\nu}_\tau) + \tau^- \ (\to \nu_\tau + \text{single charged hadron + possible additional neutrals})$$

the number of corrected events is given by:

$$N_{eh} = \int Ldt\ \sigma(e^+e^- \to \tau^+\tau^-)\ 2\ B_e\ B_h\ A_{eh}$$

where: N_{eh} is the sum of the eh events for $N_\gamma = 0$ and $N_\gamma > 0$

$\int Ldt$, σ are the same as before

B_h is the branching ratio for the decay $\tau \to$ single charged hadron + neutrals

A_{eh} is the acceptance of the apparatus for eh events,[21] calculated assuming only $\tau \to \pi\ \nu_\tau$, $\rho\ \nu_\tau$ contribute to two-prong eh events. We expect these decays to contribute 73% of the decays $\tau \to$ single charged hadron + neutrals.[23]

Using $B_e = (21.6 \pm 5.3)\%$, which is the result from the previous section, we can calculate B_h from our data. The results are given in Table III. Again, the three values of B_h are in good agreement. Combining the data and including an estimated 20% systematic error, we obtain:[22]

$$\boxed{B_h(\tau \to \text{single charged hadron + neutrals}) = (43 \pm 18)\%}$$

This is in agreement with the theoretical expectation of 45%.[23]

D. Momentum and Coplanarity Distributions. Figures 5(a)-5(c) show the corrected momentum distributions for the hadrons, muons and electrons in all the anomalous two-prong events, in terms of the variable r, defined as

$$r = \frac{p - p_o}{p_{max} - p_o}$$

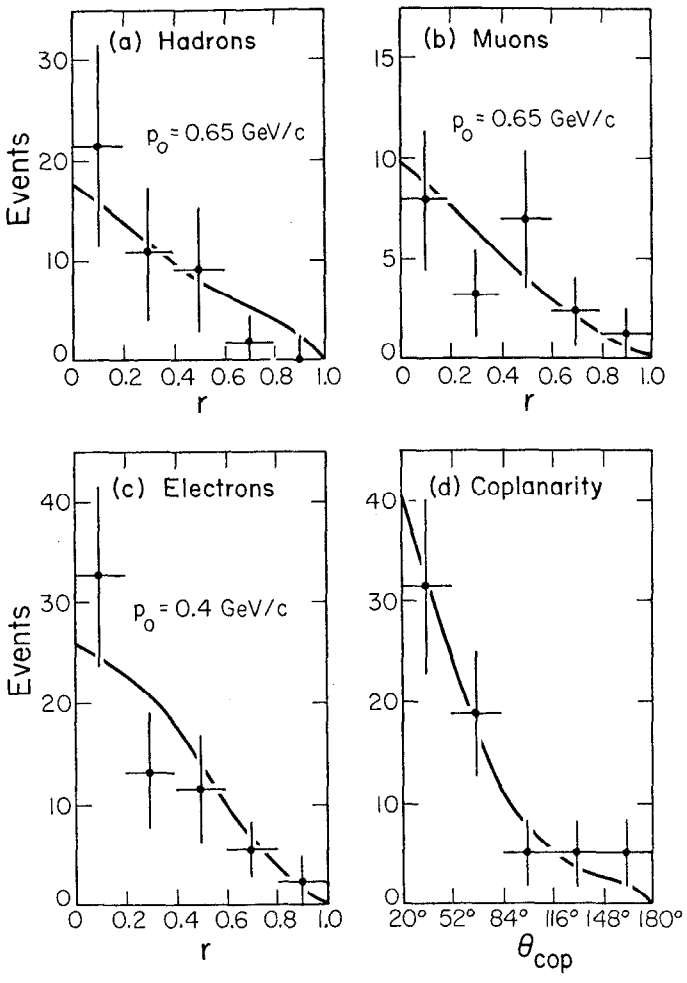

Fig. 5 The distributions of the momentum variable $r \equiv (p-p_o)/(p_{max}-p_o)$ for a) the hadrons, b) the muons, and c) the electrons in the eμ and eh anomalous two-prong events. In (d) we have the coplanarity angle distribution for all the anomalous two-prong events. Data from all three energy regions have been combined. The curves show the expected distributions assuming heavy lepton production and decay.[21] They are normalized to the total number of events in each plot.

where: p = momentum of the particle

p_o = cut-off momentum (0.4 GeV/c for electrons; 0.65 GeV/c for muons and hadrons)

p_{max} = maximum momentum allowed in τ decay.[21]

Figure 5(d) shows the corrected coplanarity angle distribution for all the anomalous two-prong events.

The curves in Figure 5 show the expected momentum and coplanarity distributions assuming heavy lepton production and decay.[21] They are normalized to the total number of events in each plot. It is seen that the data are consistent with the heavy lepton hypothesis.

It should be stated again that in our measurement of the branching ratios we have assumed that a heavy lepton is the only source of the two-prong events, and have ignored a possible contribution from semi-leptonic decays of charmed particles. Thus, strickly speaking, the measured branching ratios should be considered as upper limits.

V. MULTIPRONG EVENTS[24]

A. Event Sample. We recall from Section I that the "multiprong" events are of the type:

$$e^+e^- \to e^\pm + (\geq 2 \text{ charged particles}) + n \cdot \gamma, \text{ with } n \geq 0$$

At least three charged particles are detected, and the electron is always identified in the lead-glass wall.

I will present here the results of the multiprong event analysis for data taken in four different center-of-mass energy ranges:[25]

$E_{c.m.}$ range (GeV)	Average $E_{c.m.}$ (GeV)	$\int$ Ldt (pb^{-1})
3.76-3.79	3.774	1.28
4.1 -4.2	4.16	1.01
4.4 -5.7	4.9	3.46
6.4 -7.4	7.0	5.37

Since the lowest $E_{c.m.}$ range is essentially at the top of the $\psi(3772)$ resonance, which decays into $D\bar{D}$,[26,27] the interpretation of the multiprong events there in terms of the semi-leptonic decay of the charmed D meson is quite straightforward. In the other $E_{c.m.}$ ranges, the interpretation is more complicated because a) we aren't sure of the exact production mechanism of D mesons (i.e. $e^+e^- \to DD^*$, D^*D^*, $D^*D^*\pi\pi$, ...), and b) there might be other charmed particles produced, such as F mesons or charmed baryons. The best we can do at this point in the analysis is to measure an average semi-leptonic branching ratio for "charmed particles" into electrons for each of the three highest center-of-mass energy ranges.

The multiprong events are selected using the following criteria:

1) The momentum of the particle in the lead-glass wall is > 300 MeV/c.

2) The particle in the lead-glass wall is identified as an electron using the criteria discussed in Section III.A. for multiprong events.

3) At least two other charged particles are detected in the Mark I detector or the lead-glass wall.

4) For the $E_{c.m.}$ range 3.76-3.79 GeV only, the momentum of each particle in the event (except the one identified as the electron) must be less than the maximum momentum kinematically allowed for D meson decay.

5) The event is rejected:

a) If any particle in the event has a momentum greater than half the beam energy, and is coplanar with any other particle in the event within 10°, or

b) If any two particles in the event each have a momentum greater than half the beam energy, and any particle in the event (other than the one in the lead-glass wall) is identified as an electron by the Mark I detector.

Both of the criteria in 5) above were designed to eliminate QED events like $e^+e^- \to e^+e^-\gamma$ or $e^+e^-\gamma\gamma$, with one or both photons converting to an e^+e^- pair. These events are commonly called "multiprong Bhabha events."

For each center-of-mass energy range, the number of multiprong events which satisfy all of the above criteria are listed in the first line of Table IV under the heading of electron candidates.

Table IV. Multiprong events. See text for event selection criteria and discussion of backgrounds. $\sigma_e(p_e > 300$ MeV/c) is the cross section for multiprong events with an anomalous electron of momentum > 300 MeV/c, after the heavy lepton contribution is subtracted. These results are preliminary.

	Center-of-mass energy range (GeV)			
	3.76-3.79	4.1-4.2	4.4-5.7	6.4-7.4
Electron candidate events	55	54	139	146
Background events	23 ± 2	19 ± 2	52 ± 5	58 ± 6
Corrected events	46 ± 12	50 ± 12	119 ± 20	113 ± 19
Expected events from heavy lepton τ	0	6 ± 2	21 ± 6	18 ± 5
$\sigma_e(p_e > 300$ MeV/c) in nb	1.13±0.34	1.31±0.39	0.82±0.20	0.47±0.11

The expected number of background events from the backgrounds discussed in Section III. C. (i.e. from hadron misidentification, pion and kaon decay, and asymmetric photon conversions or Dalitz decays) are listed in the second line of Table IV. It is seen that ~ 40% of the electron candidates are due to background.

After subtracting the background events from the electron candidates, and correcting for the electron detection efficiency ($\bar{\varepsilon}$ ~ 75%) discussed in Section III. B., one has the number of corrected events shown in the third line of Table IV.

The production and decay of heavy leptons (τ) will contribute a small number of events to the multiprong events, as we have seen in Section I that the branching ratio for $\tau \rightarrow$ ($\geq$ 2 charged particles) + neutrals is ~15%.[23] Using this branching ratio, we have calculated[21] the expected contribution of the τ to the corrected events, and this is listed in line 4 in Table IV. It is seen that the τ contribution is typically ~15%.

Subtracting the τ contribution from the number of corrected events, and then correcting this result for a) the solid angle of the lead-glass wall (0.055 sr), b) for the detection efficiency of the other particles besides the electron (typically ~75-85%), and c) for several efficiencies for the data cuts whose product is ~80%, we can use the integrated luminosities given at the beginning of this Section to calculate the cross sections for multiprong events with an electron of momentum greater than 300 MeV/c. These are listed in the last line of Table IV. It is seen that we observe a substantial anomalous electron signal in all four energy ranges.

The momentum distributions for the electrons in the multiprong events are presented in Figure 6. The data in Figure 6 have been corrected for backgrounds and efficiencies, but the ~15% contamination due to the heavy lepton (τ) contribution at the higher center-of-mass energies has not been subtracted. It is seen that the electron spectrum hardens with increasing center-of-mass energy, and that there are indications that the peak momentum might be shifting slightly higher at the same time.

B. B(D$\rightarrow$eX) at the ψ(3772). The lowest center-of-mass energy range in this analysis, 3.76-3.79 GeV, corresponds to the ψ(3772) resonance.[15] The ψ(3772) appears to decay almost entirely into $D\bar{D}$,[26,27] which strongly suggests that the multiprong events at the ψ(3772) come from the decay of charmed D mesons

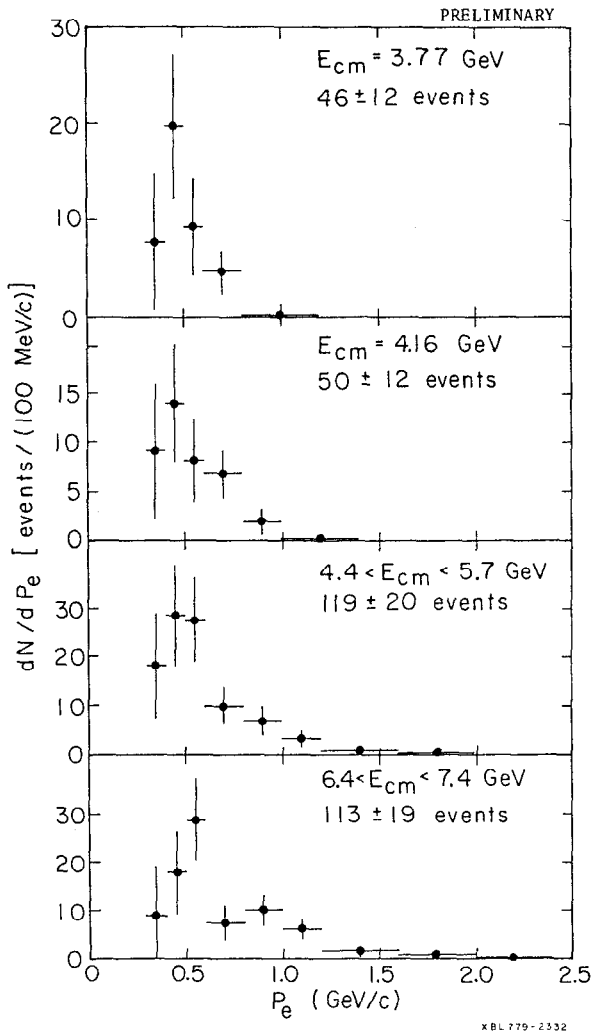

Fig. 6 The corrected momentum distributions above 300 MeV/c for the electrons in the multiprong events, for the four center-of-mass energy regions. The data are corrected for backgrounds and efficiences, but not for the ~15% heavy lepton contribution in the three highest energy regions.

via reaction (2) in Section I (with n = 0). In Figure 7 we show again our corrected momentum distribution for the electrons in the multiprong events at the $\psi(3772)$, along with the momentum spectra expected from D meson production in $e^+e^- \to \psi(3772) \to D\bar{D}$ with subsequent semi-leptonic decay into $\pi e\nu_e$, $Ke\nu_e$ or $K^*e\nu_e$ (for both V + A and V - A forms for the current which couples D to K*).[28] The data are consistent with the Cabibbo-favored decay modes $D \to Ke\nu_e$ (confidence level = 49%), $D \to K^*e\nu_e$ (V-A) (CL=54%) or $D \to K^*e\nu_e$ (V+A) (CL=79%), but are inconsistent with coming entirely from the Cabibbo-suppressed mode $D \to \pi e\nu_e$ (CL=2%). The data are also inconsistent with the purely leptonic decay $D \to e\nu_e$ which would produce a flat electron spectrum from about 810 MeV/c to 1080 MeV/c. If we combine the $Ke\nu_e$ and $K^*e\nu_e$ (V-A) spectra for a fit to the data, we find the $Ke\nu_e$ fraction to be (45±35)%.

Assuming that the multiprong signal at the $\psi(3772)$ comes entirely from D meson production and decay,[29] and that the $\psi(3772)$ decays entirely into $D\bar{D}$, we can calculate the semileptonic branching ratio for D meson decay into an electron plus other particles:

$$B(D \to eX) = \frac{\sigma_e(p_e > 300 \text{ MeV/c})/A(p \text{ cut})}{\sigma(D)}$$

where

$\sigma_e(p_e > 300 \text{ MeV/c}) = 1.13 \pm 0.34$ nb from Table IV

A(p cut) is the correction for the part of the electron spectrum which falls below our cutoff value of 300 MeV/c. As a model, we take the average of the decay spectrum for $D \to Ke\nu_e$ and $K^*e\nu_e$(V-A) as shown in Figure 7. We obtain A(p cut) = 0.82

$\sigma(D)$ is the cross section for D production, which we have previously determined to be 20.6 ± 4.3 nb.[26]

We thus find:[30] $\boxed{B(D \to eX) = (6.7 \pm 2.4)\%}$

C. B(charmed particles → eX) at several $E_{c.m.}$ As we discussed, it is only possible to give an average semi-leptonic branching ratio for "charmed

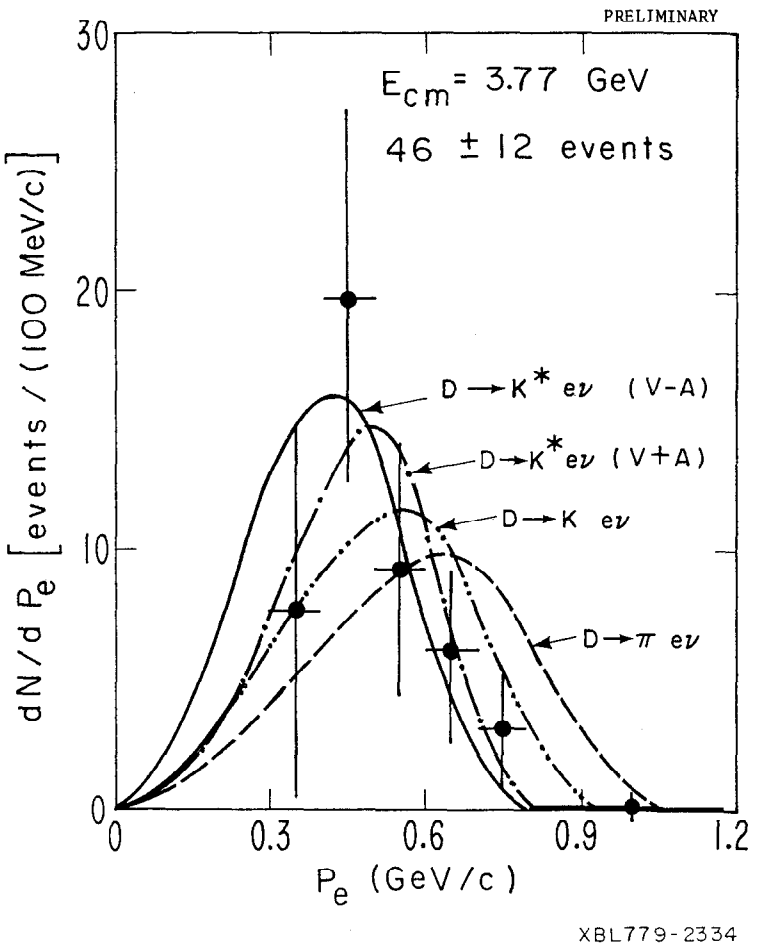

Fig. 7 The corrected momentum distribution above 300 MeV/c for the electrons in the multiprong events at the $\psi(3772)$. The curves show the electron momentum spectra expected from D meson production (via $e^+e^- \to D\bar{D}$) and decay (via $D \to \pi e\nu_e$, $Ke\nu_e$ and $K^*e\nu_e$), based on the calculations of Ali and Yang.[28] The curves are normalized above 300 MeV/c to the total number of events.

particles" into electrons for each of the three highest center-of-mass energy ranges, because we can't separate D decays from other charmed particle decays in our data. We write:

$$B(c \to eX) = R_e/2\ R_{charm}$$

where: $c \equiv$ "charmed particles"

$$R_e = \frac{\sigma_e(p_e > 300\ \text{MeV/c})/A(p\ \text{cut})}{\sigma(e^+e^- \to \mu^+\mu^-)}$$

$$R_{charm} = \frac{\text{cross section for production of a pair of charmed particles}}{\sigma(e^+e^- \to \mu^+\mu^-)}$$

To evaluate R_e we again need A(p cut), which is the correction for the part of the electron spectrum which falls below our cutoff value of 300 MeV/c. To determine A(p cut) we need to know the momentum spectrum of the electron in the "charmed particle" decays, and we need to know how the "charmed particles" are produced so that we can properly Lorentz boost the spectra. As an approximation we have chosen a reasonable production process for D meson production for each of the four center-of-mass energy ranges, and assumed the D's decay to $Ke\nu_e$ or $K^*e\nu_e$(V-A). The assumed production processes are:[31]

$E_{c.m.}$ (GeV)	Production Process
3.772	$D\bar{D}$
4.16	D^*D^*
4.4-5.7	D^*D^*
6.4-7.4	$D^*D^*\pi\pi$

The resulting spectra are shown in Figures 8-10, along with our data.[28] The agreement is satisfactory, and we average the $Ke\nu_e$ and $K^*e\nu_e$(V-A) spectra to obtain A(p cut), and thus R_e. The result is the first column in Table V.

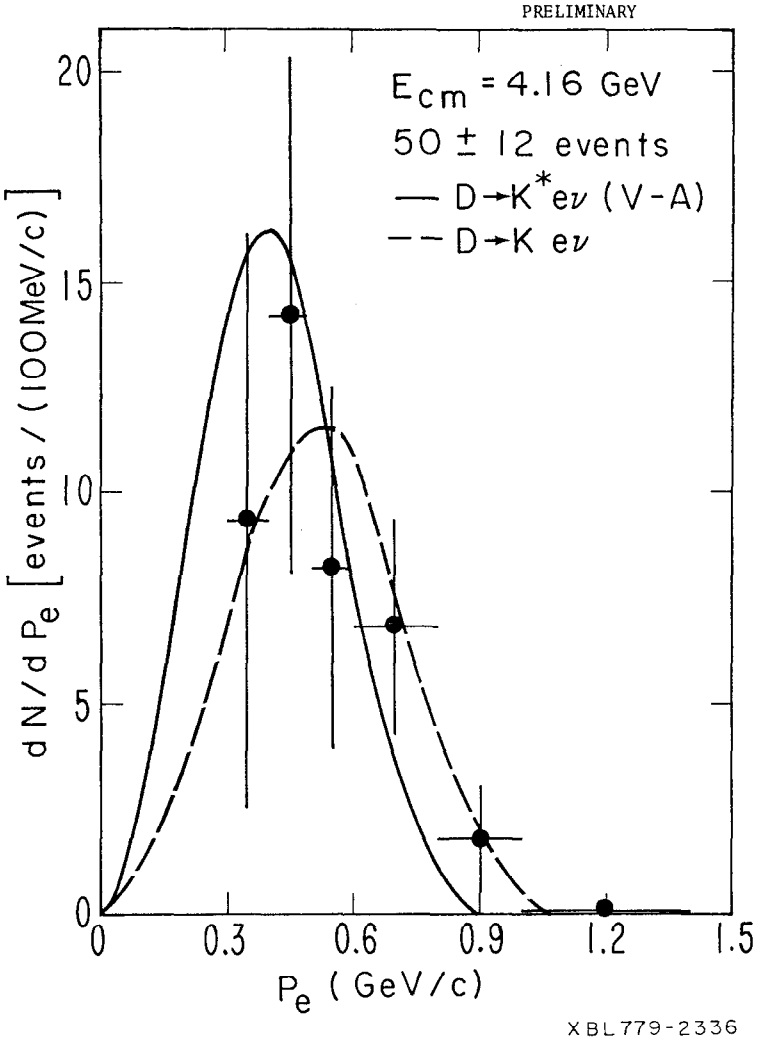

Fig. 8 The corrected momentum distribution above 300 MeV/c for the electrons in the multiprong events at $E_{c.m.}$ = 4.16 GeV. The ~15% heavy lepton contribution has not been subtracted. The curves show the electron momentum spectra expected from D meson production (via $e^+e^- \to D^*D^*$) and decay (via $D \to Ke\nu_e$ and $K^*e\nu_e$ (V-A)), based on the calculations of Ali and Yang.[28] The curves are normalized above 300 MeV/c to the total number of events.

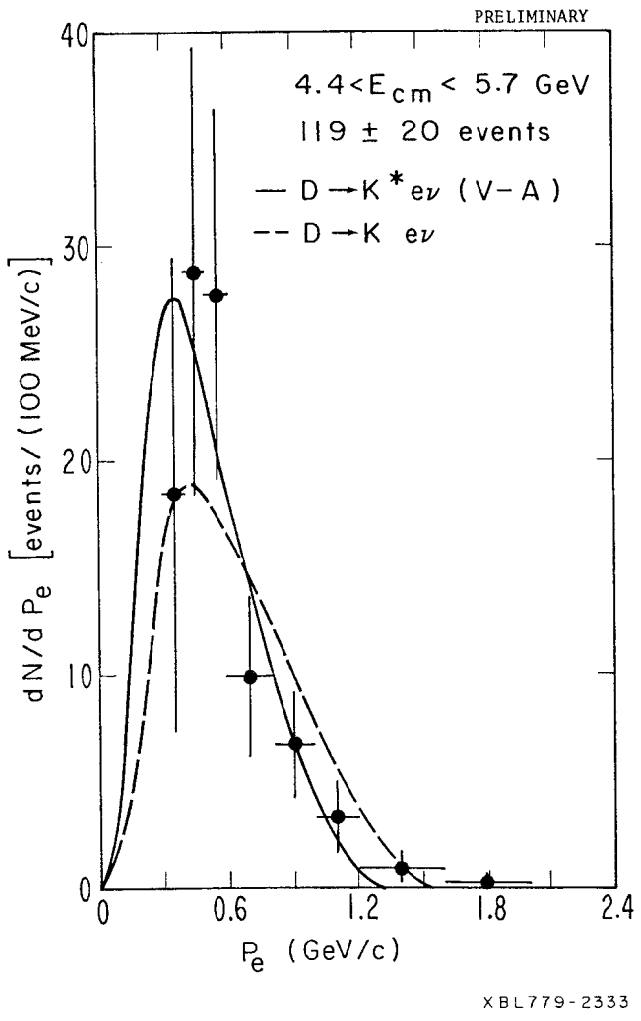

Fig. 9 The corrected momentum distribution above 300 MeV/c for the electrons in the multiprong events in the $E_{c.m.}$ region 4.4-5.7 GeV. The ~15% heavy lepton contribution has not been subtracted. The curves show the electron momentum spectra expected from D meson production (via $e^+e^- \to D^*D^*$) and decay (via $D \to Ke\nu_e$ and $K^*e\nu_e$(V-A)), based on the calculations of Ali and Yang.[28] The curves are normalized above 300 MeV/c to the total number of events.

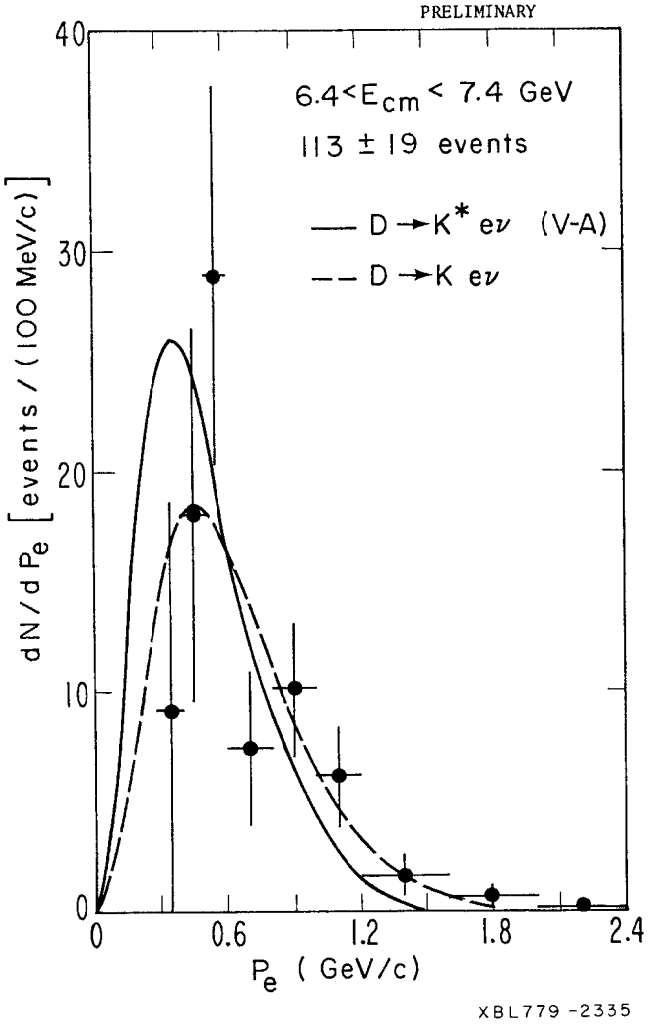

Fig. 10 The corrected momentum distribution above 300 MeV/c for the electrons in the multiprong events in the $E_{c.m.}$ region 6.4-7.4 GeV. The ~15% heavy lepton contribution has not been subtracted. The curves show the electron momentum spectra expected from D meson production (via $e^+e^- \to D^*D^*\pi\pi$) and decay (via $D \to Ke\nu$ and $K^*e\nu_e$(V-A)), based on the calculations of Ali and Yang.[28] The curves are normalized above 300 MeV/c to the total number of events.

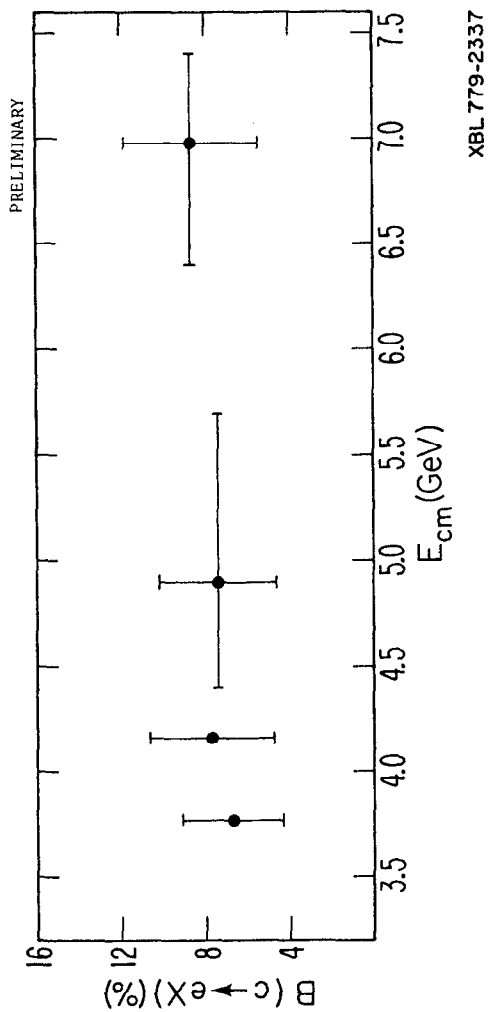

Fig. 11 The semi-leptonic branching ratio of charmed particles into electrons as a function of the center-of-mass energy.

Table V. Multiprong events. For definitions of the quantities, see the text. The results are preliminary.

$E_{c.m.}$ range (GeV)	R_e	R_{charm}	$B(c \to eX)$ (%)
3.76-3.79 [ψ(3772)]	0.23±0.07	1.7±0.3	6.7±2.4
4.1-4.2	0.32±0.10	2.1±0.5	7.7±3.0
4.4-5.7	0.28±0.07	1.9±0.5	7.4±2.8
6.4-7.4	0.33±0.08	1.9±0.4	8.7±3.2

To evaluate R_{charm} we assume:

$$R_{charm} = R - R_\tau - R_{old}$$

where:

$R = \sigma(e^+e^- \to \text{hadrons})/\sigma_{\mu\mu}$

R_τ is the contribution to R from $e^+e^- \to \tau^+\tau^-$, and equals $\frac{\beta}{2}(3-\beta^2)$ with $\beta = v_\tau/c$.

We assume m_τ = 1.9 GeV.

R_{old} is the constant value of R below the charm threshold. We take R_{old} = 2.6.

The values of R_{charm} so determined are listed in the second column in Table V.[32]

Having R_e and R_{charm}, we thus can calculate $B(c \to eX)$, which is listed in the last column in Table V. Figure 11 shows $B(c \to eX)$ as a function of the center-of-mass energy. There does not seem to be any large variation of the branching ratio with energy.

The values of $B(c \to eX)$ obtained here agree within errors with those obtained at DORIS,[13,33] but seem to be systematically lower. This is probably due to the long standing fact that the measurements of the total hadronic cross

section (and thus R) at SPEAR with the Mark I detector have always been higher then those measured at DORIS.[34]

VI. SUMMARY.

1) We observe anomalous electron production in two-prong events which is consistent with the heavy lepton hypothesis. Assuming all these events arise from the production and decay of a heavy lepton, τ, we have measured the branching ratios:[22]

$$B_e(\tau \to e\nu_e\nu_\tau) = (21.6 \pm 5.3)\%$$

$$B_h(\tau \to \text{single charged hadron + neutrals}) = (43 \pm 18)\%$$

2) We observe anomalous electron production in multiprong events. At the $\psi(3772)$ the electron momentum spectrum is consistent with the Cabibbo-favored semi-leptonic decays of the charmed D meson, and using efficiencies averaged over $D \to Ke\nu_e$ and $K^*e\nu_e$(V-A), we have measured the semi-leptonic branching ratio of the D into electrons:[30]

$$B(D \to eX) = (6.7 \pm 2.4)\%$$

For higher center-of-mass energies we have obtained average semi-leptonic branching ratios for charmed particles into electrons under similar assumptions. Our preliminary results are:

$E_{c.m.}$ (GeV)	$B(c \to eX)(\%)$
4.1-4.2	7.7 ± 3.0
4.4-5.7	7.4 ± 2.8
6.4-7.4	8.7 ± 3.2

I sincerely acknowledge the large contribution that has been made by the members of the Lead-Glass Wall collaboration[1] in obtaining the results presented here. I also thank Mrs. Josephine Barrera for her help in typing this paper.

REFERENCES AND FOOTNOTES

1. The members of the Lead-Glass Wall collaboration are: A. Barbaro-Galtieri, R. Ely, J. M. Feller, A. Fong, P. Lecomte, R. J. Madaras, T. S. Mast, M. T. Ronan, R. R. Ross, B. Sadoulet, T. G. Trippe, V. Vuillemin, (Lawrence Berkeley Laboratory and Department of Physics, University of California at Berkeley); J. M. Dorfan, G. J. Feldman, G. Hanson, J. A. Jaros, B. P. Kwan, A. M. Litke, D. Lüke, J. F. Martin, M. L. Perl, I. Peruzzi, M. Piccolo, T. P. Pun, P. A. Rapidis, D. L. Scharre (Stanford Linear Accelerator Center and Department of Physics, Stanford University); B. Gobbi, D. H. Miller (Department of Physics and Astronomy, Northwestern University); S. I. Parker, D. E. Yount (Department of Physics and Astronomy, University of Hawaii).

2. Results from the same experiment on non-leptonic decays of D mesons are presented by G. J. Feldman in these Proceedings.

3. J.-E. Augustin et al., Phys. Rev. Lett. 34, 233 (1975); G. J. Feldman and M. L. Perl, Phys. Reports 19C, 233 (1975), Appendix A; F. Vannucci et al., Phys. Rev. D15, 1814 (1977).

4. M. L. Perl et al., Phys. Rev. Lett. 35, 1489 (1975)

5. M. L. Perl et al., Phys. Letters 63B, 466 (1976).

6. A. Barbaro-Galtieri et al., Lawrence Berkeley Laboratory report number LBL-6458 (1977) and Stanford Linear Accelerator Center report number SLAC-PUB-1976 (1977), to be published in Phys. Rev. Lett.

7. M. Cavalli-Sforza et al., Phys. Rev. Lett. 36, 558 (1976); see also an interpretation of these data by G. Snow, Phys. Rev. Lett. 36, 766 (1976).

8. G. J. Feldman et al, Phys. Rev. Lett. 38, 117 (1977)

9. M. L. Perl et al., Stanford Linear Accelerator Center report number SLAC-PUB-1997 (1977) and Lawrence Berkeley Laboratory report number LBL-6731 (1977), submitted to Phys. Letters.

10. J. Burmester et al., Phys. Letters 68B, 297 (1977).

11. J. Burmester et al., Phys. Letters 68B, 301 (1977).

12. R. Brandelik et al., DESY report DESY 77/36 (1977).

13. Recent DESY results on anomalous electron production in electron-positron annihilations are presented by W. de Boer in these Proceedings.

14. The predictions are based on Y. S. Tsai, Phys. Rev. D4, 2821 (1971), and H. B. Thacker and J. J. Sakurai, Phys. Letters 36B, 103 (1971), as discussed by G. J. Feldman in Proceedings of the 1976 Summer Institute on Particle Physics (SLAC, 1976), also issued as SLAC report number SLAC-PUB-1852 (1976).

15. P. A. Rapidis et al., Phys. Rev. Lett. 39, 526 (1977).

16. R. F. Althaus et al., IEEE Trans. Nucl. Sci. NS-24, 218 (1977) and NS-24, 408 (1977)

17. More details on the lead-glass detector can be found in J. Feller et al., Lawrence Berkeley Laboratory report number LBL-6466 (1977).

18. R. J. Madaras et al., Lawrence Berkeley Laboratory report number LBL-6767 (1977), in preparation.

19. Two of the anomalous two-prong events have both the electron and the other particle identified in the lead-glass wall.

20. After we published our two-prong event results (see Reference 6), we found that the $\int$ Ldt that we had used was too small by about 8%. The integrated luminosities listed here are the correct ones for the two-prong event analysis.

21. We take the properties of the heavy lepton, τ, to be: $m(\tau) = 1.9$ GeV, $m(\nu_\tau) = 0.0$, V-A weak interaction coupling.

22. Because of the 8% correction in $\int$ Ldt (see Reference 20), these branching ratios are 4% smaller than the ones published in Reference 6.

23 See Table I in Section I.

24. The results of the multiprong event analysis in this written version of my talk are different (by less than one-half the quoted errors) from the results I originally presented. This is because a) the analysis now includes a larger data sample, and b) the analysis has been improved since the talk.

25. The integrated luminosities here are different than for the two-prong event analysis, because of slightly different data samples.

26. I. Peruzzi et al., Stanford Linear Accelerator Center report number SLAC-PUB-2012 and Lawrence Berkeley Laboratory report number LBL-6755 (1977).

27. See G. J. Feldman's talk in these Proceedings.

28. The electron momentum spectra (for D's at rest) are taken from the calculations of A. Ali and T. C. Yang, Phys. Letters 65B, 275 (1976) and A. Ali, private communication. We then Lorentz boost them with a Monte Carlo program to take into account the D momentum.

29. If the $\psi(3772)$ is above the threshold for $\tau^+\tau^-$ production, an anomalous electron signal may also arise from decays of the heavy lepton τ. From *preliminary measurements on eμ events at the $\psi(3772)$* (see M. L. Perl, Proceedings of the 1977 International Symposium on Lepton and Photon Interactions at High Energies, Hamburg, 1977, to be published) we estimate that 6% of the anomalous electron events can come from this source. Taking account of $\tau^+\tau^-$ production would also lead to a decrease in the value of $\sigma(D)$ by about 12%; the net effect is to raise our value for the branching ratio of D to electrons from 6.7% to 7.1%. For additional information on eμ and eh two-prong events at $E_{c.m.} = 3.77$ GeV (with the electron in the LGW), see the talk of A. Barbaro-Galtieri, Proceedings of the 1977 International Symposium on Lepton and Photon Interactions at High Energies, Hamburg, 1977, to be published.

30. This is a preliminary value. The final value is (7.2 ± 2.8)%, which was obtained after this paper was written. See J. Feller et al., Lawrence Berkeley Laboratory report number LBL-6772 (1977).

31. The production process for the center-of-mass energy 3.772 GeV is listed here only for completeness. We saw in Section V.B. that the $\psi(3772)$ decays almost entirely into $D\bar{D}$ (see References 26 and 27).

32. The results for the $\psi(3772)$ were discussed in Section V.B., and are listed here only for completeness. R_{charm} for the $\psi(3772)$ is obtained by dividing the experimentally measured cross section for D production, $\sigma(D)$, by $2\sigma_{\mu\mu}$. See reference 26 for $\sigma(D)$.

33. W. Braunschweig et al., Phys. Letters 63B, 471 (1976); J. Burmester et al., Phys. Letters 64B, 369 (1976); R. Brandelik et al., DESY preprint DESY 77/41 (1977).

34. See the talks of V. Luth and W. de Boer in these Proceedings.

REVIEW OF DILEPTON PRODUCTION AT HIGH ENERGY

Melvyn Jay Shochet
Enrico Fermi Institute, University of Chicago
Chicago, Illinois 60637

I. INTRODUCTION

Dilepton production in hadron-hadron collisions at high energies has been studied by a large number of experimental groups at Brookhaven, CERN, Fermilab, and Serpukhov. This work has had three major motivations. Firstly, a number of experiments investigated the origin of single direct leptons. These are known to be produced over a wide kinematic region with a production cross-section $\sim 10^{-4}$ that of single pion production.[1] Secondly, dimuon production has been studied in order to determine the properties of the high mass dimuon continuum. Tests have been made to determine whether this production is consistent with a simple model of quark anti-quark annihilation. If this is so, properties of the quarks within the nucleons can be determined from the data. Finally, dileptons have been used to study the production of high mass vector resonances. Searches in the leptonic decay mode are necessitated by the very large backgrounds in the hadronic modes due to normal multi-particle hadronic production.

In the following sections, these three aspects of dilepton studies will be discussed in turn.

II. ORIGIN OF SINGLE DIRECT LEPTONS

There are three possible origins of single direct leptons: (1) They may result from the weak decay of short-lived particles such as charmed particles. In this case the charged lepton would be accompanied by a neutrino and thus not appear in the dilepton spectrum. (2) They

may result from the electromagnetic decay of low mass objects such as $\rho, \omega, \phi, \psi \to \mu^+\mu^-$ or $\eta \to \gamma\mu^+\mu^-$. Thus there would be a charged lepton pair of low invariant mass. (3) They may result from the electromagnetic decay of high-mass objects. An example is the Drell-Yan mechanism[2] in which a quark and anti-quark annihilate into a virtual photon which materializes as a lepton pair.

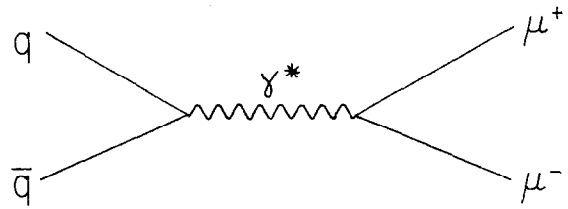

The origin of low and moderate $p_\perp$ direct leptons will now be discussed after which high $p_\perp$ direct leptons will be considered.

A. Low-Moderate $p_\perp$

A Chicago-Princeton group[3] (CP-II) working with the Chicago Cyclotron spectrometer at Fermilab has measured dimuon production over a large range of invariant mass ($M_{\mu\mu}$), Feynman x (x_F), and transverse momentum ($p_\perp$). They used these cross-sections to calculate the dimuon contribution to the single direct muon yield. Figure 1 shows their apparatus which had good acceptance over the range

$$0.3 < M_{\mu\mu} < 12 \text{ GeV/c}^2$$
$$0.15 < x_F < 1$$
$$0 < p_\perp < 4 \text{ GeV/c}$$

Proportional chambers in front of as well as in the middle of the hadron absorber improved the mass resolution at low mass and removed background from muons produced in the absorber.

Figure 2 shows data taken with a 150 GeV incident proton beam. In order to compare the single muon spectrum calculated from these data

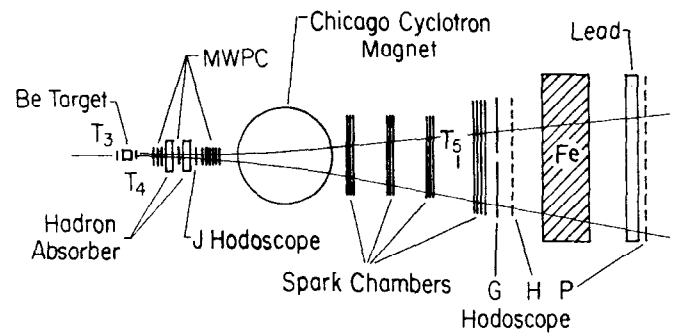

Fig. 1. The Chicago Cyclotron Spectrometer

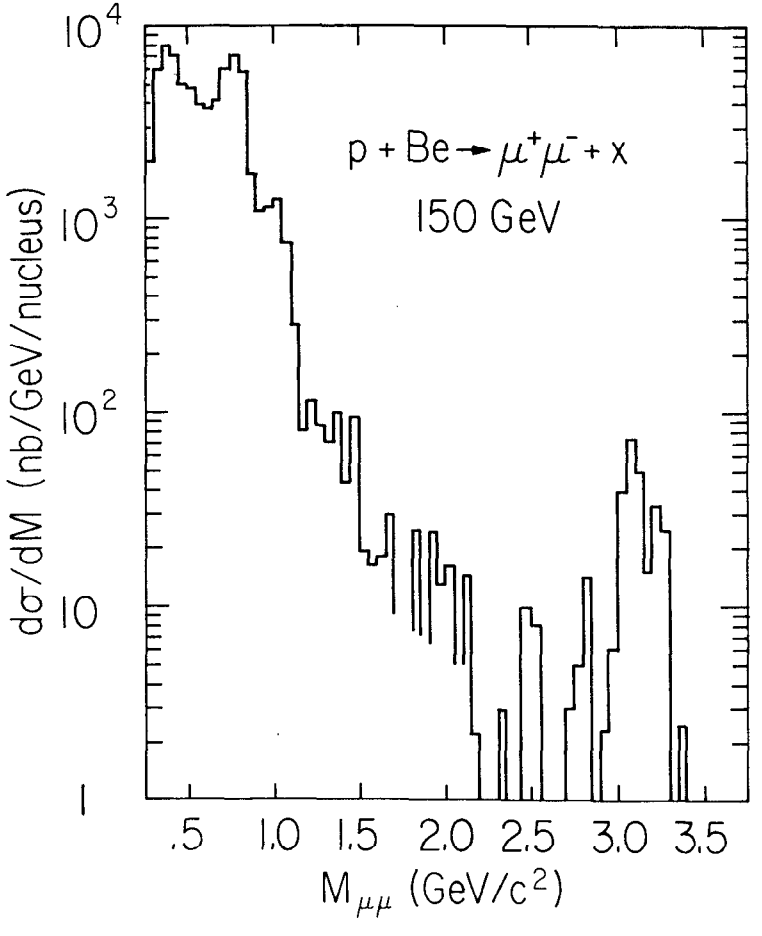

Fig. 2. CP-II Dimuon spectrum.

with results from direct muon experiments, the CP-II data had to be extrapolated to $x_F = 0$. The assumptions $\frac{d\sigma}{dx_F} \alpha (1-x_F)^c$ and $\frac{d\sigma}{dy}$ = constant for $x_F < 0.15$ gave similar results, while the parameterization $E\frac{d^3\sigma}{dp^3} \alpha (1-x_F)^c$ produced higher single muon cross-sections at $x_F = 0$. Since the latter predicted more single direct muons than were observed, the first parameterization was used. The authors also assumed an isotropic decay distribution in the dimuon center-of-mass. They found, however, that a $(1 + \cos^2\theta^*)$ distribution would change the results by <10%.

Figure 3 shows the results of their calculations. The contributions to the single direct muon cross-section from the J/ψ, all vector mesons (ρ, ω, ϕ, J/ψ), and vector mesons plus the observed low-mass continuum are plotted. These results are compared with existing data[4-7] in Fig. 4. Within the uncertainties shown, low mass dimuons can account for all the observed single direct muons at low to moderate transverse momenta. The uncertainties are large enough, however, to accommodate a significant contribution (~30%) from other sources.

The CP-II group also used their data to calculate the contribution of dimuons to single direct muons in the forward direction ($p_\perp < 0.6$ GeV/c, $0.1 < x_F < 0.6$). They found that the low mass continuum made the dominant contribution and that dimuons could again account for the direct muons observed by their group and by Leipuner et al.[8]

Additional information on the origin of single direct muons at low to moderate $p_\perp$ comes from the Yale-BNL-Fermilab collaboration. The dimuon contribution to the direct muon cross-section in the forward direction was determined by measuring both single muons and dimuons in scintillation counter hodoscopes located downstream of a target and hadron absorber at Fermilab.[8] Since their counter array did not extend far in the vertical direction, they had to calculate the fraction of

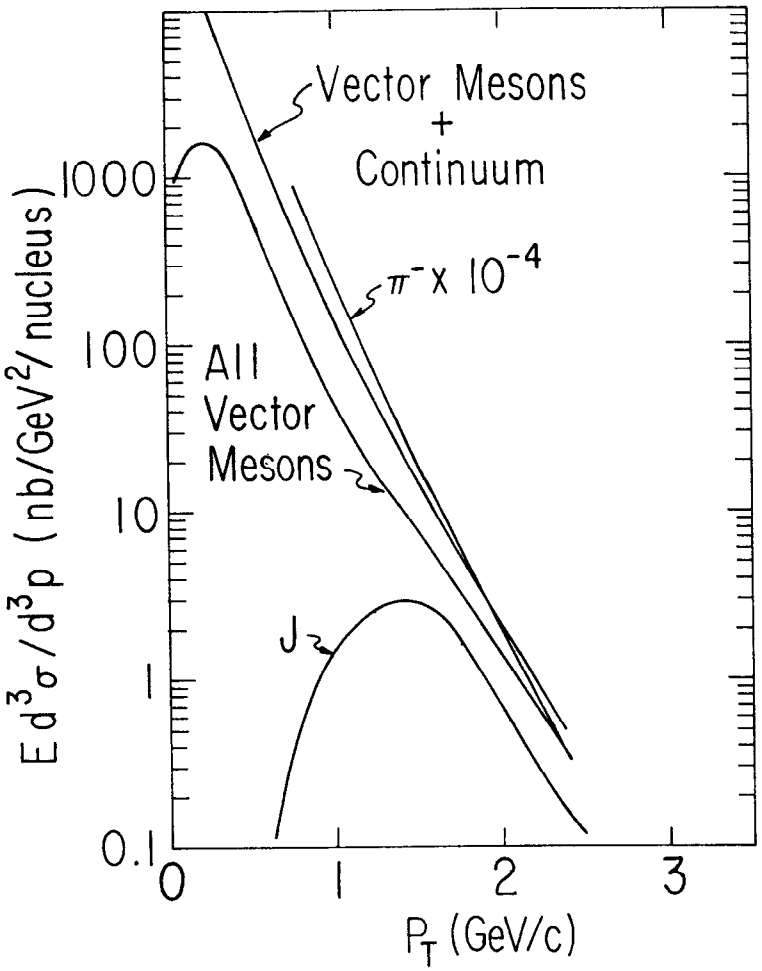

Fig. 3. Contributions to the single direct muon spectrum calculated from the CP-II dimuon spectrum. The single π^- cross-section is shown for comparison.

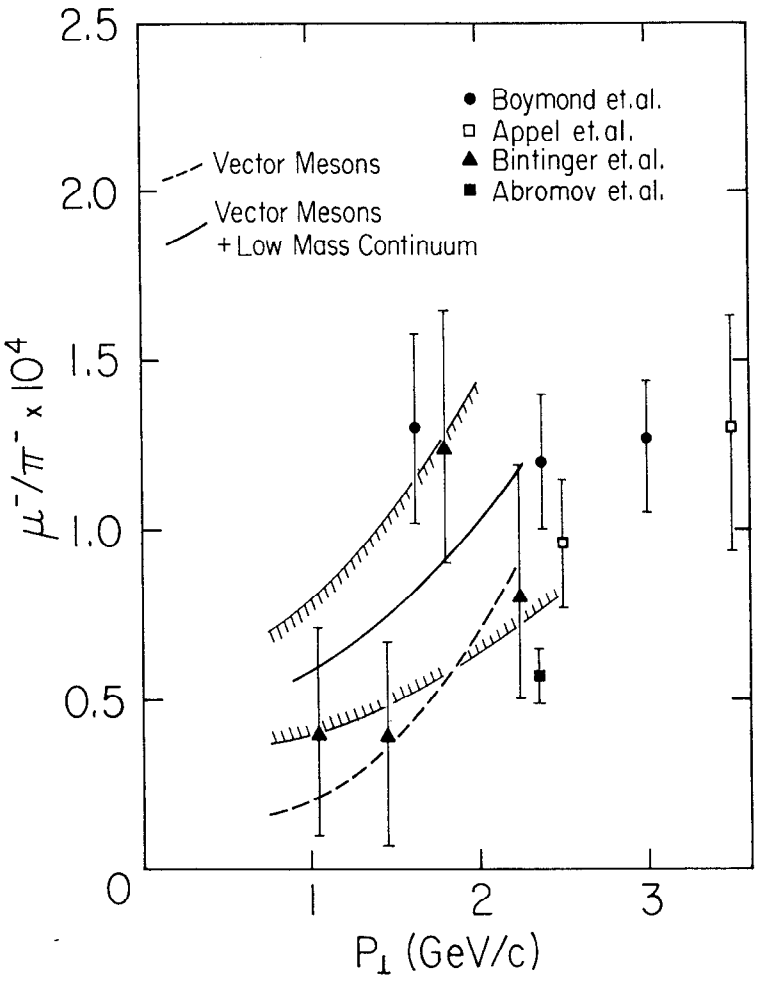

Fig. 4. Calculated μ^-/π^- ratio compared with existing data.

muon pairs for which the second muon missed the detector. The correction factor depended most strongly on the x_F distribution of the muons. Their measured x_F distribution resulted in a correction which increased the dimuon yield by approximately a factor of 11. They concluded that (1) μ pairs/single μ's $\simeq$1, and (2) the single μ rate was approximately ten times larger than they calculated from reasonable ρ, ω production. These conclusions are in qualitative agreement with those of the CP-II group.

The same group also measured the polarization of single direct μ^+ in 400 GeV p-Cu collisions.[9] An aluminum-scintillator polarimeter was used with a 30 gauss precession field to obtain a measured analyzing power of 0.185 ± 0.01. If direct muons have an electromagnetic origin, then one would expect zero polarization due to parity conservation. If direct muons are rather produced by the V-A weak decay of a heavy particle, a polarization of +1.0 would be expected for the anti-fermion μ^+. The experimental results are P = 0.00 ± 0.10 at x_F = 0.46, $p_\perp$ = 0 and P = -0.135 ± 0.20 at x_F = 0.07, $p_\perp$ = 2.15 GeV/c. These results are consistent with an electromagnetic origin for direct muons, but in disagreement with results of Anisimova et al.[10] that P = -0.85 ± 0.36 at $p_\perp$ = 2.8 GeV/c for 70 GeV incident protons.

Finally, there are electron data from the double-arm spectrometer of the CERN-Columbia-Rockefeller-Saclay group at the ISR.[11] They present 95% confidence level upper limits for the contribution of e^+e^- pairs to single direct electrons of $p_\perp$ >1.3 GeV/c.

Mass (GeV/c^2)	Fraction of Single Electron Yield
0.4	<0.064
0.5	<0.104
0.6	<0.178
0.7	<0.512
0.8	<1.61
0.9	<2.73
1.0	<4.45

Their sensitivity allows them to make a significant statement only below the ρ mass. In this region their result is consistent with the CP-II data.

B. High $p_\perp$

A Chicago-Princeton collaboration (CP-I) working in the proton area at Fermilab has studied the high mass dimuon contribution to direct muons at high $p_\perp$ by asking the following question: What fraction of the time is a direct μ accompanied by a high $p_\perp$ μ on the other side of the beamline?[12]

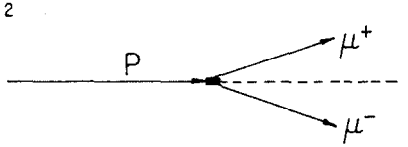

They used the small aperture precision magnetic spectrometer which had previously found direct muons produced at large $p_\perp$. This detector provided an excellent direct muon trigger: 60% - 80% of detected muons were direct rather than from π or K decay. To detect coincident muons on the other side of the beamline, the Multihole Spectrometer (MHS) was built (see Fig. 5). It consisted of 10 liquid scintillation counters (12' x 4') placed in 20' deep holes in the ground. The 6 meter earth shield between the incident beamline and the MHS provided a minimum transverse momentum requirement ($p_\perp$ > 3.2 GeV/c) for any muon reaching an MHS counter. The MHS covered 5% of 4π solid angle in the center of mass and had a mass acceptance typically 2 GeV/c^2 FWHM centered on 2 $p_\perp^s$, where $p_\perp^s$ is the transverse momentum of the muon detected in the precision spectrometer. Results obtained with 400 GeV incident protons are tabulated below.

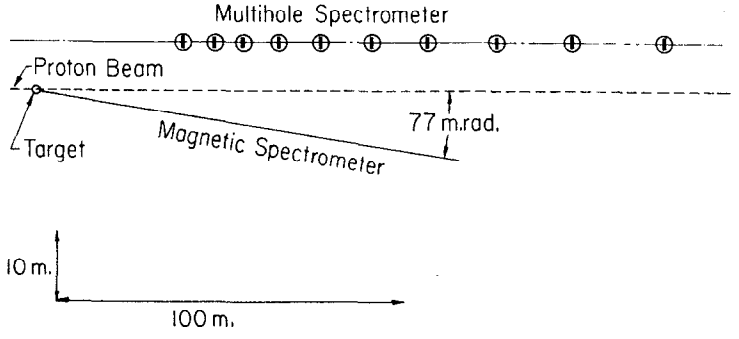

Fig. 5. Schematic of CP-I apparatus.

$p_\perp$	$\langle M_{\mu\mu} \rangle$	Fraction of Direct Muons with Count in MHS
3.9 GeV/c	7.7 GeV/c^2	1.0 ± 0.2%
4.6	8.8	4.1 ± 0.4
5.4	10.0	13.2 ± 2.4
6.2	11.3	14.9 ± 4.8

High mass dimuons are seen to be an increasingly important source of single direct muons as $p_\perp$ is increased. In order to determine the total fraction of high $p_\perp$ direct muons produced as high mass pairs, the above results must be corrected for the finite acceptance of the MHS. This correction depends strongly on the mean transverse momentum of the dimuons. If, for example, $\langle p_\perp \rangle_{\mu\mu} \simeq 0$, then the second muon would lie in the plane defined by the proton beam and the precision spectrometer. In that case the detection efficiency of the MHS would be very high. The mean dimuon $p_\perp$ was determined from the data to be

$$\langle p_\perp \rangle_{\mu\mu} = 1.25 \pm 0.3 \text{ GeV/c}.$$

If the spectrum is parameterized by a simple exponential

$$\frac{d\sigma}{dp_\perp{}^2} \propto e^{-2p_\perp/\langle p_\perp \rangle}$$

it is found that all direct muons at high $p_\perp$ can be accounted for by high mass dimuons. This conclusion varies somewhat if the form of the distribution is changed, but even the most conservative extrapolation finds high mass μ pairs responsible for >30% of high $p_\perp$ direct μ's.

C. CONCLUSION

The evidence from both low-moderate $p_\perp$ and high $p_\perp$ experiments supports the hypothesis that dileptons are responsible for most single lepton production. There is, however, still room for some contribution from weak decays ($\ell\nu$). Results from experiments addressing this question explicitly should be available during the coming year.

One kinematic region of direct lepton production has not been addressed by these dilepton studies. This is the low-$p_\perp$ low-x_F region, where two groups[13,14] have reported a large increase in the e/π ratio as $p_\perp$ drops from 1 GeV/c to 0.

III. PROPERTIES OF THE DIMUON CONTINUUM

The dimuon continuum is of interest for two purposes, what might be called engineering and scientific. The engineering aspect requires a single question to be answered: What will the intermediate vector boson production cross-section be at the proposed high energy p-p and $\bar{p}$-p colliding beam machines? The connection between W production and virtual γ (or equivalently dilepton) production at the same mass is made through CVC.[15] Thus the atomic number dependence of dilepton production must be determined so that the available data on heavy targets can be extrapolated to the p-p case. In addition the scaling properties of the data must be measured so that the data can be extrapolated to the $M_{\mu\mu}$ and $\sqrt{s}$ appropriate to the colliding beam experiments.

The major scientific question being asked is whether the data are consistent with simple quark anti-quark annihilation and if so, what can be learned about the quarks? In this connection, both Drell-Yan scaling and the transverse momentum distribution of dileptons will be discussed.

A. A Dependence

The atomic number (A) dependence of dimuon production is plotted in Fig. 6.[3, 12, 16, 17] Each point represents cross-sections which have been fit to a power law in A. The power increases from ~2/3 at low mass until at high mass it is consistent with a transparent nucleus, i.e., $A^{1.0}$. Although this result can be used to extrapolate cross-sections to the p-p case, the data are not precise enough to help us in

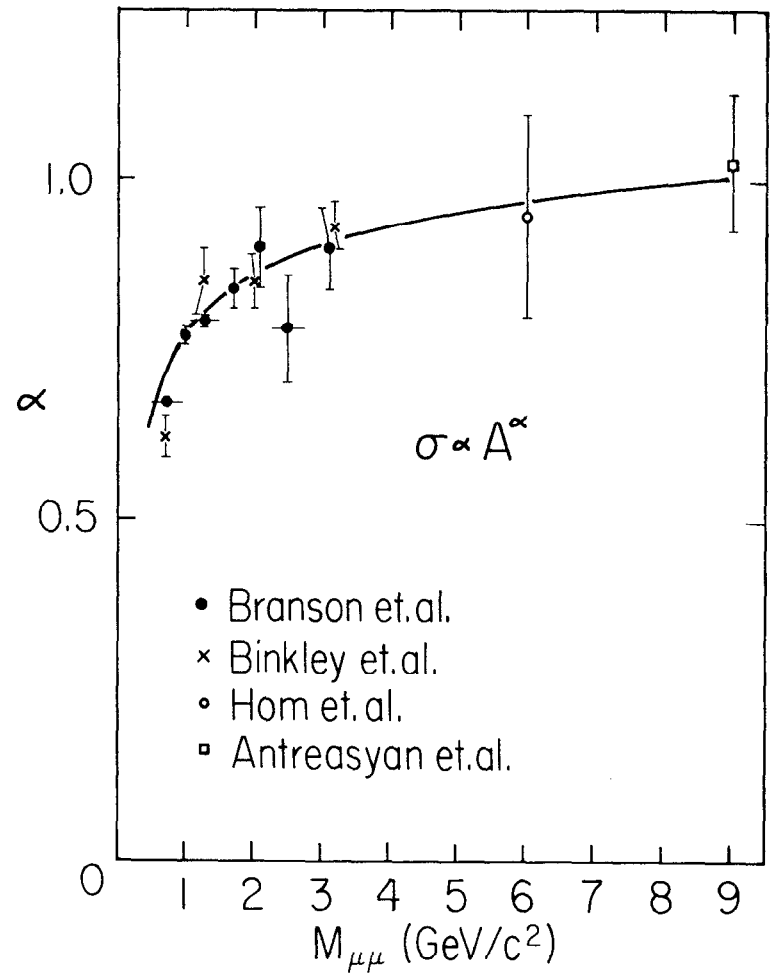

Fig. 6. Atomic number dependence of dimuon production.

understanding the anomalous A dependence observed in single hadron production at high $p_\perp$.[18]

B. Scaling

In the Drell-Yan picture, i.e., electromagnetic annihilation of point particles, the differential cross-section can be written down from simple dimensional arguments:

$$\frac{d\sigma}{dM} = \frac{1}{M^3} f\left(\frac{M}{\sqrt{s}}\right)$$

The cross-section is M^{-3} (to get the proper dimensions) times a function of the dimensionless variable $M/\sqrt{s}$, which is the fraction of the center of mass energy carried by the lepton pair. Since most of the experiments have taken data only in the central region, an alternative scaling form is used:

$$\left.\frac{d^2\sigma}{dMdy}\right)_{y=0} = \frac{1}{M^3} g\left(\frac{M}{\sqrt{s}}\right)$$

The Chicago-Princeton group, CP-I, tested scaling during the past year by taking data at three center-of-mass energies.[12] Figure 7 shows the clear dependence of the differential cross-section on center of mass energy. If scaling occurs, then plotting $M^3\ d^2\sigma/dMdy)_{y=0}$ versus $M/\sqrt{s}$ should produce a single curve with no dependence on $\sqrt{s}$. Figure 8 shows that within the statistical accuracy of the data scaling is verified. It should be noted that the experiment was designed to measure a continuum and therefore it averages over resonance structure. The data thus must be corrected for the 9.5 GeV/c^2 enhancement.[19] The 400 GeV data can be corrected exactly since the cross-section for the enhancement has been measured at that energy. Unfortunately such measurements have not yet been made at 200 GeV or 300 GeV. If it is assumed that the excitation curve for the upsilon has the same shape as that for the J/ψ, the corrected CP-I results are as shown in Fig. 9.

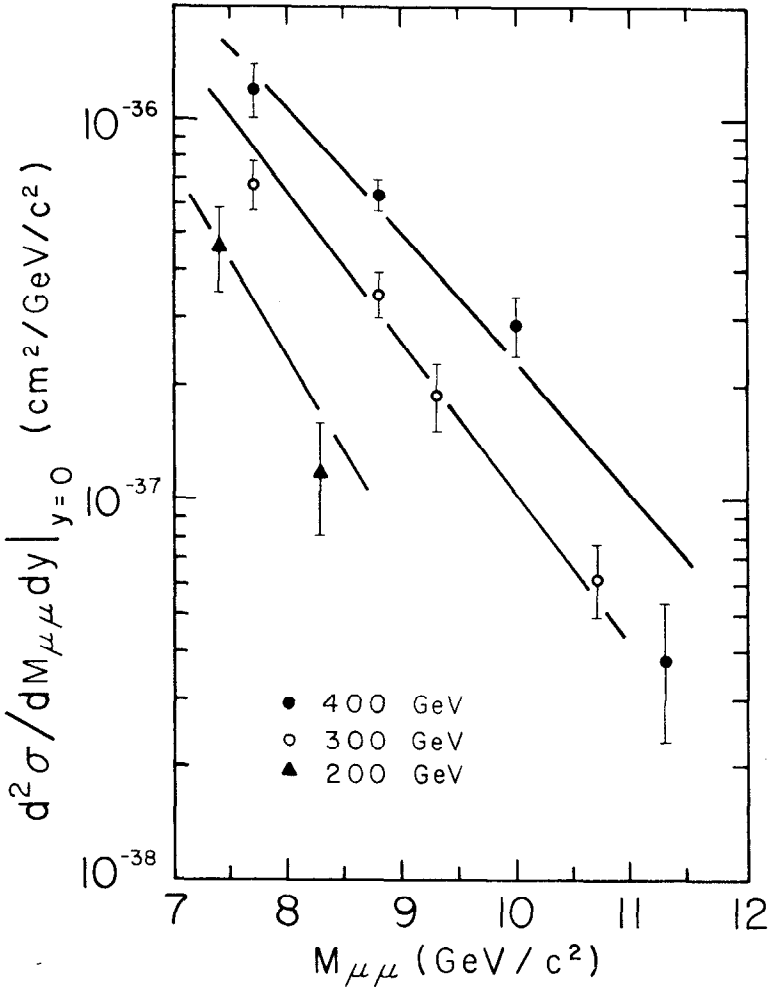

Fig. 7. Dimuon cross-sections from the CP-I group.

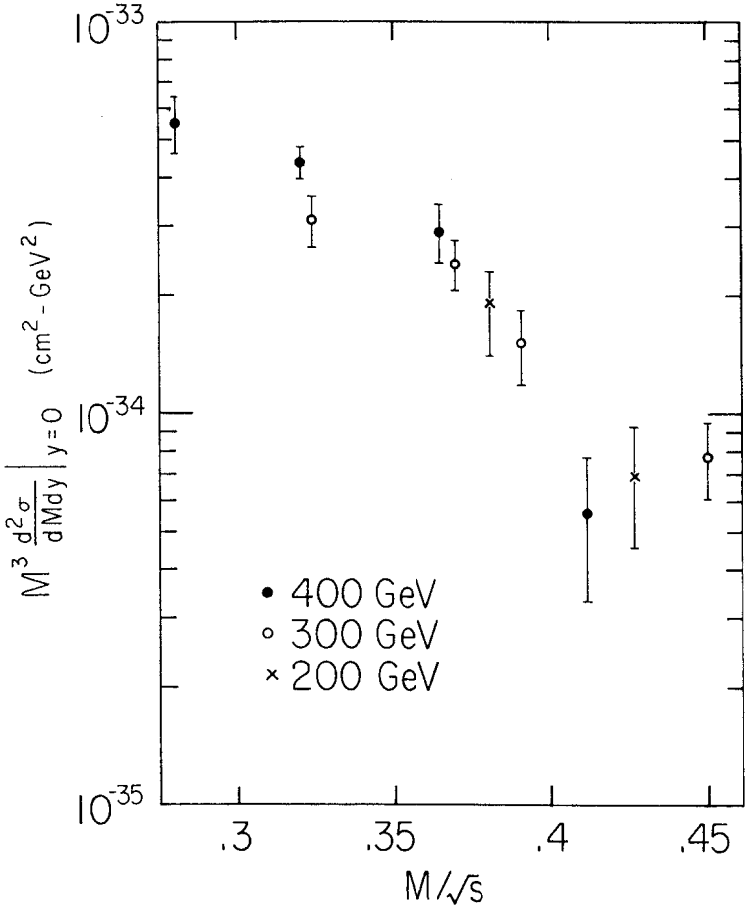

Fig. 8. The scaling properties of the CP-I data.

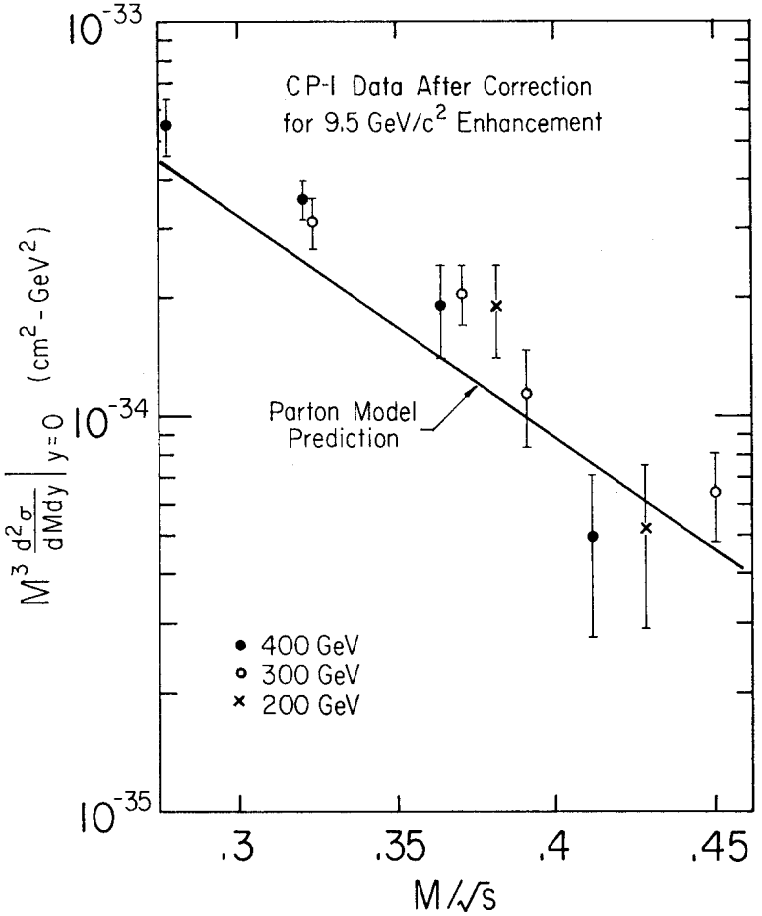

Fig. 9. Corrected CP-I data.

There is still good agreement with the scaling hypothesis. Figure 9 also shows a parton model prediction[20] for dimuon production. The data agree quite well both in shape and magnitude with the prediction.

A scaling plot with all high mass dimuon data[12, 19, 21] is shown in Fig. 10. The ISR data from the CBSY group are preliminary upper limits. A single exponential fits the high mass data quite well. The lower mass data of the CP-II group are also shown on the plot. They lie considerably above the high mass data at the same $M/\sqrt{s}$. This points out the danger in trying to extrapolate from the low mass region.

Additional information on the mechanism for dilepton production comes from the dependence of the production cross-section on incident particle. The CP-II group has compared dimuon production by π^+ and π^- incident on an isoscaler target. If production proceeds via the strong interaction, then isospin invariance requires

$$\frac{\sigma(\pi^+ C \to \mu^+\mu^- X)}{\sigma(\pi^- C \to \mu^+\mu^- X)} = 1$$

If the production mechanism is quark anti-quark electromagnetic annihilation, then

$$\frac{\sigma(\pi^+ C \to \mu^+\mu^- X)}{\sigma(\pi^- C \to \mu^+\mu^- X)} = \frac{Q_d^2}{Q_u^2} = \frac{1/9}{4/9} = 0.25$$

in the region where valence quarks dominate. The data are shown in Fig. 11. The cross-sections in the resonance regions are consistent with strong production, while the continuum data just below and above the J/ψ lie below 1.0. Although the mass range doesn't extend very high and the error bars are large, the data do suggest that the ratio is heading down toward 1/4. The CP-II group will have a run this fall which should extend the results up to much higher mass.

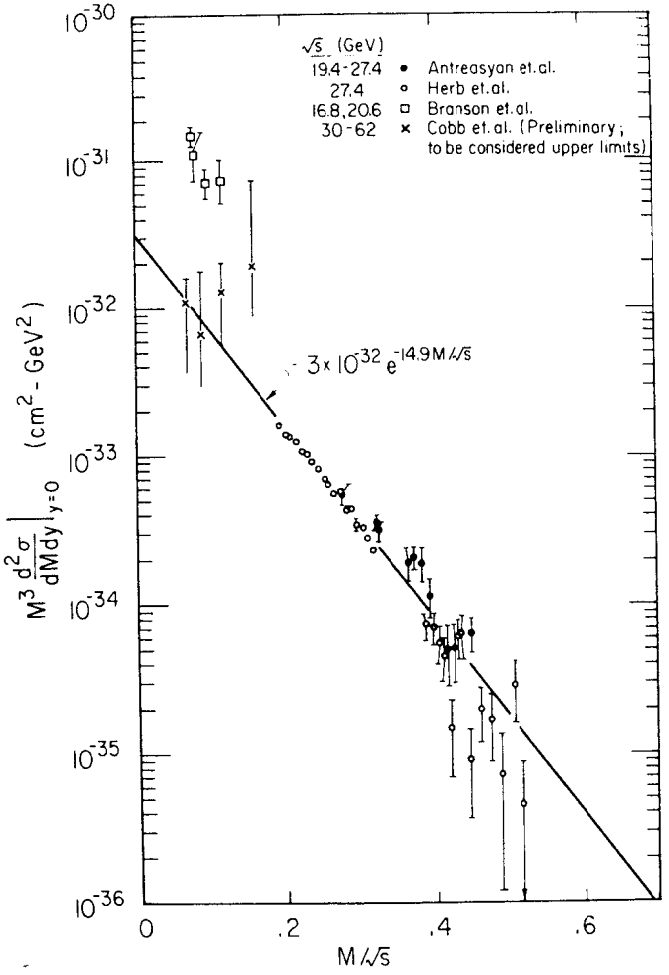

Fig. 10. Scaling curve.

C. Transverse Momentum Distribution of Dimuons

In the most naive parton model one would expect $\langle p_\perp \rangle_{\mu\mu} \approx \sqrt{2} \times 300$ MeV/c $\approx$450 MeV/c. The data (Fig. 12)[3, 12, 17, 22] show a much larger

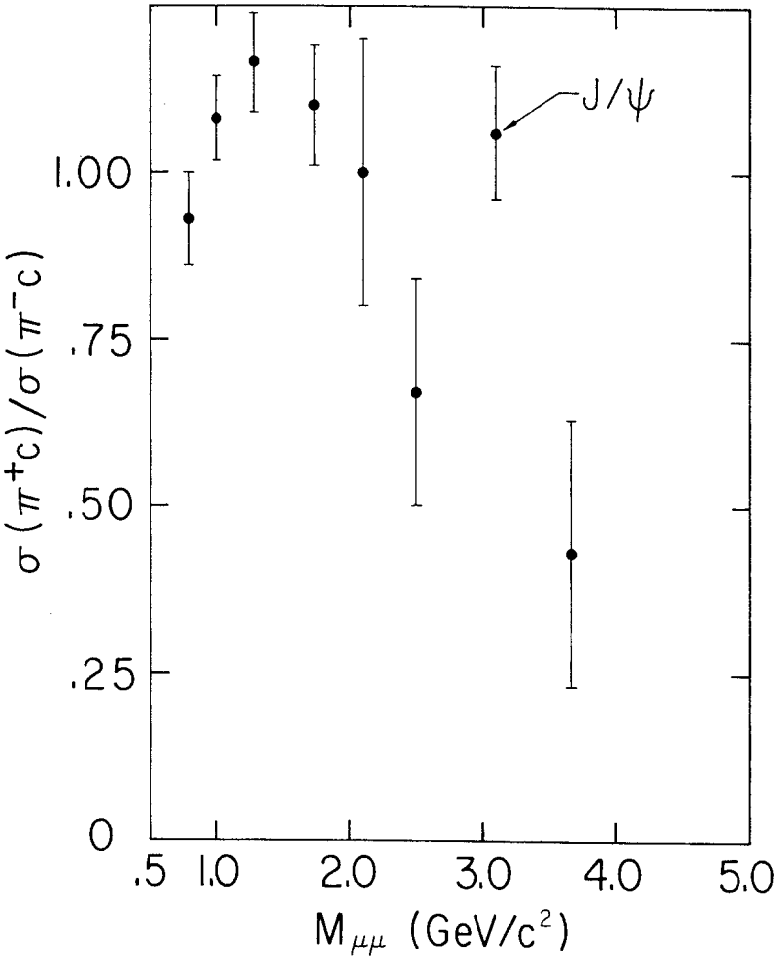

Fig. 11. CP-II data on dimuon production with incident pions.

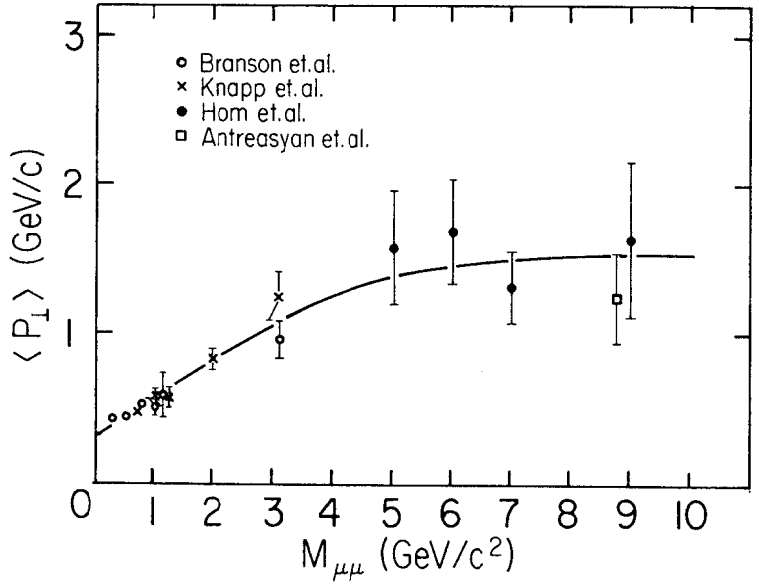

Fig. 12. Mean transverse momentum of dimuons.

$\langle p_\perp \rangle$. At low mass the mean transverse momentum is indeed small; at higher mass $\langle p_\perp \rangle$ increases and finally levels off at the surprisingly large value of $\simeq$1.5 GeV/c. A number of theorists[23] have noted that in more sophisticated models, dimensional counting and/or asymptotic freedom lead to a $\langle p_\perp \rangle$ increasing with $M_{\mu\mu}$ and then flattening out. One note of caution: the rise in $\langle p_\perp \rangle$ is in the low mass region. The production mechanisms there may be very different than in the high mass region. Thus existing data might not contradict a model in which electromagnetic $q\text{-}\bar{q}$ annihilation produced μ pairs with $\langle p_\perp \rangle$ = 1.5 GeV/c independent of mass.

IV. STUDY OF HIGH MASS RESONANCES

There is now a great deal of data on hadronic production of the J/ψ as a function of center of mass energy. The major problem is to determine the mechanism responsible for this production. Two popular models are quark fusion[24] and gluon fusion.[25] In the former a quark and an anti-quark fuse strongly to produce the J/ψ. In the latter two gluons form a positive charge conjugation state which then decays to J/ψ. The state which dominates has a mass between the ψ and ψ'. Thus it can decay to ψ but not to ψ'. This is used by the gluon fusion proponents to explain the fact that ψ is produced with a much larger cross-section than is ψ'.

The excitation curve for the J/ψ is shown in Fig. 13.[3, 11, 26-30] Rather than plotting $Bd\sigma/dy)_{y=0}$ versus $\sqrt{s}$ as is normally done, the cross-section is plotted here versus $M/\sqrt{s}$, the fraction of the center of mass energy carried off by the ψ. All the data from BNL to ISR energies fit a single exponential. The meager ψ' data also shown in Fig. 13 allow an exponential with the same slope as the ψ. If the branching ratios are removed and the cross-sections are multiplied by M^2 to get a dimensionless form (in the spirit of Drell-Yan scaling), the results

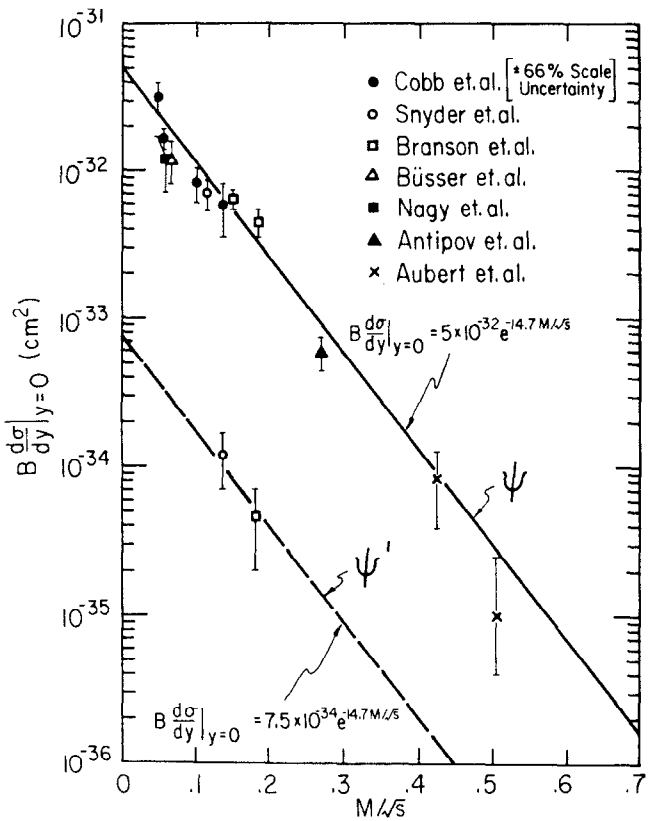

Fig. 13. Excitation curves for the ψ and ψ'.

obtained are

$$M^2 \left.\frac{d\sigma}{dy}\right)_{y=0} (\psi) = 6.9 \times 10^{-30}\, e^{-14.7\, M/\sqrt{s}}$$

$$M^2 \left.\frac{d\sigma}{dy}\right)_{y=0} (\psi') = 1.1 \times 10^{-30}\, e^{-14.7\, M/\sqrt{s}}$$

The normalization for ψ' is approximately a factor of 6 below that of the ψ.

In order to study the connection between J/ψ production and continuum dimuon production, the data from Figs. 10 and 13 have been replotted in Fig. 14 where the difference in overall normalization has been removed. The continuum data and J/ψ data fall on the same curve! The shapes of the two cross-sections are the same; the relative normalization is

$$\frac{M^3 \left.\frac{d^2\sigma}{dMdy}\right)_{y=0}^{[\text{continuum}]}}{M^2 \left.\frac{d\sigma}{dy}\right)_{y=0}^{[J/\psi]}} \approx \frac{1}{200}$$

This strongly suggests that J/ψ production and high mass continuum dimuon production proceed via the same mechanism, the only difference being the coupling: electromagnetic for the continuum, strong for the J/ψ. If, on the other hand, the continuum and J/ψ are produced from different constituents (e.g., q-$\bar{q}$ for the continuum, gluon-gluon for the J/ψ), then the overlap integral of the quark and anti-quark distribution functions would have to be the same as that for two gluons.

This view that ψ production proceeds via a quark anti-quark interaction is supported by recent results from the SPS.[31] The Ω spectrometer was used with incident $\pi^{\pm}$, $K^{\pm}$, p, $\bar{p}$ at 40 GeV to study J/ψ production. The relative cross-sections obtained are

$$\sigma(\pi^-)/\sigma(K^-)/\sigma(\bar{p}) = 1/1.0 \pm 0.3/1.0 \pm 0.3$$

$$\sigma(\pi^+)/\sigma(\pi^-) = 0.87 \pm 0.14$$

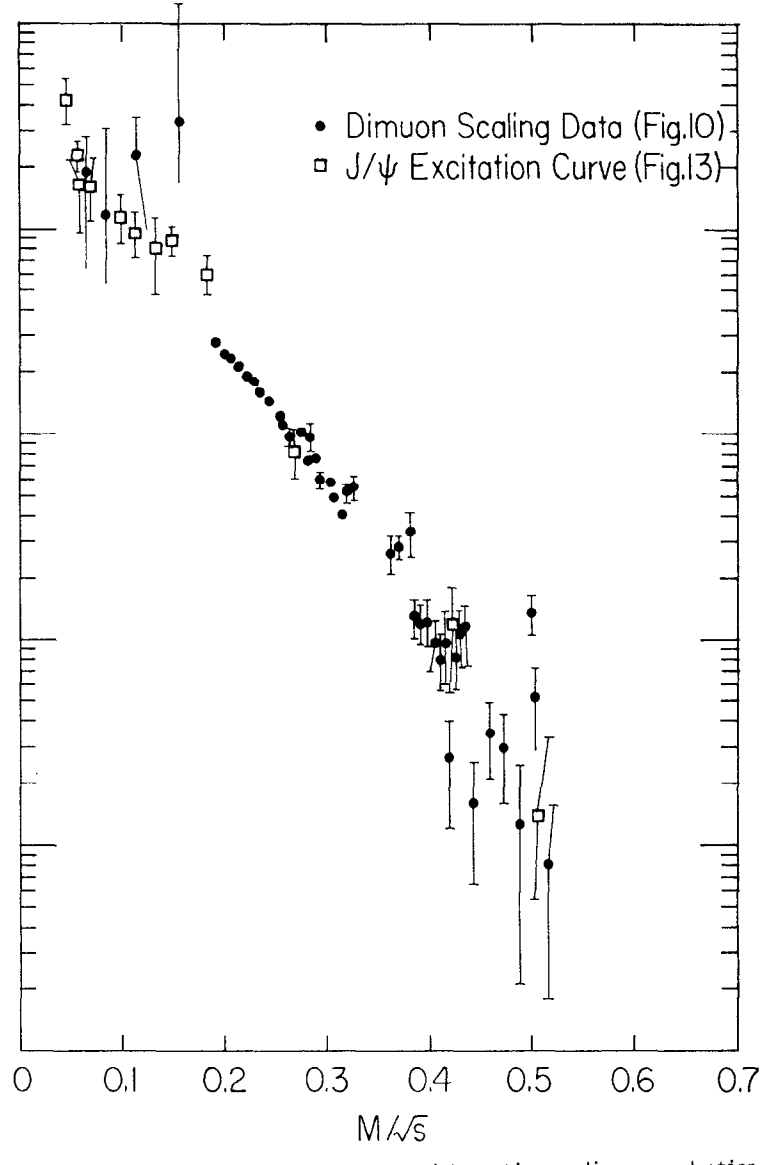

Fig. 14. Comparison of J/ψ production with continuum dimuon production.

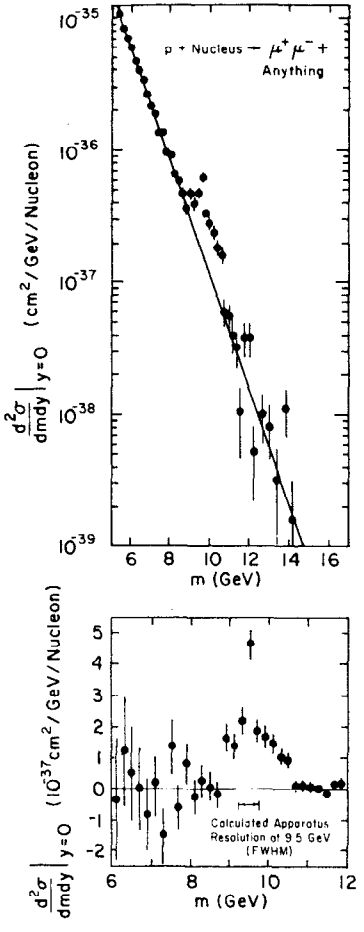

Fig. 15 The 9.5 GeV/c^2 enhancement.

$$\sigma(K^+)/\sigma(K^-) = 0.85 \pm 0.50$$

$$\sigma(p)/\sigma(\bar{p}) = 0.15 \pm 0.08$$

The much smaller p induced cross-section can be explained since the proton has no valence anti-quark with which to annihilate a quark in the target nucleon.

Finally, a word about the recently announced dimuon resonance at 9.5 GeV/c^2 [19] (see Fig. 15 and the talk given by W. Innes at this meeting). The width of the enhancement is significantly larger than the experimental resolution. The authors have tried single and double gaussian fits and find neither to be satisfactory. In fact Eichten and Gottfried expected three narrow peaks in the region.[32] The resolution of the experiment is at present being improved. If this proves not to be sufficient to resolve the structure, there is no proposed experiment I know of which will have the necessary resolution. We might then have to wait for PETRA/Cornell/PEP to find the answer.

Thus we have another example of what can be learned by studying dilepton production in hadron collisions. There are still many unanswered or partially answered questions. Some information will come from the experiments currently analyzing data, while other answers await the even more sensitive experiments now being planned.

ACKNOWLEDGEMENTS

I am indebted to Bob Palmer and Bill Willis who kindly allowed me to use preliminary data. I would also like to thank Jim Cronin and Henry Frisch for many stimulating discussions on dilepton production.

REFERENCES

1. See for example, P. A. Piroué, Review of Direct Lepton Production in Hadron Collisions, Princeton University Preprint, 1976.

2. S. D. Drell and T. M. Yan, Phys. Rev. Lett. 25, 316 (1970).

3. J. G. Branson et al., Phys. Rev. Lett. 38, 457 (1977) and J. G. Branson et al., Phys. Rev. Lett. 38, 1334 (1977). These articles contain references to the other publications of the group.

4. J. P. Boymond et al., Phys. Rev. Lett. 33, 112 (1974). A correction to the normalization was noted in Ref. 1.

5. J. A. Appel et al., Phys. Rev. Lett. 33, 722 (1974).

6. D. Bintinger et al., Phys. Rev. Lett. 35, 72 (1975).

7. V. V. Abramov et al., Phys. Lett. 64B, 365 (1976).

8. L. B. Leipuner et al., Phys. Rev. Lett. 35, 1613 (1975).
H. Kasha et al., Phys. Rev. Lett. 36, 1007 (1976).

9. L. B. Leipuner et al., Phys. Rev. Lett. 36, 1011 (1976).
M. J. Lauterbach et al., Phys. Rev. Lett. 37, 1436 (1976).

10. N. Z. Anisimova et al., Phys. Lett. 65B, 85 (1976).

11. F. W. Büsser et al., Nuclear Physics B113, 189 (1976).

12. D. Antreasyan et al., Phys. Rev. Lett. 37, 1451 (1976).
D. Antreasyan et al., Princeton University Preprint CP 77-6 (to be published).

13. E. W. Beier et al., Phys. Rev. Lett. 37, 1117 (1976).

14. L. Baum et al., Phys. Lett. 60B, 485 (1976).

15. Y. Yamaguchi, Nuovo Cimento 43, 193 (1966).

16. M. Binkley et al., Phys. Rev. Lett. 37, 571 (1976).

17. D. C. Hom et al., Phys. Rev. Lett. 37, 1374 (1976).

18. L. Kluberg et al., Phys. Rev. Lett. 38, 670 (1977).

19. S. W. Herb et al., Phys. Rev. Lett. 39, 252 (1977).

20. G. Farrar, Nuclear Physics B77, 429 (1974).

21. J. H. Cobb et al., Preliminary results supplied by R. Palmer and W. Willis. These data points are to be considered upper limits.

22. M. Binkley et al., Phys. Rev. Lett. 37, 574 (1976).

23. M. Duong-van, Preprint SLAC-PUB-1819 (1976).
J. B. Kogut, Phys. Lett. 65B, 377 (1976).
J. F. Gunion, Phys. Rev. D15, 3317 (1977).
I. Hinchliffe and C. H. Llewellyn Smith, Phys. Lett. 66B, 281(1977).
P. V. Landshoff, Phys. Lett. 66B, 452 (1977).

24. There are two quark anti-quark fusion models. One model assumes c and $\bar{c}$ quarks from the incident hadrons fuse to produce the J/ψ. This model is discussed in:
M. B. Green et al., Nuovo Cimento 29A, 123 (1975).
J. F. Gunion, Phys. Rev. D12, 1345 (1975).
A. Donnachie and P. V. Landshoff, Nuclear Physics B112, 233 (1976).
The other model assumes that a non-charmed quark and anti-quark from the incident hadrons annihilate to form the J/ψ. See:
H. Fritzsch, Phys. Lett. 67B, 217 (1977).
It is the latter model which would most naturally have the similarity to Drell-Yan dimuon production shown in Fig. 14.

25. M. B. Einhorn and S. D. Ellis, Phys. Rev. D12, 2007 (1975).
S. D. Ellis et al., Phys. Rev. Lett. 36, 1263 (1976).
C. E. Carlson and R. Suaya, Phys. Rev. D14, 3115 (1976).

26. J. J. Aubert et al., Phys. Rev. Lett. 33, 1404 (1974). Also, S.C.C. Ting, Proceedings of the International Conference on High Energy Physics, Palermo, Italy (1975).

27. E. Nagy et al., Phys. Lett. 60B, 96 (1975).

28. Yu. M. Antipov et al., Phys. Lett. 60B, 309 (1976).

29. H. D. Snyder et al., Phys. Rev. Lett. 36, 1415 (1976).

30. J. H. Cobb et al., Phys. Lett. 68B, 101 (1977).

31. M. J. Corden et al., Phys. Lett. 68B, 96 (1977).

32. E. Eichten and K. Gottfried, Phys. Lett. 66B, 286 (1977).

RECENT RESULTS FROM THE OMEGA SPECTROMETER

D. Treille

CERN

The Omega Spectrometer has been described many times[1]. Let us just recall that it is a large magnet (fig. 1) filled with optical chambers with particle identification downstream and quite sophisticated trigger possibilities. At the PS time it was fed by an unseparated hadron beam which was used between 3 and 19 GeV/c. We shall describe later the Ω at SPS.

PS Results

Table 1 gives the list of experiments which were performed at the Ω PS. All of them have given results.

The first two triggered Ω on slow particle (n and p respectively). They studied processes with large cross sections but the trigger had a small acceptance. Therefore their sensitivity does not exceed a few hundred events/μb. Nevertheless quite interesting results were obtained. They have been described elsewhere[2].

I would rather focus on the experiments with a forward trigger and show a few of their results.

Consider first the coupled experiments:

Fast proton and Exotics (fig. 2)

Using π's as incident particles they triggered the Ω on a forward proton of large momentum ($> p_{inc}/2$). Due to the small cross section of such a process, to the large acceptance and purity of the trigger and to the large statistics accumulated, the sensitivity, after all processing losses, was still above 1 evt/nanobarn, even for complicated 4 or 6 prongs channels. Table 2 illustrates the great variety of channels which have been processed up to now.

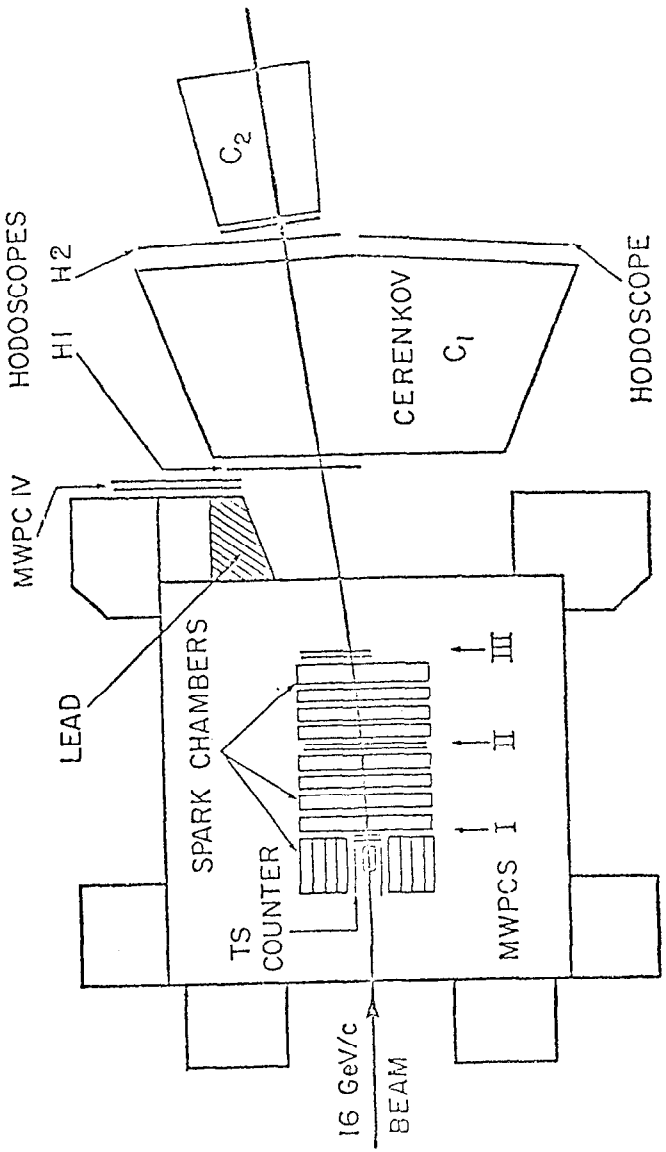

FIG. 1

TABLE 1

PHYSICS AT PS

CERN CODE	NICKNAME	COLLABORATION	DATE OF RUN
S112	"slow n"	Birmingham-Rutherford-Tel Aviv-Westfield	Aug. Dec. 73 Oct. 74
S113	"slow p"	Bari-Bonn-Daresbury-Liverpool-Milan	Aug. Oct. 73
S114	"fast Λ"	CERN-ETH-Freiburg-Saclay	June 73 Oct. 73-Oct. 74
S115	"fast $\bar{\Lambda}$"	DESY-Glasgow	Aug. 73 - Mar. 74
S117	"fast p"	CERN-College de France- Ecole-Polyth. Orsay	Apr. June 74 Oct. Nov.
S139	"rare decays"	Bari-Bonn-CERN-Glasgow-Daresbury-Liverpool-Milano-Purdue-Vienna	Nov. 74 Dec. 74
S133	"$\pi\pi$"	CERN-Saclay	Apr. Dec. 74
S116	"K^*"	CERN-ETH	Aug. 74
S148	"$K\bar{K}\pi$"	Aachen-CERN-ETH-Haifa	June 75
S145	"exotics"	CERN-College de France-Ecole Polyth.-Orsay	Apr. 75
S146	"charm"	All Groups	Mar. 75 Apr. 75

11 Experiments (20 different conditions of beam and trigger) from June 1973 to June 1975. ($\lesssim$ 200 days of run). Good efficiency $\Omega \sim 80\%$. Ω+ users $\sim 60\%$.

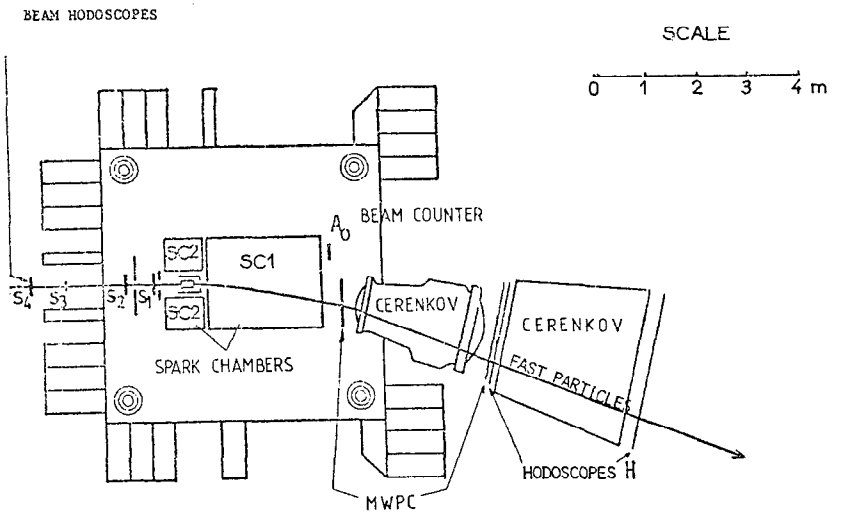

Fig. 2

TABLE 2

LIST OF THE CHANNELS PROCESSED IN THE "FAST PROTON" EXPERIMENT

-- inclusive p_f

-- elastic backward

-- $\pi^- p \rightarrow p_f \bar{P}$

-- $\pi^- p \rightarrow p_f \rho^-$

-- $\pi^- p \rightarrow (p\pi^-)_f \pi^o$

-- $\pi^- p \rightarrow p_f \pi^+\pi^-\pi^-$

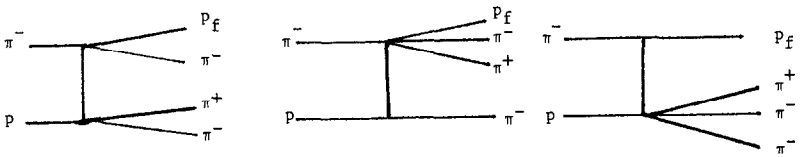

-- $\pi^- p \rightarrow (p_f\pi^-)_f \begin{matrix}\omega_o \\ \eta_o\end{matrix}$

-- $\pi^- p \rightarrow p_f\pi^-\bar{p}p$

$p_f \pi^-\pi^o \bar{p}p$

-- $\pi^- p \rightarrow p_f \pi^+\pi^-\pi^-\pi^o$

$\rightarrow p_f (5\pi)$

etc. . . .

For the channel $\pi^- p \to (p\pi^-)_{forward}\ \pi^0$ [3a] the effective mass of the forward system is shown in fig. 3. It exhibits a first unexpected and yet not understood result: while the spectrum is dominated by heavy N*'s the forward production of the Δ is suppressed by a large factor (40) compared to what one could wait for. This feature is present in many other channels. Fig. 4 illustrates the fact that, in the channel $\pi^- p \to p_f \pi^+ \pi^- \pi^-$, [3b] for all three of the main configurations (see table 2), the dominating process is quasi two body production involving resonances, like

$$\pi^- p \to N^*_f\ \rho$$
$$\pi^- p \to p_f A_2, \text{ etc...}$$

Fig. 5 in particular exhibits - with the cuts indicated - evidence for the backward production of the controversial A_1, at 1070 MeV/c^2. With such a limited statistics no Ascoli type of analysis is possible. So this is not a proof of the existence of the A_1 as a genuine resonance. On the other hand it is difficult to reproduce such a structure by any mechanism like the backward equivalent of a Deck effect.

Fig. 6 showing the backward ω_0 signal from $\pi^- p \to (p\pi^-)(\pi^+\pi^-\pi_0)$ proves that the spectrometer has reached the level of clean 1C physics for rather complicated topologies.

If we now turn to the channel $\pi^- p \to p_f \pi^- p\ \bar{p}$ we encounter there another surprise. Figs. 7 and 8 shows, with different types of cuts, the presence in the backward $\bar{p}p$ system of two (maybe three) narrow resonances. At least for the upper one, one cannot exclude zero natural width. These resonances appear only in association with forward Δ and N^*_{1520}: the relative importance of the Δ and the absence of the N^*_{1680} can be understood by pure kinematics and do not contradict the result of Fig. 3. The cross sections, if one takes into account u_{min} effects and if one assumes a substantial branching ratio of the narrow objects into $p\bar{p}$, are quite compatible with baryon exchange. No spin determination is possible. Details can be found in (4).

A similar experiment proposed for Omega prime (see below) should improve the statistics by an order of magnitude.

Figs. 9 and 10 show one of the results [5] of the Rare Decays experiment obtained in the channels

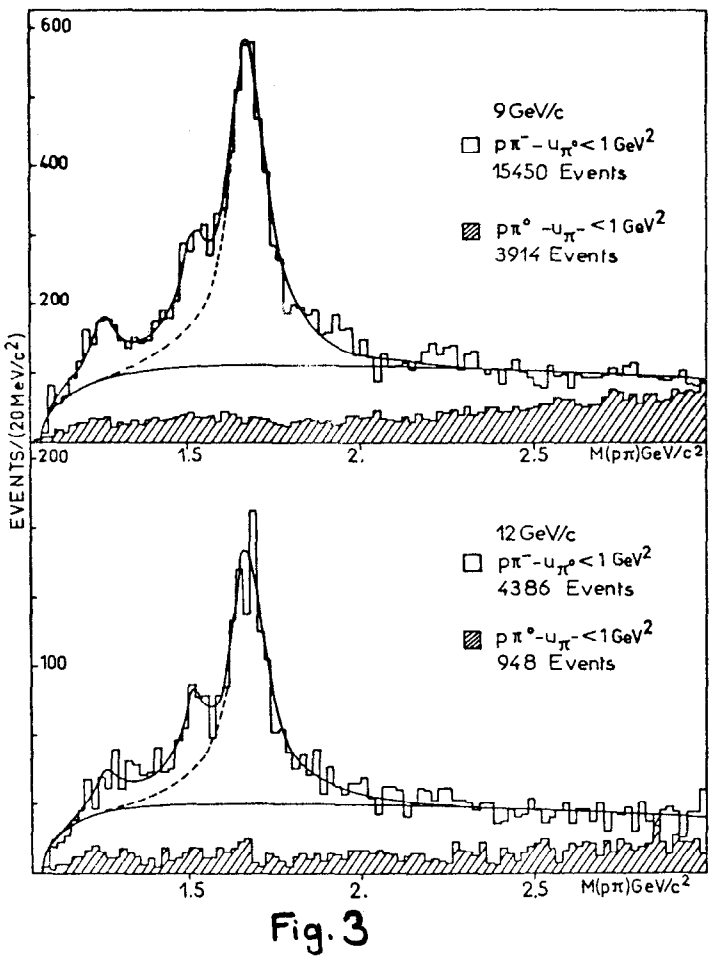

Fig. 3

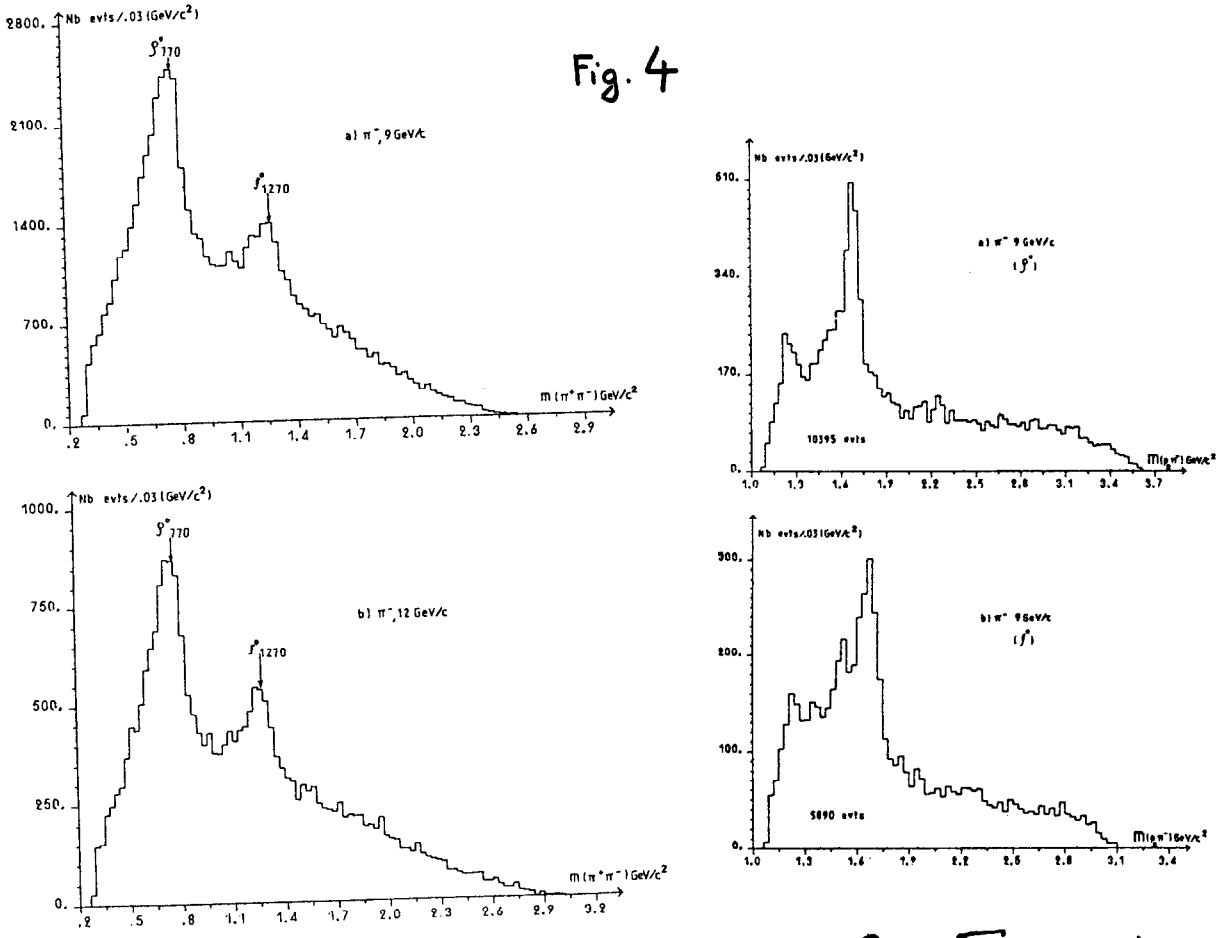

Fig. 4

$\rho^0\pi^-$, N^* out

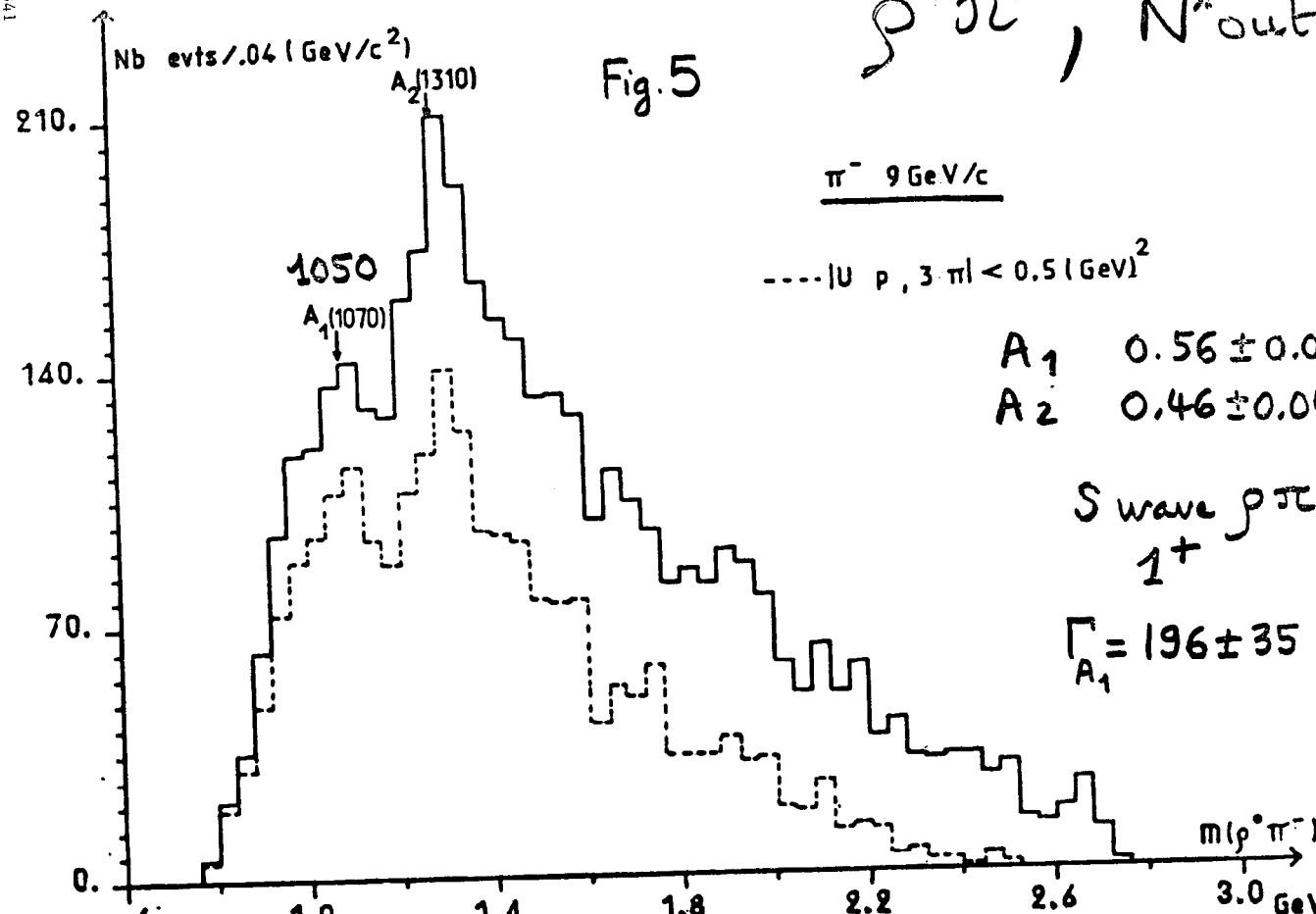

Fig. 5

π^- 9 GeV/c

---- |U p, 3 π| < 0.5 (GeV)²

A_1 0.56 ± 0.04 μb

A_2 0.46 ± 0.04 μb

S wave $\rho\pi$

1^+

Γ_{A_1} = 196 ± 35 Mev

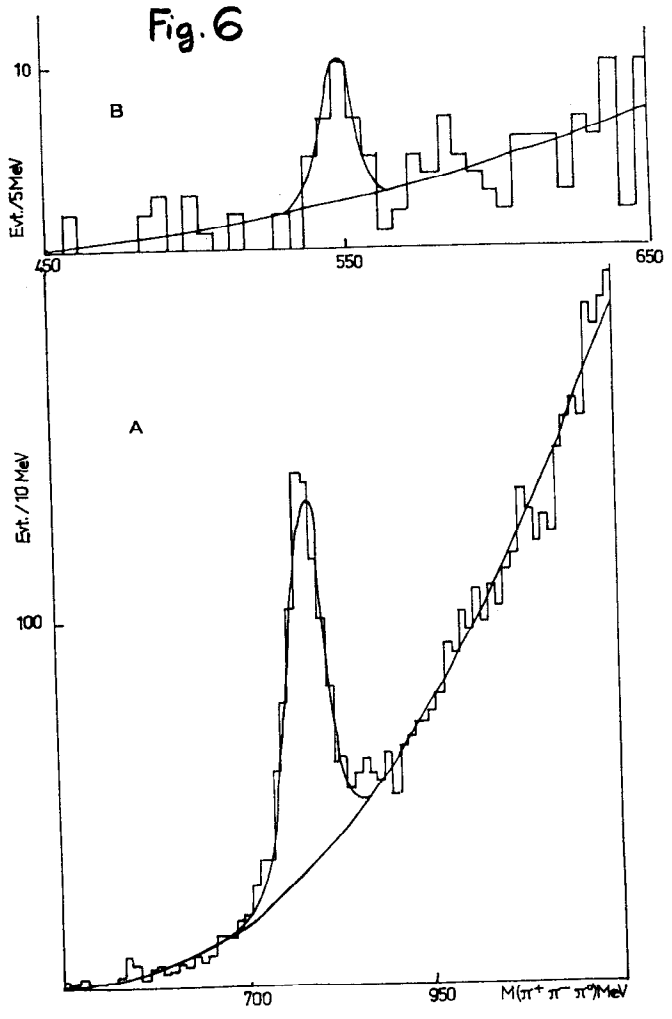

Fig. 6

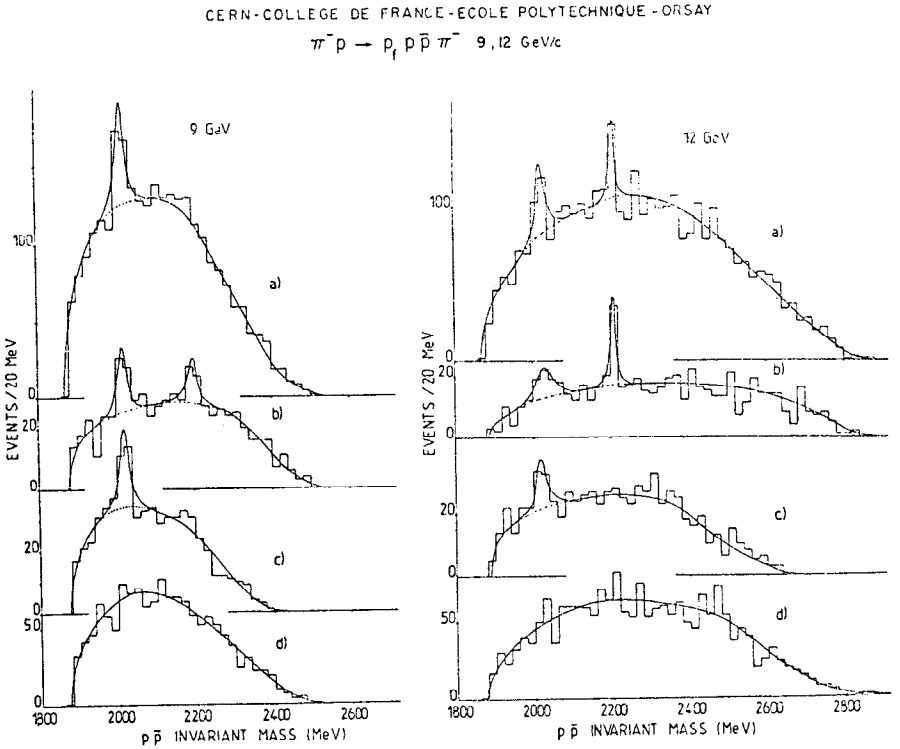

Fig. 7

$\bar{p}p$ invariant mass distributions for (a) all events, (b) events with $p_f\pi^-$ in the $\Delta^0(1232)$ region, (c) events with $p_f\pi^-$ in the $N^0(1520)$ region, and (d) events not included in (b) or (c). The curves represent the result of fits to 1 or 2 BW's + smooth background.

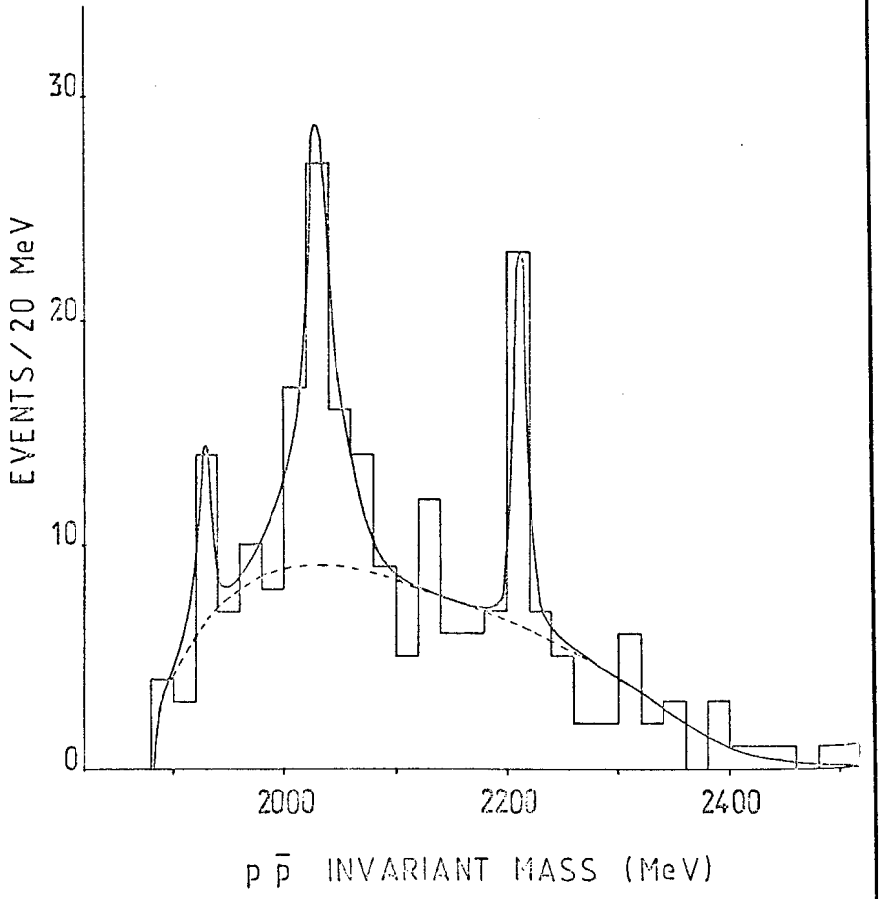

Fig.8

BARI-BONN-CERN-DARESBURY-GLASGOW-LIVERPOOL-MILAN-PURDUE-VIEN

16 GeV/c $\pi^- p$

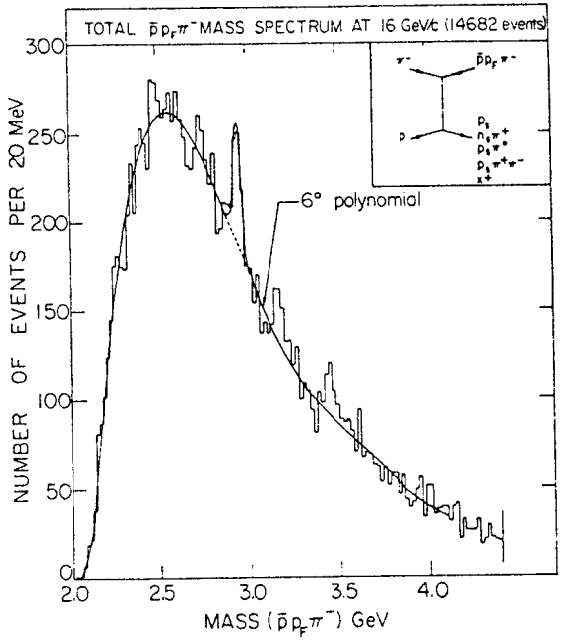

fig.9

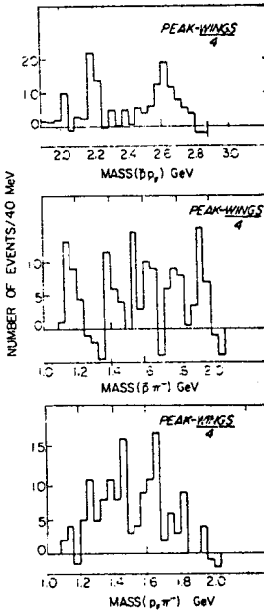

fig.10

9. Total $\bar{p}p_F\pi^-$ mass distribution and **10.** background subtracted $\bar{p}p_\pi$, $\bar{p}\pi^-$ and $p_F\pi^-$ mass distributions for the 2.95 GeV peak. The curve represents the result of a fit to a Gaussian + background polynomial.

$\pi^- p \to (p\bar{p}\pi^-)_{forw}\ X^+$ at 16 GeV/c

where X includes p, $n\pi^+$, $p\pi^0$, $p\pi^+\pi^-$ and positive systems of low mass (< 2 GeV). In the $(p\bar{p}\pi^-)$ effective mass a narrow peak is visible at 2.95 GeV/c^2. The corresponding cross section is $\sim$ 1μb. In fig. 10 it is shown that the $p\bar{p}$ system from this peak exhibits at least the 2.2 resonance.

These results, combined with several other ones[6] suggest that a rich spectroscopy could well exist in the $B\bar{B}$ channels. Its connection with baryonium or related ideas[7] is very likely. May be we are approaching from the long sought solution to the $B\bar{B}$ duality catastrophy.

The results from the Exotic search have been published[8]. Several other channels have been explored since. No signal is seen at a sensitivity level which represents a gain of at least one order of magnitude over past experiments. Nevertheless a more refined theoretical analysis is still needed to know if this sensitivity is sufficient to disprove the existence of exotic mesons: basically the problem is that, for the moment, the expected cross section for backward production of exotics of high mass cannot be safely deduced from the measured cross section for backward production of known non exotic mesons.

Fig. 11 shows another result from the Rare Decays experiment. The channel is $\pi^- p \to K^+K^-n$. The K^+K^- effective mass spectrum shows the h meson and a possible new structure at 2.2 GeV/c.

The results of the Charm search have been also published[9]. The limits given on charm production, especially for exclusive channels, are certainly impressive from the experimental point of view. But they are still well above what one can now foresee for charm production in hadronic collisions at such a modest energy.

An interesting by product of the Charm experiment was a test of the Zweig rule for strangeness[10].

Considering the 4C 6 prongs channels

$\pi^- p \to K^+K^-\pi^+\pi^-\pi^- p$ at 19 GeV/c

$\to K^+K^-K^+K^-\pi^- p$

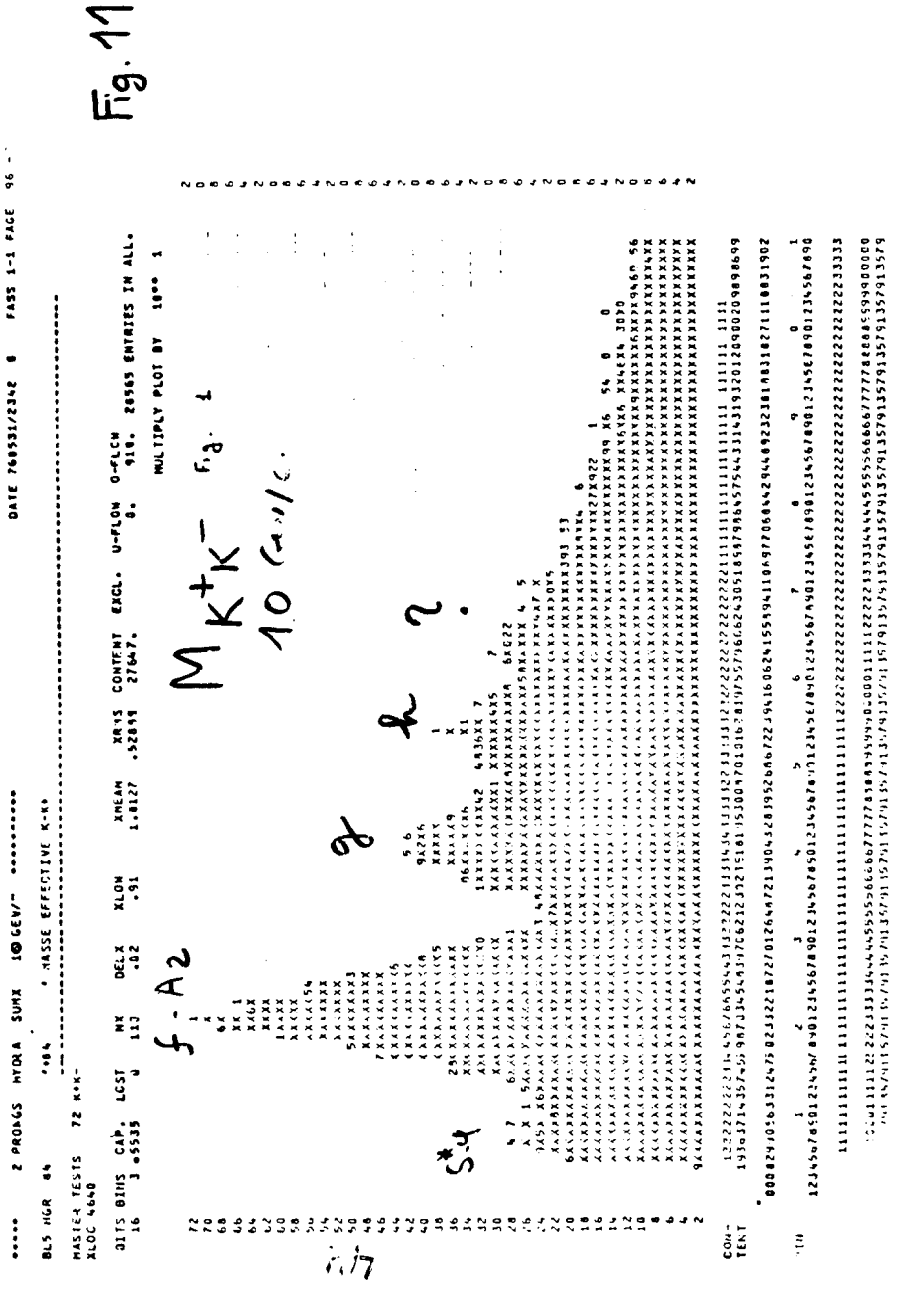

One can summarise the results by the three ratios:

(1) $\frac{\phi\ \pi\pi\pi p}{\omega\ \pi\pi\pi p} \sim 0.5\ \%$

(2) $\frac{\phi\ K^+K^-\pi^-p}{\rho^0K^+K^-\pi^-p} = 0.45\ ^{+\ 0.25}_{-\ 0.15}$

(3) $\frac{\phi\ \pi^+\pi^-\pi^-p}{\phi\ K^+K^-\pi^-p} = 1.7\ ^{+\ 0.9}_{-\ 0.5}$

(1) confirms the smallness of a Zweig forbidden process and

(2) shows that two Zweig allowed processes are of the same order of magnitude.

However (3) illustrates the fact that at 19 GeV it costs 2 orders of magnitude to produce an extra pair of kaons. Therefore, even with a perfectly correct Zweig rule, it would not be wise, if you want to discover strangeness, to trigger on a ϕ.

Finally Figs. 12 and 13 show results from the V^0 trigger experiments. In the $K^0\bar{K}\pi$ system D and E mesons are seen. In the non diffractive $\bar{K}^0\pi\pi$ system clear evidence for a 3^- K* at 1800 MeV is presented.

SPS Results

Fig. 14 shows the modified Ω spectrometer used at the SPS. It is fed by two converging beams

- an 80 GeV e/γ beam
- a 40 GeV hadron beam which will be separated next spring with the help of two supraconducting deflectors.

The main part of the program is devoted to photoproduction, with an emphasis on the study of charmed states, and a parallel attempt to measure charm life time using emulsions. No result is yet available.

Meanwhile a simpler experiment[11] - which gave the first results of the SPS - has been completed. It was a dimuon production by all kinds of hadrons (p, $\bar{p}$, $K^\pm$, $\pi^\pm$) present in the unseparated hadron beam at 40 GeV. The set up is shown in Fig. 15. The incident flux was $3\ 10^6$ particles per pulse or $\sim 10^7$/second. The main results are shown in Fig. 16 and,

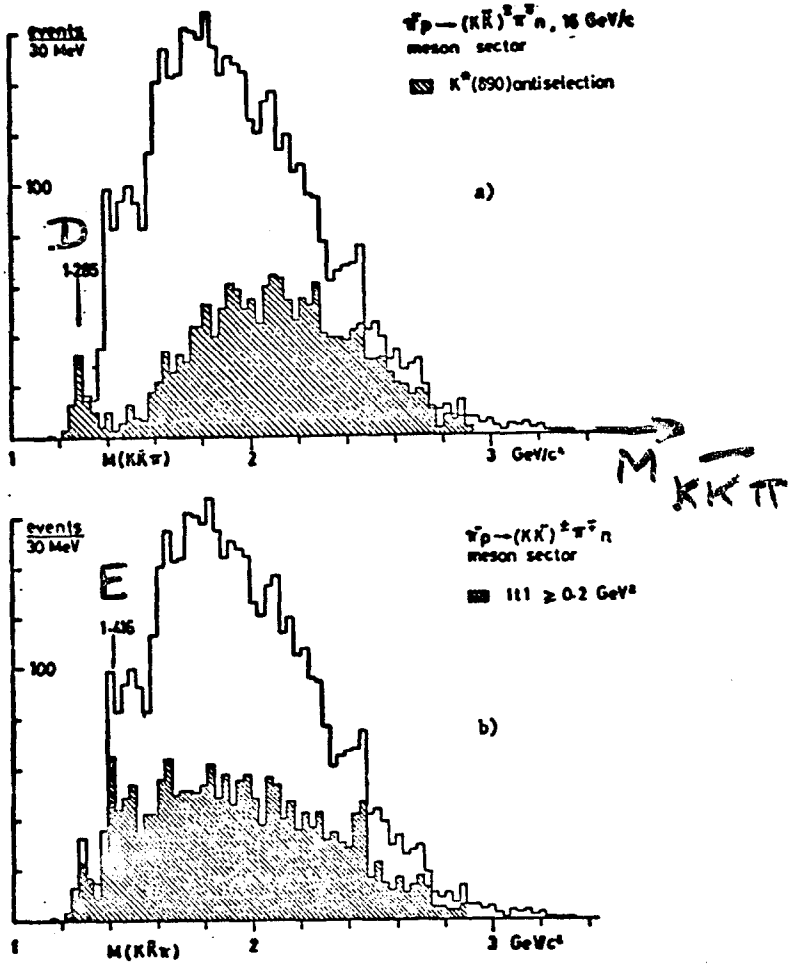

Fig. 12 $(K\bar{K}\pi)^0$ mass spectrum from $\pi^-p \to K\bar{K}\pi n$ at 16 GeV/c showing the effect of cuts and evidence for the D(1285) and E(1420) mesons.

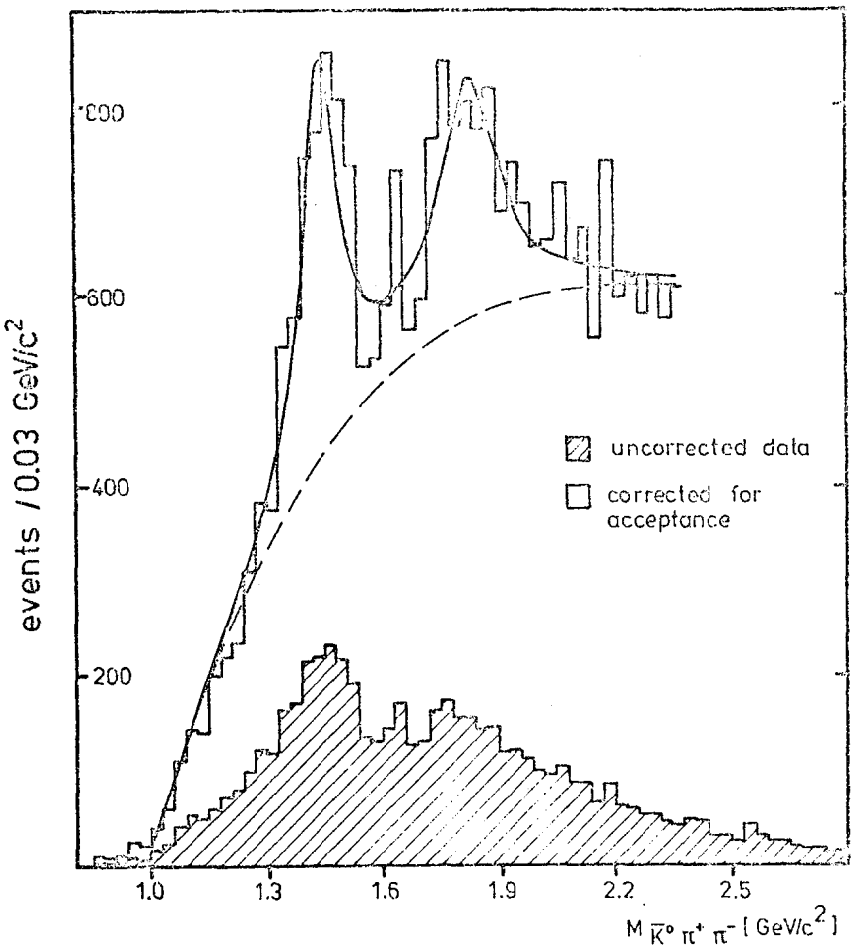

Fig.13 ($\bar{K}^0 \pi^+ \pi^-$) - Mass corrected for acceptance

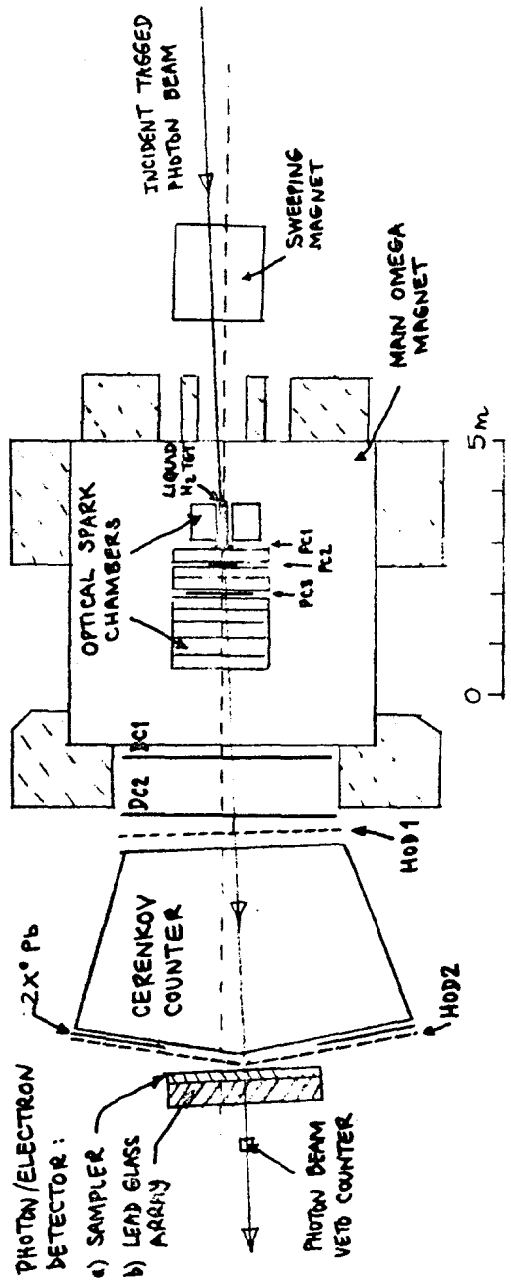

Fig.14 Layout of the SPS Omega spectrometer for the photoproduction charm search experiment

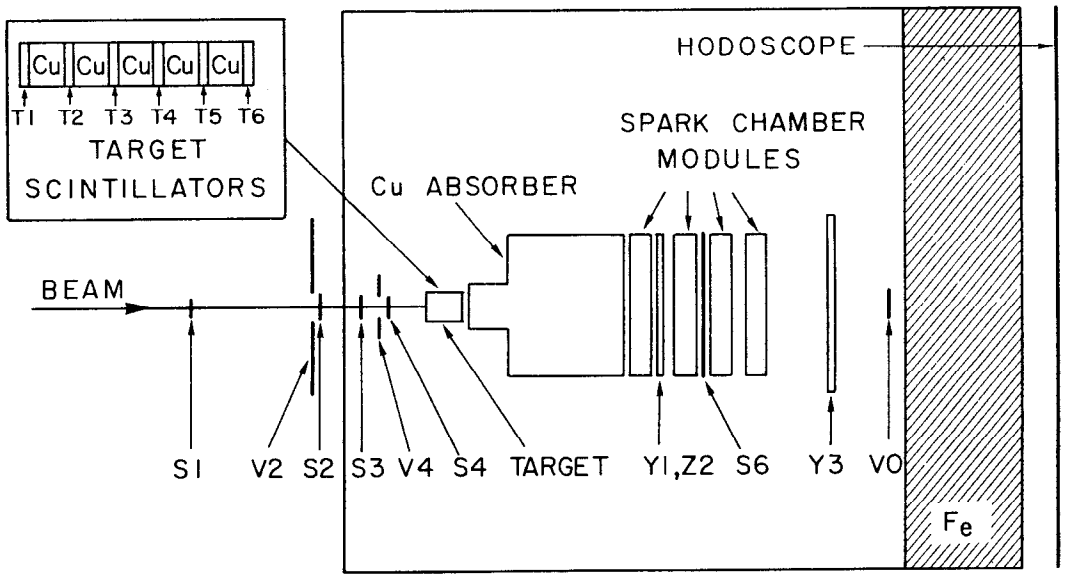
Cu Cu Cu Cu Cu
T1 T2 T3 T4 T5 T6
TARGET
SCINTILLATORS
HODOSCOPE
SPARK CHAMBER
MODULES
Cu ABSORBER
BEAM
S1 V2 S2 S3 V4 S4 TARGET Y1,Z2 S6 Y3 V0
Fe

Fig. 15

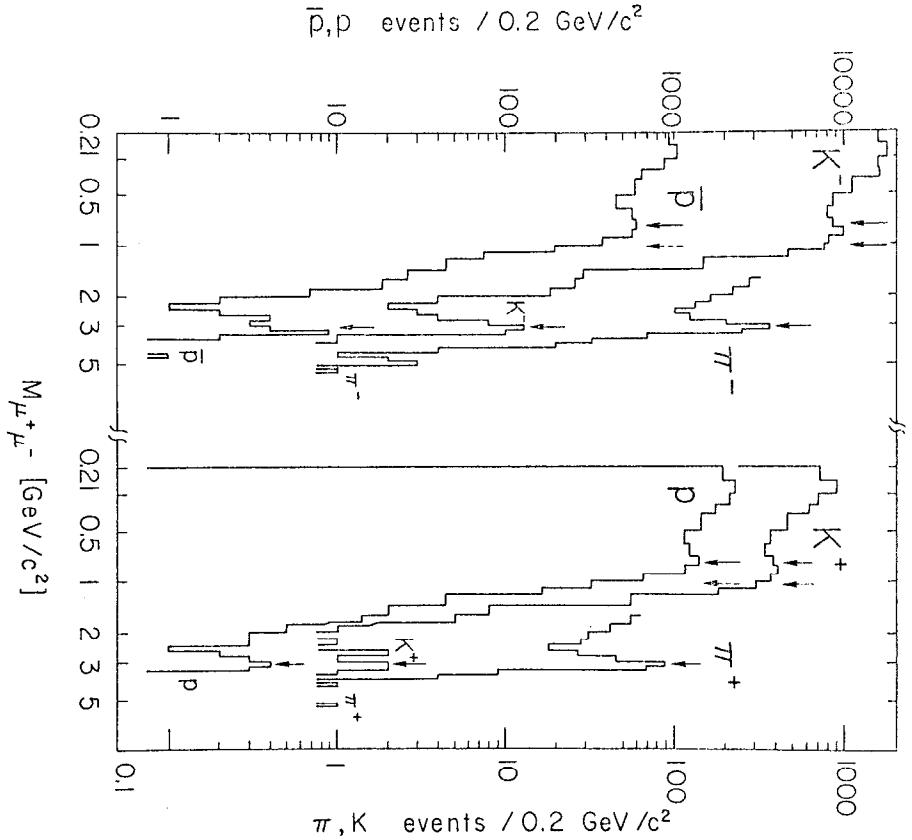
p̄,p events / 0.2 GeV/c²
Mμ⁺μ⁻ [GeV/c²]
π,K events / 0.2 GeV/c²
K⁻
p̄
K⁻
π⁻
π⁻
p
K⁺
p
K⁺
π⁺
π⁺

Fig. 16

for the ψ, can be summarized by the ratios

$$\sigma(\pi^-) : \sigma(K^-) : \sigma(\bar{p}) = 1 : 1.0 \pm 0.3 : 1.0 \pm 0.3$$

$$\frac{\sigma(\pi^+)}{\sigma(\pi^-)} = .87 \pm .14 \qquad \frac{\sigma(K^+)}{\sigma(K^-)} = 0.85 \pm 0.5$$

$$\frac{\sigma(p)}{\sigma(\bar{p})} = 0.15 \pm 0.08$$

The last ratio indicates that at our energy protons are less efficient than $\bar{p}$ or π's to produce ψ's, as expected from quark fusion models. Other results on the ψ and on the continuum are available, but for the rare particles the statistics is extremely poor. For π's Fig. 17 shows the x distribution of produced ψ's: it is not centered at zero, as expected if the valence antiquark of the meson have a higher mean x than the valence quarks of the nucleon target. Fig. 18 shows our results on the dimuon continuum induced by π's. The comparison to the proton induced continuum is striking. A similar experiment which should yield 10 times more events and therefore allow a detailed study of antiproton induced dimuons will be run next year.

Future

It is planned to replace the optical chambers of the Ω MWPC's. Details can be found in (12). This is called the Ω prime project. With other changes (a 3rd drift chamber, another Cerenkov counter, improved data acquisition, etc.) and new beams - for instance a much more intense e/γ beam (200 GeV max. momentum) - it will represent a major improvement.

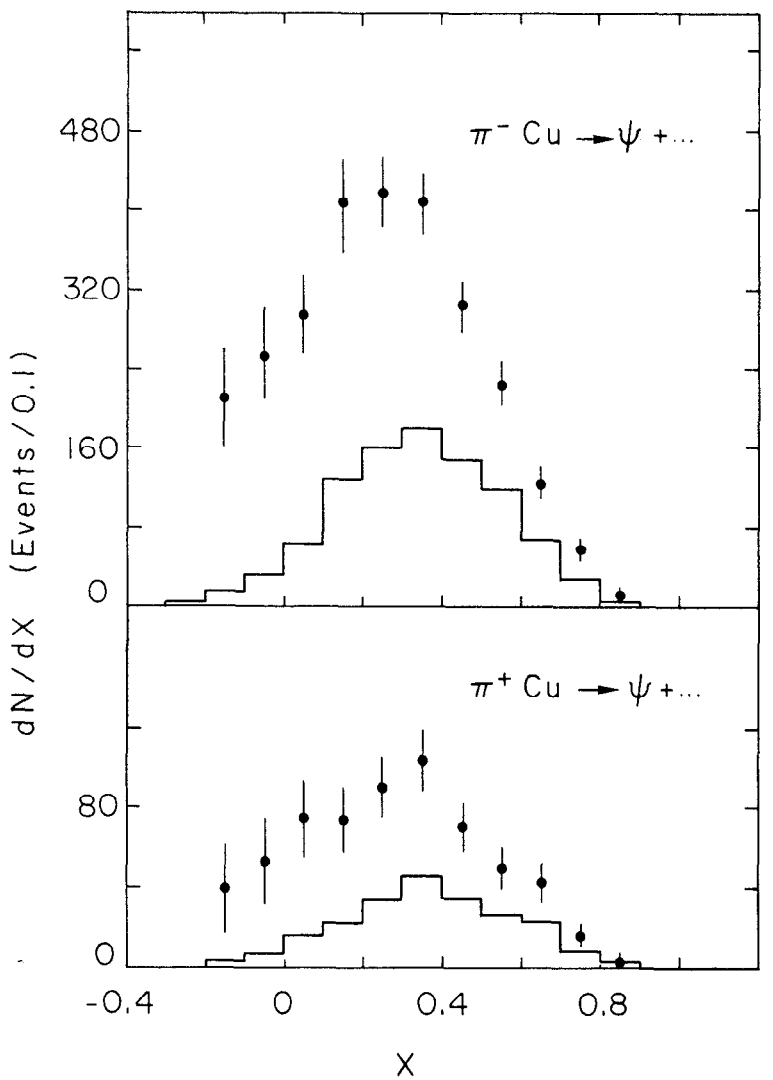

Fig. 17

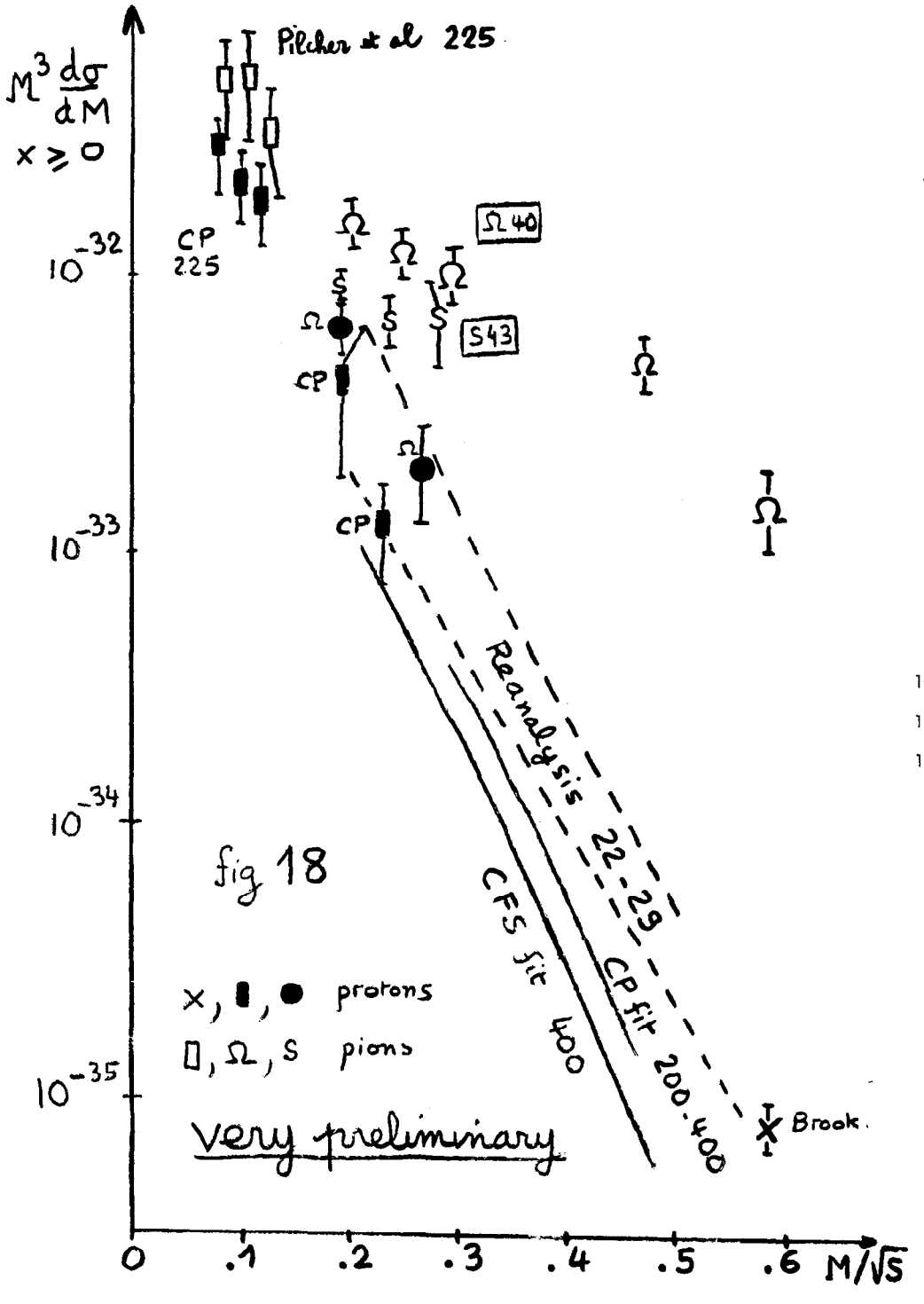

References

1) See for instance SLAC Topical Conference, August 1974.

2) J.D. Dowell. Invited talk at Boston Conference (1977).

3a) Baryon exchange in $\pi^- p \to N^{*0}\pi^0$ - LPNHE/X/77.

b) A. Ferrer. Thesis. LAL Orsay (1977).

4) Benkheiri et. al. LAL Orsay P-1977/3 (1977).

5) C. Evangelista et. al. CERN/EP/Phys. 77-24.

6) L. Montanet. Exp. review of the $B\bar{B}$ interaction. CERN/EP/Phys. 77-22.

7) See for instance G.F. Chew, in "Antinucleon-nucleon Interactions", 3rd European Symposium, Stockholm 1976, Pergamon Press, 515.

8) J. Boucrot et. al. Nuclear Physics B121 (1977) 251-269. See also Physics Letters. Vol. 64B no. 1, p.107.

9) Charm Search in 19 GeV/c $\bar{p}$ exclusive reactions. Nuclear Physics B111 (1976) 189.

10) Physics Letters Vol. 65B no. 1 (1976).

11) Physics Letters Vol. 68B no. 1 (1977) p.96

12) CERN/SPSC/77-70, SPSC T17.

EXTRAORDINARY HADRONS*

R. L. Jaffe†

Center for Theoretical Physics
Laboratory for Nuclear Science and Department of Physics
Massachusetts Institute of Technology
Cambridge, Massachusetts 02139

*This work is supported in part through funds provided by ERDA under Contract EY-76-C-02-3069.*000.

†A. P. Sloan Foundation Fellow

Talk presented at the 1977 SLAC Summer Institute Topical Conference on Quark and Hadron Spectroscopy, SLAC, Stanford, July 20-22, 1977

October, 1977

CTP #674

EXTRAORDINARY HADRONS

R. L. Jaffe
Center for Theoretical Physics
Laboratory for Nuclear Science and Department of Physics
Massachusetts Institute of Technology
Cambridge, Massachusetts 02139

In a conference featuring so many reports of exciting new experiments any theoretical talk will seem somewhat frivolous. This one especially: I intend to discuss exclusively hadrons which are largely unfamiliar, often unwanted, scruffy and generally disreputable. Fortunately for such a murky subject, it is amenable to systematic treatment. I will discuss hadrons in order of the number of quarks they contain:

1 QUARK: Liberated Quarks in QCD.

2&3 QUARKS: Type 2 exotics: mesons and baryons with $J^{PC}I^{G}$ not permitted by the non-relativistic quark model.

4&5 QUARKS: Type 1 exotics (and cryptoexotics): mesons made from $Q^2\bar{Q}^2$ and baryons made from $Q^4\bar{Q}$.

6 QUARKS: Dibaryons, especially the deuteron.

The motivation to study such systems as these lies in two of the ancient mysteries of the quark model: confinement and the absence of exotics. Once an embarrassment, confinement is now regarded as a triumph of the quark model (or more precisely of its possible theoretical antecedent, QCD). Suppose, however, that the existence of free, fractionally charged quarks is convincingly demonstrated. What becomes of QCD? This is the subject of the first part of this talk.

Compared to liberated quarks exotics appear prosaic. Nevertheless they are unfamiliar. The experimental evidence is limited to a pair of questionable Z*'s. The absence of prominent exotic states has always been a mystery in the quark model. Recently study of the color mediated forces between quarks has provided a possible partial explanation. In any case exotic hadrons represent rather virgin territory compared to the familiar landscape of the ordinary $Q\bar{Q}$ mesons and Q^3 baryons. Perhaps we shall learn more by understanding the gross features of the dynamics in these new sectors than by trying to settle out details of the old spectroscopy.

I. LIBERATED QUARKS IN QCD

From time to time evidence is presented for the observation of isolated fractional charge.[1] Suppose the evidence became unequivocal. Recently A. De Rujula, R. Giles and I[2] undertook to study the implications of such a possibility for QCD. The origins of QCD lie in its successful description of hadron spectroscopy, Bjorken scaling, quark statistics and so forth, not in its ability to confine quarks. Indeed no one has yet succeeded in deriving confinement in QCD. Discovery of physical ("liberated") quarks would not alter the phenomenological bases of QCD. It would remain our best framework for a discussion of quark dynamics. The question is how to accomodate the possibility of liberated quarks?

We do not challenge the belief that an exact local color gauge symmetry confines color completely. We found that a slightly broken local color gauge symmetry (main-

taining the global color symmetry) would confine color approximately: the properties of color singlet mesons and baryons remain as before, but liberated colored quarks would exist and be very massive. By means of a suitable Higg's scheme we arrange to give all eight gluons a small mass in the Lagrangian:

$$\mathcal{L}_{QCD} \to \mathcal{L}_{QCD} + \frac{1}{2}\mu^2 \sum_{a=1}^{8} A_\alpha^a A^{a\alpha} \tag{1.1}$$

We find then that the masses of liberated quarks and gluons go like $1/\mu$ for small μ:

$$\lim_{\mu\to 0} M_Q = 1/2\pi\alpha'\mu + 0(\mu^{1/3}) \tag{1.2}$$

$$\lim_{\mu\to 0} M_G = 3/4\pi\alpha'\mu + 0(\mu^{1/3}) \tag{1.3}$$

Note the inverse relation between the gluon mass in the Lagrangian (which breaks the local gauge symmetry) and the mass of a liberated gluon. For small μ and suitable choice of the Higg's potential spectroscopy is unaltered while asymptotic freedom is replaced by "temporary freedom": quarks act free down to distances of the order of $1/M_H$, M_H being the Higg's mass which is taken to be very large.

In this model liberated quarks have rather striking characteristics. First, it is likely that they will be found only on specific nuclei with baryon number $A_{MAX} \gtrsim M_Q/m_p$. Second, liberated quarks will have small production cross sections, making them hard to produce. Third, they will have large interaction cross sections making them, oddly enough, hard to see.

The origin of all these properties is the large size ($V \sim M_Q$) of liberated quarks. To study free quarks one must choose a calculable approximation scheme which describes confinement for $\mu=0$. We have chosen the MIT Bag Model.[3,4] Consider a bag of volume V containing a free quark with color charges Q_a. The classical equations of motion are:

$$\partial_\alpha F_a^{\alpha\beta} + \mu^2 A_a^\beta = g j_a^\beta \quad a = 1,2\ldots 8 \tag{1.4}$$

and

$$n_\alpha F_a^{\alpha\beta} = 0 \tag{1.5}$$

The latter, a bag boundary condition (n_α is the unit normal to the bag's surface). For the scalar potentials, A_a^o; eq. (1.4) reduces to Yukawa's equation

$$(\nabla^2-\mu^2)A_a^o = -g\rho_a \tag{1.6}$$

and eq. (1.5) reduces to a Neumann boundary condition

$$\hat{n}\cdot\vec{\nabla}A_a = 0 \tag{1.7}$$

ρ_a is the color charge density (including both quark and gluon sources) and g is the color coupling constant ($g^2=4\pi\alpha_c$). To proceed we intergrate eq. (1.6) over V,

$$\int_S \hat{n}\cdot\vec{\nabla}A_a^o d^2s - \mu^2\int_V A_a^o d^3x = -gQ_a \tag{1.8}$$

where S is surface bounding V. Eq. (1.8) contains the key to quasi-confinement. For $\mu=0$ eqs. (1.7) and (1.8) combine to give $Q_a=0$ — exact confinement. For $\mu\neq 0$ we find

$$\int_V A_a^o d^3x = gQ_a/\mu^2 \qquad (1.9)$$

A_a^o must contain a static term which diverges for small μ:

$$A_a^o \equiv \frac{gQ_a}{\mu^2 V} + \phi_a \qquad (1.10)$$

where ϕ_a is well-behaved as $\mu \to 0$. Since quantum fluctuations, time dependent surface fluctuations and the like do not change Q_a, this result is independent of these effects.

A_a^o contributes a divergent (as $\mu \to 0$) term to the mass

$$M(V) = \int_V \frac{1}{2}\mu^2 A_a^{o2} d^3x + BV + 0(1/R) \qquad (1.11)$$

$$= \frac{2\pi\alpha_c Q^2}{\mu^2 V} + BV + 0(1/R) \qquad (1.12)$$

where R is a typical linear dimension of the bag and B is the bag pressure. To balance the bag pressure on the average we require $\partial M/\partial V = 0$ which yields

$$V = \frac{1}{\mu}\sqrt{\frac{2\pi\alpha_c Q^2}{B}} + 0(\mu^{1/3}) \qquad (1.13)$$

and

$$M = \frac{1}{2\pi\alpha'\mu}\sqrt{\frac{3Q^2}{16}} + 0(\mu^{1/3}) \qquad (1.14)$$

where α' is the slope of Regge trajectories, which is calculable and given by

$$1/\alpha' = 16\pi\sqrt{\frac{2\pi\alpha_c B}{3}} \qquad (1.15)$$

in the bag model.[5] Q^2 is the quadratic Casimir for the SU(3)-color representation inside the bag:

$Q^2 = 16/3$ (QUARK)

$Q^2 = 12$ (GLUON)

$Q^2 = 40/3$ (SYMMETRIC DIQUARK ($\underline{6}$))

ETC.

There is a whole spectrum of colored states, depending on the color-representation. It can be shown that the lightest state *in each representation is stable.*[2] Excitations of a free quark will be scaled by $1/R \sim \mu^{1/3}$ and therefore lie very close together. Figure 1 shows a schematic spectrum of colored states.

Notice that this discussion made no reference to the explicit shape of the bag. This is determined by $O(\mu^{1/3})$ terms. We find that a sperical shape is preferred. The shape independence of the leading term in eq. (1.14) suggests that a string intepretation is possible. This was pointed out by Susskind[6] and is illustrated in Fig. 2. A string of length $\sim 1/\mu$ has a mass $T_o/\mu = 1/2\pi\alpha'\mu$ (T_o is the string tension), in agreement with the bag calculation.

The nuclear affinity of liberated quarks follows from their large size. The quarks in a nucleon are confined to a region of order 1fm. The mass of a nucleon is the sum of the (massless) quarks' kinetic energies. Should a nucleon be absorbed by a liberated quark (see Figure 3) the nucleon's quarks could "relax" into long wavelength modes in the liberated quark bag. Thus absorption of nucleons by a free quark is exothermic and remains so until the Fermi sea of quarks within the liberated quark exerts a degeneracy pressure comparable to B. The maximum number of baryons (A_{MAX}) which can be absorbed by a liberated quark is deter-

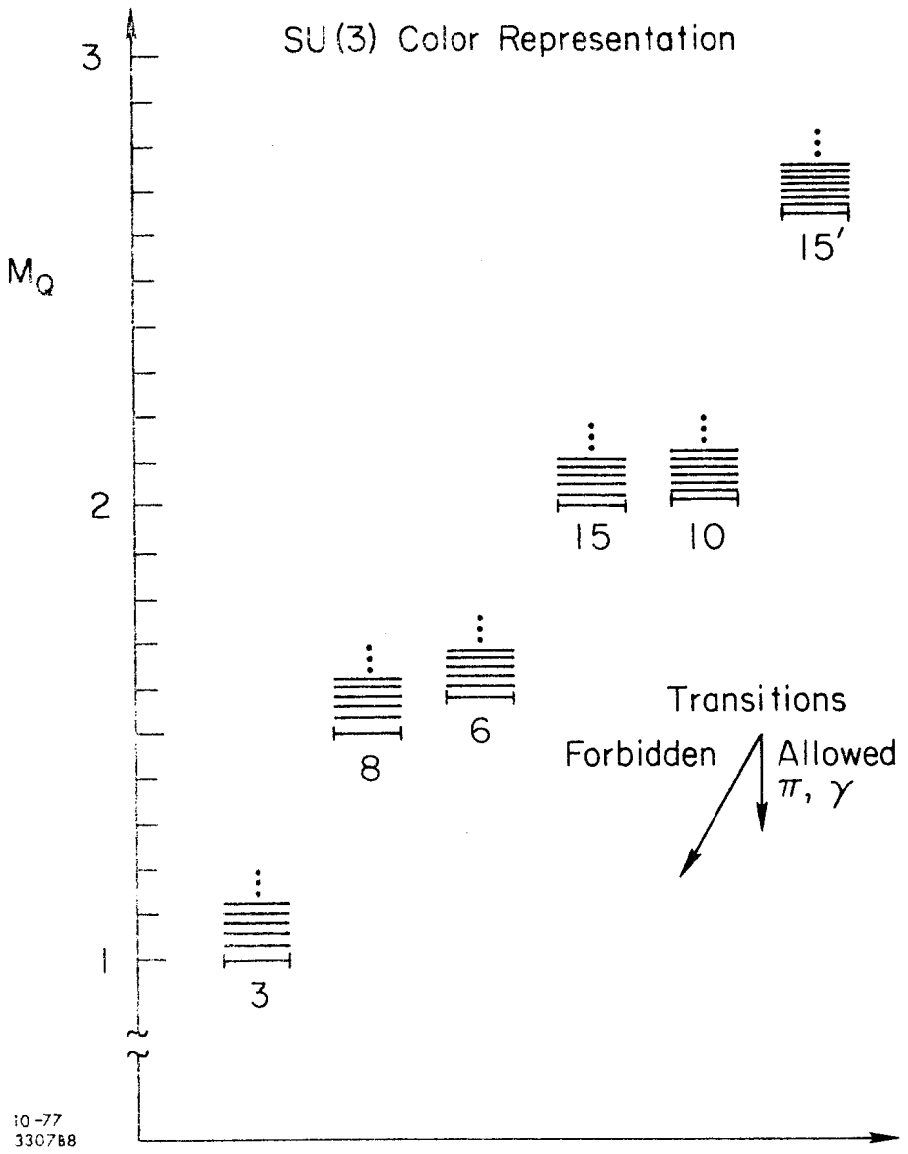

Fig. 1 The spectrum of color.

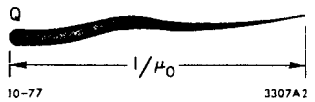

Fig. 2

A string of color flux attached to a liberated quark. The string carries tension of order T_o and peters out over a distance $1/\mu$.

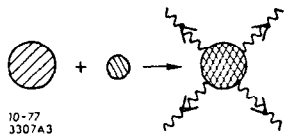

Fig. 3

Absorption of a color singlet nucleon by a liberated color triplet quark accompanied by release of energy (photons, pions).

mined by μ (or M_Q) and by α_c.[2] For the bag model value of α_c we find

$$A_{MAX} \cong .8M_Q/m_p \tag{1.16}$$

We call A_{MAX} the "appetite" of a liberated quark. The system of quark plus A-nucleons does not resemble an ordinary nucleus. It is a single bag with large, fractional baryon number and charge, which we call a quark-nucleon complex (QNC). Their properties are shown in Fig. 4. QNC's would appear as anomalously heavy nuclei. For example if M_Q=100GeV then A_{MAX}=85, $Z(A_{MAX}) = 36+Z_Q$ and $M(A_{MAX}) \approx$ 161GeV. So a 100GeV quark at its appetite has the charge of krypton but the mass of dysprosium (!). With fractional charge it probably has chemistry unlike anything else.

Quark cross sections are determined by geometry. A liberated quark is a large region of hadronic matter (mostly gluon fields). We expect total cross sections of the order $V^{2/3}$. Comparing the quark-proton cross section to the proton-proton cross section we find

$$\sigma_{TOT}(Qp) = \frac{1}{4}\left[\left(\frac{2M_Q}{M_p}\right)^{2/3} + 1\right]\sigma_{TOT}(pp) \text{ for } M_Q >> M_p \tag{1.17}$$

A 100GeV quark will have a total cross section about 10 times the total pp-cross section.

Their size makes quarks hard to produce. They are <u>not</u> pointlike. Consider, for example $e^+e^- \to Q\bar{Q}$, as shown in Figure 5. For large q^2 the time-like form factor should have the same q^2-dependence as the space-like form factor. From the space-like viewpoint the form factor measures the

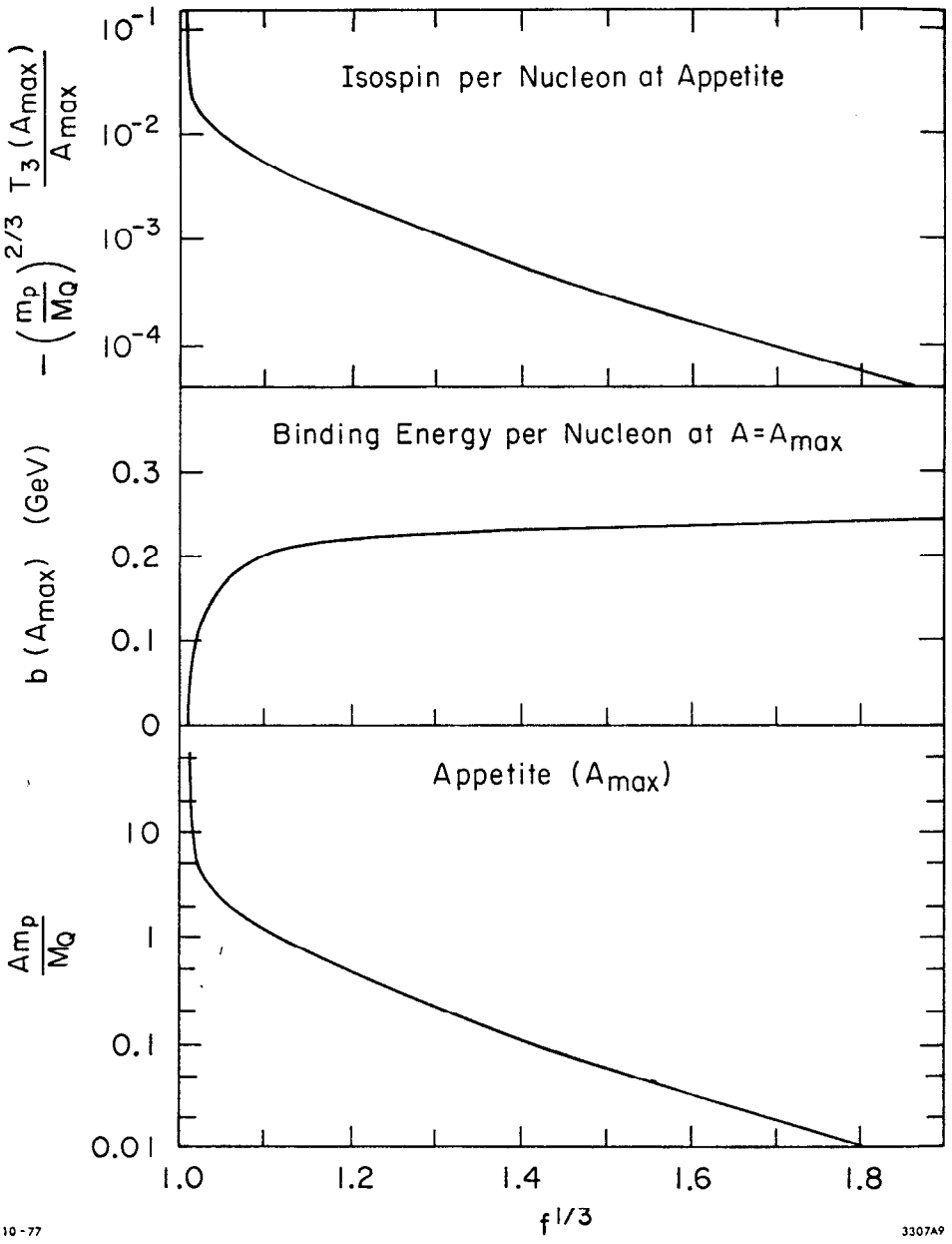

Fig. 4

Properties of quark nucleon complexes. Plotted versus atomic number (A) in units of m_p/m_Q are a) The isospin per nucleon of the most stable QNC for each A; b) The binding energy per nucleon: $b(A) \equiv m_p - (E-M_Q)/A$; and c) The separation energy of the last nucleon: $S(A) \equiv m_p - \partial E/\partial A$.

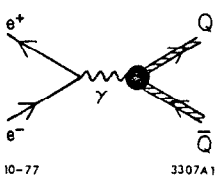

Fig. 5

$e^+e^- \to Q\bar{Q}$

amplitude for the hadronic fields to maintain phase coherence after absorbing some large momentum "kick". This should be scaled by R. We expect a form factor of the form

$$F_Q(q^2) \sim \frac{1}{(1+q^2\langle R^2\rangle/6)^p} \tag{1.18}$$

where p=1 or 2 (in analogy to other hadronic form factors). A similar result may be reached entirely in the timelike regime. The argument is outlined in Fig. 6. When a $q\bar{q}$ pair is created the gluon mass, μ, may be ignored until the separation of the pair is of order $1/\mu$. The smaller μ the more likely that an additional $q\bar{q}$-pair will be created in the flux tube connecting the original separating pair. As soon as an additional pair is created one has mesons, not liberated quarks. Again we have concluded that as $\mu \to 0$ (or $R \to \infty$) quarks will become increasingly difficult to produce. We found that accelerator quark searches put only a limit or 2 to 3 GeV on the mass of liberated quarks.

Finally the model has profound consequences for quark searches in stable matter. Any liberated quarks left over at the creation of the universe would be found only very near their appetite. The reason is that for the first 10^3 seconds there was an intense flux of low energy neutrons. A liberated quark would quickly eat its fill of neutrons (note protons would not do because of the coulomb barrier about a growing QNC) while β-decaying toward the stability liné shown in Fig. 4. So "primordial" quarks would all be found very nearly at their appetite, ie on very specific substances. Thus a quark search in one material would not bound the abundance of quarks in a different substance.

Quarks created after the big bang, by some high energy astrophysical process, would be less likely to reach their appetite. The size of $\sigma(Qp)$ insures that passing through the earth's atmosphere the quark would acquire several units of baryon number. Thus a quark-cosmic ray would be unlikely to have charge 1/3.

To summarize: everything we know about ordinary hadrons and QCD is consistent with the existence of free quarks of mass greater than 2-3GeV. In the context of approximate QCD, liberated quarks are hard to make, hard to see and likely to be found in specific nuclear systems. Although exact QCD and exact confinement are aesthetically more attractive, it is well to remember that the existence of liberated quarks is still very much an open question.

II. $Q\bar{Q}$ AND Q^3 EXOTICS

I wish to return now to the everyday world of color singlet hadrons. In the non-relativistic quark model (NRQM) certain combinations of J, P and C are forbidden to the $Q\bar{Q}$-system. Specifically $J^{PC}=0^{--}$ and the sequence 0^{+-}, 1^{-+}, 2^{+-}, etc. cannot be realized in the NRQM. Though there are no analogous rules in the Q^3-system, certain SU(6) multiplets are not expected at low mass. The NRQM ground state is the familiar L=0[56]. The first excitation could, in principle, be either L=1[70] or L=1[56]. In the NRQM the latter is a spurious state corresponding to an excitation of the three quark center of mass. A real L=1[56] multiplet occurs first at the level of three oscillator quanta. The only state in an L=1[56] which does not also occur in the L=1[70] is a $\Delta(5/2^-)$. Existence of a light $\Delta(5/2^-)$ should therefore be regarded as peculiar from the standpoint of the NRQM. As a class these peculiar $Q\bar{Q}$ and Q^3-states are known type II exotics.[7]

Type II exotics are of interest because they are to be expected in relativistic quark models. None of the selection rules of the previous paragraph can be proved unless quark-quark interactions are instantaneous. Type II exotics may be excitations of quarks relative to self-consistent field variables, such as occur in the Bag model;[8] they may be bound states of $Q\bar{Q}$ plus a gluon;[9] or they may be multiquark states (eg $Q^2\bar{Q}^2$).[10] Type II exotics also arise in Bethe-Salpeter treatments of the $Q\bar{Q}$-bound state.[11]

Characteristically Type II exotics are heavier than their non-exotic analogs. Rebbi found the exotic L=1[56] to be heavier than the non-exotic L=1[70]. Horn and Mandula's $Q\bar{Q}g$ exotic 2^{+-} state is heavier than the non-exotic 2^{++} $Q\bar{Q}$-state. Relativistic quark models mimic the spectrum of the non-relativistic model, but only up to a point. At some level Type II exotics ought to make their appearance.

There is one ambiguous piece of experimental evidence on the subject. A $\Delta(5/2^-)$ state at about 1925 MeV has been suspected for some time. The phase shift analysis of Cutkowsky et al[12], appears to confirm this. NRQM enthusiasts[13] claim this is not too low for a non-exotic $\Delta(5/2^-)$ from a multiplet with three oscillator quanta. It seems unlikely the question can be settled in the baryon sector.

Unfortunately the experimental difficulties in the

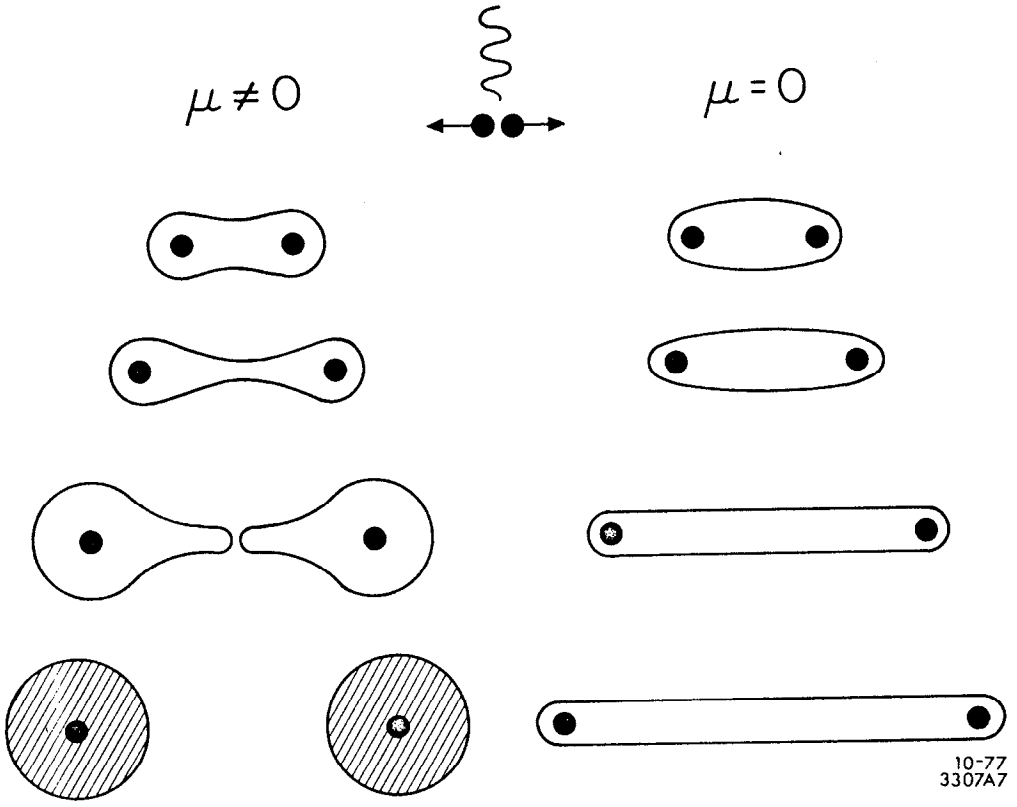

Fig. 6

Evolution of a $Q\bar{Q}$ pair produced in e^+e^--annihilation. The dominant process, the breakdown of the interquark color field into $Q\bar{Q}$ pairs, is not shown. For $\mu \neq 0$ the quarks may separate far enough for the hadron to fission, resulting in the liberation of quarks. For $\mu=0$ the color field strength does not weaken as the interquark separation increases, and quarks remained confined.

meson sector are formidable. There is no evidence for Type II exotic mesons but little evidence against them in the mass range in which they may be expected. They don't couple to easily observed meson-meson channels. A $J^{PC}=2^{+-}$ state would appear in the $\rho\pi$ or $\omega\pi$ P-wave. A $J^{PC}=0^{+-}$ state would appear in the $B\pi$ or $A_1\pi$ P-wave. Furthermore Type II exotics are not expected to be light (say M>1500 MeV for the 0^{+-} and 2^{+-} states listed above). Perhaps the J/ψ or ψ' can be used as a source of Type II exotics. One could, for example, look for the decay $J/\psi \to \pi(2^{+-})$. The matter of Type II exotics mesons is of great theoretical importance but remains largely unexplored both theoretically and experimentally.

III. MULTIQUARK EXOTICS IN THE BAG VERSION OF QCD

A persistent mystery of the quark model is why prominent hadrons appear to consist of $Q\bar{Q}$ and Q^3 but never more than three quarks. [Of course nuclei violate the rule and will figure in this story] In 1966 Nambu[14] pointed out the saturation properties of Coulomb-like SU(3)-color forces: two color singlets exert no strong, confinement-related forces on one another. In 1972 Lipkin[15] pointed out that this could account for the absence of strong attractive forces in exotic channels. These discussions ignore color-magnetism.

The effect of color-magnetic forces[16] between color singlet baryons and mesons is to <u>systematically</u> make <u>exotic</u> multiquark ($Q^m\bar{Q}^n$ with n+m>3) states heavier, while making cryptoexotic multiquark states ($Q^m\bar{Q}^n$ with n+m>3 <u>but not in an exotic flavor representation</u>) lighter. As a result exotic multiquark states are above important decay thresholds hence broad, if indeed they are resonant at all.[17] Cryptoexotics, on the other hand, may be light enough to be bound against dissociation decays, hence narrow and perhaps prominent.

By color magnetism I mean the spin-color dependent interaction arising from one-gluon exchange illustrated in Fig. 7. The justification for treating the gluon exchanges perturbatively lies in the Bag Model. The superstrong, long-range confining color forces are replaced by the bag pressure, leaving only shorter range gluon exchanges for which the coupling constant may be consistently taken to be small. The contribution of Figure 7 to the quark-quark interaction energy is given by

$$\Delta E = -\alpha_c M \sum_{a=1}^{8} \vec{\sigma}_1 \cdot \vec{\sigma}_2 \lambda_1^a \lambda_2^a \qquad (3.1)$$

where λ_i^a, a=1,2..8 (σ_i^k, k=1,2,3) are the color (spin) matrices of the ith quark. α_c is the color fine structure constant and M is a reduced matrix element depending (via bag wavefunctions) on quark masses but not on colors and spins.

The important effects of color magnetism can be read off eq. (3.1). Two quarks may couple to a $\bar{3}$ or 6 of color and a spin singlet or triplet. The table below shows the possible values of $\Delta E/\alpha_c M$.

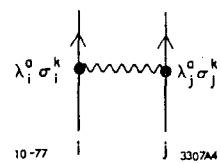

Fig. 7

Lowest order color magnetic interaction between two quarks (i and j). The exchanged gluon couples to the product of the quark's color (λ^a) and spin (σ^k).

TABLE I

	COLOR STATE	SPIN STATE	$\Delta E/\alpha_c M$	FLAVOR SYMMETRY REQUIRED BY FERMI STATISTICS
SYMMETRIC IN COLOR & SPIN	$\bar{3}$	1	-8	ANTISYMMETRIC
	6	3	-4/3	
ANTISYMMETRIC IN COLOR & SPIN	$\bar{3}$	3	+8/3	SYMMETRIC
	6	1	+4	

The interaction is attractive in antisymmetric flavor states and repulsive in symmetric flavor states. Consequently the low energy states of any multiquark system will occur when the greatest number of quarks (and antiquarks) are antisymmetrized in flavor. Among u, d, and s quarks such states are never exotic no matter how many quarks they contain. Exotic states are drawn from the second two rows of Table I and are heavier by virtue of the repulsive color-magnetic interactions.

Perhaps the most interesting implication of this analysis is the possibility that there may be light cryptoexotic mesons and baryons which have been misclassified as $Q\bar{Q}$ or Q^3 states because of their non-exotic quantum numbers. To be systematic consider one sector at a time.

A. $Q^2\bar{Q}^2$

Old Quarks

Among the "old" (u,d,s) quarks the lightest $Q^2\bar{Q}^2$ multiplet is a $J^{PC}=0^{++}$ nonet with masses predicted to lie between 650 and 1100 MeV[18]. These may be identified with the known scalar mesons as shown in Table 2. Usually these

TABLE II

QUARK CONTENT	PREDICTED MASS (MeV)	ASSIGNMENT	COMMENTS
$u\bar{u}d\bar{d}$	650	$\varepsilon(700)$	Identified with the broad low mass $\pi\pi$ enhancement
$\frac{1}{\sqrt{2}}(u\bar{u}+d\bar{d})s\bar{s}$	1100	$S^*(993)$	Trouble for the $Q\bar{Q}$ model because it couples to KK
$u\bar{d}s\bar{s}$	1100	$\delta^+(976)$	
$u\bar{s}d\bar{d}$	850	$\kappa(?)$	Identified with the broad low mass $K\pi$ enhancement

mesons are classified as P-wave $Q\bar{Q}$-states with peculiar singlet-octet mixing and accidental degeneracies. The $Q^2\bar{Q}^2$ assignment is more natural. We are led to predict an entire extra nonet of 0^+-mesons — the real $Q\bar{Q}$ P-waves — presumably heavier and hidden beneath the f, A_2, K**. There is some evidence for these states which was reviewed by Lieth last year at Brookhaven.[19]

New Quarks

States of the form $c\bar{c}q\bar{q}$ (with q an "old" quark) have been proposed by many authors.[20] Most have studied P-waves with an eye to explaining the extra bumps in $\sigma(e^+e^-\to\text{hadrons})$ above 4. GeV. Recently De Rujula and I[21] have studied the S-wave $q\bar{q}c\bar{c}$ system. We find a host of states in the 3.5-4.0 GeV range most of which are broad into $J/\psi\pi$, $\eta_c\eta$ etc. One or two $J^P=1^+$ states may be narrow and may be seen at the 1% level (branching ratio) in monochromatic pion decays of excited 1^- charmonium states.

Charmed $Q^2\bar{Q}^2$ States

Lipkin[22] has pointed out that the flavor SU(4) analog of the 0^+-nonet ground state of $Q^2\bar{Q}^2$ is a 0^+ - 36-plet which does contain certain exotic, charmed mesons: notably a state $\tilde{F}$ with quark content $sc\bar{u}\bar{d}$. This isosinglet with C=-S would be narrow if $M(\tilde{F})<M(D)+M(K)$. Non-leptonic weak decays of the $\tilde{F}$ lead to rather bizarre signatures such as $\tilde{F}\to K^+K^+\pi^-\pi^-$. Bag model calculations involving only one heavy quark are as yet too crude to provide a reliable estimate of $M(\tilde{F})$. Also in the lightest 0^+ multiplet are a set of isospin 1 F-like states (with C=S=±1) with quark content $F_1^{0,+,++}=(cd\bar{u}\bar{s}, cs(u\bar{u}+d\bar{d})/\sqrt{2}, cu\bar{d}\bar{s})$ and their antiparticles $F_1^{0,-,--}$. These states would be less likely to be stable since they may decay strongly to $F\pi$ if $M(F_1)\geq M(F)+M(\pi)$.

$Q^2\bar{Q}^2$ States in the Baryon-Antibaryon System

It has long been anticipated that $Q^2\bar{Q}^2$ resonances would be prominent in the $B\bar{B}$ system[23]. That expectation is conveniently summarized by the Harari-Rosner diagram (Fig. 8). This system has been studied in depth in the context of the Dual Resonance Model[24]. Until recently the problem of classifying the expected resonances in the language of the quark model had not been tackled. The bag model provides a unified, if approximate, description of hadrons containing many quarks and is well suited to describing the $Q^2\bar{Q}^2$ configurations which couple to $B\bar{B}$. Johnson and Thorn[5] studied bags with high angular momentum. A picture of a deformed, spinning bag is shown in Fig. 9. Johnson and Thorn showed that for large J gluon flux lines carry nearly all the hadron's energy and momentum and asymptotically that $J \approx \alpha' M^2+\alpha_0$. The Regge slope, α', could be calculated and was found to be a linear function of the "color-charge"

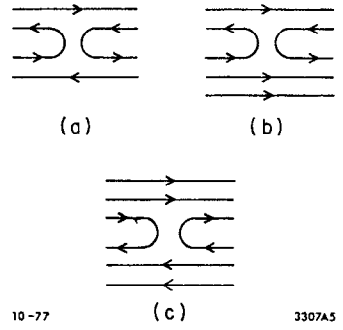

Fig. 8

Haran-Rosner diagrams for meson-meson, meson-baryon and baryon-antibaryon scattering.

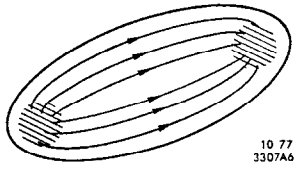

Fig. 9

A high angular momentum, deformed bag. The quarks on either end are connected by color electric flux lines which carry most of the energy and angular momentum.

on either end of the spinning bag. Since the high-J $Q^2\bar{Q}^2$ states reached from the $B\bar{B}$ channel have a color triplet and antitriplet on either end (see Fig. 8) just like ordinary mesons and baryons, Johnson and Thorn concluded the slope of $Q^2\bar{Q}^2$ states prominent in $B\bar{B}$ would be .9 GeV^{-2}.

To aid experimentalists in unravelling the $B\bar{B}$ system it would be desirable to have a checklist of the prominent $Q^2\bar{Q}^2$ states to be expected. In Regge language one would like to know the slopes, intercepts and $B\bar{B}$ couplings of the prominent $Q^2\bar{Q}^2$ resonances. A first attempt at checklist was constructed[25] by combining the slopes of Johnson and Thorn[5], with intercepts estimated from the study of S-wave $Q^2\bar{Q}^2$-states[16], and couplings estimated with the ^3P_o model of Micu, and Colglazier and Rosner[26]. Of course, there are a myriad of distinct $Q^2\bar{Q}^2$ trajectories. Fortunately most are found to couple only weakly to $B\bar{B}$ and many more are too low to be excited if resonance formation is predominantly peripheral.

An indication of the sort of information contained in this checklist is given by Figure 10. There are shown the $Q^2\bar{Q}^2$ trajectories which couple to $N\bar{N}\to\pi^+\pi^-$ in the $L_{N\bar{N}} = J+1$ channel. Of the many trajectories only the highest two couple strongly to $N\bar{N}$. One predicts prominent resonances with $J^{PC}I^G = 3^{--}1^+, 4^{++}0^+$ and $5^{--}1^+$ at 2270, 2460 and 2730 MeV respectively. Recently Carter et al[27] have reported states with these quantum numbers at 2150, 2310 and 2480 MeV.

B. $Q^4\bar{Q}$

This sector has only been studied qualitatively.[28] The lightest multiplet in the bag model appears to be a $J^P = 1/2^-$ flavor SU(3) nonet with masses ranging from 1350 to

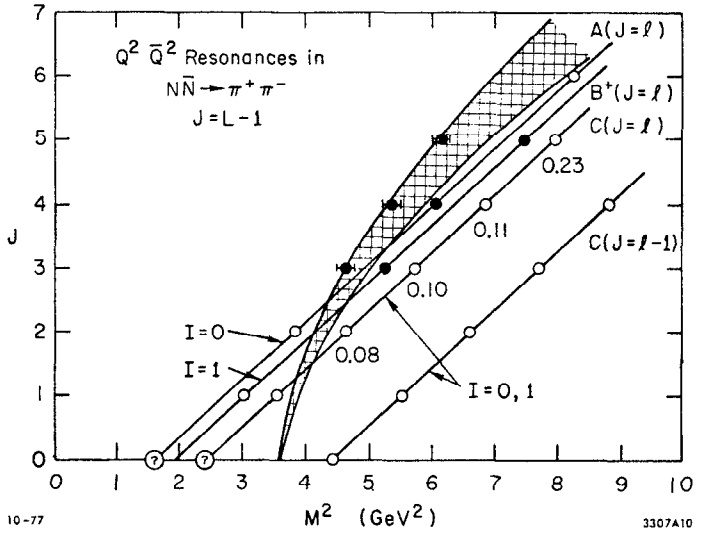

Fig. 10

$Q^2\bar{Q}^2$ trajectories from Ref. 25 which couple to both $N\bar{N}$ and $\pi^+\pi^-$ in the J=L-1 channel of $N\bar{N}$. The trajectory labels (A, B^+, C) refers to quark content; ℓ refers to the relative angular momentum between Q^2 and $\bar{Q}^2$. The strength of the C-type trajectory relative to the A or B^+ is given. The cross-hatched curve indicates peripheral kinematics for the $B\bar{B}$ system. The data are from Ref. 27 and the states marked with filled circles are candidates for the observed resonances.

1900 MeV. Only the Λ and Σ-like members (with quark content $\frac{1}{\sqrt{2}}$ uds$(u\bar{u}+d\bar{d})$ and udsu$\bar{d}$ (etc.)) of the nonet might be expected to be prominent. [The nucleon-like state (with quark content uudss$\bar{}$) couples strongly to ΣK and Nη but not to Nπ.] It is tempting to identify the "Λ" with the problematic Λ(1405). This raises more problems than it resolves since there is no candidate for a nearby "Σ" to identify as the udsu$\bar{d}$ state, nor is there an excess $\Lambda(1/2^-)$ to assign to Q^3 L=1 [70] in place of the Λ(1405).

Exotic $Q^4\bar{Q}$ states lie higher than the $1/2^-$ nonet ground state. The model appears to predict negative parity Z*'s (uudd$\bar{s}$ etc.) well below 2 GeV. The only strong experimental candidates[29] for a Z*'s, the P01 and P13 have positive parity. This may be a clue to the proper interpretation of S wave multiquark states to which I shall return shortly.

C. Q^6—Dibaryons

The general argument outlined above, applied to a six quark system, predicts the ground state to be a $J^P=0^+$, flavor SU(3) singlet (as antisymmetric as possible).[30] An SU(3) flavor singlet dibaryon would have strangeness - 2 and couple to ΛΛ,ΣΣ and NΞ. The bag model estimate of its mass is 2150 MeV, less than $2M_\Lambda$. If a dihyperon of this mass exists it would be stable, decaying weakly to NΣ and NΛ. The bag model mass estimate should not be taken too literally. If the dihyperon (H) were above $2M_\Lambda$ it would appear as an enhancement in dilambda mass spectra. If the H were less massive than M(N)+M(Λ) it would be stable except against second order weak processes and would appear as a heavy, very long lived neutral particle.

In the spectrum of six-quark, S-wave bags a state with the quantum numbers of the deuteron appears first at 2165 MeV, almost 300 MeV above the mass of a proton and neutron. This system is classically unstable against fission into a proton and neutron. In light of this it is tempting to reinterpret the object at 2165 MeV as evidence for a short range repulsion in the n-p system rather than as a n-p resonance.

Recently DeTar[17] has made this picture more precise. He has studied the six quark bag system in a Born-Oppenheimer approximation. He identifies neutron and proton collective coordinates, fixes the relative n-p separation and finds approximate solutions to the bag equations by variational methods. The result is an internuclear potential shown in Fig. 11. The spherical bag calculation of 2165 MeV M_p is the value of the n-p potential at zero separation. DeTar's calculation follows the potential out to about 1fm. Beyond this the 6 quark bag fissions, a process which his variational description of the bag's surface is not rich enough to describe. The short range repulsion and intermediate range attraction found by DeTar are, of course, well known features of the phenomenological n-p interaction.

It is tempting to extend DeTar's prescription to other multiquark sectors. Suppose we assume that any sperical (S-wave) multiquark configuration more massive than its classical dissociation decay channels is actually a signal of a short range repulsive interaction. Multi-

quark states below dissociation thresholds would be stable or resonant, eg. the H at 2150 MeV. Since color magnetism systematically makes exotic multiquark states heavy we are led to expect repulsive interactions in exotic S-wave channels, eg. in the I=2 $\pi\pi$ S-wave or in negative parity Z^* channels. S-wave cryptoexotics, which are systematically made lighter by color magnetism on the other hand actually appear as resonances. Tests of this speculation await an understanding of the dynamical effects of multiquark states on ordinary meson-meson and meson-baryon scattering.

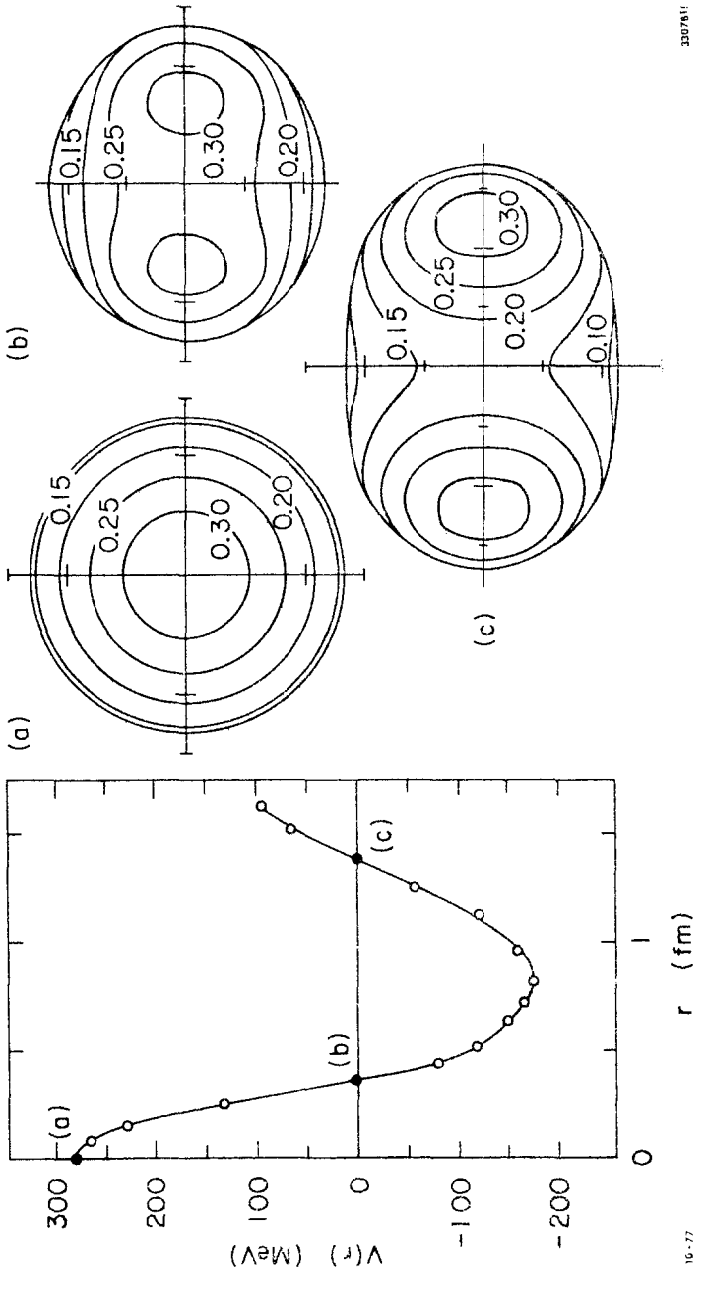

Fig. 11 The nucleon-nucleon potential V(r) from the calculation of DeTar[17]. The configurations labelled A, B and C show the shape of the 6-

FOOTNOTES AND REFERENCES

1. First by Millikan himself (Phil. Mag. 19, 209 (1920)), most recently by G. S. LaRue, W. M. Fairbank and A. F. Hebard, Phys. Rev. Letters 38, 1011 (1977). See the contribution of W. M. Fairbank to this conference.
2. A. DeRújula, R. C. Giles and R. L. Jaffe, MIT Preprint MIT-CTP-635, June 1977.
3. A. Chodos, R. L. Jaffe, K. Johnson, C. B. Thorn and V. F. Weisskopf, Phys. Rev. D9, 3471 (1974); T. A. DeGrand, R. L. Jaffe, K. Johnson and K. Kiskis, Phys. Rev. D12, 2060 (1975).
4. S. D. Drell has dubbed this application of the bag model: "the MIT-semipermeable membrane". This is slightly misleading since no colored fields permeate the bag.
5. K. Johnson and C. B. Thorn, Phys. Rev. D13, 1934 (1976).
6. L. Susskind, Harvard University Loeb Lectures, Spring 1977.
7. For a review see J. L. Rosner, Physics Reports 11C, 189 (1974).
8. T. A. DeGrand and R. L. Jaffe, Ann. Phys. (N.Y.), 100, 425 (1976); T. A. DeGrand, Ann. Phys. (N.Y.) 101, 496 (1976); C. Rebbi, Phys. Rev. D14, 2362 (1976).
9. D. Horn and J. Mandula, Cal. Tech Preprint, January 1977.
10. S. F. Tuan, Phys. Rev. D15, 3478 and references cited therein.
11. M. Krammer and H. Krasemann, DESY preprint DESY 77/34, June 1977; see also M. Krammer, Acta Phys. Austr. 40, (1974) 187.
12. R. Cutkowsky, et al., p. 49, in Proceedings of the Topical Conference on Baryon Resonances, July 1976, R. T. Ross and D. H. Saxon eds. (Rutherford Laboratory, Chilton, Didcot, 1977); R. Cutkowsky and R. E. Hendrick, Phys. Rev. D16, 786, 793 (1977).
13. R. Horgan, P. 435 in Proceedings of the Topical Conference on Baryon Resonances, July 1976, R. T. Ross and D. H. Saxon eds. (Rutherford Laboratory, Chilton, Didcot, 1977); R. H. Dalitz, R. R. Horgan and L. J. Reinders, Oxford University Preprint, OXFORD-TP 52/77.
14. Y. Nambu in Preludes in Theoretical Physics, A. deShalit, H. Feshbach and L. Van Hove, eds (North Holland, Amsterdam, 1966).
15. H. J. Lipkin, Phys. Letters 45B, 267 (1973).
16. R. J. Jaffe, Phys. Rev. D15, 267, 281 (1977).
17. C. DeTar, MIT Preprints, MIT-CTP-630 and 631, 1976.
18. R. L. Jaffe and K. Johnson, Phys. Letters, 60B, 201 (1976).
19. D. W. G. S. Lieth, talk presented at the 1976 Meeting of the APS Division of Particles and Fields, Brookhaven, October 1976.
20. L. Okun and M. B. Voloshin, Zh. Eksp. Theor. Fiz. 23, 369 (1976) [JETP Lett. 23, 333 (1976)]; M. Bander, G. L. Shaw, P. Thomas and S. Meshkov, Phys. Rev. Letters 36, 695 (1976); C. Rosenzweig, Phys. Rev. Letters 36, 697 (1976); N. P. Chang and C. S. Nelson

CUNY Report No. CCNY HEP 76-341; S. Nussinov and D. P. Sidhu, unpublished.

21. A. DeRújula and R. L. Jaffe, in Proceedings of the 1977 Experimental Meson Spectroscopy Conference (to be published) MIT preprint MIT-CTP-658.
22. H. J. Lipkin, in Proceedings of the 1977 Experimental Meson Spectroscopy Conference (to be published).
23. J. L. Rosner, Phys. Rev. Letters 21, 950 (1968).
24. For a review see G. F. Chew, p. 515 in "Antinucleon-nucleon Interactions, Proceedings of the Third European Symposium", 1976 (Pergammon Press, Oxford, 1977).
25. R. L. Jaffe, MIT preprint MIT-CTP-657.
26. L. Micu, Nuc. Phys. B10, 521 (1969); E. W. Colglazier and J. L. Rosner, Nucl. Phys. B27, 349 (1971).
27. A. A. Carter et al., Rutherford Laboratory Preprint RL-77-002/A January 1977.
28. R. L. Jaffe, p. 455 in Proceedings of the Topical Conference on Baryon Resonances, July 1976, R. T. Ross and D. H. Saxon eds. (Rutherford Laboratory, Chilton, Didcot, 1977).
29. B. R. Martin, P. 409 in Proceedings of the Topical Conference on Baryon Resonances, July 1976, R. T. Ross and D. H. Saxon eds. (Rutherford Laboratory, Chilton, Didcot, 1977).
30. R. L. Jaffe, Phys. Rev. Letters, 38, 195, 617 (E), 1977.

PROGRESS IN K* SPECTROSCOPY[†]

T. A. Lasinski
Stanford Linear Accelerator Center
Stanford University, Stanford, California 94305

ABSTRACT

Recent results from high statistics K* spectroscopy experiments are reviewed. The spin parity assignment of 3^- for the $K_N(1800)$ seems now established. A new, extensive $K\pi$ partial wave analysis gives evidence for a new S-wave state at $\sim$ 1420 MeV with a comparatively narrow width of $\sim$ 250 MeV; there is also evidence for a second, inelastic P-wave state at $\sim$ 1650 MeV and width $\sim$ 300 MeV in two of the four solutions of this analysis. Three partial wave analyses of the diffractively produced $K\pi\pi$ system all show evidence for the existence of two Q mesons. One of these, $Q_1(1290)$ decaying principally to ρK, seems well established. Although less certain due to complications of background (Deck) effects, the existence of the other state, $Q_2(1400)$ decaying principally to $K^*\pi$, is substantiated by several model fits to the partial wave results. An intriguing by-product of these $K\pi\pi$ partial wave results is the evidence for a radial excitation of the kaon at $\sim$ 1400 MeV.

[†]Work supported by The Department of Energy.

Introduction

Progress in K* spectroscopy during the last few years is reviewed. This progress is based principally on high statistics data from spectrometer experiments coupled with the refined techniques of two- and three-body partial wave analyses. The success of these K* spectrometer experiments suggests that future efforts of this type will go a long way to unraveling the resonance structure in the $K\pi$ and $K\pi\pi$ mass regions of 2 GeV and above.

Since the time of the first K-beam bubble chamber exposures,[1] our expectations in K* spectroscopy have been those of the quark model.[2] The K* states expected from the quark model are illustrated in Fig. 1. Also indicated are the generally accepted[3] K* states. Although the κ (1250), $J^P = 0^+$, is listed here, it must be noted that its broad width has always made resonant interpretation pragmatic in much the same sense as for the $\pi\pi$ analogue ϵ (700) or ϵ(1200). It is, of course, strictly wrong to say that the states shown in Fig. 1 are the only K* candidates. There is considerable evidence[3] from earlier experiments for many additional K* states.

Evidence for a state at $\sim$ 1800 MeV has been reported by several groups.[4] It would be the SU(3) partner of the g(1680), $J^P = 3^-$, in the $\pi\pi$ system. There is some indication[5] of a state at 2200 MeV, which could be a partner of the recently established h(2040) with $J^P = 4^+$. The reluctance to accept these effects as resonances is due to low statistical significance of the signals and, with the exception of one experiment[6] on the K*(1800), the lack of spin-parity information. There have been no claims for the existence of a second $J^P = 1^-$ K*. This would be the analogue of the ρ'(1600) and a possible radial excitation of the K*(890).

There exists a wealth of information[3] on the possible existence of unnatural spin-parity state ($P = -(-1)^J$) from structure seen in $K\pi\pi$ final state. Thus, for

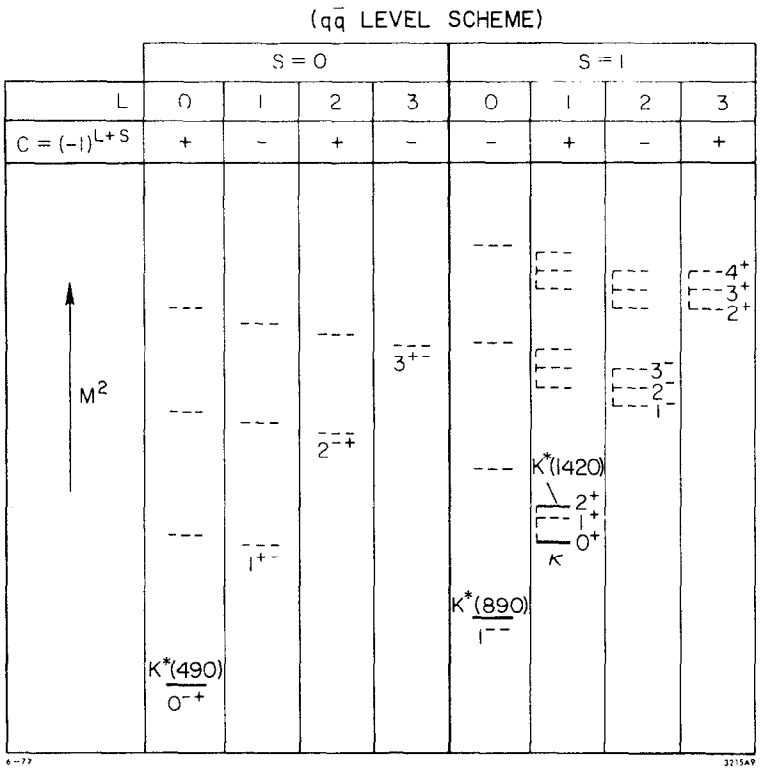

Fig. 1 Quark model level diagram showing well established (1975) K* states.

example, there is no question that $K^{\pm}\pi^{+}\pi^{-}$ mass spectra in $K^{\pm}p \to K^{\pm}\pi^{+}\pi^{-}p$ show a broad bump in the region of 1200-1400 MeV. In addition, there is good evidence that most of the data in this region are consistent with a $J^P = 1^+$ assignment for the $K\pi\pi$ system with a dominant $K^*\pi$ mode. Comparisons of many such spectra further indicate that this broad bump may indeed resolve into two structures.[7] It has always been tempting to associate these structures, known as Q mesons, with the two lowest lying axial vector states expected from the quark model. It might be naively expected that one of the Q's, with $J^{PC} = 1^{+-}$, would be the SU(3) partner of the well-known[3,8] B meson, while the other, with $J^{PC} = 1^{++}$, would be the partner of the infamous A_1.[9]

Beyond the usual qualms over statistical significance, there are dynamical reasons barring the ready acceptance of the Q's as resonances. It is well known that a physically very real mechanism,[10] known as the Deck effect, can produce a low mass $K\pi\pi$ enhancement in reactions like $K^{\pm}p \to K^{\pm}\pi^{+}\pi^{-}p$. Indeed, the Deck effect yields not only a broad Q-like enhancement but also predicts the dominance of the $1^+ K^*\pi$ system. Accepting the evidence[7] for a two-peak structure in the Q region, could it be that one of these is "Deck" and the other, a resonance? Furthermore, although one generally thinks in terms of π-exchange Deck effects leading to $K^*(\pi p)$ final states, there must surely exist some sort of K-exchange effect leading to $\rho(Kp)$ final states. As the $K^*\pi$ and ρK thresholds are different, could it be that the "two-peak" structure in the Q meson is simply the result of two competing Deck effects? Indeed one may argue that something more than the existence of bumps in the low mass $K\pi\pi$ spectrum is needed to claim the existence of even one Q meson.

Although K* spectroscopists have long used the quark model as a guide in their searches, it is only recently that our faith in that model has been reaffirmed owing to the striking successes of ψ/χ spectroscopists. In Fig. 2 we summarize the level structure of known ψ/χ states.[11] The comparison to the K* spectroscopy of Fig. 1 is almost embarrassing. First there exists not only one radial excitation of the $J^P = 1^-$ state at 3100 MeV but most likely an entire tower of such states up to 4400 MeV. In addition, note that the even C-parity axial vector state $\chi(3510)$ is well established. While its spin is known only by a process of elimination, the mass of the $\chi(3450)$ suggests that it is most likely a radial excitation of the ground state, $J^{PC} = 0^{-+}$, $\chi(2800)$.

In what follows we shall consider how well the new information on K* states obtained in the past few years can emulate the success of ψ/χ spectroscopy. This information is naturally divided experimentally into two general areas. We will first consider the $K\pi$ final states which yield information exclusively on natural spin-parity ($P = (-1)^J$) resonances. Here we will find that by far the most interesting results come from the most extensive $K\pi$ partial wave analysis performed to date. Secondly, although some new information does exist in other channels, we consider only the results of high statistics experiments on the diffractive channels $K^{\pm}p \to K^{\pm}\pi^{+}\pi^{-}p$. Experience, sometimes codified as the Morrison rule, tells us that the $K\pi\pi$ system in such reactions consists almost exclusively of unnatural spin-parity states. Here, too, as in the case of $K\pi$ scattering, it is only after a thorough partial wave analysis has been performed that the most interesting spectroscopy results come to light.

K* Production: Bump Hunting in Moments

There are presently several large spectrometer experiments at various stages of analysis studying $K\pi$ scattering. The majority of the resonance spectroscopy results we will discuss here are from the SLAC 13-GeV/c experiment, the analysis of which is essentially complete. Acceptance corrected moments and

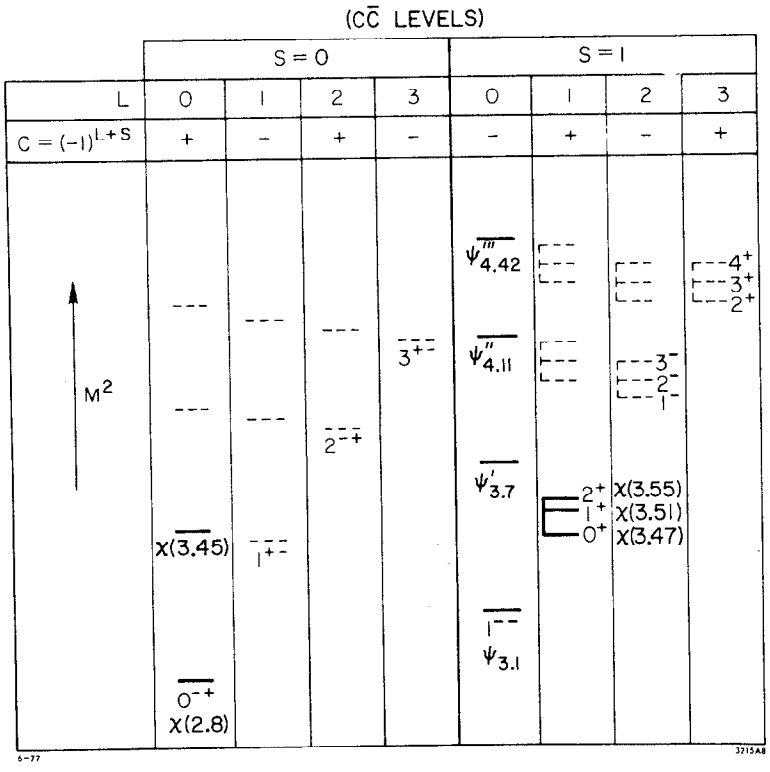

Fig. 2 Quark model level diagram showing the ψ/x states (1977).

a complete Kπ partial wave analysis[12] have been obtained from the SLAC data for the following channels:

$K^- p \to K^- \pi^+ (n)$	48,000 events
$K^+ p \to K^+ \pi^+ (n)$	14,000 events
$K^+ p \to K^+ \pi^- (\Delta^{++})$	102,000 events
$K^- p \to K^- \pi^- (\Delta^{++})$	26,000 events

Acceptance corrected moments have recently become available[13] from a University of Geneva experiment at 10 GeV/c:

$K^+ p \to K^0_s \pi^+ p$	46,000 events
$K^- p \to K^0_s \pi^+ p$	18,000 events

An amplitude analysis studying the production systematics of these quasi-elastic channels has also just been finished[14]; a complete Kπ partial wave analysis should follow shortly.

A BNL-Brandeis-CUNY-U. Mass.-U. Penn. collaboration has obtained[15] some 80,000 events on $K^- p \to K^- \pi^+ n$ at 6 GeV/c in Brookhaven's MPS. Acceptance corrected moments for these data should be available shortly.

The first sign of resonance production is the observation of bumps in invariant mass spectra. Some information on the spin of these effects can then be found by observing the same bump in even-order moments of the decay angular distribution.

The Kπ mass spectrum, $\langle Y_2^0 \rangle$ and $\langle Y_4^0 \rangle$ t-channel moments from the SLAC data on $K^- \pi^+ n$ are shown in Fig. 3. The well-known K*(890) and K*(1420) are quite apparent in the mass spectrum. Note that the 890 bump is seen in $\langle Y_2^0 \rangle$ but not in $\langle Y_4^0 \rangle$ indicating a $J^P = 1^-$ assignment. The 1420 bump

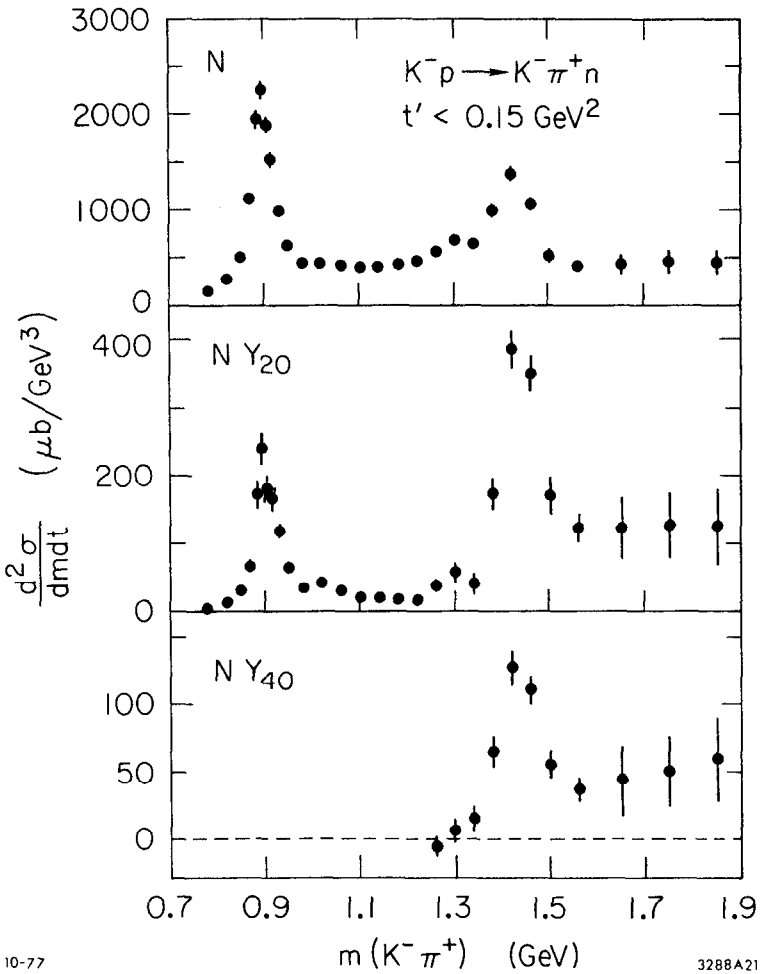

Fig. 3 Typical acceptance corrected mass spectrum, Y_{20} and Y_{40} moments from the SLAC 13 GeV/c experiment.

appears in both the $\langle Y_2^0 \rangle$ and $\langle Y_4^0 \rangle$ moments indicating a spin of at least 2. Turning to Fig. 4, we see that the 1420 bump does not appear in $\langle Y_6^0 \rangle$, indicating a $J^P = 2^-$ assignment. Notice, however, that a broadish (~ 200 MeV) bump has developed in $\langle Y_6^0 \rangle$ at ~ 1780 MeV. This and the correlations with the $\langle Y_4^0 \rangle$ and $\langle Y_5^0 \rangle$ moments constitute the SLAC evidence[16] for a $J^P = 3^-$ state, K*(1780), with a width of ~ 200 MeV. However, the precise width of this state is difficult to determine from the SLAC data due to low acceptance at masses above 1800 MeV.

Further evidence[13,17] for the 3^- assignment for the K*(1780) comes from the $\langle Y_6 \rangle$ moments of the Geneva experiment at 10 GeV/c, as shown in Fig. 5. In the first publication[17] on these data, the Geneva group estimated a width of ~ 100 MeV. However, a subsequent analysis[13] seems to indicate a broader width of ~ 180 MeV.

Both the SLAC and Geneva experiments clearly indicate the existence of a state at ~ 1800 MeV most likely with $J^P = 3^-$. Because of limited acceptance beyond 1800 MeV and the ambiguities of background subtractions, it is difficult to make a good determination of the width, though 100 MeV would certainly seem a lower limit. A best estimate[18] for the K*(1780) parameters, using the leading edge of the $\langle Y_6 \rangle$ moments from these experiments, yields

$$m(1780) = 1780 \pm 15 \text{ MeV}$$

$$\Gamma_{tot}(1780) = 180 \pm 35 \text{ MeV}$$

Information on the $K\pi\pi$ decays of the K*(1780) should be available shortly from two spectrometer experiments now under analysis. In Fig. 6 is shown a preliminary report[19] of the BNL-CUNY $\bar{K}^{*0}\pi^+\pi^-$ mass spectrum at 6 GeV/c in in the MPS. A peak at ~ 1700 MeV with a width of less than 100 MeV is evident. Note, however, that these data have <u>not</u> been corrected for acceptance in all

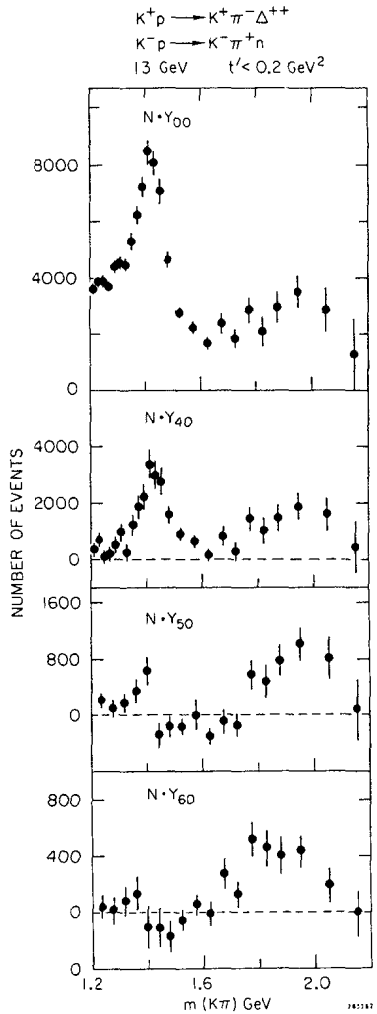

Fig. 4 Higher moments from the SLAC experiment indicating a broad state at ~1780 MeV.

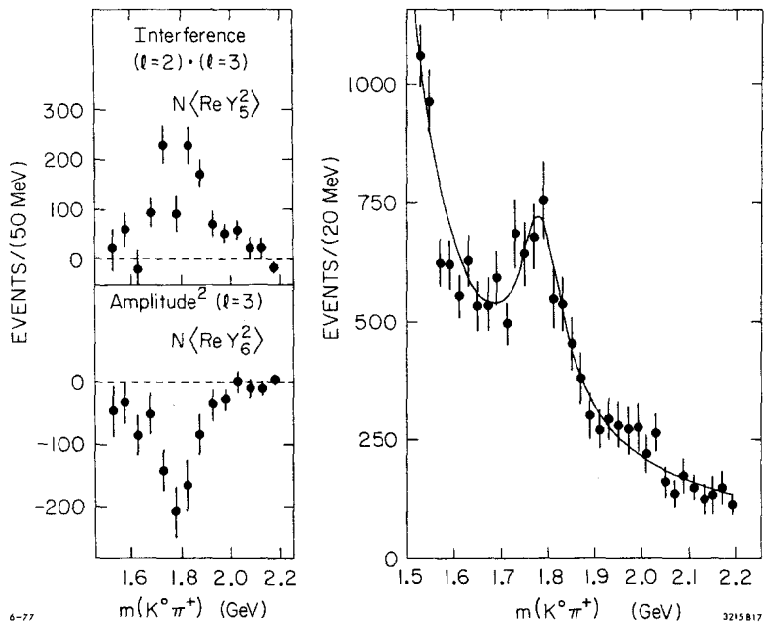

Fig. 5 Evidence from the Geneva 10 GeV/c experiment on $K^+p \rightarrow K^\circ\pi^+p$ for K* (1780).

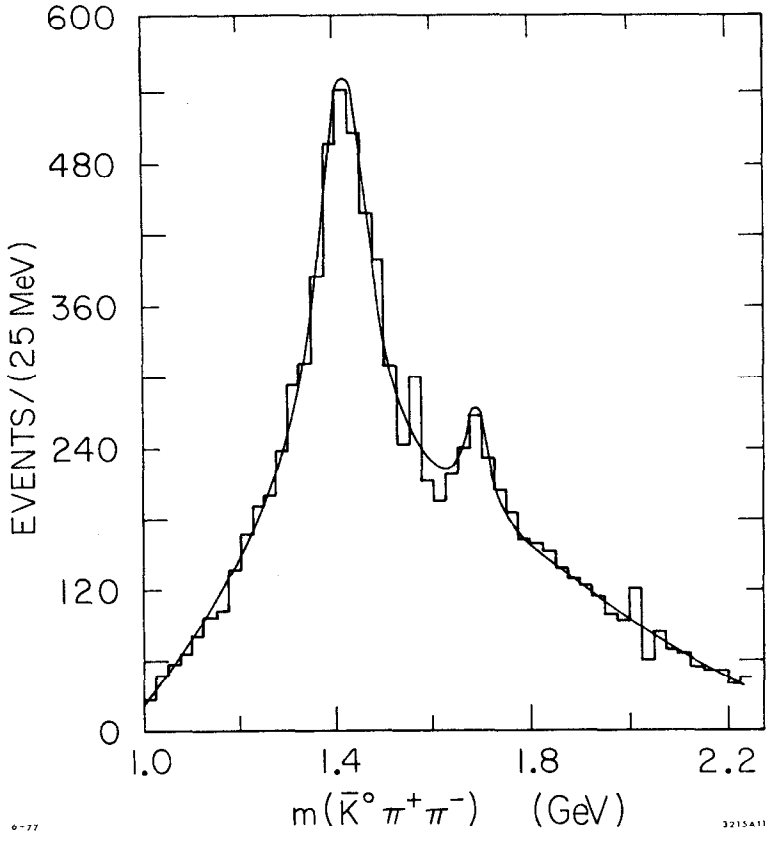

Fig. 6 The $\bar{K}^0\pi^+\pi^-$ spectrum from a BNL-CUNY experiment at 6 GeV/c.

kinematic variables. This fact is best emphasized by considering the preliminary results of the Aachen-Geneva-Zurich experiment at 10 GeV/c[20], Fig. 7, in the CERN Ω for the same mass spectrum. Even in the uncorrected data, one sees a broad peak beginning at 1750 MeV with a width of over 100 MeV. From a fit to the corrected spectrum, Aachen-Geneva-Zurich find the parameters

$$m = 1812 \pm 28 \text{ MeV and } \Gamma = 181 \pm 24 \text{ MeV}$$

in substantial agreement with the SLAC and Geneva results for the 2-body decay. A preliminary 3-body partial wave analysis by this group suggests a spin of $J^P = 3^-$.

Kπ Phase Shift Analysis

As illustrated above, much can be learned by a cursory investigation of the moments of the Kπ angular distribution. In particular, the so-called leading or peripheral states appear as bumps in specific moments; that is, at a given Kπ mass, a bump in the highest non-zero, even order moment tends to signal a resonance. Thus at ~ 900 MeV the clear spike in the dominant $\langle Y_2^0 \rangle$ corresponds to the P-wave, $J^P = 1^-$ K*(890). By 1400 MeV it is the $\langle Y_4^0 \rangle$ which dominates and we have clear evidence for the D-wave, $J^P = 2^+$K*(1420). Lastly, once the vagaries of statistics and acceptance are overcome, we find at 1800 MeV, with the dominance of the $\langle Y_6^0 \rangle$ moment, evidence for an F-wave, $J^P = 3^-$K*(1780) state.

Experience[3] from πN, $\bar{K}$N, and ππ spectroscopy teaches us that such straightforward discovery of resonances becomes ever more unlikely with increasing mass. There is a definite, well known[3] tendency for leading states to become both more inelastic and broader. In addition, this experience also tells us that states of roughly similar mass to the leading states can be expected to be hidden

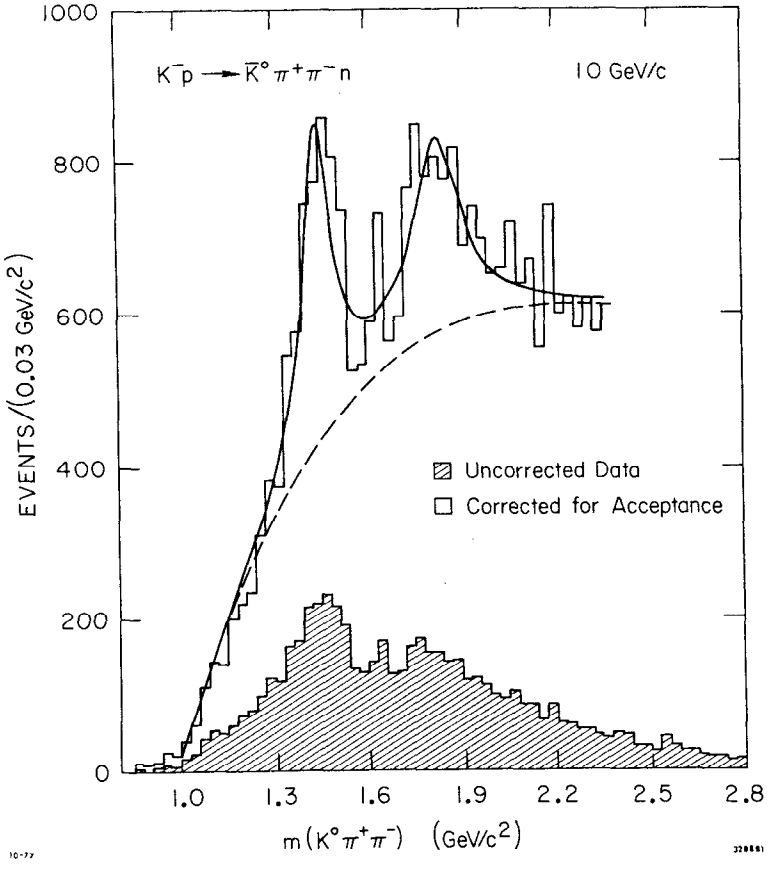

Fig. 7 Preliminary $\bar{K}^0\pi^+\pi^-$ spectrum from an Aachen-Geneva-Zurich experiment at 10 GeV/c.

in the interferences among the leading states. Indeed, it is precisely these so-called lower lying states expected in the quark model which are generally the last to be found.

To find these states, it is necessary to use all the information available in the moments of the $K\pi$ angular distribution. This is accomplished by performing a partial wave analysis on the moments. Such an analysis has recently been completed[12] by Estabrooks and Martin using the SLAC 13-GeV/c data shown in Fig. 8.

To appreciate fully the results of this analysis, it is useful to review briefly the procedure developed by Estabrooks and Martin.[21] The observed moments can be expressed in terms of the partial wave amplitudes as

$$\sum_{LM} \langle Y_{LM} \rangle Y_{LM}(\theta\,\phi) = \Big| \sum_{\ell m} T_{\ell m}(m_{K\pi},\, t)\, Y_{\ell m}(\theta\,\phi) \Big|^2 \qquad (1)$$

where $\theta\,\phi$ are the $K\pi$ decay angles in either the t- or s-channel system. Note that we have suppressed nucleon helicity labels in Eq. (1) for simplicity. In practice, careful assessment[22,23] of positivity constraints and the importance of non-π-exchange processes must be made to limit the number of nucleon helicity amplitudes. One then assumes, guided in part by Watson's theorem, that the amplitudes factorize,

$$T_{\ell m}(m_{K\pi},\, t) \propto P_{\ell m}(t,\, m_{K\pi})\, e^{i\delta_\ell} \sin\delta_\ell\,(m_{K\pi}) \qquad (2)$$

The phase shifts $\delta_\ell(m_{K\pi})$ (and η_ℓ in the inelastic region above ~ 1200 MeV) are the unknowns of the $K\pi$ scattering we are after. The parameters $P_{\ell m}(t, m_{K\pi})$ characterize the production of the $K\pi$ system—π exchange, ρ exchange, etc; note that the $P_{\ell m}$ could be functions of the $K\pi$ mass, presumably due to absorptive effects.

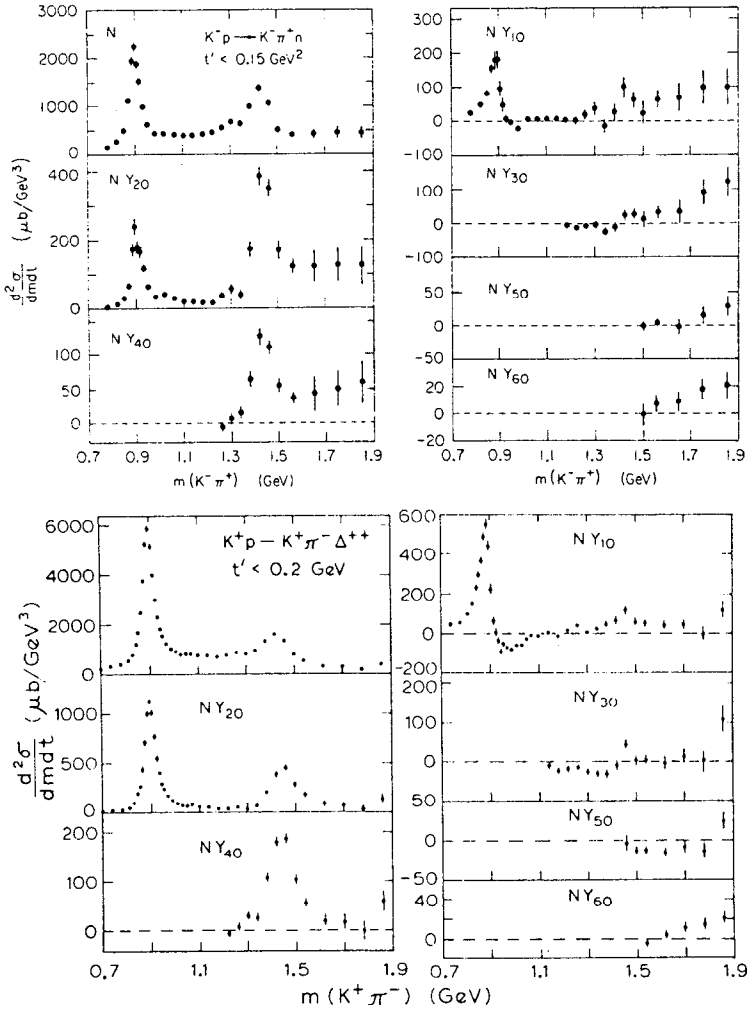

Fig. 8 Mass spectra and M=0 moments from the SLAC 13 GeV/c experiment used for an extensive Kπ partial wave analysis.

The analysis proceeds by first determining the nature of the production amplitudes, $P_{\ell m}(t, m_{K\pi})$. This is done by fixing $m_{K\pi}$ to the value of well-known peripheral states such as K*(890) or K*(1420). A detailed study of the t-dependence of the moments yields a parametrization for $P_{\ell m}(t)$ and the knowledge of its Kπ mass dependence. Even though this is a spectroscopy conference, it would be sinful not to show at least one of the lovely production distributions so necessary to elucidate the production systematics ($P_{\ell m}$). In Fig. 9 the SLAC data at 13 GeV/c are compared to ANL (EMS) data[24] at 4 GeV/c for $\bar{K}^*(890)$ n production. This particular combination of moments is designed to isolate the π-exchange contributions (the $P_{\ell 0}$ (t)). In the forward direction we see a clear turnover and a definite overlapping of the distributions. As the cross sections have been scaled by P^2_{LAB}, we have the classical signal of π-exchange dominance in the nucleon-helicity flip amplitudes. The separation of these distributions at large -t indicates the presence of other exchanges whose contributions change with energy. The production systematics of the Kπ system have been thoroughly studied in the SLAC data for both the neutron and Δ^{++} channels.[22,23] One obtains from these studies a relatively compact parametrization for the $P_{\ell m}(t, m_{K\pi})$ of Eq. (2).

Having fixed the production piece of the amplitude, we are ready to consider what follows for the Kπ scattering as characterized by the phase shifts and inelastics. Note that although the production systematics of the neutron and Δ^{++} data are quite different,[22,23] the Kπ scattering aspect must in principle be the same. Such an analysis has recently been completed by Estabrooks and Martin using the SLAC data. In addition to the $K^{\pm}\pi^{\mp}$ final state, data on the exotic states of $K^{\pm}\pi^{\pm}$ from the same experiment have also been analyzed. There are no large surprises here, other than the fact that the I = 3/2, S-wave phase shift is systematically somewhat larger (in magnitude) than previously thought.[12]

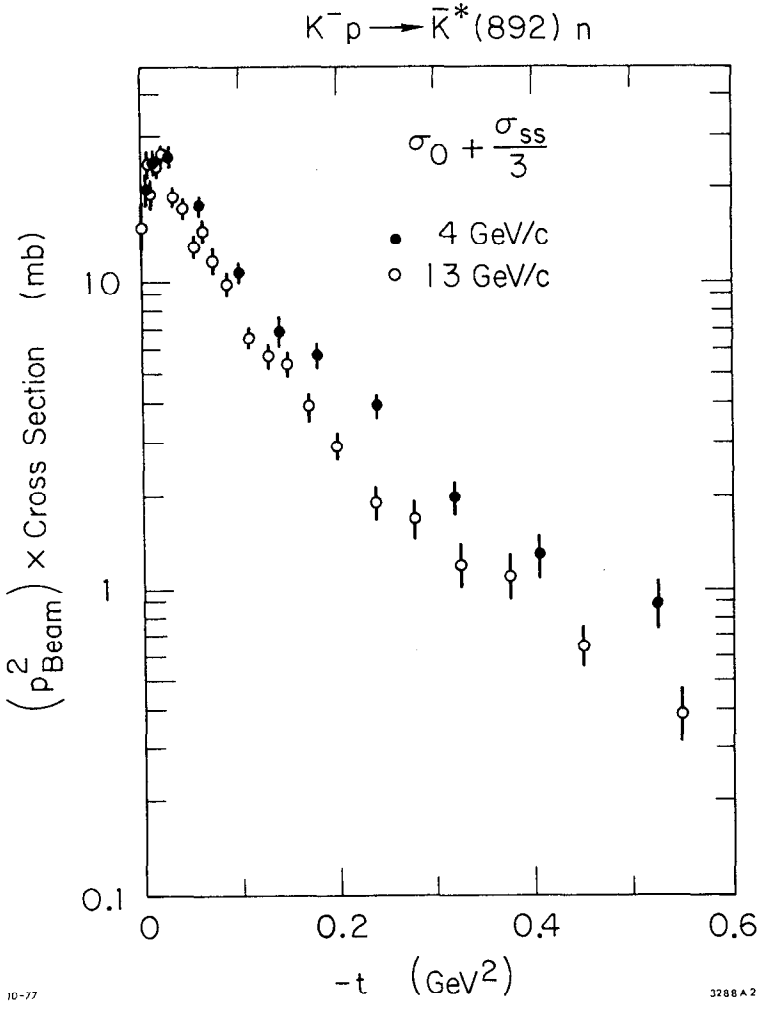

Fig. 9 Comparison of the ANL 4 GeV/c and SLAC 13 Gev/c production distributions for K*(890) via "π-exchange."

Below ~ 1400 MeV Kπ mass, the I = 1/2 solution of the partial wave analysis is essentially unique. As the S and P waves are elastic, these Kπ amplitudes are uniquely determined. Above ~ 1400 MeV with the onset of D and F waves, and corresponding Barrelet zeroes, there are four solutions. In this case, while magnitudes of the partial waves are determined, only the relative phases amongst them are found. The entire analysis is summarized[12] in Fig. 10. Note that the magnitudes plotted correspond to $\sqrt{2\ell+1}$ of the conventional Argand (unit) amplitude and that I = 3/2 effects (essentially S-wave) have not been unfolded. Additionally, in the regions of K*(1420) and the K*(1780), the relative phases—here labeled δ—have been fixed by these leading states. This is indicated by the Breit-Wigner phase motion in the bottom two rows of Fig. 10. There are many intriguing aspects of these results. Note that in all four solutions the S-wave intensity undergoes a precipitous drop just beyond 1400 MeV. In solutions B and D, note that in the region of 1600 MeV the P-wave intensity suddenly increases. How are we to understand these curious effects ?

Argand Plots for Kπ Scattering

To assess the physical implication of these results, it is extremely useful to transform them into the more conventional representation of the Argand plot. Doing this is not completely straightforward. We shall first review the assumptions and guidelines for such a transformation.

As noted above, the first problem to overcome is the fact that only relative phases are measured at Kπ masses at and beyond the K*(1420). Having established the most likely nature of the leading K*(1420) and K*(1780) resonances, it seems safe to set relative phases by assuming a Breit-Wigner behavior for these states. At this point we may also correct for the S-wave and I = 3/2

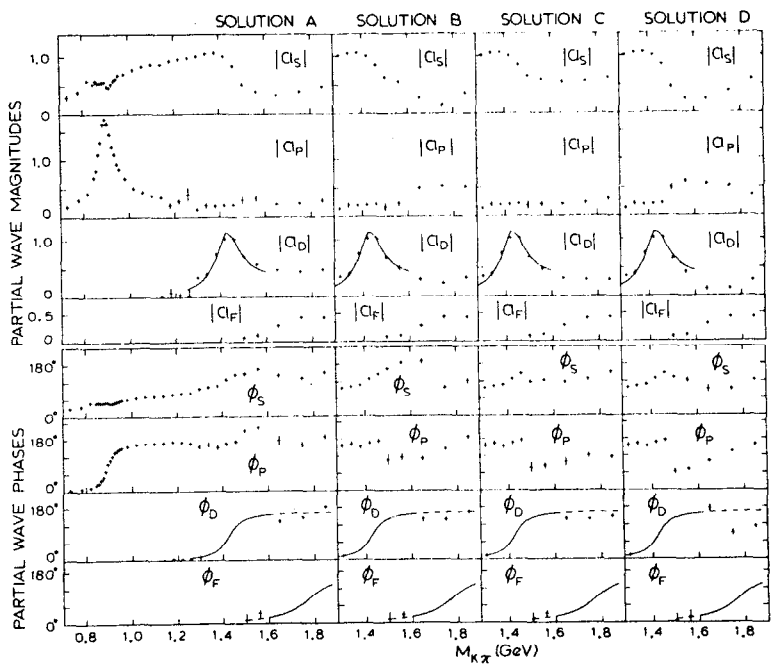

Fig. 10 Amplitudes and relative phases for $K\pi$ scattering from an analysis of the SLAC 13 GeV/c data. Above 1.3 GeV, phases are set by the Breit-Wigner behavior of K*(1420) and K*(1780); I=3/2 effects have not been unfolded.

contribution; recall that the exotic channel has been analyzed in the same experiment.

This takes us only a little beyond Fig. 10. To proceed further, we must realize that in the high mass region there still remains a choice to be made in the overall phase at each mass bin. This uncertainty is such that once we choose the absolute phase for any one partial wave, then the phases of the other partial waves are immediately determined. Two essential criteria were used in choosing this absolute phase:

(1) At each $K\pi$ mass the smallest possible rotation in overall phase is made such that all partial waves lie on or within their respective unitary circle.

(2) The leading states, the D-wave K*(1420) and the F-wave K*(1780), look like (inelastic)resonances in their Argand plots.

The first criterion is common sense, but it need not lead to the correct picture. For example, should we rotate only to get waves on the unitary circle or should we require some waves to be inelastic? It is here where the second criterion is important. From the known inelastic modes[3] of the K*(1420) and the $K\pi\pi$ data for the K*(1780), we have some limits on the inelasticity of these states. This information tells us that the overall rotation must bring these waves within the unitary circle. That the final results for the D and F waves look like inelastic Breit-Wigner resonances we take as God-given.

We now turn to the results of such an exercise in the case of solution B, the others being done elsewhere.[12] In addition to the procedure outlined above, one further thing has been done. For $K\pi$ masses above 1500 MeV, the partial wave analysis was repeated in overlapping mass bins. This was done to introduce some smoothing into the analysis so that the choice of rotation phase would be

more obvious in the high mass region. Although susceptible to the caprices of statistical fluctuations, this is perhaps the least biased method of smoothing.

In Fig. 11-d, à la the Particle Data Group,[25] we show the Argand diagram along with its imaginary and real projections vs Kπ mass for the F-wave. Owing to criterion (2), it is of little surprise that we find a circle in the Argand plot; note that the analysis stops at 1900 MeV as statistics are insufficient to produce a stable partial wave decomposition. From the imaginary projection, we see that the elasticity is just above .15 and the full width ~ 200 MeV. Note the concurrence of a peak in the imaginary part and zero in the real part at about 1800 MeV indicate the mass of this state.

Turning to the D-wave in Fig. 11-c, we again find no surprises given criterion (2); we do see, however, an even more textbook-like example of an inelastic resonance. A careful inspection of the peak in the imaginary part indicates a mass of 1435 MeV. This statistically significant shift from the nominal[3] 1420 value is indeed higher than the value seen in mass spectra for the SLAC experiment. The elasticity of just above .45 (after some interpolation) and width of ~ 100 MeV are consistent with previous estimates. Note the classical oscillation of the real part, first positive and then negative, about the mass of 1440 MeV.

We now turn to the P-wave in Fig. 11-b. It is emphasized that what we find here in the region of 1400 to 1800 MeV is a direct consequence of what we have supposed to be the behavior of the leading D- and F-waves. Starting at low Kπ mass we see a classic elastic Breit-Wigner, the K*(890). Recall that the solution is unique below ~ 1400 MeV. As we go higher in mass, we see a second loop in the Argand circle. The corresponding imaginary projection shows a bump at ~ 1600 MeV with a width of ~ 300 MeV and an elasticity of just above .25.

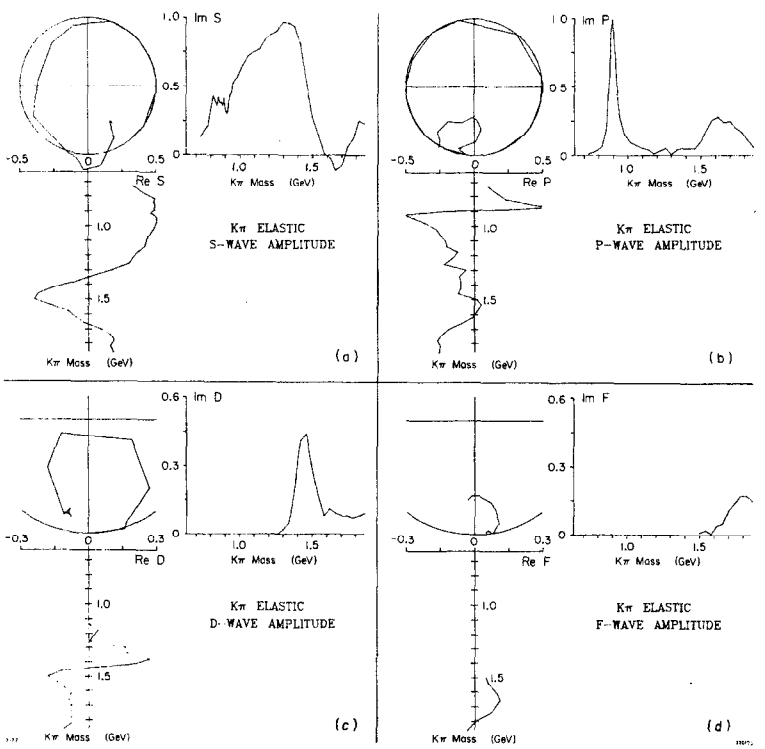

Fig. 11 Argand plots and projections for the I=1/2 partial waves from solution B of the SLAC 13 GeV/c data.

Although the real part at this mass does show the expected oscillatory behavior, notice that it is displaced to the negative side of the axis; presumably the second P-wave resonance is somewhat distorted from the simple Breit-Wigner shape due to the high mass "tail" of the K*(890). This new state, K*(1650) with $J^P = 1^-$, is present in two of the four solutions of the SLAC data. It is assigned most probably in the quark model as a radial excitation but could also be a member of L = 2 multiplet.

We finally turn to the I = 1/2 S-wave in Fig. 11-a. As has been known for some time,[3] the S-wave moves rather slowly in the Argand plot from threshold to $\sim$ 1300 MeV where the phase shift finally reaches 90^o. This corresponds in the projections of Fig. 14 to the point where the imaginary part is ~ 1.0 and the real part ~ 0. It is this effect which is referred to as κ (1250). The new feature found in the analysis of the SLAC data is the sudden speed-up of the Argand plot in the region 1300 - 1600 MeV, corresponding to the precipitous drop of the imaginary part and the negative-then-positive oscillation of the real part. These rapid variations certainly signal a resonance. But how are its parameters to be estimated? First, we must remember that this amplitude is already strongly attractive by 1300 MeV; put another way, the new effect above 1300 MeV must be "sitting" on a large background due to the old κ (1250). With this in mind, we may argue that the resonant effect in the 1300 - 1600 MeV region is best viewed by rotating Fig. 11-a by 90^o. If this is done, we may estimate from the real part (now the imaginary part!) a mass of $\sim$ 1450 MeV, a width of $\sim$ 250 MeV and an elasticity of just under 1.0. Note, too, that from this point of view, the imaginary part of the amplitude indicates the oscillatory behavior of the real part of a Breit-Wigner, albeit displaced from zero.

There are two additional points to make with regard to the S-wave solution. First, this new κ (1425) will peak in the mass spectrum at the nominal location of the K*(1420). Recall that the D-wave solution indicates a mass of 1435 for the K*(1420). When the cross sections of these partial waves are added, the observed peak in the mass spectrum is more consistent with the 1420 value. This is a noteworthy example of how the decidedly non-linear behavior of low partial waves can distort the correct mass of leading states. The second comment, returning to Fig. 11-a, is that we have appeared to have broken one of our rules for obtaining these Argand plots. At $\sim$ 1600 MeV the amplitude has an excursion outside the Argand plot, corresponding to a negative imaginary part. The size of the excursion is some measure of the systematic uncertainty of the S-wave in this high mass region. Note, however, that the systematic uncertainty of the P and F waves need not be as great as those signals are considerably larger. In short, all that can be conservatively said about the S-wave for Kπ masses above $\sim$ 1550 MeV is that its Argand motion has slowed quite considerably as compared to that in the 1300 - 1550 MeV region.

Summary and Comments on Kπ Scattering

We have summarized the information on resonances coming from complete particle wave analysis of the SLAC data in Table 1. The new information is the evidence for a comparatively narrow S-wave at $\sim$ 1425 MeV and the existence of a second P-wave state at $\sim$ 1650 MeV. The spread in elasticities for the new S-wave state corresponds to whichever of the four solutions is chosen. As mentioned before, the second P-wave state appears in only two of the four solutions.

There is a remarkable similarity between the Kπ partial wave solutions of the present analysis and those for the $\pi\pi$ system presented some time ago by Estabrooks and Martin.[26] In Fig. 12 we have Argand plots (scaled to $\sqrt{2\ell+1}$

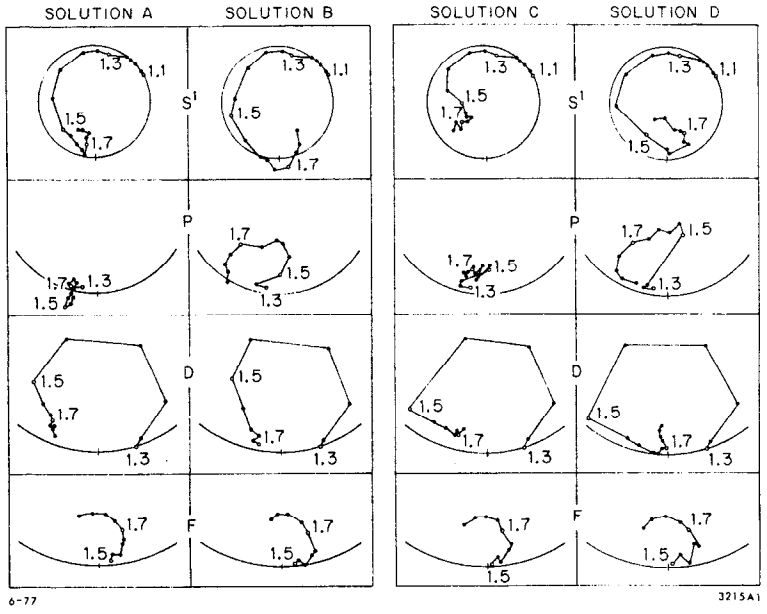

Fig. 12 Argand plots for the I=1/2 partial waves for the four solutions of the SLAC 13 GeV/c data.

Table 1

Resonances and parameters resulting from an analysis of the SLAC 13-GeV/c Kπ data. The comment "bump" indicates that resonant interpretation follows almost immediately from a cursory study of the moments; PWA signifies that resonance interpretation is suggested only after a careful partial wave analysis.

Name	J^P, Wave	Mass (MeV)	Width (MeV)	Elasticity	Comment
K*(890)	1^-, P	892	55	1.0	Bump
κ (1250)	0^+, S	~1250	>400 ?	1.0	PWA; resonant interpretation questionable
κ (1425)	0^+, S	1425	~250	0.5 - 0.9	PWA; in all solutions
K*(1435)	2^+, D	1435	100	.49	Bump; PWA for mass
K*(1650)	1^-, P	1650	~300	~0.3	PWA; in two of four solutions
K*(1780)	3^-, F	1780	175	~0.2	Bump

of the unitary circle) for all four solutions in the Kπ system. The corresponding results for the $\pi\pi$ system are shown in Fig. 13. In both figures the S-wave reveals a narrow effect (κ (1425) or S*(990)) superimposed upon a large attractive background (κ (1250) or $\epsilon(600)/\epsilon(1200)$). In the P-wave, both channels indicate a second $J^P = 1^-$ state in two of the four solutions. Note that in both cases, the second P-wave lies just below the leading F-wave and well above the D-wave states. The well-known trend for high-spin leading states to become both broader and more inelastic with increasing mass is well illustrated by D- and F-waves.

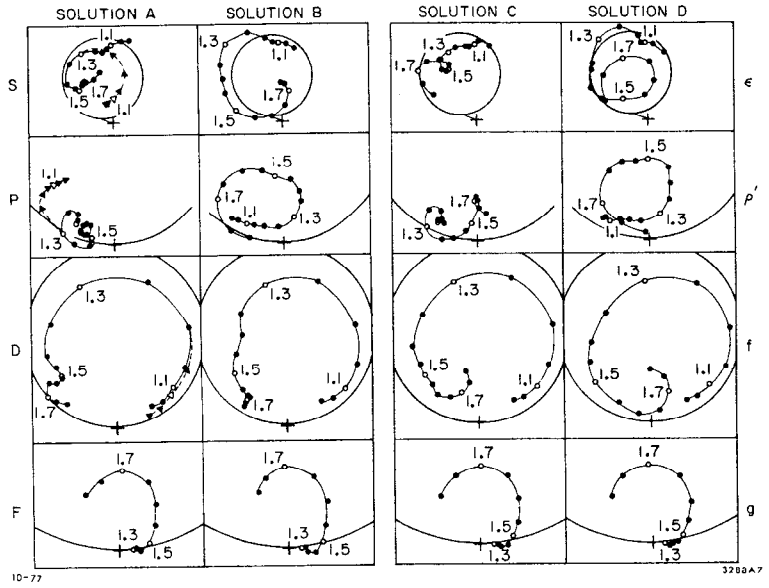

Fig. 13 Argand plots for $\pi\pi$ (nonexotic) partial waves for the four solutions of the CERN-Munich 17 GeV/c data.

Indeed, if we knew nothing of symmetry schemes such as SU(3), these detailed, dynamical similarities between the $K\pi$ and the $\pi\pi$ partial waves would quickly reveal them to us!

$K\pi\pi$ Production

The most dramatic results in $K^* \to K\pi\pi$ spectroscopy have recently come from three different experiments studying the diffractive reactions $K^{\pm}p \to (K\pi\pi)^{\pm}p$. The SLAC 13-GeV/c spectrometer experiment[27] studied both charged states

$$K^+p \to K^+\pi^+\pi^-p \qquad 72{,}000 \text{ events}$$
$$K^-p \to K^-\pi^+\pi^-p \qquad 56{,}000 \text{ events}$$

Combining the data from three bubble chamber experiments at 10, 14, and 16 GeV/c, Otter et al.[28] studied the negative charged state in both 4-prong and 2-prong V^0 topologies:

$$\left.\begin{aligned} K^-p &\to K^-\pi^-\pi^+p \\ &\to \bar{K}^0\pi^-\pi^0p \end{aligned}\right\} \sim 8000 \text{ events after cuts}$$

More recently, the ACNO (Amsterdam-CERN-Nijmegen-Oxford) collaboration presented preliminary results[29] on the same topologies at 4.2 GeV/c:

$$\left.\begin{aligned} K^-p &\to K^-\pi^-\pi^0p \\ &\to \bar{K}^0\pi^-\pi^0p \end{aligned}\right\} \sim 15{,}000 \text{ events after cuts}$$

All groups performed three-body partial wave analyses of their data. The SLAC data were analyzed with the so-called amplitude approach of the LBL-SLAC program[30] while the latter two groups used the density matrix approach of the Illinois (Ascoli) program. Within the limits of the different statistics of the three data samples, the results are for the most part in good agreement. An intriguing exception to this statement comes in a comparison of the ACNO

4.2-GeV/c results with those of the higher energy analyses. While the over-all features of the partial wave mass spectra are similar, certain details of the ACNO results could indicate energy dependent differences in the production mechanisms involved. As the ACNO results are still preliminary, we must await their final results before concluding the existence of such effects.

As a reminder of the notation in 3-body partial wave analysis, we show the conventional picture in Fig. 14. It is emphasized that Fig. 14 is only a picture; the details and approximations of such an analysis are discussed extensively elsewhere.[31] The notation for a given partial wave is

$$J^P M^\eta \text{ (Isobar) } L \ .$$

We suppose some $K\pi\pi$ state is produced with spin-parity J^P in magnetic substate M. The state then decays to some isobar (e.g., K*, ρ, ϵ, or κ) and a bachelor meson with relative orbital angular momentum L. The two-body mass effects of the isobar are imposed either by means of Breit-Wigners for simple systems (K*, ρ) or by means of the known $K\pi/\pi\pi$ phase shifts for more complicated systems (ϵ, κ). The index η is a well-defined discrete quantum number corresponding to reflection invariance of the three-body decay amplitude in the production plane.[32] In the high energy limit it may be associated with the naturality of the exchanged system[33] producing the $K\pi\pi$ final state ($\eta = (-1)^{J_{exch}} P_{exch}$). Using this notation, we would refer to the Q meson as $1^+ 0^+ K^*\pi S$ and to the K*(1420) as $2^+ 1^+ K^*\pi D$.

To get an overview of the spin states involved, we show in Fig. 15 the mass spectrum and total J^P (summed over isobars and M) contributions from the SLAC analysis[34] for the $(K\pi\pi)^+$ system. The broad Q bump from 1.2 to 1.4 GeV/c stands out clearly in the total mass spectrum; the second bump at $\sim$ 1.7 GeV

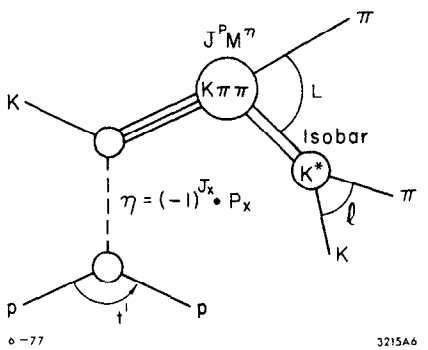

Fig. 14 Schematic illustration of the labels for three body partial wave amplitudes in production experiments.

corresponds to the L region. Below the total mass spectrum, we see that 1^+ is indeed dominant in the Q region, although 0^- becomes equally important just beyond 1.4 GeV. Note the intriguing hint of a second 1^+ bump at $\sim$ 1.7 GeV. The small 2^+ signal appears just where we expect; it is only about 5% of the total cross section. At the bottom of Fig. 15, we see the remaining contributions to the L region. The 2^- shows a broad peak from 1.65 to 1.85 GeV, and there is a hint of a peak in 3^+ at $\sim$ 1.8 GeV. A very similar picture emerges for the $(K\pi\pi)^-$ system as seen in the data of a bubble chamber collaboration,[35] Fig. 16. Indeed, if one is optimistic there is even a K*(1780) signal to be seen, though the evidence is marginal.

Were this χ spectroscopy where backgrounds are either small or well understood, we would be happy to accept these J^P bumps as resonances. Unfortunately, as mentioned in the Introduction, effects associated with the Deck mechanism preclude such straightforward conclusions. In particular, the Deck effect tells us[36] that a K*(890) and a π in an S-wave will yield a bump with $J^P = 1^+$ just above threshold, say at $\sim$ 1.2 GeV. Similarly a K*(1420) and a π in an S-wave will yield a 2^- bump precisely in the L-region. It is evident that to see whether there is any resonant signal amidst this Deck background we must go further. We must subdivide the total J^P contents into their individual isobar contributions. We must study whether any relative phase motion exists between distinct amplitudes and whether such phase behavior is characteristic of resonances.

The $J^P = 1^+ K^*\pi$ and ρK Partial Waves

In Fig. 17 we show some of the $K^*\pi$ partial waves measured in the t-channel from the SLAC analysis.[27] Underneath each partial wave mass spectrum is shown the phase of the indicated wave relative to $1^+0^+K^*\pi$ (for which, of course,

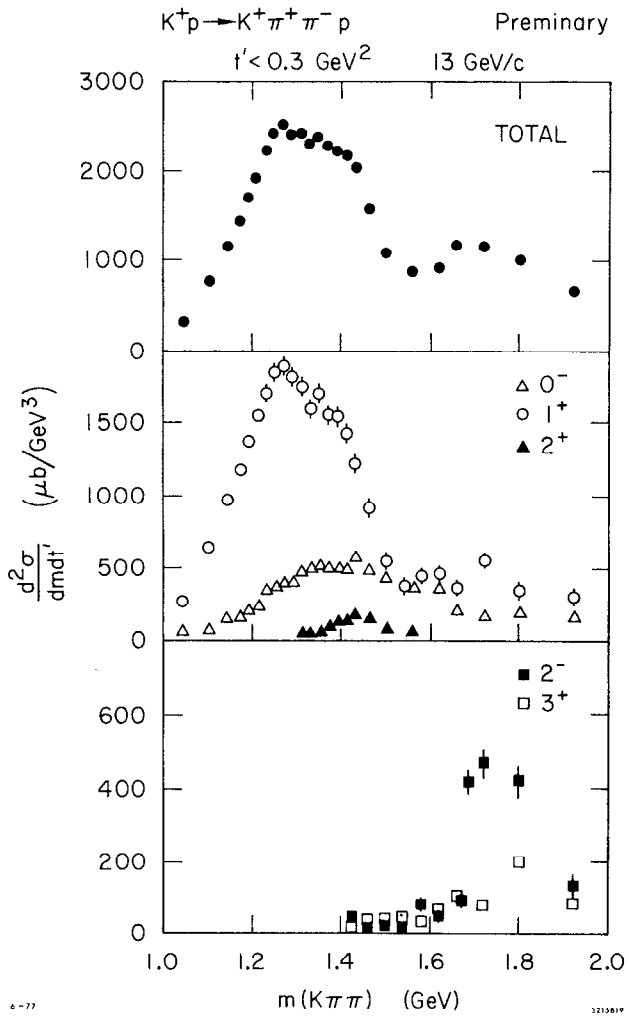

Fig. 15 Mass spectrum and total J^P (summed over M^2 and isobars) for the SLAC 13 GeV/c K^+ data.

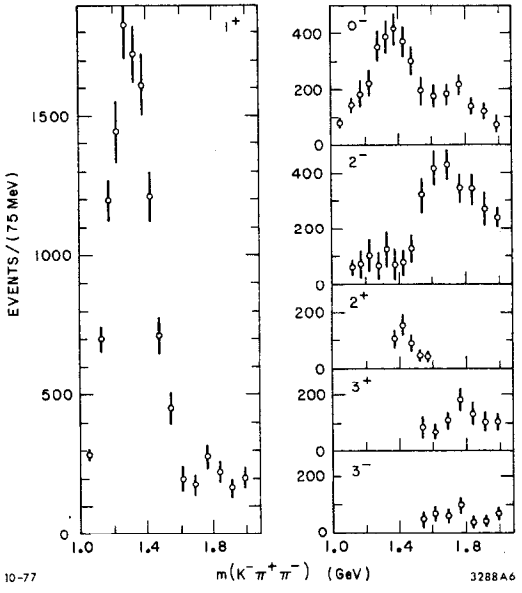

Fig. 16 Total J^P mass spectra from a K^- bubble chamber collaboration. (Ref. 35)

no relative phase is shown). The $1^+0^+K^*\pi$ spectrum for the K^+ data shows a peak at ~ 1.2 GeV and a shoulder at ~ 1.38 GeV; the same spectrum for the K^- data, however, shows two peaks at these masses. The small crosses in the K^- figures denote ambiguous, lower likelihood solutions; no such ambiguities have been observed in the K^+ data or in the K^- data above 1.3 GeV. The contribution of the $1^+1^+K^*\pi$ wave (Fig. 17-c, -d) is only about 10% that of $1^+0^+K^*\pi$; this ratio indicates the production mechanism is roughly t-channel helicity conserving. In Fig. 17-e and -f are seen definite signals corresponding to the K*(1420). Notice that in the region of good signal ($\gtrsim 20\,\mu b/GeV^3$), the phase relative to $1^+0^+K^*$ does not exhibit the expected Breit-Wigner motion.

The $1^+\rho K$ partial waves are shown in Fig. 18. As before, the phases shown are measured relative to the dominant $1^+0^+K^*\pi$ wave. What we see here is extremely different from the $1^+K^*\pi$ system of Fig. 17. First the K^+ and K^- results are essentially the same. Secondly, there is only one single peak at $\sim$ 1.27 GeV with a width of ~ 0.15. Thirdly, there is very pronounced relative phase motion: a forward motion for $1.2 < m(K\pi\pi) < 1.35$ GeV and a backward motion for $m(K\pi\pi) > 1.35$ GeV. Lastly, the ratio of M = 1 to M = 0 cross section is only about 1/3; this, in fact, indicates that the production mechanism for these waves conserves s-channel helicity.[27,28]

An attempt to tie all these observations together with a simple qualitative model is instructive. First we assume the presence of a Deck contribution[37] which peaks at ~ 1.2 GeV and whose amplitude has a constant absolute phase at all $K\pi\pi$ masses. We also suppose the Deck effect is present principally in the $K^*\pi$ channel. Next we assume the presence of two Q mesons with rather unique couplings. We take Q_1 to be at ~ 1.28 GeV with a coupling only to the ρK channel. For Q_2, at ~ 1.39 GeV, we assume a coupling only to $K^*\pi$. Both states would have widths of $\lesssim 0.2$ GeV.

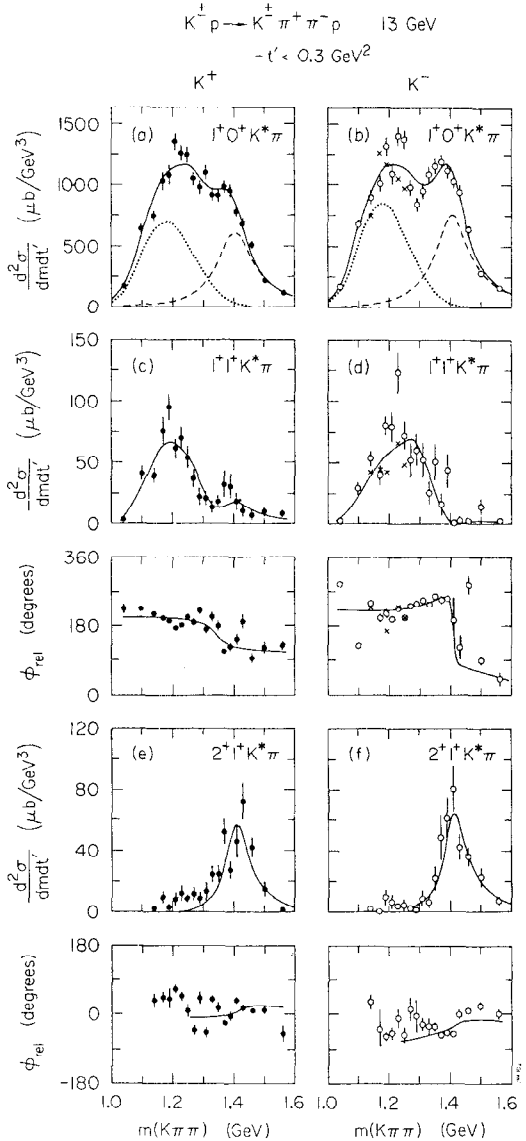

Fig. 17 Some $K^*\pi$ waves from the SLAC experiment. Phases are measured relative to $1^+0^+K^+\pi^+$. The curves correspond to the simple model discussed in the text.

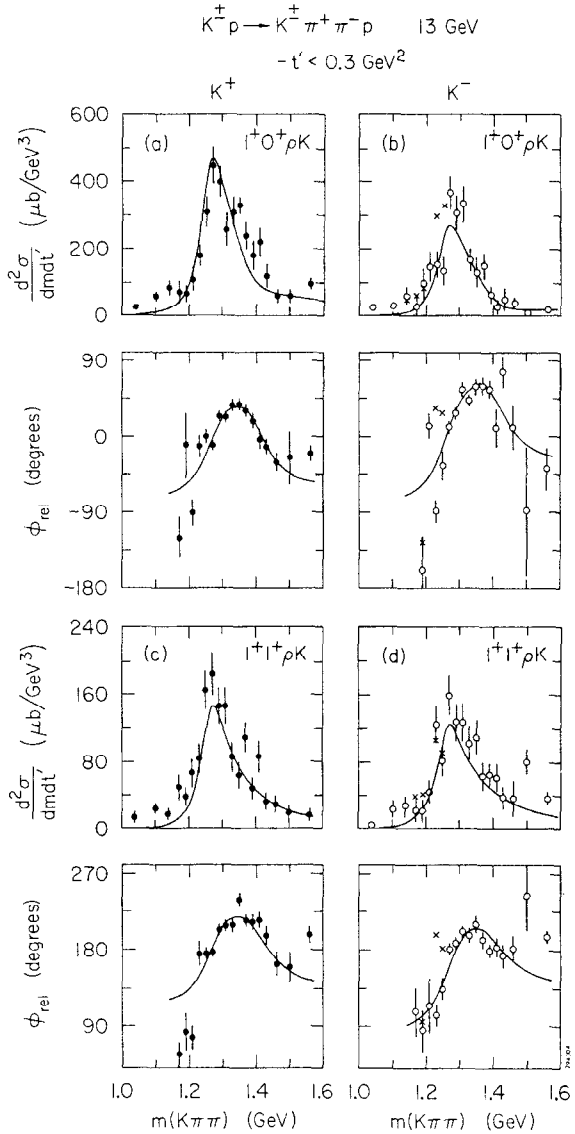

Fig. 18 The $1^+\rho K$ waves from the SLAC experiment. Phases are measured relative to $1^+0^+K^+\pi$. The curves correspond to the simple model discussed in the text.

By construction this simple picture could describe the peaks observed in the mass spectrum. The choice of couplings and the constant phase of the Deck amplitude yield a description of the observed phase motion. Thus, in the region of Q_1, ~ 1.28 GeV, we expect to see the phase for $1^+\rho K$ move forward relative to $1^+K^*\pi$ because Q_1 decouples from $K^*\pi$. Similarly, in the region of Q_2, ~ 1.39 GeV, we expect to see the same phase move backwards, since Q_2 does not couple to ρK and since we are well beyond the mass of Q_1 so that its absolute phase is now moving slowly. These arguments are illustrated in Fig. 19. Note that if Q_1 and Q_2 had the same mass and width (solid and dotted curves), then the relative phase would be constant (zero in Fig. 19). However, suppose Q_2 had a larger mass and a different production phase as indicated by the dashed curve. In this case the relative phase (dot-dashed) would be just like that observed in Fig. 18.

There is a further consequence for phases from this simple picture. In Fig. 20, we show the $2^+1^+K^*$ wave ($K^*(1420)$) in greater detail for the K^- data of SLAC[27] and that of Otter et al.[28] Again the phase is measured relative to $1^+0^+K^*\pi$. The dashed curve is the expected phase motion if the $1^+0^+K^*\pi$ wave had a constant absolute phase; the solid curve is the behavior expected if the phase of $1^+0^+K^*\pi$ wave were that of a resonance with mass ~ 1.38 GeV and width $\sim .28$ GeV.

Quantitative Description of the $J^P = 1^+$ Waves

Of course, such qualitative arguments must be taken with a grain of salt until they can be shown to reproduce the quantitative features of the data. With this in mind, the SLAC group have fit[38] a simple model to their partial wave data. The essential ingredients of their model are contained in the following

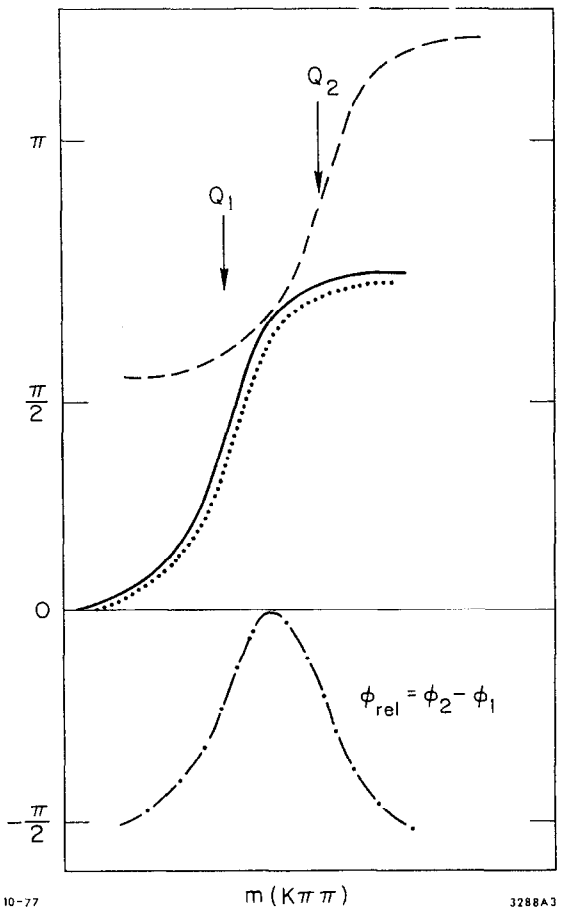

Fig. 19 Illustration of the qualitative description of the $1^+\rho K(\phi_2)$, $1^+0^+K^*\pi$ (ϕ_1) relative phase motion.

equations:

$$A(1^+K^*\pi) = D\, e^{-\left(m^2 - m_0^2\right)/\sigma^2} + A_{Q_1} \frac{\gamma^{(1)}_{K^*}}{BW(Q_1)} + A_{Q_2} \frac{\gamma^{(2)}_{K^*}}{BW(Q_2)}$$

$$A(1^+\rho K) = A_{Q_1} \frac{\gamma^{(1)}_{\rho}}{BW(Q_1)} + A_{Q_2} \frac{\gamma^{(2)}_{\rho}}{BW(Q_2)}$$

Here BW denotes the usual denominator of a Breit-Wigner amplitude. The production amplitudes, A_{Q_1} and A_{Q_2}, are taken to be complex numbers; note they are the same for $1^+K^*\pi$ and $1^+\rho K$. The γ denote different (real) couplings for Q_1, Q_2 and the $K^*\pi$, ρK channels. The Deck contribution, which exists only to the $K^*\pi$ channel, is parametrized as a real amplitude with Gaussian shape.

The results of fits to the SLAC data with such expressions are shown in Fig. 17 and 18. The $1^+\rho K$ mass spectra are essentially described by a single Breit-Wigner corresponding to $Q_1(1290)$ since $\gamma^{(2)}_{\rho} \approx 0$. The phase of $1^+\rho K$ relative to $1^+K^*\pi$ is reproduced much as the qualitative model suggests. In the $1^+0^+K^*\pi$ channel we see general agreement, though the peaks at ~ 1.2 GeV are not quite filled out. A somewhat more flexible background (Deck) parametrization could accomplish this. The relative contributions of background and $Q_2(1390)$ are indicated by dotted and dashed lines, respectively. As there is essentially no contribution from $Q_1\left(\gamma^{(1)}_{K^*} \approx 0\right)$ to $K^*\pi$, nearly half the cross section for $1^+0^+K^*\pi$ in the Q region is due to the interference of background and Q_2.

Despite the attractive simplicity of this model, there exists several criticisms which must be noted. In the first place, the SLAC model adds linearly the contributions of nearby resonances; it is well known[39] that the simple addition of resonance contributions produces an amplitude inconsistent with unitarity. Secondly, the Gaussian background is at complete odds with the first-order expectations[40] of the Deck amplitude. Not only is it too narrow but the shape of its leading and falling edges are also just the opposite that of the Deck mechanism. Lastly, the linear addition of background to resonance contributions is certainly not what we would expect from a proper treatment of final state interactions.[41]

These issues have been addressed in two independent studies of the SLAC results. Bowler[42] has produced a model which combines two resonances in a unitary fashion and properly incorporates Deck effects through final state interaction theory. His Deck amplitude is constrained to have the known[40] shape, but he leaves its strength and phase free. These unknowns as well as the resonance parameters are found by fitting his model to the SLAC data. Although there are some differences in detail, the resonances he finds are quite similar to those of the SLAC model. In addition, Bowler argues that a quantitative description of the SLAC data with only one Q meson is extremely unlikely.

Using a similar model, Basdevant and Berger have also studied the SLAC results. Their work differs from Bowler's principally in their attitude towards the Deck amplitude, which from the very outset they take as fixed in magnitude, shape and phase. In their initial effort,[43] they argued that the SLAC data could be described using the Deck amplitude and only one resonance, $Q_1 = Q_B$. Although this particularly transparent model suggests many of the features of the SLAC data, it can by no means be considered a quantitative description. More recently, through work[44] on the A_1, Basdevant and Berger have come to suspect[45] the existence of a second Q meson. One of the problems with the Deck amplitude is that its high mass tail simply does not fall off as rapidly as the $K\pi\pi$ data do in the region above 1.4 GeV. Indeed, to remove this problem they now believe a

second Q is needed to "eat out" this Deck tail through the mechanism of final state interaction.

There is an emerging consensus that a quantitative description of the SLAC data will require the existence of two Q mesons. Of course, the parameters of these states may depend on the specific details of the Deck amplitude. With this cautionary remark in mind, we turn to a discussion of the parameters of Q_1 and Q_2 and their SU(3) implications.

SU(3) Systematics of Q Mesons

In an attempt to incorporate the systematic uncertainties mentioned in the last section, the SLAC group have presented[46] a set of parameters for Q_1 and Q_2 which average the results of their fit and that of Bowler. The results are given in Table 2.

Table 2

Summary[46] of the partial widths for $Q_1(1290)$ and $Q_2(1400)$. A best estimate for the masses of the states are $m(Q_1) = 1290 \pm 3(25)$ MeV and $m(Q_2) = 1400 \pm 3(10)$ MeV. Units are MeV.

State	Total	$K^*\pi$	ρK	ωK	$\kappa\pi$	ϵK
$Q_1(1290)$	210 ± 80	12 ± 12	100 ± 35	32 ± 11	35 ± 13	29 ± 10
$Q_2(1400)$	190 ± 65	154 ± 52	2 ± 1	~ 0	~ 0	31 ± 11

The $\kappa\pi$ and ϵK modes are seen directly in the SLAC experiment[47]; the ωK modes are inferred[48] from the results of Ref. 49. Note that although the principal mode of Q_1 is to ρK, this channel is responsible for only half the total width.

Given these results we may now discuss the SU(3) classification of Q_1 and Q_2. In the context of a broken symmetry such as SU(3), it was realized long ago[50] that the physical Q's would be mixtures of Q_A and Q_B, the octet partners of the A_1 and B mesons. In the usual manner, the Q_1 and Q_2 states are mixtures of Q_A and Q_B states governed by an angle θ_Q. One of the ways we sense this mixing in the physical world is through a study of the various decay rates for the Q's. This is illustrated in Table 3, where we give the decay amplitudes

Table 3

SU(3) decay amplitudes for Q_1 and Q_2. The couplings g_A and g_B are the F-type and D-type couplings for vector-pseudoscalar decays of the A_1 and B octet states, respectively. The Q_A-Q_B mixing angle is θ_Q.

MODE	Q_1	Q_2
$K^*\pi$	$\frac{1}{2} g_A \cos\theta_Q + \frac{3}{\sqrt{20}} g_B \sin\theta_Q$	$-\frac{1}{2} g_A \sin\theta_Q + \frac{3}{\sqrt{20}} g_B \cos\theta_Q$
ρK	$\frac{1}{2} g_A \cos\theta_Q - \frac{3}{\sqrt{20}} g_B \sin\theta_Q$	$-\frac{1}{2} g_A \sin\theta_Q - \frac{3}{\sqrt{20}} g_B \cos\theta_Q$

for Q_1 and Q_2 to ρK and $K^*\pi$. The constants g_A and g_B are the F-type and D-type couplings of the A_1 and B nonets, respectively.[51] As a simple example of how things go, suppose $g_A \approx -g_B$ and $\theta_Q \approx 45^o$. To make the arithmetic even easier, let's set $1/2 \approx 3/\sqrt{20}$. We find immediately that Q_1 has zero coupling to $K^*\pi$, that Q_2 has zero coupling to ρK, and that the other couplings are equal, though of opposite sign. Note that this is precisely the decoupling scheme which was central to the SLAC interpretation of the relative $1^+\rho K - 1^+0^+K^+\pi$ phase motion.

A quantitative analysis for g_A, g_B and θ_Q proceeds as follows. Making

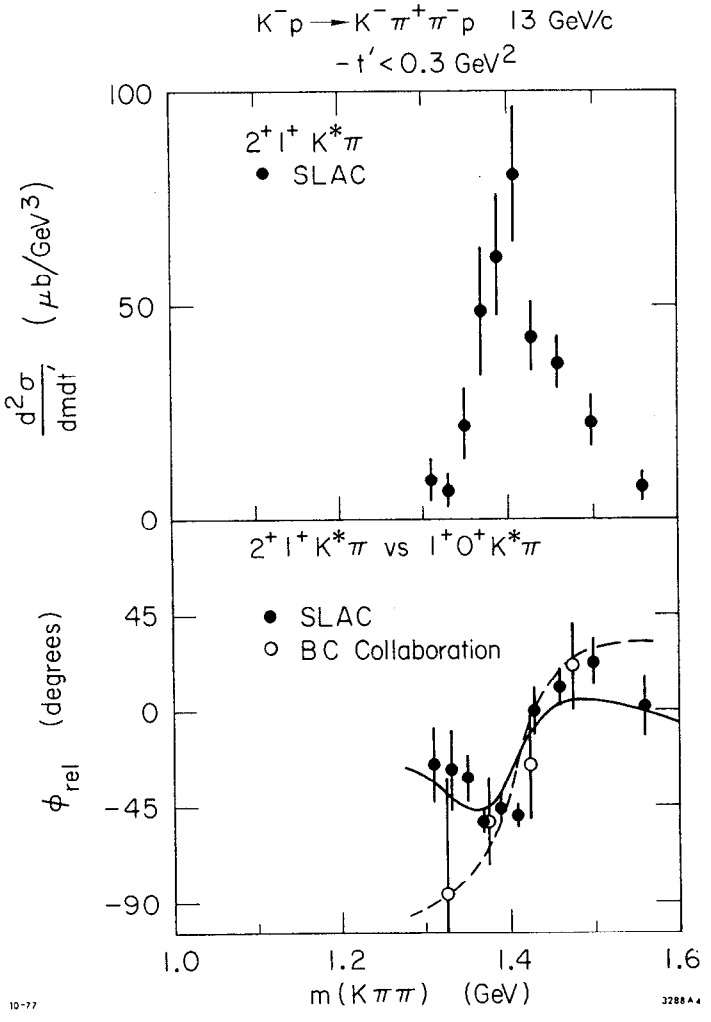

Fig. 20 The $2^+1^+K^*\pi$ wave in greater detail. The solid curve corresponds to the difference between Breit-Wigner phases for $K^+(1420)$ and $Q_2(1400)(1^+0^+K^*\pi)$ with a 280 MeV width. The dashed curve corresponds to a constant phase for $1^+0^+K^*\pi$.

some definition of phase space[46,48]

$$\Gamma = (q/m^2)\ \gamma^2$$

we obtain an estimate of γ from the known partial widths, Γ, for axial vector meson decays. Expressions such as those in Table 3 are readily found[3,46] for the various decay amplitudes in terms of the octet couplings and various mixing angles. A least squares fit of the expressions to our estimates for the γ yields a best estimate of g_A, g_B and θ_Q. Note (see Table 3) that for a given value of θ_Q, the decay amplitudes are linear in g_A and g_B. We may assess the quality of such a fit by seeing how well bands representing the measured amplitudes intersect on a plot of g_A vs g_B. This is illustrated in Fig. 21. The best estimate for the S-wave axial vector couplings (for vector pseudoscalar decays) and mixing angle are

$$g_A = +1.7 \pm 0.2\ \text{GeV}, \qquad g_B = -0.83 \pm 0.03\ \text{GeV}, \qquad \theta_Q = 41^\circ \pm 4^\circ\ .$$

The value of g_B is essentially determined by the S-wave width of $B \to \omega\pi$. The broadness of the bands for the principal Q decays, $Q_1 \to \rho K$ and $Q_2 \to K^*\pi$, reflects the systematic uncertainties in these rates. Given these uncertainties, the SU(3) consistency of the Q decays is quite satisfactory.

Knowledge of g_A and θ_Q permits us to estimate some of the parameters of the elusive A_1. We start with the width to $\rho\pi$,

$$\Gamma(A_1 \to \rho\pi) = \frac{2}{3} g_A^2 \left(q/m_{A_1}^2\right)\ .$$

Without a knowledge of the A_1 mass, all we can do is set limits on this rate,

$$300 < \Gamma(A_1 \to \rho\pi) < 450\ \text{MeV}$$

for an A_1 mass in the range 1.1 to 1.5 GeV. Considerably more information is

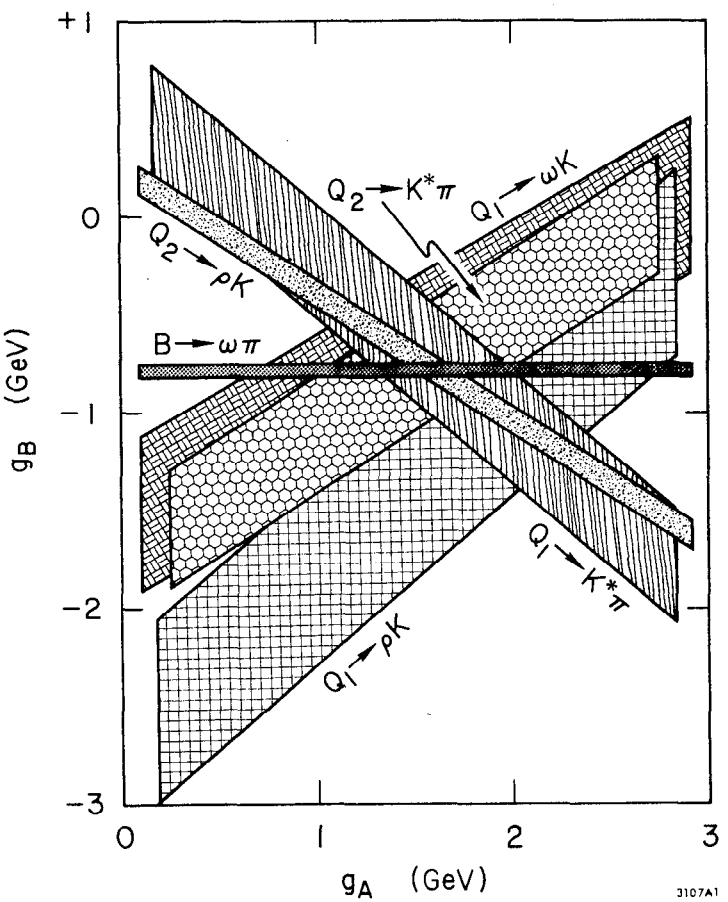

Fig. 21 g_A vs. g_B plot for θ_Q=42°. The bands correspond to measured amplitudes for various s-wave decays of axial vector mesons.

needed to estimate the A_1 mass. Taking into account singlet-octet mixing, the mass formula for the A_1 is $A_1^2 = 4Q_A^2 - 3\left(E^2\cos^2\theta_{ED} + D^2\sin^2\theta_{ED}\right)$. Here we have used particle names for masses and denote the $J^{PC} = 1^{++}$ isoscalars by E and D with a mixing angle θ_{ED}. From the masses of Q_1, Q_2 and the value of θ_Q, we know[46] that $Q_A \sim 1.34$ GeV. The D meson at 1.28 GeV most likely has $J^{PC} = 1^{++}$; the E meson at 1.42 GeV could have $J^{PC} = 1^{++}$, though $J^{PC} = 0^{-+}$ is by no means excluded. Assuming the E meson is indeed an axial vector, we may estimate[46] $|\theta_{ED}| \approx 75^\circ$ from its $K^*\bar{K}$ rate. Bringing all this information, we find

$$A_1 \sim 1.47 \text{ GeV} .$$

The result of this straightforward arithmetic is unfortunately somewhat disturbing. Note that we find $m(A_1) > m(Q_A)$! Every other known meson octet has the isospin one-half multiplet heavier than the isovector multiplet. There are other reasons for not taking $A_1 \sim 1.47$ GeV too seriously at the present time; namely, the properties of the E meson are simply not as well known as we would like. As noted earlier, if the E does not have $J^P = 1^+$, the entire calculation is meaningless. Furthermore, even if the E is an axial vector, there is new evidence[52] that suggests its other parameters could be quite different from the nominal values[3] used to estimate θ_{ED}. There are indications that the E's width could be > 100 MeV, while its branching fraction to $K^*\bar{K}$ could be as large as 90%. In addition, there is some concern that the estimate of g_A is too large. A careful inspection of Fig. 21 reveals that the rate for $Q_1 \to \rho K$ is "pulling" the fit towards larger values of g_A. Note that in determining the decay amplitude for $Q_1 \to \rho K$, we have made a definition of phase space for the ρK system. Unfortunately, although the prescription used[48] is reasonable, definitions for

phase space involving extended objects like the ρ are not unique. Suffice it to say that uncertainties in the parameters of the E as well as the value of g_A can all conspire to yield a value of $|\theta_{ED}| \approx 0$. This, in turn, gives $m(A_1) \approx 1.05$ GeV!

A Radial Excitation of the Kaon

Perhaps the most startling result of the SLAC experiment is its evidence[53] for the existence of a $J^P = 0^-$ state at 1.4 GeV. The first piece of evidence for such a state is from the peaks in the $0^- \epsilon K$ mass spectra shown in Fig. 22-a and -b). To appreciate the relative phase information shown, it is useful to review what we have discussed earlier. Recall that we have argued the existence of a state $Q_2(1400)$ with essentially no coupling to ρK. If the 0^- bump were a resonance, we would expect to see little phase motion between $0^- \epsilon K$ and $1^+ 0^+ K^* \pi$. This, indeed, is precisely what is found.[27,28,47] This fact, in itself, is already evidence that the $0^- \epsilon K$ amplitude has a moving, possibly resonant absolute phase. To make that phase motion evident, we turn to the $Q_1(1290)$ with its principal ρK decay mode. As we believe this state resonates at ~ 1.29 GeV, the absolute phase of the $1^+ \rho K$ amplitude should be moving slowly in the 1.4 GeV $K\pi\pi$ mass region. Thus, if the $0^- \epsilon K$ bump resonates, we would expect to see Breit-Wigner motion of the $0^- \epsilon K$ phase measured relative to $1^+ \rho K$. This is precisely what is seen in Fig. 22-a and -b! Note, too, that we would also expect the $2^+ 1^+ K^* \pi$ wave to show a similar behavior, as illustrated in Fig. 22-c and -d.

Were it not for the ever-present Deck effect, the evidence presented in Fig. 22 for a radial excitation of the kaon would be conclusive. However, the Deck model will be severely pressed to explain the observations discussed above. The evidence for phase motion is not the only challenge. The production distributions for the $0^- \epsilon K$ waves are much steeper than expected from the Deck model, their exponential slopes being $\sim 14 - 16$ (GeV)$^{-2}$. Additionally the 0^- system couples quite

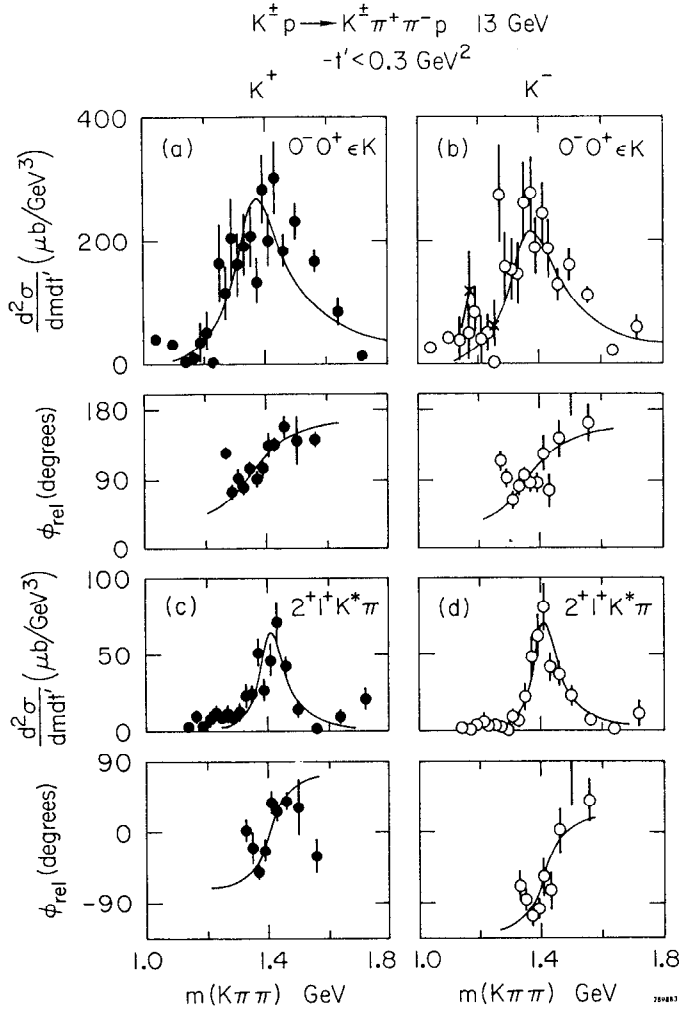

Fig. 22 The SLAC evidence for a radial excitation of the kaon in the $0^- \epsilon K$ wave. Phases are measured relative to $1^+ 0^+ \rho K$.

strongly to the $K^*\pi$ system. Such P-wave states are expected[10,36,40] to be much lower in cross section than is observed. It will indeed be interesting to see whether the present evidence for a 0^- state at 1.4 GeV survives a careful scrutiny in light of the Deck model.

Summary of the Status of K* Spectroscopy

The recent results in K* spectroscopy are summarized in Table 4.

Table 4

Summary of K* resonances. Note that parameters are given for Q_A and Q_B; information for the physical Q's is given in Table 2. For states found in $K\pi$ partial wave analyses, the elasticity x is also indicated.

J^P	Name	Mass (MeV)	Width (MeV)	Decay Modes
0^-	K	494	-	-
	K	1405 ± 15	230 ± 20	$K\epsilon$, $K^*\pi$, $K\rho$ ($K\omega$)
1^+	Q_A	1340 ± 30	≥ 250 ± 60	$K^*\pi$, $K\rho$, $K\epsilon$, $\kappa\pi$, $K\omega$
	Q_B	1355 ± 30	≥ 110 ± 10	$K^*\pi$, $K\rho$, $K\epsilon$, $\kappa\pi$, $K\omega$
0^+	κ	1250	> 400	$K\pi$ ($\pi \approx 1.0$)
	κ'	1425 ± 10	250 ± 50	$K\pi$ (x = 0.5 to 0.9), ...
1^-	K*	896 ± 1	55 ± 1	$K\pi$ ($x \approx 1.0$)
	K*'	1650 ± 50	275 ± 50	$K\pi$ ($x \sim 0.3$), ...
2^+	K**	1435 ± 1	100 ± 4	$K\pi$ (x = .49), $K^*\pi$, $K\rho$
3^-	K***	1780 ± 15	175 ± 35	$K\pi$ ($x \sim .2$), $K\pi\pi$, ...

There is little new about our old friends K(494), K*(890), and K*(1420), except that the mass of the latter state is more likely 1435. As mentioned earlier, the origin of this shift in mass lies in the evidence for κ (1425) which appears in all four partial wave solutions of the SLAC data. If one insists on calling κ (1250) a resonance, there are now perhaps too many S-wave $K\pi$ states. This is reminiscent of the confusing situation in $\pi\pi$ S-wave system with $\epsilon(600)$, $\epsilon(1200)$, and S*(990)! The K*(1780) must now be considered established with $J^P = 3^-$; there remains some doubt about its width. The existence of a second $J^P = 1^-$ state, K*(1650), in two solutions to the SLAC data is again reminiscent of the $\pi\pi$ situation. The acceptance of this state will most likely follow that of the $\rho'(1600)$.

Great strides have been made in the realism of Q mesons. There is general acceptance of at least one Q meson (Q_1); even Deck's staunchest defender believes in Q_B! Skepticism remains as to the existence of Q_2. However, all quantitative attempts to date to understand the diffractive $K\pi\pi$ partial wave results require its existence. Note that the parameters for Q_A and Q_B are given in Table 4. The indicated total widths are lower limits since an SU(3) analysis of the $\kappa\pi$ and ϵK modes is difficult given the present status of the 0^+ nonet. It is interesting that Q_B tends to have half the total width of Q_A; the comparative broadness of Q_A may explain the difficulty in pinning down the A_1. The evidence for the K'(1405) is an intriguing by-product of the partial wave analysis leading to the Q mesons. Although this evidence is persuasive, it most likely will not be taken as conclusive until the implications of the Deck model are more clearly understood for the $0^- K\pi\pi$ system.

To conclude, let us consider how well the recent results in K* spectroscopy do in filling out the expected quark levels. We show these levels and the K* candidates in Fig. 23.

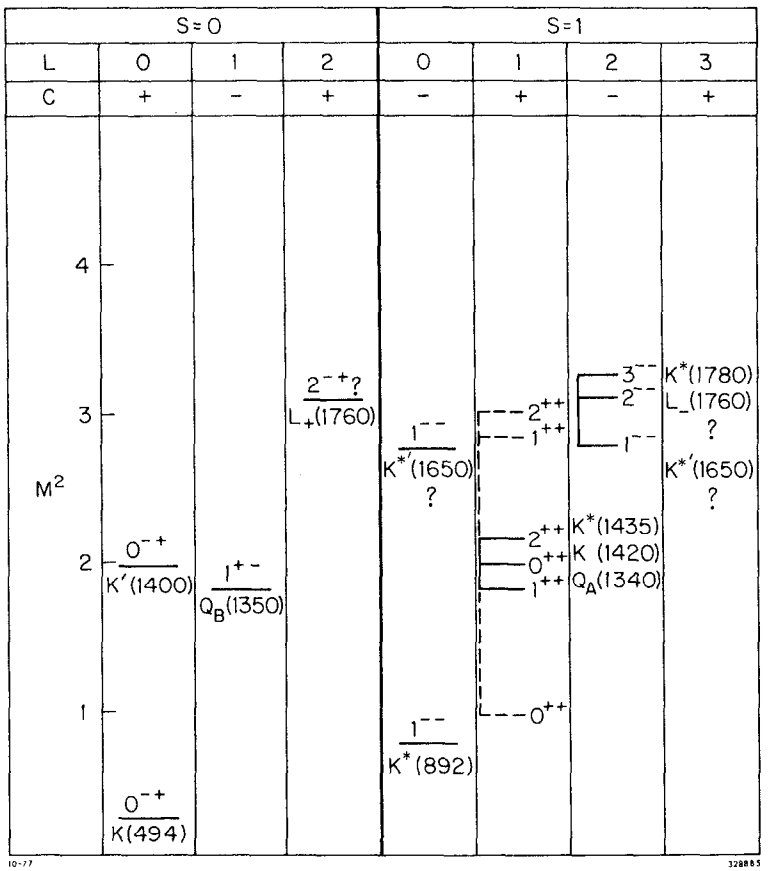

Fig. 23 Quark model level diagram illustrating the present status (1977) of K* spectroscopy.

The long suspected K*(1780) seems now established and is most likely the L=2 state. The K*'(1650) could either be a member of this multiplet or a radial excitation of the K*(892); it is thus shown in both the L=0 and L=2 columns for total quark spin S=1. While we've presented no evidence for the L mesons, other than a broad $J^P = 2^-$ bump, we indicate roughly where they could be in both C even and odd, L=2 multiplets. We might guess their ultimate story to be quite similar to that of the Q's, mixing and all.

With the evidence for $Q_A(1340)$, we can, for the first time in K* spectroscopy, consider filling out the L=1, S=1 quark multiplet. There is, however, still a problem here. If we assign the new κ (1420) to the 0^+ state, then the level spacing 1, 0, 2 is at odds with probably any simple potential model which would have 0, 1, 2. Is it that we have to take the so-called κ (1250) more seriously as a resonance? Is it that the κ (1420) is actually the lowest state of a radially excited L=1, S=1 multiplet? These questions are illustrated by the dashed lines in Fig. 23. Clearly a detailed study of K* spectroscopy at 1800 MeV and above might answer these questions. For the time being, we must take heart from the results of χ spectroscopy that the situation in the lowest lying L=1, S=1 multiplet will eventually be clarified.

Turning to the quark spin zero levels, we note that the spin of the K'(1400) bump is well determined, unlike that of $\chi(3.45)$. Indeed, there is even supporting phase evidence for a resonance interpretation. It is only the remote possibility of a "Deck explanation" which bars immediate acceptance of the K'(1400) as a radial excitation of the kaon. Finally, we end with a word of encouragement for our colleagues, the χ spectroscopists. The old spectroscopy seems to have no problem finding its lowest lying $J^{PC} = 1^{+-}$ states; both the B meson and, now,

$Q_B(1350)$ are well established. We have full confidence that, with a bit of effort, the new spectroscopy will find its missing axial vector.

Acknowledgment

I gratefully thank my colleagues R. Carnegie, R. Cashmore, W. Dunwoodie, P. Estabrooks and D. Leith for their advice, criticism, tutoring and *kvetches*.

REFERENCES

1. G. Goldhaber in Proc. of the XIIIth Int. Conf. on High-Energy Physics, U. of Calif. Press, 1967.
2. R. H. Dalitz in Proc. of the XIIIth Int. Conf. on High-Energy Physics, U. of Calif. Press, 1967.
3. Particle Data Group, Rev. Mod. Phys., No. 2, Part II, 51 (1976).
4. D. D Carmony et al., Phys. Rev. Letters 27, 1160 (1971).
   A. Firestone et al., Phys. Letters 36B, 513 (1971).
   M. Aguilar et al., Phys. Rev. Letters 30, 672 (1973).
   M. Spiro et al., Phys. Letters 60B, 389 (1976).
5. D. Lissauer et al., Nucl. Phys. B18, 491 (1970).
   P. Slattery, U. Rochester preprint, UR-875-332 (1971).
6. See Firestone, et al., ref. 4.
7. For example, A. Firestone in Experimental Meson Spectroscopy, Ed. by C. Baltay and A. H. Rosenfeld, Columbia U. Press, 1970.
8. The best results on the B meson are probably V. Chaloupka et al., Phys. Letters 51B, 407 (1974), and S. U. Chung et al., Phys. Rev. D11, 2426 (1975).
9. The A_1 situation is summarized on pages S112 - S113 of ref. 3. More recent experimental results may be found in R. Hemingway's talk.
10. See, for example, E. Berger in Three Particle Phase Shift Analysis and Meson Resonance Production, Ed. by J. Dainton and A. Hey, Daresbury Lab., 1975.
11. G. J. Feldman and M. L. Perl, SLAC-PUB-1972, sub. to Phys. Reports(1977).
12. P. Estabrooks et al., SLAC-PUB-2004, sub. to Nucl. Phys. B (1977).
13. R. Baldi et al., CERN/U. of Geneva preprint, sub. to European Conf. on Particle Physics, Budapest (1977).

14. R. Baldi et al., CERN/U. of Geneva preprint, sub. to Phys. Letters (1977).
15. S. U. Chung, private communication.
16. G. W. Brandenburg et al., Phys. Letters 60B, 478 (1976).
17. R. Baldi et al., U. of Geneva preprint (1976).
18. W. M. Dunwoodie, private communication and results presented at the Chicago APS Meeting, 1977.
19. A. Etkin et al., Phys. Rev. Letters 36, 1482 (1976).
20. Aachen-Geneva-Zurich Collaboration, paper sub. to the European Conf. on Particle Physics, Budapest (1977).
21. P. Estabrooks and A. D. Martin, Nucl. Phys. B95, 322 (1975).
22. P. Estabrooks et al., Phys. Letters 60B, 473 (1976).
23. P. Estabrooks et al., Nucl. Phys. B106, 61 (1976).
24. A. B. Wickland et al., Argonne National Lab preprint (1977).
25. Courtesy of R. Kelley, Particle Data Group.
26. P. Estabrooks and A. D. Martin, Nucl. Phys. B95, 322 (1975).
27. G. W. Brandenburg et al., Phys. Rev. Letters 36, 703, 706 (1976).
28. G. Otter et al., Nucl. Phys. B106, 77 (1976).
29. Results from the Amsterdam-CERN-Nijmegen-Oxford collaboration presented by R. Hemingway at the Experimental Meson Spectroscopy Conf., Northeastern University, Boston, 1977.
30. M. Tabak et al., LBL-3010, SLAC-PUB-1462 (1974).
D. Herndon et al., Phys. Rev. D11, 3165 (1975).
31. J. D. Hansen et al., Nucl. Phys. B81, 403 (1974); see also Three Particle Phase Shift Analysis and Meson Resonance Production, Daresbury Lab. Report DL/R34, Ed. by J. B. Dainton and A. J. G. Hey, 1975.
32. See, for example, S. U. Chung and T. L. Trueman, Phys. Rev. D11, 633 (1975).
33. G. Cohen-Tannoudji et al., Nuovo Cimento 55A, 412 (1968).
34. See ref. 27; the high mass results are unpublished, preliminary results.
35. ABCLV Collaboration of 10-, 14-, and 16-GeV/c bubble chamber results, presented at the European Conf. on Particle Physics, Budapest (1977).
36. See ref. 10 and G. Ascoli et al., Phys. Rev. D8, 3894 (1973).
37. These features of the Deck amplitude correspond roughly to those discussed in ref. 10 and 36.
38. R. K. Carnegie et al., Nucl. Physics B, 1977 (to appear).
39. R. H. Dalitz and R. G. Moorhouse, Proc. Roy. Soc. London A318, 279 (1970); C. J. Goebel and K. W. McVoy, Phys. Rev. 164, 1932 (1967).
40. L. Stodolsky, Phys. Rev. Letters 18, 973 (1967); see also ref. 10 and 36.
41. J. D. Jackson, appendix to an article in Dispersion Relations, Scottish University Summer School, Ed. by G. R. Screaton (1960).
42. M. G. Bowler, Phys. Journ. G3, 775 (1976).
43. J.-L. Basdevant and E. L. Berger, Phys. Rev. Letters 37, 977 (1976).
44. J.-L. Basdevant and E. L. Berger, Phys. Rev. D16, 657 (1977).
45. E. Berger, Private Communication, (1977).
46. R. K. Carnegie et al., Phys. Letters 68B, 287 (1977).
47. G. W. Brandenburg et al., in preparation.
48. W. M. Dunwoodie and T. A. Lasinski, SLAC Group B, Physics Note No. 60 (1976).
49. ABCLV and BBCMS collaboration, CERN/EP/PHYS (1976).
50. H. J. Lipkin, Phys. Rev. 176, 1709 (1968) and references therein.
51. The results discussed here are for S-wave decays; there is no evidence for D-wave Q decays.
52. R. J. Hemingway, Review talk at the European Conf. on Particle Physics, Budapest, (1977).
53. G. W. Brandenburg et al., Phys. Rev. Letters 36, 1239 (1976).

NEW RESULTS FROM OLD SPECTROSCOPY

R.J. Hemingway(*)

CERN, Geneva, Switzerland

ABSTRACT

A report is presented of some of the major experimental results during the last year in the field of old spectroscopy.

(*) Permanent address from September 1977, Department of Physics, Carleton University, Ottawa, Ontario, Canada.

1. INTRODUCTION

The non-relativistic quark model provides a simple scheme in which hadron classification can be discussed. In this model a classical meson is represented as a $q\bar{q}$ pair where each q has three flavours (p, n, λ). The SU(3) structure $3 \otimes 3 = 8 \oplus 1$ thus provides nonets naturally. Under orbital excitation L = 0, 1, 2, ... the meson quantum numbers follow $P = (-1)^L$, $\vec{J} = \vec{L} + \vec{S}$ [S being the $q\bar{q}$ spin 0, 1] , $C = (-1)^{L+S}$ and $G = (-1)^{L+S+I}$. Under radial excitation the quantum numbers remain unchanged, but the nonet is repeated at increased mass. Fig. 1 shows how the meson spectrum is expected to look in a simple harmonic oscillator potential. The niceties of such a scheme are: (a) all established classical mesons have a home - not too many states have been found, (b) no evidence exists for CP exotics i.e. mesons with natural parity and CP odd, or mesons with $J^{PC} = 0^{--}$ and (c) no evidence exists for flavour exotics i.e. states that cannot be made with $q\bar{q}$ (eg. I = 2, Y = 0 or I = 3/2, Y = 1).

To appreciate the rate of advance of meson spectroscopy, fig. 1(a) shows the states considered to be well established in the January 1967 edition of the PDG. Where the quantum number assignment is complete, the state is included in the relevant nonet. One should remark that even ten years ago considerable evidence existed for the δ, S^*, A_1, A_3, Q, L, B, D, E, g, K^{**}, and the $\bar{p}N$ total cross section bumps S, T, and U. Fig. 1(b) shows how this pattern had extended by April 1976 - in particular, members of the L = 2 and 3 supermultiplets and a possible radial excitation (ρ') had been added. To achieve a satisfactory advance in the meson spectrum it is essential that existing states be understood, that the supermultiplets be completed up to L = 2, and that the L = 0 radial excitation be established. This poses the following problems:

(a) The resonant nature of the low mass threshold enhancements must be established A_1, Q_A, Q_B $[J^P = 1^+]$ and A_3, $Q_{A'}$, $Q_{B'}$ $[J^P = 2^-]$.

(b) The quantum numbers of the non-classified states must be established η', δ, D, E, $\omega(1675)$ and $K_N(1800)$.

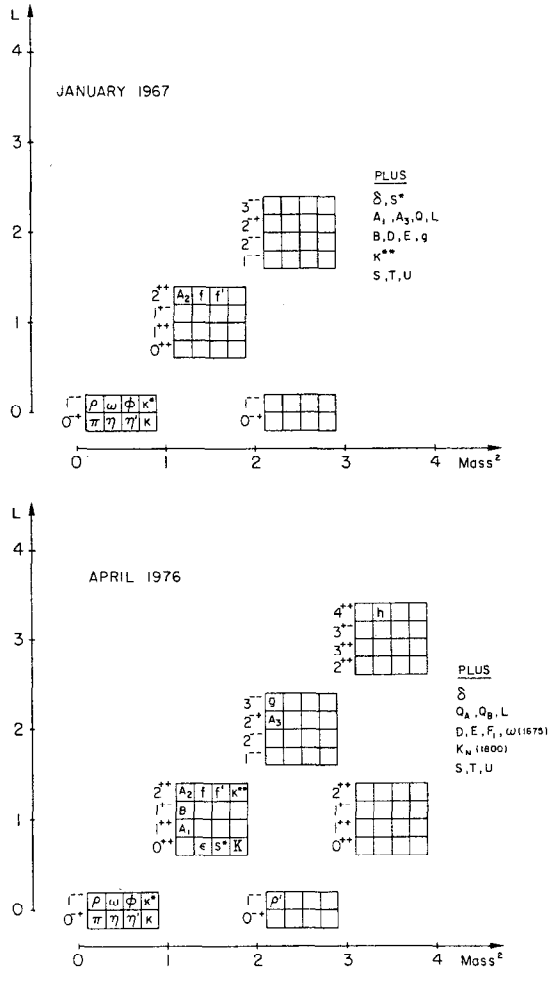

Fig. 1

Meson states from the Particle Data Group tables of January 1967 and April 1976.

(c) The resonant nature, the mass, width and couplings of the entire scalar nonet must be clarified δ, ε, S^*, κ.

(d) The seven missing members of the L = 1 supermultiplet must be found, in particular the two I = 0 $J^{PC} = 1^{+-}$ states [the other five are presumed to be δ, D, E, Q_A, Q_B].

(e) The fourteen missing members of the L = 2 supermultiplet must be found.

(f) The existence of radial excitations must be established $[\rho, \omega, \phi, K^*]'$ with $J^{PC} = 1^{--}$ and $[\pi, \eta, \eta', K]'$ with $J^{PC} = 0^{-+}$.

(g) The high mass structures in $\bar{p}N$ must be understood.

In the following report we will discuss several new results pertaining to the above problems. At the end of the meson section we will return again to the classsification scheme. To avoid repetition, those topics covered by T. Lasinski (K^* spectroscopy) and D. Trielle (CERN Ω Group) are not included here.

2. VECTOR MESON PRODUCTION - DESY, ORSAY, FRASCATI

A DESY-Frascati group at DESY have studied the photo-production off hydrogen of e^+e^- pairs at 7.2 GeV/c in a double-arm magnetic spectrometer [1]. This system enables the interference between the Bethe-Heitler and Compton amplitudes to be evaluated. The relevant interference spectra, with each arm at 13^o, 15^o, 16^o and 19^o wrt the beam, are shown in fig. 2(a). Other than the ρ/ω and ϕ peaks, a considerable excess of events is observed at higher masses - indicating possible ρ' production. More interestingly is the occurrence of a peak, especially in the 15^o data, at $\sim$ 1100 MeV with $5 \leq \Gamma \leq 30$ MeV. Fig. 2(b) shows a summary of the old plus new data - the statistical evidence for the 1100 MeV peak being 5.2 standard deviations.

An Orsay group have provided possible evidence for an excited ω state produced by e^+e^- collisions in DCI [2]. Their large solid angle detector is able to detect both charged particles and γ's. The excitation function for production of 3 or 4 charged tracks plus 1 or 2 γ's, a configuration

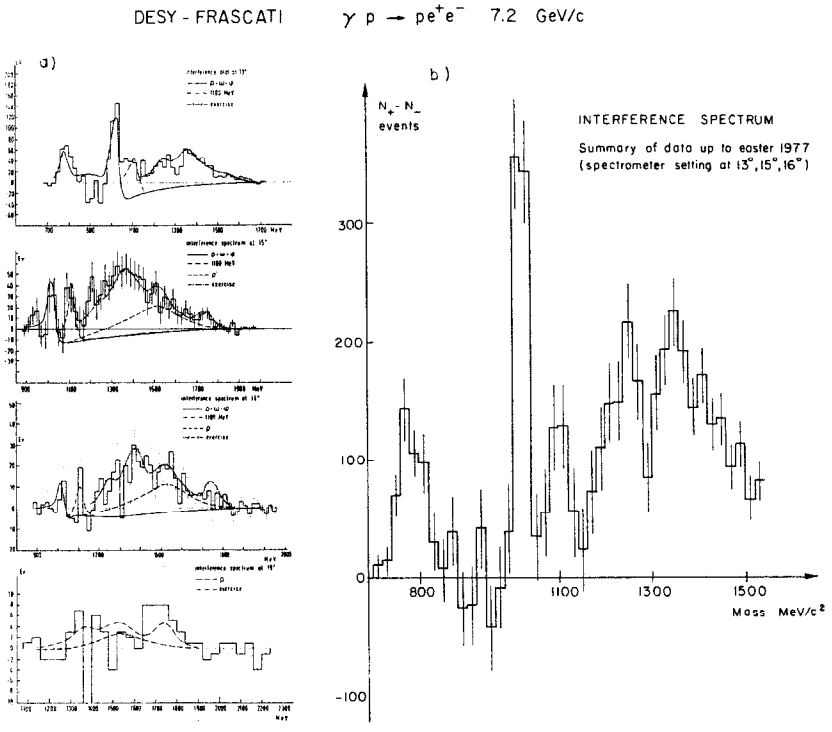

Fig. 2

Interference spectra at (a) 13^o, 15^o, 16^o and 19^o together with (b) a recent summary. The curves represent the results of fits to the data.

consistent with $\pi^+\pi^+\pi^-\pi^-\pi^o$, shows a Breit-Wigner form with M = 1778 ± 14 and Γ = 150 ± 40 MeV (fig. 3(b)). Neither the 4π (ρ'?) nor the 6, 7π configurations exhibit the same bump (figs 3(a), 3(c)). This ω', if confirmed, would probably be in the same nonet as the ρ'(1600).

From Frascati all three detection systems have reported evidence for a narrow structure near 1820 MeV [3]. Fig. 4(a) shows the results from the MEA detector with a data selection requiring $\geq$ 3 charged tracks. The narrow peak has been parametrerised to yield M = 1821 ± 16 MeV and Γ = 31 ± 15 MeV. Both the $B\bar{B}$ and $\gamma\gamma 2$ detectors confirm the narrow effect, the $\gamma\gamma 2$ group showing that the signal exists in three- or four-charged tracks plus at least one γ [i.e. $2\pi^+2\pi^-\pi^o$] and not in events without associated γ's [i.e. $2\pi^+2\pi^-$]. At the Budapest conference new data near 1500 MeV from the three systems were presented for the $\geq$ 2 charged track yield and again all three observe a narrow effect with M $\sim$ 1498 MeV and width $\Gamma \sim$ 5 MeV [4]. As an example, the data of the $B\bar{B}$ group is shown in fig. 4(b).

It is clear that the above vector meson situation is complicated and that evidence exists for surprisingly new structures. If these structures are confirmed, our naive ideas of classification may have to change in order to accommodate them

3. EVIDENCE FOR A $J^P = 3^+$ S-WAVE $(g\pi)^+$ THRESHOLD ENHANCEMENT

Recent results from the Columbia group [5] demonstrate clearly the phenomenon of low mass threshold enhancements. Fig. 5 shows data from the reaction $\pi^+p \to p\pi^+\pi^+\pi^-$ at 13 GeV/c taken in the SLAC 82" HBC with 43 events/μb. Selecting $\pi^+\pi^-$ within the ρ, f and g results in the $\pi^+\pi^+\pi^-$ exhibiting threshold enhancements A_1(M $\sim$ 1100, $\Gamma \sim$ 300), A_3(M $\sim$ 1700, $\Gamma \sim$ 300) and A_4(M $\sim$ 2200, $\Gamma \sim$ 300). A PWA of the 3π system, fig. 6, shows the corresponding spin-parity structures to be $1^+S(\rho\pi)$, $2^-S(f\pi)$ and $3^+S(g\pi)$. The 3^+ bump has a Breit-Wigner shape with M = 2214 ± 15, Γ = 355 ± 21 MeV. None of the structures show the requisite phase variation characteristic of resonance behaviour.

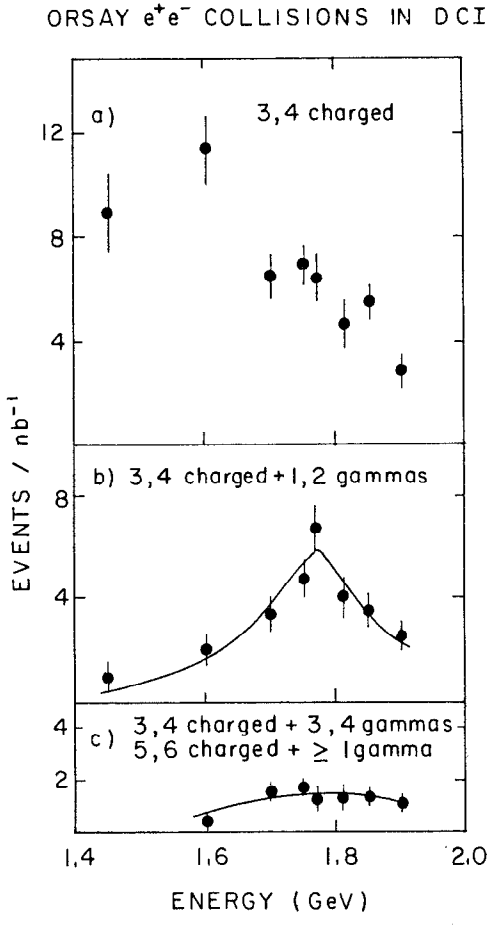

Fig. 3

Evidence for ω'(1780). The solid curve in (b) corresponds to a BW + quadratic background fit. The solid curve in (c) represents a quadratic background only.

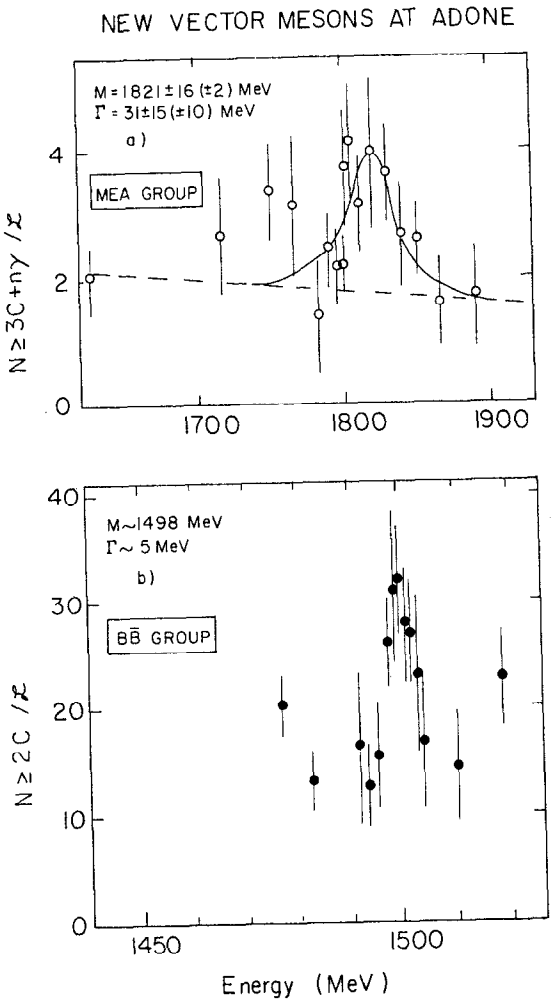

Fig. 4

Recent results from Frascati (a) yield (events/nb^{-1}) of ≥ 3 charged tracks from the MEA detector and (b) yield of ≥ 2 charged tracks from the $B\bar{B}$ detector. The curve in (a) is the result of a straight-line + BW fit.

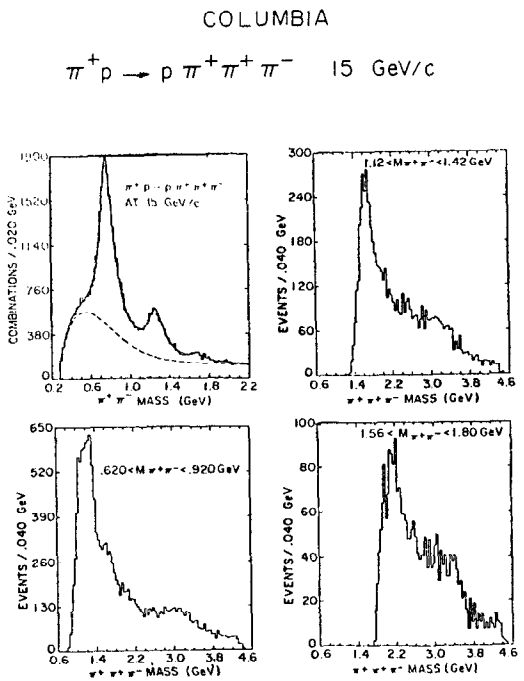

Fig. 5

Invariant mass distributions of 2π and 3π. The 3π distributions have M(2π) selected in the ρ, f or g regions.

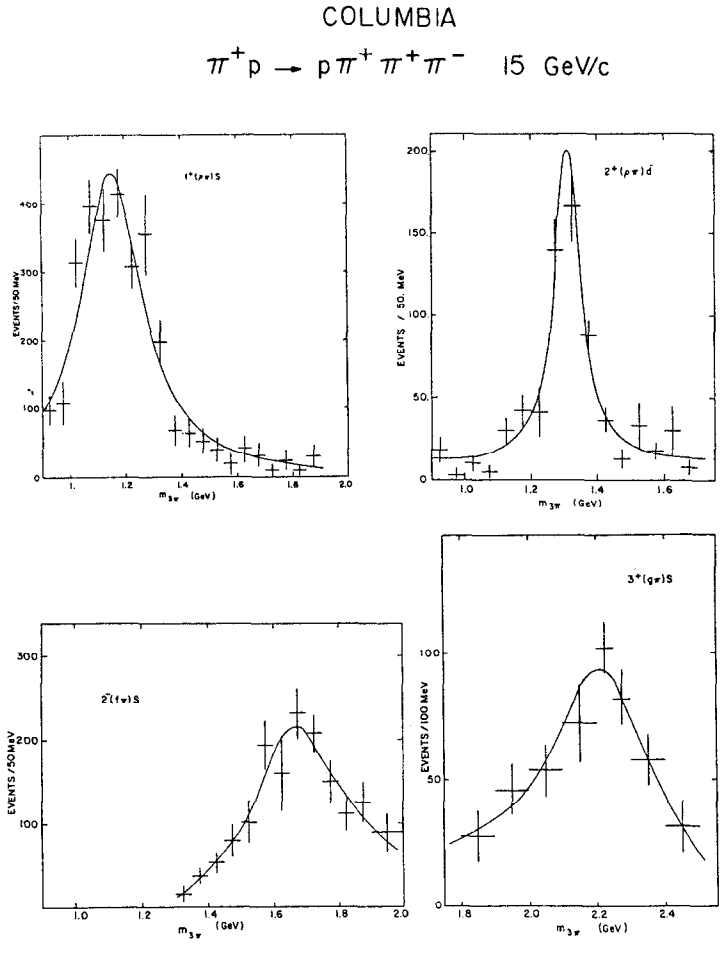

Fig. 6

Selected waves from the 3π partial wave decomposition. The curves represent the result of a fit to a BW + smooth polynomial background.

A similar gπ effect has been reported by the IHEP-CERN Collaboration [6] in an analysis of their 25 GeV/c $\pi^- p \rightarrow \pi^-\pi^-\pi^+ p$ data taken with the boson spectrometer in 1970-1972. Selecting events with a leading π^+ shows clearly the ρ, f, g and h in the 2π spectrum (fig. 7(a)). Again the gπ distribution shows a threshold enhancement (fig. 7(b)). The decay distributions are consistent with acceptance corrected expectations for a $J^P = 3^+$ state (figs 7(c-f)).

4. EVIDENCE FOR PHASE VARIATION OF A_1 AND A_3

The continual absence of phase variation for the A_1 in diffractive 3π production has spurred the analysis of non-diffractively produced 3π systems. In the charge exchange reaction $\pi^+ p \rightarrow \Delta^{++}\pi^+\pi^-\pi^0$ at 15 GeV/c the Columbia group have performed a PWA of the $\pi^+\pi^-\pi^0$ system [5]. The partial wave decomposition of the 3π spectrum (fig. 8(a)) is shown in fig. 8(b). Although the NP states $2^+(A_2)$ and $3^-(\omega(1675))$ exhibit typical BW behaviour in magnitude and phase (not shown), the 1^+ state is small and structureless and shows no phase variation. The Amsterdam-CERN-Nijmegen-Oxford Collaboration have performed a PWA of the $\pi^+\pi^-\pi^0$ system in the hypercharge exchange reaction $K^- p \rightarrow \Lambda 3\pi$ at 4.2 GeV/c [7]. Fig. 9 shows the partial wave decomposition - the NP states again being prominent. The 1^+ states, both I = 0 and I = 1, show no clear evidence for resonant structure and neither do they exhibit phase variation (not shown).

The saviour of phase variation may be in an analysis of coherent 3π production from complex nuclei. A CERN-ETH-IC-Milano Collaboration using an optical spark chamber system have accumulated 60 K events of the type $\pi^- A \rightarrow \pi^-\pi^-\pi^+ A$ using nine different targets Be-Pb at three incident momenta 8.9, 12.9 and 15.1 GeV/c [8]. Dividing the data into a coherent sample (typically $t' = t^* < 0.035$ GeV^2) and an incoherent sample ($t^* < t' < 0.5$ GeV^2), fig. 10 shows the respective partial wave decomposition. A careful analysis of the coherent data has shown two ambiguous phase solutions in the A_1 region, of which one (favoured by the authors) shows in fig. 11(a) a resonance behaviour for 1^+S. The constancy of phase between 1^+S and

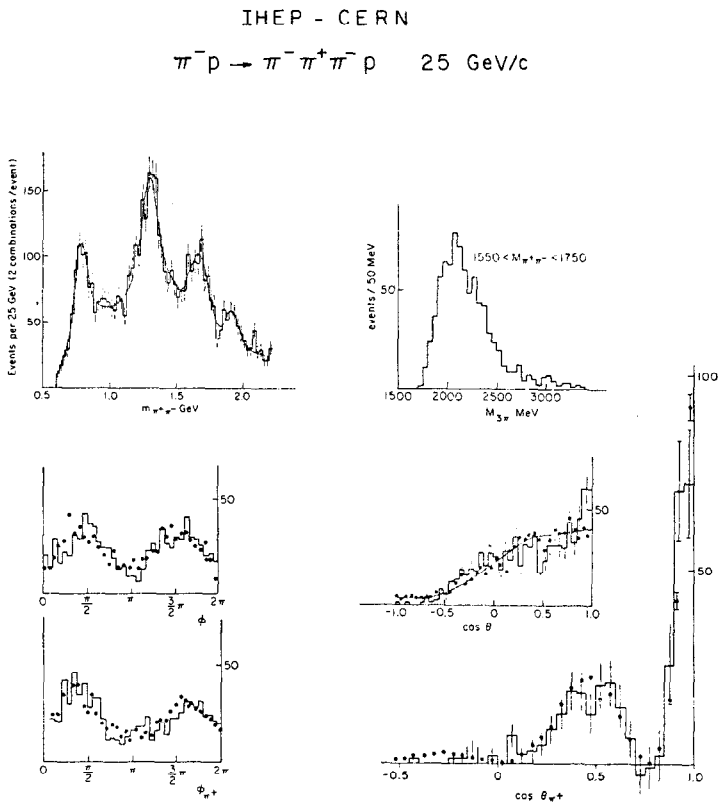

Fig. 7

Invariant mass distributions of 2π and 3π, and $g\pi$ decay distributions. ϕ, cos $\theta(\phi_{\pi^+}$, cos $\theta_{\pi^+})$ represent the $A_{f} \to g\pi$ $(g \to \pi\pi)$ decay angles compared to Monte-Carlo predictions for a $J^P = 3^+$ state.

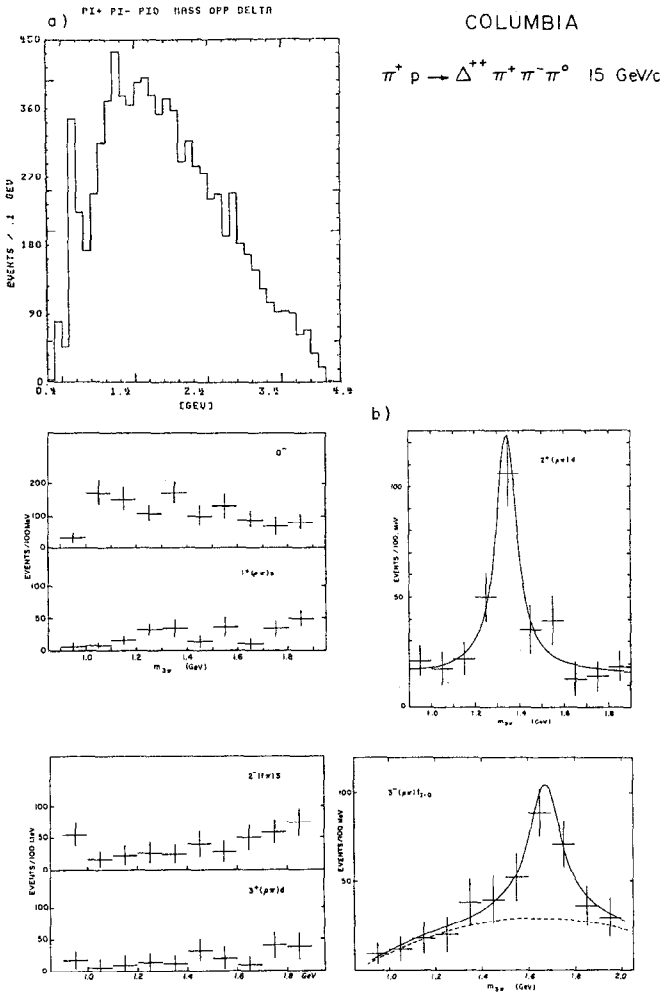

Fig. 8

(a) Invariant mass distribution of $\pi^+\pi^-\pi^0$ and (b) prominent contributions to the partial wave decomposition. The curves represent the result of BW+background fits.

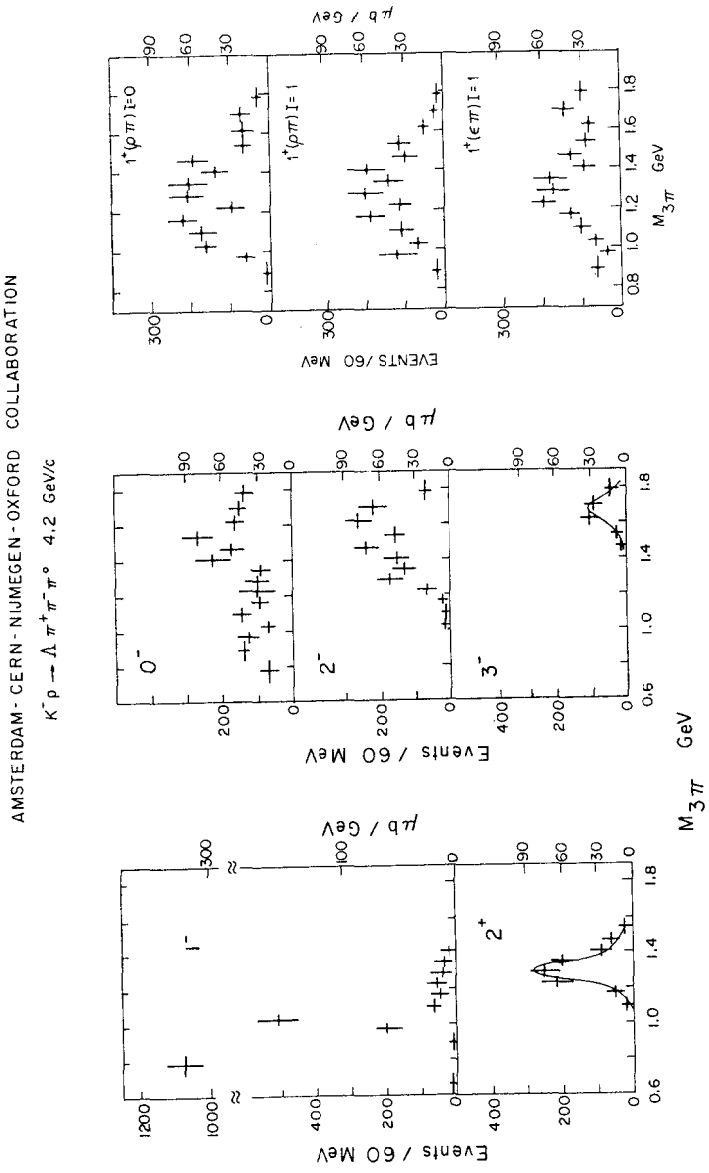

Fig. 9

Partial wave cross-sections as a function of $M(\pi^+\pi^-\pi^0)$. Curves in the 2^+ and 3^- spectra correspond to BW shapes with masses and widths from the PDGT.

1^+P implies that 1^+P also resonates. Fig. 11(b) shows for both samples resonant phase behaviour for 2^-S and 2^-P (with amplitudes of opposite sign) and also for the A_2 2^+D. The mass and width parameters of the A_1 and A_3 are somewhat uncertain since they are strongly influenced by the form of the dipion parametrization and by the nuclear form factor.

5. BARYON EXCHANGE PRODUCTION OF A_1

The Amsterdam-CERN-Nijmegen-Oxford Collaboration have reported evidence in a large statistics (128 events/μb) bubble chamber experiment for a $1^+\rho\pi$ enhancement produced via baryon exchange in the reaction $K^- p \to \Sigma^- \pi^+ \pi^+ \pi^-$ at 4.2 GeV/c [9]. Fig. 12(a) shows the Chew-Low plot for their sample of 13 K events - one sees an accumulation at small $K^- \to \Sigma^-$ momentum transfer for $M(3\pi) \sim 1$ GeV. This is seen more clearly in fig. 12(b) where the 3π mass spectrum is shown for $t_{K\Sigma} < 0.7$ GeV^2. Two enhancements are visible - one at $M(3\pi) \sim 1$ GeV, the second near the A_2 position, and both remain when a ρπ selection is made. A fit to this distribution has given the parameters of the lower mass bump $M = 1041 \pm 13$ MeV, $\Gamma = 230 \pm 50$ MeV. By parametrizing the Dalitz plot population in terms of Zemach amplitudes the 3π partial wave decomposition has been extracted - and is shown in fig. 13. Only the $1^+S(\rho\pi)$ wave contributes significantly in the 1 GeV region, its size and position corresponding well with the bump in the 3π mass spectrum. The total cross section for the reaction $K^- p \to \Sigma^- A_1$, $A_1 \to \rho\pi$ is measured to be 7.2 ± 1.0 μb.

In the talk by Treille evidence was presented for backward A_1 production, with a similar mass and width, observed in $\pi^- p$ interactions at 9 GeV/c and 12 GeV/c [10].

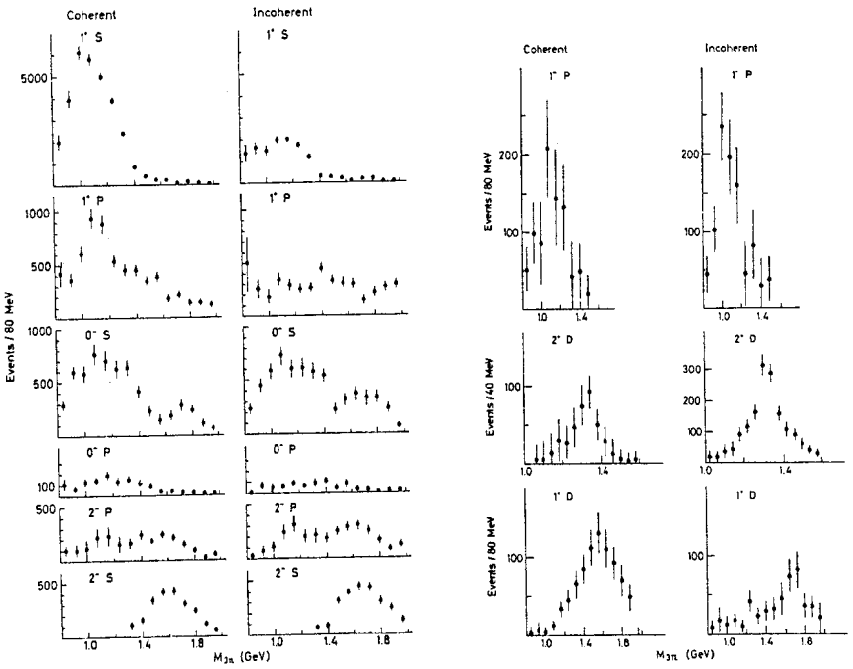

Fig. 10

Partial wave decomposition of both coherent and incoherent 3π samples

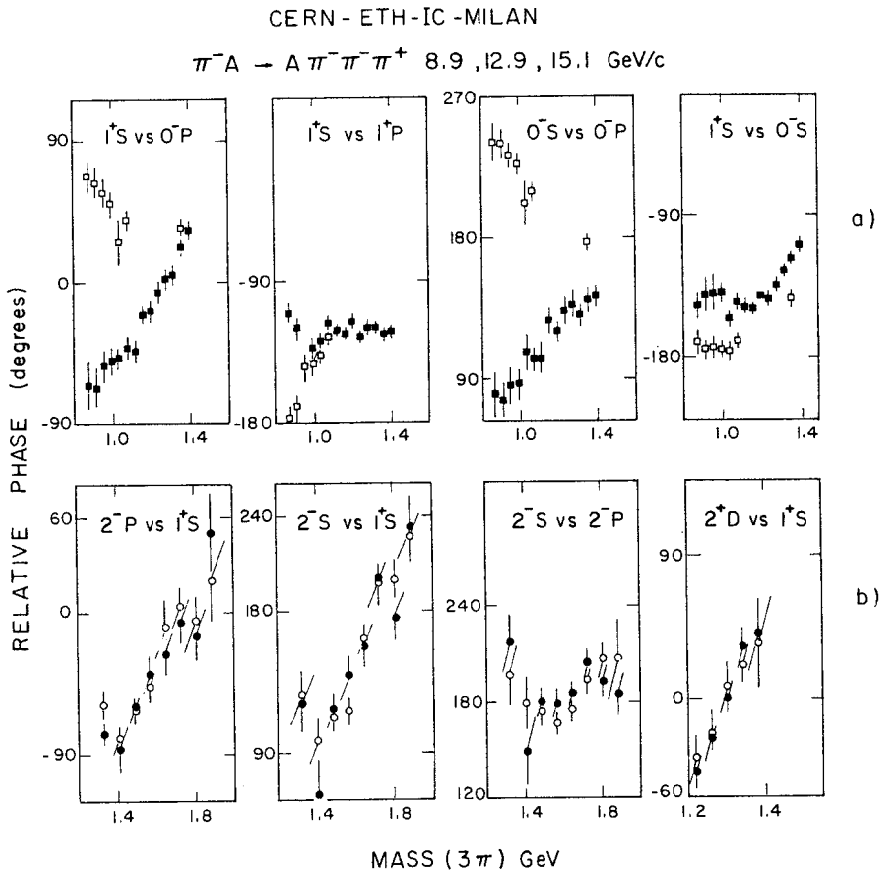

Fig. 11

Selected relative phase variations. The solid (open) points in (a) represent solution 1 (2) for the coherent sample. The solid (open) points in (b) correspond to the coherent (incoherent) samples.

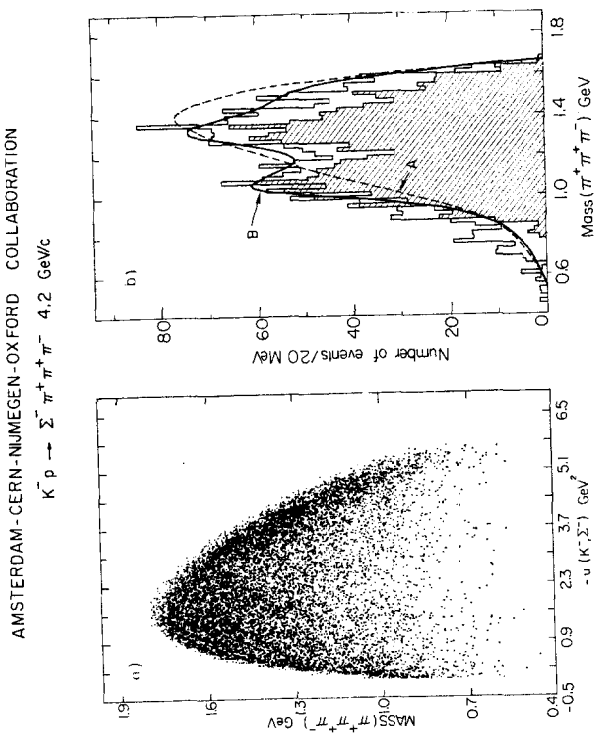

Fig. 12

(a) Chew-Low plot and (b) 3π mass distribution with $u < 0.7$ GeV^2. The shaded distribution represents ρπ and the solid (dotted) curve corresponds to a fit including (excluding) A_1 and A_2

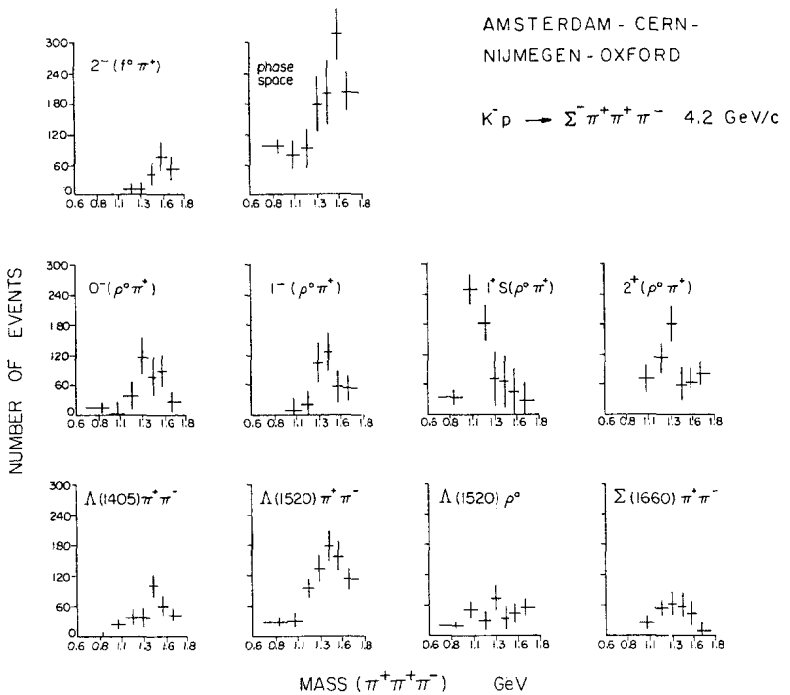

Fig. 13

Minimum complexity partial-wave decomposition of the 3π system with $u < 1.2$ GeV.

6. THE DEMISE OF THE $F_1(1540)$

A Bombay-CERN-Collège de France-Madrid Collaboration has found no evidence of $F_1(1540)$ production in a 22 events/μb exposure of $\bar{p}p$ interactions at 760 MeV/c [11]. A comparison of this new data, 4517 events of the type $\bar{p}p \to K_1^o(K^o)\pi^+\pi^-$, with the original evidence for the F_1, 1305 events at 700 MeV/c, is shown in fig. 14. The clear discrepancy has led to a reanalysis of the original data - the end result being that the original evidence was a systematic effect due to event misidentification. It is perhaps indicative that very little supporting evidence exists in the literature.

7. FIRST EVIDENCE FOR A $J^P = 4^+$ I = 1 STATE

The University of Geneva-CERN group have obtained evidence for a $J^P = 4^+$ I = 1 state observed in the reaction $\pi^- p \to K_s^o K^- p$ at 10 GeV/c [12]. Data have been taken in the University of Geneva two-arm spectrometer in which the forward arm with no magnetic momentum analysis allows a large solid angle acceptance. In the t-range 0.05 - 1.0 GeV^2, 75 10^6 triggers with ⩾ 3 forward tracks have yielded 40 K events of the type $\pi^- p \to K_s^o K^- p$. Fig. 15(a) shows the acceptance corrected mass spectrum after removing events with $M(pK^-) < 1.9$ GeV to eliminate Y^* reflection at high $K_s^o K^-$ mass. The A_2 and g peaks are clearly seen together with an indication of a third bump ∿ 1.9 GeV. Fig. 15(b) shows the Y_6, Y_7 and Y_8 moments plotted in 50 MeV bins in the higher mass region. Clear indication of resonant behaviour is visible at ∿ 1.9 GeV, especially in the Y_7^o and Y_8^o moments - thus implying J ⩾ 4. Such a behaviour has been interpreted by the authors as evidence for an I = 1, $J^P = 4^+$ object with M ∿ 1950 MeV and Γ ∿ 150 MeV. This state would naturally be the I = 1 companion of the h meson.

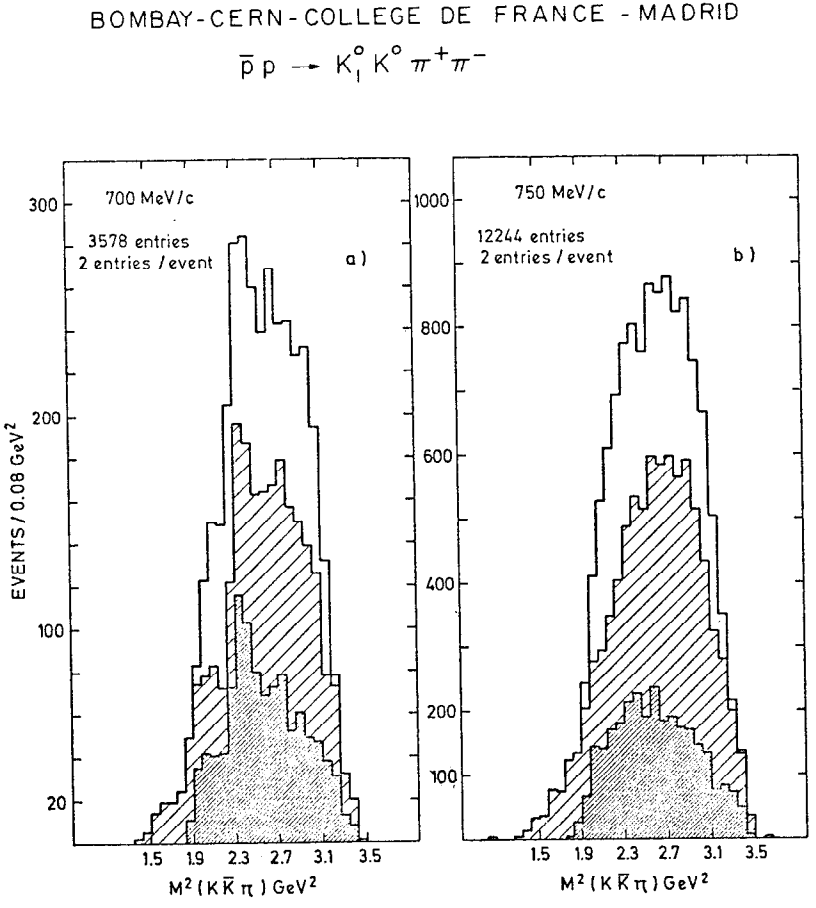

Fig. 14

Invariant mass^2 distribution for the $K^o\bar{K}^o\pi^\pm$ system. The hatched distribution remains when $K^*\bar{K}^*$ events are removed. The darker distribution results from the further requirement of at least one K^*.

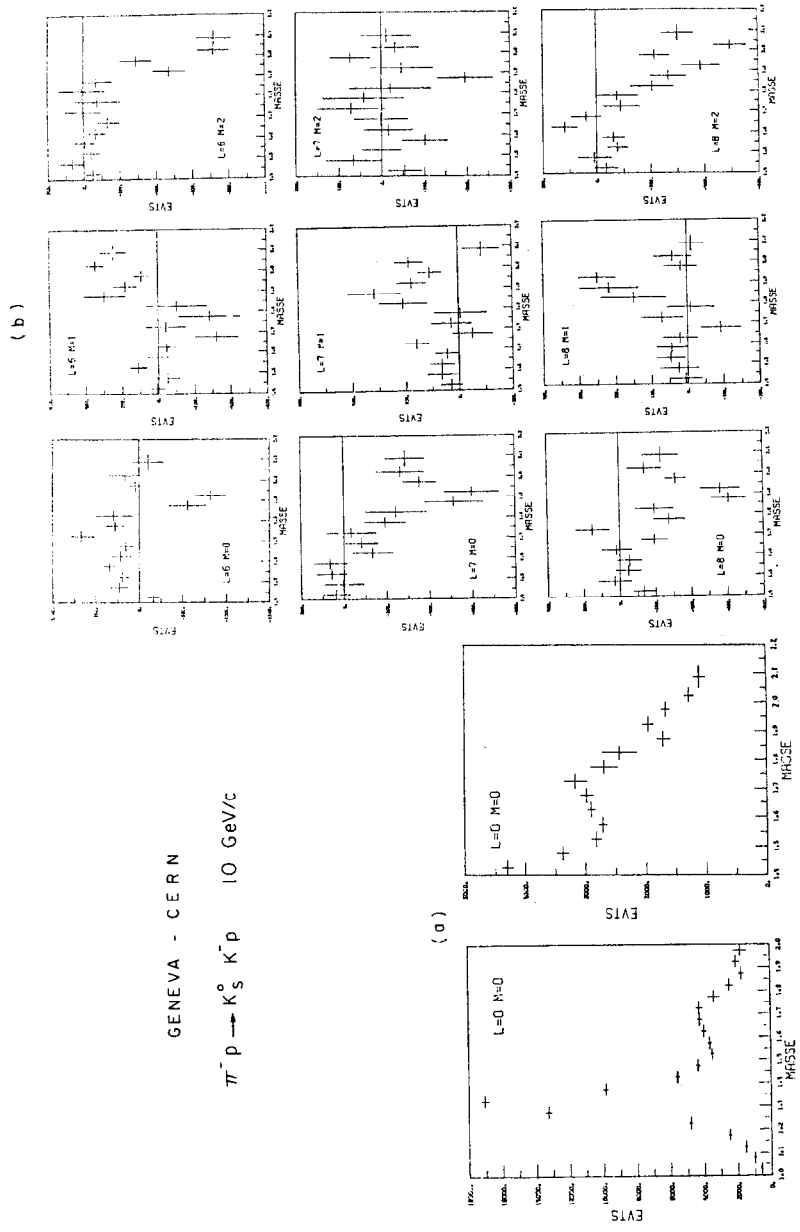

Fig. 15 Evidence for a $J^P = 4^+$, I = 1 state. (a) Acceptance corrected $K^0_S K^-$ mass spectrum and (b) Y_6, Y_7, Y_8 moments.

8. BARYON EXCHANGE PRODUCTION OF Q_1

The most detailed analysis of diffractive $K\pi\pi$ in the Q mass region has been performed by the SLAC spectrometer group with their high statistics data on the reactions $K^{\pm}p \rightarrow K^{\pm}\pi^+\pi^- p$ at 13 GeV/c [13]. A model dependent analysis of these results by the SLAC group [14] and by Bowler [15] has been shown to adequately describe the data in terms of two resonating 1^+ waves with the following parameters [16]

	Mass	$\Gamma(K^*\pi)$	$\Gamma(K\rho)$	$\Gamma(K\omega)$	$\Gamma(K\pi)$	$\Gamma(K\varepsilon)$	Γ_{TOTAL}
Q_1	$\sim$ 1290	12 ± 13	100 ± 35	32 ± 11	35 ± 13	29 ± 10	$\sim$ 208
Q_2	$\sim$ 1400	154 ± 52	2 ± 1	$\sim$ 0	$\sim$ 0	31 ± 11	$\sim$ 187 .

In contrast to the above 2Q picture, non-diffractive $K\pi\pi$ production has consistently shown only a single Q type bump with a mass in the range 1235-1300 MeV, and always with a width $\lesssim$ 100 MeV. A recent bubble chamber experiment by the ANL-Michigan State group has shown evidence for a $K\pi\pi$ bump (mainly in $K^+\pi^+\pi^-$) at 1273 ± 9 MeV with a width of 66 ± 35 MeV from an analysis of the reaction $\bar{p}p \rightarrow K^+K^-\pi^+\pi^-$ at 2.32 GeV/c [17]. The Bergen-CERN-Collège de France-Madrid-Stockholm Collaboration have obtained evidence for a $K\pi\pi$ bump at 1272 ± 6 MeV with a width of 114 ± 21 MeV from the hypercharge exchange reaction $\pi^- p \rightarrow \Lambda(K\pi\pi)^0$ at 3.9 GeV/c [18].

In a baryon exchange reaction, where we expect Deck-type complications to be small, the Amsterdam-CERN-Nijmegen-Oxford Collaboration have obtained clear evidence in $K^- p$ reactions at 4.2 GeV/c for Q-production [19]. With an exposure sensitivity of 133 events/μb the following final states have been investigated $\Xi^- K^+\pi^+\pi^-$ (2463 events), $\Xi^- K^0_1\pi^+\pi^0$(820), $\Xi^-\pi^+$MM(1716) and $\Xi^- K^+$MM(1039). Fig. 16(a) shows the Chew-Low plot for the reaction $K^- p \rightarrow \Xi^- K^0_1\pi^+\pi^0$ where one sees an accumulation at small $K^- \rightarrow \Xi^-$ momentum transfer in the mass region 1.2 - 1.3 GeV. Fig. 16(b) shows the total $K\pi\pi$ mass spectrum (except K^+MM) with the momentum transfer restriction $u(K^- \rightarrow \Xi^-) < 1.5$ GeV^2. A clear enhancement is seen - and a Breit-Wigner plus polynomial background parametrization yields M = 1276 ± 5 MeV and

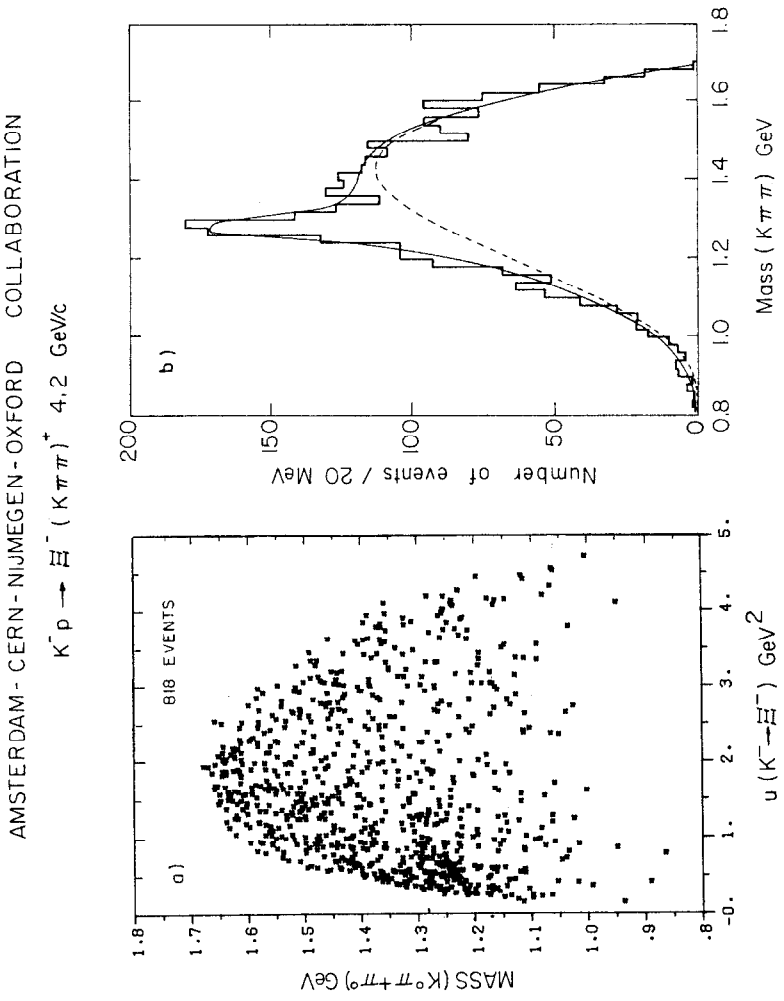

Fig. 16

(a) Chew-Low plot for the $K^{o}\pi^{+}\pi^{o}$ system and (b) $(K\pi\pi)^{+}$ mass spectrum from the reactions $K^{-}p \to \Xi^{-}K^{+}\pi^{+}\pi^{-}$, $\Xi^{-}K^{o}\pi^{+}\pi^{o}$ and $\Xi^{-}\pi^{+}MM$ with $u < 1.5$ GeV^2. The solid curve represent the result of a fit to a BW + polynomial background (dotted).

$\Gamma = 78 \pm 20$ MeV. The application of a multi-channel likelihood fit shows the data to be compatible with an $I = \frac{1}{2}$ $K\pi\pi$ effect with dominant $K\rho$ decay. The cross section for the process $K^{-}p \to Q_1^{+}\Xi^{-}$, $Q_1^{+} \to K\rho$ is determined to be 4.5 ± 1.0 μb.

Thus, if these non-diffractive experiments are seeing the Q_1 (consistent mass), then two problems arise - why is the width different, and where is the Q_2?

A narrow structure in K3π at 2600 MeV

The CERN-Mons-Imperial College-Brussels-Orsay Collaboration have reported evidence for a narrow peak in $K^{o}\pi^{\pm}\pi^{+}\pi^{-}$ at 2600 ± 10 MeV coming from an analysis of 12 GeV/c $\bar{p}p$ in BEBC [20]. From the topology 6-prongs + V^{o}, 587 events have been isolated for the reactions $\bar{p}p \to K_s^{o}3\pi^{+}3\pi^{-}$ + neutrals and $\bar{p}p \to K_s^{o}K^{\pm}\pi^{\mp}2\pi^{+}2\pi^{-}$ + neutrals. In both the combinations $K^{o}\pi^{+}\pi^{+}\pi^{-}$ and $K^{o}\pi^{-}\pi^{-}\pi^{+}$ a peaking is seen near 2600 MeV (fig. 17(a)), the sum spectrum showing a 5.5 standard deviation effect in a single 30 MeV bin. With the high magnetic field and large volume of BEBC the mass resolution was found to be compatible with the width of the signal, $\Gamma \leq 18$ MeV. No evidence was found in either the recoil mass spectrum or in other mass combinations.

An identical experiment has been carried out by the Amsterdam-Helsinki-Liverpool-Stockholm Collaboration in the CERN 2m HBC [21]. Their results (fig. 17(b)) offer no positive confirmation of the 2600 MeV peak. Even allowing for the poorer resolution of the 2m HBC, the discrepancy is estimated at 1-2 standard deviations.

9. $\bar{p}p$ FORMATION - AMPLITUDE ANALYSIS

The beautiful series of formation experiments by the Queen Mary College-Rutherford-Daresbury group have provided both the differential cross section (at 20 momenta) and polarisation (at 11 momenta) in the reaction $\bar{p}p \to \pi^{+}\pi^{-}$ over the CM energy range 2020-2580 MeV. Using the

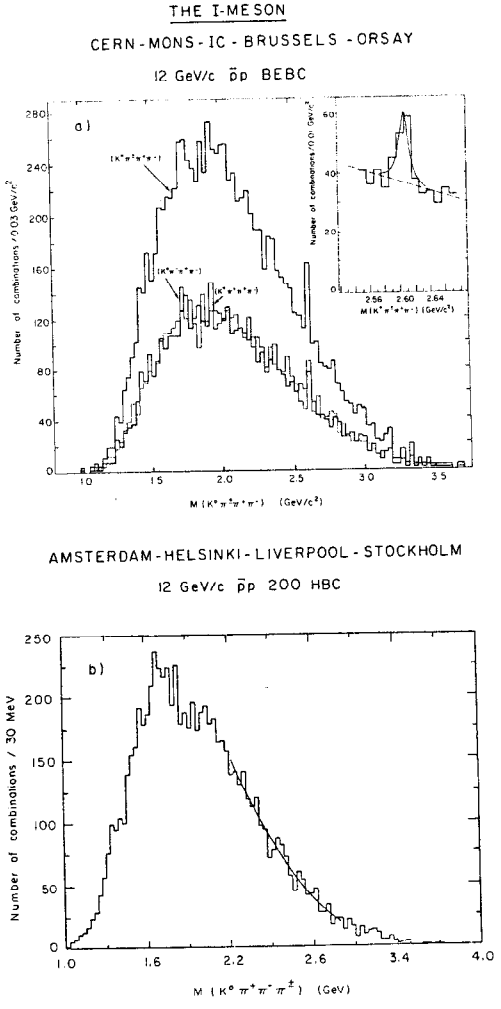

Fig. 17

Evidence for the I-meson in the invariant mass $K^0\pi^{\pm}\pi^+\pi^-$. The solid curve in (b) represents a polynomial fit to the data.

cross section zeroes as a guide, a helicity amplitude analysis has enabled a fit to the data with waves up to J = 5, the solution for J = 3, 4, 5 being unique [22]. The results of the fit are compared with the data at selected momenta in fig. 18, and yield $I^G = 1^+$ $J^{PC} = 3^{--}$ [M = 2150 ± 30, Γ = 200 ± 25], $I^G = 0^+$ $J^{PC} = 4^{++}$[M = 2130 ± 30, Γ = 210 ± 25], and $I^G = 1^+$ $J^{PC} = 5^{--}$[M = 2480 ± 30, Γ = 280 ± 25]. The mass and width of the J = 3, 4 waves are consistent with the T and U(I = 0) bumps seen in $\bar{p}N$ total cross section measurements.

If we assume that the narrow bump at ∿ 1936 MeV [the S meson] in the $\bar{p}N$ total cross section has J = 2, then a single trajectory can describe the S, T, U and V(J = 5). Fig. 19 shows that this trajectory is much steeper than that normally attributed to hadrons - thus indicating that either: (a) the states do not belong on the same trajectory or (b) the systematics of low-lying trajectories are different or (c) states coupled to the $N\bar{N}$ channel are different (e.g. $qqq\bar{q}\bar{q}$ states).

10. STATUS OF MESON SPECTROSCOPY

Fig. 20 shows an optimistic picture of the current status of classical mesons - due consideration being given to the analyses mentioned above and those discussed at this Institute by Treille and Lasinski. It is clear that a considerable advance has been made during the last year.

11. INTRODUCTION TO BARYON SPECTROSCOPY

For classical baryons the non-relativistic quark shell model with harmonic oscillator forces leads to the rather complex supermultiplet structure in fig. 21 (taken from Dalitz [23]). The lectures by Gilman at this Institute have shown how the application of symmetry considerations limits the N = 0 supermultiplet to be the SU(6) representation [56, 0^+] and the N = 1 to be the [70, 1^-]. At higher mass the situation becomes more and more complex. Along the leading trajectory the experimentally observed pattern is one of alternating 56's and 70's, namely [56, 0^+],

QUEEN MARY-RUTHERFORD-DARESBURY

$\bar{p}p \rightarrow \pi^+\pi^-$

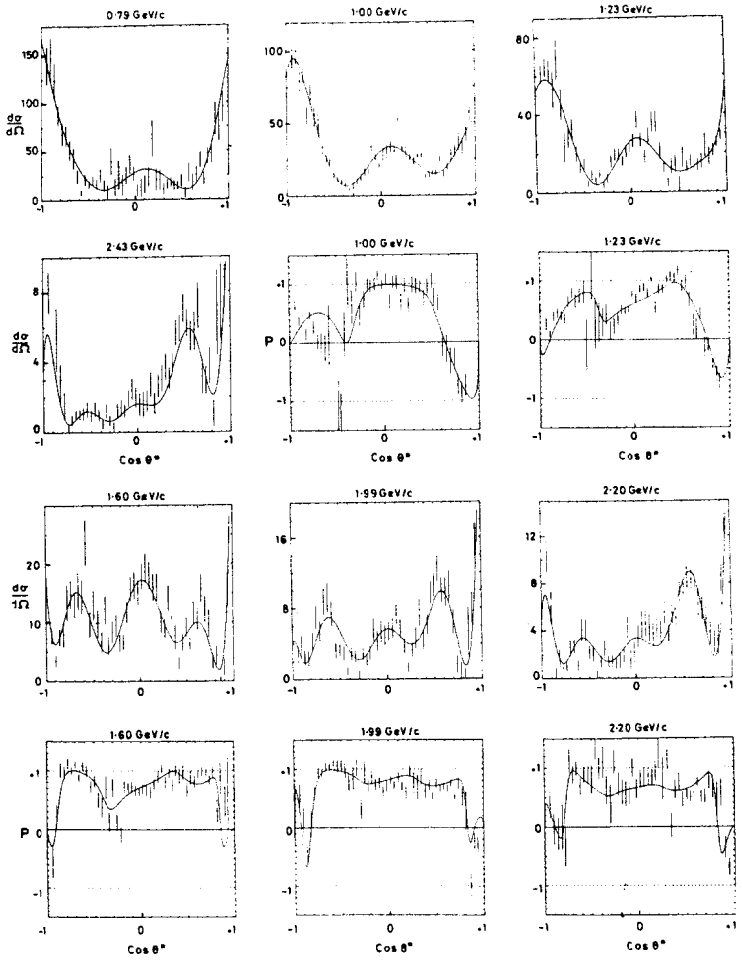

Fig. 18

Sample differential cross sections and polarisations. The curves represent the result of a helicity amplitude analysis.

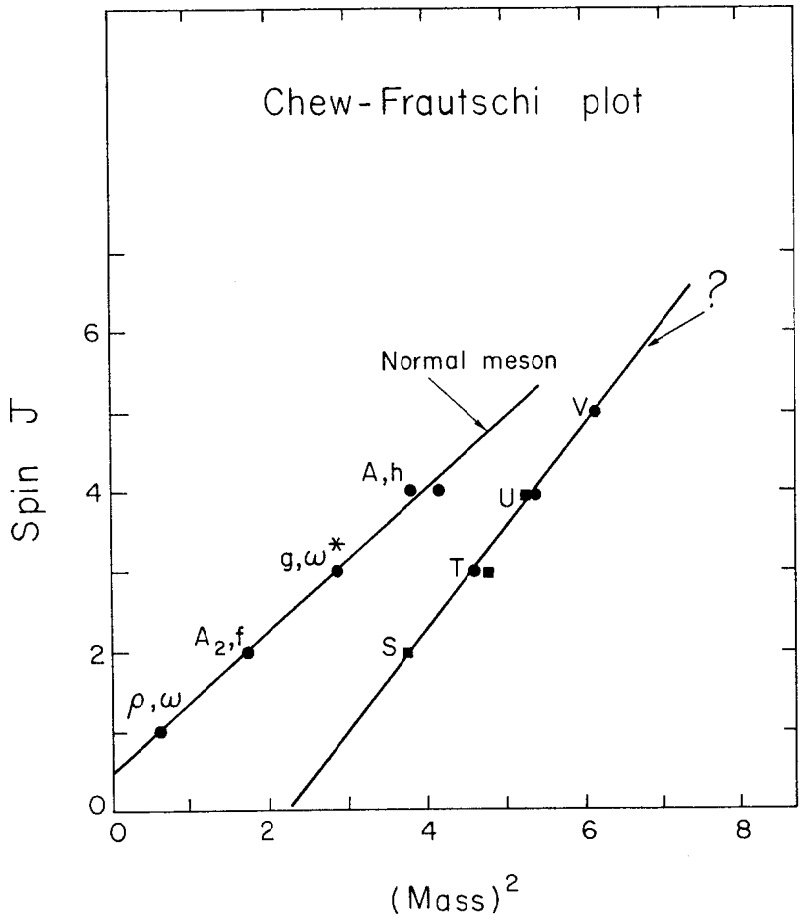

Fig. 19

Chew-Frautschi plot for selected meson states

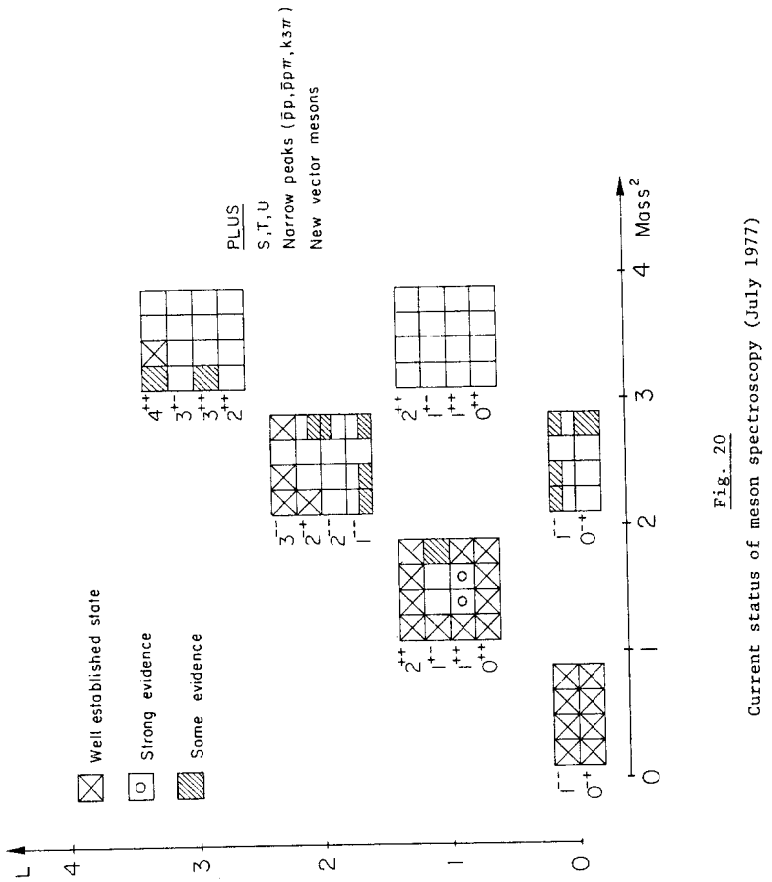

Fig. 20

Current status of meson spectroscopy (July 1977)

BARYON SPECTRUM IN QUARK SHELL MODEL

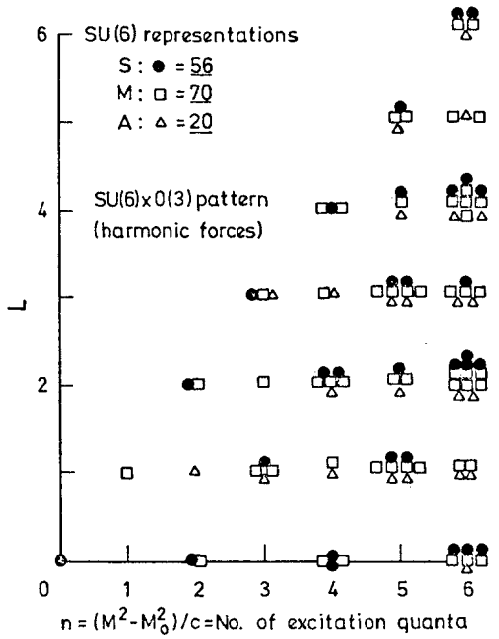

Fig. 21

Baryon spectrum in quark shell model

$[70, 1^-]$, $[56, 2^+]$, $[70, 3^-]$ etc. Evidence also exists for the ground state radial excitation $[56, 0^+]_2$ and possibly $[56, 0^+]_4$.

Conventionally the first three supermultiplets of the leading trajectory have attracted most interest as a testing ground of our ideas of baryon systematics. This is certainly due to the large number of established states with a natural home within these supermultiplets, as shown in fig. 22. The open circles, representing states which have not been found or whose status is questionable, give the following table of missing states:

	Δ	N	Σ	Λ	Ξ	Ω
$[56, 0^+]$	0	0	0	0	0	0
$[70, 1^-]$	0	$\frac{3}{2}^-$	$\frac{1}{2}^-\ \frac{1}{2}^-\ \frac{3}{2}^-$	$\frac{1}{2}^-$	$\frac{1}{2}^-\ \frac{1}{2}^-\ \frac{1}{2}^-\ \frac{3}{2}^-\ \frac{3}{2}^-\ \frac{3}{2}^-\ \frac{5}{2}^-$	$\frac{1}{2}^-\ \frac{3}{2}^-$
$[56, 2^+]$	$\frac{3}{2}^+$	0	$\frac{1}{2}^+\ \frac{3}{2}^+\ \frac{3}{2}^+\ \frac{5}{2}^+$	0	$\frac{1}{2}^+\ \frac{3}{2}^+\ \frac{3}{2}^+\ \frac{5}{2}^+\ \frac{5}{2}^+\ \frac{7}{2}^+$	$\frac{1}{2}^+\ \frac{3}{2}^+\ \frac{5}{2}^+\ \frac{7}{2}^+$.

It is clear that, whereas the S = 0 states are in excellent shape, the S ≠ 0 states need a considerably increased experimental effort, particularly for the S = −2 and S = −3 states.

For the S = 0 and S = −1 states, where detailed partial wave analyses have been performed, one may reasonably ask the question: where are the missing states? Various explanations can be proposed - the coupling to the elastic channel may be very small, the states may be very broad, or the states may be very narrow. For the S = −2 and −3 states, the lack of reliable information stems from the fact that these states can only be observed in production experiments where they are produced with very small cross sections. The need for very high statistics production experiments is therefore essential - to determine at least some of the S = −2 and −3 states, and perhaps to indicate the missing S = 0 and −1 states.

In what follows, we will discuss recent $\bar{K}N$ total cross section measurements and then give some flavour of what can be learned from huge production experiments. We avoid formation studies completely - the recent Oxford Baryon Conference [24] should be consulted for a full appreciation of the state of the art.

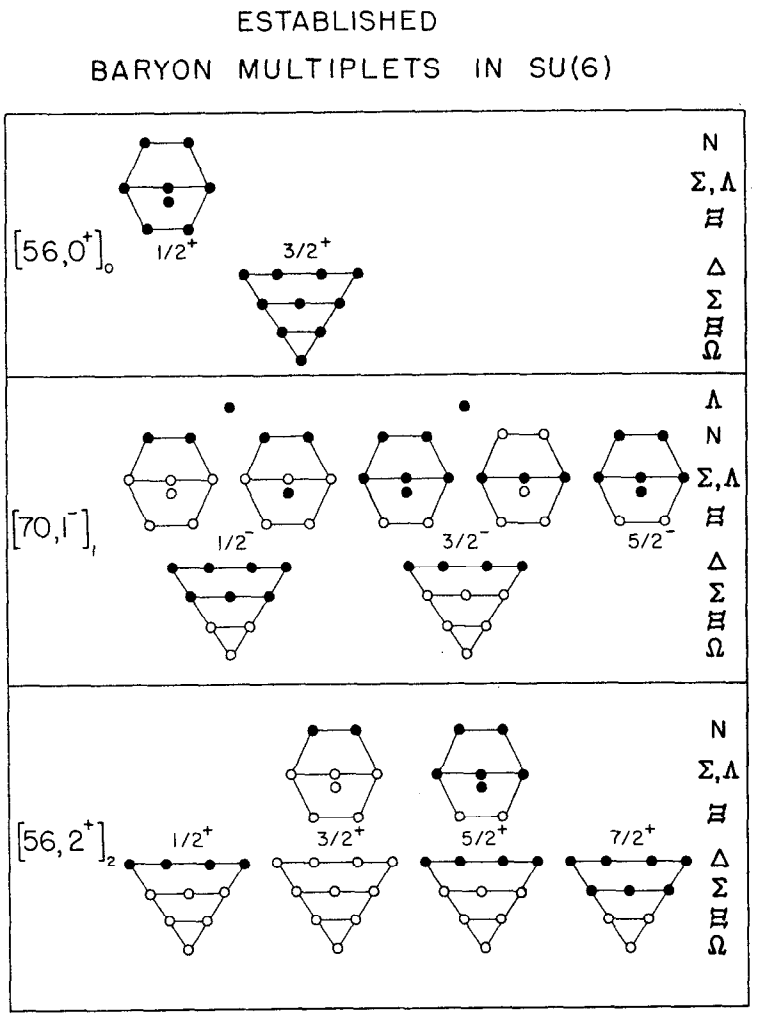

Fig. 22

Current status of the leading baryon supermultiplets. Solid points correspond to well-established states.

12. STRUCTURE IN $\bar{K}N$ TOTAL CROSS SECTION

Recent high precision measurements of the $\bar{K}N$ total cross sections below 1.1 GeV/c at BNL have observed several structures which could be Y^* resonances [25]. The unfolded I = 0 and I = 1 contributions are shown in fig. 23. The data have been fitted with a momentum dependent background together with a sum of Breit-Wigner forms which yield the following parameters:

ISOSPIN	MASS	WIDTH	$(J + \frac{1}{2})x$	ESTABLISHED STATES
0	1646 ± 7	20	0.04	
0	1692 ± 4	38	0.48	$\Lambda(1670)S_{01}$, $\Lambda(1690)D_{03}$
0	1735 ± 5	28	0.29	
1	1583 ± 4	15	0.06	
1	1608 ± 5	15	0.06	
1	1633 ± 10	10	0.04	
1	1670 ± 4	52	0.23	$\Sigma(1670)D_{13}$
1	1715 ± 10	10	0.30	

All the structures have a significance of more than five standard deviations except $\Lambda(1646)$ and $\Sigma(1633)$ which are $\sim$ 3 standard deviations. The step in I = 1 at $\sim$ 1550 MeV has not been parameterized due to the undertainty of the cross sections below the energy range covered. Assuming the structures to be genuine, the probability that they would have been seen in past formation experiments is small since they have small widths, small elasticities, or both. The indications are therefore that the Y^* spectrum in this energy region may be much richer than was originally believed.

13. A NEW Σ AT 1550 MeV

The Amsterdam-CERN-Nijmegen-Oxford Collaboration have reported evidence for an I = 1 enhancement at a mass of 1550 MeV in both $\Lambda\pi$ and $\Sigma\pi$ from an analysis of the reactions $K^-p \to (\Lambda, \Sigma^o)\pi^{\pm}K^{\mp}K_1^o$ at 4.2 GeV/c [26]. With a sensitivity of 100 events/μb for events where both V^o decays are seen,

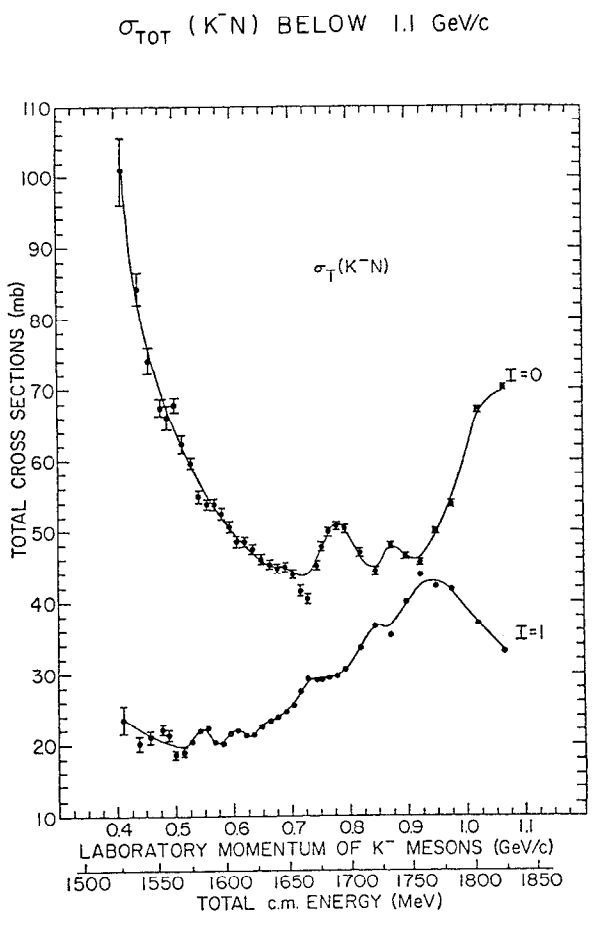

Fig. 23

Total K^--nucleon cross sections for the I = 0 and I = 1 isotopic-spin states. The curves are the results of fits including BW's and a background.

fig. 24 shows the combined $\Lambda\pi$ and $\Sigma\pi$ mass spectrum with the selection of forward hemisphere for $(\Lambda, \Sigma^o)\pi^-$ and backward hemisphere for $(\Lambda, \Sigma^o)\pi^+$. A clear $\Sigma(1385)$ is seen together with a six-standard deviation enhancement at $\sim$ 1550 MeV. Fitting the distribution with a background polynomial plus two BW functions, yields M = 1553 ± 7 MeV, Γ = 79 ± 29 MeV for the Σ_{1550}. The production cross section is estimated at $\sim$ 7 μb and the decay rate $\Sigma\pi/(\Lambda\pi + \Sigma\pi)$ to be 0.4 ± 0.2.

14. A NON-CHARMED BARYON NEAR 2260 MeV

The same collaboration have found significant evidence for a non-charmed Σ state [27] whose mass and width are compatible with the recently reported narrow antibaryon state in the wide-band photon beam at Fermilab [28]. Analysis of the reactions $K^-p \to \Sigma^-\pi^+\pi^+\pi^-\pi^o$ (39 K events) and $K^-p \to \Sigma^+\pi^-\pi^+\pi^-\pi^o$ (30 K events) displays abundant $\omega(783)$ production. Fig. 25 shows background subtracted $\Sigma\omega$ mass distributions where peripheral cuts have been made to isolate forward $\Sigma^-\omega$ and backward $\Sigma^+\omega$. A peaking is observed in each distribution close to 2.26 GeV and both peaks have widths consistent with Γ < 75 MeV.

This observation should encourage further investigation of high mass baryons decaying into two-body systems with high thresholds eg. $(\Lambda, \Sigma)\phi$, $\Xi\omega$, $\Lambda(1405)\omega$ etc.

15. PROGRESS IN Ξ SPECTROSCOPY

Fig. 26 shows the latest results on S = −2 mass combinations with charge = −1 from the Amsterdam-CERN-Nijmegen-Oxford Collaboration studying 4.2 GeV K^-p interactions with a sensitivity of 128 events/μb. The two prominent structures above the well-established $\Xi(1530)$ are $\Xi(1820)$, seen dominantly in ΛK^-, and $\Xi(2030)$ dominantly in $(\Sigma K)^-$. Properties of these states, whose status can now be taken as well-established, are summarised below [29, 30].

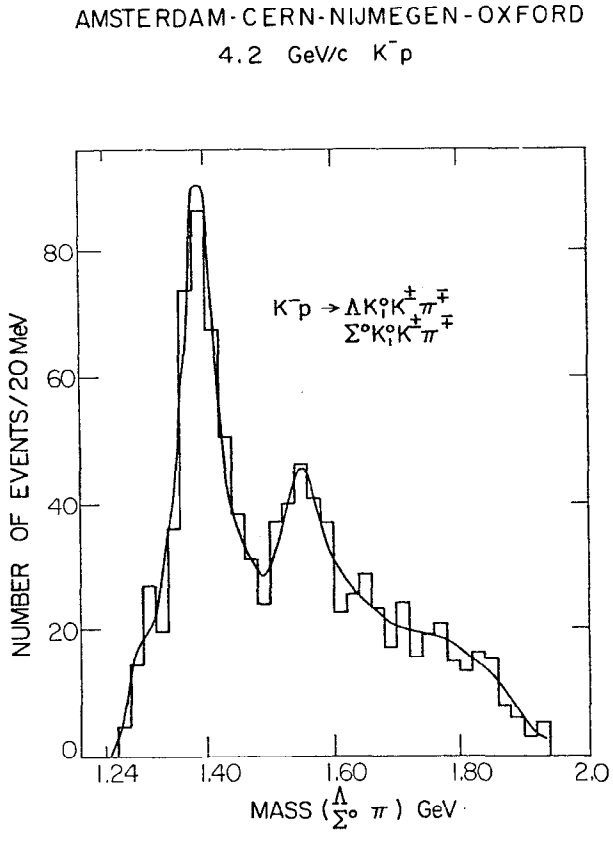

Fig. 24

Invariant mass distribution of $\Lambda(\Sigma^o)\pi^-$ in the backward hemisphere + $\Lambda(\Sigma^o)\pi^+$ in the forward hemisphere. The curve is the result of a fit with 2 BW's and a polynomial background.

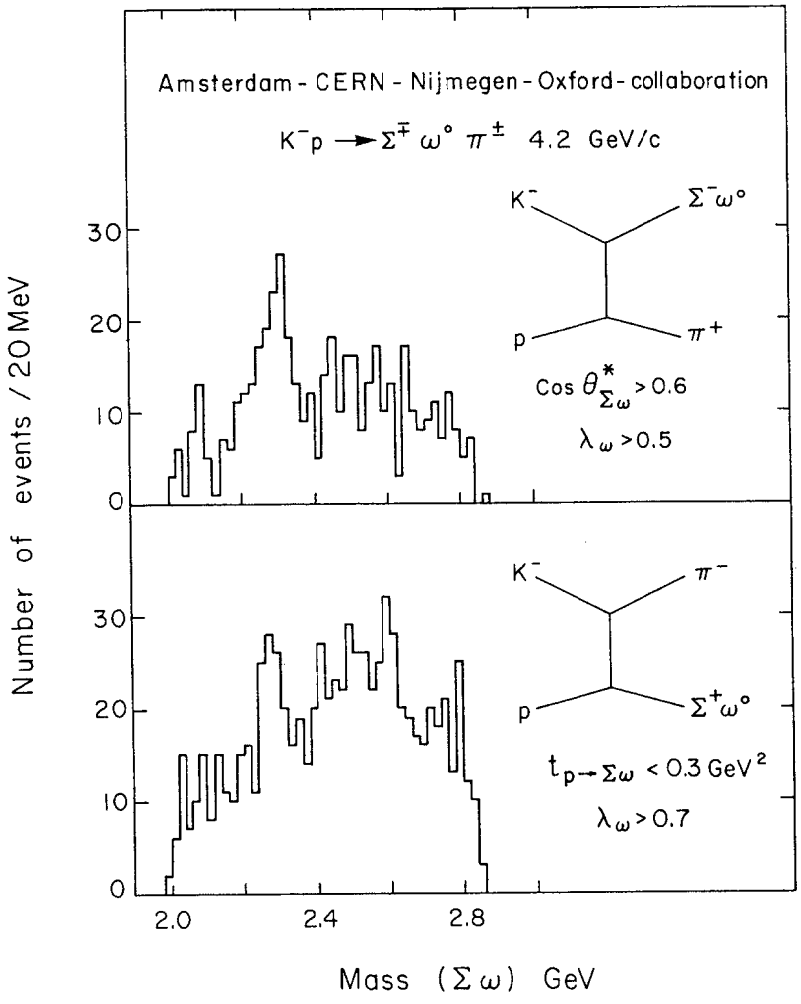

Fig. 25

Invariant mass distribution of $\Sigma\omega$. (a) $\Sigma^-\omega$ in the forward direction, and (b) $\Sigma^+\omega$ in the backward direction. In both cases a cut has been made on the ω decay matrix element to reduce background.

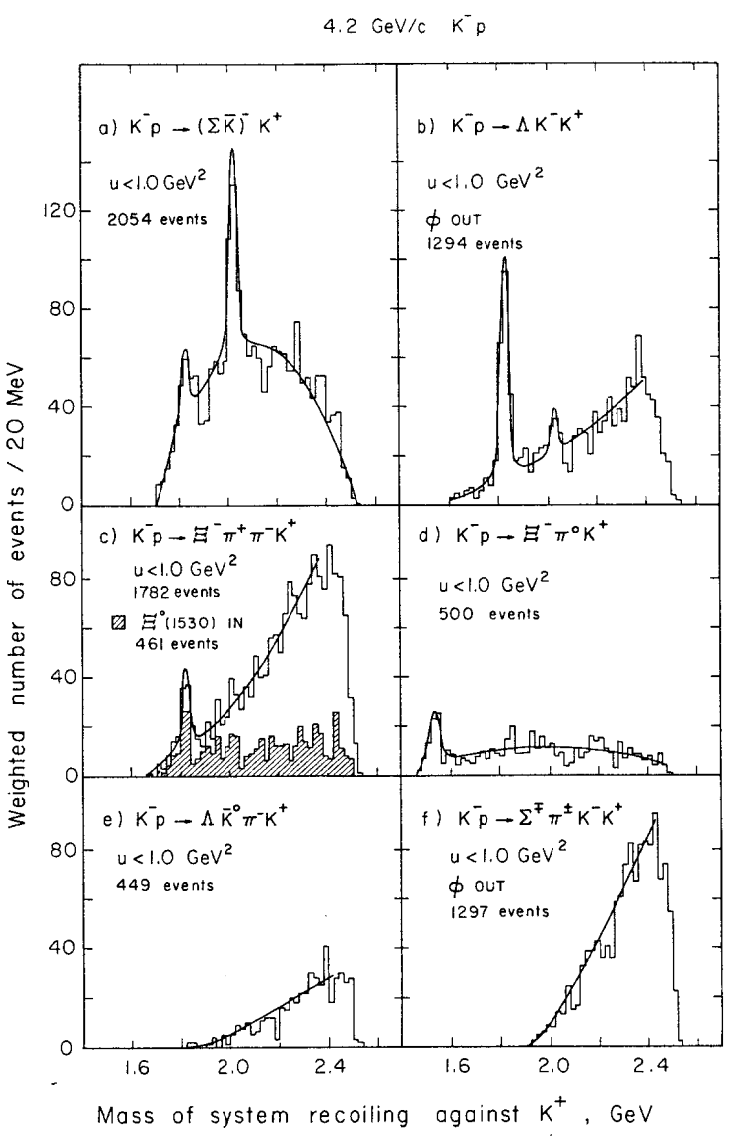

Fig. 26

Mass spectra of different S = -2 particle combinations. The superimposed curves are the results of fits to BW forms plus a polynomial background.

	MASS (MeV)	WIDTH (MeV)	SPIN	RELATIVE DECAY RATES $\Lambda\bar{K}$	$\Sigma\bar{K}$	$\Xi\pi$	$\Xi^*_{1530}\pi$
$\Xi(1820)$	1823 ± 2	21 ± 7	> 1/2	1	0.24 ± 0.10	< 0.36	1.0 ± 0.3
$\Xi(2030)$	2024 ± 2	16 ± 5	> 3/2	0.22 ± 0.09	1	< 0.19	< 0.25

where the spin restrictions were based on minimum complexity decay moment evaluations.

With final data now available the J^P determination of the $\Xi(1820)$ has been reinvestigated. By comparing the decay moments of the two major decay channels $\Lambda\bar{K}^-$ and $\Xi(1530)\pi$ (fig. 27(a, b)) where the daughter baryons have different J^P, it is possible to define a χ^2 test as a function of $\Xi(1820)$ spin [31]. Fig. 27(c, d) shows clearly that the data are consistent with the J = 3/2 assignment (probability $\sim$ 50%), whereas higher spins have a much lower confidence level ($\lesssim$ 1% for J $\geq$ 5/2).

This experiment is in the process of investigating several other final states and should continue to improve our knowledge of Ξ resonances in the mass range 1.5 - 2.5 GeV.

16. THE SPIN OF THE Ω^-

Although the Ω^- is considered to be well-established and to belong to the $3/2^+$ decuplet of the ground state [56, 0^+], its spin-parity has never been measured. The Aachen-Berlin-CERN-London-Vienna Collaboration have now accumulated 101 Ω^- decays in K^-p reactions at 10 and 16 GeV/c [32]. Fig. 28 shows the corrected helicity decay angular distribution of the Ω^- sample together with the result of a fit to the form $I(\cos\theta^*) \propto (1 + \beta \cos^2\theta^*)$. The spin = 1/2 prediction of $\beta = 0$ is clearly ruled out (probability < 0.1%), whereas the data are in good agreement with spin = 3/2 (probability $\sim$ 70%).

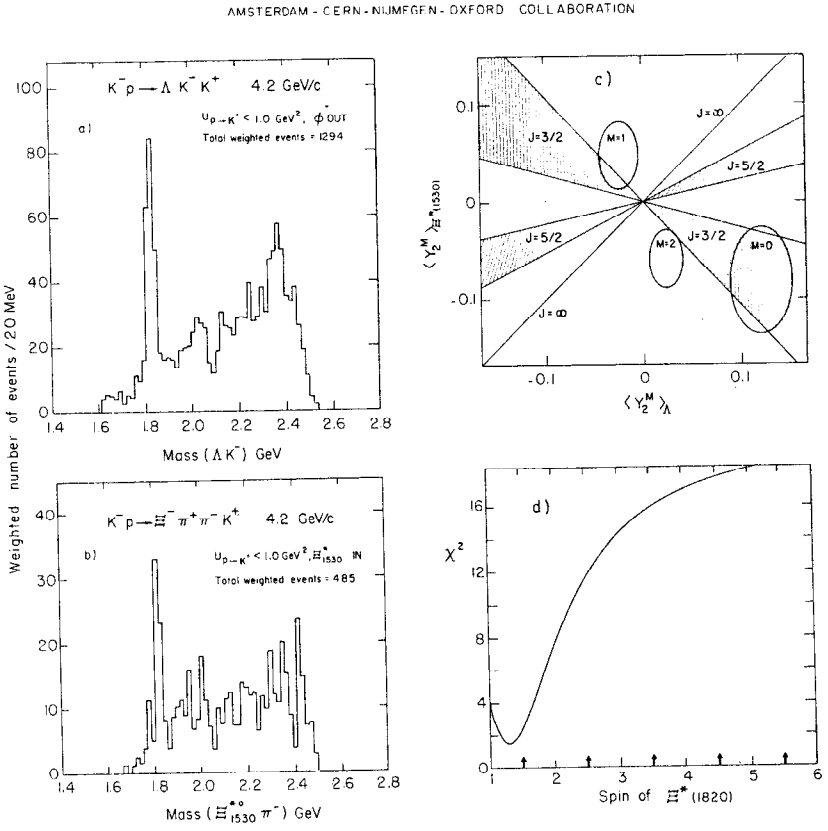

Fig. 27

Effective mass distributions (a)ΛK^-, (b) $\Xi^{*o}_{1530}\pi^-$. The experimental decay moments with L = 2 in the u-channel helicity frame are shown in (c), and the variation of chi-square with Ξ^*1820) spin in (d)

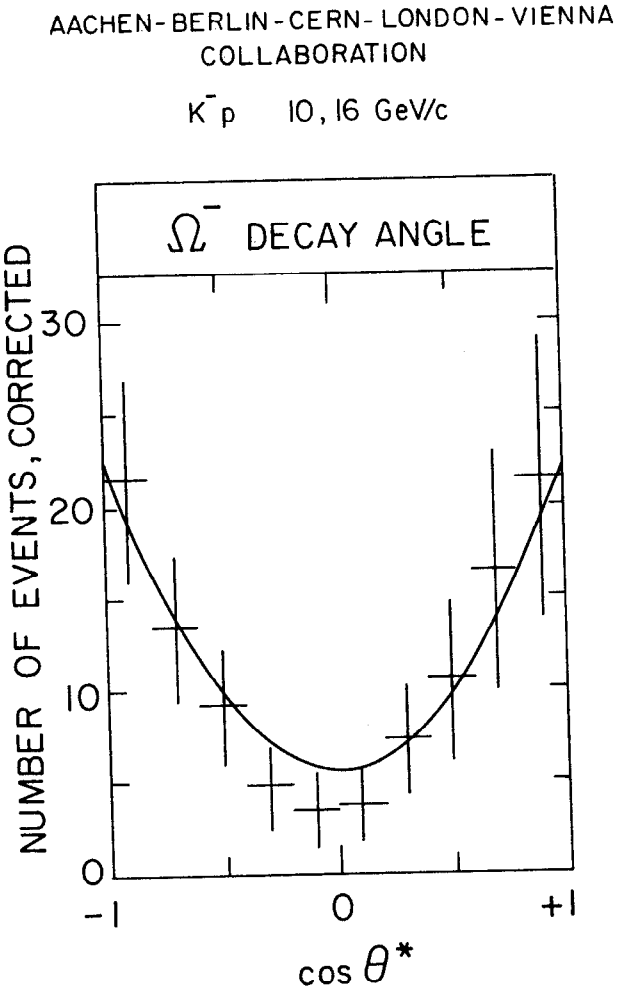

Fig. 28

Helicity decay angular distribution for 101 Ω^- events. The curve is described in the text.

17. FUTURE OUTLOOK

Together with the talks of Treille and Lasinski, this report shows that a considerable advance has been made in experimental old spectroscopy during the last twelve months. For the big spectrometers which are currently beginning to show their true worth, several problems remain to be solved, in particular:

- In the baryon spectrum many states are still required to complete the $[70, 1^-]$ and $[56, 2^+]$ multiplets. Our current understanding of baryon systematics is heavily weighted towards S = 0 states, and it is therefore possible that the consolidation of the S ≠ 0 states may show several surprises. Furthermore, the completion of the spectrum up to N = 2 requires the additional multiplets $[70, 2^+]$, $[20, 1^+]$ and $[70, 0^+]$, for which very few states currently exist (and none for $[20, 1^+]$ which cannot decay into the usual two-body channels, $35 \otimes 56 \notin 20$).

- In the meson spectrum an important question concerns the existence of radial excitations $[\rho, \omega, \phi, K^*]'$ and especially $[\pi, \eta, \eta', K]'$ whose members cannot be placed in alternative multiplets. The new data from DESY, Orsay and Frascati together with $K\pi$, $\pi\pi$ and $K\pi\pi$ phase shift analyses have given encouraging signs that these nonets do indeed exist. With forthcoming data on the D and E mesons, the only states in bad shape (really missing) in the L = 1 supermultiplet are the two I = 0 members of the B nonet. Where are they? Considerable effort should now be directed into filling out the L = 2 supermultiplet - at least 8 out of the 16 states are completely missing. Finally, the narrow peak structures observed in $\bar{p}p$, $\bar{p}p\pi$ and $K3\pi$, if confirmed, may open a new avenue of spectroscopy.

Acknowledgements

I would like to thank my colleagues at CERN for their help and support in preparing this talk. In particular, I wish to thank Mike Losty and Mike Pennington for the innumerable discussions on aspects of meson spectroscopy.

REFERENCES

[1] S. Bartalucci et al., Nuovo Cimento 39A (1977) 374 and Systematic Search for New Vector Mesons in the Mass Range up to 2 GeV, paper submitted to Budapest Conference, 1977.

[2] G. Cosme et al., Phys. Letters 67B (1977) 231.

[3] B. Esposito et al., Phys. Letters 68B (1977) 389;
C. Bacci et al., Phys. Letters 68B (1977) 393;
G. Barbiellini et al., Phys. Letters 68B (1977) 397.

[4] G. Capon, Recent Results at Adone, invited talk at Budapest Conf. 1977.

[5] C.V. Cautis, thesis University of Columbia 1977, R1097, CU327, Nevis 221.

[6] Yu. M. Antipov et al., Nucl. Phys. B119 (1977) 45.

[7] M. Cerrada et al., A Partial Wave Analysis of the 3π System in the Reaction $K^- p \to \pi^+\pi^-\pi^0\Lambda$ at 4.2 GeV/c, CERN/EP/PHYS 77-9.

[8] J. Pernegr et al., Evidence for Resonance Behaviour of A_1 and A_3 Mesons Coherently Produced on Nuclei, paper submitted to the Budapest Conference, 1977.

[9] Ph. Gavillet et al., Backward Production of a Spin Parity $1^+\rho\pi$ Enhancement at 1.04 GeV, CERN/EP/PHYS 77-15.

[10] A. Ferrer et al., Backward A_1 and A_2 Production in $\pi^- p \to p\pi^+\pi^-\pi^-$ at 9 GeV/c and 12 GeV/c, paper submitted to the Budapest Conference, 1977.

[11] M. Cerrada et al., Search for the $F_1(1540)$ Meson in $\bar{p}p$ Annihilations at 750 MeV/c, to be submitted to Nucl. Phys B.

[12] R. Baldi et al., Meson Resonance Production in $\pi^- p \to K^0_s K^- p$ at 10 GeV/c, paper submitted to the Budapest Conference, 1977.

[13] G.W. Brandenburg et al., Phys. Rev. Letters 36 (1976) 703 and 1239.

[14] R.K. Carnegie et al., SLAC-PUB-1767.

[15] M.G. Bowler, Journal of Phys. G3 (1977) 775.

[16] R.K. Carnegie et al., Phys. Letters 68B (1977) 287.

[17] C.K. Chen et al., ANL-HEP-PR-77-22.

REFERENCES (Cont'd)

[18] BCCMS Collaboration, Evidence for Q-production by Hypercharge Exchange in $\pi^- p$ Interactions at 3.9 GeV/c, paper submitted to the Budapest conference, 1977.

[19] ACNO Collaboration, Observation of a ($K\pi\pi$) Enhancement Produced by Hyperon Exchange in $K^- p$ Interactions at 4.2 GeV/c, paper submitted to the Budapest Conference, 1977.

[20] A. Apostolakis et al., Phys. Letters 66B (1977) 185.

[21] G.W. Van Apeldoorn et al., A Search for the I-peak at 2.60 GeV in 12 GeV/c pp Interactions in the CERN 2m HBC, paper submitted to the Budapest Conference, 1977.

[22] A.A. Carter et al., Phys. Letters 67B (1977) 117 and 122.

[23] R.H. Dalitz in Proceedings of the Topical Conference on Baryon Resonances, Oxford, 1976.

[24] Proceedings of the Topical Conference on Baryon Resonances, Oxford, July 1976, published by the Rutherford Laboratory.

[25] A.S. Carroll et al., Phys. Rev. Letters 37 (1976) 806.

[26] ACNO Collaboration, An I = 1 Enhancement at a Mass of 1550 MeV in the ($\Lambda\pi$) and ($\Sigma\pi$) System, paper submitted to the Budapest Conference, 1977.

[27] ACNO Collaboration, Observation of a $\Sigma\omega$ Enhancement near 2.26 in $K^- p$ Interactions at 4.2 GeV/c, paper submitted to the Budapest Conference, 1977.

[28] B. Knapp et al., Phys. Rev. Letters 37 (1976) 882.

[29] J.B. Gay et al., Phys. Letters 62B (1976) 477.

[30] R.J. Hemingway et al., Phys. Letters 68B (1977) 197.

[31] ACNO Collaboration, A Spin Determination of the $\Xi^*(1820)$ Resonance, paper submitted to the Budapest Conference, 1977.

[32] ABCLV Collaboration, Spin and Lifetime of the Ω^- Hyperon, paper submitted to the Budapest Conference, 1977.

OBSERVATION OF A DIMUON RESONANCE NEAR 9.5 GeV IN 400 GeV PROTON-NUCLEUS COLLISIONS

Walter R. Innes*
Fermi National Accelerator Laboratory
Batavia, Illinois 60510

This is a report on preliminary results of a measurement of the production of high mass dimuons in proton-nucleus collisions. The sample collected to date contains 18,000 events with a mass $m_{\mu^+\mu^-}$ above 5 GeV. The mass spectrum of these events is shown in Fig. 1. Excluding the region between 8.8 and 10.6 GeV, the spectrum falls smoothly following a linear exponential curve of constant slope. While this curve predicts 719 events in the excluded region, the data contain 1397. I will first discuss how this data was obtained and then return for a closer look at the structure and discuss its possible significance.

*This talk is based on work being done by a Columbia University, Fermilab, SUNY-Stony Brook collaboration. The members of the research team are: J. A. Appel, B. C. Brown, C. N. Brown, S. W. Herb, D. C. Hom, W. R. Innes, A. S. Ito, H. Jöstlein, D. M. Kaplan, R. D. Kephart, L. M. Lederman, J. C. Sens, H. D. Snyder, K. Ueno, T. Yamanouchi, and J. K. Yoh. The work is supported in part by ERDA and the NSF.

Figure 1: Differential cross-section $d^2\sigma/dmdy$ for the reaction p + Nucleus → $\mu^+\mu^-$ + X. A linear dependence on the atomic number of the nucleus has been assumed. The curve is: $1.28\ e^{-0.93M}$.

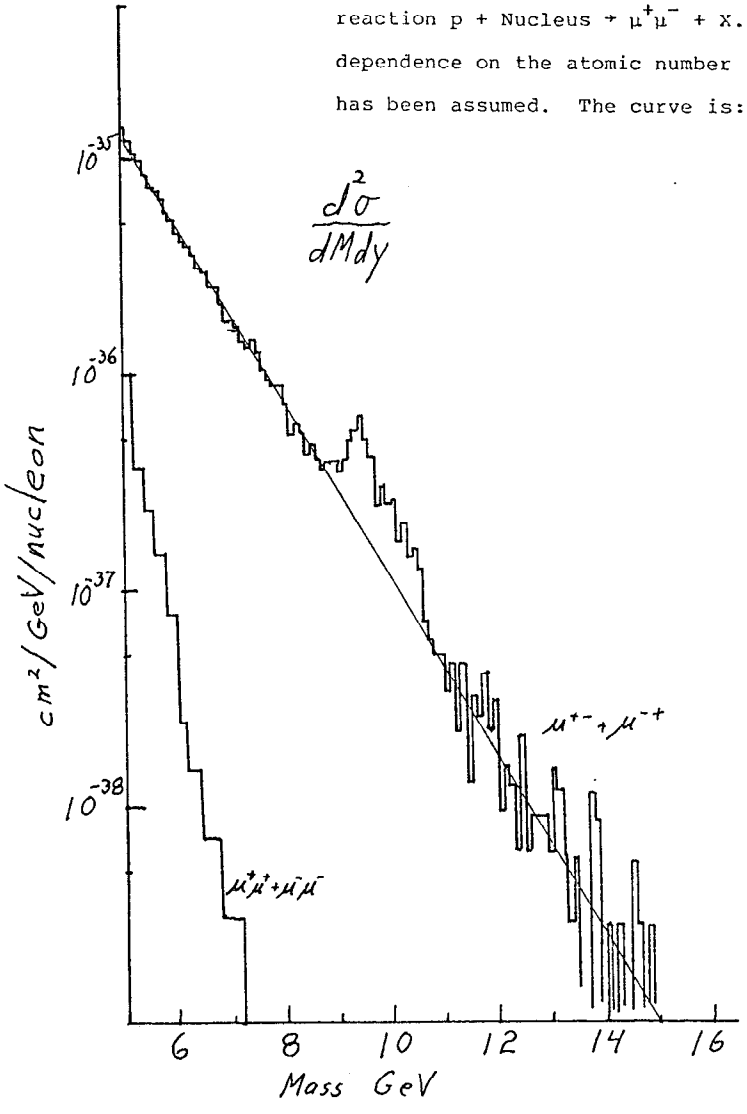

The data was taken with a double arm spectrometer located in the Proton Center Laboratory at Fermilab. A plan view of the apparatus is shown in Fig. 2. The targets were .75 mm wide and ~30% of an absorption length long. Both Cu and Pt targets were used. Proceeding downstream from the target each arm consists of: a Be hadron absorber, an Fe collimator, a vertically bending air gap dipole magnet with a maximum P_t -kick of 1.2 GeV, planes of plastic scintillators and proportional wire chambers (PWC's), a solid steel dipole magnet bending in the direction opposite to the air dipole with a P_t-kick of 1 GeV, and finally more scintillators and PWC's. Be was used as the hadron absorber to retain good resolution by minimizing multiple scattering. (Be has a favorable ratio of absorption lengths to radiation lengths.) The first 30 cm of Be could be exchanged for Cu permitting a doubling of beam intensity with only a small sacrifice in resolution at high masses. The PWC's determined the muon trajectory between the magnets, which combined with the assumption that the muons come from the target determined the muon momentum to about 2%. To check the target origin assumption the muon momentum was remeasured with the steel magnet to about 10%. The arms were symmetric with respect to reflection about a horizontal plane at beam height. Therefore, both signs of muons were accepted simultaneously in each arm allowing same sign

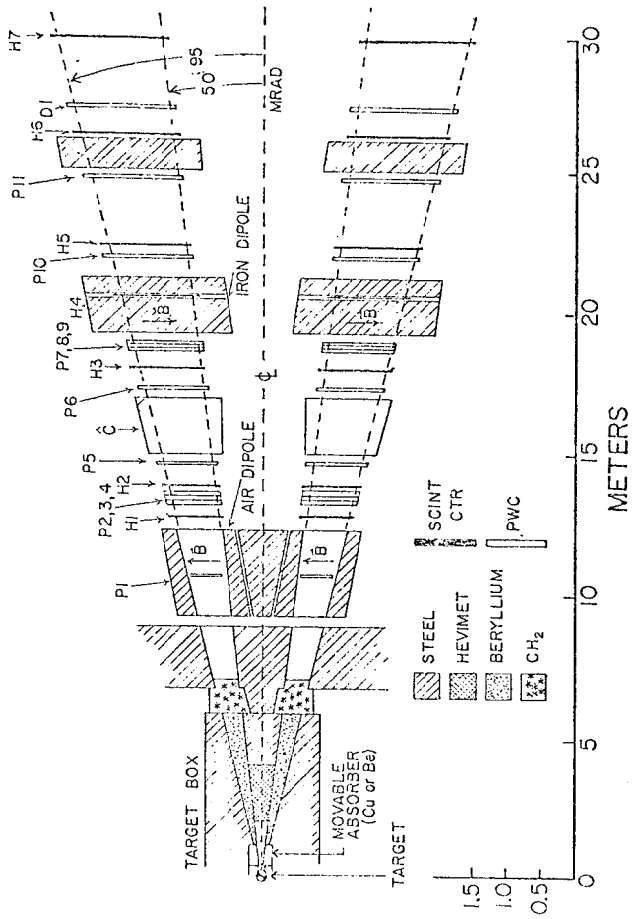

Figure 2: Plan view of the apparatus.

pairs to be obtained along with the data. The remaining critical component of the apparatus was the beam dump which consists of 2 M of W. The choice of Tungsten was essential to prevent the detectors from being flooded with muons from the dump.

The trigger consisted of the coincidence of 6 scintillator planes distributed from the exit of the air dipole magnet to the end of the arm, two of which formed horizontal roads pointing to the target. Data was typically taken with 3×10^{11} protons incident on the target per 1.2 second pulse and a pulse repetition period of about 13 sec. This intensity resulted in a singles rate of ~5 M/pulse in detector planes between the magnets and 1-2 M/pulse in planes after the steel magnet. The single arm trigger rate was 20 K/pulse and the pair trigger rate was 50/pulse. The beam intensity was limited by the singles rates in the detectors between the magnets. Approximately 1/1000 of the pair triggers were good $\mu^+\mu^-$ events with masses above 5 GeV. The remainder were primarily low mass events and events with tracks outside the fiducial volume.

Each arm accepted muons with horizontal production angles between 50 and 95 mr in the lab (70° - 110° in the C. M.). Their vertical acceptance was a function of muon momentum, reaching ±10 mr for p > 50 GeV. The lowest momentum accepted was 10 GeV. Because the acceptance of each arm was near 90° in the C. M., the acceptance of muon pairs

was confined to a small region of C. M. rapidity between ±0.3 units. For this reason cross-sections are quoted as $d\sigma/dy$ at $y = 0$.

The pair acceptance in P_t for different ranges of muon pair invariant mass is shown in Fig. 3. Note that for high masses the acceptance was reasonably good out to P_t's as large as are likely to occur. The overall pair acceptance as a function of mass for three different excitations of the air dipole magnet is shown in Fig. 4. The excitation used for most of the data in Fig. 1 was 1500 amps. Note that above 7 GeV the acceptance was nearly constant. In order to calculate these pair acceptances a decay angle distribution proportional to $1 + \cos^2\theta$ in the S channel helicity frame was assumed. The overall acceptance was not sensitive to this assumption. Different assumptions do result in small changes in the dependence of invariant cross-sections on P_t, e.g. the alternate assumption of an isotropic decay distribution would change an $e^{-1.2\ P_t}$ dependence into $e^{-1.0\ P_t}$.

The mass resolution as a function of mass is shown in Fig. 5. The solid curve is for the first 30 cm of hadron absorber being Cu, the dashed curve is for an all Be absorber, and the dotted curves show various contributions to the error. Since it is near the target, the choice of Cu or Be for the first section of absorber affects only the opening angle measurement. Because this is the dominant contribution to the combined error only at low mass, the

Figure 3: Pair acceptance as a function of P_t for various mass ranges.

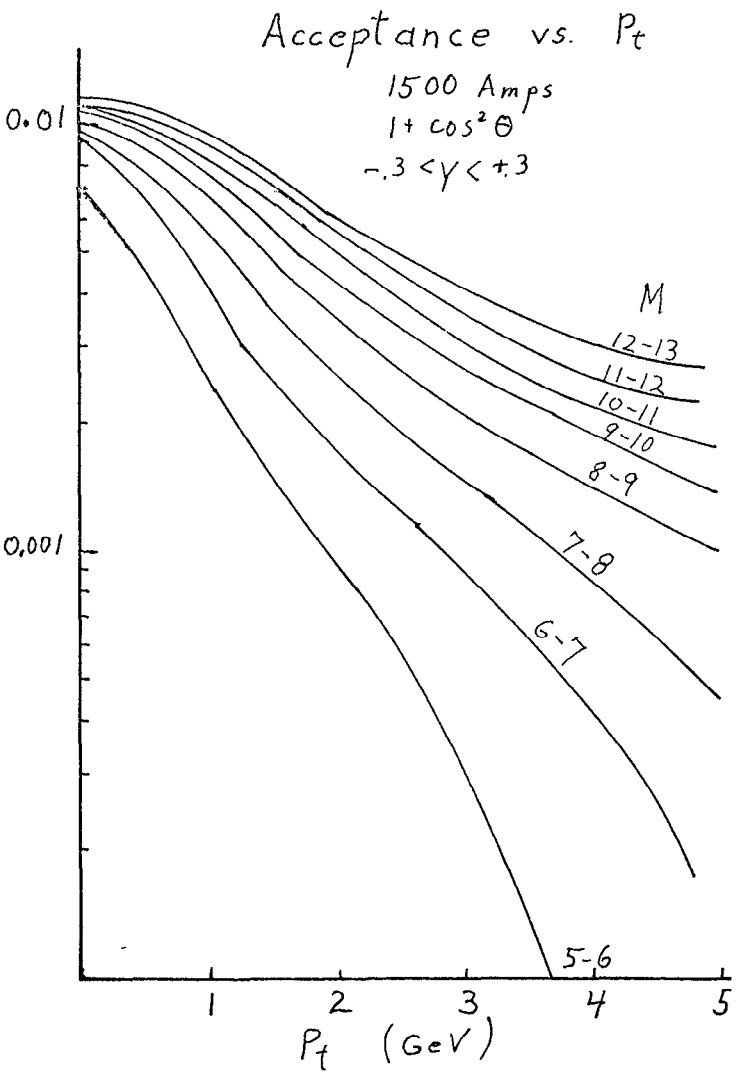

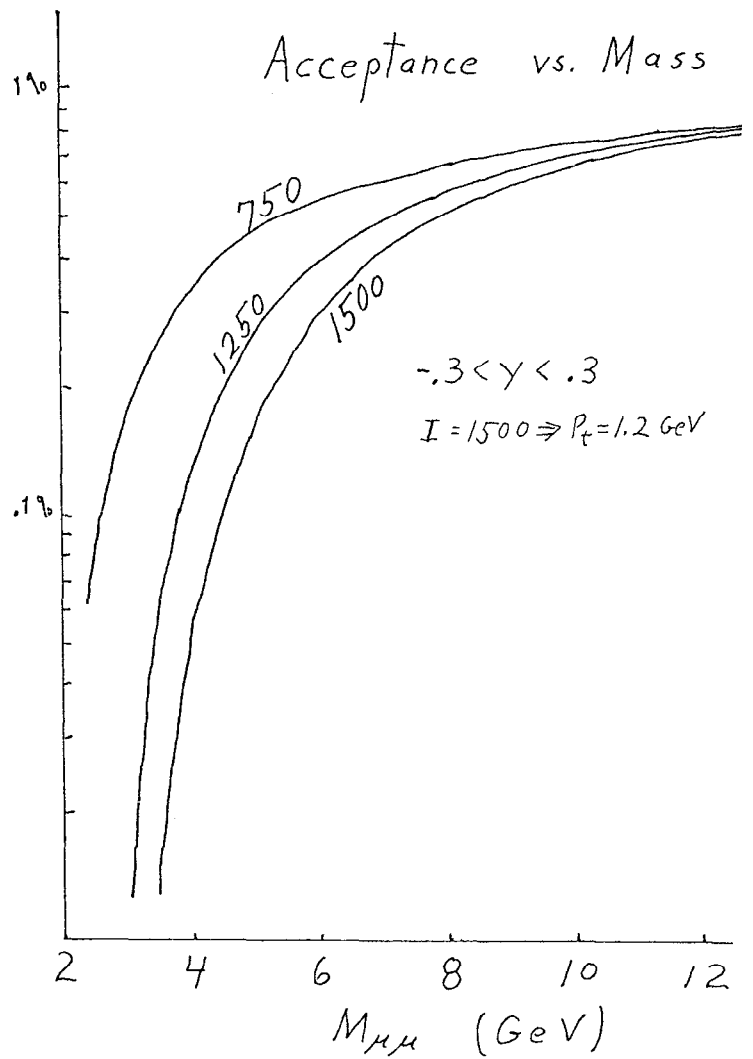

Figure 4: Pair acceptance as a function of mass.

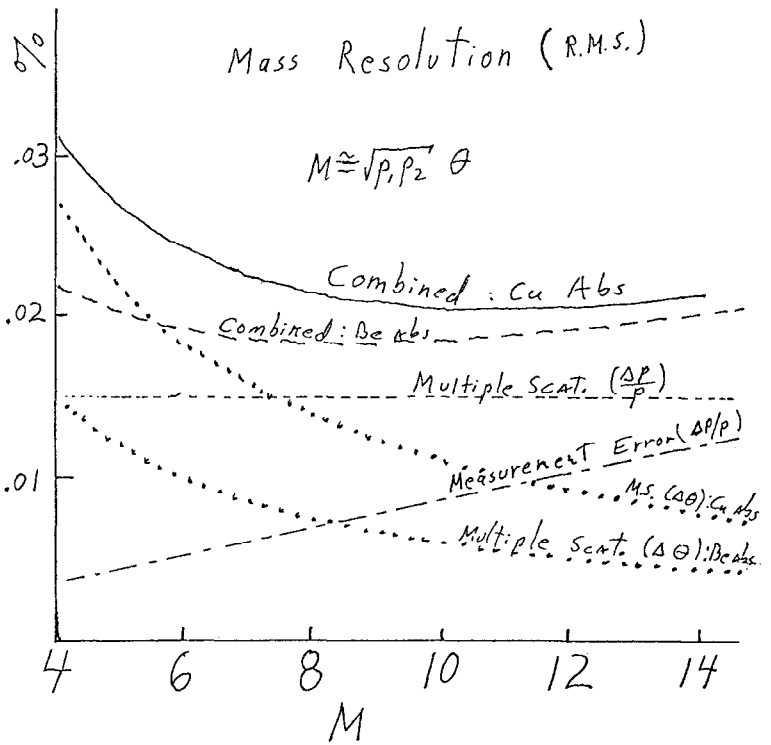

Figure 5: Mass resolution as a function of mass. Solid curve is for Cu absorber, dashed curve is for Be absorber, dotted curves are for various contributions as labeled.

resolution at high mass is not strongly affected. Figure 6 shows an event distribution for masses in the J/ψ region. We see clearly separated J/ψ and ψ' peaks with the expected widths. Expected and observed J/ψ widths for several air magnet excitations are shown in Table I.

Table II depicts a history of the data taken to date. During 600 hours of running 3.2×10^{16} protons were incident on the target resulting in 1×10^{16} interactions. Most of the data was taken with the Pt target, Cu absorber, and maximum excitation of the air magnet, i.e., the highest luminosity configuration.

To calculate cross-sections, the following corrections for apparatus efficiencies were made:

1) targeting ... 0.98 ± 0.02;
2) trigger and reconstruction ... 0.85 ± 0.10;
3) cuts on detectors behind the steel magnet ... 0.85 ± 0.10;
4) single track/arm requirement ... 0.90 ± 0.03.

These result in an overall efficiency correction of 0.64 ± 0.15.

Figure 7 shows the effect of these cuts on a typical event distribution. A 9-10 GeV enhancement is already prominant in the raw data. It becomes better defined when fiducial cuts are applied so that only well measured events are retained. With all cuts applied the enhancement is more prominant yet. Also shown are the same charge events.

TABLE I

J/ψ Resolution

(GeV r.m.s.)

Air Magnet Current	Predicted	Observed
750A	0.113	0.115
1000A	0.093	0.089
1250A	0.083	0.095

TABLE II

Date	Hours	Beam	Tgt.	Abs.	Mag. Curr.
5/14-6/05	180	8×10^{15}	Cu	Cu	1500A
6/05-6/12	70	2.5×10^{15}	Cu	Cu	1250A
6/12-6/19	50	1.6×10^{15}	Pt	Be	1250A
6/19-7/10	300	2.1×10^{16}	Pt	Cu	1500A
Total	600	3.2×10^{16}			

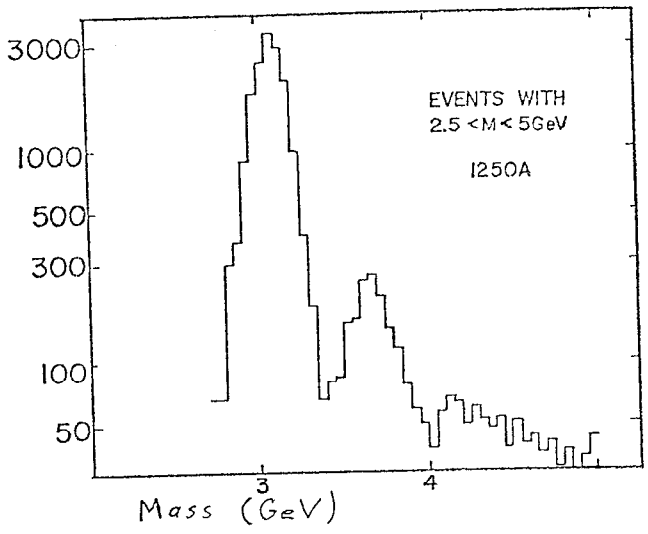

Figure 6: Mass distribution in the J/ψ region from air magnet excitation of 1250A.

Figure 7: Event distributions for various cuts: A) $\mu^+\mu^- + \mu^-\mu^+$, B) $\mu^+\mu^+ + \mu^-\mu^-$. This data is from the Cu target, Cu absorber, 1500A sample.

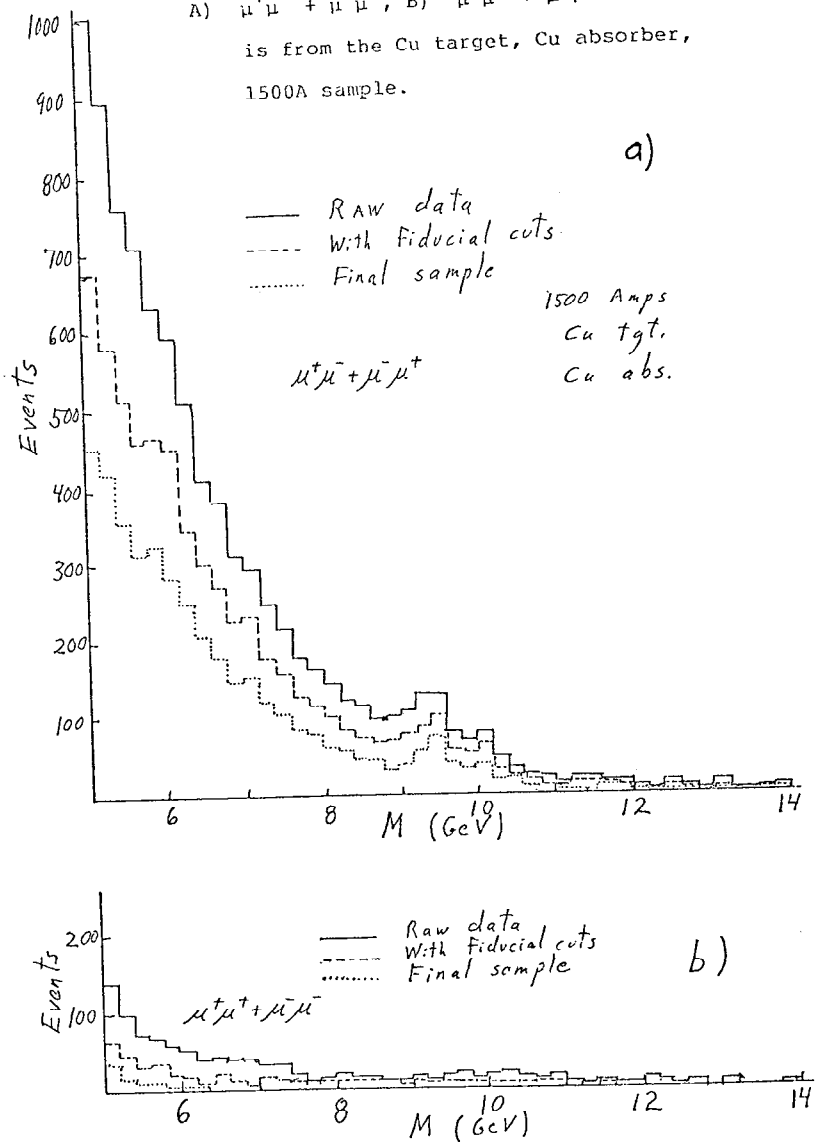

These events disappear as cuts are applied. If the ratio of pair cross-section to the product of single arm cross-sections is independent of particle type and charge for hadrons in the relevant kinematic region, then the hadron induced background plus muon accidentals satisfies the relation:

$$N_{+-} + N_{-+} = 2\sqrt{N_{++}N_{--}} \simeq N_{++} + N_{--} \quad .$$

The above premise has been shown to be true to the requisite accuracy in a previous experiment by this collaboration.[1] Therefore such background is negligible in this experiment (see again Fig. 1).

Checks were performed to verify that the origin of the 9-10 GeV enhancement was not apparatus. Data was taken with the air magnet excited to 1250 amps (1.0 GeV P_t-kick). This resulted in the spectrum shown in Fig. 8. The enhancement was present with same mass and cross-section. The confirmation of the target origin of the muons was checked using the PWC's located at the center of the air magnet. These chambers enabled a second remeasurement of the muon momentum. The apparatus was uniformly illuminated at all masses. A target out run yielded no events when 200 would have been obtained with target in. Subsets of data (current, time, absorber, target) yielded the same fit parameters. Paired muons from different events generated a smooth $d\sigma/dmdy$ curve.

Figure 8: Cross-section from the 1250A sample.

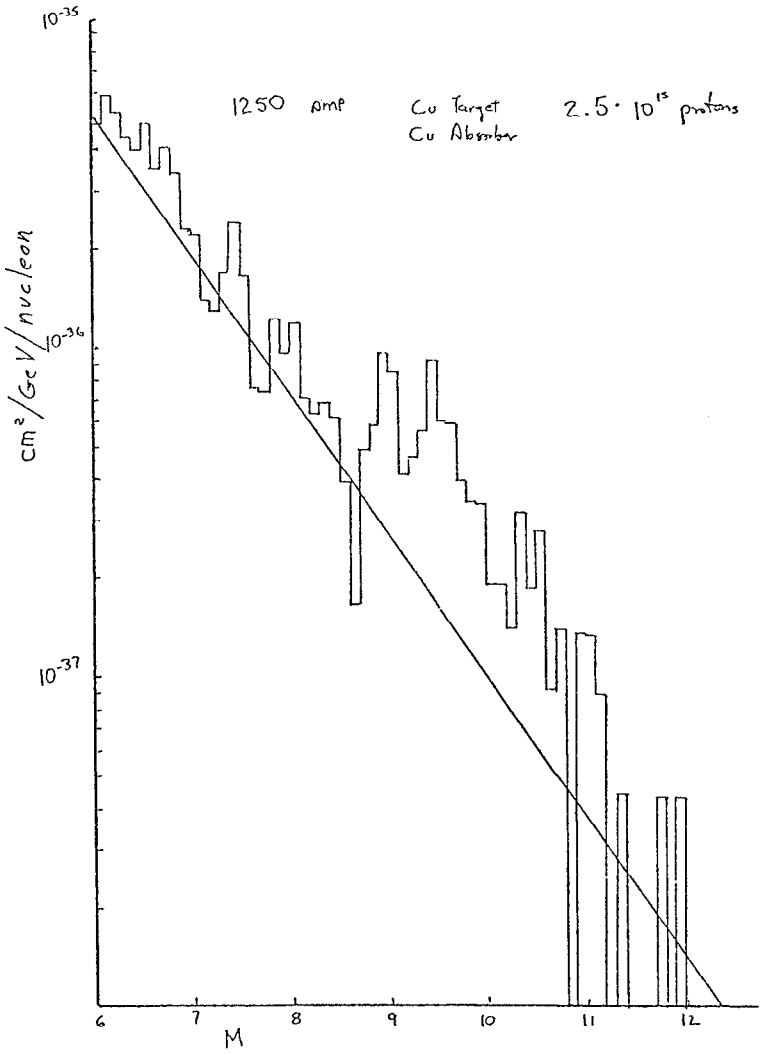

Return now to Fig. 1 for a closer look at the data. Fitting the region from 6-8.8 and 10.6-12 GeV with form Ae^{-bM} yields the result: A = 1.28 ± .03 nb, b = 0.93 ± .03 GeV^{-1}. χ^2 is 48 for 50 degrees of freedom. Subtracting this fit from the data yields the residual cross-section in Fig. 9. If this residual cross-section is fit with a single gaussian of arbitrary mass, width, and amplitude the result is: M = 9.5 ± .03 GeV, width (rms) = 0.47 ± .03 GeV, $\left.\frac{d\sigma}{dy}\right|_0$ = 0.31 ± .02 pb. χ^2 is 63 for 15 degrees of freedom, and the fit looks very bad. The curve in the figure is a fit using two gaussians whose widths are fixed at the experimental resolution of 2.1%. The fit parameters are: 1) M = 9.43 ± .02 GeV, $d\sigma/dy$ = 0.20 ± .02 pb; 2) M = 10.14 ± .04 GeV, $d\sigma/dy$ = 0.07 ± .01 pb. χ^2 is 29.2 for 14 degrees of freedom. While the confidence level of this fit is only about 1% it looks reasonable.

Following the suggestion of our paper of last year, the research team has decided to call the primary peak the T(9.4).[2]

A possible explanation of this resonance and its structure is that it is a bound state of a new quark and its anti-quark. Eichten and Gottfried[3] have predicted the level spacings of such a system based on charmonium and asymptotic freedom within the framework of a static-potential model. They predict a spacing of 0.44 GeV between the first and second states and 0.32 GeV between the second and third.

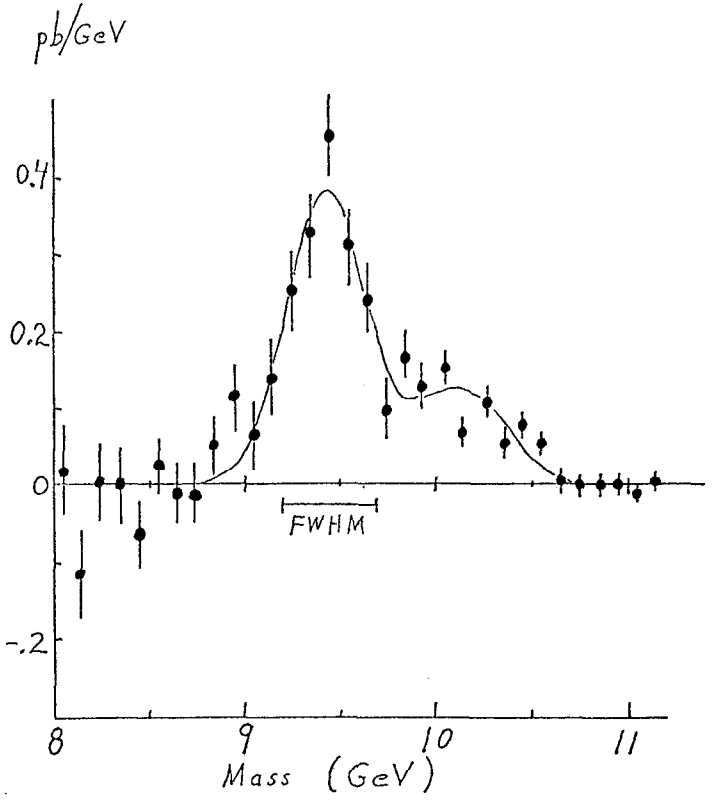

Figure 9: Cross-section in Fig. 1 with the continuum ($1.28\ e^{-0.93M}$) subtracted. The curve is the two gaussian fit.

A fit with three gaussians whose widths are fixed at 2.1% r.m.s. and whose spacings are fixed to Eichten and Gottfried's predictions yields: 1) M = 9.42 ± .02 GeV, $d\sigma/dy$ = .20 ± .02 pb; 2) $d\sigma/dy$ = 0.024 ± .012 pb; 3) $d\sigma/dy$ = .057 ± .010 pb. χ^2 is 26.7 for 14 degrees of freedom. This fit is nearly identical to the two gaussian fit. The ratios of $d\sigma/dy$ of 1:0.12:0.24 are not consistent with the quark-antiquark model on which the spacings were based. Therefore, the two peak fit is the more likely representation of the data. This suggests that if the system is an "onium" that the spacings are wider than those expected with the static potential used by Eichten and Gottfried. These fits are summarized in Table III.

Pursuing the quark-antiquark assumption we can ask what the expected $B \cdot d\sigma/dy$ would be. Cahn and Ellis[4] relate σ_Υ to σ_ψ with a gluon annihilaiton plus cascade model:

$$gg \to \chi_b \to \Upsilon\gamma.$$

They find: $$\sigma_\Upsilon = \frac{Mx_c^4}{Mx_b^4} \frac{Q_b^2}{Q_c^2} \frac{K_b^2}{K_c^2} \sigma_\psi,$$

and: $$B_{\Upsilon \to \mu\mu} \propto Q_b^2 \sim .1 \quad .$$

This implies $B_{\mu\mu}\ \sigma_\Upsilon \sim .4$ pb if $Q_b = -1/3$. This is in reasonable agreement with the data. $Q_b = 2/3$ would predict 6.4 pb.

TABLE III

Fit Results

	1	2	3
M_1	9.5 ± .03	9.43 ± .02	9.42 ± .02 GeV
$B \frac{d\sigma}{dy}_1$	0.31± .02	0.20 ± .02	0.20 ± .02 Pb
width (rms)	4.9 ±0.3	2.1	2.1%
M_2	-	10.14 ± .04	9.86 GeV
$B \frac{d\sigma}{dy}_2$	-	0.07 ± .01	0.024± .012 Pb
M_3	-	-	10.18 GeV
$B \frac{d\sigma}{dy}_3$		-	0.057± .010 Pb
χ^2/DF	63/15	29.2/14	26.7/14

Cahn and Ellis also predict an integrated cross-section of ~200 nb MeV for Q = -1/3 in e^+e^- annihilation. This should make such a resonance easy to see if not as convenient to study as charmonium.

Figure 10 shows the scaling form of the J/ψ production cross-section plotted as a function of $\sqrt{\tau} = M/\sqrt{S}$. Also marked is where on this curve T production at Fermilab falls. It is about equivalent to J/ψ production at Brookhaven indicating that considerably larger cross-sections might be expected at the ISR or Isabelle.

The continuum has not been studied as carefully as the resonance(s) but some preliminary indications may be of interest. $d\sigma/dmdy$ is consistent with reasonable Drell-Yan predictions. Some typical P_t distributions are displayed in Fig. 11. The curve through the mass 5-6 GeV points is $1/(P_t^2 + 2.25)^3$. The higher mass points break more sharply at low mass but are consistent with this form for $P_t > 1.5$ GeV. Mean P_t as a function of mass is shown in Fig. 12. $< P_t >$ appears to have leveled off after a rising at lower masses.[5]

As I talk data continues to be accumulated. In August when the accelerator begins a six week shut-down 50% more data should be on tape. In addition target atomic number dependence studies will have been done. When the machine resumes operation S dependence (200 and 300 GeV operation) will be measured. After that we will make apparatus modifications which we hope will improve the resolution by a factor of 2.

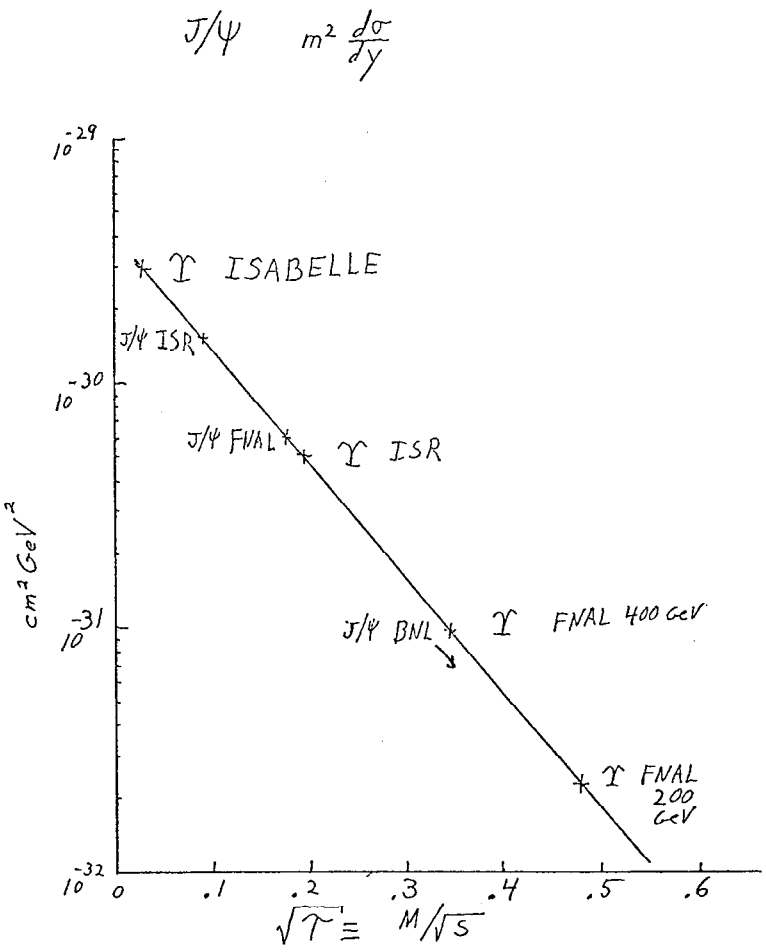

Figure 10: $M^2 d\sigma/dy$ for J/ψ production. Shown are the ϒ values for T production at various accelerators.

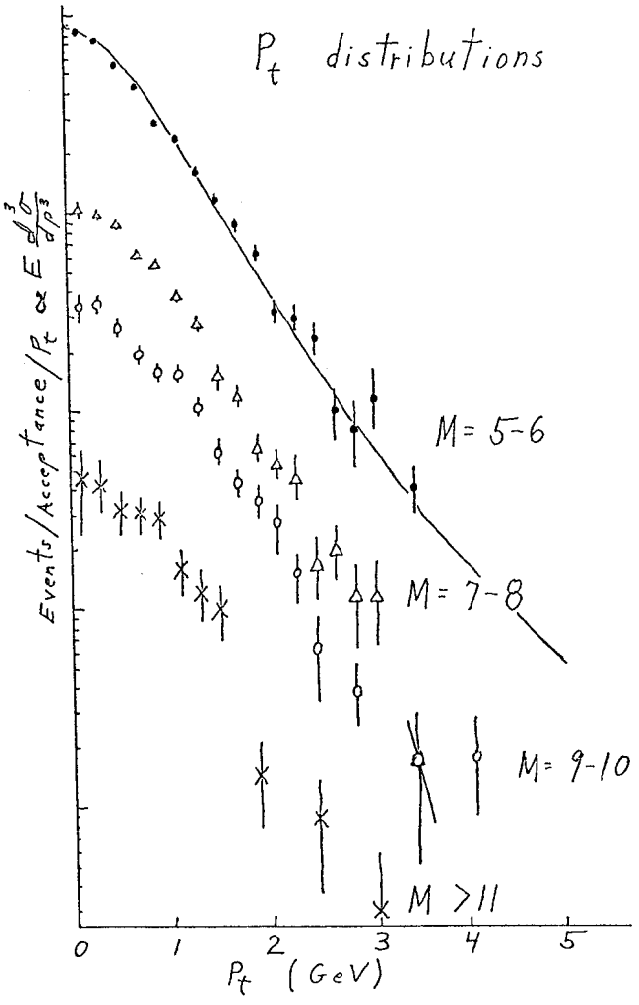

Figure 11: P_t distributions for various masses. The curve is α $1/(2.25 + P_t^2)^3$.

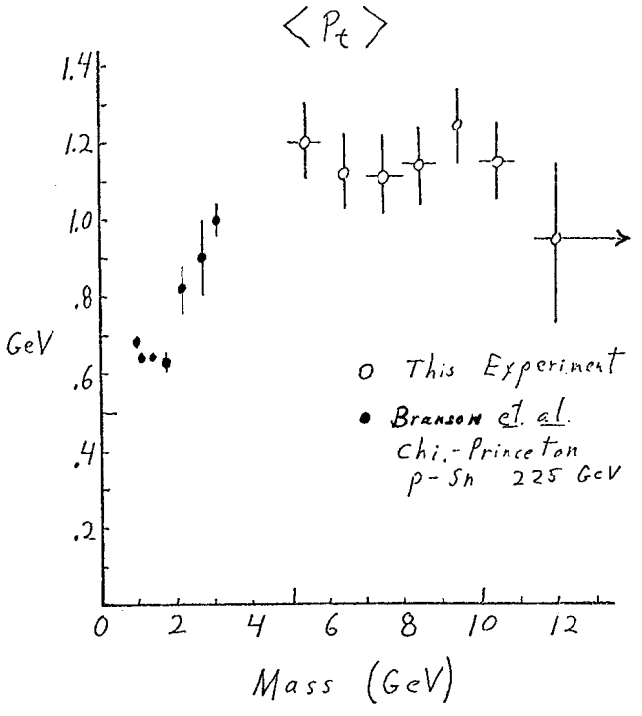

Figure 12: Mean P_t as a function of mass. The low mass points are from Ref. 5.

A preliminary version of this work is being published.[6] A paper based on all data through August will be submitted in early fall.[7]

REFERENCES

[1]R. Fisk, et al., to be published.

[2]D. Hom, et al., PRL 36, 1236 (1976).

[3]E. Eichten and K. Gottfried, Phys. Lett., 66B, 286 (1976).

[4]R. Cahn and S. Ellis, UMHE 76-45.

[5]Branson et al., 38, 1334 (1977).

[6]S. Herb, et al., PRL, 39, 252 (1977).

[7]W. Innes, et al., to be submitted to PRL.

MULTIMUON PRODUCTION BY HIGH ENERGY NEUTRINOS

A. Benvenuti, D. Cline, P. Cooper, M. Heagy, R. Imlay,
M.E. Johnson, T.Y. Ling†, R. Lundy, A.K. Mann, P. McIntyre,
S. Mori, D.D. Reeder, J. Rich, C. Rubbia, R. Stefanski and D. Winn

Fermilab
P.O. Box 500
Batavia, Illinois 60510

Department of Physics
Harvard University
Cambridge, Massachusetts 02138

Department of Physics
University of Pennsylvania
Philadelphia, Pennsylvania 19104

Department of Physics
Rutgers University
New Brunswick, New Jersey 08903

Department of Physics
University of Wisconsin
Madison, Wisconsin 53706

Presented by T.Y. Ling† University of Pennsylvania

†Present Address: Department of Physics, Ohio State University,
Columbus, Ohio 43210

Introduction

One of the most interesting discoveries in recent years has been the production of multilepton events by high energy neutrinos. Dimuon events were first observed by the HPWF Collaboration at Fermilab in 1974.[1] The characteristics of the dimuons as well as the observed rate in targets of different density[2] led the experimenters to conclude that the dimuon events were due to the production and weak semileptonic decay of new hadron(s) carrying a new quantum number. Dilepton production from other neutrino experiments[3-8] confirmed the earlier HPWF observation. With the discovery of the D-mesons from e^+e^- collisions[9], it became clear that the new quantum number was indeed 'CHARM' as originally conjectured by Glashow, Iliopoulous and Maiani.[10]

In this talk I will report the observation and characteristics of six neutrino induced events each with three muons in the final states (trimuon events). The properties of some of these trimuon events strongly indicate that the source of these events involves new physics beyond charm.

Detector

The original HPWF detector[11] has been substantially modified and now consists of three separate target detectors and two large magnetic spectrometers. This new detector is schematically shown in Fig. 1. The three target-detectors have different densities: ~ 8 gm/cm^3 for the three sections of the Fe target (FeT), total mass 250 metric tons; ~ 0.8 gm/cm^3 for the 12 modules of the liquid scintillator calorimeter (LiqC), total mass 45 metric tons; and ~ 3 gm/cm^3 for the 10 modules of Fe-plate calorimeter (FeC), total mass 90 metric tons. Wide gap optical spark chambers are inserted throughout the entire detector to provide visual information about an event. The LiqC and the FeC provide timing information and determine the hadronic energy deposited in them with uncertainties of 15% and 20%, respectively. The 8-meter diameter magnetic muon spectrometer measures the charge and momentum of wide angle ($\lesssim 600$ mrad) muons of momentum as low as 3 GeV/c. The 8m and 4m spectrometers together provide approximately $\pm$ 15% momentum resolution. A large area, 35 cm x 35 cm grid, liquid scintillation counter hodoscope in the 8 m spectrometer, and counters in the 4 m spectrometer furnish trigger requirements for one and two muon final states in addition to other triggers based on a minimum energy deposition in LiqC or FeC.

Data

The data reported here were acquired from a run in December 1976. The incident neutrino-antineutrino mixed beam was obtained from quadrupole triplet focusing of the secondary hadrons produced by 400 GeV protons. The ν_μ and $\bar{\nu}_\mu$ spectrum is shown in Fig. 2. Note that above 100 GeV there is very little $\bar{\nu}_\mu$ flux, the beam consists predominantly of ν_μ.

Four of the six observed trimuon events are shown in Fig. 1 and Fig. 3 - 5. The events are sketched on the detector as shown. In each case three penetrating tracks emerging from a common vertex were observed in the spark chambers. Three times minimum ionizing signals were observed in the calorimeter for each of these events as indicated by the pulse height distributions. The range and energy loss together unambiguously identify these tracks as muons. The measured muon momentum and sign of electric charge and labeled for each muon. The most striking event of the six, event 119-017911 is shown in Fig. 5. This event originated in the FeC.

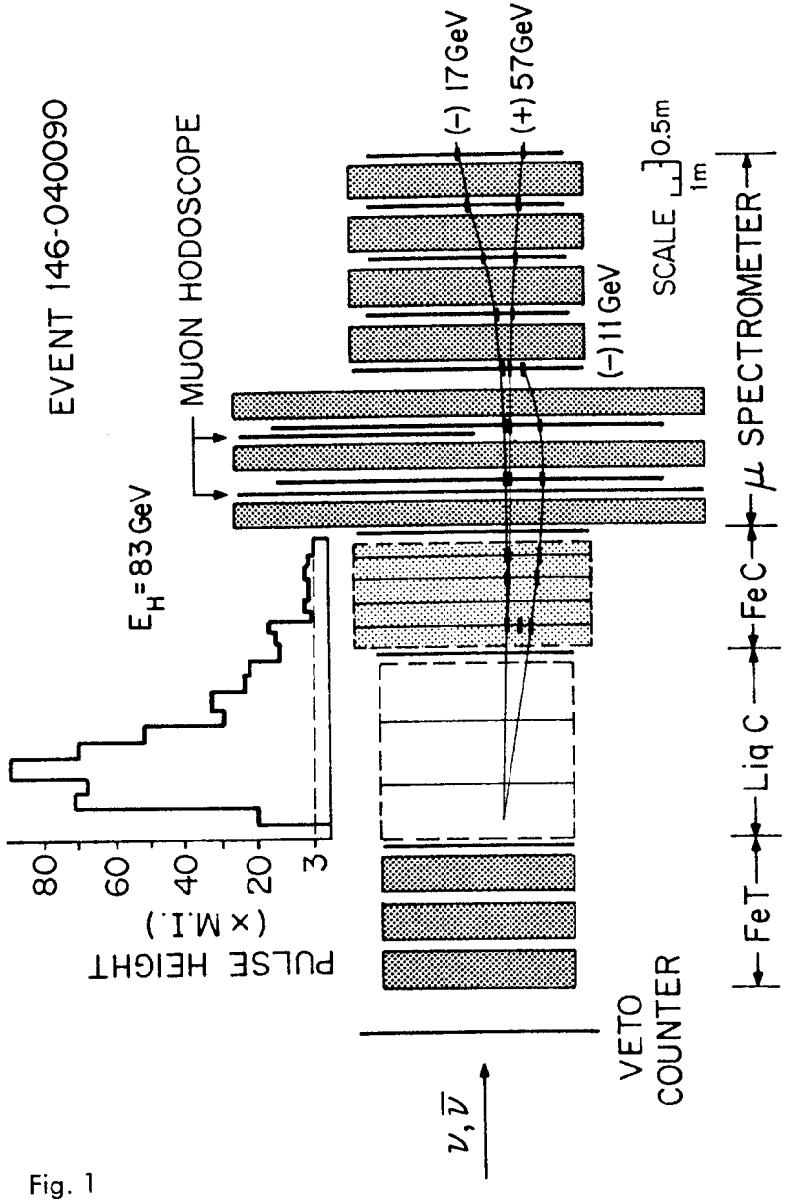
EVENT 146-040090
MUON HODOSCOPE
(-) 17 GeV
(+) 57 GeV
(-) 11 GeV
SCALE 0.5m 1m
E_H = 83 GeV
PULSE HEIGHT (× M.I.)
80
60
40
20
3
μ SPECTROMETER
Fe C
Liq C
Fe T
VETO COUNTER
ν, ν̄

Fig. 1

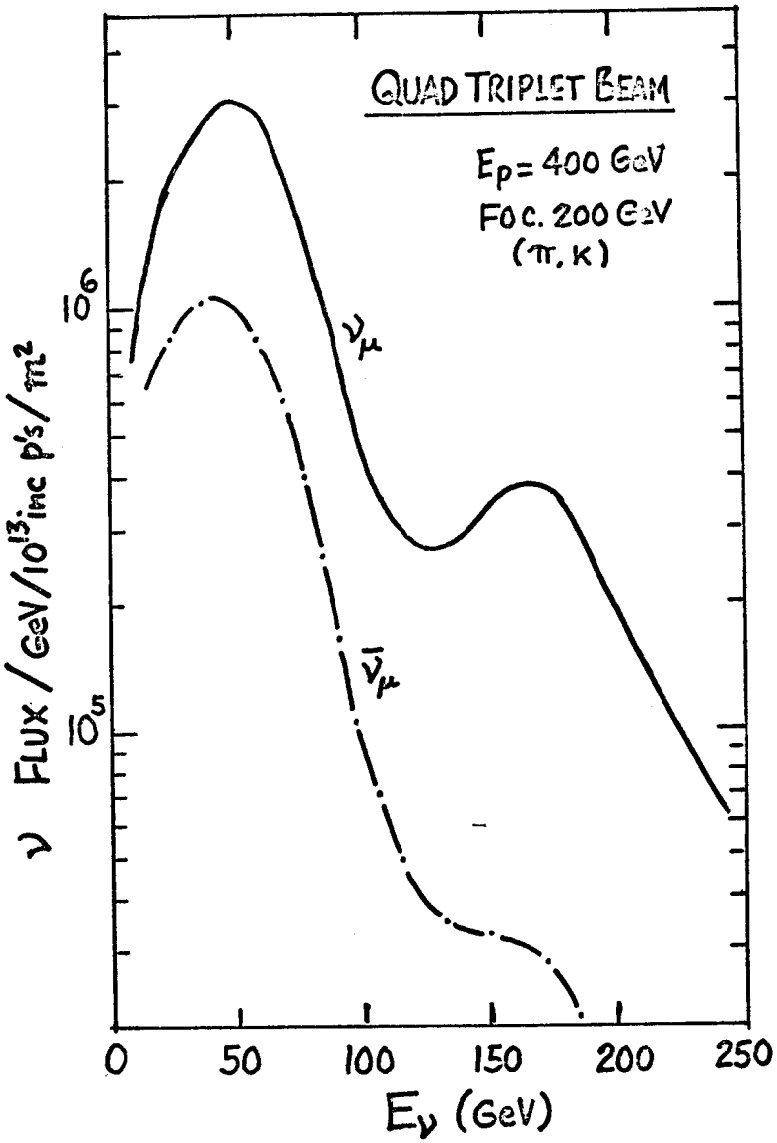
QUAD TRIPLET BEAM
E_p = 400 GeV
Foc. 200 GeV
(π, K)
ν_μ
$\bar{\nu}_\mu$
ν FLUX / GeV / 10^{13} inc p's / m²
10^6
10^5
0
50
100
150
200
250
E_ν (GeV)

Fig. 2

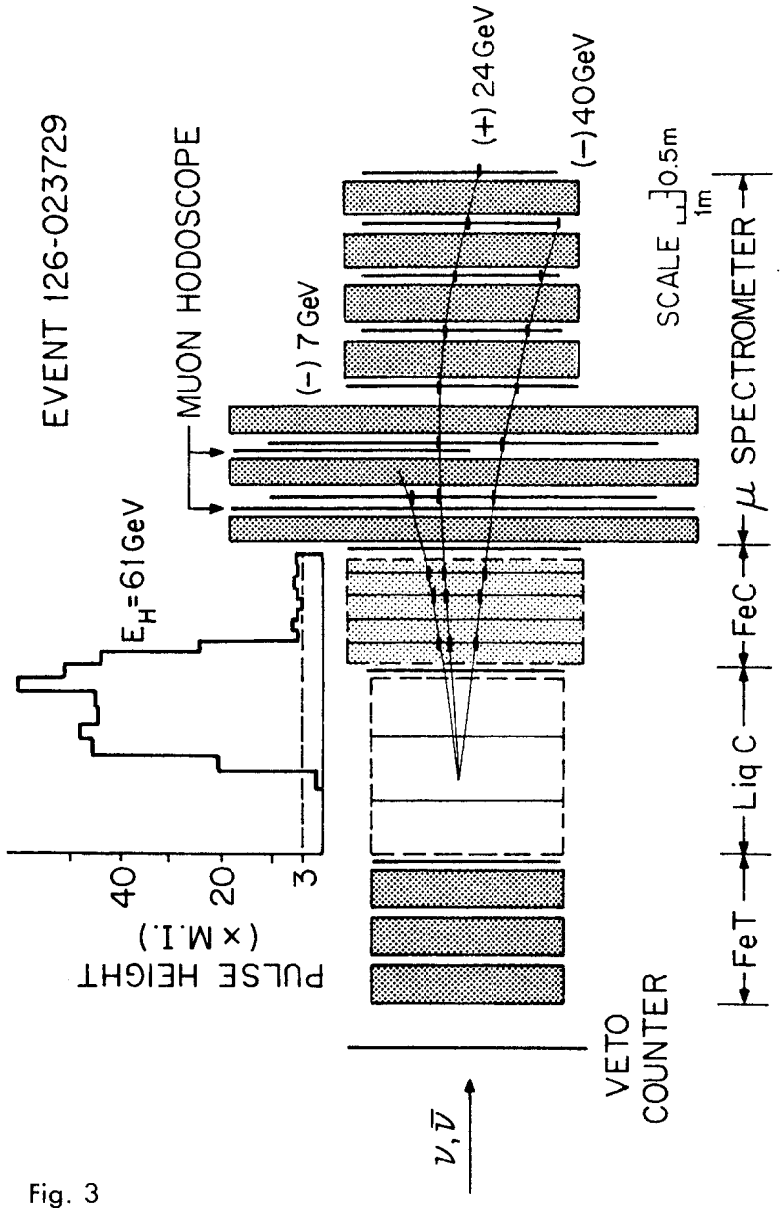
EVENT 126-023729
MUON HODOSCOPE
E_H=61GeV
(-) 7 GeV
(+) 24GeV
(-) 40GeV
SCALE 0.5m 1m
PULSE HEIGHT (× M.I.)
40
20
3
VETO COUNTER
FeT
Liq C
FeC
μ SPECTROMETER
ν, ν̄

Fig. 3

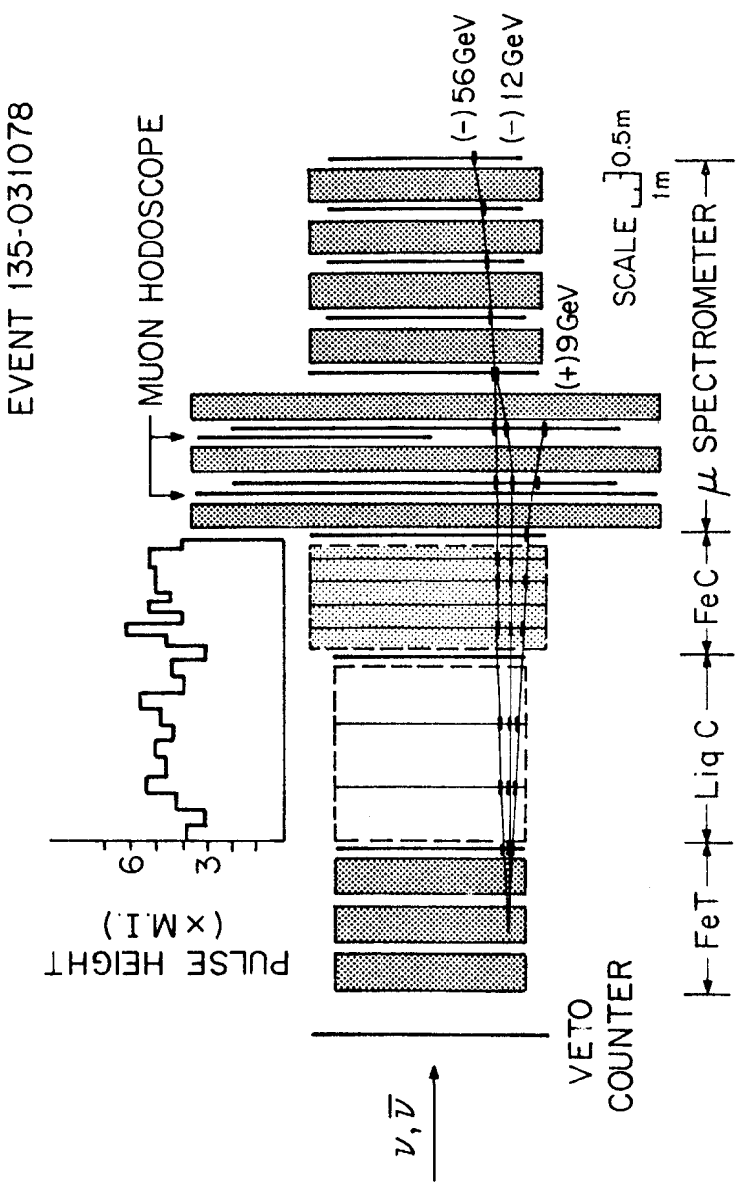
EVENT 135-031078
MUON HODOSCOPE
(-) 56GeV
(-) 12GeV
(+) 9GeV
SCALE 0.5m 1m
PULSE HEIGHT (× M.I.)
6
3
VETO COUNTER
FeT
Liq C
FeC
μ SPECTROMETER
ν, ν̄

Fig. 4

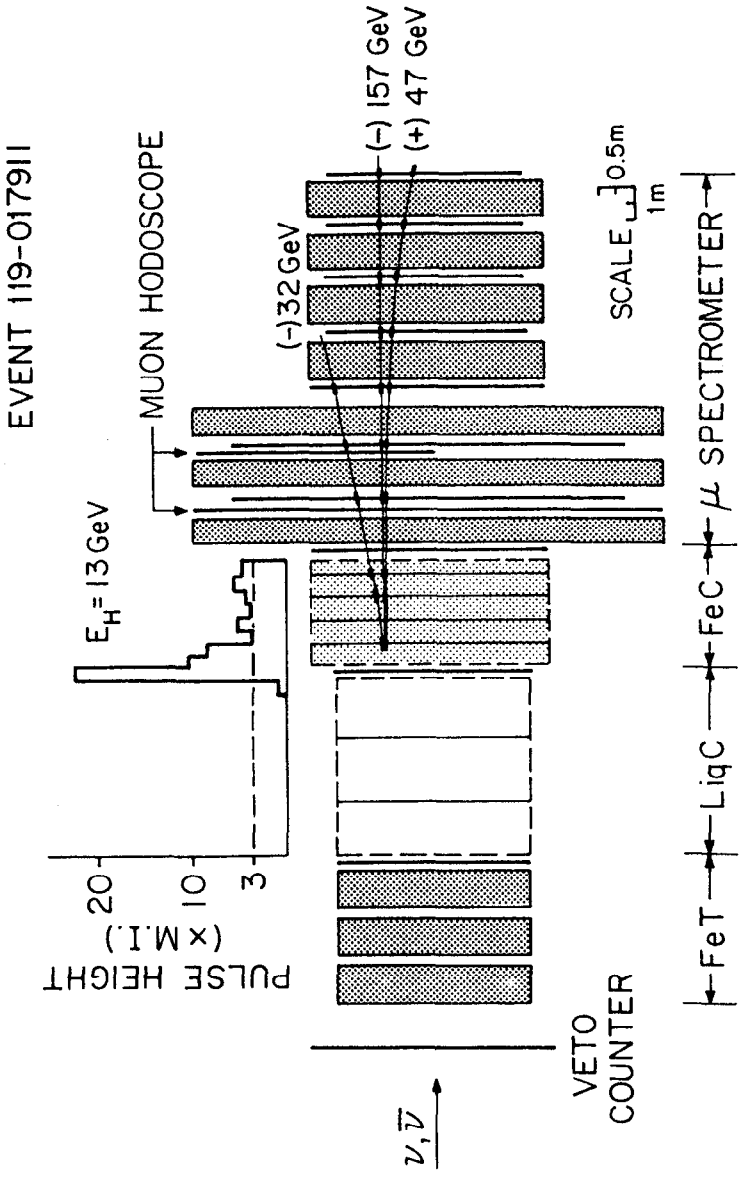

Fig. 5

TABLE 3

Event	$\mathcal{D}$ /10^{-4}
58	< 0.03
119	0.003
126	0.1
135	0.02
138	0.09
146	0.005

TABLE I - Properties of the Observed Trimuon Events.

RUN FRAME	TGT MOD	ENERGY(GeV) E_{vis}	ENERGY(GeV) E_H	MOMENTUM(GeV) MU(1)	MU(2)	MU(3)	ANGLE(mrad) θ_{12}	θ_{13}	θ_{23}	INVAR.MASS(GeV/c^2) M_{12}	M_{13}	M_{23}	M_{123}
58 796791	FeT 2	$\gtrsim$ 82	-	(-) 52 ± 7	(-) 20 ± 5	(+) >10	36	29	58	1.2 ±0.4	>0.64	>0.82	>1.6
119 017991	Liq 12	249 ± 25	13 ± 2	(-) 157 ± 24	(-) 32 ± 6	(+) 47 ± 8	67	16	77	4.7 ±0.9	1.4 ±0.9	3.0 ±0.5	5.8 ±1.3
126 023729	Liq 6	131 ± 13	61 ±10	(-) 40 ± 6	(-) 6 ± 4	(+) 24 ± 4	204	113	149	3.2 ±1.0	3.5 ±0.5	1.8 ±1.2	5.1 ±1.6
135 031078	FeT 2	$\gtrsim$ 82	-	(-) 57 ± 9	(-) 14 ± 2	(+) 11 ± 6	39	51	24	1.1 ±0.3	1.3 ±0.8	0.3 ±0.2	1.7 ±0.9
138 032717	FeT 3	$\gtrsim$ 48	-	(-) 29 ± 4	(-) 4 ± 1	(+) 15 ± 2	266	110	272	2.9 ±0.3	2.3 ±0.3	2.2 ±0.2	4.3 ±0.5
146 040090	Liq 2	168 ± 15	83 ±12	(-) 17 ± 3	(-) 11 ± 3	(+) 57 ± 7	46	37	68	0.6 ±0.2	1.2 ±0.3	1.7 ±0.4	2.2 ±0.5

All three muons have momenta above 30 GeV. While the combined energy carried by the three muons exceeds 200 GeV, the hadronic energy deposited is only 13 GeV.

Tables 1 and 2 list the properties of the six trimuon events. Observe that three of these events occur in FeT, two in LiqC and one in FeC. One common property of these events is the high total visible energy measured. For the three events which occur in the calorimeter, one measures the hadronic energy and the resulting total visible energy, $E_{vis} \equiv E_h + E_{\mu 1} + E_{\mu 2} + E_{\mu 3}$, is well above 100 GeV. The distribution in E_{vis} is shown in Fig. 6. Another common property is the small opening angles between the muons.

It is difficult to specify the rate of trimuon production accurately because the detection and reconstruction efficiencies are not accurately known yet. However, it seems reasonable to make a rate comparision with opposite sign dimuons observed in the same run. We obtain a rate

$$\left[R(\mu\mu\mu)/R(\mu\mu)\right]_{E_{vis} > 100\ GeV} \sim 0.05,$$

with no corrections for relative scanning, detection or reconstruction efficiencies.

Possible Origins of the Trimuons

There are several possible origins of the trimuon events. These possibilities are discussed below.

(A) Accidental space-time coincidence of a dimuon event with a muon from a single muon event. The three muons are in time within 200 nsec while the beam spill length is $\sim$2msec, the probability of chance coincidence in time of a dimuon and a single muon is therefore $\sim 10^{-3}$. Similarly, since the neutrino beam profile is roughly the cross section of the detector, the probability of chance coincidence in space is given by the ratio of the

Table II. Momentum Components of the Three Muons of Each Trimuon in Table I.

RUN FRAME	MOMENTUM (GeV/c)								
	P_{x1}	P_{y1}	P_{z1}	P_{x2}	P_{y2}	P_{z2}	P_{x3}	P_{y3}	P_{z3}
58* 796791	-	-	-	-	-	-	-	-	-
119 017991	2.5 ±0.4	0.79 ±0.2	157 ±24	-0.63 ±0.1	2.0 ±0.5	32 ±6	0.46 ±0.06	-0.45 ±0.07	47 ±8
126 023729	0.18 ±0.07	-3.3 ±0.3	40 ± 6	1.04 ±0.8	0.23 ±0.3	6 ±4	0.51 ±0.14	0.71 ±0.04	24 ±4
135 031078	0.20 ±0.07	0.54 ±0.07	57 ± 9	-0.49 ±0.06	0.08 ±0.07	14 ±2	-0.42 ±0.50	-0.20 ±0.40	11 ±6
138 032717	-0.71 ±0.03	1.10 ±0.02	29 ± 4	0.65 ±0.13	-0.67 ±0.13	4 ±1	-1.40 ±0.3	-0.69 ±0.12	15 ±2
146 040090	0.9 ±0.04	-0.03 ±0.04	17 3	0.74 ±0.14	-0.52 ±0.08	11 ±3	0.85 ±0.08	0.01 ±0.05	57 ±7

*Event obtained in test run when 90° stereo view not accurately aligned.

volume into which the three muons are extrapolated to the total detector volume. This ratio is about 6 x 10^{-3}. Taking the dimuon rate of 10^{-2} per single muon, we obtain the probability per single muon event that a trimuon event is an accidental space-time coincidence to be $\sim 2x0.01x10^{-4}x6x10^{-3} \sim 10^{-8}$. This is to be compared with the observed trimuon rate of $\sim 10^{-4}$ per single muon. We conclude that this is not the source for the trimuons.

(B) Decay in flight of a pion or a kaon in the hadronic cascade of a dimuon event. The probability for this source can be calculated for each of the trimuon events. Briefly, the probability is given by $\mathcal{P} = 10^{-2} \int f(z) \left(\frac{\lambda abs}{\lambda decay}\right)$; where $f(z) = 2\, e^{-8z}$ is the probability of producing a π^- with $E_\pi - /\nu \geq z$ and ν is the total hadronic energy. This z-distribution, as shown in Fig. 7, was measured in a bubble chamber neutrino experiment by Berge et al.[12] The calculated probabilities are shown in Table 3. We conclude from the small probabilities that it is very unlikely that all 6 trimuons are caused by pion or kaon decay from a dimuon event.

(C) Direct muon pair production at the hadron vertex similar to the yield of prompt muon pairs observed in hadron-hadron collisions. Trimuon data is compared with data for the process $\pi N \to \mu^+\mu^- +$ anything from the Chicago-Princeton collaboration.[13] Fig. 8a shows the invariant mass distribution of the μ-pair from Ref. 13. It is observed that the mass distribution falls by 4 orders of magnitude between 0 and 2 GeV/c^2. Fig. 8b shows the invariant mass distribution between opposite sign muons for the trimuon events. No sharp peaking of $M_{\mu^-\mu^+}$ near 0 is observed, contrary to the hadron data. Fig. 9a shows the distribution in $p_\perp$ of the muon pair in the hadron data. The $p_\perp$ distribution of the muon pair with respect to W-direction, assuming one of the μ^- being the leading muon, is shown in Fig. 9b.

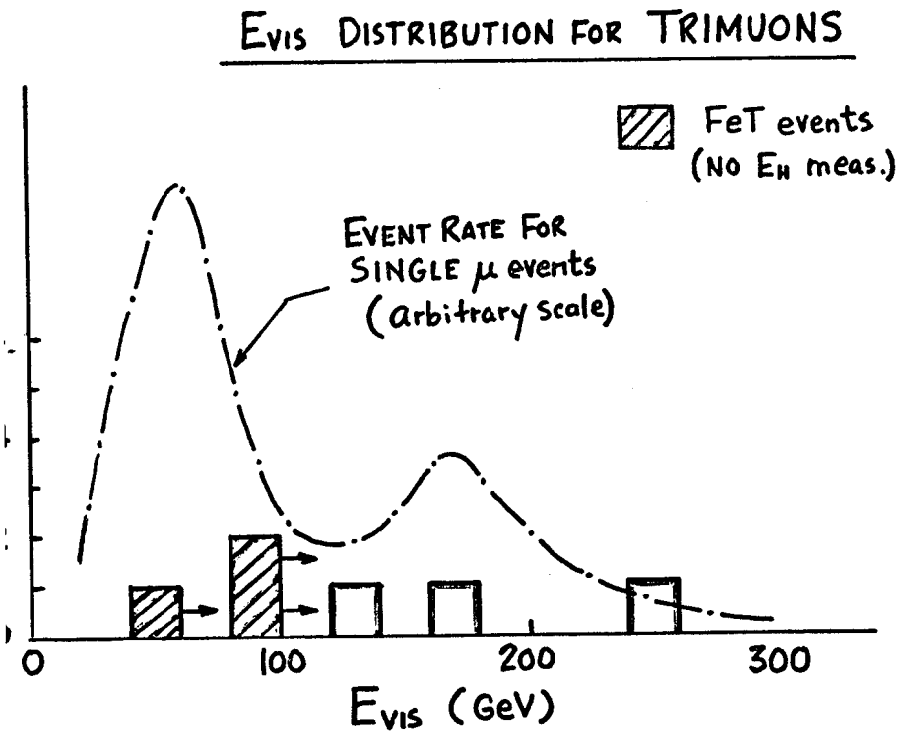
E_VIS DISTRIBUTION FOR TRIMUONS
FeT events
(NO E_H meas.)
EVENT RATE FOR
SINGLE μ events
(arbitrary scale)
0
100
200
300
E_VIS (GeV)

Fig. 6

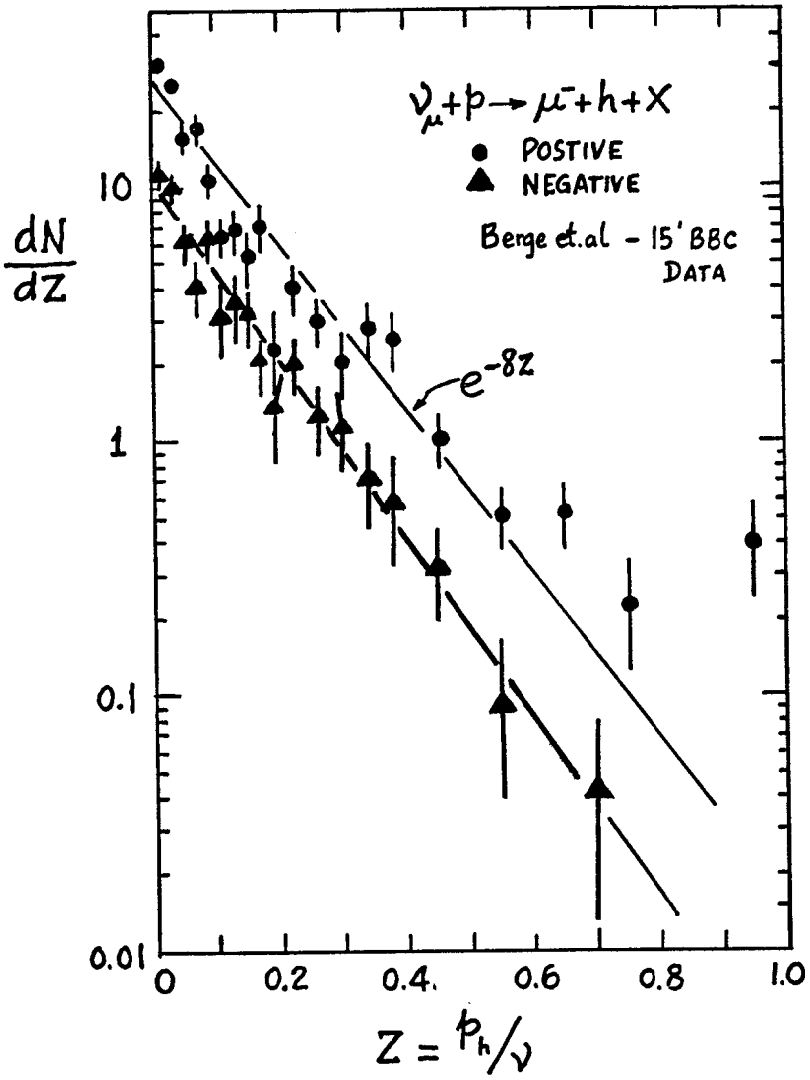
ν_μ+p→μ⁻+h+X
POSTIVE
NEGATIVE
Berge et.al - 15' BBC
DATA
dN/dz
e^-8z
10
1
0.1
0.01
0
0.2
0.4
0.6
0.8
1.0
Z = p_h/ν

Fig. 7

Anderson et.al.
Phys. Rev. Lett. 37, 799 (1976)

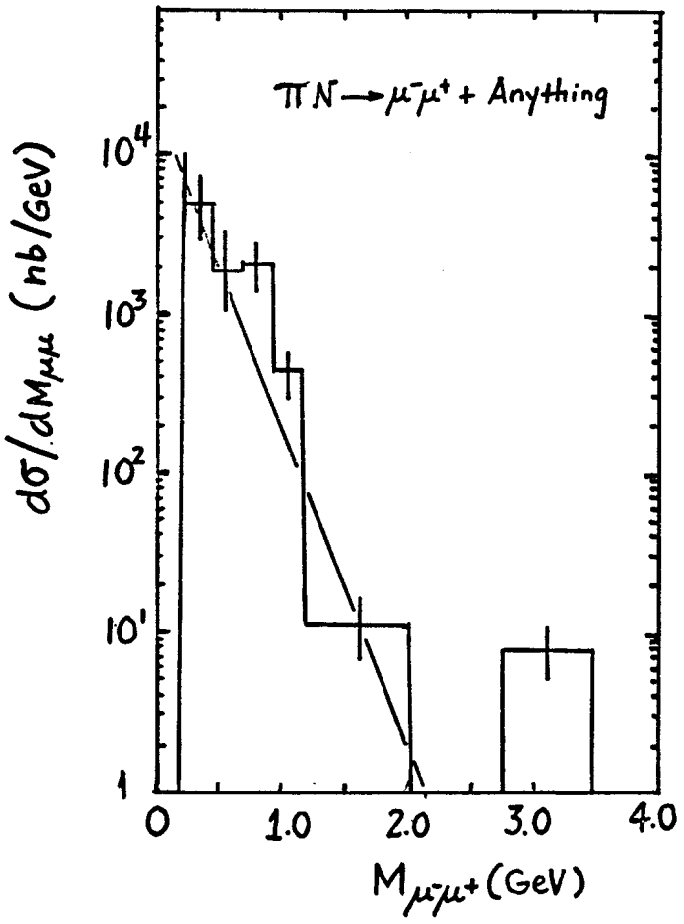

FIG. 8a

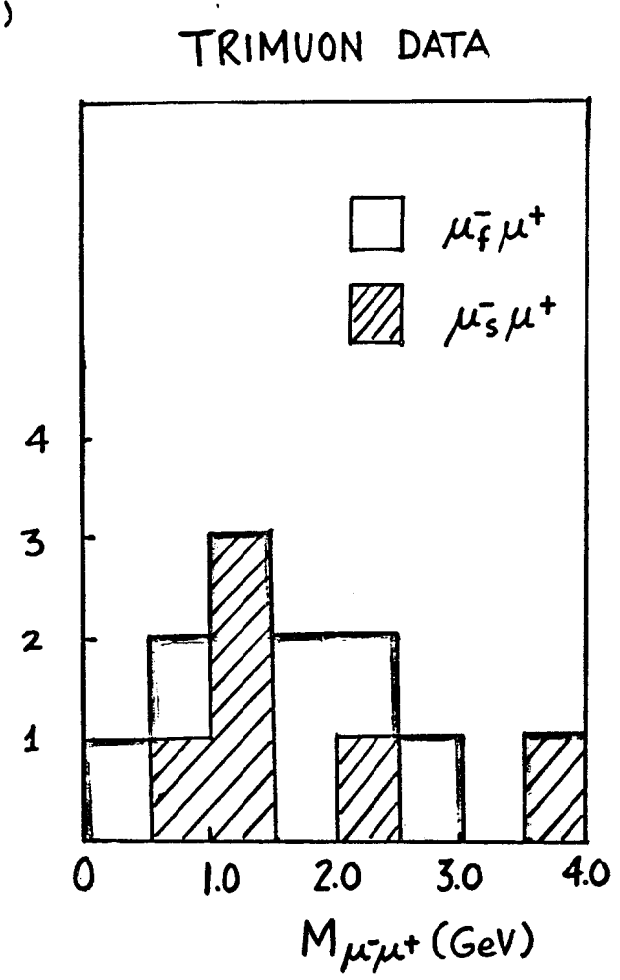

FIG. 8b

$\pi Be \rightarrow \mu^-\mu^+ + Anything$

Anderson et.al., Phys. Rev. Lett. 37, 799 (1976)

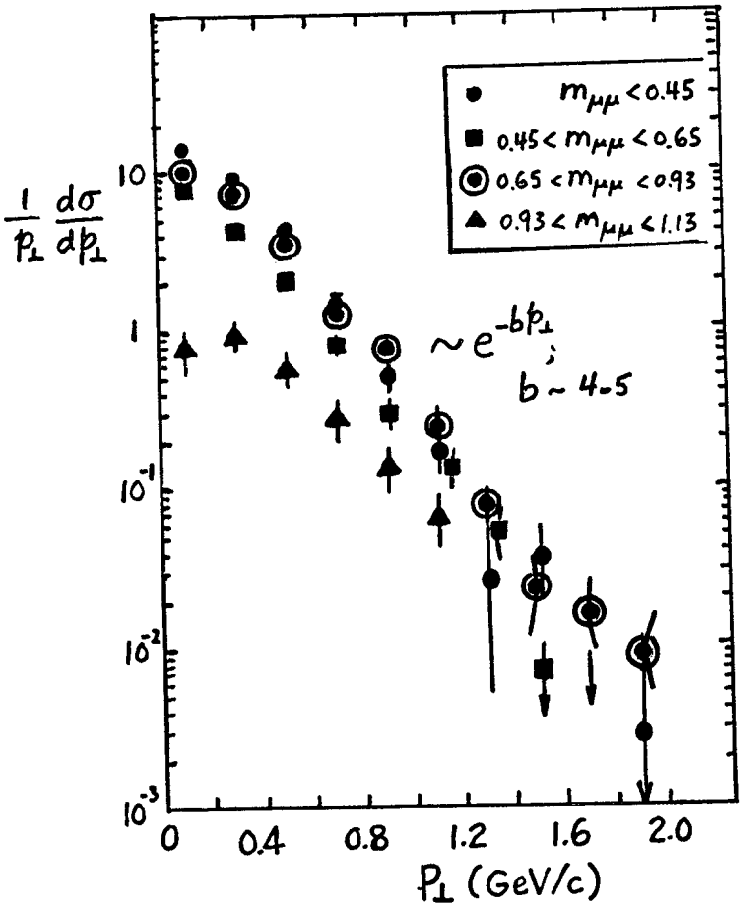

$\langle p_{\perp\,pair} \rangle \sim 0.4$ GeV

FIG. 9a

TRIMUON DATA

$\langle p_{\perp\,pair} \rangle \sim 2$ GeV

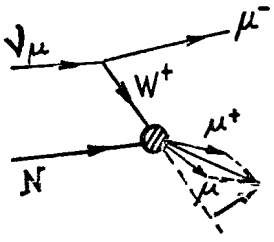

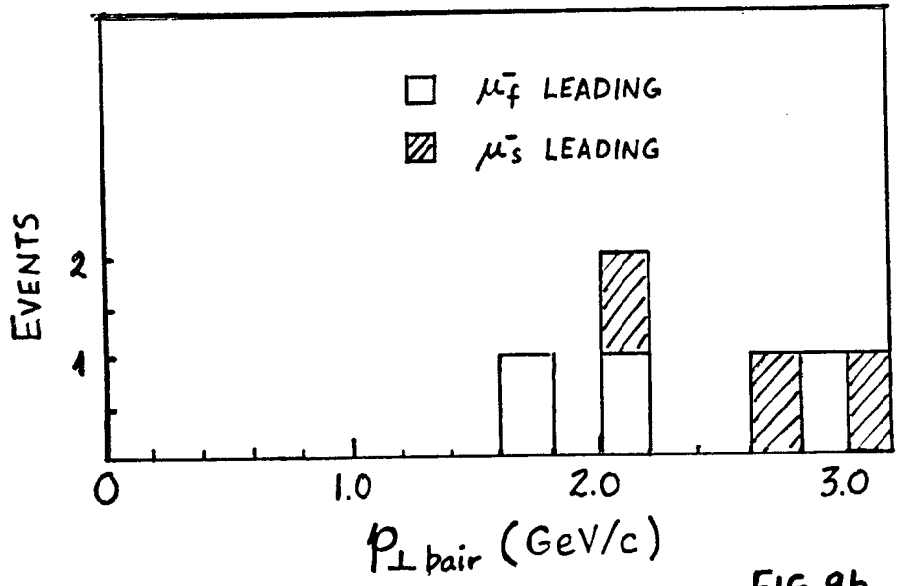

FIG. 9b

Again the sharp fall in $P_\perp$ of the hadron data is not observed in the trimuon data. The average $p_\perp$ for the hadron data is about 0.4 GeV/c while the average $p_\perp$ for the trimuon data is about 2 GeV/c. These marked differences between direct muon pair production and the trimuon events rule out direct muon pair production at the hadron vertex as the sole source for trimuons.

(D) Associated charm production through charge current interaction with subsequent semileptonic decay of both the c and $\bar{c}$ particles:

i.e. $\nu_\mu + N \rightarrow \mu^- + c + \bar{c}$ + anything

$\qquad\qquad\qquad\qquad\qquad \bar{c} \rightarrow \mu^- \nu + x$

$\qquad\qquad\qquad\qquad c \rightarrow \mu^+ \nu + x'$

- *For this process we expect the following characteristics:* (i) low energy muons from the c and $\bar{c}$ decays, since the c or $\bar{c}$ particles are produced at the hadron vertex with some fragmentation function $f(z)$, or in other words, they must share with other hadrons produced the total energy transfer $\nu = E_\nu - E_{\mu(\text{leading})}$ to the hadron vertex; (ii) Small $p_\perp$ of each of the extra muons with respect to the W-direction; (iii) Azimuthal symmetry about the W-direction for the extra muons since the c and $\bar{c}$ particles are produced uncorrelated at the hadron vertex. To examine whether the trimuon events exhibit the above properties, we compare the trimuon data with opposite sign dimuon data since the bulk of the $\mu^+\mu^-$ data are believed to be due to single charm production. In Fig. 10 we show the scatter plot of p_s versus $p_{s\perp}$ (with respect to the W-direction). The subscript s refers to 'secondary' muon, i.e. the μ^+ for the dimuons; the μ^+ and the non-leading μ^- for the trimuon events. The dimuons, shown as solid dots, tends to cluster in the region of low p_s and low $p_{s\perp}$ as expected for a hadronic origin such as single charm production. In contrast, the trimuons have much broader p_s and $p_{s\perp}$ distribution as shown by the open circles and triangles

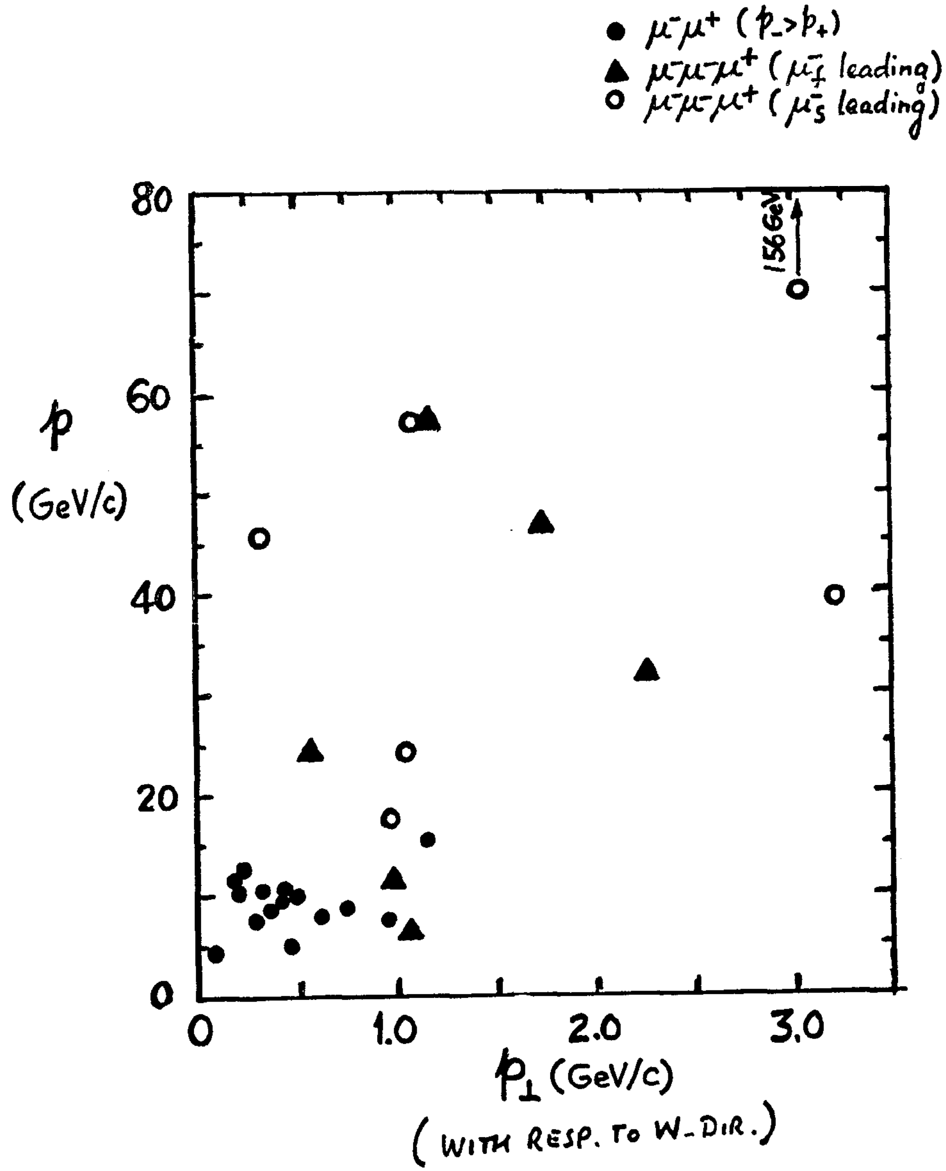

FIG. 10

Another interesting difference between the dimuons and the trimuons is the distribution of the azimuthal angle between the leading and the secondary muon(s), as shown in Fig. 11. The dimuon $\Delta\phi$ distribution shows a clear peaking at 180° as expected for charm production but the trimuon distribution is flat. The azimuthal angle $\Delta\gamma$ calculated about the W-direction reveal just the opposite. Namely, a flat distribution for the dimuons and a distribution skewed toward small $\Delta\gamma$ for the trimuons as shown in Fig. 12. These distinctive differences between the trimuon and the dimuon data lead us to conclude that Associated Charm Production is an unlikely source for trimuons.

(E) Production and Decay of the D° meson - This is the process

$$\nu_{\mu} + N \rightarrow \mu^{-} D^{\circ} + \text{anything}$$
$$\qquad\qquad\quad \lfloor\!\rightarrow \mu^{-}\mu^{+} + x$$

The only decay mode of the D° which resulted in two extra muons, i.e. $D^{\circ} \rightarrow \mu^{+}\mu^{-} + x$, is a decay process which involves charm changing neutral current. However, if charm changing neutral current did exist, there would be substantial $D^{\circ} - \bar{D}^{\circ}$ mixing which has not been observed in $e^{+}e^{-}$ experiments.[14] Hence this is also an unlikely source for trimuons.

(F) Production and Sequential Decay of New Hadron; i.e. the process

$$\nu_{\mu} + N \rightarrow \mu^{-} A\, x$$
$$\qquad\qquad\quad \lfloor\!\rightarrow \mu^{+}\nu B$$
$$\qquad\qquad\qquad\quad \lfloor\!\rightarrow \mu^{-}\nu\, C$$

We note that if the new hadron A were produced with a 'soft' fragmentation function $f(z)$; i.e. the function $f(z)$ is a rapidly decreasing function of z similar to ordinary hadron or charm production, then all the arguments

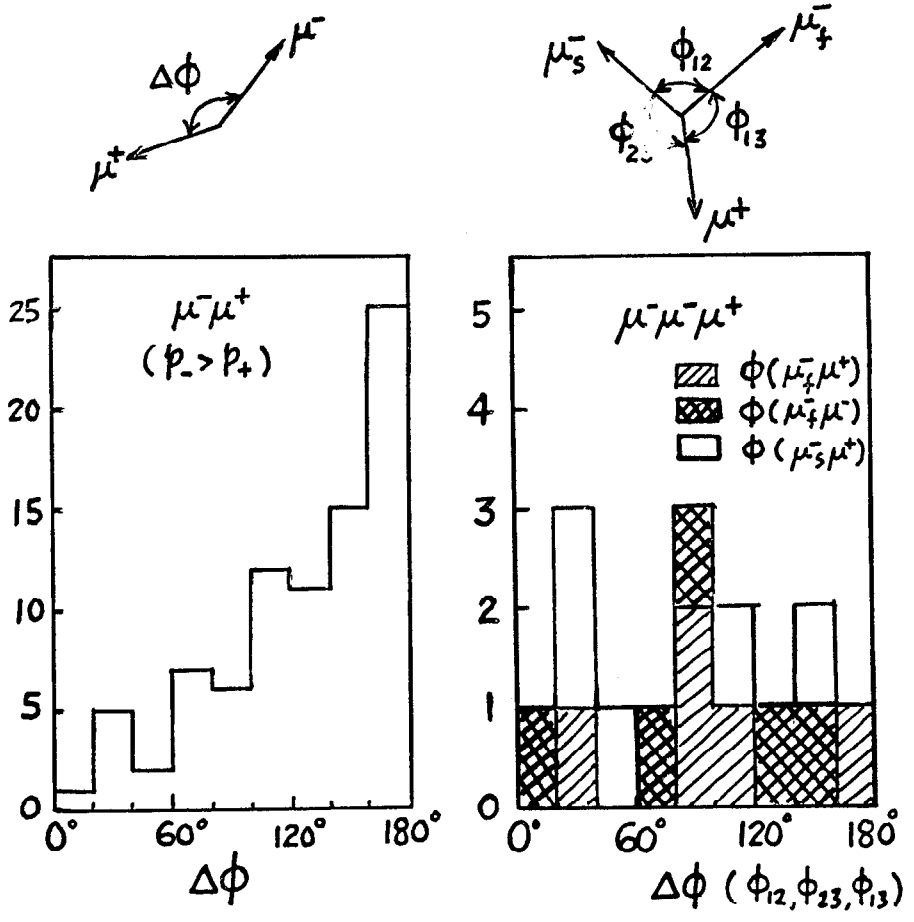

FIG. 11

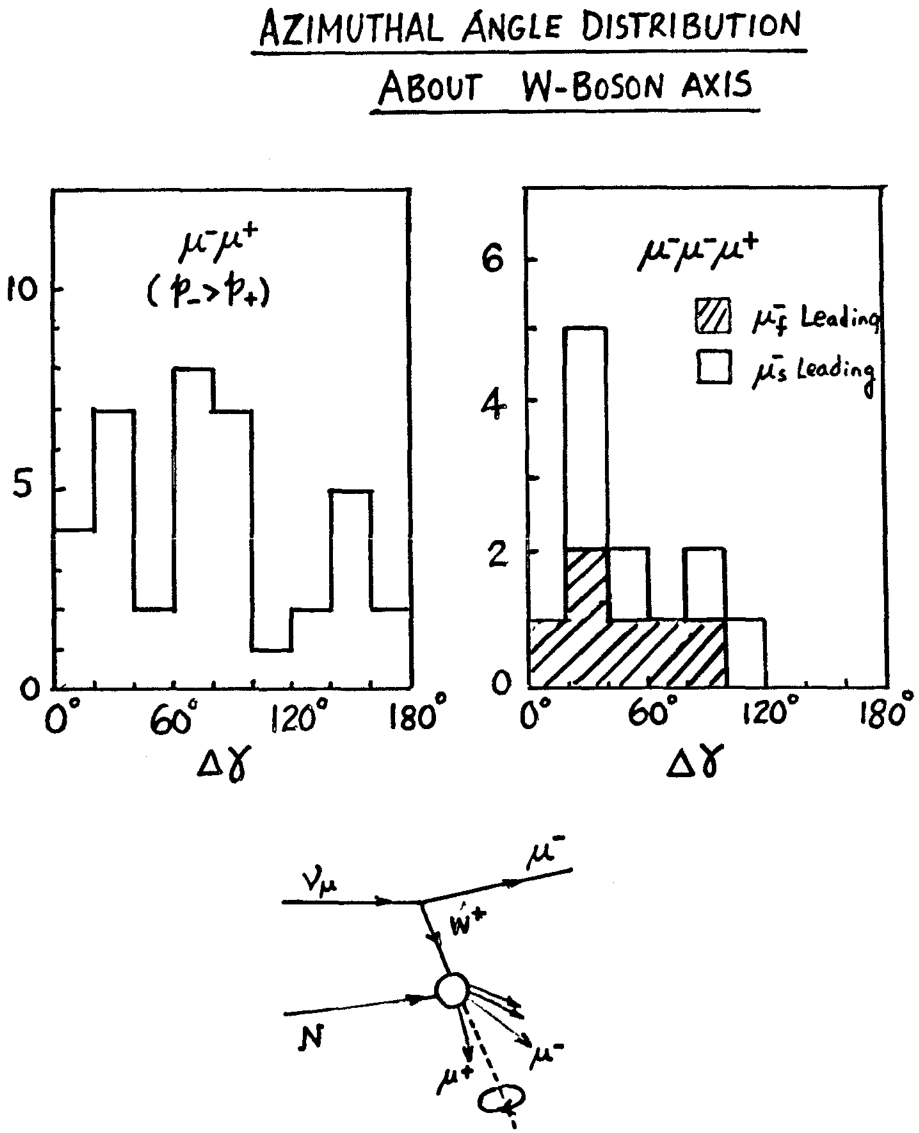

FIG.12

presented in (D) apply here. In such case, this process would be ruled out as the source for the trimuons.

There are theoretical considerations[15], however, that suggest that if the new hadron A were very massive ($M_A >> 1$ GeV), the fragmentation function $\mathfrak{f}(z)$ might be peaked near z = 1. If this were the case, then the arguments given in (D) do not follow. Consequently this mechanism can not be ruled out as a possible source for the trimuons.

(G) Production and Cascade Decay of New Heavy Leptons.

The possibility that all six trimuon events are due to the production of a heavy lepton which in turn decays into three muons is small since no enhancement is observed in the trimuon mass distribution. (See Fig. 13), even though the statistics is poor. The alternative involves two new leptons, a massive charged lepton M^- which decays into a lighter neutral lepton L^o. The process which gives rise three muons is

$$\nu_\mu + N \to M^- + x$$
$$\quad \hookrightarrow L^o + \mu^- + \bar{\nu}_\mu$$
$$\qquad \hookrightarrow \mu^- + \mu^+ + \nu_\mu$$

Phenomenological calculations[16] which involve simple assumptions have been carried out to compare with the data. The trimuon data appears to be qualitatively consistent with this hypothesis. However the data should not be taken as evidence for the existence of the heavy leptons, since the inference is an indirect one and the statistics of the data is very limited so far.

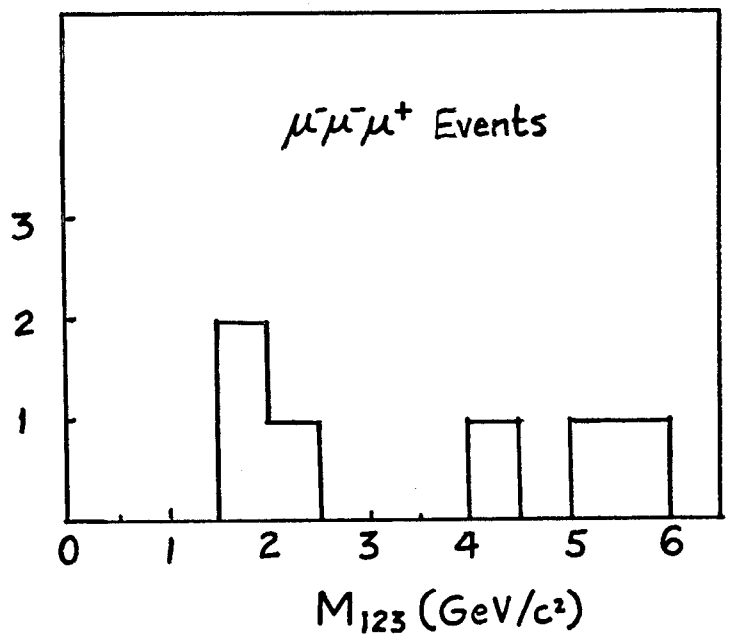

Fig. 13

Conclusion

In summary, we have observed six neutrino-induced events which have three muons identified in the final state. The rate and the characteristics of these trimuon events can not be accounted for by any conventional mechanism. New physics beyond charm is almost certainly needed to explain the trimuon phenomenon. The production of a point-like heavy particle, either a new hadron produced at $z \sim 1$ or a new heavy lepton, followed by their cascade decay into semi-leptonic final states are possible sources of the trimuons. Nevertheless, the interpretation of the trimuons is still an open problem. It may turn out that none of the above mentioned mechanisms is the true source for the trimuons.[17] More data, which we hope to collect in the coming run at Fermilab, will certainly shed more light onto the understanding of this interesting phenomenon.

References

1. A Benvenuti et al, Phys. Rev. Lett 34, 419 (1975).

2. A. Benvenuti et al, Phys. Rev. Lett. 35, 1199 (1975); Phys. Rev. Lett. 35, 1203 (1975).

3. B.C. Barish et al, Phys. Rev. Lett 36, 939 (1976).

4. H. Deden et al, Phys. Lett 58B, 361 (1975).

5. J. von Krogh et al, Phys. Rev. Lett 36, 710 (1976).

6. J. Blietschu et al, Phys. Lett. 60B, 207 (1976).

7. J.P. Berge et al, Phys. Rev. Lett. 38, 266 (1977).

8. C. Baltay et al, Phys. Rev. Lett 39, 62 (1977).

9. E.G. Cazzoli et al, Phys. Rev. Lett 34, 1125 (1975); G. Goldhaber et al., Phys. Rev. Lett 37, 255 (1976).

10. S.L. Glashow, J. Iliopoulous and L. Maiani, Phys. Rev. D2, 1285 (1970).

11. A. Benvenuti et al, Nucl. Instru. Meth. 125, 447 and 457 (1975).

12. B. Roe, Proc. of the XVIII International Conference on High Energy Physics, Tbilisi, U.S.S.R. July 1976 (to be published).

13. K.J. Anderson et al, Phys. Rev. Lett 37, 799 (1976).

14. Goldhaber et al, SLAC-Pub-1973.

15. J.D. Bjorken 'Properties of Hadron Distribution in Reactions Containing Very Heavy Quarks' SLAC Preprint (1977).

16. V. Barger et al, University of Wisconsin Report Nos. COO-595, 596. C.H. Albright et al, Stony Brook Report No. ITP-SB-77-25 (1977).

17. M. Barnett and L-N Chang, SLAC-Pub-1932 (1977).

Neutrino Production of "New" Particles in Bubble Chambers

N. P. Samios

Physics Department
Brookhaven National Laboratory
Upton, New York

Today I will discuss some results from the study of neutrino interactions above 1 GeV, the relevance being the utility of such investigations for unearthing new phenomena. To begin with, I wish to note in Table I, the variety of experimental searches and their relevance.

TABLE I

$\Delta S = -\Delta Q$	Baryon Charm Σ_c^{++}, Λ_c^+
Di-leptons $(\mu^- e^+)$	Charm Production
$\Delta S = +\Delta Q = 1 (S = +1)$	Production Off Sea
Tri-leptons $(\mu^- e^+ e^-)$	Possible Heavy Leptons
Single e^+, e^- production by ν_μ	τ(1.9 GeV) muon number

In particular the experimental results that I will review involve visual techniques, namely bubble chambers. These are listed below along with the approximate number of events:

Exposure	Events	Strength	
7' ν H_2D_2	1,000 events	Kinematics	1-20 GeV
15' ν H_2-N_e heavy	50,000 events	Rate	10-200 GeV
15' ν H_2-N_e light	5,000 events		
15' $\bar{\nu}$ H_2-N_e heavy	3,000 events		
15' ν H_2-N_e light	1,000 events		

It would be advantageous at this point to briefly review the Glashow-Iliopoulos-Maiani (GIM) model predictions as far as old fashioned leptonic decays are concerned as well as for the implications in high energy neutrino reactions. The leptonic currents charged j^+ and neutral j^o are given by

$$j^+ = \nu_e \bar{e} + \nu_\mu \bar{\mu}$$

$$j^o = \nu_e \bar{\nu}_e + \nu_\mu \bar{\nu}_\mu - e\bar{e} - \mu\bar{\mu}$$

with the corresponding quark (hadronic) currents by

$$J^+ = (u\bar{d} + c\bar{s})\cos\theta + (u\bar{s} - c\bar{d})\sin\theta$$

$$J^o = u\bar{u} + c\bar{c} - d\bar{d} - s\bar{s}$$

and θ being the Cabbibo angle.

The old results (pre-charm) were that the leptonic decays of strange particles were suppressed compared to non-strange, i.e., $\Lambda \to pe\bar{\nu}$ involved $s\bar{u}\sin\theta$ while ordinary neutron decay $n \to pe\bar{\nu}$ had $d\bar{u}\cos\theta$; and $\Delta S = -\Delta Q$ (hadron) was not allowed, i.e., $\Sigma^+ \not\to ne^+\nu$. The introduction of charm had the further consequence of not allowing $\Delta S = 1$ $\Delta Q=0$ currents, thereby suppressing $K_L^o \to \mu^+\mu^-$. In addition non-strangeness changing neutral currents are allowed and have been observed, $\nu p \to \nu p$. The consequences for neutrino reactions are striking. This is due to the $c\bar{s}\cos\theta$ and $c\bar{s}\sin\theta$ couplings. As such $\Delta S = -\Delta Q$ reactions can occur via the production of charm and it's subsequent decay into strange particles. There are several mechanisms for production of charm particles and they and their characteristics are enumerated below.

A) Single strange particle production off valence quarks by ν's. In this instance charm is produced by the $d\bar{c}\sin\theta$ coupling with subsequent $c\bar{s}\cos\theta$ decay. As such the characteristics are:

1) $\Delta S = -\Delta Q$; 2) one strange particle/event; 3) valence quark interaction; 4) rate $\simeq \sin^2\theta \simeq 6\%$ and 5) leptonic decays involving e^+ only. Possible reactions are $\nu p \to \mu^- \Sigma^+ \pi^+$ or $\nu n \to \mu^- \Lambda^o \pi^+$.

B) Production from the sea. This can occur from the $(s\bar{s})$ or $(c\bar{c})$ sea via the $(c\bar{s})\cos\theta$ coupling, leaving a $c\bar{s}$ hadronic final state. Again charm should decay with the same coupling. The characteristics of such events would then be: 1) two strange particles/event; 2) production from the sea, small x; (3) leptonic decays involving only e^+; 4) rate small but unknown.

C) Associated charm production off valence quarks. This mechanism involves the ordinary $u\bar{d}\cos\theta$ coupling but picks up a $(c\bar{c})$ from the sea, analogous to associated strange particle production in which an $(s\bar{s})$ arises from the sea. In this case there will be 1) two strange particles per event; 2) valence distribution; 3) both e^+ and e^- leptonic decays and 4) unknown but probably low rate.

I now turn to a discussion of several experimental results, the first being those derived from the BNL 7-foot bubble chamber. I would be remiss in my charge as a lecturer in this summer school if I didn't begin with a few brief comments on a very significant event, found, analyzed, and published several years ago which I believe constituted the first evidence for bare charm. This is shown in Fig. 1 and the reaction is

$$\nu p \to \mu^- \Lambda^o \pi^+\pi^+\pi^+\pi^-$$

with the $\Lambda^o \to p\pi^-$.

Since the working liquid in the 7-foot bubble chamber was hydrogen this event is highly kinematically constrained. In particular the transverse momentum is balanced, the mass of the initiating particle is

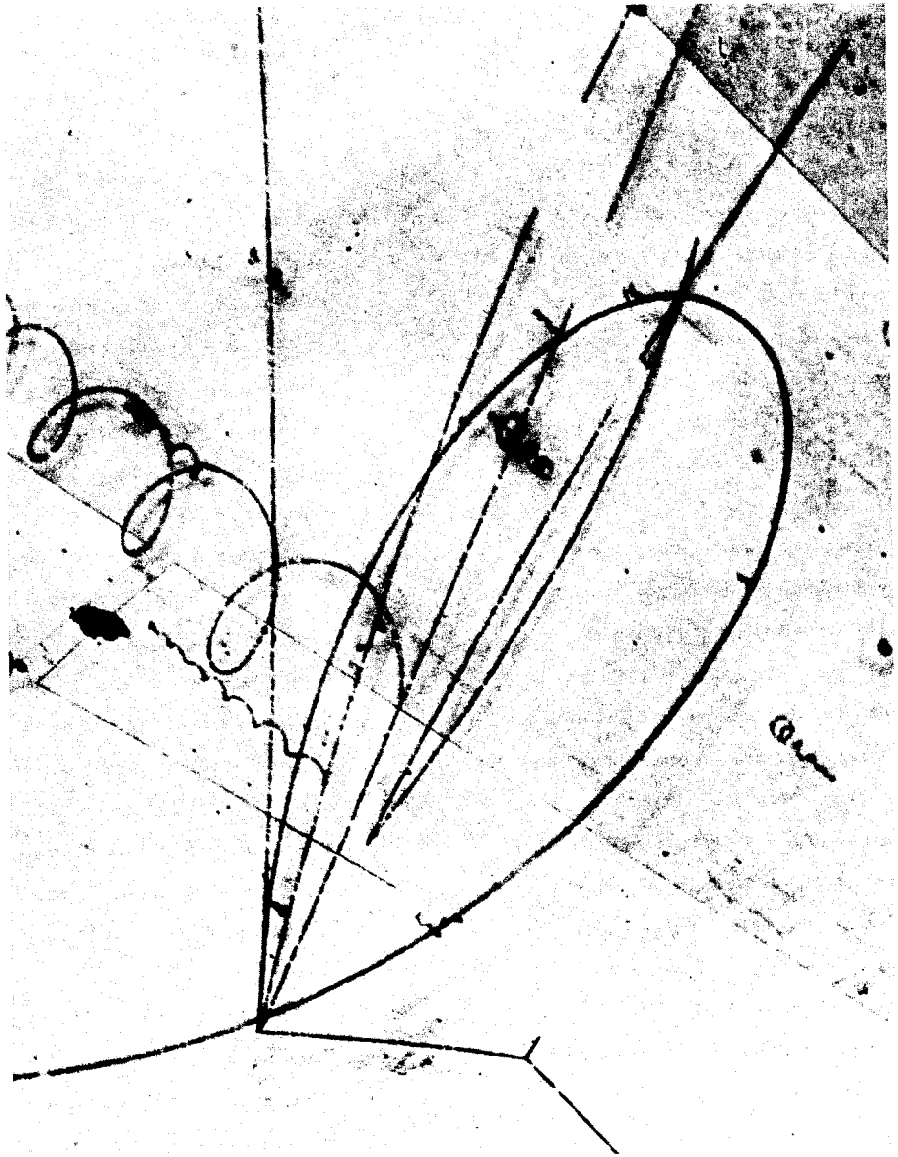

FIGURE 1

is zero (as expected for a ν) if the positively charged group are π's, and non-physical if any one is assumed to be a K^+. Furthermore the three positive tracks are identified as π^+'s by the decay of one, the interaction of the second and a δ ray on the third. All alternative explanations are extremely unlikely, by a factor of 10^{-4} - 10^{-5}.

Since there is only a single strange particle with S = -1 (Λ^o) in the final state this is a clear example of $\Delta S = -\Delta Q$. However as noted earlier this is precisely the expected signature of charm production. The charm masses can be determined since these involve non-leptonic decays. The effective $\Lambda\pi^+\pi^+\pi^+\pi^-$ mass was 2426 $\pm$ 12 MeV. We ascribe this to the charm analogue of the Σ^+ which we call the Σ_c^{++}(cuu). This in turn can decay strongly via π^+ emission to the Λ_c^+ (cud) which in turn decays weakly into $\Lambda\pi^+\pi^+\pi^-$. There are three possible masses for the Λ_c^+, 2260, 2099, and 2088 MeV; however, the preferred value is 2260 $\pm$ 20 MeV, utilizing the theoretical prediction of Glashow of $\Delta M(\Sigma_c^{++} - \Lambda_c^+)$ = 160 MeV. The rate is also roughly that expected from charm production and decay, in that of the 1,000 charged current events observed only 150 are above threshold for charm production, and the one observed event is equivalent to half a dozen when one corrects for unseen particles and decays. These two numbers yield a production rate of 4%--a Cabbibo rate. All in all, a picturesque, clear example of bare charm baryon production and two new particles for the price of one event.

For completeness I note that a few events with single (S = +1) strange particles in final states have been observed from a total of 10 associated strange particle events. Such events must of necessity be produced off the sea quarks and not valence quarks. As such the production rate for such positive strange events is not negligible, being of the order of 10% of total strange particle production.

At this point I would like to discuss the bubble chamber di-lepton results, the experiment with the most data being the BNL-Columbia exposure with the 15-foot bubble chamber in the broadband horn focussed neutrino beam at Fermi-Lab. This particular experiment used 400 GeV protons, 10^{13} protons/pulse with the peak of the neutrino spectrum at 25 GeV but extending to 200 GeV. The liquid mixture was 64% Neon and 36% Hydrogen. The total mass is 28 tons, a density of 0.8 gm/cm^3, a radiation length of 40 cm and an interaction length of 125 cm--indeed a formidable detector. The data to be discussed involves 45,000 pictures taken in May 1976, with one interaction per picture, this film having been double scanned for di-lepton events. The electron identification is rather straight forward, the signature being either one or more bremsstrahlungs or the curling up of a minimum track--two signatures being required for acceptance. In addition a momentum cut of greater than 300 MeV/c was also applied. The correction of 85 $\pm$ 5% for detection efficiency for electrons was determined by an examination of externally converted e^+e^- pairs. A μ^- was defined as a negative track that left the chamber without interacting. Since the interaction length is 125 cm and the average path length for charged tracks was 200 cm, $e^{-2/1.5}$=25% of the tracks will not interact and 75% will interact. With these definitions, 81 di-lepton (μ^-e^+) events have been observed, i.e., $\nu Ne \to \mu^-e^+$ anything. The main background sources are twofold; 1) π^- punch thru. This amounts to 9 $\pm$ 8 events as determined from the ratio of leaving to interacting positive tracks. 2) Asymmetric Dalitz pairs. A correction of 3 $\pm$ 3 events was evaluated from a measurement of 1,000 such pairs. In order to

measure a rate there are several other corrections: a) scanning efficiency 90 $\pm$ 5%; b) fiducial volume 85%, and c) normalization 46,000 pictures x .6 ν events/picture. As such

$$\text{Rate } \frac{\mu^- e^+}{\mu^-} = \frac{(81\text{-}9\text{-}3)\ 1/.85x1/.9}{46{,}000 \times .6 \times .85} = .5 \pm .15$$

The momentum distribution of the μ^- and e^+ as well as the incoming energy distribution for these 81 events is shown in Fig. 2. One notes the neutrino energy reflects that expected from the known neutrino flux and that the average μ^- momentum is much larger than that for the e^+ by a factor of $\simeq$ 6.

A careful examination of these 81 events revealed 15 strange particles. This consisted of 10 $K^0_s \to \pi^+\pi^-$, 3 $\Lambda^0 \to p\pi^-$ and two ambiguous events (either Λ^0 or K^0_s). This number of 15 is increased to 50 upon correction for neutral decay modes and lifetime effects. As such the ratio of neutral strange particles with di-leptons to all di-lepton events is 50 $\pm$ 14/81 = .6 $\pm$ .2. It should be noted that ordinary visible strange particles are 6% such that .06(81)=5 events were expected, with 15 observed, di-lepton events being clearly associated with strangeness. Furthermore if charged and neutral strange particle production were equal there would be 1.2 strange particles per di-lepton event implying production from sea as well as valence quarks.

In Fig. 3 we display the relevant kinematic variables for these 81 events, x_{vis}, y_{vis} and W the total hadron mass. The solid curves in the x_{vis} and y_{vis} distributions denote those for the ordinary charge current events. One notes they are rather similar; however, the di-lepton events can accommodate up to 25% production from the sea (i.e., peaking at small x_{vis}). For completeness we also display the (V^0e^+) effective mass which is a lower limit since both the non-visible decay

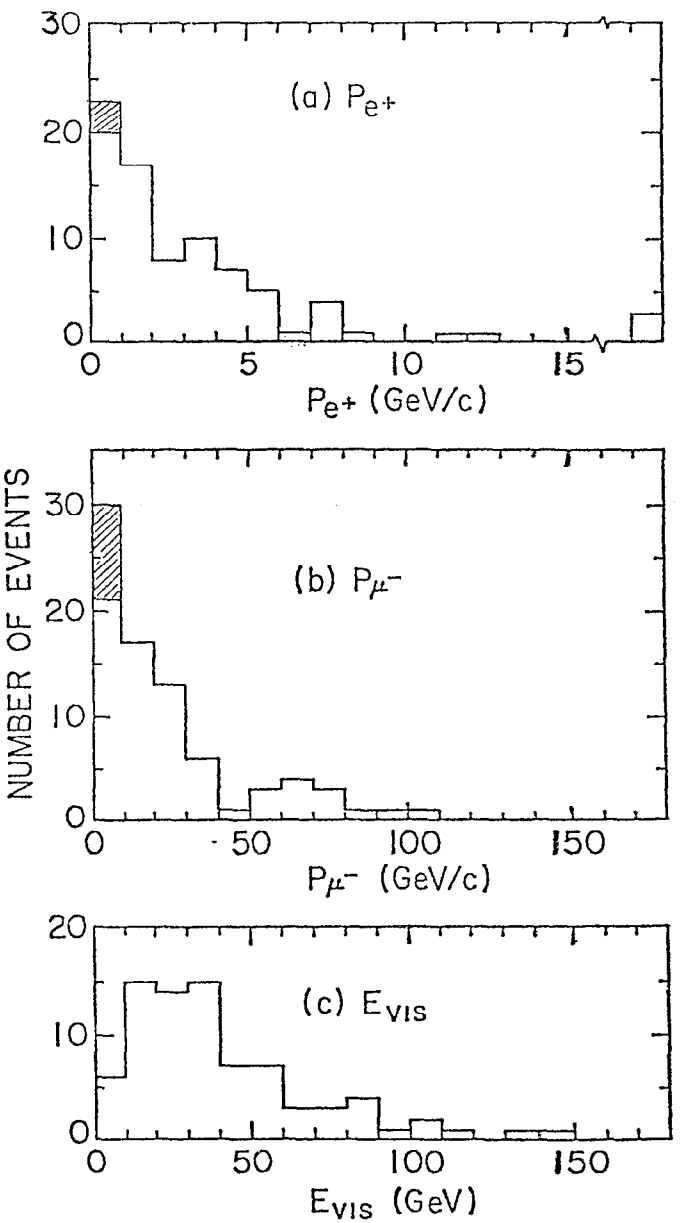

FIGURE 2

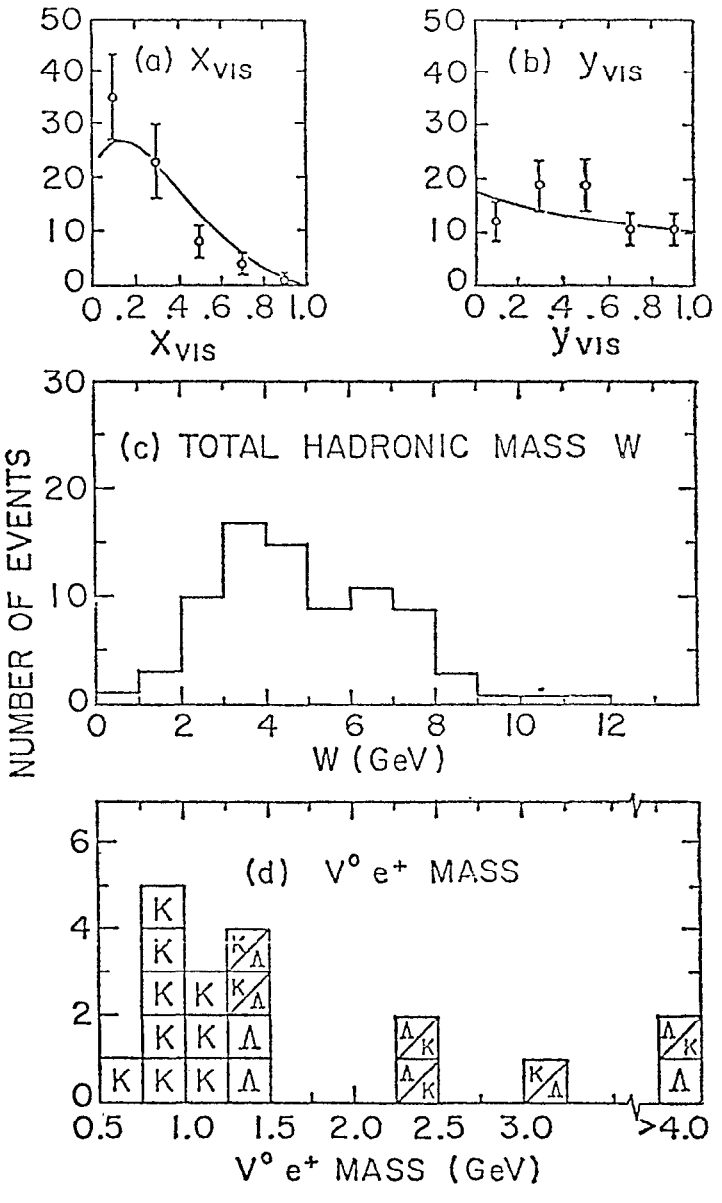

FIGURE 3

ν as well as possible π's are omitted from consideration. Again a substantial fraction are less than 2.5 GeV, consistent with charm decay. As a final comment we plot the pertinent di-lepton angular distribution in Fig. 4. One notes the (e^+, π^-) peaks at 180° as does the (π^-, hadron) distribution in contrast to the (e^+, hadron) which is flat. Again this is consistent with charm production. In fact the rate, momentum and mass distribution, strange particle content and angular distribution of these di-lepton events are all consistent with charm production.

There are several other experiments that have bearing on this general question of di-lepton events and strange particle production. There are listed in Table II along with their yield and rates. One sees that where comparisons can be made the di-lepton rate is between 0.3-0.8% of the charged current yield--with general agreement among all experiments considering the different experimental conditions and cuts. However in the V^0 content there is a possible discrepancy between the BCHW experiment and the BNL-Columbia result, 1.84 versus .6, a difference of $1.2 \pm .6$, a 2σ effect. This is a matter of clear importance and additional data will be needed to clarify the situation.

Of equal or possibly greater importance is the search for the non-leptonic decay of charm. A priori one expects low rates. As noted earlier, the GIM model would yield production rates at the few percent level and this is compounded by the numerous available decay channels for particles with masses of 2 GeV as well as totally charged versus neutral decay modes. One can easily get only a few events per thousand or ten thousand, as such large data samples are clearly desirable and necessary. One notes in passing the SPEAR experience of

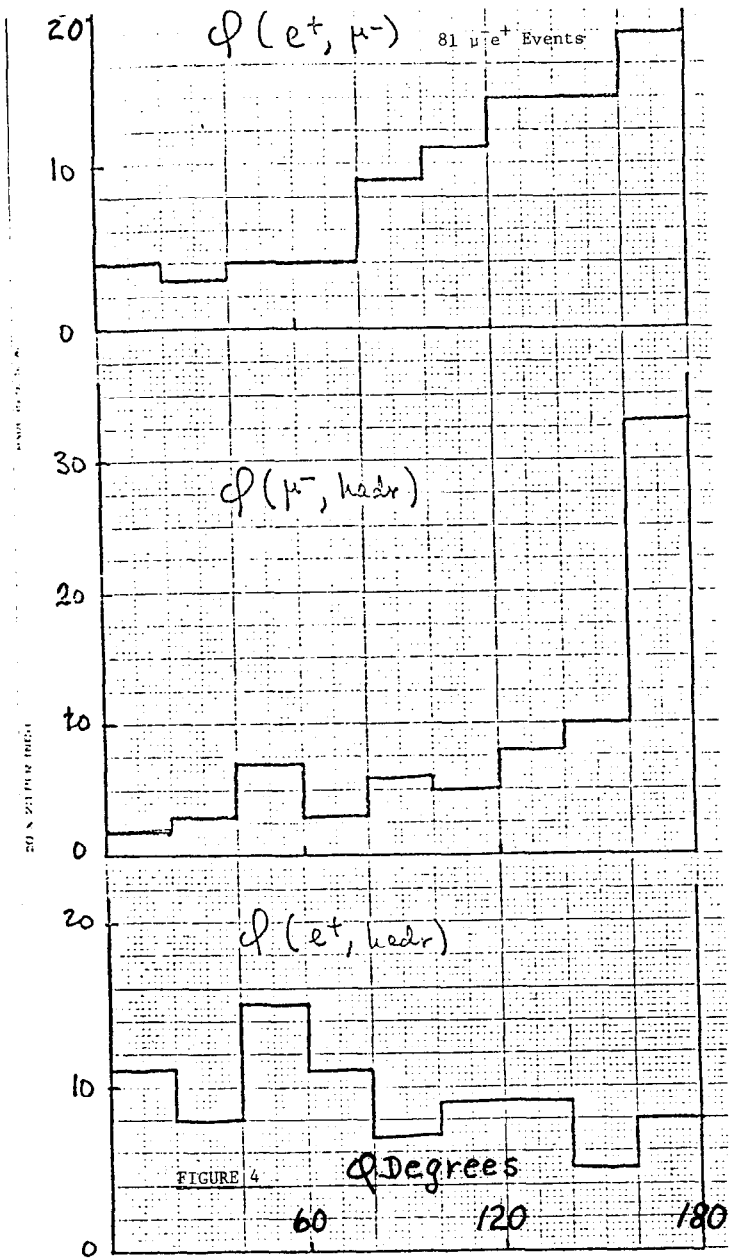

FIGURE 4

TABLE II

COMPARISONS $\nu_\mu + N \rightarrow \mu^- e^+ + ...$

Experiment	Liquid	$\mu^- e^+$ Events	$\mu^- e^+/\mu^-$ %	V°'s	$(SP)^o$/EV	Total SP/EV
B.C.H.W.*	21% Ne	17	.8 ± .3	11	$1.84^{+.6}_{-.5}$	3.7
BNL-Columbia	64% Ne	81	.5 ± .15	15	.6 ± .2	1.2
Gargamelle	Freon	19	.31 ± .13	3	.6	1.2
Berkeley-Seattle		6	.4 ± .2	$1\{K^o_{+1K^+}$		
1A ($\mu^-\mu^+$)			.8 ± .3	-		
			$\bar{\nu} + N \rightarrow \mu^+ e^-$			
Fermilab-Michigan-U.S.S.R.	21%	≤1	≤.5%			
Berkeley-Hawaii-Seattle	64%	3	.10 ± .10			

* Berkeley-CERN-Hawaii-Wisconsin

75,000 hadron events in order to obtain a few hundred visible charm particles. In this vein I wish to give a preliminary report on the evidence for D^o production in the BNL-Columbia experiment which involved heavy neon in the 15-foot chamber. In effect, from a sample of 22,000 charged current events, 1300 strange particle events have been analyzed. The first effect to show up has been evidence for $D^o \to K^o_s \pi^+ \pi^-$ inclusive production, an excess of 25 events corresponding to a 2.5 standard deviation. This is shown in Fig. 5 where a clear fluctuation is observed in the 1800-1880 MeV bin. If one compares this signal with the charged leptonic decay ($K^o e+\nu$) of 10 events, they are of comparible magnitude with a possible excess of the former. There are ≃ 70,000 charged current events on hand, needless to say strong efforts are being expended in searches for the expected other boson (F^+, D^*, F^+) and baryon ($\Lambda_c^+, \Sigma_c^{++}$) charm particles.

A subject of considerable recent interest has been that of heavy leptons, as such the relevance of tri-lepton production. The most sensitive search in the BNL-Columbia experiment is for $\mu^- e^+ e^-$ final state. No such events have been found in a sample of 81 $\mu^- e^+$ events. This yields a value <2% for 90% confidence to be compared with a reported rate of 5% which would have resulted in the observation of four events instead of zero. There was also a null result for the $\mu^-\mu^+\mu^-, \mu^- e^+ \mu^-$ and $\mu^-\mu^+ e$ modes ($p_e > .3$ GeV $p_\mu > 4$ GeV); however, these have a poorer detection efficiency (≃40%) and are thus less sensitive. Single electron (e^+, e^-) production by muon neutrinos is also of relevance. 160 events with a single e^- and no μ^- candidate have been observed. Most if not all are due to electron neutrinos in the beam; however, this number can be used to demonstrate that the muon number of the conjectured τ(1.9 GeV) is different than ν_μ.

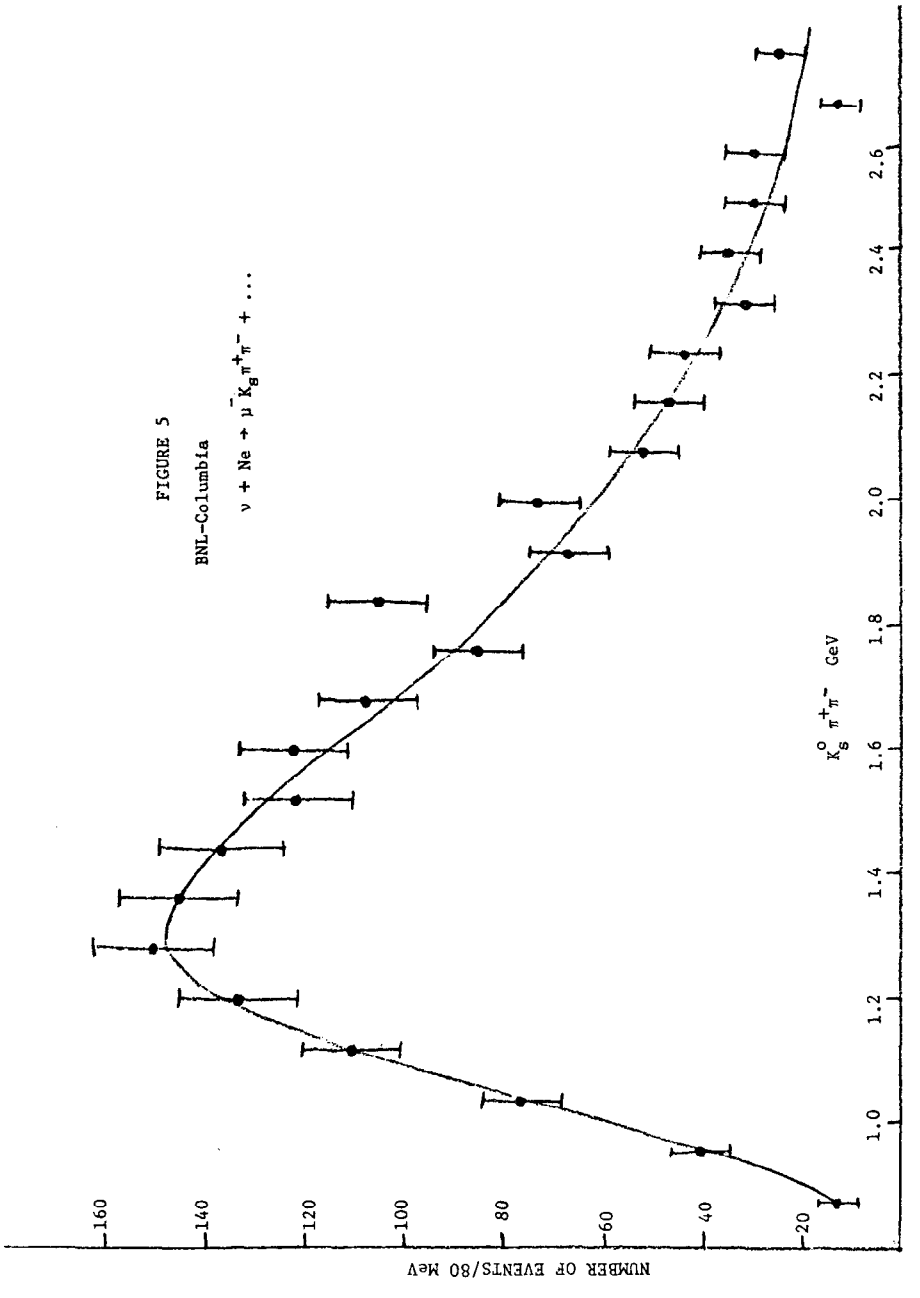

This comes about because if the μ and τ are the same in coupling and lepton number then of the order of 2,000 single e^- should have been observed, in contrast to the maximum of 160. For completeness we also note the observation of 23 single e^+ events (no μ^-) again from a total of 22,000 charged current events. The relevance here is limits on charm changing neutral currents.

I close with noting the successes arising from the study of high energy neutrino interactions--observations of bare baryon charm, di-leptons associated with strange particles--all consistent with charm production, evidence for interaction from sea as well as valence quarks, possible evidence for D^o production and some comments and limits on the production of heavy leptons. The further exploration and exploitation of neutrino reactions will, I believe, add immeasurably to the above list.

Acknowledgement:

The research described above is clearly the work of a large body of people. In particular I wish to acknowledge the efforts of the BNL and Columbia Groups involving R. Palmer, C. Baltay and A. M. Cnops, P. L. Connolly, S. A. Kahn, H. G. Kirk, M. J. Murtagh, T. T. Tso, D. Caroumbalis, H. French, M. Hibbs, R. Hylton, M. Kalelkar, W. Orance, E. Schmidt.

Results of the CERN-Dortmund-Heidelberg-Saclay Neutrino Counter Experiment*

F. Eisele

Dortmund, September 1977

Invited talk at the SLAC Summer Institute on Particle Physics

July 18-22, 1977

* This experiment was performed by the following group: M. Holder, J. Knobloch, J. May, H.P. Paar, P. Palazzi, F. Ranjard, D. Schlatter, J. Steinberger, H. Suter, H. Wahl, S. Whitaker, E.G.H. Williams, CERN; F. Eisele, C. Geweniger, K. Kleinknecht, G. Spahn, H.-J. Willutzki, University Dortmund; W. Dorth, F. Dydak, V. Hepp, K. Tittel, J. Wotschak, University Heidelberg; A. Berthelot, P. Bloch, B. Devaux, M. Grimm, J. Maillard, B. Peyaud, J. Rander, A. Savoy-Navarro, R. Turlay, CEN Saclay; F. Navarria, Bologna

Introduction

Results are presented on charged current, neutral current and multimuon events induced by neutrino and antineutrino narrow band beams in the CDHS-Neutrino counter detector. The overall strength and the differential y-distribution of neutral and charged current interactions are investigated to determine the fraction of right handed and left handed constituents inside the nucleon as a function of the neutrino energy in the interval $0 < E_\nu < 200$ GeV. Direct tests on new particle production are performed based on the observation of $\sim$ 300 events with more than one muon in the final state.

I Experimental Configuration

The experiment has been performed at the CERN SPS neutrino facility in the period from December 76 to March 77. Neutrino interaction were recorded in a massive iron target-detector exposed to narrow band neutrino and antineutrino beams which cover neutrino energies from zero to 200 GeV.

I.1 Detector[1)]

The detector has been designed for optimum detection of multimuon events. Its outstanding features are thus the very large muon acceptance, high density and high target mass. The detector is capable to measure and identify any number of muons and to measure the total energy of hadronic showers. An overall view of the detector is shown in figure 1. It consists of 19 similar moduls and 19 interspaced driftchambers, where each module acts as target, hadron

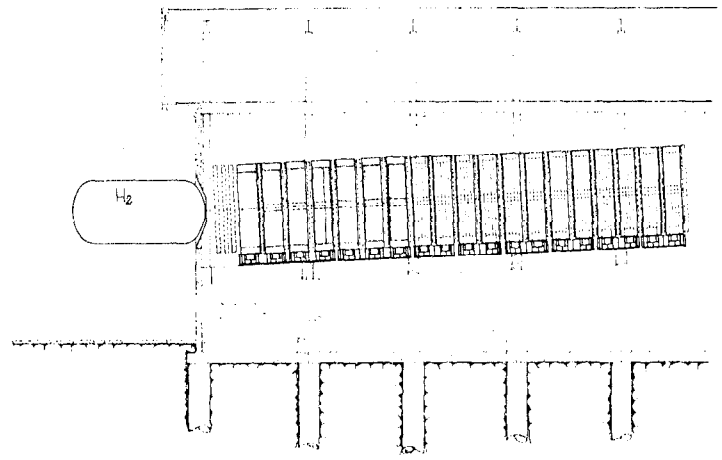

Fig. 1 : Side view of the CDHS neutrino detector

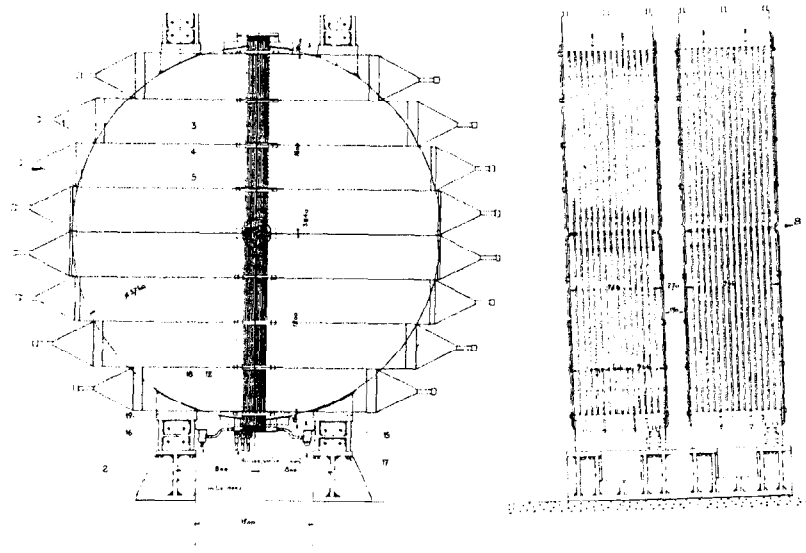

Fig. 2 : Front and side view of one module

calorimeter, muon identifier, and part of the muon spectrometer. A schematic view of one module is shown in figure 2. It is a large torodial magnet and sampling calorimeter with a total thickness of 75 cm iron, a radius of 1.85 m and a total weight of 66 tons.

The iron is subdivided in 15(5) plates of 5(15) cm thickness with plastic scintillators between two successive plates to sample the total energy deposited in the module. Muon tracks are measured between two adjacent modules by 3 gap driftchambers with a spatial resolution of < 1 mm. Multimuon tracks can be resolved provided their spacial separation is at least 1 cm.

A summary of some basic properties of this detector is given in table I.

Table I: Basic properties of CDHS-neutrino detector

	total length	21,75 m
	total length of iron	14,25 m
	diameter	3,85 m
	total mass	1250 tons
	magnetic field	1,65 tesla
	Number of phototubes	2400
	Number of driftchamber planes	57
Target:		
	fiducial volume	∿ 800 tons
	average density	5,2 g/cm^3

calorimeter:

$$\frac{\Delta E_h}{E_h} = \frac{.9\ (1.5)}{\sqrt{E\,(\mathrm{GeV})}}$$

sampling calorimeter (iron + plastic scintillator) with 5(15) cm sampling thickness

muon spectrometer:

$$\frac{\Delta p_\mu}{p_\mu} = \frac{.2}{\sqrt{L_{Fe}\ (\mathrm{m})}} \simeq 10\ \%$$

$$\Delta\theta_\mu \simeq \frac{.2}{p_\mu\,(\mathrm{GeV/c})}$$

good muon acceptance: $\theta_\mu \lesssim 400$ mrad

A very important property of this detector is its very large solid angle for muon detection. This point is illustrated in figure 3 where the region of good muon acceptance (> 50 %) is shown in the x-y plot for charged current inclusive interactions and compared to the μ-acceptance of the first generation experiments at NAL.

2. Neutrino beam[2)]

The data has been taken with 200 GeV narrow band neutrino and antineutrino beams. A layout of the CERN SPS neutrino facility is shown in figure 4. The primary protons have an energy of 400 GeV. A narrow momentum band of pions and kaons is selected and focussed towards the detector with small beam divergence before they enter the decay region. Some of the more important properties of the beam are given in table II.

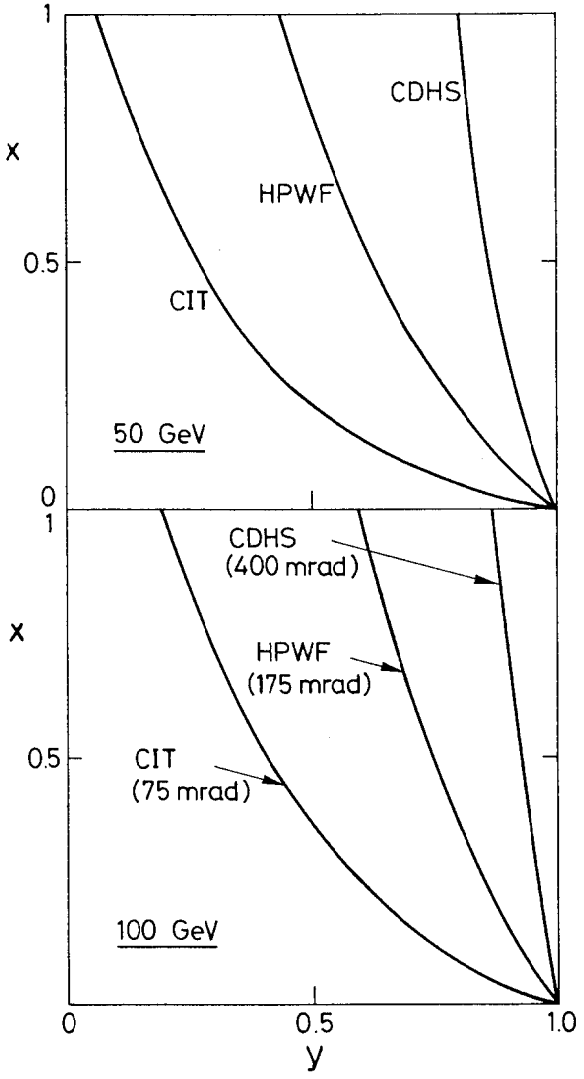

Fig. 3 : Muon acceptance for charged current events in the x-y plot for CDHS and first generation NAL experiments.

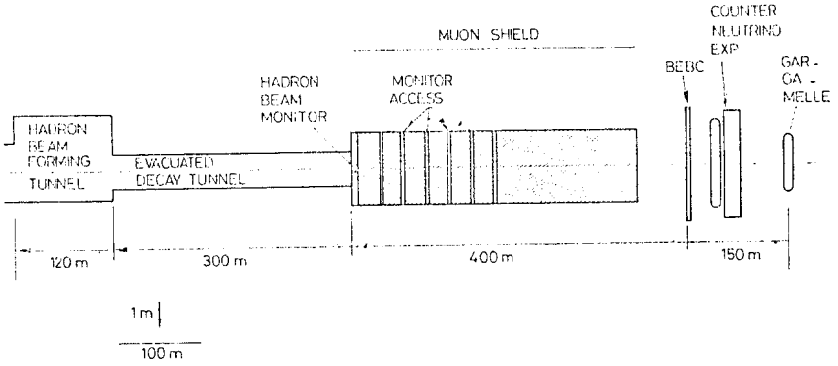

Fig. 4 : Layout of CERN SPS neutrino facility

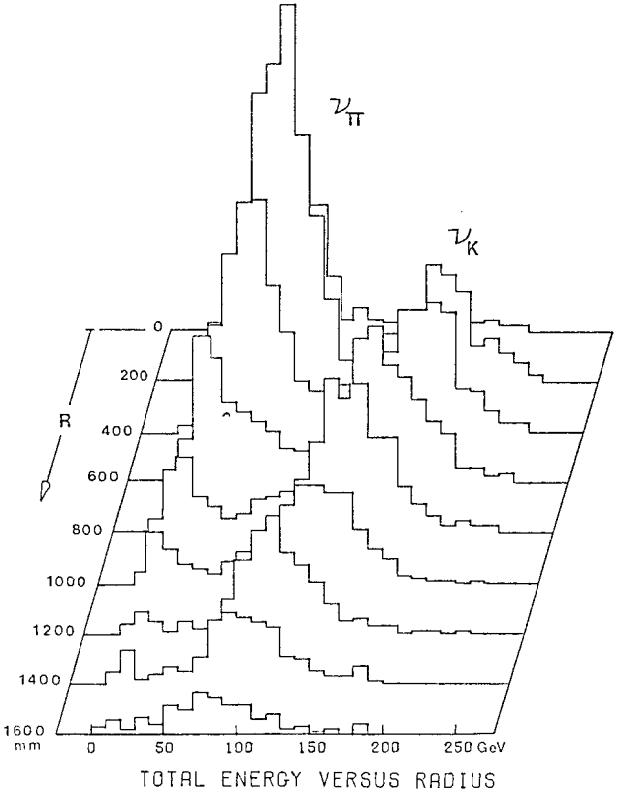

Fig. 5 : Correlation between radial vertex position in the CDHS detector and the incident neutrino energy for narrow band neutrino beam

Table II: Properties of the neutrino beam

Proton energy	400 GeV
average proton intensity	$\sim 2 \times 10^{12}$ ppp
parent energies	200 ± 14 GeV
beam divergence	.18 mrad horizontal .24 mrad vertical
length of decay volume	300 m
average distance target detector	620 m
angular ν acceptance of detector	3 mrad
short spill	23 μsec
beam composition	measured by differential $\check{C}$-counter
negative beam	$K^-: \pi^- = .054:1$
Positive beam	$K^+: \pi^+ : p^+ = .16 : 1 : 4.6$
absolute ν-flux measurement:	three independent methods
i)	beam current transformer BCT
ii)	hadron absorption calorimeter
iii)	muon flux measurement by solid state detectors

For the analysis of neutrino interactions this beam offers essential advantages over wide band or high band beams.

a) The shape of the neutrino spectrum is determined essentially by the well known beam geometry. The only uncertainty remaining from the hadron production is the ratio of pions and kaons which is measured by a differential $\check{C}$-counter.

b) Since the bulk of the neutrinos is due to twobody decays of fixed momentum particles the neutrino angle relative to the beam line is correlated to its energy and can be measured event by event in the detector from the radial displacement of the vertex.

The correlation of neutrino energy with the radial vertex position is shown in figure 5. For a given radial bin the neutrino energy is known up to a π/K ambiguity. This property of the beam is used for the analysis of neutral current events and for the absolute energy calibration of the apparatus.

c) The neutrino energy spectrum seen by our detector covers the whole energy range from $0 < E_\nu < 200$ GeV with similar intensity (figure 6a, b).

d) The absolute neutrino flux is measured by three independent ways and should be known to better than 10 %.

Summary

The outstanding features of this experiment are the high mass, high density detector with very large radius. This results in an excellent muon angular acceptance. The total neutrino energy spectrum up to $E_\nu = 200$ GeV is covered at the same time with similar intensity. Relative flux measurements are easy since they depend only on the beam geometry apart from the π/K ratio.

Compared to first generation neutrino counter experiments we have the advantage of substantially higher statistics and smaller systematic uncertainties.

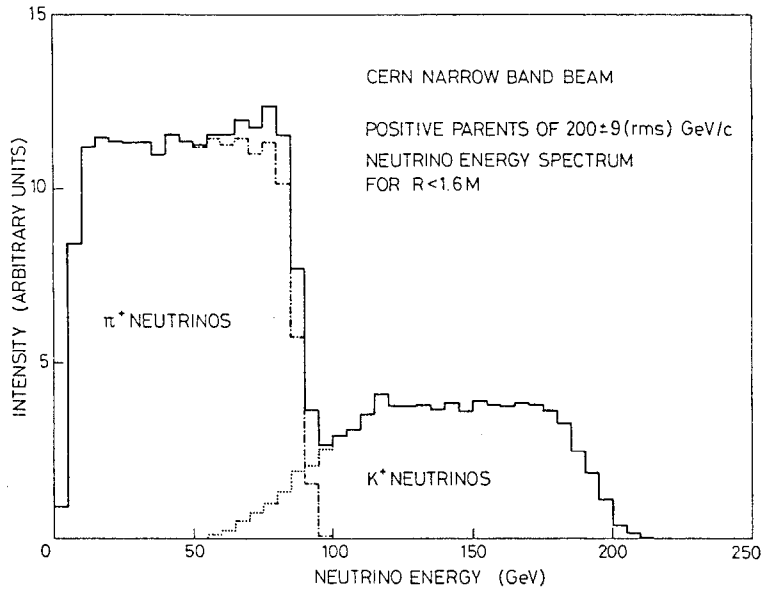

Fig. 6a : Neutrino spectrum

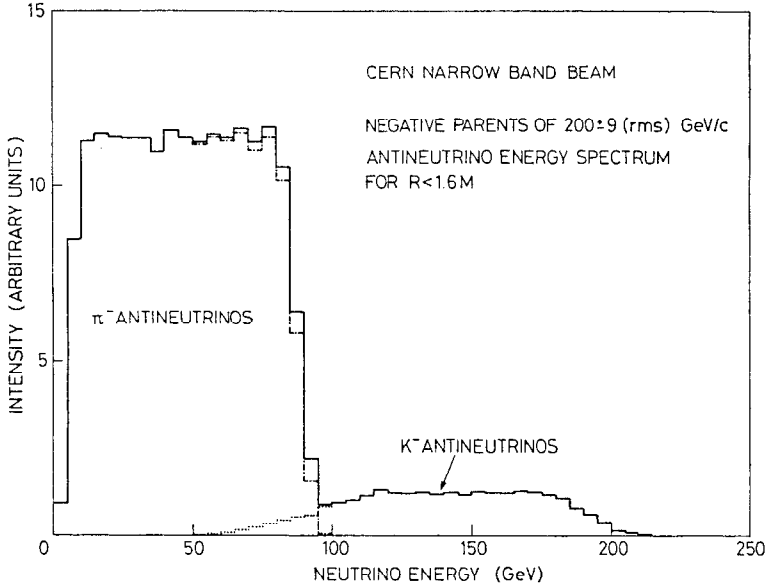

Fig. 6b : Antineutrino spectrum

II Experimental results

II.1 Event selection and statistics

A summary of the data taken in the 200 GeV narrow band beams is given in table III. The trigger required for this experiment was equivalent to demanding a hadron shower energy of $E_H \gtrsim 3$ GeV or a single muon with momentum above $\sim$ 3 GeV/c.

Table III: Event statistics

	neutrino	antineutrino	
Data taking	4 weeks	8 weeks	
Protons on target	3×10^{17}	6×10^{17}	
charged current	12000	5400	E_ν < 100 GeV
events ($\nu N \to \mu X$)	16000	2500	E_ν > 100 GeV
Neutral current events	8600	2900	
Multimuon events			
$\nu + N \to \mu^+\mu^- + X$	257	58	
$\to \mu^-\mu^- + X$	47	0	
$\to \mu^+\mu^+ + X$	0	9	
$\to \mu\mu\mu + X$	2	0	

The basic information available for one event is displayed in figure 7 for the example of a dimuon event where the top row gives the pulseheight in the scintillators and the three lower rows give the coordinates measured in the three views of the driftchambers.

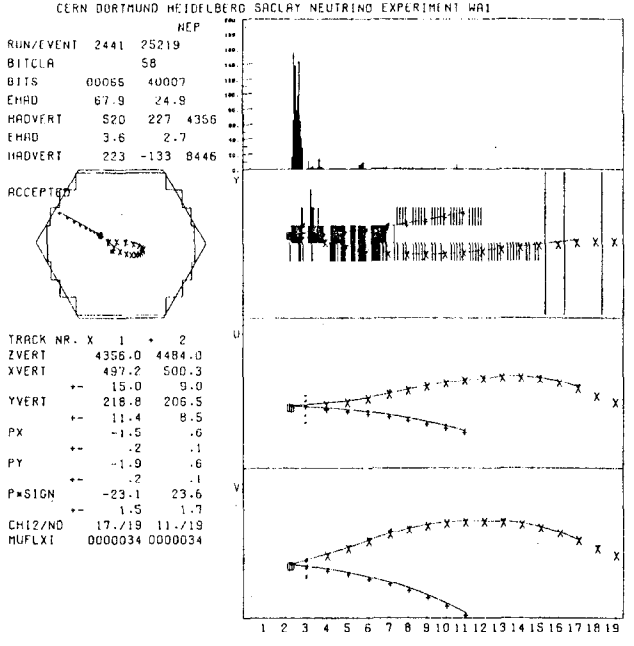

Fig. 7 : Example of a dimuon event as reconstructed by computer. On the left a front view of the event. On the right side views of module 1-19 with scintillator pulse height (top row) and the coordinated in the three driftchamber projections (y,u,v).

II.2 First results for inclusive charged current interactions[3)]

1. Predictions of the quark parton model

It has been shown by first generation experiments[4)] that the simplest version of the quark parton model gives a reasonable good description of inclusive neutrino interactions at low and moderate energies. Given the high statistics and the broad energy range of our experiment however, we have to analyse the data in a more general way allowing for scaling violations and other deviations from the quark parton model. Whereas this is a long term program that requires refined analysis and detailed understanding of small experimental effects, a quick look on the rough features of our data is sufficient to detect the very large effects expected if a new right handed quark with a mass less than $\sim$ 10 GeV would be produced. Experimental evidence for such a process has been reported in references [5,6)].

The standard spin 1/2 quark parton model gives the following differential distributions of the scaling variable $y = E_h/E_\nu$

$$\frac{d\sigma_\nu}{dy} = \frac{G^2 ME_\nu}{\pi} \left(Q + \bar{Q}(1-y)^2\right) \qquad (1)$$

$$\frac{d\sigma_{\bar{\nu}}}{dy} = \frac{G^2 ME_\nu}{\pi} \left(\bar{Q} + Q(1-y)^2\right) \qquad (2)$$

and the ratio of total cross sections

$$\frac{\sigma_{\bar{\nu}}}{\sigma_\nu} = \frac{1}{3} \frac{Q + 3\bar{Q}}{Q + 1/3\,\bar{Q}} \qquad (3)$$

In this notation $Q(\bar{Q})$ is the fraction of the nucleon momentum carried by quarks (antiquarks). It is common practice to define also a shape parameter B

$$B = 1 - \frac{2\bar{Q}}{Q}$$

which is related to the amount of antimatter in the nucleon.

The production of a new right handed quark (b-quark) from a valence quark would contribute in the same way as the scattering off antiquarks and would thus show up as a strong apparent increase of the fraction of right handed constituents above threshold.

It should be noted from relations (1) - (3) that the presence of right handed constituents gives a drastic effect in antineutrino interactions whereas the effect in neutrino interactions is rather small.

2. Results

The emphasis of our first analysis was to look for large deviations from the standard quark parton model especially in the energy dependence. Following the procedure of ref. [5] we just plot the average inelastic <y> in the scaling region ($x < 0.6$) as a function of energy without any correction for acceptance and resolution (figure 8). To give an estimate of the small effect of acceptance and resolution for this experiment we have also given in the figure the predictions of the standard model with B = 0.8 including these effects.

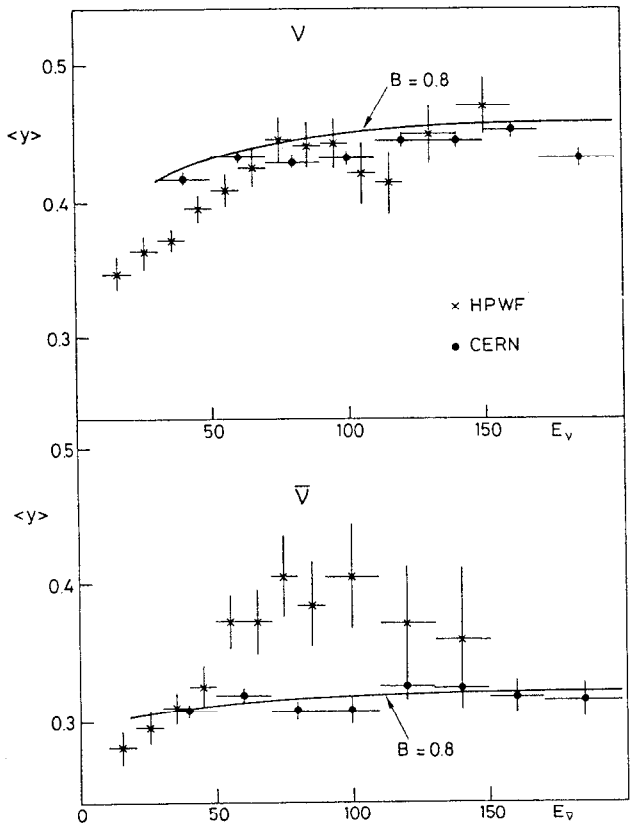

Fig. 8 : Average inelasticity <y> for neutrino and antineutrino data as measured by the CDHS experiment compared to same data of reference [5]. The data is uncorrected for acceptance and resolution and only statistical errors are given.
The solid lines are the predictions of the standard quark parton model with B = 0.8 for the CDHS experiment.

The data follow nicely the shape of these predictions indicating that the shape of the y-distributions is compatible with no energy dependence in disagreement with reference[5].

A further easy check can be made by evaluating the ratio of antineutrino to neutrino total cross section. For energies below E_ν = 80 GeV neutrinos and antineutrinos are coming from π-decays only, thus their energy spectrum is identical and there is no relative flux uncertainty apart from one factor common to all energies which is known to ± 10 % (see section I.2). The same is true for energies above E_ν = 100 GeV where the neutrinos are due to K-decays only. To get the relative flux for E_ν < 80 GeV and E_ν > 100 GeV we need however one additional quantity, the ratio of kaon to pion production for positive and negative beams which is also known to better than 10 %. The small differences in acceptance for neutrino and antineutrino data have been corrected by a Monte Carlo calculation.

Our measured cross-section ratio is shown in figure 9 together with the results of reference[6]. Within statistical errors the data are compatible with no energy dependence. The overal flux uncertainty of ± 10 % occurs as a scale error and is irrelevant for the present discussion.

Finally for easier comparison with other experiments we have calculated the shape parameter B from the average <y> values of the antineutrino data which are much more sensitive than the neutrino data. The result is shown in figure

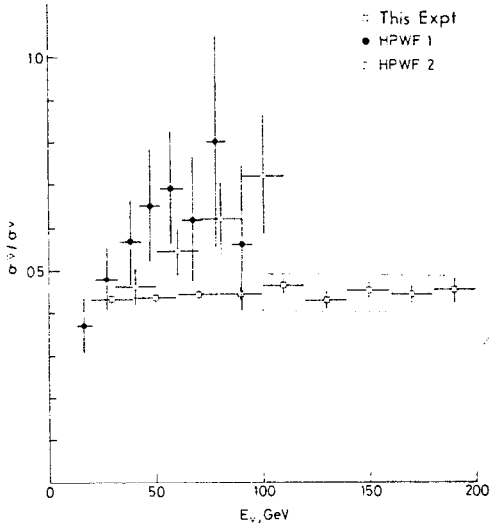

Fig. 9 : Ratio of total antineutrino to neutrino cross sections for this experiment compared to the data of reference[6]. The shaded area indicates the systematic uncertainty in the K/π ratio

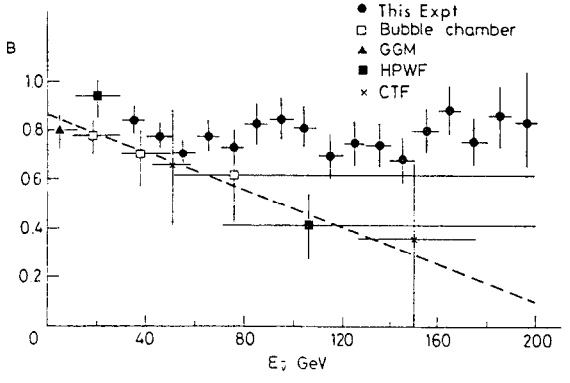

Fig. 10 : The shape parameter B determined from antineutrino data compared to earlier measurements

10 and compared to published results of other experiments.

3. Conclusions

Our data has been analysed to look for large deviations from the distributions observed at low energies. This analysis is straightforward and does not require any large corrections due to the high acceptance and the easy flux measurement of this experiment. Though it would be premature to draw conclusions on the actual value of B or on possible sclaing violations without a better understanding of systematic uncertaintics, there is no way how any conceivable experimental bias could produce a strong energy dependence or prevent us to see a "high y anomaly" of the sort and magnitude reported by the HPWF group[5,6].

Our conclusions are thus:

i) our data are compatible with no energy variation of $\langle y \rangle$ and $\sigma_{\bar{\nu}}/\sigma_{\nu}$ within statistical errors in the energy range $30 < E_{\nu} < 200$ GeV

ii) the rough features of the data are consistent with the predictions of the standard (V-A) quark parton model

$\therefore$ We do not see any evidence for the "high y anomaly"

II.3 Results for inclusive neutral current interactions[7]

1. Experimental data and method of analysis

The experimental quantities available in our experiment to study neutral current (NC) interactions are the hadron energy and the radial vertex position which is related to the neutrino energy (section I.2). The analysis is based on a direct comparison with charged current(CC) interactions using only the ratios of NC to CC event rates R_{ν} ($R_{\bar{\nu}}$) as a function of the neutrino energy and the scaling variable $y = E_h/E_{\nu}$. This has the advantage that some experimental uncertainties become less important since NC and CC events share the same neutrino spectrum and much of the selection procedure.

Neutral current events are separated from charged current events using the event length distribution shown in figure 11a, b. Due to the large diameter of our detector the bulk of the CC events with short event length is due to stopping muons from the high y region. The number of CC events below the NC signal is thus easily obtainable from the measured population in the "monitor region" indicated in figure 11 and a straightforward short distance extrapolation to the NC signal region using a Monte Carlo simulation. In addition to the charged current subtraction a series of other corrections has to be applied to clean up the NC and CC signals. To reduce background and to ensure full trigger efficiency a hadron energy $E_H > 12$ GeV was required. All corrections are summarized in table IV. The systematic uncertainties are

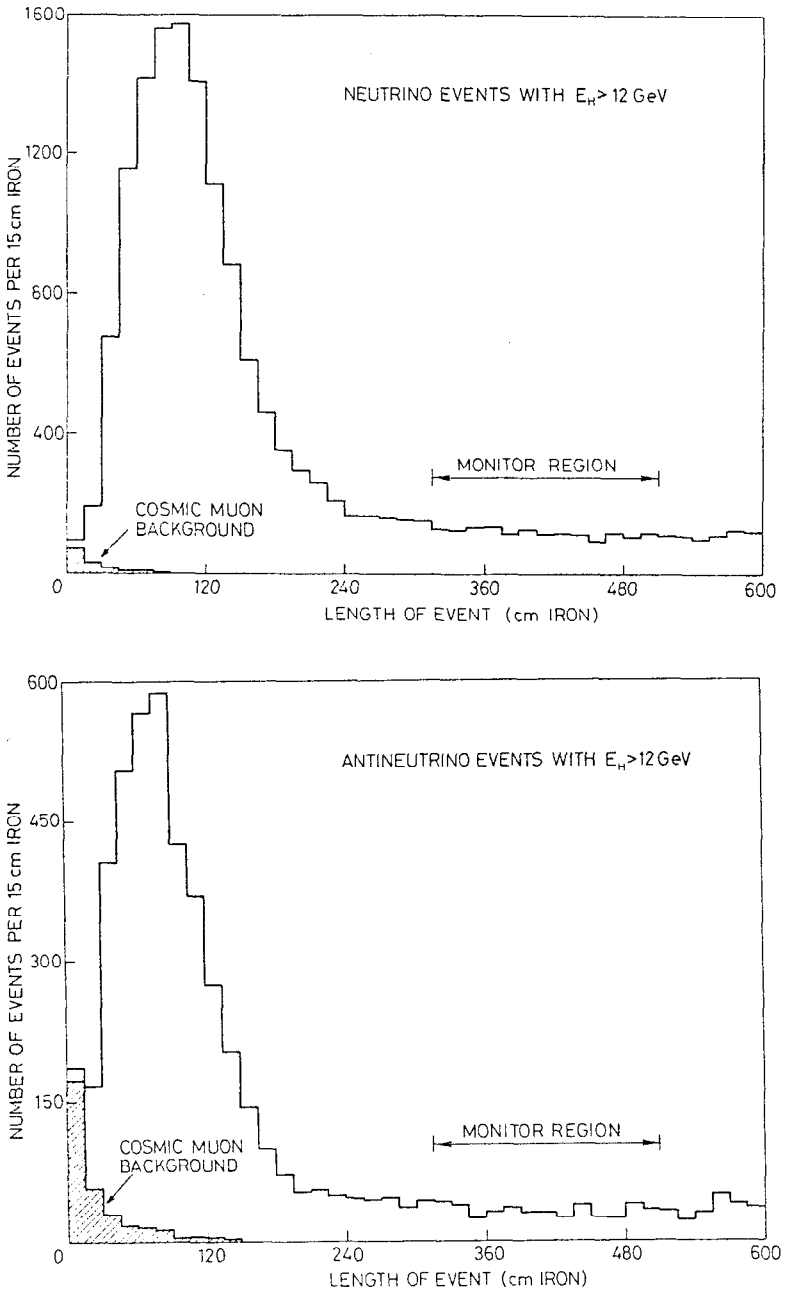

Fig.11: Event length distribution for neutrino and antineutrino data.

mainly due to the CC subtraction for neutrinos and due to the wide band beam subtraction for antineutrinos. The estimates of the systematic errors have been included in the final error.

Table IV: Summary of data reduction for NC and CC event for E_H > 12 GeV

	Neutrinos	Antineutrinos
NC candidates	10770 ± 104	3314 ± 58
Cosmic-ray background	-59 ± 7	-119 ± 10
WBB background	-286 ± 126	-646 ± 116
CC background	-1493 ± 64	-235 ± 49
NC with L < 16 and L > L_{cut}	+150	+43
K_{e3} correction	-1008	-154
NC signal	8074 ± 156	2203 ± 130
CC candidates	26509 ± 163	6483 ± 81
WBB background	-239 ± 117	-323 ± 83
CC extrapolation	+1467 ± 64	+253 ± 42
NC with L > L_{cut}	-134	-35
CC signal	27603 ± 211	6378 ± 123
NC/CC (error only statistical)	0.293 ± 0.006	0.346 ± 0.021
NC/CC (final result, systematic error included	0.293 ± 0.010	0.35 ± 0.03

For the detailed analysis of differential distributions the events have been grouped into a 20 x 4 matrix according to their hadron energy and their radial position in the detector. The analysis makes use of the fact that for each radial bin the incident neutrino spectrum is known and these spectra are different for the four radial bins (see section I.2). The measured ratios of NC to CC events for neutrino and antineutrino data are shown in figure 12a, b. It can be seen that these ratios do not change drastically with hadron energy or with radius so that one can conclude immediately that the NC and CC distributions do not differ greatly.

The analysis of these ratios is performed by comparing Monte Carlo calculations with the data where these calculations are used to transform a given distribution in the variables E_ν and y to the hadron energy - radial bin matrix using the properties of the neutrino beam, the experimental cuts and the resolution or our detector.

2. Cross section ratios for neutrinos and antineutrinos

The ratios R_ν and $R_{\bar{\nu}}$ averaged over all energies are obtained from table IV without any theoretical assumptions.

$$R_\nu = .30 \pm .01 \qquad \text{for } E_H > 12 \text{ GeV}$$

$$R_{\bar{\nu}} = .35 \pm .03$$

The average energies are $\langle E_\nu \rangle$ = 110 GeV and $\langle E_{\bar{\nu}} \rangle$ = 90 GeV.

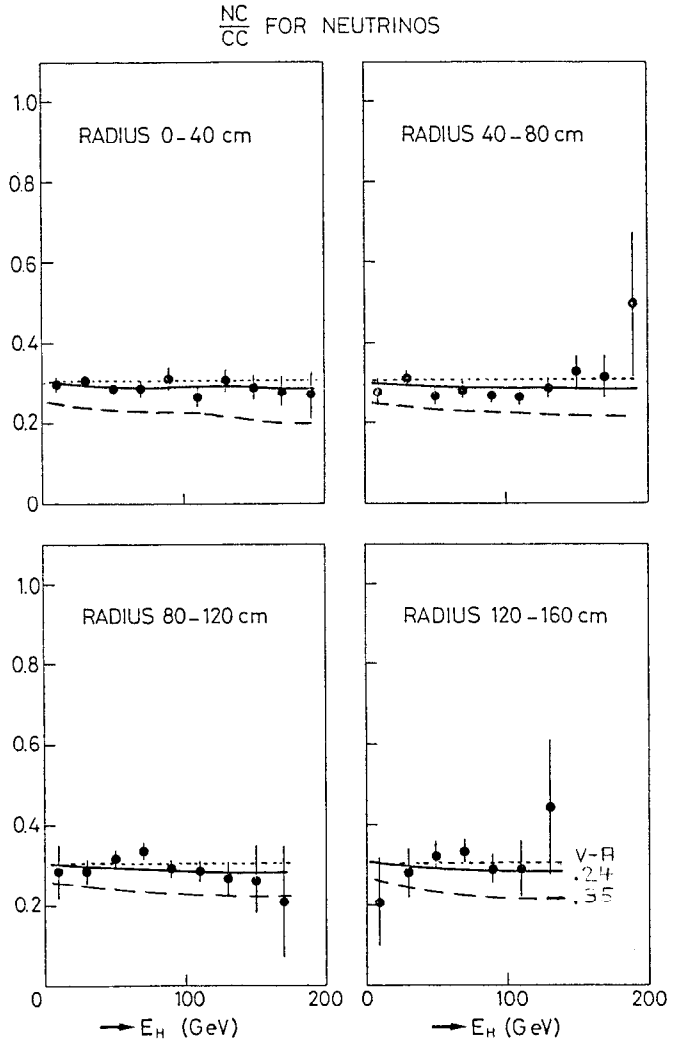

Fig. 12a: Neutral to charged current ratios versus hadron energy for neutrinos in four radial bins. The solid line is the best fit for the Weinberg-Salam model ($\sin^2\theta_W$ = 0.24), the expected distributions for $\sin^2\theta_W$ = 0.35 and the V - A prediction are also given (-- $\sin^2\theta_W$ = 0.35,...,V - A)

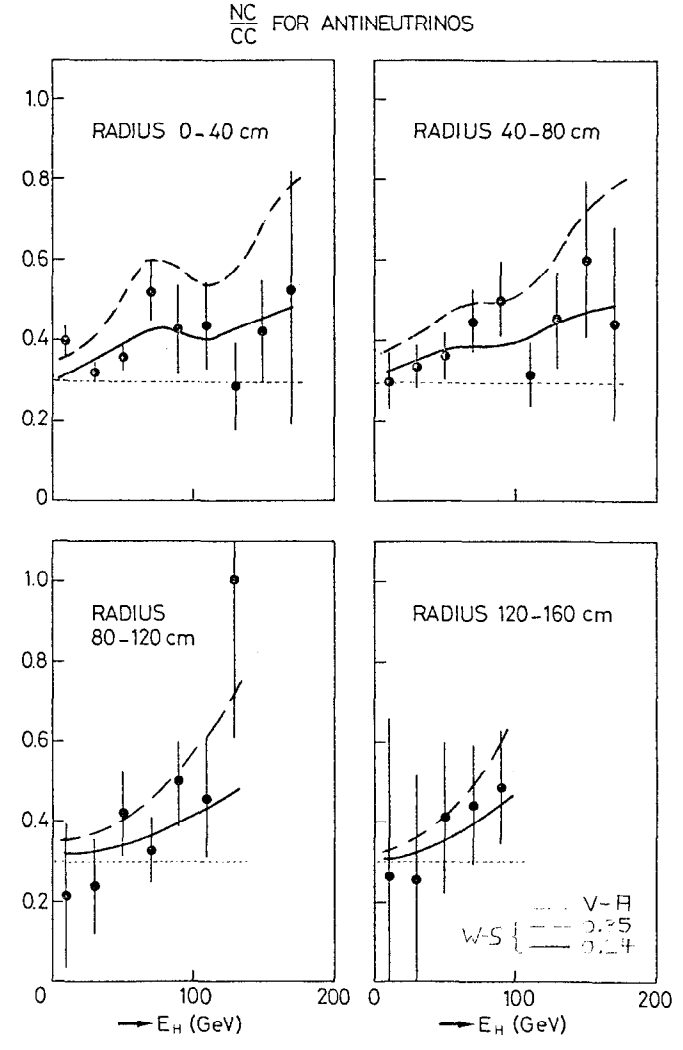

Fig. 12b: Neutral to charged current ratios versus hadron energy for antineutrinos and four radial bins. The solid line is the best fit for the Weinberg - Salam model ($\sin^2\theta_w = 0.24$), the expected distributions for $\sin^2\theta_w = 0.35$ and the V - A prediction are also given (-- $\sin^2\theta_w = 0.35$,..., V - A)

3. Shape of y-distributions and energy dependence

To get this information, the data have to be compared with a definite functional form of the y-distributions. We have chosen the form suggested by the quark parton model. The validity of our conclusions is however more general than that of the specific model. We have used the following parametrization

$$R_\nu\ (E_\nu, y) = (1 + \alpha_{CC}/3)\ \frac{A_L^\nu + A_R^\nu\ (1-y)^2}{1 + \alpha_{CC}\ (1-y)^2}$$

$$R_{\bar\nu}\ (E_{\bar\nu}, y) = (\alpha_{CC} + 1/3)\ \frac{A_L^{\bar\nu}\ (1-y)^2 + A_R^{\bar\nu}}{(1-y)^2 + \alpha_{CC}}$$

with separate coefficients A_L, A_R for neutrino and antineutrino data. Using the fitted values of A_L, A_R we can also obtain the integrated ratios R_ν^C, $R_{\bar\nu}^C$ corrected for the hadron energy cut $E_H > 12$ GeV:

$$R_\nu^C = A_L^\nu + A_R^\nu/3; \qquad R_{\bar\nu}^C = A_L^{\bar\nu}/3 + A_R^{\bar\nu}$$

In order to study the possible energy dependence of R_ν^C and $R_{\bar\nu}^C$ the data are fitted with two sets of parameters A_L, A_R, one for $E_\nu < 100$ GeV and the other for $E_\nu > 100$ GeV. The results of this fit are summarized in table V. The errors include the estimate of the systematic error. For comparison the purely statistical errors are given in brackets.

Table V: Fit results for the energy dependence and y-distribution of NC to CC cross section ratios

	Neutrinos	Antineutrinos
E_ν > 100 GeV $\langle E_\nu \rangle$ = 150 GeV	R_ν = .296±.013(0.10)	$R_{\bar\nu}$ = .34±.03(.019)
E_ν < 100 GeV $\langle E_\nu \rangle$ = 60 GeV	R_ν = .293±.017(.012)	$R_{\bar\nu}$ = .35±.06(.045)
$\frac{R(E_\nu > 100)}{R(E_\nu < 100)}$	.99 ±.07 (.06)	1.03±.18(.14)
all energies	R_ν = .295±.010(.006)	$R_{\bar\nu}$ = .34±.03(.017)
α_{CC} = .10	$A_R^\nu/A_L^\nu - \alpha_{CC}$ = .09±.18	$A_R^{\bar\nu}/A_L^{\bar\nu} - \alpha_{CC}$ = .10±.07
α_{CC} = .15	$A_R^\nu/A_L^\nu - \alpha_{CC}$ = .09±.19	$A_R^{\bar\nu}/A_L^{\bar\nu} - \alpha_{CC}$ = .14±.11

The data do not favour a substantial energy dependence. The experimental shape of the y-distribution for NC is compatible with that of CC interactions.

4. Spacetime structure of NC interactions

Information on the spacetime structure of NC interactions can be obtained from our data within the framework of specific theoretical models. We have analysed our data in the framework of the quark parton model assuming only vector V and axial vector A contributions. The parametrization for the y distribution has the following form:

$$\text{NC} \begin{cases} \frac{d\sigma_\nu}{dy} \propto A_L \{1 + \frac{A_R}{A_L}(1-y)^2\} \\ \frac{d\sigma_{\bar\nu}}{dy} \propto A_L \{\frac{A_R}{A_L} + (1-y)^2\} \end{cases} \quad (1)$$

$$\text{CC} \begin{cases} \frac{d\sigma_\nu}{dy} \propto 1 + \frac{\bar Q}{Q}(1-y)^2 \\ \frac{d\sigma_{\bar\nu}}{dy} \propto \frac{\bar Q}{Q} + (1-y)^2 \end{cases} \quad (2)$$

where the overall strength and the y-distribution for neutrino and antineutrino neutral currents are described by only two parameters A_L and A_R. These can be related to the coupling strengths of (V-A)- currents $A_- = [C_V - C_A]^2$ and (V+A)-currents $A_+ = [C_V + C_A]^2$

$$A_L = A_- + A_+ \frac{\bar Q}{Q}$$
$$A_R = A_+ + A_- \frac{\bar Q}{Q}$$

Weinberg - Salam model

The Weinberg - Salam model gives the following relations between the (V - A) and (V + A) couplings:

$$A_+ = \frac{5}{9}\sin^4\theta_w$$
$$A_- = \frac{1}{2} - \sin^2\theta_w + \frac{5}{9}\sin^4\theta_w$$

Determination of the V,A coupling

A simultaneous fit to the neutrino and antineutrino data displayed in figure 14 leaving A_L and A_R as free parameters has the result

$$\left.\begin{aligned} \frac{A_R}{A_L} &= .187 \pm .020 \quad \text{for } \frac{\bar{Q}}{Q} = .1 \\ \text{and} \\ \frac{A_R}{A_L} &= .256 \pm .025 \quad \text{for } \frac{\bar{Q}}{Q} = .15 \end{aligned}\right\} \quad \chi^2/DF = 56.7/60$$

for two different values of the antiquark content assumed for charged current interactions.

Independent of the assumed value for $\bar{Q}/Q$ the fitted ratio A_R/A_L is significantly different from $\bar{Q}/Q$ at a level of 4 standard deviations. We thus have to conclude that assuming the parametrization of the quark parton model both V - A and V + A currents contribute to the neutral current interactions.

Test of the Weinberg - Salam model

The Weinberg angle can be easily calculated from our measured values R_ν and $R_{\bar{\nu}}$. This is shown in figure 13 together with similar measurements of other experiments[8) 9) 10)]. It can be seen that for our experiment the Weinberg angle is determined essentially from the measured value R_ν and that it is nearly independent of the value of $\bar{Q}/Q$. We find

from R_ν : $\sin^2\theta_w = .24 \pm .021$

from $R_{\bar{\nu}}$: $\sin^2\theta_w = .21 \pm .09$

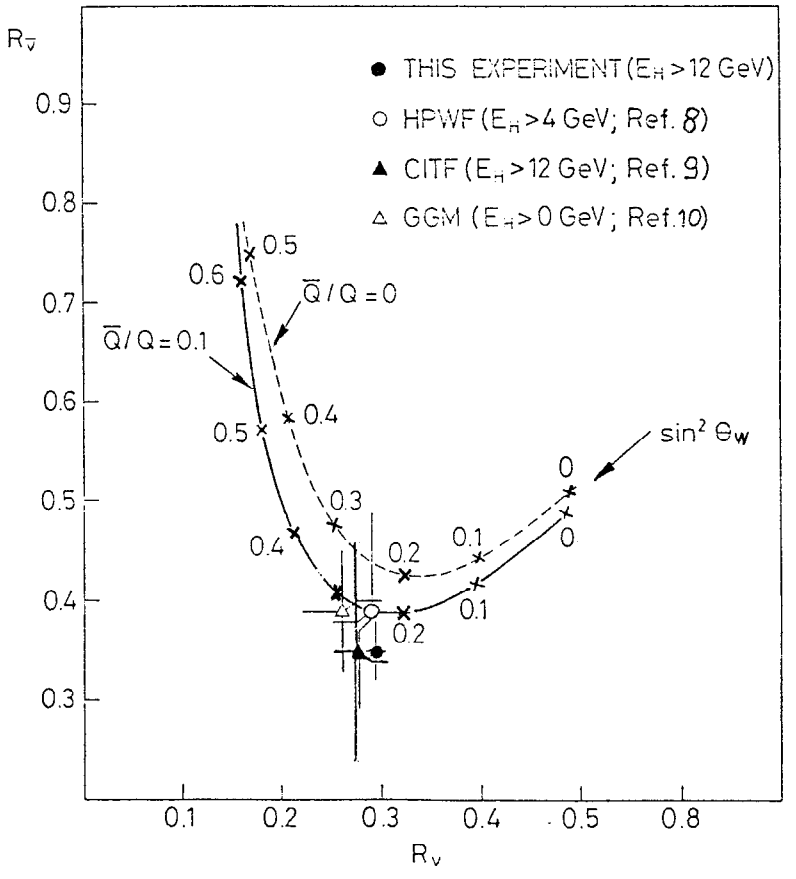

Fig.13: Comparison of R_ν and $R_{\bar{\nu}}$ with the Weinberg-Salam model. The curves shown include the effect of the hadron energy cut E_H > 12 GeV for this experiment and corrections for the neutron-proton ratio and the contribution of strange quarks.

The Weinberg angle can also be determined from the measured slopes of the y-distribution. We get

from $\frac{A_R^{\nu}}{A_L^{\nu}}$: $\sin^2\theta_W = .22^{\pm}.17$

from $\frac{A_R^{\bar{\nu}}}{A_L^{\bar{\nu}}}$: $\sin^2\theta_W = .25^{\pm}.06$

All values are in remarkable agreement giving strong support to the Weinberg-Salam model.

Finally the Weinberg-Salam model gives an excellent overall fit to both neutrino and antineutrino data with

$$\sin^2\theta_W = 0.24^{\pm} .02$$

and a χ^2 of 59 for 61 degrees of freedom. The error given is ~ 3 times larger than the statistical error and includes an estimate of systematic errors as well as the uncertainty in the total amount of the sea contribution and in the sea composition.

Discussion

Our data gives strong support for the existence of a V+A contribution in neutral current interactions with a strength that agrees well with what is expected in the Weinberg-Salam model. The Weinberg angle $\sin^2\theta_W=0.24^{\pm}.02$ found in this experiment is substantially lower than the world average of the other experiments and poses severe constraints on model builders. Therefore it may be useful to discuss the assumptions that enter into the determination of this angle.

In our experiment the Weinberg angle is determined essentially by the measured value of R_{ν} that is obtained without any theoretical assumptions. It should be noted that our value R_{ν} (and $R_{\bar{\nu}}$) is also in excellent agreement with recent results of other experiments [8)9)].

For a detailed comparison of the Weinberg-Salam model with the measured y-distributions of neutral currents we have to assume the parametrisation given by the quark parton model. This simple model is in remarkable good agreement with all features of our data as shown in figures 12a,b. Both the absolute magnitude and the shape of the y distribution for neutrino and antineutrino data are well described by the same Weinberg angle $\sin^2\theta_W=0.24$. It's very likely that the validity of this analysis goes beyond the validity of the quark parton model since the analysis is based on the ratio of NC to CC events only , thus that deviations from the model might cancel in first approximation.

Our value of $\sin^2\theta_W \simeq 1/4$ is very interesting from a theoretical point of view since the neutral current is then a composition of the third component of the charged current and of the electromagnetic current with equal strength.

II.4 Results on multimuon events

The observation of events with more than one muon in the final state is a very good signature for new particle production. New particles may be produced at the hadron or at the lepton vertex. Events of hadronic origin-i.e. production of charmed particles or even heavier quarks with subsequent semileptonic decay- generally show a large momentum asymmetry of the muons since one of the muon is the decay particle of a hadron that has to share the total hadronic energy with others. Also this decay muon has to show a correlation with the hadron shower. On the contrary events from leptonic origin - i.e. production of new heavy leptons ($\nu_\mu + N \to L^o +$ hadron, $L_o \to \mu^+\mu^-$ etc.)-show no correlation of the muons with the hadron shower and tend to produce events that are symmetric in the muon momenta.

1. Selection criteria

To detect muons with full efficiency and to measure their momentum and angle, they have to be well separated from the hadron shower. Thus a minimum of 4 driftchamber digitisations (including the shower) had to be required for each muon. This corresponds to an average momentum cutoff of 4.5 GeV/c. This unavoidable cutoff is uncomfortably high since it gives severe distortions of most of the kinematical distributions. For this reason the quantitative interpretation of the data requires comparison with detailed models of particle production.

2. Opposite sign dimuons[11)]

A total of 257 $\mu^-\mu^+$ events have been observed in the neutrino and 58 $\mu^+\mu^-$ events in the antineutrino exposure. Since the corresponding observed number of like-sign dimuon events (table III) is much smaller it is evident that most of these events are due to a prompt muon signal rather than due to π/K-decays. It has been shown earlier by other experiments[12)] that the bulk of these events it due to charm production. Thus using our data we can make detailed tests on single charm production models and look for possible other sources beyond charm. The observed $\mu^+\mu^-$ events show the following main characteristics:

i) The bulk of the events exhibits a large asymmetry in the muon momenta as shown in figure 14a,b. The wrong sign muon (μ_2) is in average much slower than the muon that has the same lepton number as the incoming neutrino. The solid curves in the figures are the predictions of the GIM-model for single charm production[13)] and agree fairly well with the measured distributions.

ii) All events, including the symmetric ($E_{\mu_1} \simeq E_{\mu_2}$), are correlated with the hadron shower. This is shown in figure 15 that shows the azimuthal angle ϕ between the two muons in a plane perpendicular to the incoming neutrino for different energy intervals of the wrong sign muon (shower direction is $\phi = 180^o$). Figure 16 gives the transverse momentum of the wrong

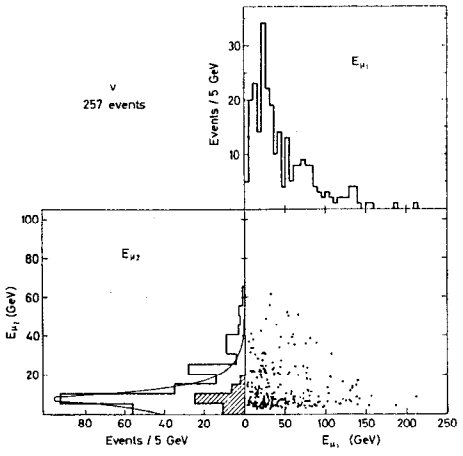

a)

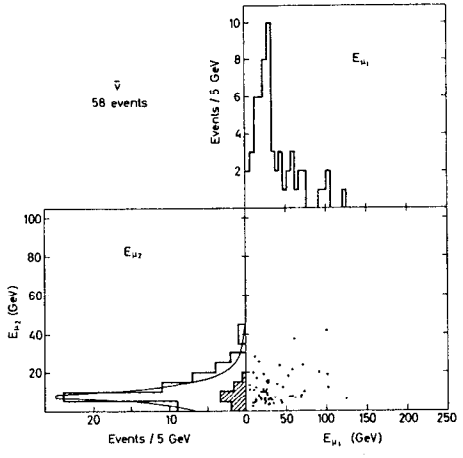

b)

Fig. 14: Scatter plots, with projections, in $E_{\mu 1}$ - $E_{\mu 2}$ plane, for for neutrinos and antineutrino events. In the $E_{\mu 2}$ projection the $\pi \to \mu$ and $K \to \mu$ decay background is shown, as well as the prediction of a charm model, normalized to the total event number.

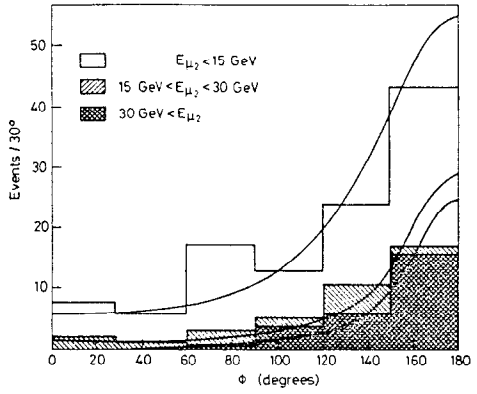

Fig.15: Azimuthal angle between the two muons for different energies of the wrong sign muon compared to the prediction of the GIM model (solid lines)

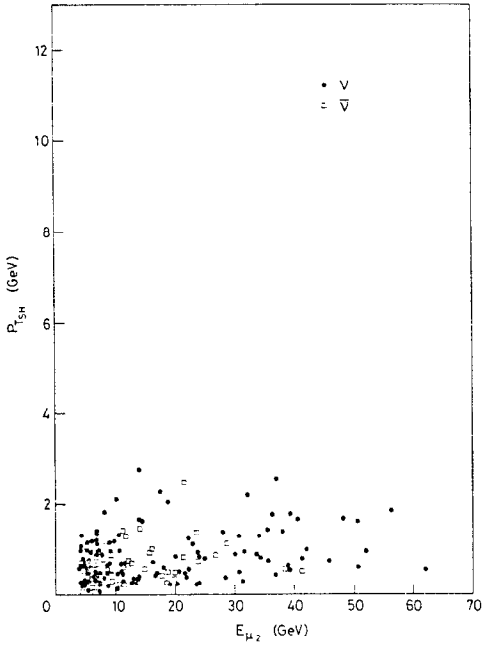

Fig.16: Transverse momentum of the wrong sign muon relative to the shower direction versus its energy

The outstanding features predicted by this model are

i) the y-distributions are flat for both neutrino and antineutrino charm production

ii) the x-distribution is significantly different for neutrinos and antineutrinos

The y-distributions are shown in fig. 17. They are heavily distorted due to the momentum cutoff for the second muon. Antineutrino and neutrino data are however very similar and agree fairly well with the expected distribution from the GIM-model (solid line). The x-distributions (fig. 17) are indeed significantly different for neutrinos and antineutrinos. They are compared with the measured "sea" and "valence" distributions from ordinary charged current events. The antineutrino distribution agrees well with a pure sea-distribution whereas the neutrino distribution is a mixture of sea and valence distributions. These observations give very strong support to the GIM-model. Comparing the observed dimuon rates from neutrino and antineutrino using $\sin^2\theta_c = .057$ we can evaluate the fraction of momentum carried by strange quarks. We find

$$\xi_s = .034$$

leading to a total expected charm production of about 9 % for both neutrinos and antineutrinos relative to charged current events. Using the expected rate and the calculated efficiency for muon detection we can compare it to the observed rate of $\mu^+\mu^-$ - events to get an estimate of the leptonic branching ratio. This gives

$$B_\mu \approx 0.15.$$

sign muon relative to the shower direction versus its total energy E_{μ_2}. The average transverse momentum is independent of E_{μ_2} as expected from hadronic production of fixed mass particles.

In summary we may conclude that we see no evidence for new particle production at the lepton vertex and that the kinematical distributions of the events observed are consistent with the expectations of single charm production.

Detailed test of GIM-model

Single charm production in the GIM-model is due to three processes that are bound to have definite production rates and scaling distributions.

Process	production rate	main characteristics
1. $\nu_\mu + d \to \mu^- + c$	$\sin^2\theta_c \cdot B_\mu$	flat in y; valence distribution in x
2. $\nu_\mu + s \to \mu^- + c$	$\cos^2\theta_c \cdot B_\mu \cdot \xi_s$	flat in y
3. $\bar{\nu}_\mu + \bar{s} \to \mu^+ + \bar{c}$		sea distribution peaked at small x

θ_c = Cabbibo angle

B_μ = effective muonic branching ratio of charmed particles

$\xi_s = \frac{Qs}{Qd}$ = fraction of momentum carried by strange quarks relative to d- quarks

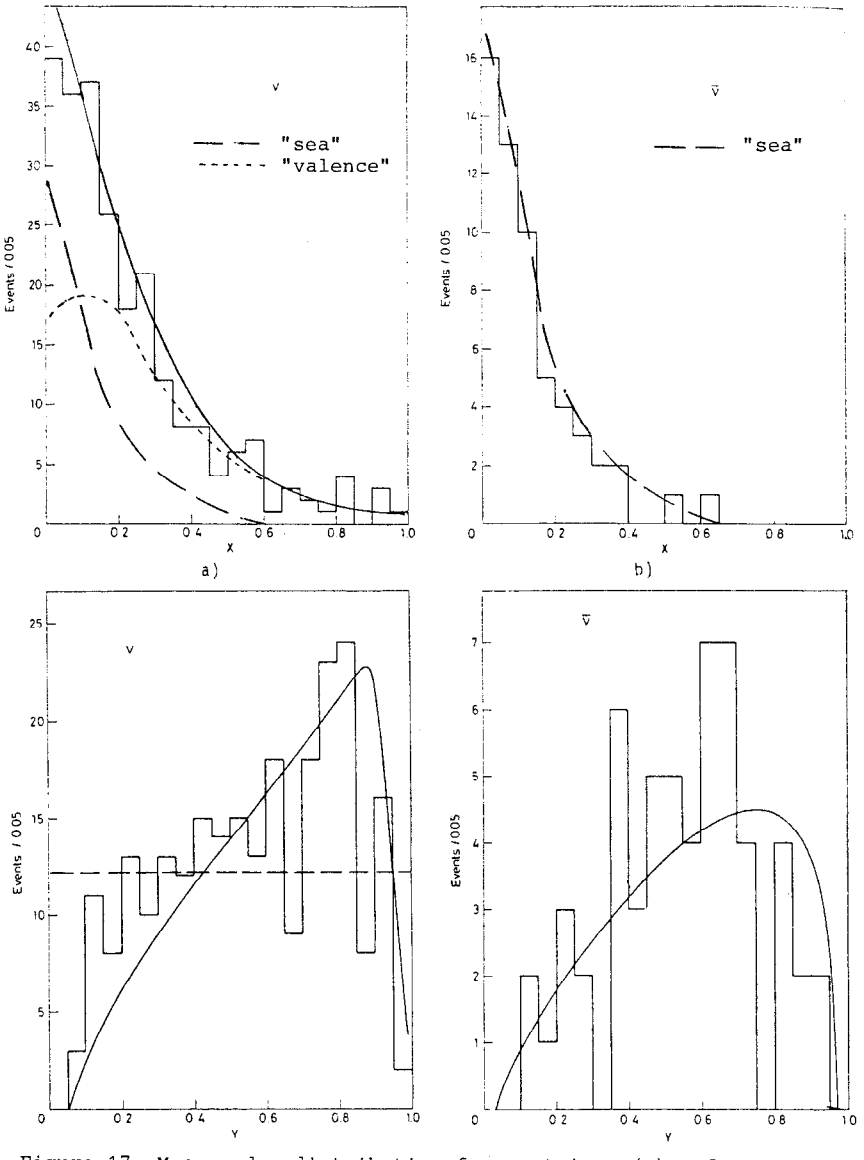

Figure 17: Measured x-distribution for neutrinos (a) and antineutrinos (b) compared to GIM-model predictions (— — "sea", ------ "valence", —— "sea+valence" in the ratio .057:.034, where the shape of sea and valence distributions is taken from CC antineutrino and neutrino events)
c,d: Y-distributions compared to GIM-model prediction (——).

The opposite dimuon data are thus in excellent agreement with the predictions of the GIM - single charm production model. No other sources of dimuons are needed to explain the data.

3. Like-sign dimuon events

The observed events are dominated by π/K-decay background. This background has been calculated including the cascade effect in iron and should be reliable to about ± 30 %. Table VI summarises the event numbers

Table VI Summary for like-sign dimuon events

	neutrino	antineutrino
observed	47 $\mu^-\mu^-$	9 $\mu^+\mu^+$
calculated background	30	5
above background	17 ± 10	4 ± 3

There are no events with outstanding kinematical properties. The scatterplot of the muon energies is shown in figure 18. All events are very asymmetric and the distribution of the slow muon is as expected from π/K decay (shaded area). The transverse momentum P_T of the slow muon perpendicular to the plane made up by the incident neutrino and the fast muon is shown in figure 19. There is no sign of events with two fast muons or with a large transverse momentum P_T as would be expected in heavy lepton cascade models.

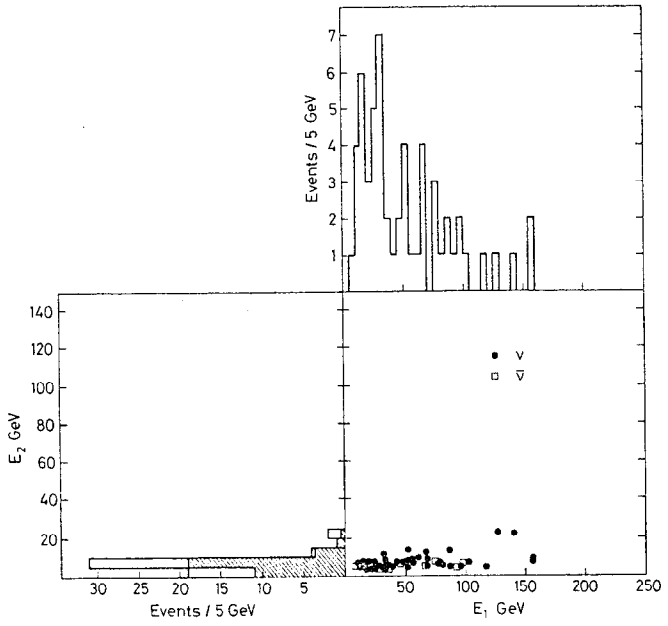

Figure 18: Energies of the two muons for like-sign dimuons (▨ expected for π/K-decays).

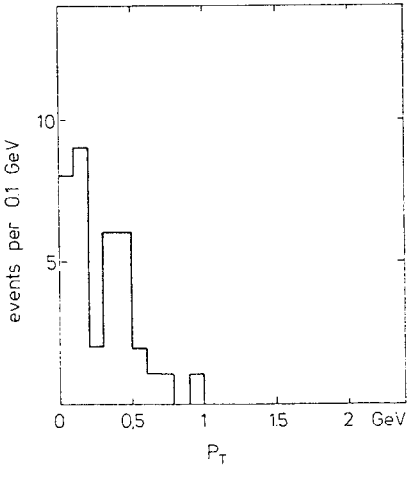

Figure 19: Transverse momentum of the slow muon perpendicular to the neutrino-fast muon plane.

The events above background (uncertain) may however be due to associated charm production. Using this hypothesis we estimate that the total rate of associate charm production is of the order of 0.5 to 1 % at E_ν = 100 GeV.

III. Conclusions

From the data of the CDHS experiment presented in this talk we can draw the following conclusions:

i) the standard quark parton model with 4 quarks is in fairly good agreement with the data,

ii) charged current events are consistent with pure V - A coupling,

iii) neutral currents consist of both V-A and V+A currents,

iv) no additional quarks or leptons are required to explain the data.

Though nothing really exciting has been observed until now we may very well expect some surprises in the course of a detailed analysis of our charged current data. If new particles are produced in neutrino interactions we will also have a good change to see a signal in our wide band beam running that has just started. The emphasis there is on the detection of multimuon events with high statistics ($\sim$ 150 $\mu^+\mu^-$/day) and at higher energies.

References:

1) M. Holder et al: A detector for high energy neutrino Interactions , submitted to Nuclear Instrum. methods.

2) J. May et al, "Narrow bard neutrino beam running and monitoring" internal report CERN, GP 4/77

3) M. Holder et al, Phys.Rev. Letters, 39, 433 (1977)

4) D.H. Perkins, Proc. 1975 Internat. Symposium on Lepton and Photon Interactions at High Energies, Stanford, 1975, P. 571

5) A. Benvenuti et al, Phys.Rev. Letters 36, 1478 (1976)

6) A. Benvenuti et al, Phys.Rev. Letters 37, 189 (1976)

7) M. Holder et al: Measurement of neutral current interactions in narrow band neutrino and antineutrino beams , submitted to Phys.Letters B.

8) P. Wanderer et al, Measurement of the neutral current interactions, preprint HWPF - 77/1, submitted to Phys. Rev. D.

9) F.S. Merritt et al, Differential cross - sections for inclusive neutral current interactions at high energies, CALT 68-600 preprint.

10) J. Blietschau et al, Nuclear Physics B 118,218 (1977)

11) M. Holder et al, Phys. Letters B 69 ,377,(1977)

12) A. Benvenuti et al, Phys.Rev. Lett. 35, 1199, 1203 and 1249 (1975)

13) L.M. Sehgal and P.M. Zerwas, Nucl.Phys. B108, 483 (1976)

14) M. Holder et al, Like - sign dimuon events produced in narrow-band neutrino and antineutrino beams. submitted to Phys.Letters B.

PARTICIPANTS

A:

Julio Abad
University of Wisconsin
Department of Physics
Madison, Wi. 53706

E. Abers
Univ. of California
Department of Physics
Los Angeles, Ca. 90024

Moshe Aelion
Stanford Linear Accelerator Center
Bin 81
Stanford, Ca. 94305

S. Alam
Stanford Linear Accelerator Center
Bin 95
Stanford, Ca. 94305

John Alcock
Bristol Univ.
Physics Dept.
Bristol BS8 ITL England

William Ash
Stanford Linear Accelerator Center
Bin 60
Stanford, Ca. 94305

Patrick Aurenche
Ecole Polytechnique
Centre de Physique Theorique
Route de Saclay
F-91120 Palaiseau, France

B:

Belal Baaquie
Stanford Linear Accelerator Center
Bin 81
Stanford, Ca. 94305

Howard C. Baker
Berea College
Physics Dept.
Berea, Ky. 40403

James S. Ball
University of Utah
Physics Department
Salt Lake City, Ut. 84112

Vernon Barger
University of Wisconsin
Physics Department
Madison, Wi. 53706

Dana Beavis
University of California
Physics Department
Riverside, Ca. 92502

Shelomo I. Ben-Abraham
Ben Gurion University of Negev
Physics Department
P. O. Box 653
84120 Beer-Sheva, Israel

Shahar Ben-Menahem
Stanford Linear Accelerator Center
Bin 81
Stanford, Ca. 94305

E. Berger
Argonne National Laboratory
9700 So. Cass Avenue
Argonne, Il. 60439

H. H. Bingham
Lawrence Berkeley Laboratory
Berkeley, Ca. 94720

J. Bjorken
Bin 81
Stanford Linear Accelerator Center
Stanford, Ca. 94305

Richard Blankenbecler
Stanford Linear Accelerator Center
Bin 81
Stanford, Ca. 94305

Craig Blocker
Lawrence Berkeley Laboratory
Berkeley, Ca. 94720

E. Bloom
Stanford Linear Accelerator Center
Bin 98
Stanford, Ca. 94305

W. De Boer
Deutsches Elektronen Synchrotron
Notkestiegl
D-2000 Hamburg 52, Germany

Fritz W. Bopp
Gesamthochschule Siegen
Fachbereich fur Physik
Holderlinstr. 3
Postfach 210209
D-5900 Siegen 21, Germany

Jacques M. Bouchez
Stanford Linear Accelerator Center
Bin 78
Stanford, Ca. 94305

David Brayshaw
Stanford Linear Accelerator Center
Bin 81
Stanford, Ca. 94305

Marty Breidenbach
Stanford Linear Accelerator Center
Bin 96
Stanford, Ca. 94305

Stan Brodsky
Stanford Linear Accelerator Center
Bin 81
Stanford, Ca. 94305

K. Wyatt Brown
California Institute of Technology
Physics Department
Pasadena, Ca. 91125

Karl Brown
Stanford Linear Accelerator Center
Bin 72
Stanford, Ca. 94305

Walter Bruckner
Lawrence Berkeley Laboratory
Berkeley, Ca. 94720

Warren Buck
State University of New York
Physics Department
Stony Brook, NY. 11794

F. Bulos
Stanford Linear Accelerator Center
Bin 95
Stanford, Ca. 94305

Kirk Bunnell
Stanford Linear Accelerator Center
Bin 65
Stanford, Ca. 94305

C:

Robert N. Cahn
University of Michigan
Physics Department
Ann Arbor, Mi. 48104

Robert K. Carnegie
Carleton University
Physics Department
Ottawa, On. Canada K1S 5B6

J. Terry Carroll
Stanford Linear Accelerator Center
Bin 78
Stanford, Ca. 94305

Arthur S. Cary
California Polytechnic State University
Physics Department
San Luis Obispo, Ca. 93407

Ron Cassell
Stanford Linear Accelerator Center
Bin 65
Stanford, Ca. 94305

Bill Caswell
Brown University
Department of Physics
Providence, RI. 02912

Vlada Chaloupka
Stanford Linear Accelerator Center
Bin 78
Stanford, Ca. 94305

Lai-Him Chan
Louisiana State University
Physics and Astronomy Department
Baton Rouge, La. 70803

Lay Nam Chang
Stanford Linear Accelerator Center
Bin 81
Stanford, Ca. 94305

Wang Kong Cheung
University of Pennsylvania
Physics Department
Philadelphia, Pa. 19174

C. Y. Chien
Stanford Linear Accelerator Center
Bin 62
Stanford, Ca. 94305

Norman H. Christ
Columbia University
Physics Department
New York, NY. 10027

B. Kent Clark
Florida State University
Physics Department
Tallahassee, Fl. 32306

James Clendenin
Yale University
Physics Department
New Haven, Ct. 06520

J. Cleymans
University Bielefeld
Faculty of Physics
Postfach 8640
D-4800 Bielefeld 1, Germany

Mark Coles
Lawrence Berkeley Laboratory
Berkeley, Ca. 94720

Guido Cosenza
University di Napoli
Istituto di Fisica Teorica
Mostra d'Oltremare, Pad. 19
I-80125 Naples, Italy

R. L. Cottrell
Stanford Linear Accelerator Center
Bin 96
Stanford, Ca. 94305

Brian Couchman
CERN
1211 Geneva 23
Switzerland

Robert Cousins
Stanford Linear Accelerator Center
Bin 62
Stanford, Ca. 94305

D. Coyne
Stanford Linear Accelerator Center
Bin 98
Stanford, Ca. 94305

Ronald L. Crawford
Department of Natural Philosophy
University of Glasgow
Glasgow G128QQ, Scotland

Thomas Curtright
University of California
Physics Department
Padadena, Ca. 91125

D.

Murray S. Daw
California Institute of Technology
Physics Department
Pasadena, Ca. 92664

Christopher M. Debeau
University of California
Physics Deaprtment
Irvine, Ca. 92664

N. G. Deshpande
University of Oregon
Institute of Theoretical Science
Eugene, Or. 97403

H. DeStaebler
Stanford Linear Accelerator Center
Bin 96
Stanford, Ca. 94305

Alain Diamant-Berger
Stanford Linear Accelerator Center
Bin 63
Stanford, Ca. 94305

Patrick Dishaw
Stanford Linear Accelerator Center
Bin 63
Stanford, Ca. 94305

Jonathan Dorfan
Stanford Linear Accelerator Center
Bin 61
Stanford, Ca. 94305

Sidney Drell
Stanford Linear Accelerator Center
Bin 81
Stanford, Ca. 94305

William Dunwoodie
Stanford Linear Accelerator Center
Bin 62
Stanford, Ca. 94305

Minh Duong-van
Stanford Linear Accelerator Center
Bin 65
Stanford, Ca. 94305

Stanley Durkin
Stanford Linear Accelerator Center
Bin 62
Stanford, Ca. 94305

E.

Tohru Eguchi
Stanford Linear Accelerator Center
Bin 81
Stanford, Ca. 94305

Martin B. Einhorn
University of Michigan
Physics Department
Ann Arbor, Mi. 48104

F. Eisele
University of Dortmund
Institüt fur Physik
Baroper Str.
Postfach 50 05 00
D-4600 Dortmund-Hornbruch,
Germany

James R. Elliott
University of Illinois
Physics Department
Urbana, Il. 61801

F.

C. W. Fabjan
CERN
CH-1211 Geneva 23,
Switzerland

W. M. Fairbank
Stanford University
Physics Department
Stanford, Ca. 94305

Gary Feldman
Stanford Linear Accelerator Center
Bin 61
Stanford, Ca. 94305

Joseph Feller
Lawrence Berkeley Laboratory
Berkeley, Ca. 94720

A. Fernandez-Pacheco
Stanford Linear Accelerator Center
Bin 81
Stanford, Ca. 94305

R. Clive Field
Stanford Linear Accelerator Center
Bin 78
Stanford, Ca. 94305

G. H. Fischer
Stanford Linear Accelerator Center
Bin 95
Stanford, Ca. 94305

Abraham Fong
Lawrence Berkeley Laboratory
Berkeley, Ca. 94720

Barry A. Freedman
Massachusetts Institute of Tech..
Physics Department
Cambridge, Ma. 02139

Lenore Friedlaender
Oberlin College
Box 841
Oberlin, Ohio 44074

David Fryberger
Stanford Linear Accelerator Center
Bin 20
Stanford, Ca. 94305

G.

J. Gayser
Stanford Linear Accelerator Center
Bin 96
Stanford, Ca. 94305

Paolo Gensini
Instituto Di Fisica Universita
I73100 Lecce, Italy

Eldad Gildener
University of California, San Diego
Physics Department
B-019
La Jolla, Ca. 92093

Roscoe Giles
Massachusetts Institute of Technology
Physics Department
Canbridge, Ma. 02139

Fred Gilman
Stanford Linear Accelerator Center
Bin 81
Stanford, Ca. 94305

Thomas Glanzman
Duke University
Physice Department
Durham, NC. 27706

Bruno Gobbi
Northwestern University
Department of Physics
Evanston, Il. 60201

G. Godfrey
Stanford Linear Accelerator Center
Bin 81
Stanford, Ca. 94305

Gerson Goldhaber
Lawrence Berkeley Laboratory
Berkeley, Ca. 94720

T. J. Goldman
Los Alamos Scientific Laboratory
P. O. Box 1663
Los Alamos, NM. 87544

Gary R. Goldstein
Tufts University
Physics Department
Medford, Ma. 02155

A. Gonidec
Stanford Linear Accelerator Center
Bin 96
Stanford, Ca. 94305

Richard J. Gonsalves
Institute for Advanced Study
Princeton, NJ. 08540

A. T. Goshaw
Duke University
Physics Department
Durham, NC. 27706

K. Gottfried
Cornell University
Laboratory of Nuclear Studies
Ithaca, NY. 14853

Thomas Gottschalk
University of Wisconsin
Physics Department
Madison, Wi. 53706

Garland Grammer
University of Illinois
Physics Deaprtment
Box 4348
Chicago, Il. 60608

John Greenhalgh
Stanford University
Department of Physics
Stanford, Ca. 94305

Jose Grifols
Stanford Linear Accelreator Center
Bin 81
Stanford, Ca. 94305

John F. Gunion
University of California
Physics Department
Davis, Ca. 95616

H.

Howard Haber
University of Michigan
Physics Deaprtment
Ann Arbor, Mi. 48104

U. Hahn
University Freiburg
Physikalisches Institute
Hermann-Herder Strasse 3
D-7800 Freiburg i. Br, Germany

Anne Hall
Stanford Linear Accelerator Center
Bin 63
Stanford, Ca. 94305

Robert P. Hamilton
Lawrence Berkeley Laboratory
Berkeley, Ca. 94720

James E. Hanlon
State University of New York
Physics Department
Stony Brook, NY. 11794

Gail Hanson
Stanford Linear Accelerator Center
Bin 61
Stanford, Ca. 94305

Haim Harari
Weizmann Institute of Science
Physics Department
Rehovoth, Israel

John Hauptman
University of California
Physics Department
Los Angeles, Ca. 90024

Mitsuo Hayashi
Stanford Linear Accelerator Center
Bin 81
Stanford, Ca. 94305

Ken Hayes
Stanford Linear Accelerator Center
P. O. Box 4349
Stanford, Ca. 94305

Richard J. Hemingway
Stanford Linear Accelerator Center
Bin 62
Stanford, Ca. 94305

R. E. Hendrick
Carnegie Mellon University
Physics Department
Pittsburbh, Pa. 15213

Thomas Himel
Stanford Linear Accelerator Center
Bin 95
Stanford, Ca. 94305

Minoru Hirayama
Toyama University
Department of Physics
Toyama 930, Japan

David Hitlin
Stanford Linear Accelerator Center
Bin 95
Stanford, Ca. 94305

Hanna J. Hoffman
Rutherford High Energy Laboratory
Chilton
Didcot, Oxon. OX11 0OX, England

Alan Honma
Stanford Linear Accelerator Center
Bin 62
Stanford, Ca. 94305

Ron Horgan
Stanford Linear Accelerator Center
Bin 81
Stanford, Ca. 94305

Charles P. Horne
Lawrence Berkeley Laboratory
Berkeley, Ca. 94720

Monowar Hossain
University of Texas
Center for Particle Theory
Austin, Tx. 78712

Richard J. Hughes
University of Liverpool
Dept. Appl. Math Theor. Phys.
P. O. Box 147
Liverpool, L69 3BX, England

Benedikt Humpert
Stanford Linear Accelerator Center
P. O. Box 4349
Stanford, Ca. 94305

David Hutchinson
Stanford Linear Accelerator Center
Bin 62
Stanford, Ca. 94305

I.

Walter Innes
Fermilab
P. O. Box 500
Batavia, Il. 60510

David Iskandar
University of Oregon
Institute of Theoretical Science
Eugene, Or. 97403

J.

Robert Jaffe
Massachusetts Institute of Technology
Physics Department
Cambridge, Ma. 02139

John Jaros
Stanford Linear Accelerator Center
Bin 61
Stanford, Ca. 94305

J. Johnson
Stanford Linear Accelerator Center
Bin 94
Stanford, Ca. 94305

William B. Johnson
Stanford Linear Accelerator Center
Bin 62
Stanford, Ca. 94305

Daniel L. Jones
University of California
Physics Department
Davis, Ca. 95616

Michael K. Jones
University of Hawaii
Physics Department
Honolulu, Hi. 96822

Steve Jones
Vanderbilt University
Physics Department
Nashville, Tn. 37235

Hans Jostlein
State University of New York
Physics Department
Stony Brook, NY. 11794

Ilmun Ju
University of Oregon
Institute of Theoretical Science
Eugene, Or. 97403

K.

John Kadyk
Lawrence Berkeley Laboratory
Berkeley, Ca. 94720

John Kafka
State University of New York
Physics Department
Stony Brook, NY 11794

Sinan Kaptanoglu
Stanford Linear Accelerator Center
Bin 81
Stanford, Ca. 94305

Robert Kelly
Lawrence Berkeley Laboratory
Berkeley, Ca. 94720

Rosemary G. Kennett
California Institute of Technology
Physice Department
Pasadena, Ca. 91125

Robert W. Kenney
Lawrence Berkeley Laboratory
Berkeley, Ca. 94720

C. Kiesling
Stanford Linear Accelerator Center
Bin 98
Stanford, Ca. 94305

J. D. Kimel
Florida State University
Physics Department
Tallahassee, Fl. 32306

Jasper Kirkby
Stanford Linear Accelerator Center
Bin 63
Stanford, Ca. 94305

Janos Kirz
State University of New York
Physics Department
Stony Brook, NY. 11794

Leslie Klein
400 F High Point Drive
Hartsdale, NY. 10530

Winston Ko
University of California
Phyiscs Department
Davis, Ca. 95616

Eleizer Kogan
Weizmann Institute of Science
Rehovot,
Israel 00197

In Gyu Koh
Korea Advanced Institute of Science
Physics Department
P. O. Box 150
Chongyangni, Seoul, Korea

Edward Kolb
University of Texas
Center for Particle Theory
Austin, Tx. 78712

Wolf D. Kollmann
Stanford Linear Accelerator Center
Bin 98
Stanford, Ca. 94305

David Koltick
University of Michigan
Physics Department
Ann Arbor, Mi. 48104

M. Krammer
Deutsches Elektronen Synchrotron
Notkestieg 1
D-2000 Hamburg 52, Germany

Arthur Kreymer
Indiana University
Physics Department
Bloomington, In. 47401

Paul Kunz
Stanford Linear Accelerator Center
Bin 62
Stanford, Ca. 94305

Betty Kwan
Stanford Linear Accelerator Center
Bin 61
Stanford, Ca. 94305

L.

Robert Lacy
201 Greenway
Lake Charles, La. 70605

Choy-Heng Lai
Fermilab
P. O. Box 500
Batavia, Il. 60510

Kwan Wu Lai
Brookhaven National Laboratory
Upton, NY. 11973

Ken Lane
Harvard University
Cambridge, Ma. 02138

Joseph E. Lannutti
Florida State University
Physics Department
Tallahassee, Fl. 32306

Peter G. LePage
Stanford Linear Accelerator Center
Bin 81
Stanford, Ca. 94305

T. Lasinski
Stanford Linear Accelerator Center
Bin 62
Stanford, Ca. 94305

K. E. Lassila
Iowa State University
Physics Department
Ames, Io. 50010

David W. G. S. Leith
Stanford Linear Accelerator Center
Bin 62
Stanford, Ca. 94305

Abraham Lesnik
Brookhaven National Laboratory
Upton, NY. 11973

Garry Levman
Argonne National Laboratory
9700 South Cass Avenue
Argonne, Il. 60439

James Lindesay
Stanford Linear Accelerator Center
Bin 81
Stanford, Ca. 94305

Ta-yung Ling
University of Pennsylvania
Physics Department
Philadelphia, Pa. 19174

Vicente Llamas
830 Baca Avenue
Las Vegas, NM. 87701

William Louis
University of Michigan
Physics Department
Ann Arbor, Mi. 48104

Dieter Luke
Stanford Linear Accelerator Center
Bin 61
Stanford, Ca. 94305

Vera Luth
Stanford Linear Accelerator Center
Bin 95
Stanford, Ca. 94305

Richard Lytel
Stanford Linear Accelerator Center
Bin 81
Stanford, Ca. 94305

M.

Ernest Ma
University of Hawaii
Physics Department
Honolulu, Hi. 96822

Rabindar Madan
North Carolina A and T
State University
Physics Department
Greensboro, MC. 27411

Leon Mandansky
Johns Hopkins University
Physics Department
Baltimore, Md.21218

R. Madaras
Lawrence Berkeley Laboratory
Berkeley, Ca. 94720

Anthony Mann
Tufts University
Physics Department
Medford, Ma. 02155

Fred Mansouri
Yale University
New Haven, Ct. 06520

Max Marshall
California Institute Technology
Physics Department
Pasadena, Ca. 91125

Francois Martin
Stanford Linear Accelerator Center
Bin 81
Stanford, Ca. 94305

Jim Martin
Stanford Linear Accelerator Center
Bin 61
Stanford, Ca. 94305

C. Matteuzzi
CERN
CH-1211 Geneva 23, Switzerland

G. May
Johns Hopkins University
Physics Department
Baltimore, Md. 21218

Aidan Mc Donald
Trinity College
School of Mathematics
Dublin 2, Ireland

Frank Merritt
Stanford Linear Accelerator Center
Bin 81
Stanford, Ca. 94305

Sydney Meshkov
National Bureau of Standards
Radiation Theory Section
Washington, DC. 21234

Donald I. Meyer
University of Michigan
Physics Department
Ann Arbor, Mi. 48104

Thomas Meyer
University of California
Physics Department
Los Angeles, Ca. 90024

Thomas Meyer
Stanford Linear Accelerator Center
Bin 62
Stanford, Ca. 94305

M. Meystayer
Stanford Linear Accelerator Center
Bin 96
Stanford, Ca. 94305

Ronald E. Mickens
Fisk University
Physics Department
Nashville, Tn. 37203

David Miller
Stanford Linear Accelerator Center
Bin 81
Stanford, Ca. 94305

Edward S. Miller
University of California, San Diego
Physics Department
B-019
La Jolla, Ca. 92093

Ross Milliken
Lawrence Berkeley Laboratory
Berkeley, Ca. 94720

Marie-Noelle Minard
Stanford Linear Accelerator Center
Bin 95
Stanford, Ca. 94305

Michiko Miyamoto
Kobe College
Physics Department
4 - 1, Okadayama
Nishinomiya, Japan 622

I. O. Moen
Trent University
Physics Department
Peterborough, Ont.,
Canada K9J 7B8

Kenneth Moffeit
Stanford Linear Accelerator Center
P. O. Box 4349
Stanford, Ca. 94305

Matias Moreno
University Nacional Autonoma de
Mexico
Instituta de Fisica
Apdo Postal 20-364
Mexico 20, D. F., Mexico

Bob Morse
Stanford Linear Accelerator Center
Bin 98
Stanford, Ca. 94305

Robert Mozley
Stanford Linear Accelerator Center
Bin 65
Stanford, Ca. 94305

J. Murray
Stanford Linear Accelerator Center
Bin 20
Stanford, Ca. 94305

N.

Ann Nelson
Stanford University
Department of Physics
Stanford, Ca. 94305

Charles A. Nelson
State University of New York
Physics Department
Binghamton, NY. 13901

Y. Jack Ng
Stanford Linear Accelerator Center
Bin 81
Stanfor, Ca. 94305

Basarab Nicolescu
Lab. de Physique Theorique des
Particules Elem.
4, Place Jussieu, Tour 16, 1 er etage
F-75230 Paris, Cedex 05, France

Peter Nicoletopoulos
Stanford Linear Accelerator Center
Bin 81
Stanford, Ca. 94305

B. P. Nigam
Arizona State University
Physics Department
Tempe, Az. 85281

Daniel E. Novoseller
452-48
California Institute of Technology
Pasadena Ca. 91125

Pierre Noyes
Stanford Linear Accelerator Center
Bin 81
Stanford, Ca. 94305

O.

Robert Oakes
Northwestern University
Physics Department
Evanston, Il. 60201

Wolfgang Ochs
Max Planck Inst. fur Phys.
Fohringer Ring 6
Postfach 40 12 12
D-8000 Munich 23, Germany

Allen Odian
Stanford Linear Accelerator Center
Bin 65
Stanford, Ca. 94305

Seiji Ono
University of California
Physics Department
Davis, Ca. 95616

R. F. Oppenheim
Yale University
Physics Department
New Haven, Dt. 06520

Harry Orbach
Stanford Linear Accelerator Center
Bin 81
Stanford, Ca. 94305

M. Oreglia
Stanford Linear Accelerator Center
Bin 81
Stanford, Ca. 94305

P.

Pong Youl Pac
Seoul National University
Department of Physics
Seoul 151, Korea

D. A. Palmer
Yale University
Physics Department
New Haven, Ct. -6520

W. K. H. Panofsky
Stanford Linear Accelerator Center
Bin 80
Stanford, Ca. 94305

Robert Panvini
Vanderbilt University
Physics Department
Nashville, Tn. 37235

Sherwood Parker
Lawrence Berkeley Laboratory
Berkeley, Ca. 94720

Richard Partridge
California Institute of Technology
Physics Department
Pasadena, Ca. 91125

Ronald F. Peierls
Brookhaven National Laboratory
Upton, NY. 11973

David Pellett
University of California
Physics Department
Davis, Ca. 95616

Martin Perl
Stanford Linear Accelerator Center
Bin 61
Stanford, Ca. 94305

Ida Peruzzi
Laboratory Nazionali di Frascati
Via E. Fermi
Frascati (Rome) Italy

Henry Pessard
Stanford Linear Accelerator Center
Bin 96
Stanford, Ca. 94305

Aihud Pevsner
Johns Hopkins University
Physics Department
Baltimore, Md. 21218

Marcello Piccolo
Lab. Nazionali di Frascati
Via E. Fermi
Frascati (Rome) Italy

David Pollard
Lawrence Berkeley Laboratory
Berkeley, Ca. 94720

Bojan Pomorisac
Johns Hopkins University
Physics Department
Baltimore, Md. 21218

R. Prepost
University of Wisconsin
Physics Department
Madison, Wi. 53706

C. Y. Prescott
Stanford Linear Accelerator Center
Bin 60
Stanford, Ca. 94305

Ting Pun
Stanford Linear Accelerator Center
Bin 61
Stanford, Ca. 94305

Q.

Helen Quinn
Stanford Linear Accelerator Center
Bin 81
Stanford, Ca. 94305

R.

Petros Rapidis
Stanford Linear Accelerator Center
Bin 61
Stanford, Ca. 94305

Blair Ratcliff
Stanford Linear Accelerator Center
Bin 62
Stanford, Ca. 94305

Mark Richardson
Harvard University
Physics Department
Cambridge, Ma. 02138

David Ritson
Stanford Linear Accelerator Center
Bin 94
Stanford, Ca. 94305

L. Rochester
Stanford Linear Accelerator Center
Bin 96
Stanford, Ca. 94305

Michael T. Ronan
Lawrence Berkeley Laboratory
Berkekey, Ca. 94720

Reinhold Rueckl
University of California
Physics Department
Los Angeles, Ca. 90024

S.

H. Sadrozinski
Princeton University
Physics Department
Princeton, NJ. 08504

Deshdeep Sahdev
Case Western Reserve University
Physics Department
Cleveland, Oh. 44106

Norisuke Sakai
Tohoku University
Physics Department
Sendai, Japan 980

N. P. Samios
Brookhaven National Laboratory
Upton, NY. 11973

Jonathan Sapirstein
Stanford Linear Accelerator Center
Stanford, Ca. 94305

David Saroff
Stanford Linear Accelerator Center
Bin 62
Stanford, Ca. 94305

T. Sato
Stanford Linear Accelerator Center
Bin 96
Stanford, Ca. 94305

Peter Scharbach
Stanford Linear Accelerator Center
Bin 81
Stanford, Ca. 94305

Dan Scharre
Stanford Linear Accelerator Center
Bin 81
Stanford, Ca. 94305

John Schied
California Institute of Technology
Physics Department
Pasadena, Ca. 91125

Rafe Schindler
Stanford Linear Accelerator Center
Bin 95
Stanford, Ca. 94305

Ivan Schmidt
Univ. Tecnica Federico Santa Maria
Casilla 110-V
Valparaiso, Chile

William Schreiber
City University of New York
Sunnyside Campus
Physics Department
Staten Island, NY.10301

K. P. Schuler
Yale University
Physics Department
New Haven, Ct. 06520

Michael Shaevitz
California Institute of Technology
Physics Department
Pasadena, Ca. 91125

Steve Shapiro
Stanford Linear Accelerator Center
Bin 62
Stanford, Ca. 94305

Gordon Shaw
University of Califirnia
Physics Department
Irvine, Ca. 92664

Edward I Shibata
Purdue University
Physics Department
Lafayette, In. 47907

M. Shochet
University of Chicago
Physics Department
Chicago, Il. 60637

Jim Siegrist
Stanford Linear Accelerator Center
Bin 95
Stanford, Ca. 94305

Dennis Silverman
University of California
Physics Department
Irvine, Ca. 92664

Peter Sixel
Tech. Hochsch. Aachen
III. Physikalisches Inst./B
D-5100 Aachen, Germany

Milton D. Slaughter
Los Alamos Scientific Laboratory
P. O. Box 1663
Los Alamos, NM. 87544

Jan Smit
University van Amsterdam
Inst. voor Theoretische Fysica
Valckenierstraat 65
1004 Amsterdam, Netherlands

Arthur Snyder
Argonne National Laboratory
9700 South Cass Avenue
Argonne Il. 60439

Miguel Socolovsky
Inst. Politecnico Nacional
Centro Invest. Estudios
Dept. de Fisica
Apartado Postal 14-740
Mexico 14, D. F., Mexico

Hi Sung Song
Seoul National University
Department of Physics
Seoul 151, Korea

Cherrill Spencer
Stanford Linear Accelerator Center
Bin 81
Stanford, Ca. 94305

Robin Staffin
Stanford Linear Accelerator Center
Bin 81
Stanford, Ca. 94305

Rob A. Stevens
Stanford Linear Accelerator Center
Bin 78
Stanford Ca. 94305

M. L. Stevenson
Lawrence Berkeley Laboratory
Berkeley, CA 94720

Ryszard Stroynowski
Stanford Linear Accelerator Center
Bin 62
Stanford, Ca. 94305

Roberto Suaya
McGill University
Physics Department
MacDonald Chemistry Building
P. O. Box 6070, Station A
Montreal, PQ, Canada H3C 3G1

Chih-Ree Sun
State University of New York
Physics Department
Albany, NY. 12222

Ben Svetitsky
Stanford Linear Accelerator Center
Bin 81
Stanford, Ca. 94305

Marek Szczekowski
Inst. for Nuclear Research
00-681 Warszawa
Hoza-69
Poland

T.

S. Tatur
Institute of Theoretical Physics
Warszawa H02A69, Poland

H. Taureg
Stanford Linear Accelerator Center
Bin 95
Stanford, Ca. 94305

R. E. Taylor
Stanford Linear Accelerator Center
Bin 96
Stanford, Ca. 94305

Hilary N. Thompson
Royal Holloway College
Mathematics Department
Englefield Green, Surrey TW20
OEX England

J. J. Thresher
Rutherford High Energy Laboratory
Chilton
Didcot, Oxon. OX11 OOX, England

John Carter Tompkins
Stanford University
High Energy Physics Laboratory
Stanford, Ca. 94305

John Townsend
Claremont College
Joint Science Department
Claremont, Ca. 91711

J. A. Travis
10695 Eloise Circle
Los Altos Hills, Ca. 90422

Daniel Treille
CERN
CH-1211 Geneva 23,
Switzerland

George Trevino
Del Mar College
Physics Department
Corpus Christi, Tx. 78404

Thomas Trippe
Lawrence Berkeley Laboratory
Berkeley, Ca. 94720

Yung Su Tsai
Stanford Linear Accelerator Center
Bin 81
Stanford, Ca. 94305

Peter Turner
Stanford Linear Accelerator Center
Bin 81
Stanford, Ca. 94305

Chia Tze
Stanford Linear Accelerator Center
Bin 81
Stanford, Ca. 94305

U.

J. Uschersohn
Nordisk Inst. Teoret. Atomfysik
Blegdamsvej 17
DK-2100 Copenhagen, Denmark

V.

Francis J. Vanhecke
Univ. Fed. do Rio Grande do Norte
Department de Fisica
CX Postal 143
Natal, RN 59000, Brazil

Jaroslav Va'vra
Carleton University
Physics Department
Ottawa, On, Canada K1S 5B6

Francesco Villa
Stanford Linear Accelerator Center
Bin 65
Stanford, Ca. 94305

Vincent Vuillemin
Lawrence Berkeley Laboratory
Berkeley, Ca. 94720

W.

Walter W. Wada
Ohio State University
Physics Department
Columbus, Oh. 43210

S. Wagner
Johns Hopkins University
Physics Department
Baltimore, Md. 21218

W. D. Walker
Duke University
Physics Department
Durhan, NC. 27706

Li-chen Wang
Stanford Linear Accelerator Center
Bin 65
Stanford, Ca. 94305

Marvin Weinstein
Stanford Linear Accelerator Center
Bin 81
Stanford, Ca. 94305

J. M. Weiss
Stanford Linear Accelerator Center
Bin 95
Stanford, Ca. 94305

Nathan Weiss
Stanford Linear Accelerator Center
P. O. Box 4349
Stanford, Ca. 94305

R. S. Willey
University of Pittsburgh
Physics Department
Pittsburgh, Pa. 15260

Petro William
Stanford Linear Accelerator Center
Bin 81
Stanford, Ca. 94305

S. H. Williams
Stanford Linear Accelerator Center
Bin 62
Stanford, Ca. 94305

Robert B. Willmann
Purdue University
Physics Department
Lafayette, In. 47907

David Wiser
Stanford Linear Accelerator Center
Bin 94
Stanford, Ca. 94305

Craig Woody
Stanford Linear Accelerator Center
Bin 62
Stanford, Ca. 94305

Y.

Kazuo Yamada
686 Minami-Otsuka
Kawagoe-Shi, Saitama-Ken
Japan

George Yost
Lawrence Berkeley Laboratory
Berkeley, Ca. 94720

Z.

P. M. Zerwas
Tech. Hochsch. Aachen
Inst. fur Theor. Physik
Schinkelstrasse 2
D-5100 Aachen, Germany